



*A National Center of Excellence in Advanced Technology Applications*

ISSN 1520-295X

---

# Seismic Vulnerability Evaluation of Axially Loaded Steel Built-up Laced Members

by

Kangmin Lee and Michel Bruneau

University at Buffalo, State University of New York

Department of Civil, Structural and Environmental Engineering

Ketter Hall

Buffalo, New York 14260

Technical Report MCEER-04-0007

June 30, 2004

This research was conducted at the University at Buffalo, State University of New York and was supported by the Federal Highway Administration under contract number DTFH61-98-C-00094.

## NOTICE

This report was prepared by the University at Buffalo, State University of New York as a result of research sponsored by the Multidisciplinary Center for Earthquake Engineering Research (MCEER) through a contract from the Federal Highway Administration. Neither MCEER, associates of MCEER, its sponsors, the University at Buffalo, State University of New York, nor any person acting on their behalf:

- a. makes any warranty, express or implied, with respect to the use of any information, apparatus, method, or process disclosed in this report or that such use may not infringe upon privately owned rights; or
- b. assumes any liabilities of whatsoever kind with respect to the use of, or the damage resulting from the use of, any information, apparatus, method, or process disclosed in this report.

Any opinions, findings, and conclusions or recommendations expressed in this publication are those of the author(s) and do not necessarily reflect the views of MCEER or the Federal Highway Administration.

## Seismic Vulnerability Evaluation of Axially Loaded Steel Built-up Laced Members

by

Kangmin Lee<sup>1</sup> and Michel Bruneau<sup>2</sup>

Publication Date: June 30, 2004

Submittal Date: September 10, 2003

Technical Report MCEER-04-0007

Task Number 094-C-3.2

FHWA Contract Number DTFH61-98-C-00094

- 1 Graduate Student, Department of Civil, Structural and Environmental Engineering, University at Buffalo, State University of New York
- 2 Professor, Department of Civil, Structural and Environmental Engineering, University at Buffalo, State University of New York

MULTIDISCIPLINARY CENTER FOR EARTHQUAKE ENGINEERING RESEARCH  
University at Buffalo, State University of New York  
Red Jacket Quadrangle, Buffalo, NY 14261

---



## Preface

The Multidisciplinary Center for Earthquake Engineering Research (MCEER) is a national center of excellence in advanced technology applications that is dedicated to the reduction of earthquake losses nationwide. Headquartered at the University at Buffalo, State University of New York, the Center was originally established by the National Science Foundation in 1986, as the National Center for Earthquake Engineering Research (NCEER).

Comprising a consortium of researchers from numerous disciplines and institutions throughout the United States, the Center's mission is to reduce earthquake losses through research and the application of advanced technologies that improve engineering, pre-earthquake planning and post-earthquake recovery strategies. Toward this end, the Center coordinates a nationwide program of multidisciplinary team research, education and outreach activities.

MCEER's research is conducted under the sponsorship of two major federal agencies, the National Science Foundation (NSF) and the Federal Highway Administration (FHWA), and the State of New York. Significant support is also derived from the Federal Emergency Management Agency (FEMA), other state governments, academic institutions, foreign governments and private industry.

The Center's Highway Project develops improved seismic design, evaluation, and retrofit methodologies and strategies for new and existing bridges and other highway structures, and for assessing the seismic performance of highway systems. The FHWA has sponsored three major contracts with MCEER under the Highway Project, two of which were initiated in 1992 and the third in 1998.

Of the two 1992 studies, one performed a series of tasks intended to improve seismic design practices for new highway bridges, tunnels, and retaining structures (MCEER Project 112). The other study focused on methodologies and approaches for assessing and improving the seismic performance of existing "typical" highway bridges and other highway system components including tunnels, retaining structures, slopes, culverts, and pavements (MCEER Project 106). These studies were conducted to:

- assess the seismic vulnerability of highway systems, structures, and components;
- develop concepts for retrofitting vulnerable highway structures and components;
- develop improved design and analysis methodologies for bridges, tunnels, and retaining structures, which include consideration of soil-structure interaction mechanisms and their influence on structural response; and
- develop, update, and recommend improved seismic design and performance criteria for new highway systems and structures.

The 1998 study, “Seismic Vulnerability of the Highway System” (FHWA Contract DTFH61-98-C-00094; known as MCEER Project 094), was initiated with the objective of performing studies to improve the seismic performance of bridge types not covered under Projects 106 or 112, and to provide extensions to system performance assessments for highway systems. Specific subjects covered under Project 094 include:

- development of formal loss estimation technologies and methodologies for highway systems;
- analysis, design, detailing, and retrofitting technologies for special bridges, including those with flexible superstructures (e.g., trusses), those supported by steel tower substructures, and cable-supported bridges (e.g., suspension and cable-stayed bridges);
- seismic response modification device technologies (e.g., hysteretic dampers, isolation bearings); and
- soil behavior, foundation behavior, and ground motion studies for large bridges.

In addition, Project 094 includes a series of special studies, addressing topics that range from non-destructive assessment of retrofitted bridge components to supporting studies intended to assist in educating the bridge engineering profession on the implementation of new seismic design and retrofitting strategies.

*The research discussed in this report was performed within Project 094, Task 094-C-3.2, “Seismic Performance of Steel Superstructures.” The objective of this research is to provide better knowledge on the seismic behavior of laced members, which can be broadly applicable to many steel truss bridges that share similar structural characteristics and details. Commonly encountered built-up brace details and configurations were collected from actual bridges that have laced members. Using this information, an experimental program was designed and conducted to investigate the hysteretic behavior of typical built-up compression members. Strength capacity of the specimens, obtained from the testing, was correlated with the predicted strength in the AISC LRFD Specifications. Assessments of hysteretic properties such as ductility capacity, energy dissipation capacity, and strength degradation after buckling of the specimen were performed. Nonlinear pushover analyses were also conducted and correlated with test results. The low cycle fatigue life of the specimens was quantified and compared with that predicted from models by other researchers. The observed cyclic inelastic behavior of the specimens showed that these latticed members can exhibit variable seismic performance and could often fail to meet the displacement demands for typical braced frames in seismic regions.*

## ABSTRACT

Built-up bracing members have been built as structural members in trusses throughout the United States. These members have typically been designed to resist wind forces, but not earthquakes. Seismic evaluation of steel built-up members is difficult due to the lack of knowledge on the cyclic inelastic behavior of these members. Although some testing of laced members has been conducted by other researchers, results to date have mostly been project specific; consequently, it is difficult to draw general conclusions from those studies. The objective of this research is therefore to provide additional knowledge on the seismic behavior of laced members, supported by experimental results, and that can be broadly applicable to many structures that share similar structural characteristics and details.

In this study, to understand how laced built-up bracing members were originally designed, design provisions and steel design textbooks published at the time when laced bracing were commonly being built, are also reviewed, along with recent research work conducted for built-up bracing members. From the survey of some of the most commonly used shapes and details that have been historically used for built-up members, a range of parameters typically encountered for built-up bracing members, including typical built-up member configurations and lacing geometry, typical  $b/t$  and  $KL/r$  ratios for the built-up members and their lacings, connection details, and other lacing characteristics, are extracted. Based on this information, a limited experimental program is designed and conducted to investigate the hysteretic behavior of typical built-up compression members, including design and quasi-static testing of the specimens.

Strength capacity of the built-up bracing specimens obtained from the testing is correlated with the strength predicted by the AISC LRFD Specification (1999). Assessments of hysteretic properties such as ductility capacity, energy dissipation capacity, and strength degradation after buckling of the specimen are performed. Non-linear pushover analyses are also conducted and correlated with test results. The low cycle fatigue life of the built-up bracing members is quantified and compared with that from the proposed models by other researchers.

From the experimental data obtained from the testing of twelve laced built-up bracing members, and analyses of these results, the experimentally obtained tensile strengths of built-up bracing members is found to be relatively well predicted using equations from the AISC LRFD Specification. When calculating the compressive strength of the built-up bracing members using the AISC LRFD Specification, the theoretical effective length factor,  $K$ , of 0.65 was found to more accurately match the experimental results for X-braced configuration. In single brace configuration, the theoretical length factor,  $K$ , of 1.0 resulted in slightly under-estimating the compressive strength for the members.

Although the laced built-up bracing members with a smaller slenderness ratio dissipated substantial energy dissipation and experienced many inelastic cycles, these members failed to reach the target ductility of 3.0 before starting to fracture. Built-up bracing members with a larger slenderness ratio had sufficient ductility to meet the ductility demand of 3.0 in most cases, although their normalized cumulative energy dissipation and fracture life capacities were much less than those with a smaller slenderness ratio. Built-up laced bracing members with a larger slenderness ratio were shown to have less ductility capacity than monolithic bracing members, while those with a smaller slenderness ratio showed ductility capacity comparable to monolithic bracing members. On average, the tested built-up bracing members with section shape “B” dissipated less normalized cumulative energy than monolithic bracing members, however those with section shape “A” dissipated slightly more normalized cumulative energy.

## **ACKNOWLEDGEMENTS**

This research was conducted by the University at Buffalo and was supported by the Federal Highway Administration under contract number DTFH61-98-C-00094 to the Multidisciplinary Center for Earthquake Engineering Research.



# TABLE OF CONTENTS

SECTION	TITLE	PAGE
<b>1</b>	<b>INTRODUCTION</b> -----	1
	1.1 Statement of the Problem and Objectives -----	1
	1.2 Scope of Work -----	1
	1.3 Outline of Report -----	2
<b>2</b>	<b>LITERATURE REVIEW</b> -----	5
	2.1 Review of Archaic Design Procedures for Laced Brace Members -----	5
	2.1.1 Section Shapes of Laced Compressive Members -----	5
	2.1.2 Design of Lacing Bars -----	7
	2.2 Survey of Recent Experimental Studies -----	10
	2.2.1 Uang and Kleiser (1997) -----	11
	2.2.2 Dameron, Maxwell, and Dunham (1997) -----	11
	2.2.3 Itani, Vesco, and Dietrich (1998) -----	12
	2.2.4 Dietrich and Itani (1999) -----	12
	2.3 Investigations of Existing Bridges -----	13
<b>3</b>	<b>EXPERIMENTAL APPROACH</b> -----	21
	3.1 Selection of Parameters -----	21
	3.2 Design of Specimens and Testing Frames -----	24
	3.2.1 Design of Specimens-----	24
	3.2.2 Design of Testing Frames -----	31
	3.2.3 Design of Foundation Beams -----	32
	3.3 Materials -----	33
	3.4 Test Set-up -----	34

## TABLE OF CONTENTS (continued)

SECTION	TITLE	PAGE
	3.4.1 Mounting of Boundary Frames and Specimens -----	38
	3.4.2 Mounting Actuator -----	38
	3.4.3 Lateral Bracing -----	38
	3.5 Instrumentation -----	39
	3.5.1 Strain gauges -----	39
	3.5.2 Temposonics and LVDTs -----	39
<b>4</b>	<b>EXPERIMENTAL OBSERVATIONS -----</b>	<b>43</b>
	4.1 Loading Programs -----	43
	4.1.1 ATC Loading Protocol -----	43
	4.1.2 Loading Histories -----	43
	4.2 Experimental Observations -----	45
	4.2.1 Bare Frame Testing -----	45
	4.2.2 Specimen Ay8-60 -----	46
	4.2.3 Specimen Ay8-120 -----	55
	4.2.4 Specimen Ay16-60 -----	58
	4.2.5 Specimen Ay16-120 -----	59
	4.2.6 Specimen By8-60 -----	64
	4.2.7 Specimen By8-120 -----	66
	4.2.8 Specimen By16-60 -----	73
	4.2.9 Specimen By16-120 -----	79
	4.2.10 Specimen Bx8-60 -----	83
	4.2.11 Specimen Bx8-120 -----	87
	4.2.12 Specimen Bx16-60 -----	92
	4.2.13 Specimen Bx16-120 -----	96

## TABLE OF CONTENTS (continued)

SECTION	TITLE	PAGE
<b>5</b>	<b>ANALYSIS OF RESULTS – HYSTERETIC BEHAVIOR</b> -----	<b>101</b>
	5.1 Data Analyses of Test Results -----	101
	5.1.1 Tension Strength -----	101
	5.1.2 Compression Strength -----	106
	5.1.3 Hysteretic Curves -----	117
	5.2 Non-linear Analyses -----	133
	5.2.1 Modeling -----	133
	5.2.2 Comparisons with Test Results -----	133
	5.3 General Observations -----	136
<b>6</b>	<b>ANALYSIS OF RESULTS – NORMALIZED COMPRESSION STRENGTH, NORMALIZED HYSTERETIC ENERGY, AND LOW CYCLE FATIGUE RESULTS</b> -----	<b>153</b>
	6.1 Energy Dissipation -----	153
	6.2 Strength Degradation -----	164
	6.3 Low Cycle Fatigue Fracture Life -----	164
	6.3.1 Tang and Goel Model -----	164
	6.3.2 Archambault et al. Model -----	166
	6.3.3 Fracture life of Built-up Specimens -----	188
	6.4 General Observations -----	193
<b>7</b>	<b>SUMMARY AND CONCLUSIONS</b> -----	<b>195</b>
	7.1 Summary -----	195
	7.2 Conclusions -----	195

## TABLE OF CONTENTS (continued)

SECTION	TITLE	PAGE
	7.3 Recommendations and Further Research -----	198
<b>8</b>	<b>REFERENCES -----</b>	<b>201</b>
<b>APPENDIX A</b>	<b>Drawings Specimens and Boundary Frames -----</b>	<b>205</b>
<b>APPENDIX B</b>	<b>Experimental Observations Made During Testing -----</b>	<b>225</b>
<b>APPENDIX C</b>	<b>Hysteretic Curves from Test Results -----</b>	<b>239</b>
<b>APPENDIX D</b>	<b>Normalized Energy Dissipation of Specimens -----</b>	<b>257</b>

## LIST OF FIGURES

FIGURE	TITLE	PAGE
2.1	Cross sections for (a – d) non-symmetric built-up latticed compression members; (e – h) symmetric built-up latticed compression members (Ketchum, 1920) -----	6
2.2	Latticed compression members (Caltrans, 1995) -----	6
2.3	Plate lacing bar -----	9
2.4	Axial and shear forces in compression member -----	9
2.5	Section shapes from the existing bridges survey -----	14
2.6	Lacing configurations -----	14
3.1	Distributions of b/t ratios and KL/r ratios -----	23
3.2	Section shapes -----	23
3.3	Design of dummy bracing members -----	28
3.4	Dummy bracing members -----	29
3.5	Detailed cross section shapes of the specimens -----	30
3.6	An example test set-up -----	35
3.7	Stress-strain curve for the angle 1 x 1 x 1/8 -----	35
3.8	Stress-strain curve for the angle 1-1/2 x 1-1/2 x 3/16 -----	36
3.9	Stress-strain curve for the angle 2 x 2 x 1/8 -----	36
3.10	Stress-strain curve for the plate with thickness of 1/8 -----	37
3.11	Stress-strain curve for the plate with thickness of 3/8 -----	37
3.12	Test set-ups -----	40
3.13	Lateral bracing -----	41
3.14	Strain gauge layouts -----	41
3.15	Temposonics and LVDT layout -----	42
4.1	ATC loading protocol (ATC, 1992) -----	44
4.2	Loading histories for “Ay” specimens -----	48
4.3	Loading histories for “By” specimens -----	49
4.4	Loading histories for “Bx” specimens -----	50

## LIST OF FIGURES (continued)

FIGURE	TITLE	PAGE
4.5	FBD for axial force corrections from SAP 2000 analysis (KL/r = 60) – example for Ay8-60 Specimen -----	51
4.6	FBD for axial force corrections from SAP 2000 analysis (KL/r = 120) – example for Ay8-120 Specimen -----	51
4.7	Test set-up for Bare Frame Test -----	52
4.8	Hysteretic curve for Bare Frame Test -----	52
4.9	Test set-up for the Ay8-60 specimen -----	53
4.10	Hysteretic curve for the Ay8-60 specimen -----	53
4.11	Observations made during testing of the Ay8-60 specimen -----	54
4.12	Test set-up for the Ay8-120 specimen -----	56
4.13	Hysteretic curve for the Ay8-120 specimen -----	56
4.14	Observations made during testing of the Ay8-120 specimen -----	57
4.15	Test set-up for the Ay16-60 specimen -----	60
4.16	Hysteretic curve for the Ay16-60 specimen -----	60
4.17	Observations made during testing of the Ay16-60 specimen -----	61
4.18	Test set-up for the Ay16-120 specimen -----	62
4.19	Hysteretic curve for the Ay16-120 specimen -----	62
4.20	Observations made during testing of the Ay16-120 specimen -----	67
4.21	Test set-up for the By8-60 specimen -----	69
4.22	Hysteretic curve for the By8-60 specimen -----	69
4.23	Observations made during testing of the By8-60 specimen -----	70
4.24	Test set-up for the By8-120 specimen -----	72
4.25	Hysteretic curve for the By8-120 specimen -----	72
4.26	Observations made during testing of the By8-120 specimen -----	74
4.27	Test set-up for the By16-60 specimen -----	76
4.28	Hysteretic curve for the By16-60 specimen -----	76
4.29	Observations made during testing of the By16-60 specimen -----	77

## LIST OF FIGURES (continued)

FIGURE	TITLE	PAGE
4.30	Test set-up for the By16-120 specimen -----	80
4.31	Hysteretic curve for the By16-120 specimen -----	80
4.32	Observations made during testing of the By16-120 specimen -----	81
4.33	Test set-up for the Bx8-60 specimen -----	84
4.34	Hysteretic curve for the Bx8-60 specimen -----	84
4.35	Observations made during testing of the Bx8-60 specimen -----	85
4.36	Test set-up for the Bx8-120 specimen -----	89
4.37	Hysteretic curve for the Bx8-120 specimen -----	89
4.38	Observations made during testing of the Bx8-120 specimen -----	90
4.39	Test set-up for the Bx16-60 specimen -----	93
4.40	Hysteretic curve for the Bx16-60 specimen -----	93
4.41	Observations made during testing of the Bx16-60 specimen -----	94
4.42	Test set-up for the Bx16-120 specimen -----	98
4.43	Hysteretic curve for the Bx16-120 specimen -----	98
4.44	Observations made during testing of the Bx16-120 specimen -----	99
5.1	Tensile strength comparisons -----	112
5.2	Effective length factor, K (specimens with $KL/r = 60$ ) -----	112
5.3	Compressive strength comparisons ( $KL/r = 60$ ) -----	113
5.4	Initial imperfection of By8-60 specimen -----	113
5.5	Theoretical K value for test specimens with $KL/r = 120$ -----	116
5.6	Compressive strength comparisons ( $KL/r = 120$ ) -----	116
5.7	Definition of experimental buckling and yield displacement ( $\delta_{b,exp}$ and $\delta_{y,exp}$ ) ---	121
5.8	Definition of equivalent horizontal frame drift ( $\Delta$ ) -----	121
5.9	Normalized hysteretic curves for Ay specimens (Element, $\delta_{b,exp}$ ) -----	122
5.10	Normalized hysteretic curves for Ay specimens (System, $\delta_{b,exp}$ ) -----	123
5.11	Normalized hysteretic curves for By specimens (Element, $\delta_{b,exp}$ ) -----	124
5.12	Normalized hysteretic curves for By specimens (System, $\delta_{b,exp}$ ) -----	125

## LIST OF FIGURES (continued)

FIGURE	TITLE	PAGE
5.13	Normalized hysteretic curves for Bx specimens (Element, $\delta_{b,exp}$ ) -----	126
5.14	Normalized hysteretic curves for Bx specimens (System, $\delta_{b,exp}$ ) -----	127
5.15	Hysteretic curves for By8-60 specimen -----	128
5.16	Theoretical displacements of upper and lower specimens -----	129
5.17	Relationship between system ductility ( $\mu_{sys}$ ) and element (1 buckled brace) ductility ( $\mu_{ele}$ ) neglecting brace strength degradation -----	129
5.18	SAP 2000 model for By16-60 specimen -----	130
5.19	Gage correction factors from SAP 2000 analyses -----	130
5.20	Tension only braced frame design -----	131
5.21	X-braced frame design -----	131
5.22	Ductility comparisons between slender and stocky braces in a X-braced frame -	132
5.23	Relationship between compressive and tensile ductility -----	132
5.24	Analyses model for DRAIN-2DX -----	134
5.25	Comparison between analysis and experimental results of Ay8-60 specimen ---	134
5.26	Comparison between analysis and experimental results of Ay8-120 specimen (Theoretical K = 1.0) -----	140
5.27	Comparison between analysis and experimental results of Ay8-120 specimen (Experimental K = 0.91) -----	140
5.28	Comparison between analysis and experimental results of Ay16-60 specimen -	141
5.29	Comparison between analysis and experimental results of Ay16-120 specimen (Theoretical K = 1.0) -----	141
5.30	Comparison between analysis and experimental results of Ay16-120 specimen (Experimental K = 0.93) -----	142
5.31	Comparison between analysis and experimental results of By8-60 specimen ---	142
5.32	Comparison between analysis and experimental results of By8-120 specimen (Theoretical K = 1.0) -----	143

## LIST OF FIGURES (continued)

FIGURE	TITLE	PAGE
5.33	Comparison between analysis and experimental results of By8-120 specimen (Experimental $K = 0.77$ ) -----	143
5.34	Comparison between analysis and experimental results of By16-60 specimen --	144
5.35	Comparison between analysis and experimental results of By16-120 specimen (Theoretical $K = 1.0$ ) -----	144
5.36	Comparison between analysis and experimental results of By16-120 specimen (Experimental $K = 0.71$ ) -----	145
5.37	Comparison between analysis and experimental results of Bx8-60 specimen ----	145
5.38	Comparison between analysis and experimental results of Bx8-120 specimen (Theoretical $K = 1.0$ ) -----	146
5.39	Comparison between analysis and experimental results of Bx8-120 specimen (Experimental $K = 0.85$ ) -----	146
5.40	Comparison between analysis and experimental results of Bx16-60 specimen --	147
5.41	Comparison between analysis and experimental results of Bx16-120 specimen -----	147
5.42	Comparison between analysis and experimental results of Bx16-120 specimen (Experimental $K = 0.76$ ) -----	148
5.43	Ductility comparisons ( $\mu_b$ ) -----	149
5.44	Ductility comparisons ( $\mu_y$ ) -----	150
5.45	Ductility comparisons ( $\mu_y^{*1}$ ) -----	151
6.1	Definition of dissipated energy ratio, $E_C / E_T$ (Lee and Bruneau, 2002) -----	155
6.2	Definition of axial displacement, $\delta$ (Lee and Bruneau, 2002) -----	155
6.3	Normalized hysteretic energy ratios in compression for Ay Specimens (Element) -----	156
6.4	Normalized hysteretic energy ratios in compression for Ay Specimens (System) -----	157

## LIST OF FIGURES (continued)

FIGURE	TITLE	PAGE
6.5	Normalized hysteretic energy ratios in compression for By Specimens (Element) -----	158
6.6	Normalized hysteretic energy ratios in compression for By Specimens (System) -----	159
6.7	Normalized hysteretic energy ratios in compression for Bx Specimens (Element) -----	160
6.8	Normalized hysteretic energy ratios in compression for Bx Specimens (System) -----	161
6.9	Normalized cumulative energy in compression (Element) -----	162
6.10	Normalized cumulative energy in compression (System) -----	163
6.11	Definition of normalized buckling capacity, $C_r'' / C_r (1^{st})$ (Lee and Bruneau, 2002) -----	167
6.12	Definition of normalized buckling capacity, $C_r'' / C_r$ (Last) (Lee and Bruneau, 2002) -----	167
6.13	Normalized buckling capacity, $C_r'' / C_r (1^{st})$ for Ay specimens (Element) -----	168
6.14	Normalized buckling capacity, $C_r'' / C_r (1^{st})$ for Ay specimens (System) -----	169
6.15	Normalized buckling capacity, $C_r'' / C_r$ (Last) for Ay specimens (Element) -----	170
6.16	Normalized buckling capacity, $C_r'' / C_r$ (Last) for Ay specimens (System) -----	171
6.17	Normalized buckling capacity, $C_r'' / C_r (1^{st}/Last)$ for Ay specimens (Element) --	172
6.18	Normalized buckling capacity, $C_r'' / C_r (1^{st}/Last)$ for Ay specimens (System) ---	173
6.19	Normalized buckling capacity, $C_r'' / C_r (1^{st})$ for By specimens (Element) -----	174
6.20	Normalized buckling capacity, $C_r'' / C_r (1^{st})$ for By specimens (System) -----	175
6.21	Normalized buckling capacity, $C_r'' / C_r$ (Last) for By specimens (Element) -----	176
6.22	Normalized buckling capacity, $C_r'' / C_r$ (Last) for By specimens (System) -----	177
6.23	Normalized buckling capacity, $C_r'' / C_r (1^{st}/Last)$ for By specimens (Element) --	178
6.24	Normalized buckling capacity, $C_r'' / C_r (1^{st}/Last)$ for By specimens (System) ---	179

## LIST OF FIGURES (continued)

FIGURE	TITLE	PAGE
6.25	Normalized buckling capacity, $C_r'' / C_r (1^{st})$ for Bx specimens (Element) -----	180
6.26	Normalized buckling capacity, $C_r'' / C_r (1^{st})$ for Bx specimens (System) -----	181
6.27	Normalized buckling capacity, $C_r'' / C_r$ (Last) for Bx specimens (Element) -----	182
6.28	Normalized buckling capacity, $C_r'' / C_r$ (Last) for Bx specimens (System) -----	183
6.29	Normalized buckling capacity, $C_r'' / C_r (1^{st}/Last)$ for Bx specimens (Element) --	184
6.30	Normalized buckling capacity, $C_r'' / C_r (1^{st} / Last)$ for Bx specimens (System) --	185
6.31	Typical cycles in a deformation history of Tang and Goel model (1987) -----	186
6.32	Equivalent conversion between hysteretic cycles and the standard cycles of Tang and Goel model (1987) -----	186
6.33	Definition of $\Delta_1$ and $\Delta_2$ (Lee and Goel model) -----	187
6.34	Experimental fracture life from hysteretic curve normalized by $\delta_y^*$ -----	189
6.35	Comparisons of fracture life of the specimens -----	191



## LIST OF TABLES

TABLE	TITLE	PAGE
2.1	Bridges investigated -----	15
2.2	Characteristics of laced built-up members -----	16
2.3	Characteristics of lacings -----	18
3.1	Summary of experimental parameters to be considered -----	22
3.2	Given specimen names -----	22
3.3	Specimen design -----	26
3.4	Coupon test results -----	34
4.1	Summary of equilibrium for converting from $P_H$ to $P_D$ (Results are from SAP2000 analyses) -----	46
5.1	Cross sectional properties of the specimens -----	103
5.2	Tensile strength comparison -----	105
5.3	Modified slenderness ratios for $B_y$ specimens per different assumptions -----	108
5.4	Effective length factor, $K$ (specimens with $KL/r = 60$ ) -----	109
5.5	Compressive strength comparison (specimens with $KL/r = 60$ ) -----	110
5.6	Buckling mode observed at its maximum compressive forces reached (specimens with $KL/r = 60$ ) -----	110
5.7	Compressive strength comparison (specimens with $KL/r = 120$ ) -----	114
5.8	Buckling mode observed at its maximum compressive forces reached (specimens with $KL/r = 120$ ) -----	115
5.9	Effective length factor, $K$ (specimens with $KL/r = 120$ ) -----	115
5.10	Ductility capacity comparisons -----	138
6.1	Cumulative energy dissipation ratios capacity of the specimens -----	154
6.2	Experimentally obtained fracture life the specimens ( $\Delta_{f,exp}$ ) -----	190
6.3	Predicted fracture life the specimens ( $\Delta_f$ and $\Delta_f^*$ ) -----	190



# SECTION 1

## INTRODUCTION

### 1.1 Statement of the Problem and Objectives

A large number of steel truss bridges have been built through out the United States, many in zones of moderate to large seismicity. These bridges have typically been designed to resist wind forces, but not earthquakes. Structural analysis of such bridges typically reveal that many key structural members along the load path followed by the seismically-induced forces may buckle, yield, or suffer brittle fracture. Built-up bracing members have been used as structural members in those bridges. These members are formed by combining rolled plate, channel, angle sections to fabricate shapes with open webs or sides. For example, channels are typically connected by bars and plates to create laced box sections to resist substantial compression forces. Tie plates (also called stay plates) are usually placed at the end of the laced member and at the intermediate lacing interruptions producing a non-uniform cross section along the span of the member.

Seismic evaluation of steel truss bridges is difficult due to the lack of knowledge on the cyclic inelastic behavior of built-up members of the type typically found in these bridges, and on the riveted connections of these members. Although some testing of bridge-specific laced members has been conducted by other researchers, results to date have mostly been project specific; consequently, it is difficult to draw general conclusions from those studies. The objective of this research is therefore to provide better knowledge on the seismic behavior of laced members, supported by experimental results, and that can be broadly applicable to many steel truss bridges that share similar structural characteristics and details.

### 1.2 Scope of Work

Commonly encountered built-up brace details and configurations, and foundation anchorage details have been collected from actual bridges through a few selected consulting firms experienced in the rehabilitation of existing bridges. A particular attention was paid to identify

those details that are germane to bridges in the Eastern United States, but given the fact that most bridges were conceived in absence of earthquake-resistant design knowledge, similar details are commonly encountered nationwide.

Using the above information, a limited experimental program was designed and conducted to investigate the hysteretic behavior of typical built-up compression members, including design and quasi-static testing of the specimens.

Strength capacity of the specimens obtained from the testing is correlated with the predicted strength from the AISC LRFD Specification (1999). Assessments of hysteretic properties such as ductility capacity, energy dissipation capacity, and strength degradation after buckling of the specimen are performed. Non-linear pushover analyses are also conducted and correlated with test results.

Finally, the low cycle fatigue life of the specimens is quantified and compared with that from the proposed models by other researchers.

### **1.3 Outline of Report**

Following this introductory section, SECTION 2 describes the literature review of laced brace members. Design provisions in the literature, particularly in steel design textbooks published at the turn of the century are described along with recent research work conducted for the major crossings in California. Drawings obtained for a few existing bridges having truss substructures (bents, towers, etc.) with laced members are also reviewed to investigate those commonly used shapes and details that have been historically used for built-up members.

SECTION 3 presents the design of built-up laced bracing members considered as part of the experimental program conducted here, using design parameters from the literature review. Details on test set-up are given along and results from coupon testing of materials used for the test specimens. The instrumentation layout is also described.

In SECTION 4, loading protocol used for quasi-static testing is discussed, followed by descriptions of observations (including some photos) made during the testing of each specimen.

SECTION 5 discusses the hysteretic behavior from the test results, including tensile and compressive strength comparison and normalized hysteretic curves of the specimens. Results from the non-linear analyses of specimens are also discussed.

SECTION 6 discusses results of the testing in a quantitative manner including energy dissipation in compression and strength degradation of compressive members. The low cycle fatigue life of test specimens is also discussed.

Summary and conclusions of this study are presented in SECTION 7 and recommendations for future research are also given.

Finally, references are in SECTION 8.



## SECTION 2

### LITERATURE REVIEW

This research focuses on the study of built-up bracing members subjected to cyclic loading. In this section, some design provisions for built-up laced members are reviewed, particularly those found in archaic steel design textbooks published at the turn of the century (Ketchum, 1920 and Kunz, 1915), along with recent research work conducted for the major crossings in California (Uang and Kleiser, 1997, Itani et al., 1998, and Dietrich and Itani, 1999). Commonly encountered built-up brace details and configurations are collected from actual bridges drawings obtained from a few selected consulting firms and departments of transportation experienced in the rehabilitation of existing bridges.

#### **2.1 Review of Archaic Design Procedures for Laced Brace Members**

To understand how laced built-up bracing members were originally designed, design provisions and steel design textbooks published at the time when laced bracing were commonly being built, were reviewed.

##### ***2.1.1 Section Shapes of a Laced Compressive Members***

Typically, laced built-up compression members were built from angles and channels connected with bars and plates by rivets to form I shapes and box shapes as shown in Figure 2.1. Note that dotted lines represent lacings in Figure 2.1. These laced built-up members have been used to resist compression and tension forces. To satisfy the requirements of codes and specifications, and increased global buckling strength could be achieved by changing the distance between the assembled parts, that is by changing cross sectional properties such as moment of inertia,  $I$  and radius of gyration,  $r$ . Tie plates (also called stay plates) were usually placed at the end of the laced compression member and at the intermediate lacing interruptions (where braces crossed) producing a non-uniform cross section along the span of the member as shown in Figure 2.2 (Caltrans, 1995).

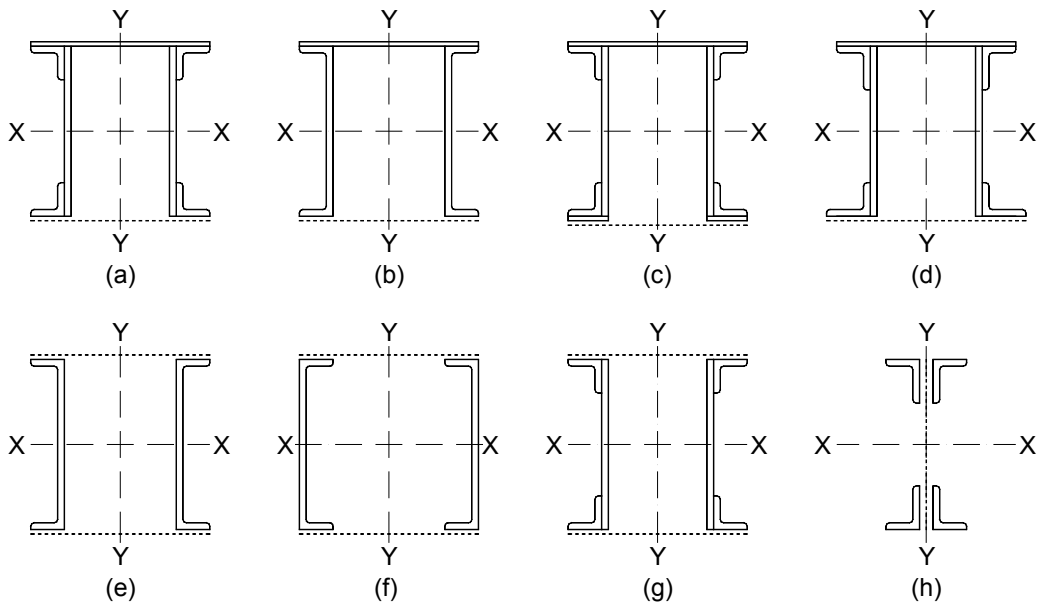


Figure 2.1 Cross sections for (a – d) non-symmetric built-up latticed compression members; (e – h) symmetric built-up latticed compression members (Ketchum, 1920) – symmetric cases considered in this study

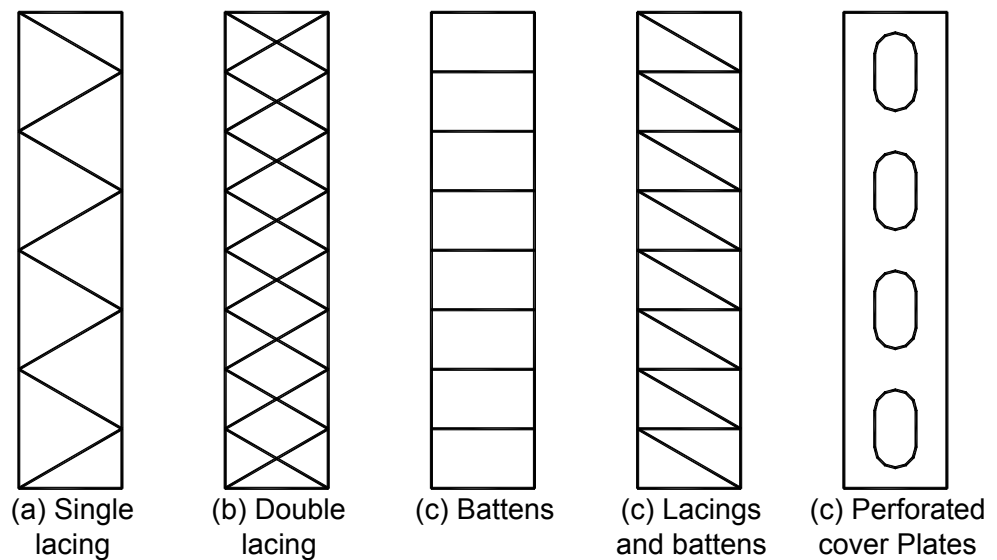


Figure 2.2 Latticed compression members (Caltrans, 1995)

### 2.1.2 Design of Lacing Bars

In a laced built-up compression members, lacing bars were used to join the parts of the member together, and make it act as a solid member to resist the shear due to bending and diagonal shear in the member. The length of lacing bars were commonly designed with a thickness of not less than 1/40 the distance between end rivets for single lacing, or 1/60 of the distance between rivets for double lacing riveted in the middle (Ketchum, 1920).

For single lacing,

$$t \geq l/40 \quad (2.1 \text{ a})$$

For double lacing,

$$t \geq l/60 \quad (2.1 \text{ b})$$

These limitations translate into slenderness limits for lacing bars. Assuming plate lacing members of rectangular cross section, with width of  $B$ , thickness of  $t$ , and length of  $l$  as shown in Figure 2.3. Considering,  $I = \frac{Bt^3}{12}$  and  $A = Bt$ , then  $t = r\sqrt{12}$ , and Eq. 2.1 can be rewritten as:

For single lacing,

$$\frac{l}{r} \leq 138.6 \quad (2.2 \text{ a})$$

For double lacing,

$$\frac{l}{r} \leq 207.8 \quad (2.2 \text{ b})$$

It was also typically required that the spacing between laces be such that the sum of the strength of the individual constituting elements of the built-up cross-section between laces be stronger than the member as a whole to prevent localized buckling of an angle, plate, or channel prior to

attaining the design compression strength of the built-up member. Specifications also required that lacing bars be at an angle with the axis of the member of 45 or 60 degrees for double and single lacings, respectively.

The design of lacing bars on compression members was largely a matter of judgment and any theory advanced can be only an approximation. A guide in designing lacing bar of heavy compression member was introduced in structural design text by Kunz (1915) and Ketchum (1920). They suggested the following, considering that any compression strength formula can be cast into the form of:

$$s_b = s - f\left(\frac{L}{r}\right) \quad (2.3)$$

where,  $s_b$  is an allowable buckling stress,  $s$  is an allowable axial stress, and  $f\left(\frac{L}{r}\right)$  denotes a certain function of  $\left(\frac{L}{r}\right)$  and may be regarded as the bending stress produced by the axial load  $P$  in the deflected column as shown in Figure 2.4 and can be presented as:

$$f\left(\frac{L}{r}\right) = \frac{My}{I} = \frac{P\delta}{S} \quad (2.4)$$

where,  $S$  is section modulus,  $S = I/y$

The shear force,  $V$  produced along the deflected compression member can be obtained by resolving the axial force,  $P$  into components parallel to the elastic deflected shape and normal to  $P$ . Assuming the elastic deflected shape to be a parabola,  $V$  can be obtained as:

$$V = P \frac{2\delta}{L/2} = \frac{4}{L} P\delta \quad (2.5)$$

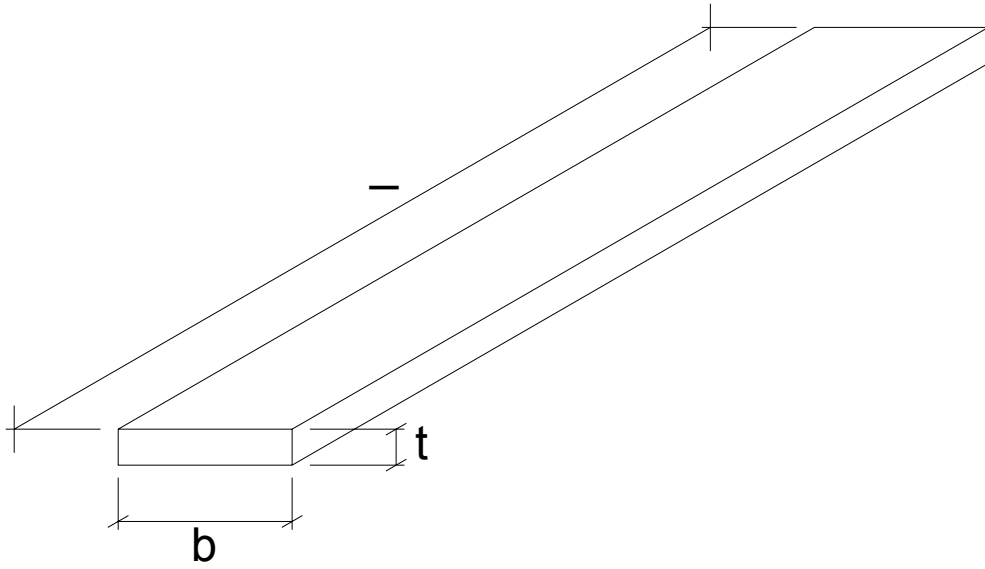


Figure 2.3 Plate lacing bar

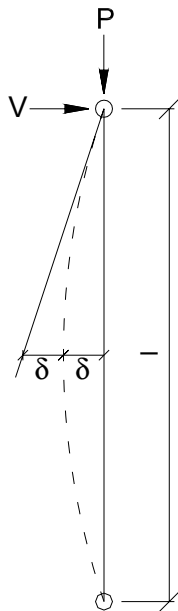


Figure 2.4 Axial and shear forces in compression member

Substituting Eq. 2.4 into Eq. 2.5:

$$V = \frac{4}{L} S f\left(\frac{L}{r}\right) \quad (2.7)$$

In old design requirements, for a concentrically loaded compressive member, the allowable buckling stress was often represented by a straight line reduction from an allowable compression stress as a function of member slenderness, such as per the formula (Ketchum, 1920):

$$s_b = 16000 - 70\left(\frac{L}{r}\right) \quad (2.8)$$

Since,  $f\left(\frac{L}{r}\right) = 70\left(\frac{L}{r}\right) s_b$  in Eq 2.8, Eq 2.7 can be rewritten as:

$$V = 280 \frac{S}{r} \quad (2.9)$$

In addition, Kunz (1915) advised to limit the allowable compressive stress in flat lacing bar to no more than  $10000 - 40\frac{L}{r}$  or to use lacing angles or channels based on the results of research by others at the time.

## 2.2 Survey of Recent Experimental Studies

The cyclic behavior of built-up laced member subjected to repeated axial loads was apparently first studied by Caltrans (1995). In this research program, the capacity of laced compression members (and their connections) used in the San Francisco-Oakland bay bridge was evaluated. In the following, parts of the Caltrans' research program relevant to the hysteretic behavior of laced members are reviewed.

### **2.2.1 *Uang and Kleiser (1997)***

Uang and Kleiser (1997) tested three one-half scale laced built-up compression members subjected to axial load eccentricities of 0, 5, and 15 inches to determine their cyclic behavior and ultimate strength. The objectives were to develop an axial force–moment (P-M) interaction relationship for these members and investigate post-buckling behavior such as strength degradation and ductility capacity under cyclic loading conditions, as well as net section fracture. Shearing effect produced by lacing was also studied.

The test results showed that compressive capacity of the laced specimens could be predicted reliably taking into account shearing effects of lacing and effective length factors. The three specimens were able to reach and exceed the axial force–moment interaction surface predicted by AISC LRFD Specification. However, because average over-strength was less than otherwise obtained for usual beam-columns (e.g. W-shapes), reduced  $\Phi$  factors were suggested to use with the AISC LRFD axial force–moment interaction formulae for the seismic retrofit design of laced members for the San Francisco–Oakland bay bridge.

### **2.2.2 *Dameron, Maxwell, and Dunham (1997)***

Dameron et al. (1997) performed pre-test analyses to predict the hysteretic behavior, capacity, and failure mode of the three built-up laced compression members tested by Uang and Kleiser (1997). In this study, three loadings conditions (monotonic compression, monotonic tension, and cyclic test loading history) were considered for each test specimen using finite element analysis software, ABAQUS. In modeling the test specimens, gussets were strengthened to prevent failure in the gusset connection regions because the research focused on the behavior of the laced built-up compression members themselves.

From the finite element analyses of the three test specimens of Uang and Kleiser (1997), it was found that although each specimen was significantly damaged early during the  $\delta/\delta_y = 1.5$  test cycle, all specimens survived this cycle without fracturing. Also comparisons between test and

analysis results showed that analyses predicted peak compressive and tension strength within 10 percents, and displacements within 15 percents. Analyses also predicted reasonably well trends in local buckling.

### **2.2.3 *Itani, Vesco, and Dietrich (1998)***

Itani et al. (1998) tested a half scale specimen that represented the diagonal member of a tower (pier) of the eastern span of the San Francisco–Oakland bay bridge. Built-up laced member specimen included representative end conditions, and were subjected to cyclic loading to determine the cyclic behavior and to evaluate the ultimate tensile and compressive capacity and post-buckling behavior of laced members with realistic end connections.

Testing revealed that, due to premature local buckling near connection, only 60 percent of the predicted compressive strength could be reached. That was consistent with predictions done for the compression strength of individual components (between laces) calculated using the AISC LRFD relationships. Itani et al. recommended to extend the stay plates of laced members as much as possible into the gusset connection to partly improve seismic performance.

### **2.2.4 *Dietrich and Itani (1999)***

Dietrich and Itani (1999) tested two half scale built-up member specimens, one with lacings and the other with perforated built-up plates, representative of diagonal members of bents in western approach spans of the Francisco – Oakland bay bridge. Cyclic testing was performed to determine the cyclic behavior of built-up laced and perforated members with representative end conditions and as well as to evaluate the ultimate tensile and compressive capacity and post-buckling behavior of laced and perforated members. Displacement ductility and energy dissipation capacities were evaluated from the test results.

Test results showed that both laced and perforated specimens were not able to reach the capacity predicted by the AISC LRFD Specification. However, perforated diagonal compression member was found to be more ductile and more capable of energy dissipation than the laced member.

### 2.3 Investigation of Existing Bridges

A survey was conducted to identify some of the most commonly used shapes and details that have been historically used for built-up members in steel truss bridge braced pier substructures. As a result of discussion with the California, Oregon, Washington, Tennessee and New York DOTs, as well as with a few consulting engineering firms, drawings were obtained from for a few existing bridges having truss substructures (bents, towers, etc.) having laced members and these are summarized in Table 2.1. This survey showed that braces in these bridges almost universally consist of laced built-up members with riveted connections. Five common cross-sectional configurations have been identified as seen in Figure 2.5. From the limited survey, it was found that section type A (equivalent to an I shape rolled section) was frequently used as diagonal bracings or struts in bridge bents and section type B was used for columns or diagonal bracings where larger compression strength is needed.

Potential failure modes of built-up laced members are global buckling (in-plane or out-of-plane of the frame) or local buckling so research focused mainly on assessing the impact of slenderness ratios,  $KL/r$ , and width-to-thickness ratios,  $b/t$ , on the seismic behavior of laced members. A summary of the values of these parameters considered for these parameters is presented in Table 2.2. It was found from the sample of bridges for which structural drawings were collected that the slenderness ratios of laced members ranged from 40 to 160 and that the width-to-thickness ratios ranged from 8 to 19. However, slenderness ratios and width to thickness ratios of most laced members were within the 60 to 120 and the 8 to 16 ranges, respectively.

Another key issue characterizing the laced built-up compression member is the lacing members themselves. Information on the lacing types, single and double lacings, and slenderness ratios,  $kl/r$ , was collected from the drawings presented in Table 2.1. Lacing forces were also calculated by the procedure described Section 2.1 to achieve an understandings of design procedures for lacing members. Information on the characteristics of lacing member investigated is summarized in Table 2.3. Lacings are classified as single and double lacings by their configurations in a laced compression member as presented in Figure 2.6. Survey showed that slenderness ratio of lacings ranged from 90 to 150 and 170 to 240 for single and double lacings,

respectively. Note that some of these lacings violate the prescribed limits of approximately 140 and 200 for single and double lacings, respectively described in Section 2.1.2. The angle between lacing and longitudinal axis of the member was found to be approximately 60 degrees for single lacings and 45 degrees for double lacings, for the bridges reviewed.

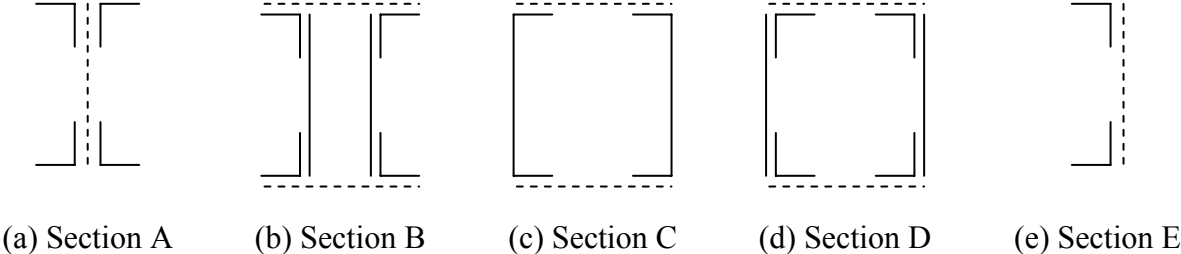


Figure 2.5 Section shapes from the existing bridges survey

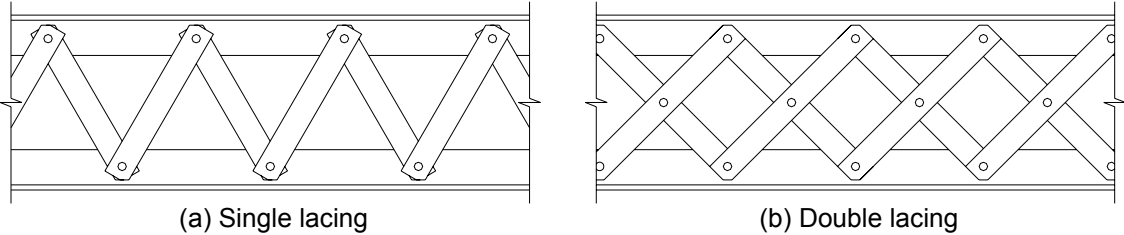


Figure 2.6 Lacing configurations

Table 2.1 Bridges investigated

<b>Bridges</b>	<b>Location</b>	<b>Designed by</b>	<b>Built in</b>	<b>Total Span feet (meter)</b>	<b>Main Span feet (meter)</b>
Rip-Van-Winkle Bridge	Between Catskill and Hudson, NY	NY State Bridge Authority	1934	5041 (1538)	800 (244)
Lincoln Tunnel Bridge	New York, NY	The Port of NY Authority	1955	467 (142)	213 (65)
North Grand Island Bridge	Between Grand Island and Niagara, NY	Hardesty & Hanover Engineering	1962	4025 (1228)	500 (153)
White Water Bridge	N.Santiam Hwy Oregon	Dept. of Agriculture	1931	330 (100)	60 (18)
F.B. Hoit Bridge	City of Tacoma, WA	Washington D.O.T.	1929	562 (171)	72 (22)
Younglove CR Bridge	City of Tacoma, WA	King County Engineering	1929	264 (81)	72 (22)
Anderson CR Bridge	Anderson CR, Canada	Waddel & Marrington	1912	910 (278)	70 (21)
River du Milieu bridge	Quebec, Canada	Dominion Bridge Co.	1908	-	225 (69)
San Francisco - Oakland Bay Bridge	San Francisco, CA	CA State Bridge Authority	1936	845 (258)	193 (59)

Table 2.2 Characteristics of laced built-up members

Bridges	Usages	Section Shape	Sections Used	B in(mm)	D in(mm)	L in(mm)	KL/r <sub>x</sub>	KL/r <sub>y</sub>	b/t
Rip-Van-Winkle Bridge	Column	B	4Ls-6x6x5/8 2PLs-24x5/8	26.0 (660.4)	24.0 609.6)	318.0 (8077.2)	72.2	40.5	9.6
	Transverse Bracing	A	4Ls-5x3 <sup>1/2</sup> x3/8	10.4 (264.2)	12.5 (317.5)	195.9 (4975.9)	35.7	81.5	13.3
	Transverse Strut	A	4Ls-5x3 <sup>1/2</sup> x3/8	10.4 (264.2)	18.0 (457.2)	214.4 (5445.8)	26.1	89.2	13.3
North Grand Island Bridge	Transverse Bracing	E	2Ls-6x3 <sup>1/2</sup> x3/8	6.0 (152.4)	21.0 (533.4)	151.8 (3855.7)	15.6	49.6	16.0
	Transverse Strut	E	2Ls-6x3 <sup>1/2</sup> x3/8	6.0 (152.4)	21.0 (533.4)	214.7 (5453.4)	22.0	70.1	16.0
	Column	B	4Ls-3 <sup>1/2</sup> x3 <sup>1/2</sup> x7/16 2PL-18x7/16	25.8 (655.3)	18.0 (457.2)	256.6 (6517.6)	53.0	21.0	7.3
Anderson Creek Bridge	Longitudinal Bracing	A	4Ls-5x3x3/8	10.4 (264.2)	17.9 (454.7)	285.7 (7256.8)	60.2	115.3	13.3
	Longitudinal Strut	A	4Ls-4x3x3/8	8.4 (213.4)	17.9 (454.7)	228.1 (5793.7)	48.3	117.8	10.7
	Transverse Bracing	A	4Ls-3 <sup>1/2</sup> x3x3/8	7.4 (188.0)	18.1 (459.7)	180.3 (4579.6)	32.2	107.9	9.3
	Transverse Strut	A	4Ls-3 <sup>1/2</sup> x3x3/8	7.4 (188.0)	14.6 (370.8)	163.1 (4142.7)	24.9	97.7	9.3

Table 2.2 Characteristics of laced built-up members (continued)

Bridges	Usages	Section Shape	Sections Used	B in(mm)	D in(mm)	L in(mm)	KL/r <sub>x</sub>	KL/r <sub>y</sub>	b/t
River du Milieu Bridge	Longitudinal Bracing	E	2Ls-7 <sup>1/2</sup> x3 <sup>1/2</sup> x8/20	7.5 (190.5)	17.9 (454.7)	308.6 (7838.4)	37.0	107.5	18.8
	Longitudinal Strut	A	4Ls-7 <sup>1/2</sup> x3 <sup>1/2</sup> x8/20	15.4 (391.2)	17.9 (454.7)	480.0 (12192.0)	57.5	141.4	18.8
	Transverse Bracing	E	2Ls-7 <sup>1/2</sup> x3 <sup>1/2</sup> x8/20	7.5 (190.5)	15.0 (381.0)	330.2 (8387.1)	47.7	115.0	18.8
	Transverse Strut	A	4Ls-7 <sup>1/2</sup> x3 <sup>1/2</sup> x8/20	15.4 (391.2)	15.0 (381.0)	365.5 (9283.7)	52.8	107.7	18.8
San Francisco Oakland Bay Bridge	Transverse Bracing	B	4Ls-3x3x5/16 2PLs-13x5/16	17.2 (436.9)	13.3 (337.8)	204.0 (5181.6)	42.2	34.2	9.6

Table 2.3 Characteristics of lacing

<b>Bridges</b>	<b>Usages</b>	<b>Section Used</b>	<b>b in (mm)</b>	<b>t in (mm)</b>	<b>Angle <math>\theta</math></b>	<b>l in (mm)</b>	<b>k<sub>l</sub>/r</b>	<b>Lacing Force kips(kN)</b>
Rip-Van-Winkle Bridge	Column	DL PL-2 <sup>1/2</sup> x1/2	2.5 (63.5)	0.5 (12.7)	45.0	32.5 (825.5)	225.4	4.25 (18.9)
	Transverse Bracing	SL PL-2 <sup>1/2</sup> x3/8	2.5 (63.5)	0.38 (9.5)	63.4	9.5 (241.3)	87.6	3.35 (14.9)
	Transverse Strut	DL PL-2 <sup>1/2</sup> x3/8	2.5 (63.5)	0.38 (9.5)	46.9	19.0 (482.6)	175.2	2.13 (9.5)
North Grand Island Bridge	Transverse Bracing	DL PL-2 <sup>5/8</sup> x3/8	2.6 (66.0)	0.38 (9.5)	45.0	25.5 (647.7)	235.2	1.26 (5.6)
	Transverse Strut	DL PL-2 <sup>5/8</sup> x3/8	2.6 (66.0)	0.38 (9.5)	45.0	25.5 (647.7)	235.2	1.26 (5.6)
	Column	SL L-3x2 <sup>1/2</sup> x3/8	N/A	N/A	57.8	18.0 (457.2)	34.5	N/A
Anderson Creek Bridge	Longitudinal Bracing	SL PL-2 <sup>1/2</sup> x3/8	2.5 (63.5)	0.38 (9.5)	61.7	16.3 (414.0)	151.0	3.37 (15.0)
	Longitudinal Strut	SL PL-2 <sup>1/2</sup> x3/8	2.5 (63.5)	0.38 (9.5)	60.1	16.6 (421.6)	153.0	2.94 (13.1)
	Transverse Bracing	SL PL-2 <sup>1/2</sup> x3/8	2.5 (63.5)	0.38 (9.5)	62.1	16.6 (421.6)	153.0	2.66 (11.8)
	Transverse Strut	SL PL-2 <sup>1/2</sup> x3/8	2.5 (63.5)	0.38 (9.5)	60.6	16.8 (426.7)	155.3	2.65 (11.8)

Table 2.3 Characteristics of lacings (continued)

<b>Bridges</b>	<b>Usages</b>	<b>Section Used</b>	<b>b in (mm)</b>	<b>t in (mm)</b>	<b>Angle <math>\theta</math></b>	<b><math>l</math> in (mm)</b>	<b><math>k_l/r</math></b>	<b>Lacing Force kips(kN)</b>
River du Milieu Bridge	Longitudinal Bracing	SL PL-2 <sup>1/2</sup> x3/8	2.5 (63.5)	0.38 (9.5)	59.3	16.1 (408.9)	149.0	2.58 (11.5)
	Longitudinal Strut	SL PL-2 <sup>1/2</sup> x3/8	2.5 (63.5)	0.38 (9.5)	59.3	16.1 (408.9)	149.0	5.16 (23.0)
	Transverse Bracing	SL PL-2 <sup>1/2</sup> x3/8	2.5 (63.5)	0.38 (9.5)	57.5	13.1 (332.7)	120.7	2.60 (11.6)
	Transverse Strut	SL PL-2 <sup>1/2</sup> x3/8	2.5 (63.5)	0.38 (9.5)	57.5	13.1 (332.7)	120.7	5.19 (23.1)
San Francisco Oakland Bay Bridge	Transverse Bracing	DL PL-1 <sup>1/2</sup> x5/16	1.5 (38.1)	0.31 (7.9)	48.0	21.5 (546.1)	237.9	1.45 (6.5)



## SECTION 3

### EXPERIMENTAL APPROACH

#### 3.1 Selection of Parameters

Drawings were obtained for a few existing bridges having truss substructures (bents, towers, etc.) with laced members as described in SECTION 2. Design provisions and steel design textbooks published at the time when laced compression members were being used, were also reviewed, along with recent research work conducted for the major crossings in California. To this end, based on representative details, an experimental program has been devised whereby several cross-sectional shapes and geometric configurations of X-bracing are explored to ascertain the inelastic deformation capability of these critical elements. This allowed to extract a range of parameters typically encountered for such members, including typical built-up member configurations and lacing geometry, typical  $b/t$  and  $KL/r$  ratios for the built-up members and their lacings, connection details, and other lacing characteristics. As a result of this work, parameters worthy of experimental consideration (and their range) have been identified as shown in Table 3.1 and Figure 3.1. While some bridges were observed to have members having  $b/t$  ratios in excess of 16, it was decided to restrict testing to specimens having  $b/t$  values of 8 and 16 on the basis that this would allow to compare the cyclic performance of members having considerably different expectations in terms of local buckling behavior. Note that the AISC recommended maximum  $b/t$  value for ductile seismic design is 7.4 for grade 50 steel. Likewise, it was judged that testing braces having slenderness,  $KL/r$  of 60 and 120 would encompass the range of member slenderness observed in bridges, while allowing comparisons of the cyclic inelastic behavior of members expected to have significantly different levels of inelastic buckling. The resulting specimens designed based on these considerations are listed in Table 3.2 and section shapes are presented in Figure 3.2. Note that only built-up members constructed of angles are considered.

The purpose of the experimental portion of this project is to evaluate the seismic vulnerability of steel built-up brace members under moderate to severe earthquakes. Therefore, the test specimens should be indicative of full-scale built-up brace members in North America.

Table 3.1 Summary of experimental parameters to be considered

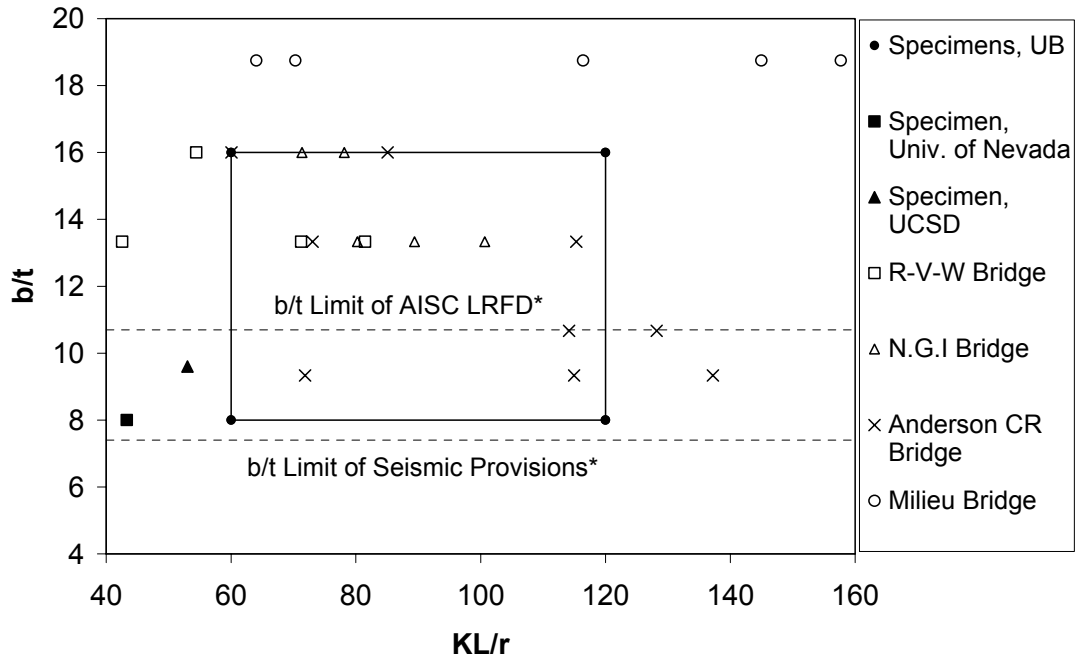
<b>Built-up Members</b>			<b>Lacings</b>		
<i>Configurations</i>	<i>b/t ratio</i>	<i>KL/r ratio</i>	<i>Type</i>	<i>Angle</i>	<i>kl/r</i>
Type "A" Type "B"	8 – 16	60 – 120	Single Lacing	60°	100 - 120

Table 3.2 Given specimen names

<b>Name</b>	<b>Section Shape<sup>*1</sup></b>	<b>Buckling Axis</b>	<b>b/t ratio</b>	<b>KL/r</b>
Ay8-60	A	Y	8	60
Ay8-120	A	Y	8	120
Ay16-60	A	Y	16	60
Ay16-120	A	Y	16	120
By8-60	B	Y	8	60
By8-120	B	Y	8	120
By16-60	B	Y	16	60
By16-120	B	Y	16	120
Bx8-60	B	X	8	60
Bx8-120	B	X	8	120
Bx16-60	B	X	16	60
Bx16-120	B	X	16	120

\*1. Section shapes are presented in Figure 3.2

## SUMMARY



$$* b/t(AISC LRFD) = \frac{76}{\sqrt{F_y}} = 10.7, \text{ where } F_y = 50\text{ksi}$$

$$b/t(AISC LRFD) = \frac{52}{\sqrt{F_y}} = 7.4, \text{ where } F_y = 50\text{ksi}$$

Figure 3.1 Distributions of b/t ratios and KL/r ratios

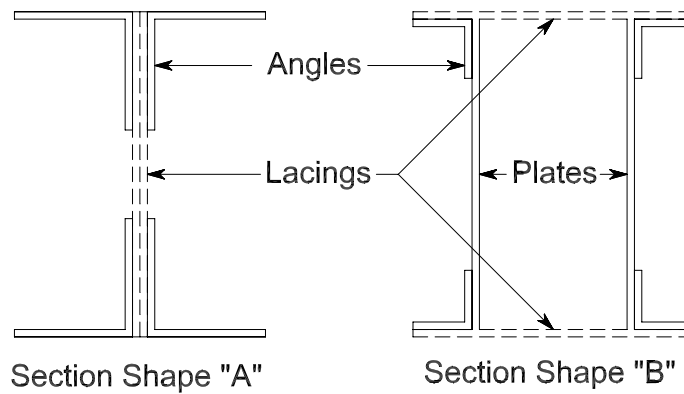


Figure 3.2 Section shapes

## 3.2 Design of Specimens and Testing Frames

Test specimens were selected with representative section shapes having slenderness ratios and width to thickness ratios as described in previous section. Compressive and tensile strength of each specimen was estimated, and considering limitations of the equipment available for quasi-static testing in the Structural Engineering and Earthquake Simulation Laboratory (SEESL) at the University at Buffalo, sizes of test specimens and frames were determined. All the detailed drawings for the specimens and elements of boundary frames are presented in Appendix A.

### 3.2.1 Design of Specimens

As shown in Figure 3.2, Ay specimens are built using four angles, and By and Bx specimens using four angles and two tie plates. Specimens were designed to have a strength less than the 250 kips (1112.5 kN), actuator capacity available in the SEESL. Considering representative cross-section aspect ratios, the largest angle size that could be used to build the specimens, and be tested with the 250 kips (1112.5 kN) actuator capacity of the SEESL, were identified. Selecting angle sections satisfying the target width to thick ratios,  $b/t$ , of 8 and 16, lead to  $1 \times 1 \times 1/8$  ( $b/t = 8$ ),  $1-1/2 \times 1-1/2 \times 3/16$  ( $b/t = 8$ ), and  $2 \times 2 \times 1/8$  ( $b/t = 16$  shapes).

Then, widths and depths of the specimens to satisfy the slenderness ratio of 120 were selected using these three angles. Note that when calculating the cross sectional properties of the specimens, the lacing members were not included, but the two tie-plates of the section shape “B” specimens were included. In these procedures, the lengths of the specimens were also limited by the maximum height of the reaction frame available at SEESL. For the specimens with section shape “B”, direction of buckling was also controlled by design by changing the width and depth of the test specimens. Note that the interest in testing section shape “B” specimens for which lacing members would be in shear, as well as others for which this would not be the case. Cross-section used were the same for the specimens having  $KL/r$  of 60 and  $KL/r$  of 120 for a given specimen name designation. For example, Ay8-60 and Ay8-120 specimens have the same cross-section.

The original idea in designing the test set-up was that specimens having  $KL/r$  of 60 would be tested in a X-shape configuration, but with one of the brace not connected at its top end. This effectively made braces with  $KL/r$  of 60 resist the tension and compression forces while the other brace in the X-braced configuration resisted no axial forces other than providing a bracing point at mid-length of the other member. The concept was then to remove the specimen having  $KL/r$  of 60 after it was tested, connect the top of the other brace, and therefore test the second specimen having  $KL/r$  of 120 without having to change the configuration the test set-up, such that two specimens could be effectively tested per test set-up configuration. However, as will be described in SECTION 4, this concept did not work as expected because was not possible to fail and fracture the specimen having  $KL/r$  of 60 without introducing possible plastic deformations in the specimen having  $KL/r$  of 120. Therefore, to be able to test the specimen  $KL/r$  of 60 without introducing damage in the other specimen in the X-braced configuration, for all subsequent tests following the Ay8 series, dummy bracing members were used to provide the bracing point at the mid-length of the  $KL/r$  of 60 specimens. These dummy bracing members were designed to provide the same in-plane and out-of-plane flexural stiffness as would be encountered in the real X-braced frame configuration as schematically presented in Figure 3.3. As shown in this figure, the required flexural stiffness of the dummy bracing member was identified as 2 times and 8 times that of the specimen for in-plane (weak axis) and out-of-plane (strong axis), respectively, and the dummy bracing members were designed satisfying this criteria.

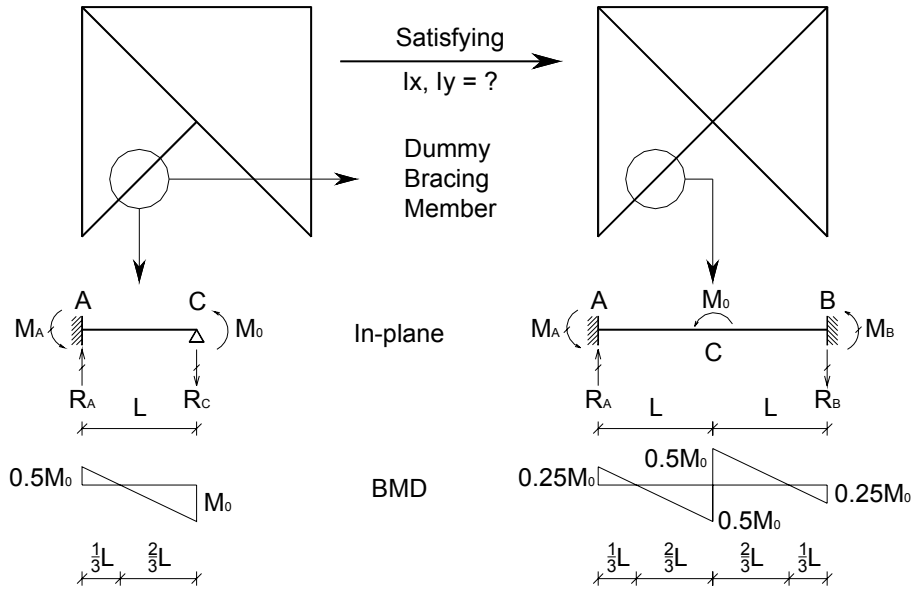
Resulting specimens are summarized with their cross sectional properties in Table 3.3. Properties of the dummy bracing members are presented in Figure 3.4. Cross sections for the specimens are presented in Figure 3.5. Detailed drawings for both specimens and dummy bracing members are also available in Appendix A.

Table 3.3 Specimen design

Specimen	Section				Height in(mm)	Local b/t	Global KL/r <sub>x</sub>	Global KL/r <sub>y</sub>	Lacing k/r
	Angles	Plates in(mm)	Width(B) in(mm)	Depth(D) in(mm)					
Ay8-60	4 - 1 <sup>1/2</sup> x1 <sup>1/2</sup> x3/16	None	3.375 (85.7)	6.5 (165.1)	46.8 (1187.9)	8.0	16.4	60.0	107
Ay8-120	4 - 1 <sup>1/2</sup> x1 <sup>1/2</sup> x3/16	None	3.375 (85.7)	6.5 (165.1)	93.5 (2375.7)	8.0	32.9	120.0	107
Ay16-60	4 - 2 x 2 x 1/8	None	4.25 (108.0)	5.5 (139.7)	55.1 (1399.1)	16.0	24.0	60.0	112
Ay16-120	4 - 2 x 2 x 1/8	None	4.25 (108.0)	5.5 (139.7)	110.2 (2798.2)	16.0	48.1	120.0	112
By8-60	4 - 1 x 1 x 1/8	0.125 (3.2)	4.75 (120.7)	4.75 (120.7)	89.7 (2279.0)	8.0	51.8	60.0	120
By8-120	4 - 1 x 1 x 1/8	0.125 (3.2)	4.75 (120.7)	4.75 (120.7)	179.5 (4558.0)	8.0	103.6	120.0	120
By16-60	4 - 2 x 2 x 1/8	0.125 (3.2)	5.25 (133.4)	5.25 (133.4)	65.2 (1655.2)	16.0	33.7	60.0	104
By16-120	4 - 2 x 2 x 1/8	0.125 (3.2)	5.25 (133.4)	5.25 (133.4)	130.3 (3310.3)	16.0	67.4	120.0	104
Bx8-60	4 - 1 x 1 x 1/8	0.125 (3.2)	4.5 (114.3)	3.0 (76.2)	65.5 (1662.9)	8.0	60.0	46.2	112
Bx8-120	4 - 1 x 1 x 1/8	0.125 (3.2)	4.5 (114.3)	3.0 (76.2)	130.9 (3325.8)	8.0	120.0	92.4	112
Bx16-60	4 - 2 x 2 x 1/8	0.125 (3.2)	6.5 (165.1)	4.125 (104.8)	90.0 (2285.7)	16.0	60.0	53.3	144
Bx16-120	4 - 2 x 2 x 1/8	0.125 (3.2)	6.5 (165.1)	4.125 (104.8)	180.0 (4571.4)	16.0	120.0	106.6	144

Table 3.3 Specimen design (continue)

Specimen	Local ( $P_{local}$ )		Global ( $P_{global}$ )		Yield ( $P_{yield}$ )		Critical ( $P_{critic}$ )		Govern by
	$P_{dia}$ kips (kN)	$P_{hor}$ kips (kN)	$P_{dia}$ kips (kN)	$P_{hor}$ kips (kN)	$P_{dia}$ kips (kN)	$P_{hor}$ kips (kN)	$P_{dia}$ kips (kN)	$P_{hor}$ kips (kN)	
Ay8-60	190.2 (846.6)	134.5 (598.6)	167.6 (745.8)	118.5 (527.4)	105.4 (469.0)	74.5 (331.7)	105.4 (469.0)	74.5 (331.7)	Yield
Ay8-120	190.2 (846.6)	134.5 (598.6)	41.9 (186.5)	29.6 (131.8)	105.4 (469.0)	74.5 (331.7)	41.9 (186.5)	29.6 (131.8)	Global
Ay16-60	43.7 (194.4)	30.9 (137.4)	153.9 (685.0)	108.8 (484.3)	96.8 (430.8)	68.4 (304.6)	96.8 (430.8)	68.4 (304.6)	Local
Ay16-120	43.7 (194.4)	30.9 (137.4)	38.5 (171.2)	27.2 (121.1)	96.8 (430.8)	68.4 (304.6)	38.5 (171.2)	27.2 (121.1)	Global
By8-60	191.6 (852.8)	135.5 (603.0)	168.8 (751.3)	119.4 (531.2)	106.2 (472.5)	75.1 (334.1)	106.2 (472.5)	75.1 (334.1)	Yield
By8-120	191.6 (852.8)	135.5 (603.0)	42.2 (187.8)	29.8 (132.8)	106.2 (472.5)	75.1 (334.1)	42.2 (187.8)	29.8 (132.8)	Global
By16-60	73.3 (326.2)	51.8 (230.6)	258.3 (1149.3)	182.6 (812.7)	162.4 (722.8)	114.9 (511.1)	162.4 (722.8)	114.9 (511.1)	Local
By16-120	73.3 (326.2)	51.8 (230.6)	64.6 (287.3)	45.7 (203.2)	162.4 (722.8)	114.9 (511.1)	64.6 (287.3)	45.7 (203.2)	Global
Bx8-60	152.2 (677.1)	107.6 (478.8)	134.0 (596.5)	94.8 (421.8)	84.3 (375.1)	59.6 (265.3)	84.3 (375.1)	59.6 (265.3)	Yield
Bx8-120	152.2 (677.1)	107.6 (478.8)	33.5 (149.1)	23.7 (105.4)	84.3 (375.1)	59.6 (265.3)	33.5 (149.1)	23.7 (105.4)	Global
Bx16-60	66.9 (297.9)	47.3 (210.7)	235.9 (1049.8)	166.8 (742.3)	148.4 (660.2)	104.9 (466.8)	148.4 (660.2)	104.9 (466.8)	Local
Bx16-120	66.9 (297.9)	47.3 (210.7)	59.0 (262.5)	41.7 (185.6)	148.4 (660.2)	104.9 (466.8)	59.0 (262.5)	41.7 (185.6)	Global



From the Boundary Condition,

$$\delta_c = 0;$$

$$\delta_B = -\frac{M_0}{2EI}L^2 + \frac{R_C}{3EI}(L)^3 = 0$$

$$\therefore R_A = -\frac{3M_0}{2L}, R_C = \frac{3M_0}{2L}$$

$$\Sigma M_A = 0;$$

$$-M_A - M_0 + R_C L = 0$$

$$\therefore M_A = \frac{1}{2}M_0$$

From the BMD

$$\theta_c = \frac{1}{EI} \left[ \left( \frac{1}{2} \right) \left( \frac{1}{2} M_0 \right) \left( \frac{1}{3} L \right) + \left( \frac{1}{2} \right) \left( M_0 \right) \left( \frac{2}{3} L \right) \right] = \frac{5M_0 L}{12EI}$$

$$\therefore M_{0,\theta=1} = \frac{12EI}{5L}$$

From the Boundary Condition,

$$\delta_B = 0;$$

$$\delta_B = -\frac{M_0}{2EI}L(4L-L) - \frac{M_B}{2EI}(2L)^2 + \frac{R_B}{3EI}(2L)^3$$

$$= \frac{L^2}{EI} \left( -\frac{3}{2}M_0 - 2M_B + \frac{8}{3}LR_B \right) = 0 \text{ --- (1)}$$

$$\theta_B = 0;$$

$$\theta_B = -\frac{M_0 L}{EI} - \frac{M_B(2L)}{EI} + \frac{R_B(2L)^2}{2EI}$$

$$= \frac{L}{EI} (-M_0 - 2M_B + 2LR_B) = 0 \text{ ---- (2)}$$

From the Eq.(1) and (2),

$$R_A = -\frac{3M_0}{4L}, R_B = \frac{3M_0}{4L}, M_A = -\frac{1}{4}M_0, M_B = \frac{1}{4}M_0$$

From the BMD

$$\theta_c = \frac{1}{EI} \left[ \left( \frac{1}{2} \right) \left( \frac{1}{4} M_0 \right) \left( \frac{1}{3} L \right) + \left( \frac{1}{2} \right) \left( \frac{1}{2} M_0 \right) \left( \frac{2}{3} L \right) \right] = \frac{5M_0 L}{24EI}$$

$$\therefore M_{0,\theta=1} = \frac{24EI}{5L}$$



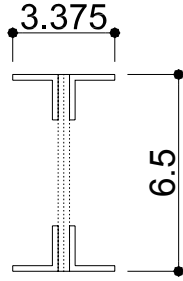
$$\delta_c = \frac{V_0 L^3}{3EI}$$

$$\therefore V_{0,\delta=1} = \frac{3EI}{L^3}$$

$$\delta_c = \frac{V_0(2L)^3}{192EI} = \frac{V_0 L^3}{24EI}$$

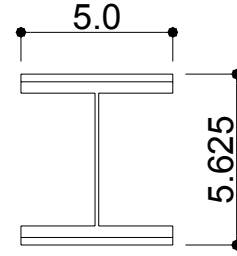
$$\therefore V_{0,\delta=1} = \frac{24EI}{L^3}$$

Figure 3.3 Design of dummy bracing members



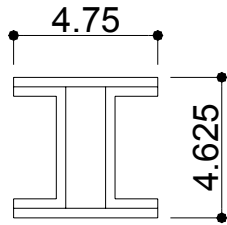
L- 1-1/2 x 1-1/2 x 3/16

(a) Dummy bracing for Ay8-60 specimen



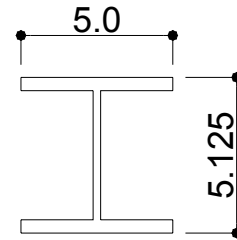
W 5x16 and PL-1/4" thk.

(b) Dummy bracing for Ay16-60 specimen



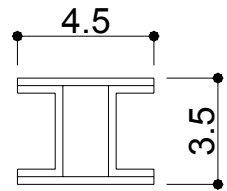
C 4x7.25 and PL-5/16" thk.

(c) Dummy bracing for By8-60 specimen



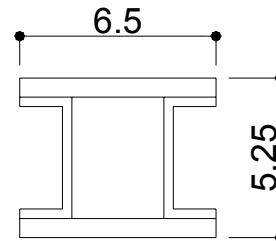
W 5x19

(d) Dummy bracing for By16-60 specimen



C 3x5 and PL-1/4" thk.

(e) Dummy bracing for Bx8-60 specimen



C 4x7.25 and PL-5/8" thk.

(f) Dummy bracing for Bx16-60 specimen

Figure 3.4 Dummy bracing members

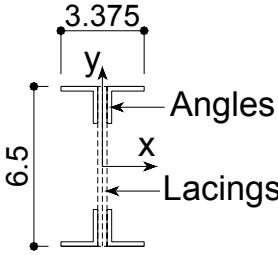
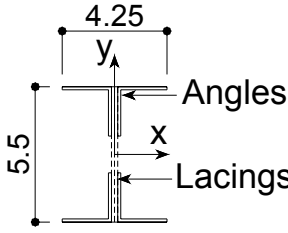
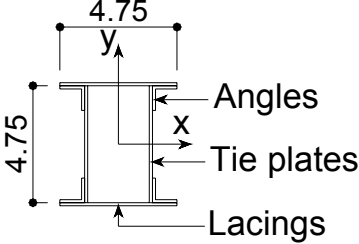
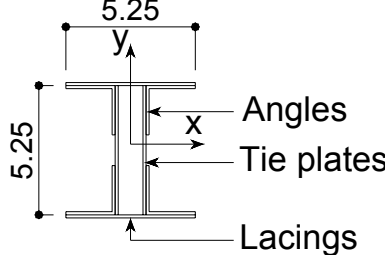
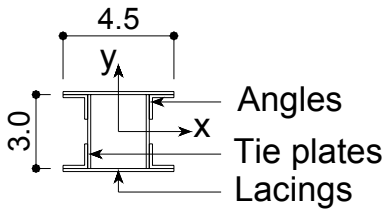
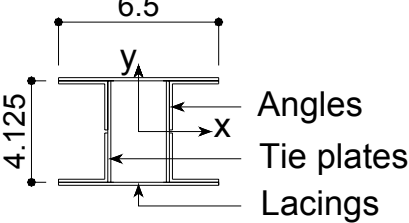
	b/t = 8.0	b/t = 16.0
Ay specimens	 <p>Ay8-60, Ay8-120  <math>4L-1 \frac{1}{2} \times 1 \frac{1}{2} \times \frac{3}{16}</math></p>	 <p>Ay16-60, Ay16-120  <math>4L-2 \times 2 \times \frac{1}{8}</math></p>
By specimens	 <p>By8-60, By8-120  <math>4L-1 \times 1 \times \frac{1}{8}</math></p>	 <p>By16-60, By16-120  <math>4L-2 \times 2 \times \frac{1}{8}</math></p>
Bx specimens	 <p>Bx8-60, Bx8-120  <math>4L-1 \times 1 \times \frac{1}{8}</math></p>	 <p>Bx16-60, Bx16-120  <math>4L-2 \times 2 \times \frac{1}{8}</math></p>

Figure 3.5 Detailed cross section shapes of the specimens

Lacings were designed with slenderness ratios between 100 and 120, recognizing the fact that slenderness of a single lacing member was limited to by archaic design requirements 140 and data for the survey of existing built-up laced members which showed lacing having slenderness ranging from 90 to 150 (mostly from 100 to 120) as compiled in Table 3.1. Angle between lacing and main member was selected as 60 degree as typically is the case for single lacing as summarized in Table 3.1. Steel plates with thickness of 1/8" (3.2 mm) were used for all the lacing members, which is identical to the thickness of the angles used for the specimens except for the Ay8 specimens.

As described in SECTION 2, hot driven riveted connections were the fasteners used for the field connections of the most built-up laced members until high strength bolts superseded them. Although riveted connections for the fabrication of the specimen would be ideal for evaluating the cyclic behavior of built-up laced member, due to difficulties in finding equipment and technicians for riveting, A307 mild carbon steel bolts were used for the connection of the specimens. A comparative study of bolted and riveted connection was conducted by Roeder et al. (1994). This experimental study indicated that the cyclic behavior of A307 mild carbon steel bolt in tightly fit connections is comparable to the inelastic behavior of riveted joints.

### ***3.2.2 Design of Testing Frames***

The scheme for the test set-up was to replicate one panel of an X-braced frame. During sway, deformation of that panel would induce brace elongation or shortening, but also flexure in the brace and beams due to panel racking (distortion). The focus of this research is on the buckling of the braces in a braced bent, and test set-up used for this research project (as shown in Figure 3.6) gives the correct racking system deformation for braces in such bents, but the beams that would be present in such braced panels are omitted for convenience (to allow testing of bigger braces for the maximum actuator force available). However, to properly distribute the lateral load to both columns and to ensure consistent racking deformations, a top beam on hinges is used as shown in Figure 3.6.

The width and height of the frames were dictated by the diagonal length of the brace specimens.

Figure 3.6 shows an example setup, illustrating terminology for the various parts of the boundary frames and test setup. The framing members around the brace specimens were designed to remain elastic under the maximum possible loading. This was done to insure the safety of the test and so that the boundary frame could be reused for the whole experimental program.

The dimensions of existing hinges available in the SEESL were considered in selecting the column dimensions; the resulting member is a W12x65. These columns were checked to remain elastic considering the maximum shear and axial forces transferred from the maximum predicted diagonal axial loads during the testing. Although the W12x65 columns are large enough to resist the maximum transferred forces, stiffeners were added at the connections between columns and gusset plates and stub-beams.

At the four edges of the boundary frames for the Ay specimens (four specimens), hinges available in the SEESL were installed and bearing capacities of these hinges were checked using the AISC LRFD Specification (1999). For the testing of the specimens with section shape “B”, new hinges designed for another experimental project in the SEESL, were used. These hinges had less slippage, and were designed to resist larger loads.

For convenience, a W12x65, identical to the columns, was used for the top beam and stub beams. For the stub beams, stiffeners were added at the connection with gusset plates.

### ***3.2.3 Design of Foundation Beams***

For the specimens with section shape “A”, a concrete foundation beam, previously used for quasi-static testing in the SEESL and slightly modified and reinforced, was secured to the 18" (460 mm) thick reinforced concrete strong floor of the SEESL using 4 prestressed, 1-1/8" (29 mm) diameter Diwidag bars. Specimens were mounted to the foundation beam using four 1-1/4" (31.8 mm) diameter high strength threaded rods embedded in the concrete foundation beam. However, during the testing of the “Ay” section shape specimens, as a consequence of excessive deformations in the concrete foundation beam, significant undesirable movements occurred in the test set-up and made data interpretation and test control challenging. After attempting a number of unsuccessful modifications to improve the concrete foundation scheme, it was

replaced by a new foundation beam made from a steel wide flange section. Conservatively, it was deemed appropriate to design the foundation beam for twice the maximum support reactions can could be developed assuming that the specimens could resist the load applied by the actuator developing its full capacity of 250 kips (1112.5 kN).

The new foundation beam was also secured to the strong floor of the SEESL using 8 prestressed, 1-1/8" (29 mm) diameter Diwidag bars. The resulting friction between the floor and beam in the maximum uplift condition was deemed insufficient to resist horizontal sliding. Therefore, the foundation beam was also connected to the bottom of the column of the existing reaction frame (on which the actuator is mounted) to create a self-reacting frame. Design loads described above dictated the use of a W14x211 section to provide sufficient flexural strength and stiffness. Additionally, 1/2" (13 mm) stiffeners were used at the loading points and strong floor tie-down locations. The beam was designed in two pieces, 74.5" (1892 mm), and 314-5/8" (7991 mm) long, each with butt-welded end-plates so that they could be bolted together. All specimen mounting and strong floor tie-down locations are on the longer segment, while the shorter section serves as the link to the column of the reaction frame. The splice between the two beam sections and the connection to the reaction frame were designed for 2.5 times the maximum actuator force. Detailed drawings of both concrete and new steel foundation beams are also available in Appendix A.

### **3.3 Materials**

Steel for the angles and plates used for the test specimens were specified to be ASTM A36 Gr. 36 (ASTM, 1997), which is a cold-rolled, carbon, chemical commercial steel sheet with no mandatory mechanical properties. ASTM states that typical mechanical properties are minimum yield strengths of 36 ksi (250 MPa), minimum tensile strength between 58 and 80 ksi (400 and 550 MPa), and elongations at fracture of 23 % in 2" (50 mm). From the angles and plates used for the specimens, coupons were fabricated and tested following the ASTM A370 standard for mechanical testing of steel products (ASTM, 1997). Results obtained from the coupon tests are summarized in Table 3.4 and Figures 3.7 to 3.11. As seen in these table and figures, the yield stresses obtained from the coupon tests were much bigger than the specified minimum yield

stresses of the ASTM A36 steel especially for the angles. Note that similar results were achieved by the other researchers who used this lower grade steel for the simulation of old types of structures.

ASTM A572 Gr. 50 steel was used for the boundary frames however, due to the need to re-use the boundary frames for additional testing, coupon tests of the frame material were not performed.

Table 3.4 Coupon test results

<b>Coupons</b>	<b><math>F_y</math> Ksi (MPa)</b>	<b><math>F_u</math> Ksi (MPa)</b>	<b><math>E</math> Ksi (MPa)</b>	<b>Usages</b>
L - 1 <sup>1/2</sup> x 1 <sup>1/2</sup> x 3/16	50.78 (349.9)	72.00 (496.1)	29871 (205811)	Ay8 type Specimens
L - 2 x 2 x 1/8	51.04 (351.7)	68.20 (469.9)	30024 (206865)	Ay16 Type, By16 type and Bx16 type Specimens
L - 1 x 1 x 1/8	52.44 (361.3)	68.91 (474.8)	30847 (212536)	By8 type and Bx8 type Specimens
1/8" thk. plate	46.81 (322.5)	55.70 (383.8)	32283 (222430)	Lacings, Tie-Plates
3/8" thk. plate	36.77 (253.3)	50.63 (348.8)	29048 (200141)	Gusset plates

### 3.4 Test Set-up

Test set-up for the whole testing program of this project was gradually changed from the smallest test set-up for the Ay8 specimen to the largest test set-up of the By8 and Bx16 specimens by increasing the width between the columns and increasing the height of the frame by adding column stub segment extensions. The resulting sequence of changes in test set-up is presented in Figure 3.12. Test set-up for the Ay16 specimen was achieved by increasing the distance between the North and South columns of the test set-up for Ay8 specimen, the very first test set-up. As described in the Section 3.2, the concrete foundation beam and bottom hinges of the SEELS

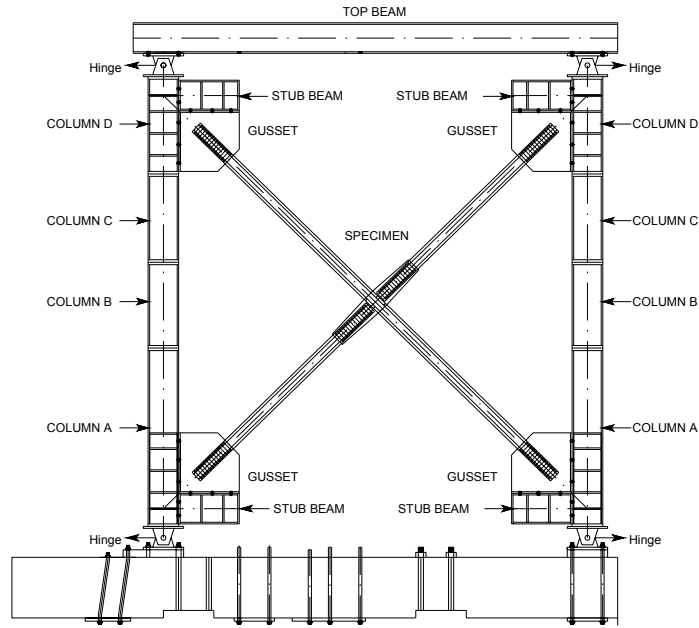


Figure 3.6 An example test set-up

Stress - Strain (L 1 x 1 x 1/8)

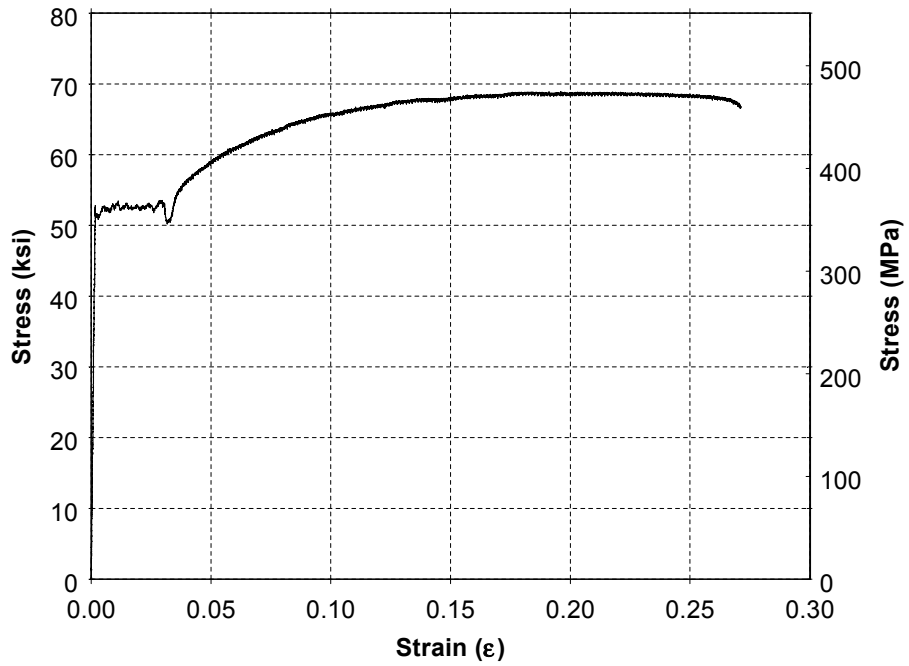


Figure 3.7 Stress-strain curve for the angle 1 x 1 x 1/8

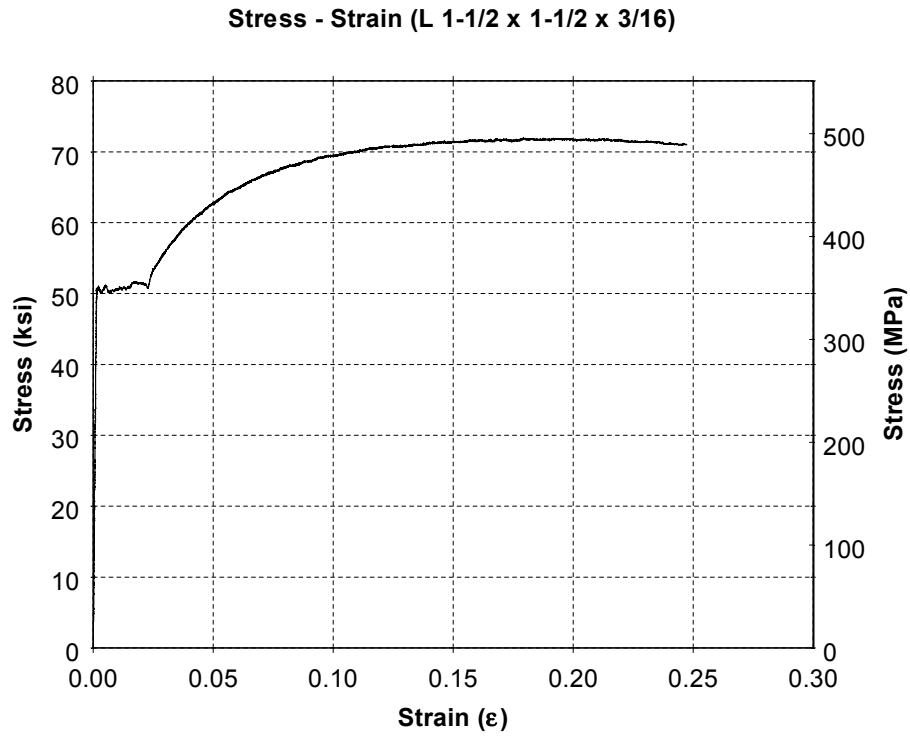


Figure 3.8 Stress-strain curve for the angle 1-1/2 x 1-1/2 x 3/16

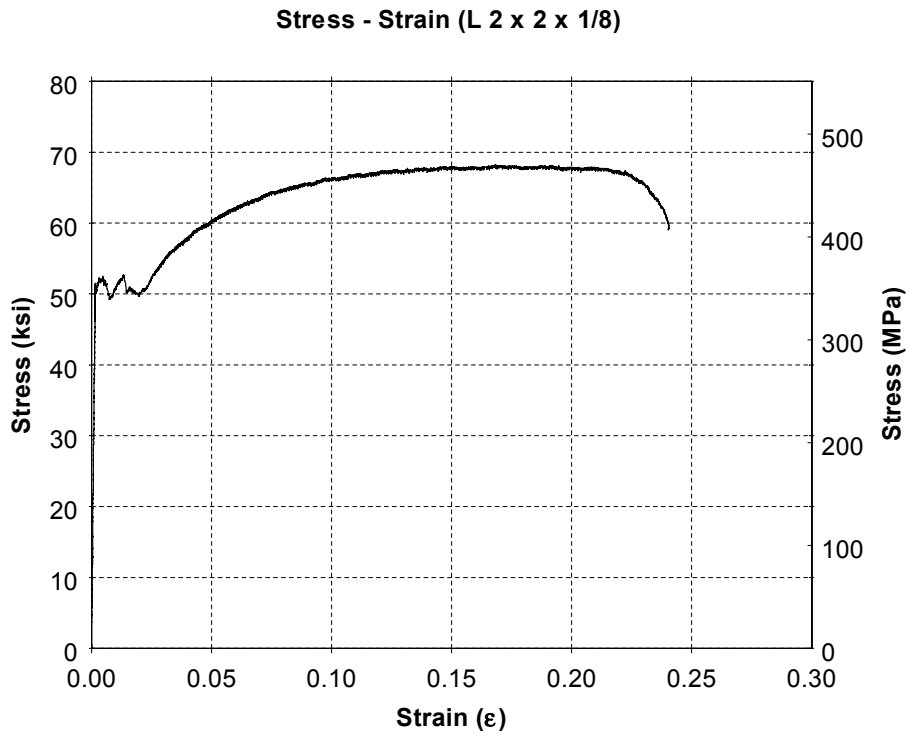


Figure 3.9 Stress-strain curve for the angle 2 x 2 x 1/8

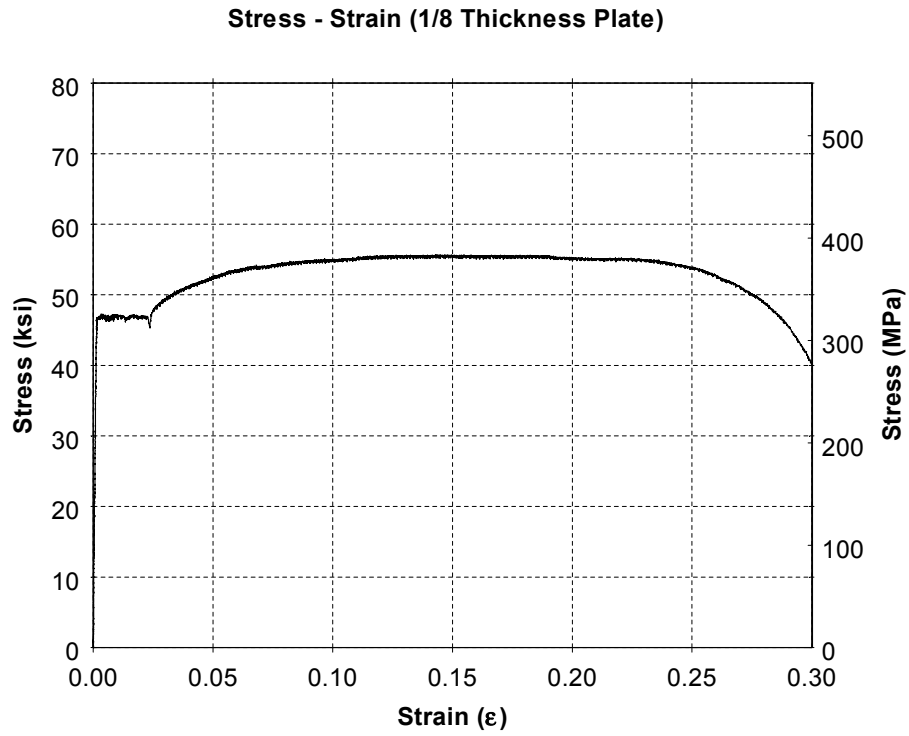


Figure 3.10 Stress-strain curve for the plate with thickness of 1/8

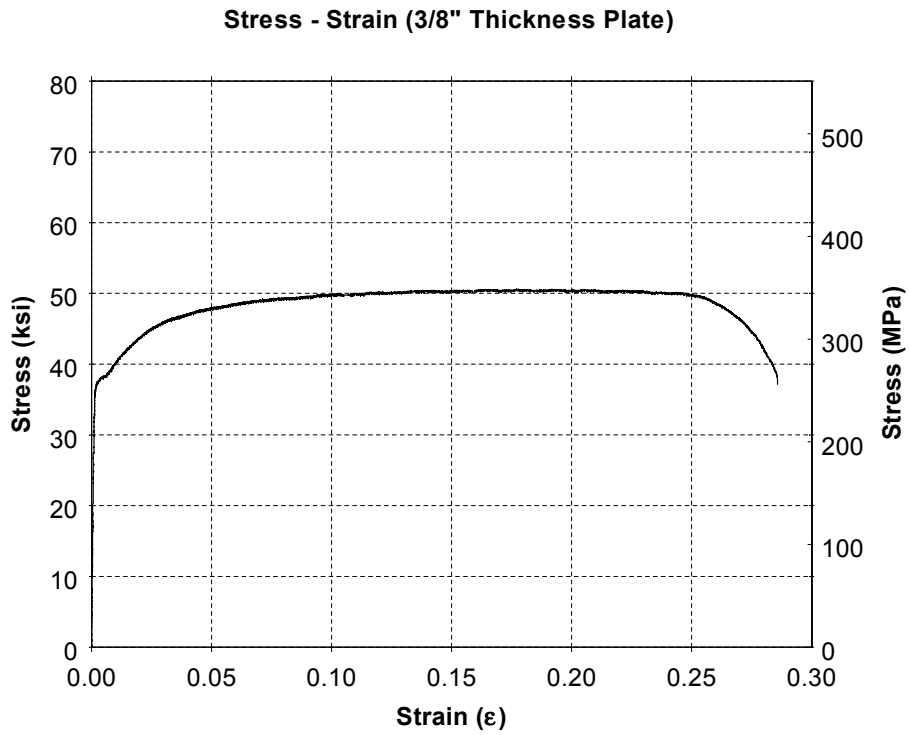


Figure 3.11 Stress-strain curve for the plate with thickness of 3/8

were replaced by the new ones before testing section shape “B” specimens. Test set-up for the By16 and Bx8 specimens were achieved by adding column extensions to the columns, as shown in Figure 3.12. Finally, the last test set-up for the specimens By8 and Bx16 was achieved by both increasing the displacement between the columns and adding another set of column extension.

### ***3.4.1 Mounting of Boundary Frames and Specimens***

Testing was performed in the SEESL at the University at Buffalo. The foundation beam was connected to the strong floor as described in Section 3.2.3. Each specimen was mounted on the hinges which were themselves mounted on the foundation beam. Four 1-1/2" (38 mm) diameter A490 bolts were used to attach each column base plate to the corresponding hinge, and then to attach each hinge to the foundation beam. All bolts (the bolts on the specimen themselves as well as bolts used to connect the two sections of the foundation beam together and the foundation beam to the reaction frame) were tightened to their specified internal tension using the “turn-of-the-nut” method described in the AISC LRFD Specifications (AISC, 1999). To achieve the torque required to reach the specified nut rotations, a HYTORC Blitz 4-A hydraulic torque wrench was used.

### ***3.4.2 Mounting Actuator***

The Miller servo-controlled static rated actuator with a load capacity of 250 kip (1110 kN) and an available stroke of 8" (200 mm) was mounted to the reaction frame using four 1" (25 mm) diameter high strength threaded rods. Four similar rods were used to connect the actuator to the test specimen. The actuator is equipped with swivels at each end and end-plates with threaded holes to accept the rods.

### ***3.4.3 Lateral Bracing***

Lateral bracing was provided to the specimen through the use of large rollers (Figure 3.13) cantilevering from frames mounted on the east and west side of the specimen and set to roll

along the middle of the web of the top beam. A gap of approximately 1/8" (3 mm) was left between the beam web and each roller so that the roller would only be engaged if the out-of-plane deflection closed that gap. The frames supporting the rollers on each side of the specimen were secured to the strong floor using high strength threaded rods.

### **3.5 Instrumentation**

#### **3.5.1 Strain Gauges**

All specimens were instrumented with CEA-06-125UW-120 strain gauges manufactured by Vishay Measurements Group Incorporated at the location of predicted maximum moment of the each specimen. The strain gauge layouts for specimens are shown in Figure 3.14. For the specimens with KL/r of 60, the maximum moment was predicted at the 0.3 and 0.6 of the center to center length of the both South and North segments of the specimen. The specimens with KL/r of 120 were instrumented with strain gauges at the quarter and half of the center to center length of the specimen, where the maximum moment was predicted.

#### **3.5.2 Temposonics and LVDTs**

The layout of the Temposonic Magnetic Strictive Transducers (Temposonics) is shown in Figure 3.15. To measure the horizontal frame drift at the loading point and bottom of the frame, Temposonics, T1 and T2 were installed. Temposonics for the measuring the axial displacement of the specimens were also installed. For the specimens with KL/r of 60, three Temposonics were installed, (labelled Tcontrol, ThalfN, and ThalfS) for measuring whole diagonal displacement, and displacement of the North and South segments of the specimens, respectively. Two Temposonics were installed to measure the diagonal axial displacements of the specimens with KL/r of 120.

Two Displacement Potentiometers (DP) were placed in strategic locations to measure the vertical and horizontal displacement of the foundation beam under the South hinge. The DP layout was the same for all specimens.

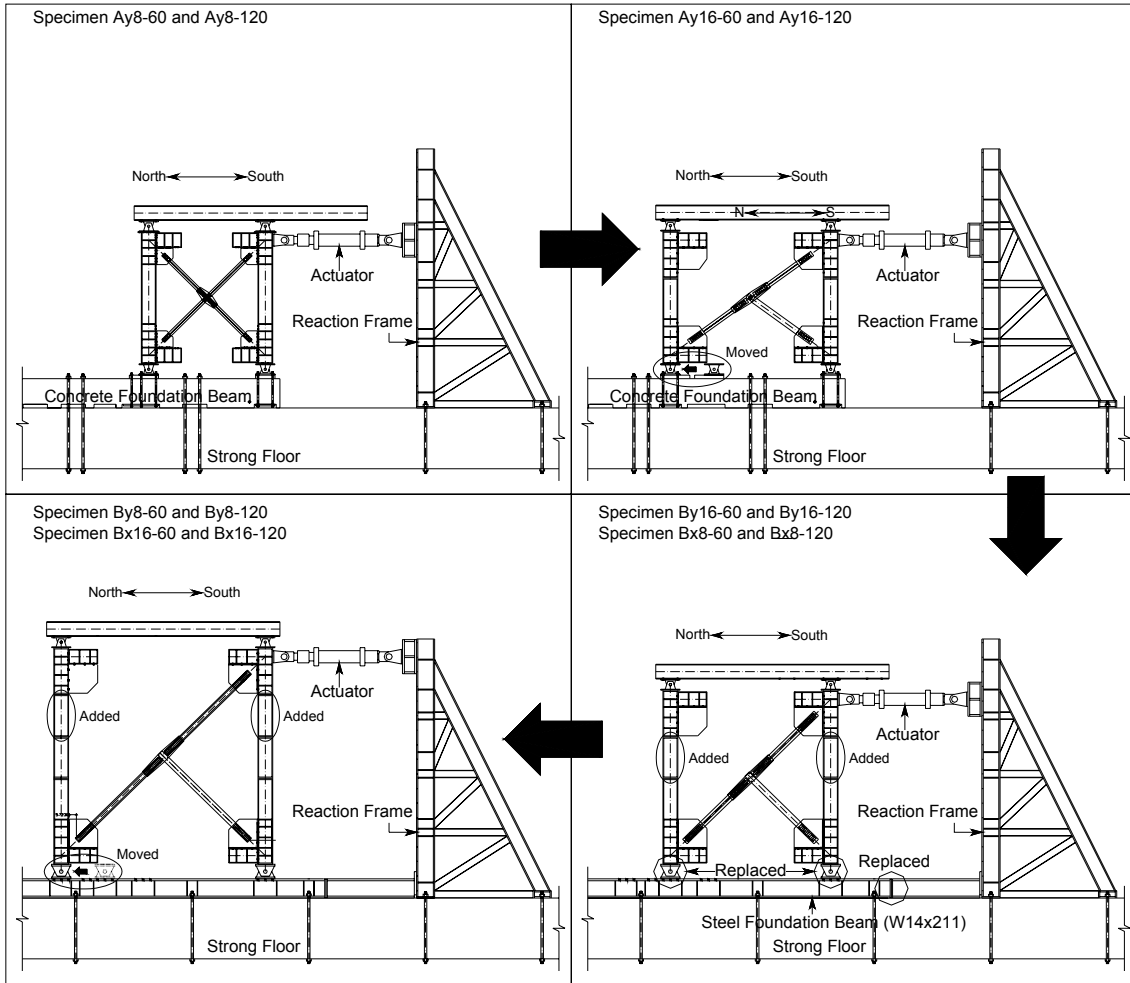


Figure 3.12 Test set-ups

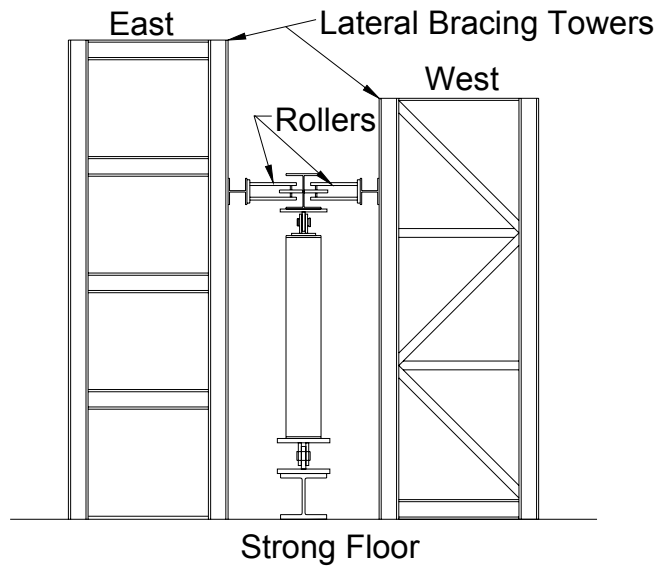


Figure 3.13 Lateral bracing

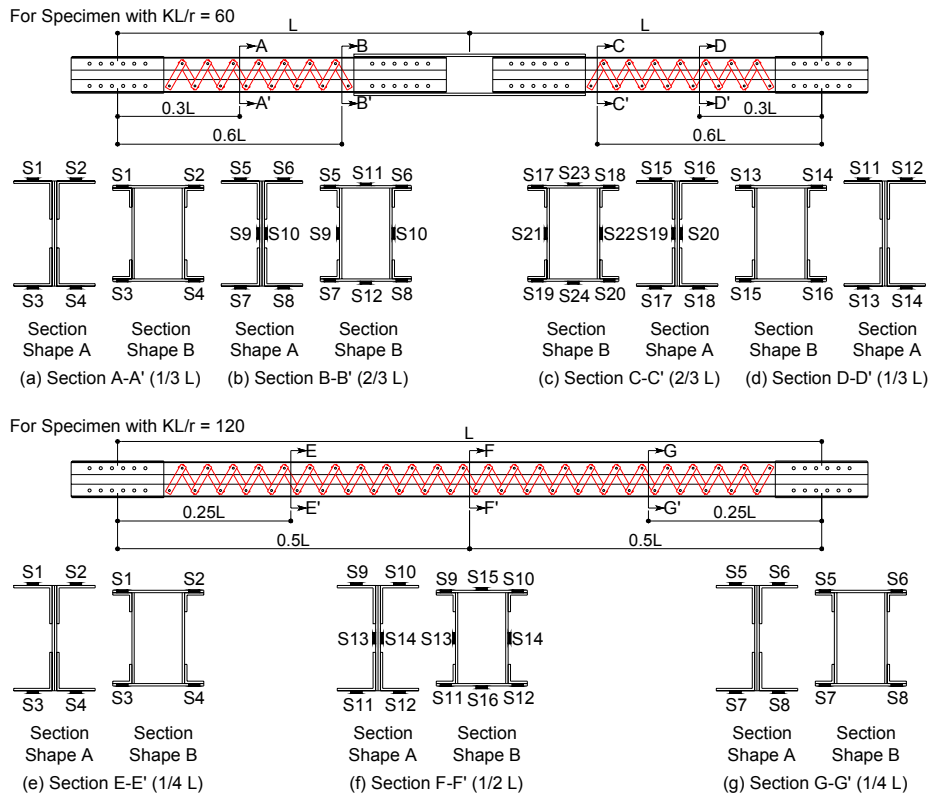


Figure 3.14 Strain gauge layouts

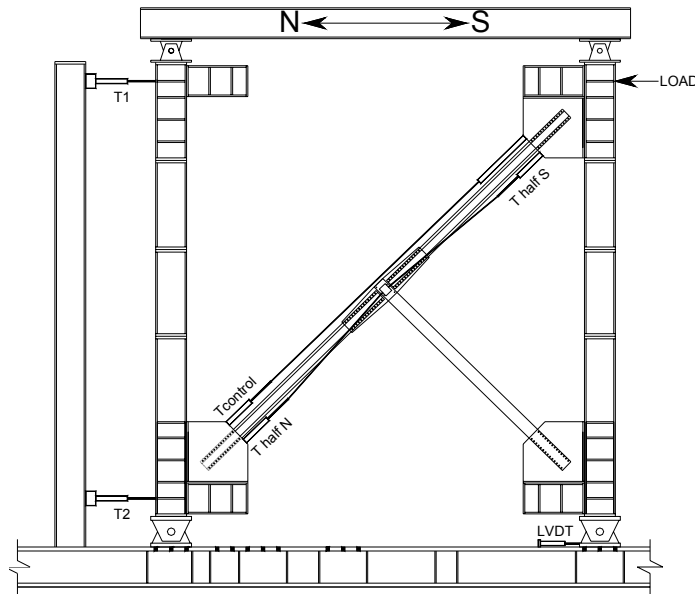


Figure 3.15 Temposonics and LVDT layout

## SECTION 4

### EXPERIMENTAL OBSERVATIONS

This section describes the loading programs and experimental observations for the twelve specimens (in the order of section shapes Ay, By, and Bx). Hysteretic curve of each specimen is presented and observations made during the test are discussed in detail, supported with pictures taken during testing. Based on the observations made in this section, analyses of results, in terms of hysteretic behaviors, comparison of analytical versus experimental tension and compression strength, and predicted hysteretic curves from existing models, will be discussed in SECTION 5. Energy dissipation, strength degradation, and low-cycle fatigue fracture life, will be also discussed in SECTION 6.

#### 4.1 Loading Programs

##### 4.1.1 *ATC Loading Protocol*

In all cyclic tests, all specimens were loaded by quasi-static cycles following the procedure of the ATC 24 loading protocol (ATC, 1992). As graphically presented in Figure 4.1, ATC 24 specifies that specimens should be subjected to three cycles at each displacement step up to three times the yield displacement, after which only two cycles are necessary. Before a specimen reaches its yield displacement ( $\delta_y$ ), it should experience three cycles at 1/3 of the yield displacement ( $1/3 \delta_y$ ) and three cycles at 2/3 of the yield displacement ( $2/3 \delta_y$ ). The third displacement step should be the yield displacement ( $\delta_y$ ), and every step after should be increasing multiples of the yield displacement ( $2\delta_y, 3\delta_y, \text{etc.}$ ).

##### 4.1.2 *Loading Histories*

The difficulty in the ATC 24 loading procedure lies in defining yield displacement before testing. Because this research focuses more on the compressive behavior of the laced built-up bracing member than on their tensile behavior, the experimentally determined displacement at the onset

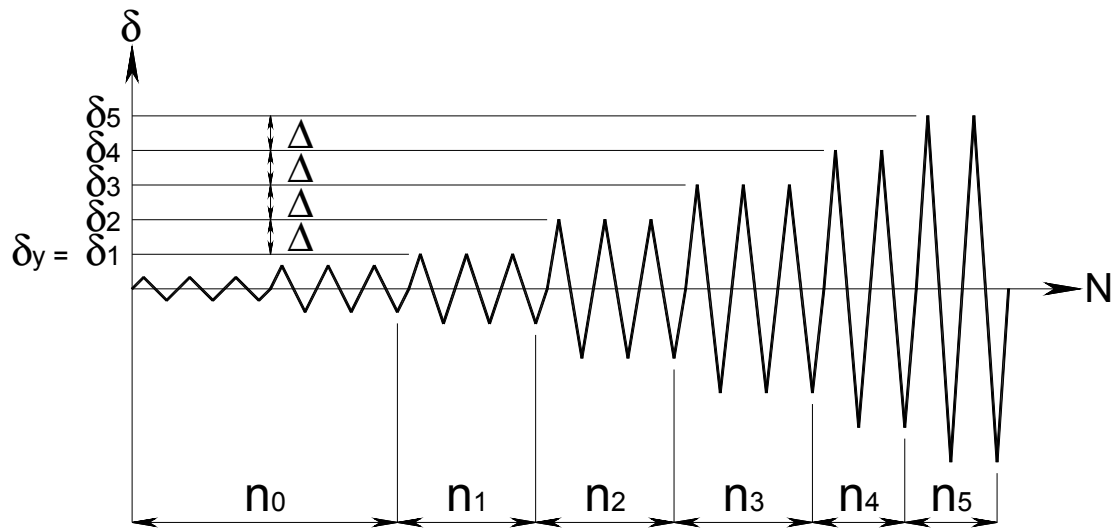


Figure 4.1 ATC loading protocol (ATC, 1992)

of buckling was substituted for the yield displacement in the above procedure. Cycles of loading up to buckling were performed using force control, then once the buckling displacement had been identified experimentally, the subsequent cycles were done using displacement control. Due to the difficulty in exactly predicting the buckling strength and corresponding displacement, the displacement steps in the elastic range did not exactly equal  $1/3$  and  $2/3$  of the buckling displacements for any given specimen. However, three cycles were still applied at each of at least two displacement steps of increasing amplitude prior to reaching the buckling displacement. Loading histories are summarized graphically in Figures 4.2 to 4.4, along with limit states discussed in their respective sections. Detailed loading history for each test is described below.

## **4.2 Experimental Observations**

The experimental observations made during testing of the twelve specimens are presented as consistently as possible over both the linear and nonlinear range. However, some unavoidable departures are introduced as aspects of the test control were improved. The experimental log book is included in Appendix B. Note that the diagonal axial forces referred to in this section are converted from the horizontal forces applied by hydraulic actuator, and diagonal axial displacements were directly measured by Temposonics displacement transducers installed diagonally as described in Section 3.4. Also note that the diagonal axial forces are not obtained from direct divisions of the horizontal forces by the cosine angle of the brace, because shear forces were introduced in the frame columns due to eccentricities between the longitudinal axes of the braces and the center of the hinges. When calculating the diagonal axial forces, corrections were made considering the complete Free Body Diagram (FBD) for the specimens validated using analysis results from SAP 2000. Resulting conversion factors are presented in Table 4.1, and example calculation and FBD in Figures 4.5 and 4.6.

### **4.2.1 Bare Frame Testing**

Though four hinges are installed in the boundary frame shown in Figure 4.7, to quantify the typical contribution of that frame on specimen behavior, one boundary frame was tested alone before mounting the very first specimen. As shown in Figure 4.8, the contribution of boundary

frame is very small (less than 0.1 kips (0.4 kN) lateral force applied at maximum actuator stroke). Consequently, the impact of boundary frame lateral-load resistance on the results is negligible and not subtracted from the test results for the specimens.

Table 4.1 Summary of equilibrium for converting from  $P_H$  to  $P_D$   
(Results are from SAP2000 analyses)

Specimen	Equilibrium	Results $P_D$
Ay8-60	$\Sigma H = 1 + 0.09 + 0.03 - 0.03 \sin \theta - P_D \cos \theta = 0$	1.50 $P_H$
Ay8-120	$\Sigma H = 1 + 0.11 + 0.008243 \sin \theta - P_D \cos \theta = 0$	1.53 $P_H$
Ay16-60	$\Sigma H = 1 + 0.09 + 0.02 - 0.02 \sin \theta - P_D \cos \theta = 0$	1.35 $P_H$
Ay16-120	$\Sigma H = 1 + 0.11 + 0.0074 \sin \theta - P_D \cos \theta = 0$	1.37 $P_H$
By8-60	$\Sigma H = 1 + 0.06 + 0.01 - 0.01 \sin \theta - P_D \cos \theta = 0$	1.47 $P_H$
By8-120	$\Sigma H = 1 + 0.06 + 0.007628 \sin \theta - P_D \cos \theta = 0$	1.49 $P_H$
By16-60	$\Sigma H = 1 + 0.07 + 0.02 - 0.03 \sin \theta - P_D \cos \theta = 0$	1.49 $P_H$
By16-120	$\Sigma H = 1.01 + 0.08 + 0.01 \sin \theta - P_D \cos \theta = 0$	1.53 $P_H$
Bx8-60	$\Sigma H = 1 + 0.07 + 0.02 - 0.03 \sin \theta - P_D \cos \theta = 0$	1.49 $P_H$
Bx8-120	$\Sigma H = 1.01 + 0.08 + 0.01 \sin \theta - P_D \cos \theta = 0$	1.53 $P_H$
Bx16-60	$\Sigma H = 1 + 0.057 + 0.02 - 0.01 \sin \theta - P_D \cos \theta = 0$	1.47 $P_H$
Bx16-120	$\Sigma H = 1 + 0.06 + 0.01 \sin \theta - P_D \cos \theta = 0$	1.49 $P_H$

#### 4.2.2 Specimen Ay8-60

Test set-up for the Ay8-60 specimen is presented in Figure 4.9. Note the unconnected upper end of one brace (Figure 4.9b) to ensure that only one brace is tested, while the other provides only lateral bracing at mid-length of the tested brace. Hysteretic curve obtained from test result is presented in Figure 4.10 in support of the following description of observations.

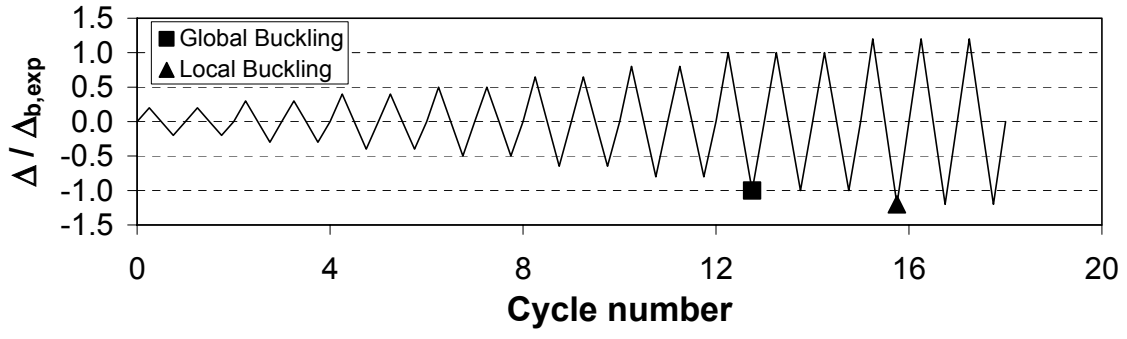
Initially, loading cycles were applied to the specimen based on theoretical calculation of elastic displacement of the specimen, and equivalent horizontal buckling frame drift ( $\Delta_b$ ) in

compression at the loading point was used for the test loading control. However, after six cycles at  $1/3 \Delta_b$  and  $2/3 \Delta_b$  (three cycles each) which were in elastic range, strains from test results were compared with results from SAP 2000 analyses. Significant discrepancies were noted as the frame proved to be very significantly more flexible as a consequence of excessive deformations in the concrete foundation beam and the hinges. Because of these relatively large differences between theoretical and experimental results, a decision was made to seek the experimental buckling frame drift,  $\Delta_{b,exp}$ , by subjecting the specimen to progressively increasing small values of the control displacement, starting from the theoretical  $2/3 \Delta_b = 0.2''$  (5.08 mm).

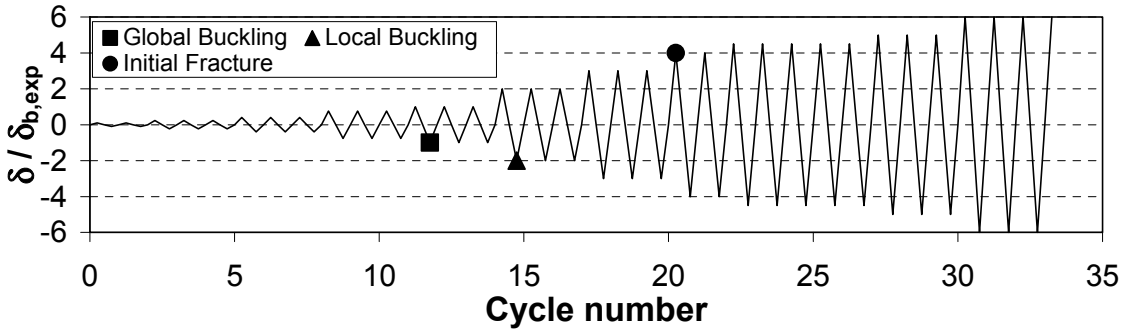
Experimental buckling drifts,  $\Delta_{b,exp}$  was identified during the first compressive displacement at  $\Delta = 1.0''$  (25.4 mm). Global buckling was observed in both the South and North segments of the specimens as shown in Figure 4.11a. During inspection of the specimen after buckling, relatively small damage on the other diagonal specimen (Ay8-120) was visually noticed. To prevent severe damage of the Ay8-120 specimen, testing was continued with a small increment of  $0.2''$  (5.08 mm) of the control displacement,  $\Delta$ .

During the first compressive cycle at  $\Delta = 1.2''$  (30.5 mm), more severe global buckling was observed as shown in Figure 4.8b. Local buckling was also observed on the angles at the plastic hinge locations at mid-length of both the South and North segments of the specimens, as shown in Figure 4.11c and 4.11d, respectively. Although the specimen had not reached fracture, testing was stopped to prevent severe damage on the Ay8-120 specimen. Note that the compressive strength had dropped to about  $1/3$  of its maximum compressive force at that point.

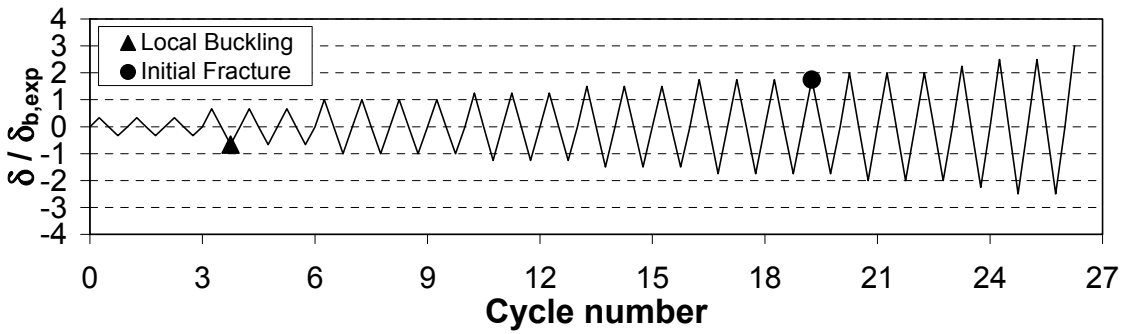
The risk of the damage to the second specimen proved to be a limiting factor in preventing testing of the specimen having a  $KL/r$  of 60 up to its fracture. It was therefore decided for all subsequent specimens having a  $KL/r$  of 60 to use a dummy member to provide mid-length bracing. Furthermore, due to a controller problem, displacement cycles were not symmetrical, and the specimen was not subjected to tensile inelastic deformations. This problem was resolved for testing of the other specimens.



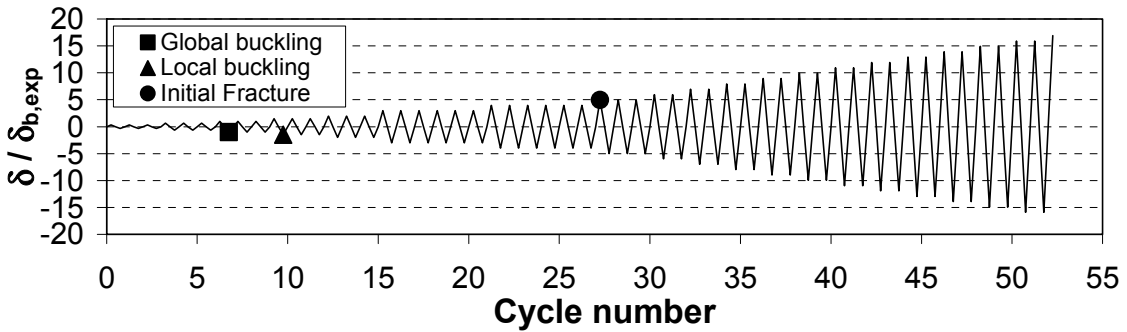
(a) Ay8-60 specimen



(b) Ay8-120 specimen

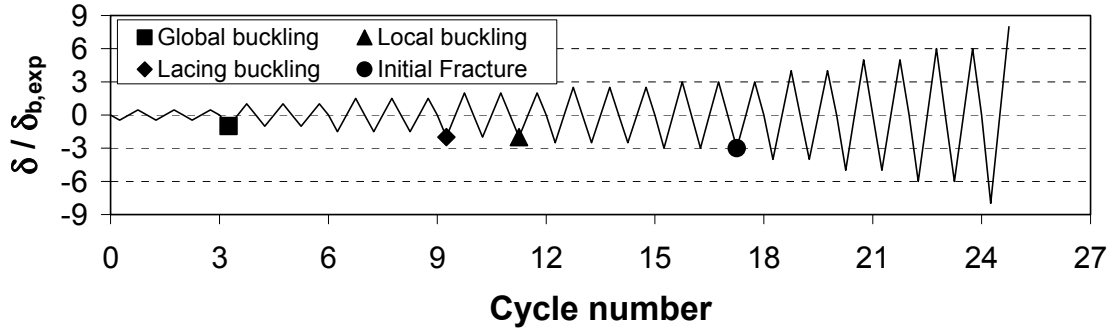


(c) Ay16-60 specimen

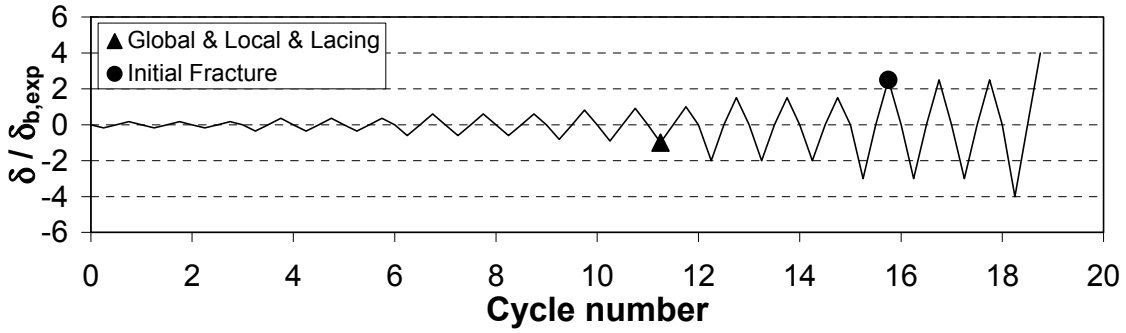


(d) Ay16-120 specimen

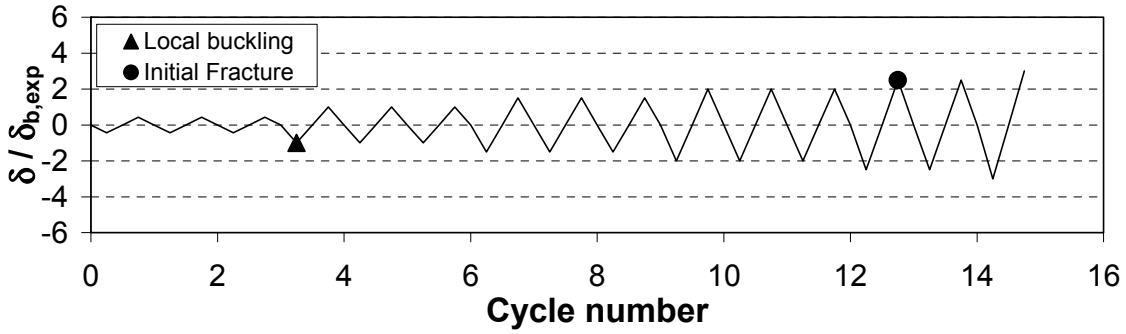
Figure 4.2 Loading histories for “Ay” specimens



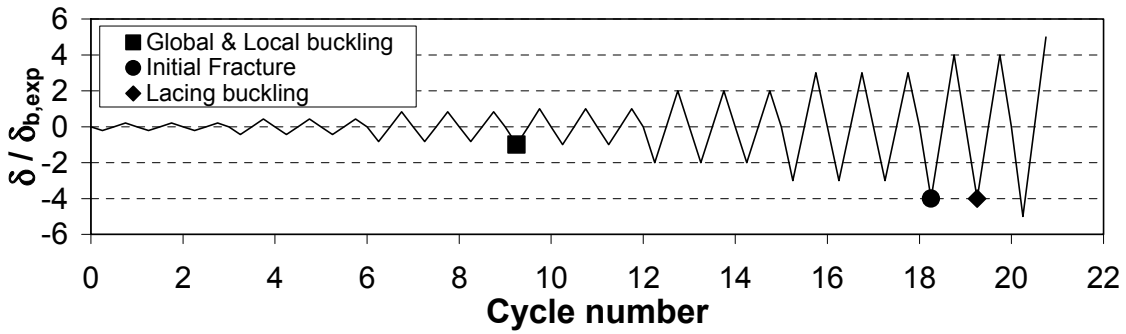
(a) By8-60 specimen



(b) By8-120 specimen

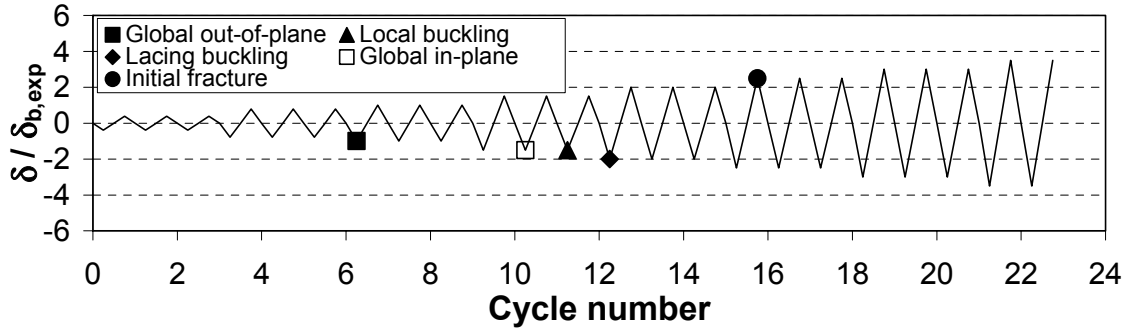


(c) By16-60 specimen

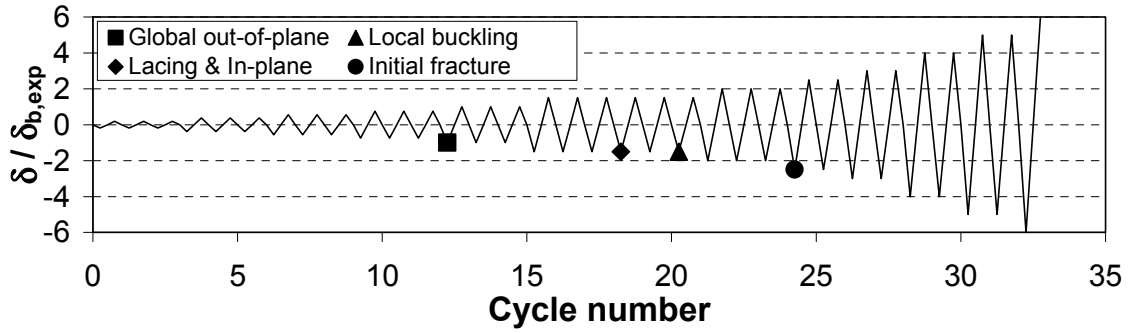


(d) By16-120 specimen

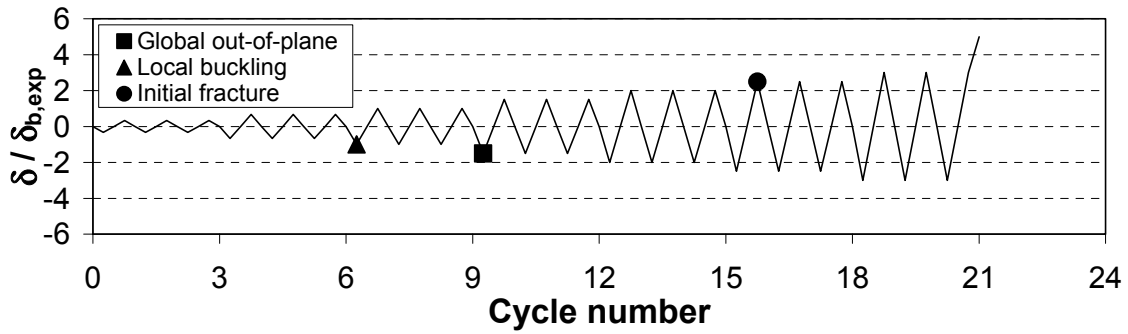
Figure 4.3 Loading histories for “By” specimens



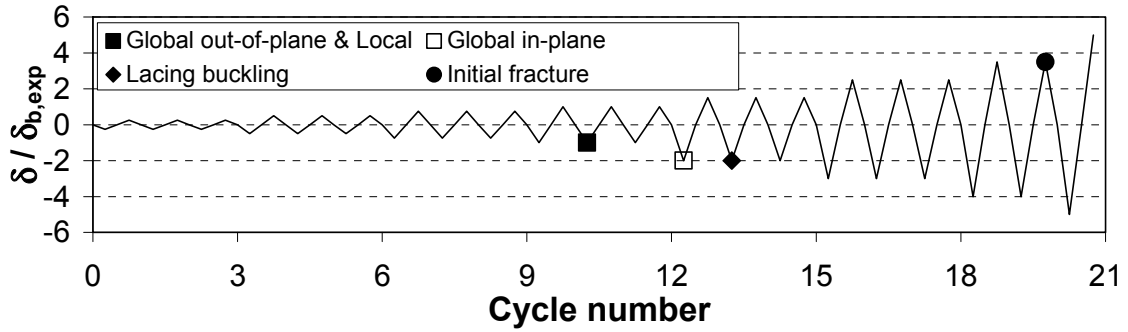
(a) Bx8-60 specimen



(b) Bx8-120 specimen

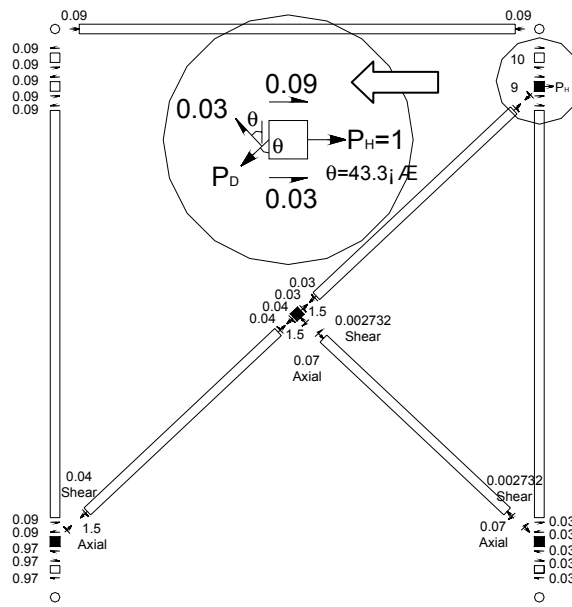


(c) Bx16-60 specimen



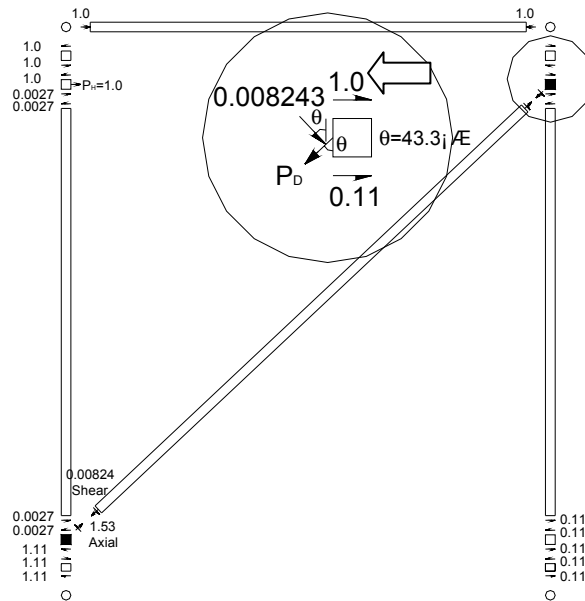
(d) Bx16-120 specimen

Figure 4.4 Loading histories for “Bx” specimens



$$\Sigma H = 1 + 0.09 + 0.03 - 0.03 \sin \theta - P_{axial} \cos \theta = 0, \quad P_{axial} = 1.51$$

Figure 4.5 FBD for axial force corrections from SAP 2000 analysis (KL/r = 60) – example for Ay8-60 Specimen



$$\Sigma H = 1 + 0.11 + 0.008243 \sin \theta - P_{axial} \cos \theta = 0, \quad P_{axial} = 1.53$$

Figure 4.6 FBD for axial force corrections from SAP 2000 analysis (KL/r = 120) – example for Ay8-120 Specimen



Figure 4.7 Test set-up for Bare Frame Test

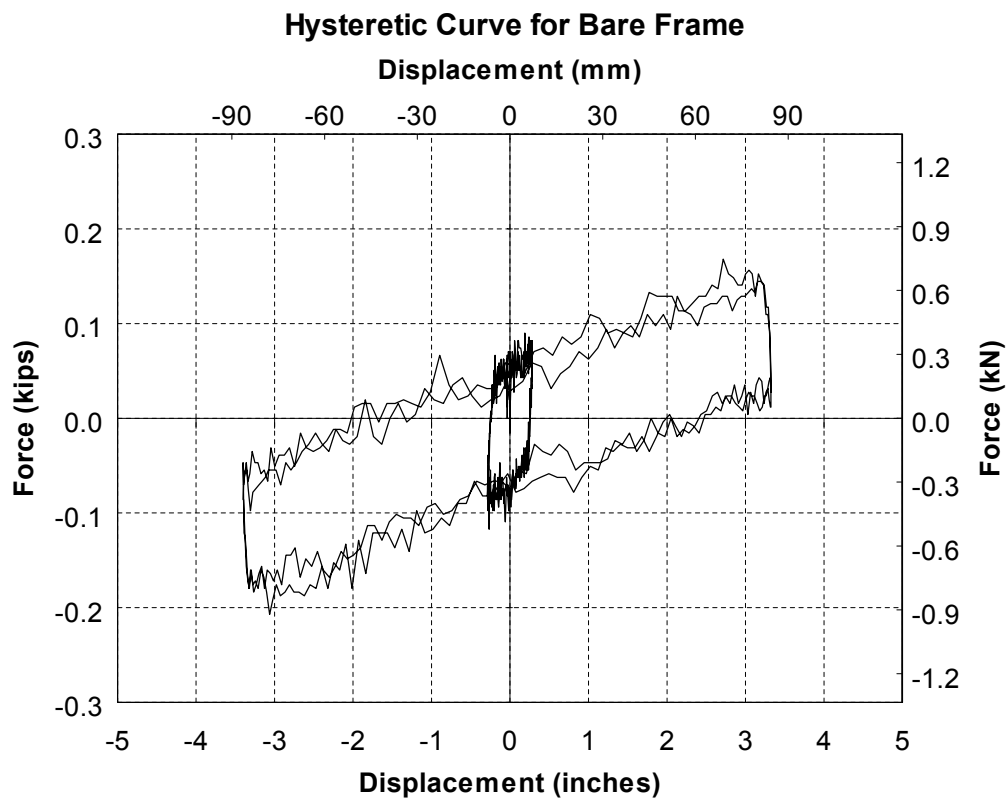


Figure 4.8 Hysteretic curve for Bare Frame Test



(a) Test set-up

(b) Unconnected end of a brace

Figure 4.9 Test set-up for the Ay8-60 specimen

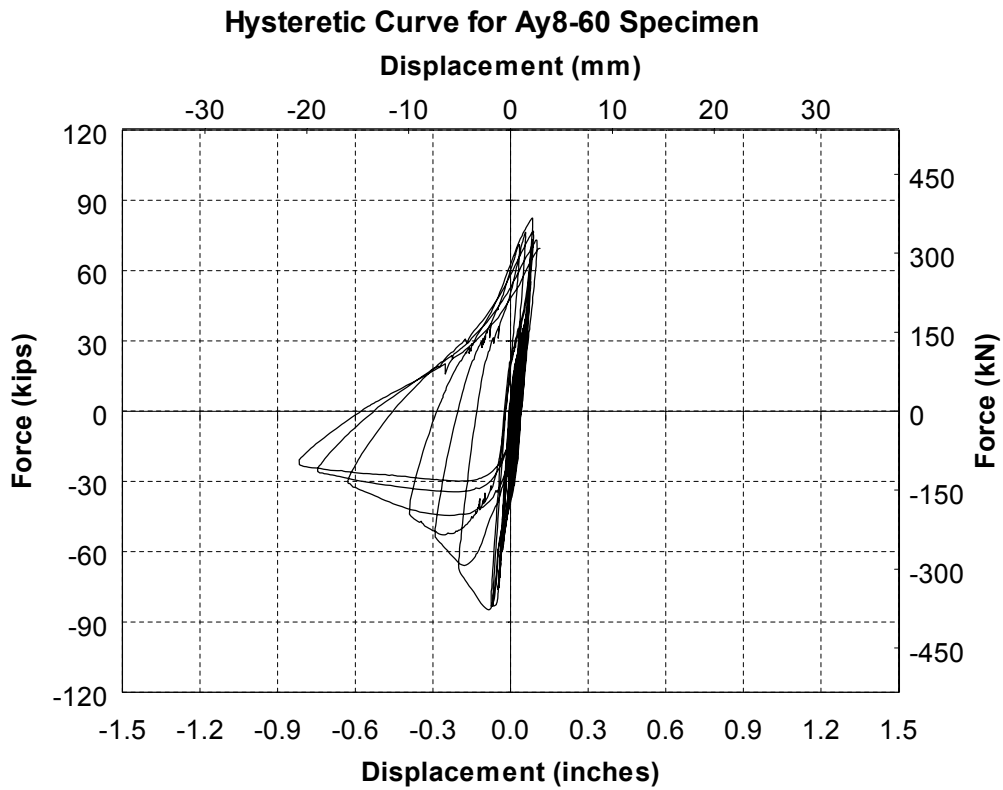
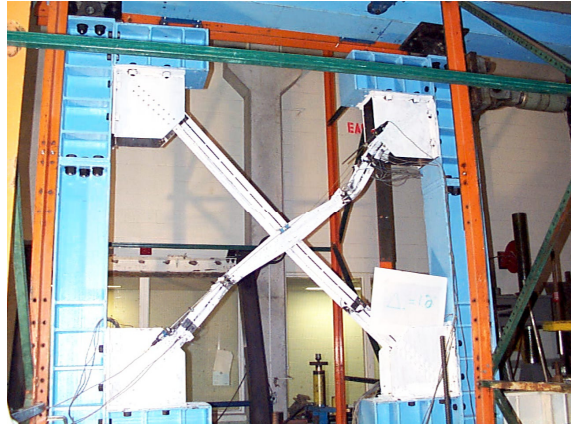


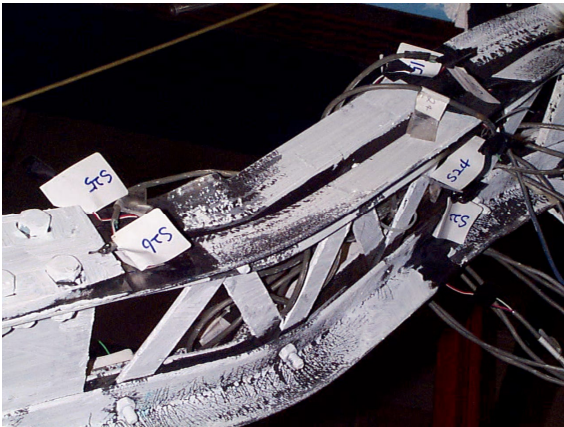
Figure 4.10 Hysteretic curve for the Ay8-60 specimen



(a) Global buckling at  $\Delta=1.0''$  (25.4mm)



(b) Global buckling at  $\Delta=1.2''$  (30.5mm)



(c) Global and local buckling at  $\Delta=1.2''$  (30.5mm), the South segment



(d) Local buckling at  $\Delta=1.2''$  (30.5mm), the North segment

Figure 4.11 Observations made during testing of the Ay8-60 specimen

### 4.2.3 Specimen Ay8-120

Testing of the Ay8-120 specimen was controlled by diagonal axial displacements of the specimen instead of horizontal frame drifts, because movement in the hinges and in the concrete foundation beam (as demonstrated during the previous test) made it too difficult to establish a reliable relationship between these two displacement measures and because the focus of this research project was more on the axial displacement behavior of the bracing member rather than on drifts of the braced frame. Test set-up for Ay8-120 specimen is presented in Figure 4.12. Hysteretic curve obtained from test result is also presented in Figure 4.13.

The calculated elastic theoretical buckling displacement ( $\delta_b$ ) was used to control the displacements for the first set of testing cycles, but no evidence of buckling or yielding was observed after 12 cycles at the theoretical  $1/3 \delta_b$ ,  $2/3 \delta_b$ ,  $1.0 \delta_b$ , and even  $2.0 \delta_b$  (3 cycles each). This was due to greater than expected flexibility of the specimen, as in all cases the corresponding applied axial brace force was less than the computed theoretical strength. During the first compressive cycle at  $2.5 \delta_b$ , global buckling at mid-length of the specimen was observed as shown in Figure 4.14a and the experimental buckling displacements,  $\delta_{b,exp} = 0.16''$  (4.1 mm) was identified. This value was then used as the reference control displacement to continuous testing per the ATC-24 protocol.

During the first compressive cycle at  $2.0 \delta_{b,exp} = 0.32''$  (8.1 mm), larger global buckling was observed at the location of initial buckling. Local buckling was also observed during this cycle at near the mid-length brace plastic hinge location. Figure 4.14b shows both global and (although hard to see) local buckling at  $2.0 \delta_{b,exp}$ .

During the first tensile cycle at  $4.0 \delta_{b,exp} = 0.64''$  (16.26 mm), initial fracture was observed on the upper angle at the global and local buckling location as shown in Figure 4.14c. Figure 4.14d shows local buckling during the first compressive cycle at  $4.0 \delta_{b,exp}$ .

Entire fracture of specimen was observed at  $6.0 \delta_{b,exp} = 0.96''$  (24.38 mm). Figures 4.11e and 4.11f show global buckling at  $5.0 \delta_{b,exp} = 0.80''$  (20.33 mm) and entire fracture of the specimen at  $6.0 \delta_{b,exp}$ , respectively.



Figure 4.12 Test set-up for the Ay8-120 specimen

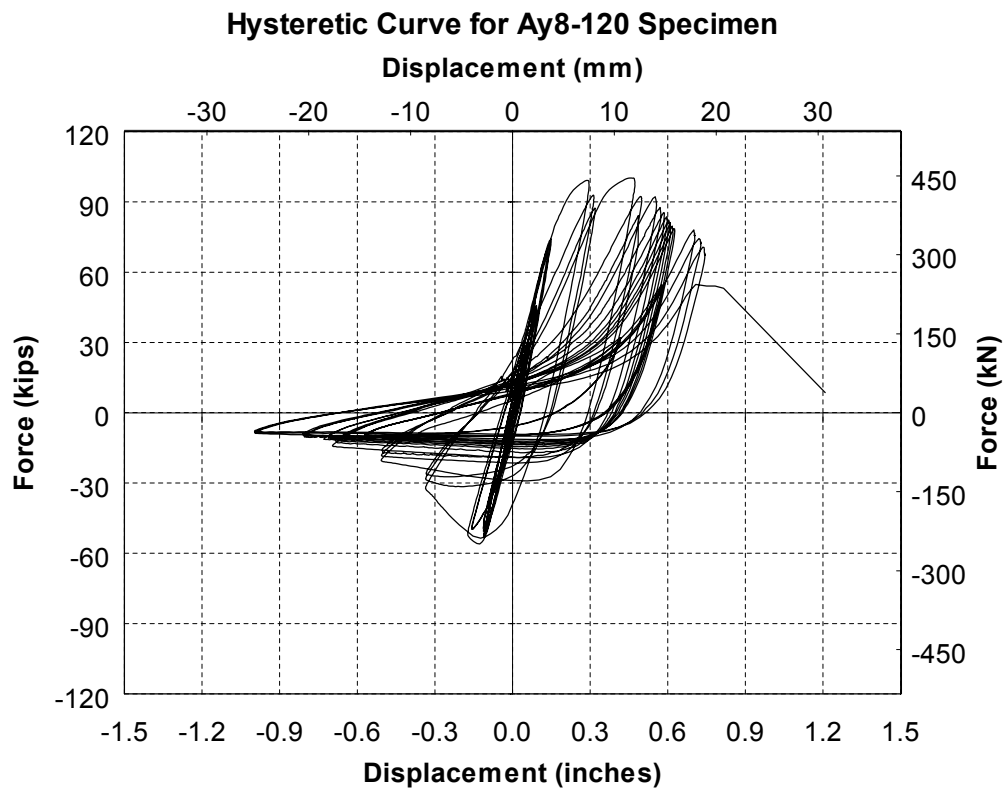


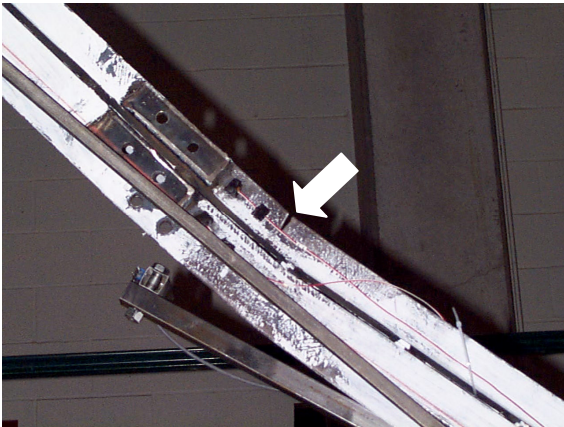
Figure 4.13 Hysteretic curve for the Ay8-120 specimen



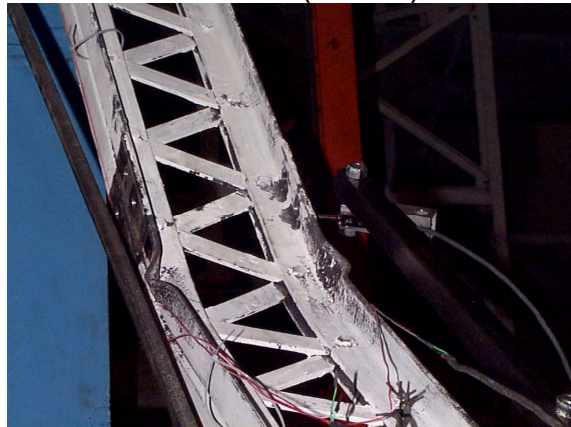
(a) Global buckling at  $\delta=0.16''$ (4.1mm)



(b) Global and local buckling at  $\delta=0.32''$ (8.1mm)



(c) Initial fracture at  $\delta=0.64''$ (16.3mm)



(d) Local buckling at  $\delta=0.64''$ (16.3mm)



(e) Global buckling at  $\delta=0.8''$ (20.3mm)



(f) Entire fractured shape

Figure 4.14 Observations made during testing of the Ay8-120 specimen

#### 4.2.4 Specimen Ay16-60

As described earlier, to prevent the damage on the other diagonal specimen (Ay16-120), a dummy brace member was used to brace specimen Ay16-60 at mid-length as shown Figure 4.15 (see Section 3.2.1), to produce two specimen segments each with  $KL/r = 60$ . Before applying horizontal forces to the frame, an axial gravity load of 56.33 kips (250.7 kN) was applied on the top beam to prevent lifting of the concrete foundation beam which was observed during testing of the Ay8-60 and Ay8-120 specimens and deemed to be partly accountable for the large discrepancy between theoretical and experimental results. Hysteretic curve from test results is presented in Figure 4.16.

Loading was controlled by diagonal axial displacement of the entire specimen, i.e., the cumulative displacement over both segments. Before the experimental buckling displacement,  $\delta_{b,exp}$ , could be identified, the theoretical one,  $\delta_b$ , was used for controlling the loading.

During the first compressive cycle at  $1.0 \delta_b = 0.22''$  (5.59 mm), local buckling was observed on the upper angles near the middle connection plate on the North specimen, as shown in Figure 4.17a. From the temposonic transducer installed for measuring the whole diagonal axial displacement of the specimen, the experimental buckling displacement was identified as  $\delta_{b,exp} = 0.22''$  (5.59 mm). The corresponding experimental buckling displacements for each of the South and North segments of the specimen were identified as  $0.11''$  (2.79 mm). From that point, loading of the specimen proceeded on the assumption that damage would concentrate on the North segment, leaving the South segment intact, and that, therefore, smaller cyclic displacement steps should be applied using total member length as a control, to indirectly control the North segment displacements. Observations confirmed that buckling, damage, and inelastic deformation concentrated only on the buckled North segment.

After the three cycles at  $1.0 \delta_{b,exp}$ , three cycles at  $\delta = 1.25 \delta_{b,exp} = 0.275''$  (6.99 mm) were applied, which was assumed to correspond to  $1.5 \delta_{b,exp}$  of the North segment and  $1.0 \delta_{b,exp}$  of the South segment. The decision to apply  $1.5 \delta_{b,exp}$  on the North segment instead of  $2.0 \delta_{b,exp}$  was for

the purpose of allowing better observations of other local buckling which might be missed if using larger displacement increments.

During the first compressive cycle at  $\delta = 1.25 \delta_{b,exp} = 0.275''$  (6.99 mm), local buckling on the lower angle near the middle connection plate and on the lower angle near the gusset-connection of the North segment of the specimen were observed as shown in Figures 4.17b and 4.17c respectively.

During the third tensile cycle at  $\delta = 1.75 \delta_{b,exp}$  (corresponding to an assumed  $2.5 \delta_{b,exp}$  of the North and  $1.0 \delta_{b,exp}$  of the South segments) =  $0.385''$  (9.78 mm), initial fracture was observed on the lower angle near the middle connection plate of the North segment of the specimen as shown in Figure 4.17d.

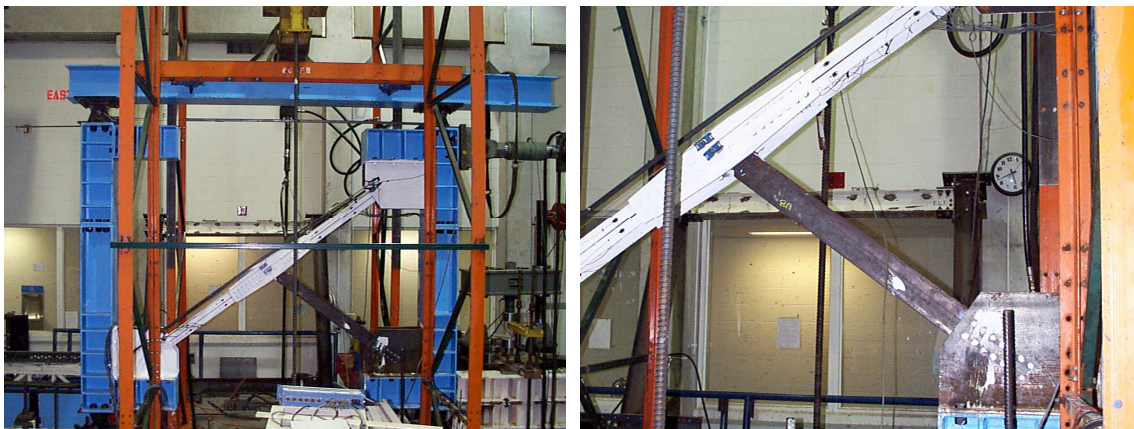
During the first tensile cycle at  $\delta = 3.0 \delta_{b,exp}$  ( $5.0 \delta_{b,exp}$  of North and  $1.0 \delta_{b,exp}$  of South specimen) =  $0.66''$  (16.76 mm), entire fracture near the middle connection plate of the North segment was observed as shown in Figure 4.17f.

#### **4.2.5 Specimen Ay16-120**

Test set-up for Ay16-120 specimen is presented in Figure 4.18 and hysteretic curve obtained from test result is presented in Figure 4.19. Testing of Ay16-120 specimen was controlled by diagonal axial displacements of specimen.

Initially, the theoretical buckling displacement ( $\delta_b$ ) was used to control the displacements for the first set of testing cycles. During the first compressive cycle at  $1.0 \delta_b$ , global buckling was observed near the mid-length of the specimen and the experimental buckling displacements,  $\delta_{b,exp} = 0.088''$  (2.22 mm) was identified.

The decision to apply  $1.5 \delta_{b,exp}$  of the specimen instead of  $2.0 \delta_{b,exp}$  was for the purpose of allowing better observations of local buckling which might be missed due to larger global buckling if using larger displacement increments.



(a) Test set-up

(b) Dummy specimen

Figure 4.15 Test set-up for the Ay16-60 specimen

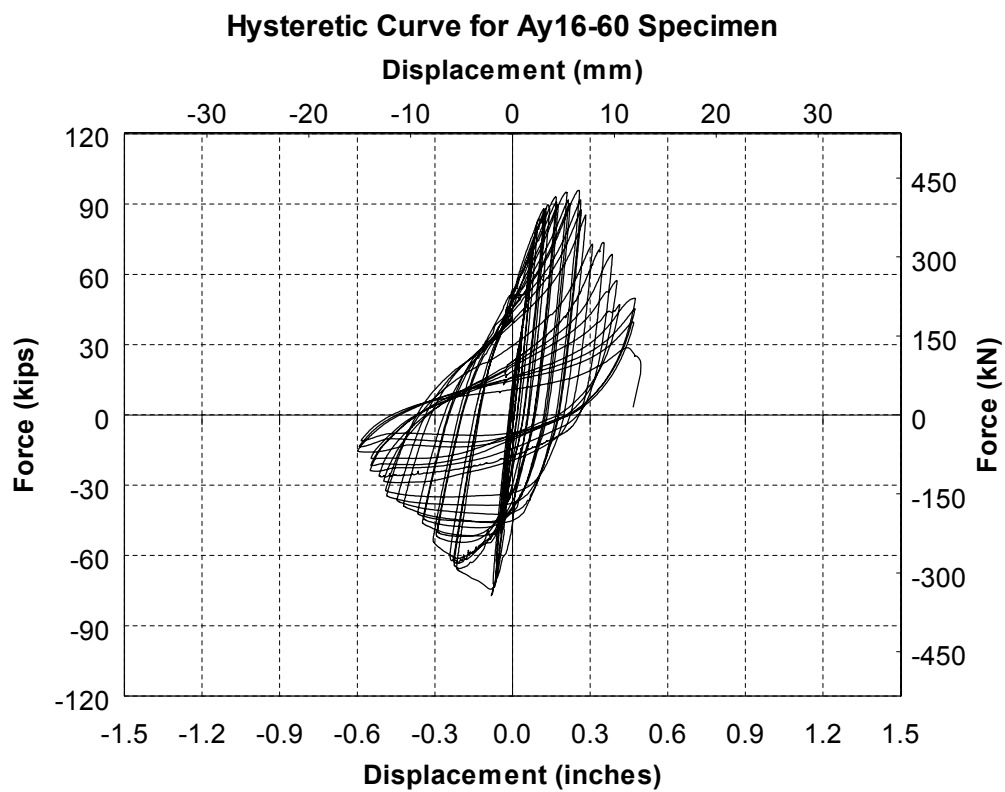
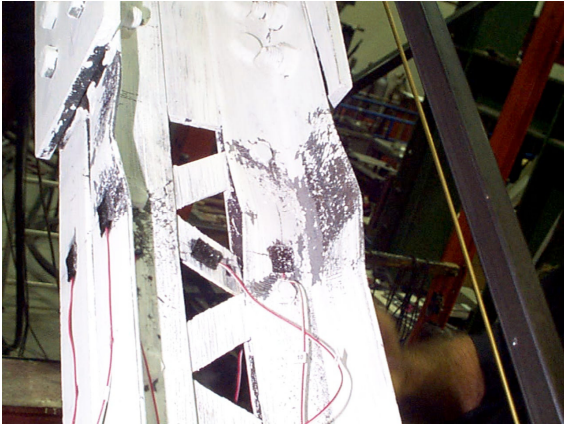


Figure 4.16 Hysteretic curve for the Ay16-60 specimen



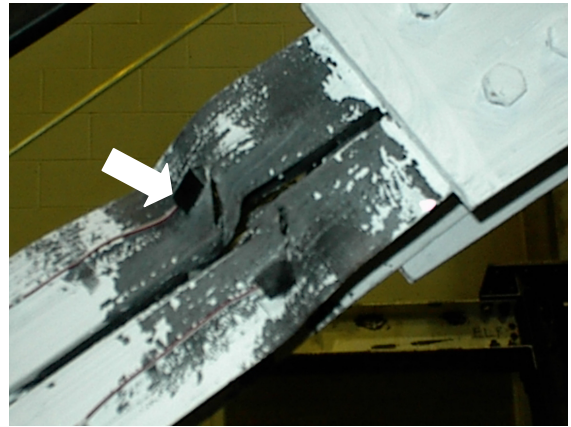
(a) Local buckling at  $\delta=0.22''$ (5.6mm)



(b) Local buckling at  $\delta=0.28''$ (7.0mm)



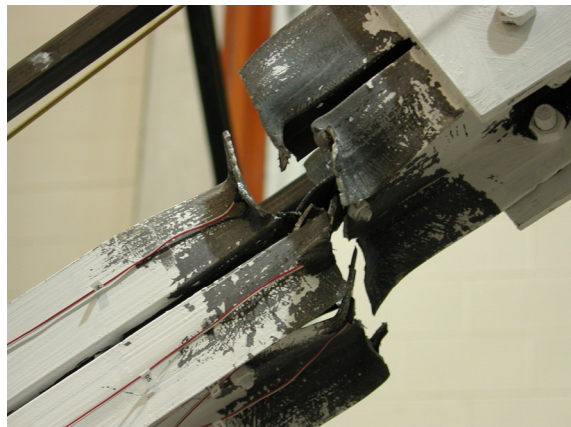
(c) Local buckling at  $\delta=0.28''$ (7.0mm)



(d) Initial fracture at  $\delta=0.39''$ (10.0mm)



(e) Global buckling at  $\delta=0.55''$ (14.0mm)



(f) Final fracture at  $\delta=0.66''$ (16.8mm)

Figure 4.17 Observations made during testing of the Ay16-60 specimen



Figure 4.18 Test set-up for the Ay16-120 specimen

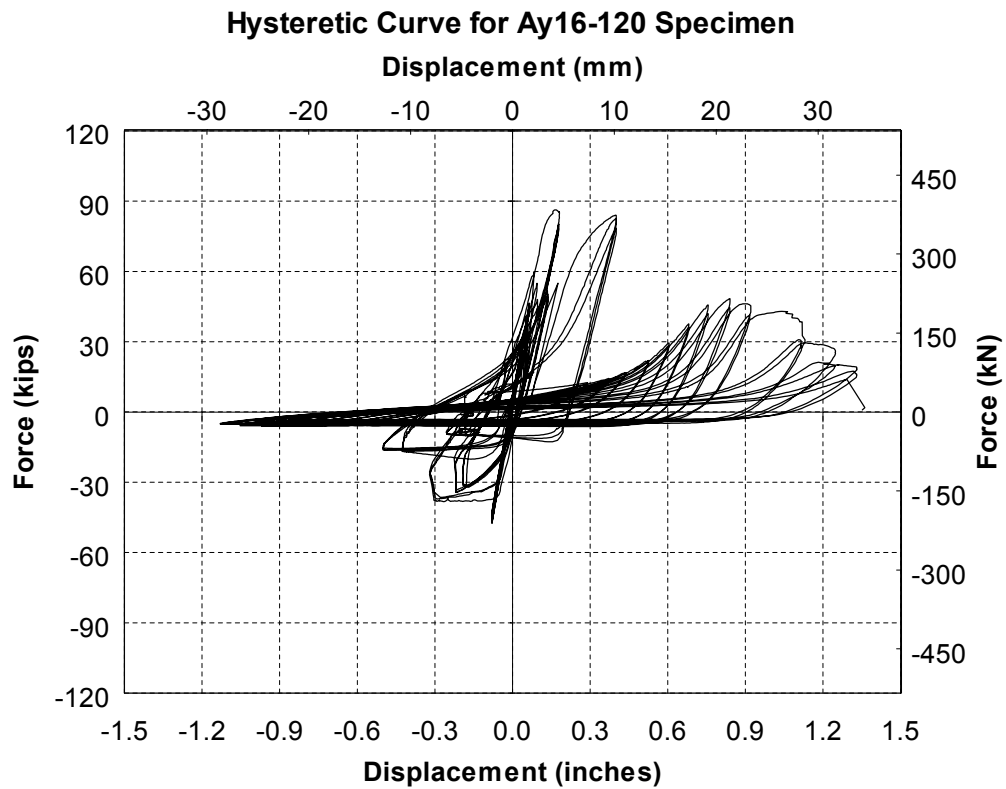


Figure 4.19 Hysteretic curve for the Ay16-120 specimen

During the first compressive cycle at  $1.5 \delta_{b,exp}$ , larger global buckling was observed at the location of initial buckling as shown in Figure 4.20a. Local buckling was also observed during this cycle on the lower angle near the mid-length brace plastic hinge location and on the upper angle near the South gusset-connection as shown in Figures 4.20b and 4.20c, respectively.

During the first compressive cycle at  $3.0 \delta_{b,exp} = 0.26''$  (6.60 mm), another local buckling was observed on the lower angle at 1/3 of member length from the South end as shown in Figure 4.20d.

After three cycles at  $3.0 \delta_{b,exp}$ , the actuator monitoring system behaved erratically during a few loading cycles, giving erroneous results that went unnoticed for a while, resulting in unexpected forces applied in compression on the specimen with large deformations at the buckling location and without data acquisition. After correcting the problem and re-initializing the testing set-up, another three loading cycles at  $3.0 \delta_{b,exp} = 0.26''$  (6.60 mm) were applied to reduce the uncertainty that might exist between before and after initialization of the testing set-up. During the first compressive cycle at these loading cycles, another local buckling was observed on the upper angle at 1/3 of member length from the South end.

During the first tensile cycle at  $5.0 \delta_{b,exp} = 0.44''$  (11.18 mm), the North top hinge was damaged at  $\delta = 0.35''$  (8.89 mm) as shown in Figure 4.20e due to eccentric axial gravity loads applied to the top beam and testing was stopped for safety purpose. After replacing the damaged hinge with a new one, remaining the axial loads, and adjusting lateral bracing to the top beam, three cycles at  $4.0 \delta_{b,exp}$  were applied to compare the effect of testing ‘with’ and ‘without’ axial loads. Comparison is presented in Figure 4.20f. In this figure, diagonal axial force and displacement from the three new cycles at  $4.0 \delta_{b,exp}$  were applied at the end of the data from the previous tensile cycle data (frame sway was observed during unloading of the gravity axial loads but not recorded by the data acquisition, resulting in an offset in data). As shown in Figure 4.20f, trends in the slope of the hysteretic curve from the three comparison cycles without axial gravity loads followed logically and closely those from the three cycles with axial gravity loads. Comparisons of the compression cycles results both with and without axial gravity loads were almost identical.

Decision was therefore made to continue testing without axial gravity loads for the rest of testing of the Ay16-120 specimen and for all following “B” shape specimens.

During the first tensile cycle at 5.0  $\delta_{b,exp} = 0.44''$  (11.2 mm), initial fracture was observed on the lower angle near the mid-length of the specimen as shown in Figure 4.17g. Another local buckling was observed on the upper angles near the North gusset-connection as shown in Figure 4.20h.

During the first tensile cycle at 11.0  $\delta_{b,exp} = 0.97''$  (24.6 mm), fractures on the upper angles near the South gusset-connection and on the lower angle at the 1/3 of member length from the South end were observed as shown in Figures 4.20i and 4.20j, respectively.

During the first tensile cycle at 12.0  $\delta_{b,exp} = 1.06''$  (26.8 mm), fractures on the lower angles near the North gusset-connection was observed as shown in Figure 4.20k

At the loading cycles of 14.0  $\delta_{b,exp} = 1.23''$  (31.3 mm), maximum actuator stroke was reached in compression, and the control displacement was increased thereon only in tension (for example, 14.0  $\delta_{b,exp}$  in tension and 13.0  $\delta_{b,exp}$  in compression).

During the first tensile cycle at 16.0  $\delta_{b,exp} = 1.41''$  (35.8 mm) in tension and 13.0  $\delta_{b,exp} = 1.144''$  (29.1 mm) in compression, lacing bolt failure near the mid-length of the specimen was observed.

During the first tensile cycle at 17.0  $\delta_{b,exp} = 1.496''$  (38.0 mm) in tension, entire fracture near the mid-length of the specimen was observed as shown in Figure 4.20l.

#### **4.2.6 Specimen By8-60**

Before the testing the By8-60 specimen, the concrete foundation beam and hinges at the bottom of the frame (which caused significantly more flexible frame response due to their excessive deformations), were replaced with a steel foundation beam and better designed new hinges. This foundation beam was connected to the large quasi-static reaction frame and strong floor as

described in SECTION 3. Connections between the steel foundation beam and hinges were done with 1-1/2" (38.1 mm) diameter A490 high strength bolts using a hydraulic torque wrench to pre-tension the bolts and prevent slippage in the connections. The steel foundation beam was also connected with the reaction frame using 1-1/2" (38.1 mm) diameter A490 high strength bolts and connected to the strong floor with prestressed 1-1/8" (38.1 mm) diameter Diwidag bar to prevent slippage and lifting of the foundation beam. These new steel foundation beam and hinges were consistently used for all the section shape B specimens. These new equipments proved effective to prevent undesirable frame deformations due to movements in the foundation beam and hinges.

For all the section shape B specimens, testing was initially controlled in relation to the lateral frame force,  $P_H$ , corresponding to the theoretical elastic brace buckling force until the experimental buckling displacements ( $\delta_{b,exp}$ ) was identified. Beyond that point, subsequent cycles were controlled using target displacements.

Test set-up for the By8-60 specimen is presented in Figure 4.21 and the hysteretic curve obtained from test result is presented in Figure 4.22.

During the first compressive cycle at  $2/3 P_H = 36$  kips (160.2 kN) corresponding to the  $2/3$  of elastic theoretical buckling displacement,  $\delta_b$ , global buckling was observed in the North segment of the specimen as shown in Figure 4.23a and the experimental buckling displacements,  $\delta_{b,exp} = 0.14$ " (3.6 mm) was identified.

Three loading cycles at  $1.5 \delta_{b,exp}$  of the specimen instead of  $2.0 \delta_{b,exp}$  were applied for better observations of local buckling and progress of global buckling. During the first compressive cycle on the way to the target value of  $1.5 \delta_{b,exp} = 0.21$ " (5.3 mm), global buckling occurred suddenly in the North segment of the specimen when the control displacement had only reached  $0.17$ " (4.3 mm).

During the first compressive cycle at  $2.0 \delta_{b,exp} = 0.28$ " (7.1 mm), buckling of the 2<sup>nd</sup> lacing on the East side of the brace and on the 6<sup>th</sup> lacing in the West side from the top of the North segment were observed as shown in Figure 4.23b. Lacing buckling gradually spread to the 2<sup>nd</sup>, 4<sup>th</sup>, and 8<sup>th</sup>

lacings on the West side and on the 3<sup>rd</sup>, 5<sup>th</sup>, and 7<sup>th</sup> lacings on the East side from the top of the North segment during the cycles at  $\delta_{b,exp} = 0.28''$  (7.1 mm). Lacing buckling caused the two channels that constituted the cross-section to move closer together, resulting in a smaller moment of inertia (I) for the specimen and consequently a greater drops in compression strength during compressive cycles. During the third compressive cycle, local buckling was observed on the upper angle near the middle connection plate as shown in Figure 4.23c.

During the second compressive cycle at  $2.5 \delta_{b,exp} = 0.35''$  (8.9 mm), a lacing bolt failure near the middle connection plate was observed in the North segment of the specimen as shown in Figure 4.23d.

During the second compressive cycle at  $3.0 \delta_{b,exp} = 0.42''$  (10.7 mm), local buckling on the upper angle near the 5<sup>th</sup> lacing from the top of the North segment was observed as shown in Figure 4.23e. During the third compressive cycle, initial fracture was observed on the lower angle near the 5<sup>th</sup> lacing from the top of the North segment as shown in Figure 4.23f. Fracture on the lower angle near the middle connection plate was also observed during this cycle as shown in Figure 4.23g.

During the first tensile cycle at  $5.0 \delta_{b,exp} = 0.70''$  (17.8 mm), the upper two angles completely fractured near the 4<sup>th</sup> and 5<sup>th</sup> lacings from the top of North segment of the specimen as shown in Figures 4.23h and 4.23i.

During the first tensile cycle at  $8.0 \delta_{b,exp} = 1.12''$  (28.4 mm), entire fracture was observed at the fracture location that initiated at  $5.0 \delta_{b,exp}$  as shown in Figure 4.23j. Figures 4.23k and 4.23l respectively show global and local buckling during the last compressive cycle before the entire fracture.

#### **4.2.7 Specimen By8-120**

Test set-up and hysteretic curve obtained from test result for the By8-120 specimen are presented in Figures 4.24 and 4.25, respectively.



(a) Global buckling at  $\delta=0.13''$ (3.3mm) near the mid-length of the specimen



(b) Local buckling at  $\delta=0.13''$ (3.3mm) near the mid-length of the specimen



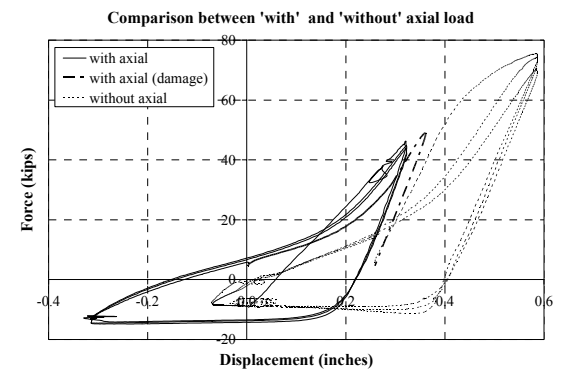
(c) Local buckling at  $\delta=0.13''$ (3.3mm) near the gusset-connection



(d) Local buckling at  $\delta=0.26''$ (6.7mm) at 1/3 of member length



(e) Damaged hinge at  $\delta=0.35''$ (8.9mm)

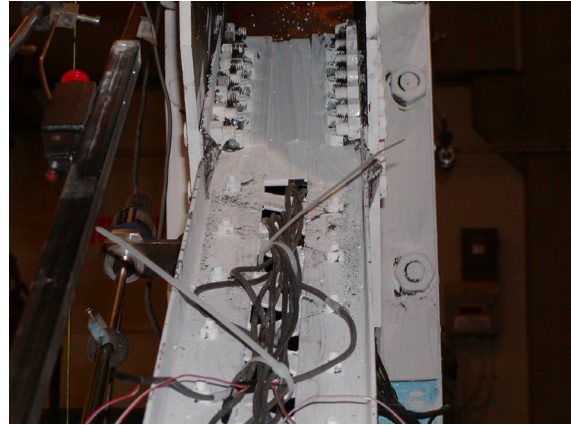


(f) Comparison between with and without axial gravity loads

Figure 4.20 Observations made during testing of the Ay16-120 specimen



(g) Initial fracture at  $\delta=0.44"$  (11.1mm) near the mid-length of the specimen



(h) Local buckling at  $\delta=0.44"$  (11.1mm) near the gusset-connection



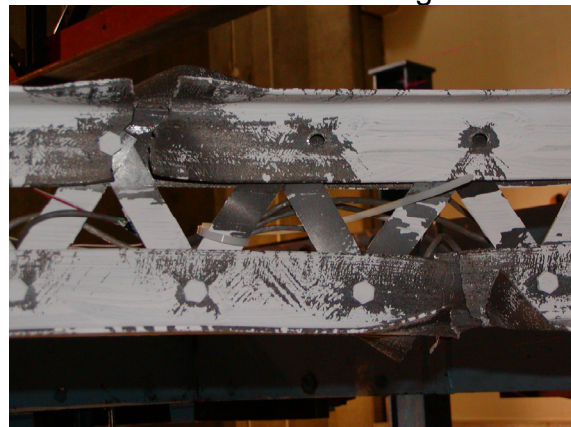
(i) Fracture at  $\delta=0.97"$  (24.5mm) near the gusset-connection



(j) Fracture at  $\delta=0.97"$  (24.5mm) at 1/3 of member length



(k) Fracture at  $\delta=1.06"$  (26.8mm) near gusset-connection



(l) Final fracture at  $\delta=1.49"$  (37.8mm)

Figure 4.20 Observations made during testing of the Ay16-120 specimen (continued)

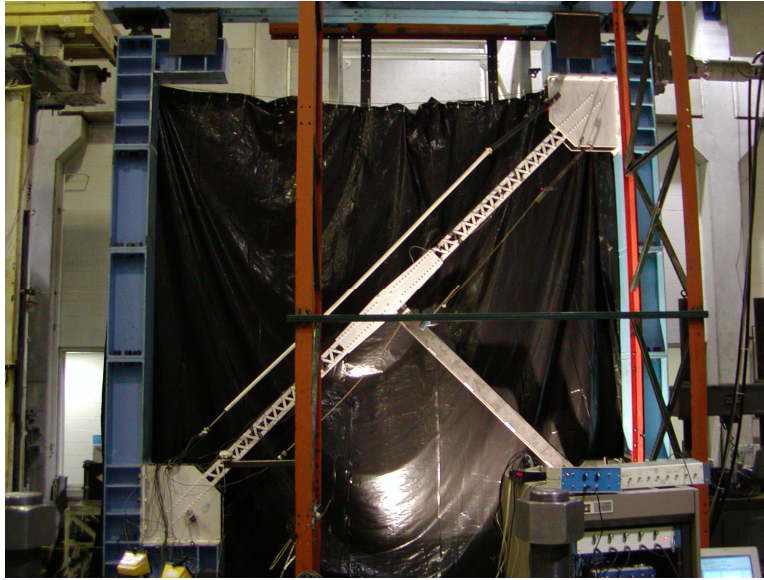


Figure 4.21 Test set-up for the By8-60 specimen

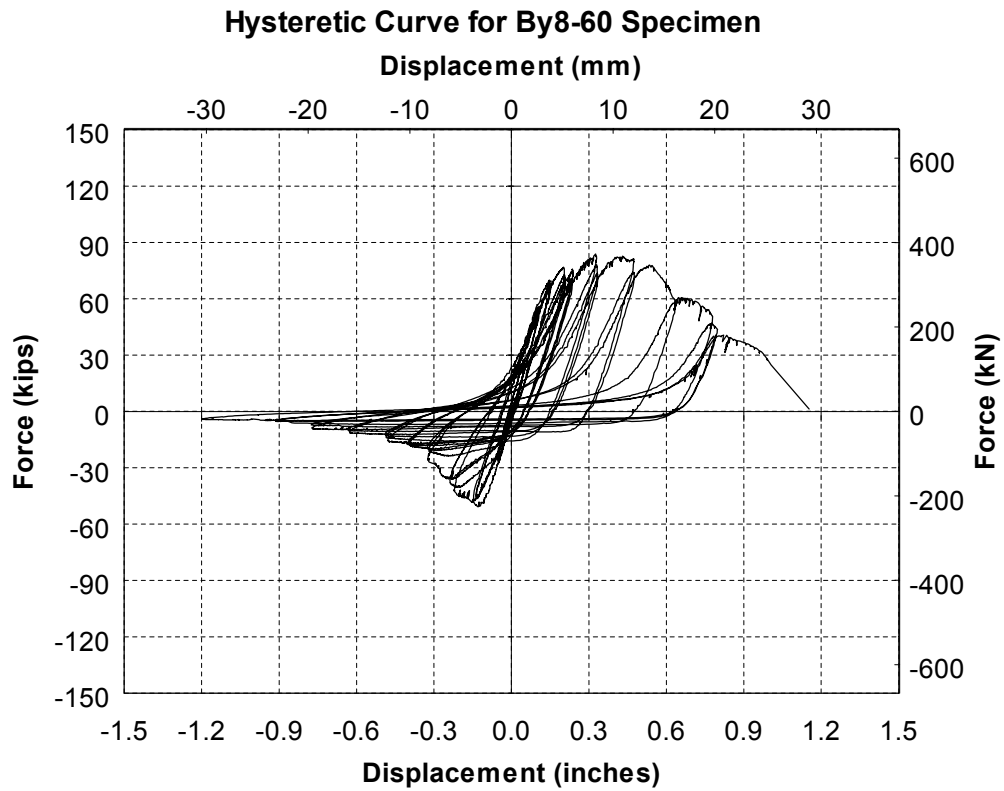
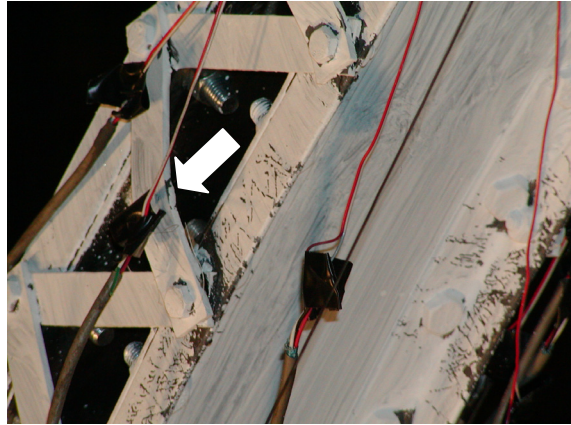


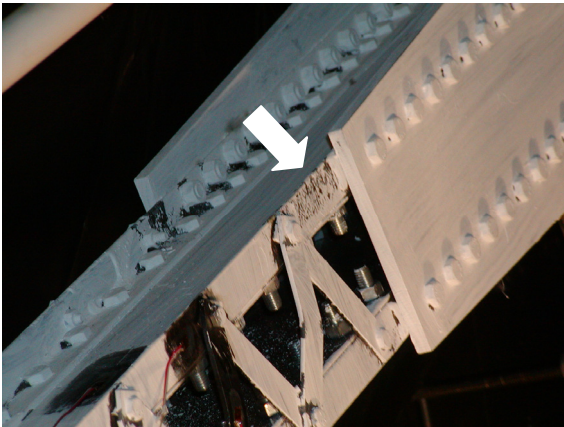
Figure 4.22 Hysteretic curve for the By8-60 specimen



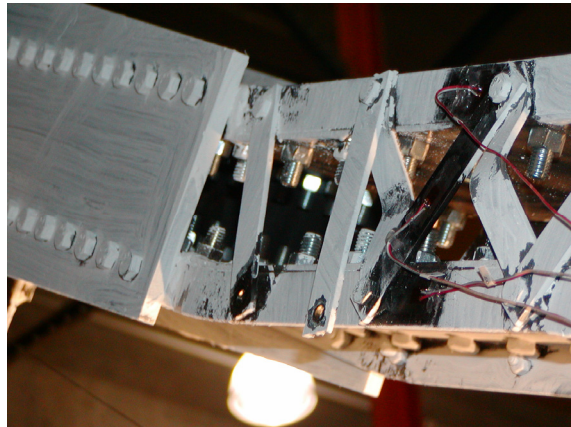
(a) Global buckling at  $\delta=0.14''$ (3.66mm)



(b) Lacing buckling at  $\delta=0.28''$ (7.1mm)



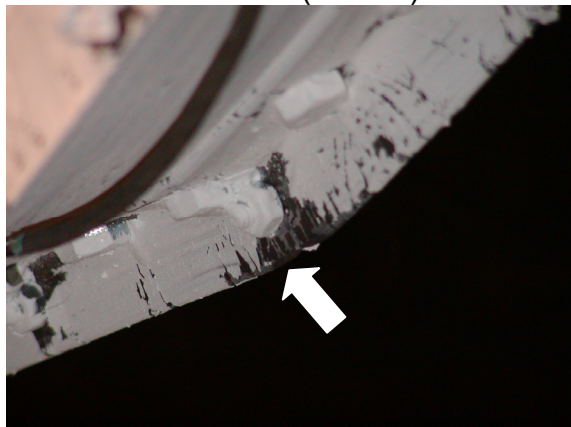
(c) Local buckling at  $\delta=0.28''$ (7.1mm)



(d) Lacing bolt failures at  $\delta=0.35''$ (8.9mm)

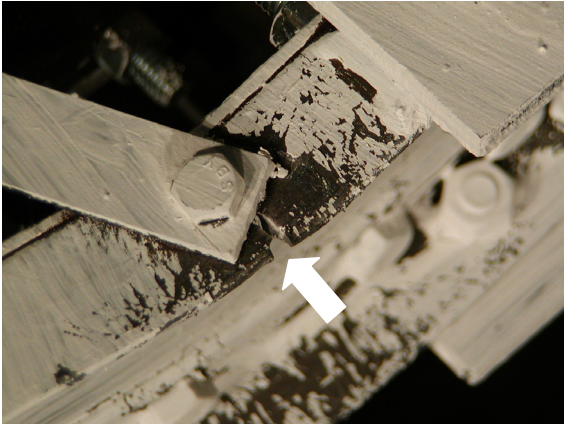


(e) Local buckling at  $\delta=0.42''$ (10.7mm)

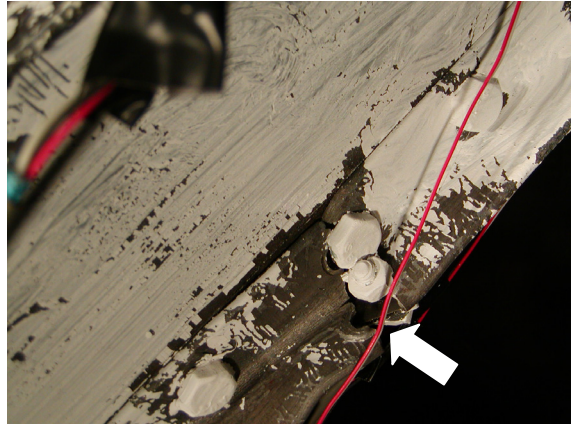


(f) Initial fracture at  $\delta=0.42''$ (10.7mm)

Figure 4.23 Observations made during testing of the By8-60 specimen



(g) Initial fracture at  $\delta=0.42''$ (10.7mm)



(h) Fracture at  $\delta=0.7''$ (17.8mm)



(i) Fracture and lacing buckling at  $\delta=0.7''$ (17.8mm)



(j) Entire fracture at  $\delta=1.12''$ (28.5mm)



(k) Global buckling at  $\delta=1.12''$ (28.5mm)



(l) Local buckling at  $\delta=1.12''$ (28.5mm)

Figure 4.23 Observations made during testing of the By8-60 specimen (continued)



Figure 4.24 Test set-up for the By8-120 specimen

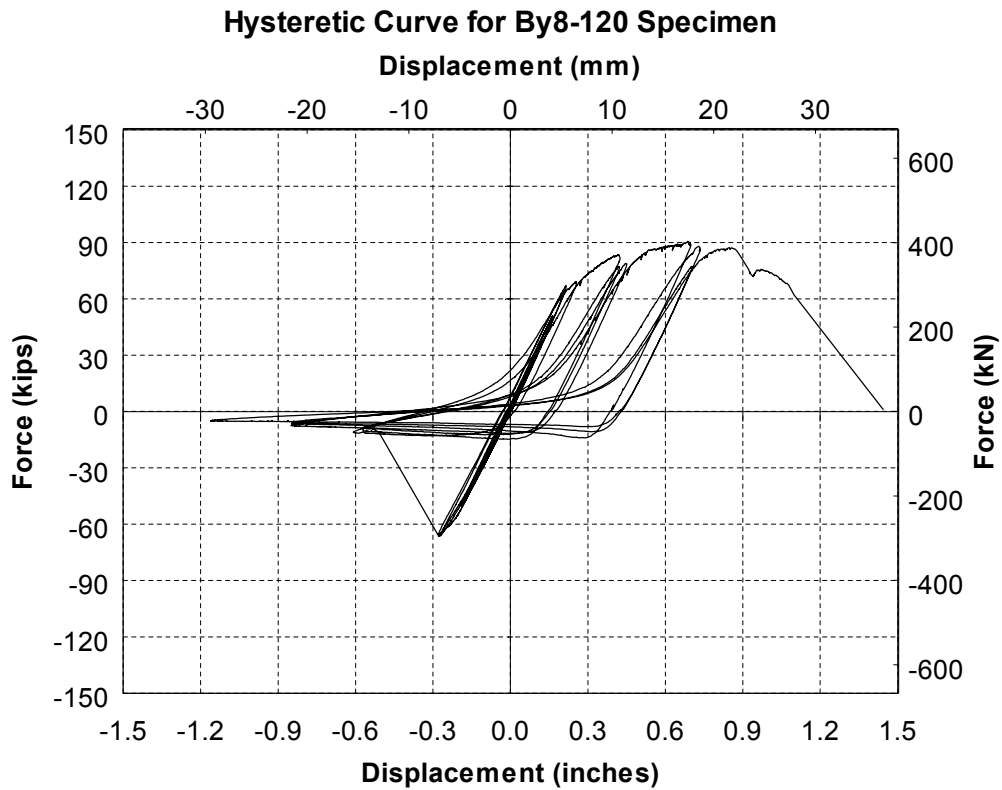


Figure 4.25 Hysteretic curve for the By8-120 specimen

The calculated frame force corresponding to the elastic theoretical buckling strength ( $P_H$ ) was used to control for the first set of testing cycles, but no evidence of buckling or yielding was observed after 9 cycles at the theoretical  $1/3 P_H$ ,  $2/3 P_H$ , and  $1.0 P_H$  (three cycles each), or even during the first cycle at  $1 \frac{1}{3} P_H = 40$  kips (178 kN). A decision was made to seek the experimental buckling displacement by subjecting the specimen to progressively increasing small values of the control force, starting from  $P_H = 42.0$  kips (186.9 kN) for the first, 44.0 kips (195.8 kN) for the second, and 46.0 kips (204.7 kN) for third loading cycle. During the third compressive cycle at 46.0 kips (204.7 kN), significant global buckling suddenly developed near mid-length of the specimen as shown in Figure 4.26a. Local and lacing buckling, and lacing bolt failures, were also observed near the global buckling location during this cycle as shown in Figures 4.26b and 4.26c and the experimental  $\delta_{b,exp} = 0.28''$  (7.1 mm) was identified.

During the first tensile cycle at  $3.0 \delta_{b,exp} = 0.84''$  (21.3 mm), initial fracture on the lower angle near the 7<sup>th</sup> lacing from the South end of the specimen was observed as shown in Figure 4.26d. During the second compressive cycle at  $0.84''$  (21.3 mm), fracture on the upper angle near the global buckling location was also observed as shown in Figure 4.26e.

During the first compressive cycle at  $4.0 \delta_{b,exp} = 1.12''$  (28.5 mm), fractures on the lower angles near the South gusset-connection were observed as shown in Figures 4.26f and 4.26g. During the first tensile cycle at this stage, entire fracture was observed at the global buckling location as shown 4.26h and 4.26i. Figures 4.26j, to 4.26l show the global and local buckling at the last compressive loading cycle before the entire fracture of the specimen.

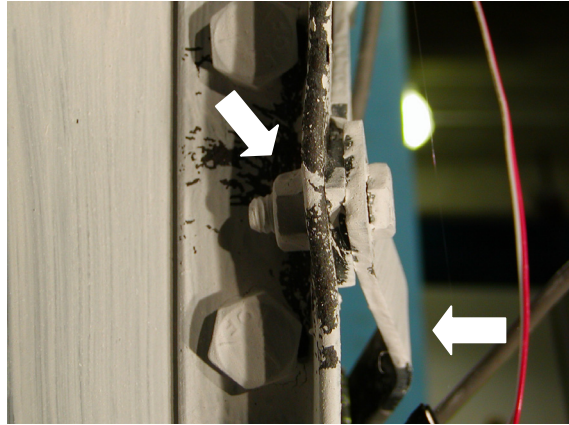
#### **4.2.8 Specimen By16-60**

Test set-up and hysteretic curve obtained from test result for the By16-60 specimen are presented in Figures 4.27 and 4.28, respectively.

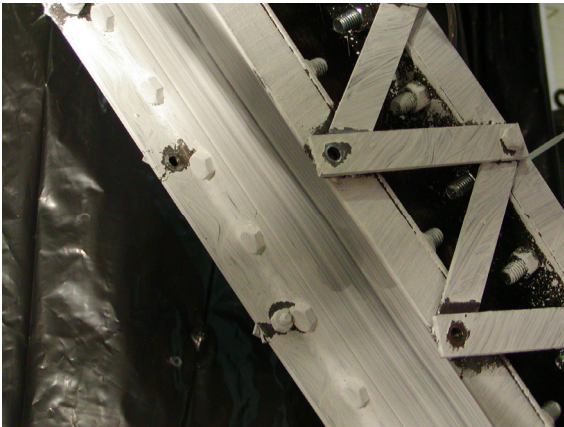
During the first compressive cycle at  $2/3 P_H = 77$  kips (342.7 kN), local buckling on the upper angle near the middle connection plate and lower angles near the gusset-connection in the North segment of the specimen were observed as shown in Figures 4.29a and 4.29b, respectively and



(a) Global buckling at  $\delta=0.28''(7.11\text{mm})$



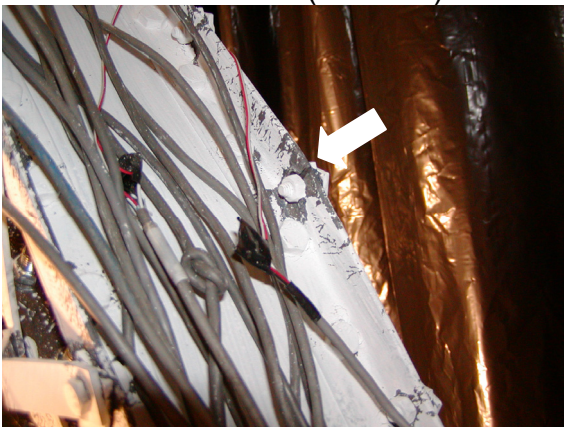
(b) Local and lacing buckling at  $\delta=0.28''(7.11\text{mm})$



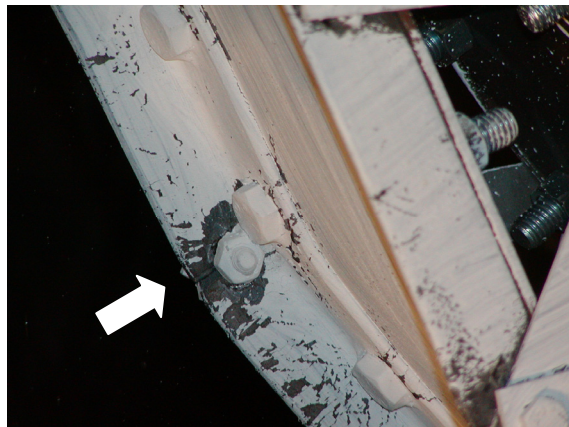
(c) Lacing bolt failure at  $\delta=0.28''(7.11\text{mm})$



(d) Initial fracture at  $\delta=0.84''(21.3\text{mm})$



(e) Fracture at  $\delta=0.84''(21.3\text{mm})$



(f) Fracture at  $\delta=1.12''(28.5\text{mm})$

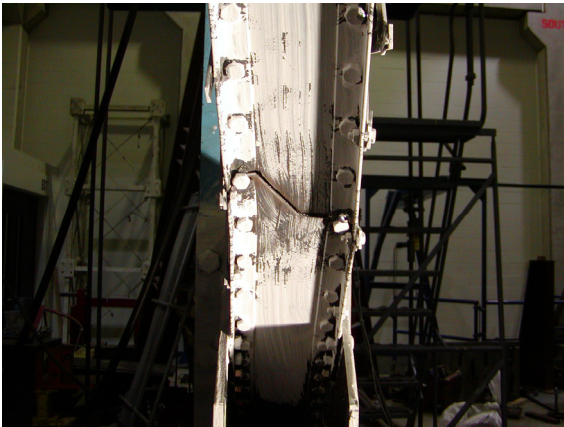
Figure 4.26 Observations made during testing of the By8-120 specimen



(g) Fracture at  $\delta=1.12''$ (28.5mm)



(h) Fracture at  $\delta=1.12''$ (28.5mm)



(i) Final fracture at  $\delta=1.12''$ (28.5mm)



(j) Local and lacing buckling at  $\delta=1.12''$ (28.5mm)



(k) Global buckling at  $\delta=1.12''$ (28.5mm)



(l) Global buckling at  $\delta=1.12''$ (28.5mm)

Figure 4.26 Observations made during testing of the By8-120 specimen (continued)

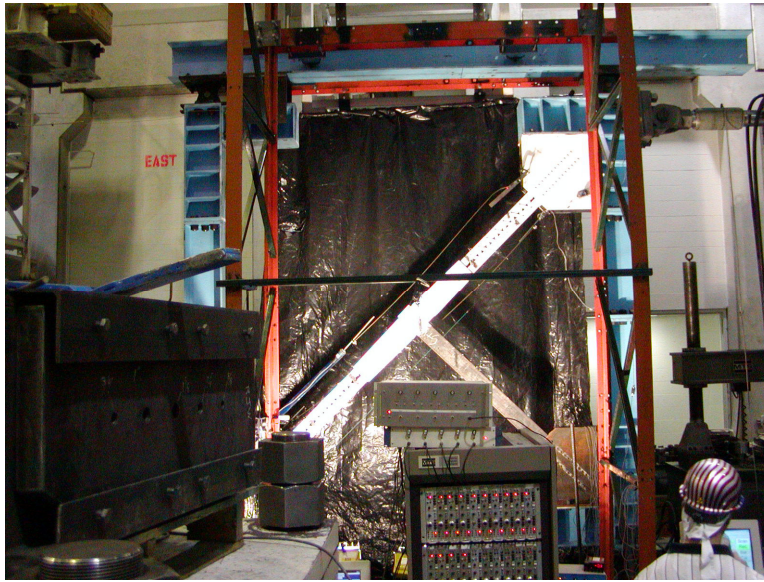


Figure 4.27 Test set-up for the By16-60 specimen

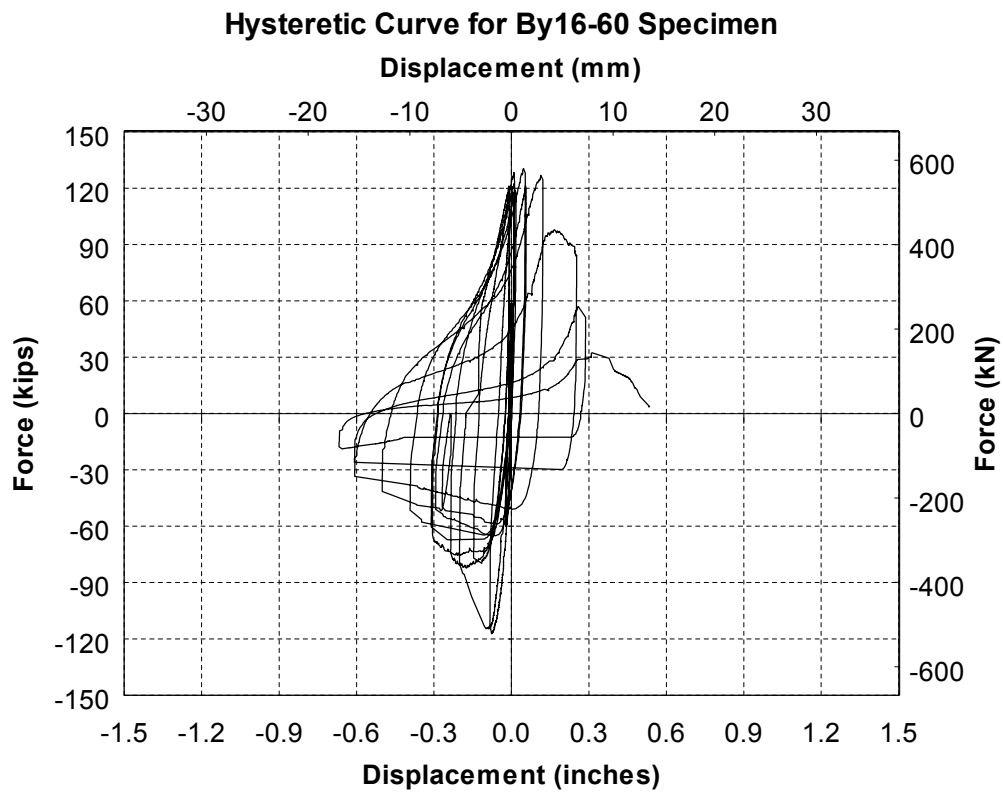
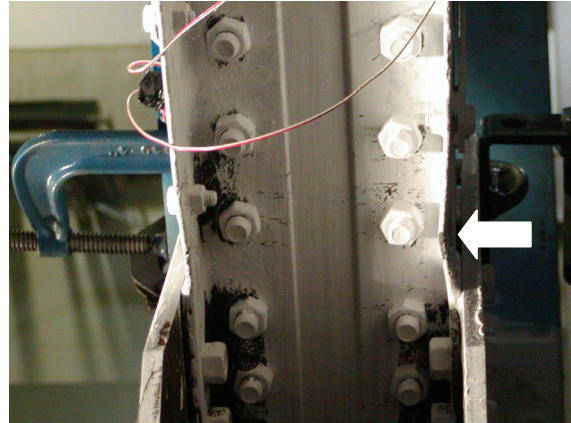


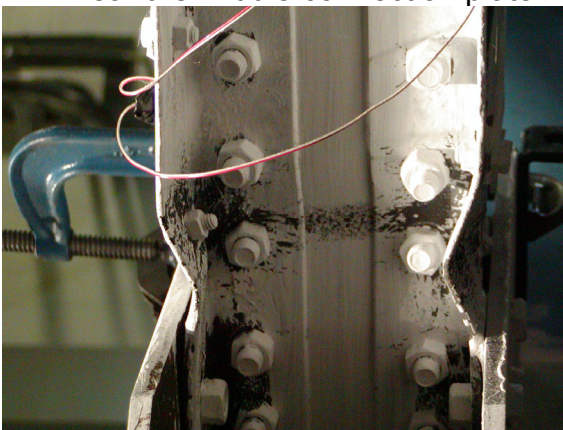
Figure 4.28 Hysteretic curve for the By16-60 specimen



(a) Local buckling at  $\delta=0.16''(4.1\text{mm})$  near the middle connection plate



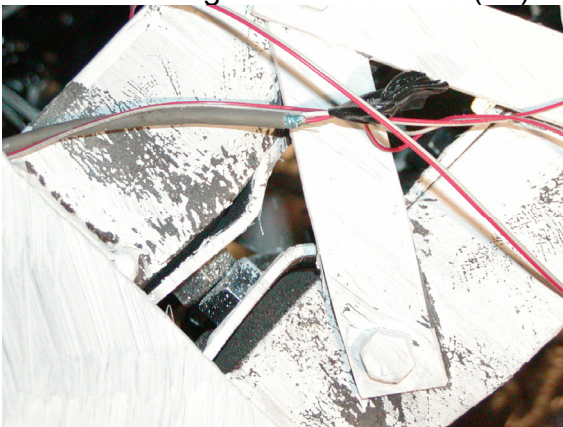
(b) Local buckling at  $\delta=0.16''(4.1\text{mm})$  near the gusset-connection (1<sup>st</sup>)



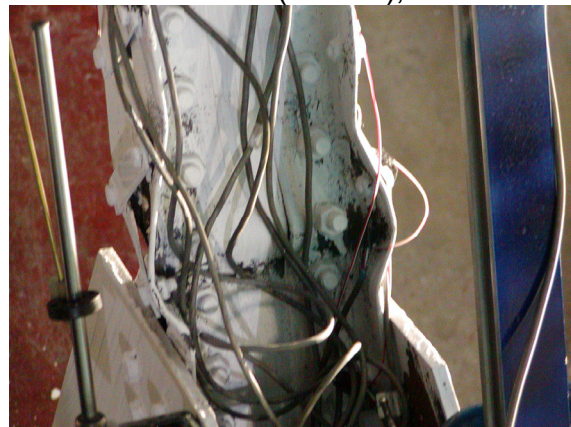
(c) Local buckling at  $\delta=0.16''(4.1\text{mm})$  near the gusset-connection (3<sup>rd</sup>)



(d) Local buckling on the plates at  $\delta=0.24''(6.1\text{mm})$ , 1<sup>st</sup>

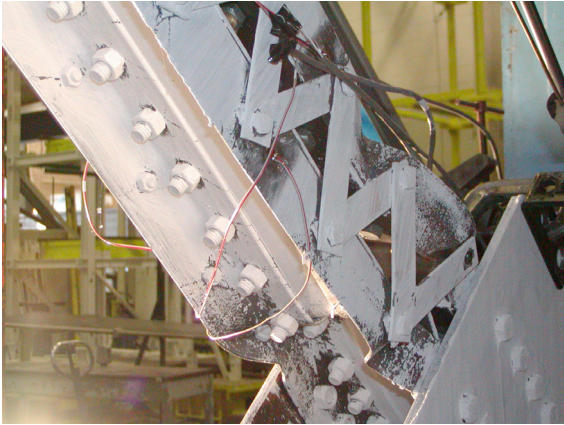


(e) Local buckling on the plates at  $\delta=0.24''(6.1\text{mm})$ , 2<sup>nd</sup>

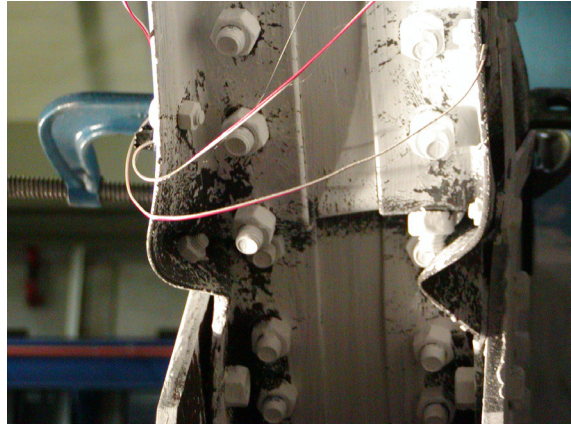


(f) Local buckling at  $\delta=0.24''(6.1\text{mm})$

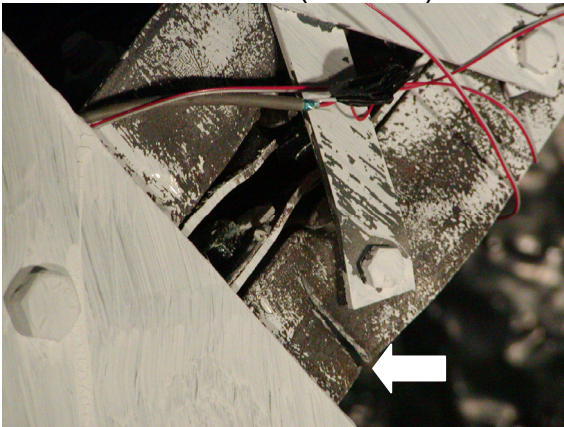
Figure 4.29 Observations made during testing of the By16-60 specimen



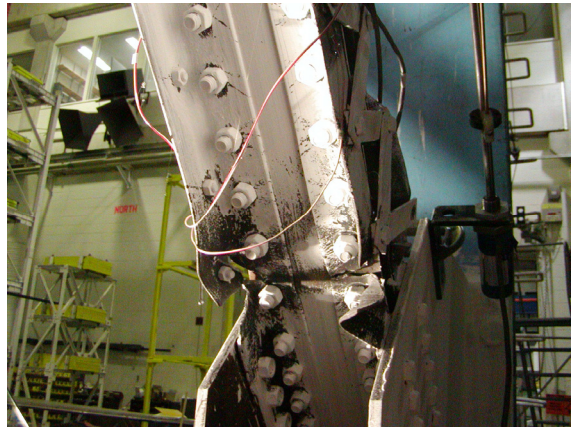
(g) Lacing bolt failure at  $\delta=0.4''$ (10.2mm)



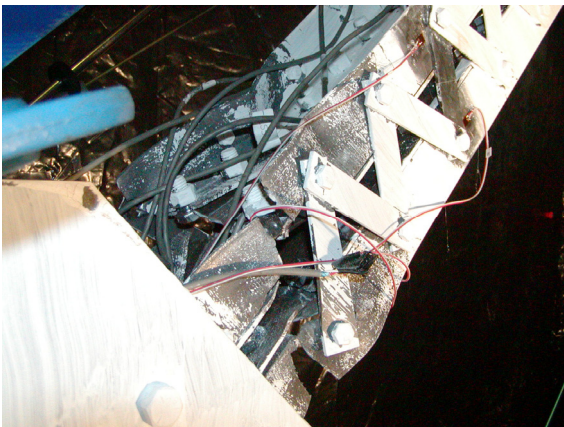
(h) Local buckling at  $\delta=0.4''$ (10.2mm)



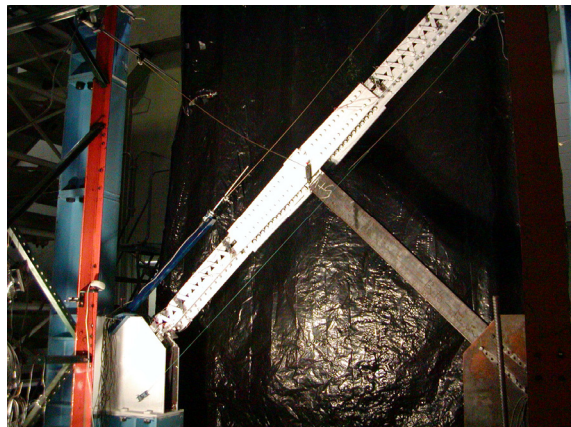
(i) Initial fracture at  $\delta=0.40''$ (10.2mm)



(j) Final fracture at  $\delta=0.48''$ (12.2mm)



(k) Final fracture at  $\delta=0.48''$ (12.2mm)



(l) Global fractured shape at  $\delta=0.48''$ (12.2mm)

Figure 4.29 Observations made during testing of the By16-60 specimen (continued)

the corresponding experimental buckling displacement,  $\delta_{b,exp} = 0.16''$  (4.1 mm) was identified. These local buckles became more severe during the following compressive loading cycles as shown in Figure 4.29c.

Three loading cycles at  $1.5 \delta_{b,exp}$  of the specimen were applied for better observations of local buckling. During the first compressive cycle at  $1.5 \delta_{b,exp} = 0.24''$  (6.1 mm), local buckling on the tie-plates near the gusset-connection in the North segment of the specimen was observed as shown in Figure 4.29d. During the second compressive cycle, local buckling on the plates was so severe that bolts on the adjacent deformed upper and lower tie-plates came in contact as shown in Figure 4.29e. During the third compressive cycle, local buckling on the upper angles near the gusset-connection in the North segment were also observed as shown in Figure 4.29f.

During the first compressive cycle at  $2.5 \delta_{b,exp} = 0.40''$  (10.2 mm), a lacing bolt failure and more severe local buckling were observed near the gusset-connection of the North segment of the specimen as shown in Figures 4.29g and 4.29h, respectively. Initial fracture was also observed on the lower angle near the gusset-connection during the first tensile cycle as shown in Figure 4.29i.

During the first tensile cycle at  $3.0 \delta_{b,exp} = 0.48''$  (12.2 mm), entire fracture was observed near the gusset-connection as shown in Figures 4.29j and 4.29k. Global view of the member deformations after the fracture is shown in Figure 4.29l.

#### **4.2.9 Specimen By16-120**

Test set-up and hysteretic curve obtained from test result for the By16-120 specimen are presented in Figures 4.30 and 4.31, respectively.

Because no evidence of buckling or yielding was observed after 9 cycles at the theoretical  $1/3$ ,  $2/3$ , and  $1.0 P_H = 60$  kips (2647.0 kN), a decision was made to seek the experimental buckling displacement by increasing small values of the control force, starting from  $P_H = 70.0$  kips (311.5 kN). During the first cycle at  $P_H = 70.0$  kips (311.5 kN), global buckling suddenly developed near the mid-length of the specimen as shown in Figure 4.32a. This resulted in a significant

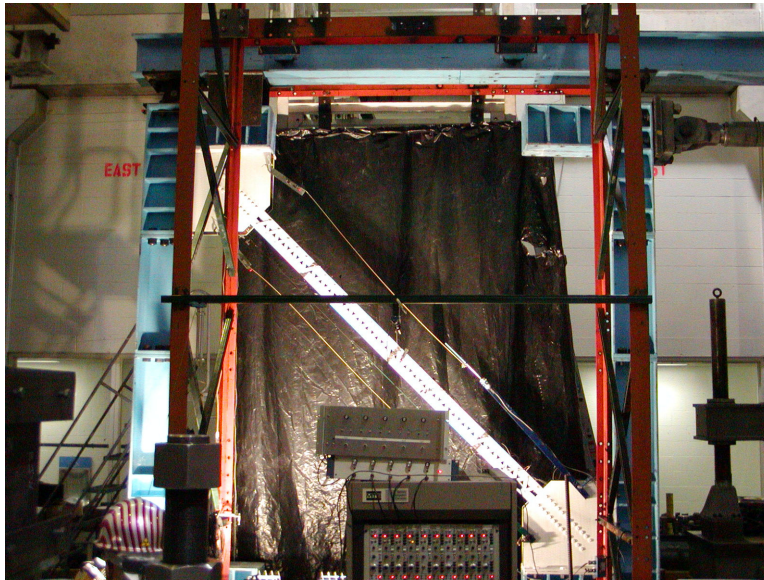


Figure 4.30 Test set-up for the By16-120 specimen

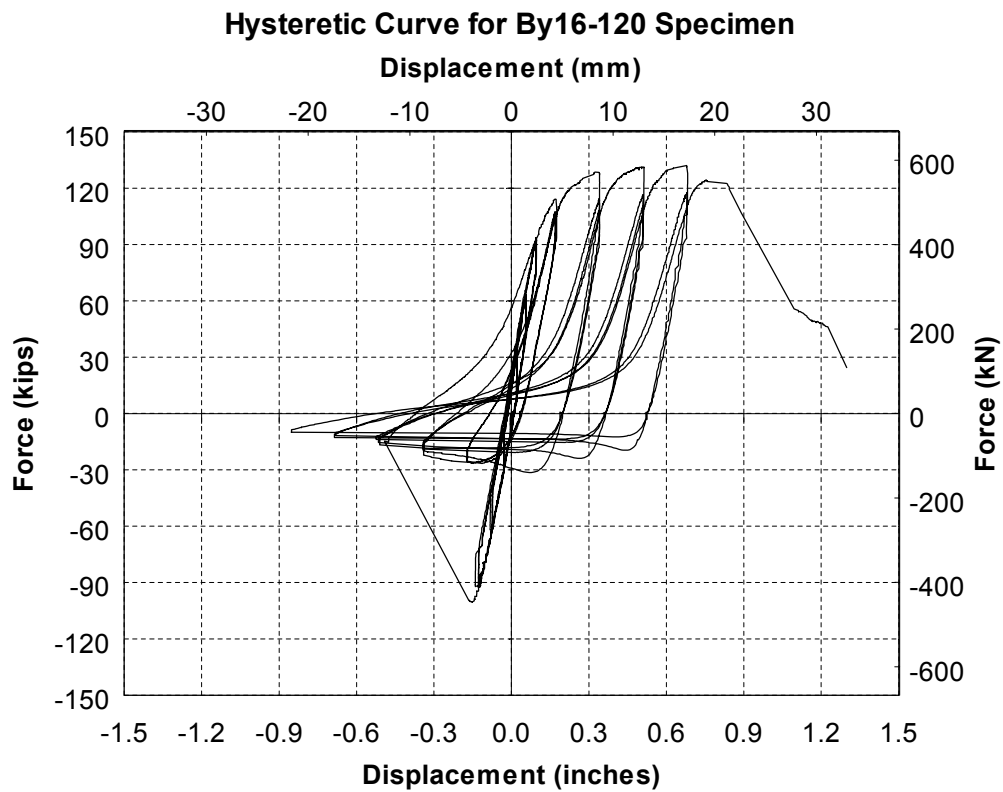
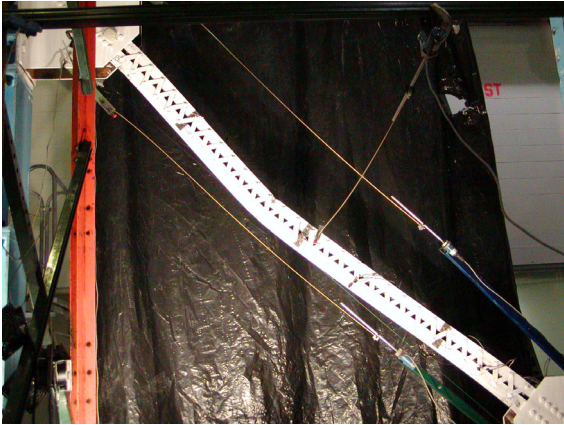


Figure 4.31 Hysteretic curve for the By16-120 specimen



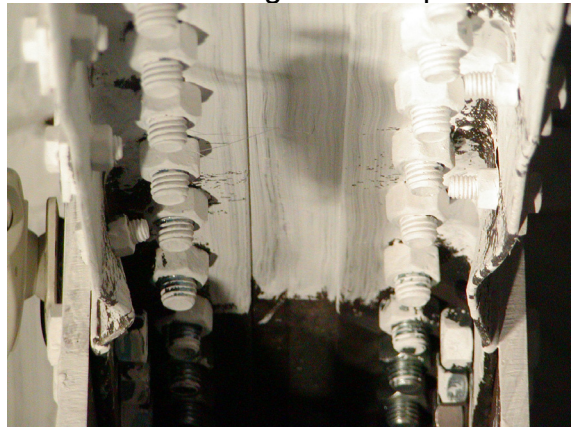
(a) Global buckling at  $\delta=0.17''$ (4.3mm)



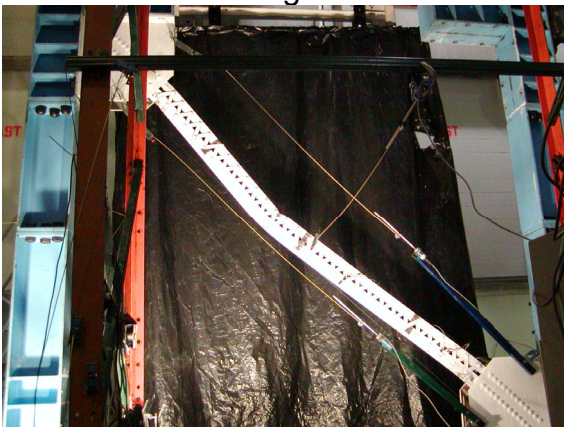
(b) Local buckling at  $\delta=0.17''$ (4.3mm) near the mid-length of the specimen



(c) Local buckling at  $\delta=0.17''$ (4.3mm) near the South gusset-connection



(d) Local buckling at  $\delta=0.17''$ (4.3mm) near the North gusset-connection

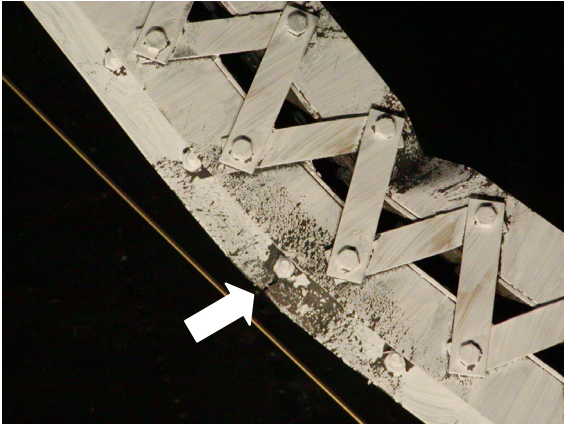


(e) Global buckling at  $\delta=0.34''$ (8.6mm)



(f) Local buckling at  $\delta=0.34''$ (8.6mm) near the mid-length of the specimen

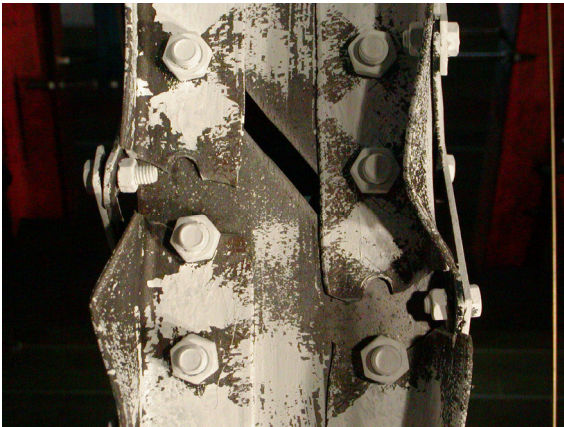
Figure 4.32 Observations made during testing of the By16-120 specimen



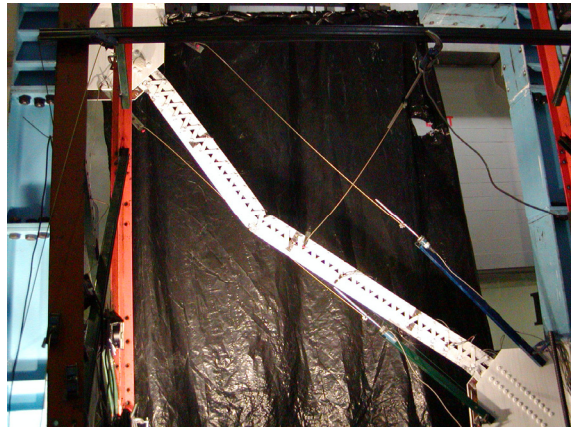
(g) Initial fracture at  $\delta=0.68''(17.3\text{mm})$



(h) Lacing buckling at  $\delta=0.68''(17.3\text{mm})$



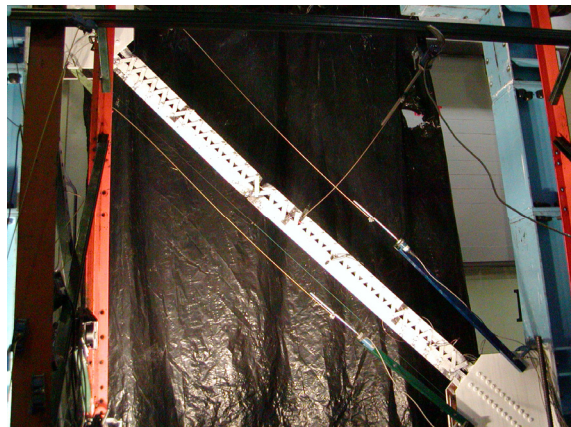
(i) Final fracture at  $\delta=0.86''(21.8\text{mm})$



(j) Global buckling at  $\delta=0.86''(21.8\text{mm})$



(k) Local buckling at  $\delta=0.86''(21.8\text{mm})$



(l) Global fractured shape at  $\delta=0.86''(21.8\text{mm})$

Figure 4.32 Observations made during testing of By16-120 specimen (continued)

overshoot beyond the control displacement that the controllers could not prevent. Local buckling was also observed at the global buckling location and near both the South and North gusset-connections as shown in Figures 4.32b to 4.32d and the experimental buckling displacement,  $\delta_{b,exp} = 0.17''$  (4.3 mm) was identified.

During the first compressive cycle at 2.0  $\delta_{b,exp} = 0.34''$  (8.6 mm), global and local buckling were getting more severe as shown in Figures 4.32e and 4.32f.

During the first compressive cycle at 4.0  $\delta_{b,exp} = 0.68''$  (17.3 mm), initial fracture on the lower angle at the mid-length of the specimen was observed as shown in Figure 4.32g. During the second compressive cycle, local buckling (on the bottom angle) and lacing buckling at the mid-length of the specimen were observed as shown in Figure 4.32h.

During the first tensile cycle at 6.0  $\delta_{b,exp} = 0.86''$  (21.8 mm), entire fracture of the lower angle at the mid-length of the specimen was observed as shown in Figure 4.32i. Figures 4.32j and 4.32k show the global and local buckling at the last compressive cycle and Figure 4.32l is showing the global deformed shape of the specimen after fracture in tension.

#### **4.2.10 Specimen Bx8-60**

Test set-up and hysteretic curve obtained from test result for the Bx8-60 specimen are presented in Figures 4.33 and 4.34, respectively.

During the first compressive cycle at 1.0  $P_H = 87.0$  kips (387.2 kN), global buckling in the South segment of the specimen was observed and the experimental buckling displacements,  $\delta_{b,exp} = 0.18''$  (4.6 mm) was identified.

Three loading cycles at 1.5  $\delta_{b,exp}$  of the specimen were applied for better observations of global and local buckling. During the first compressive cycle at 1.5  $\delta_{b,exp} = 0.27''$  (6.9 mm), global out-of-plane buckling was observed in the South segment as shown in Figure 4.35a. However, during the second compressive cycle, the out-of-plane buckling behavior permanently changed



Figure 4.33 Test set-up for the Bx8-60 specimen

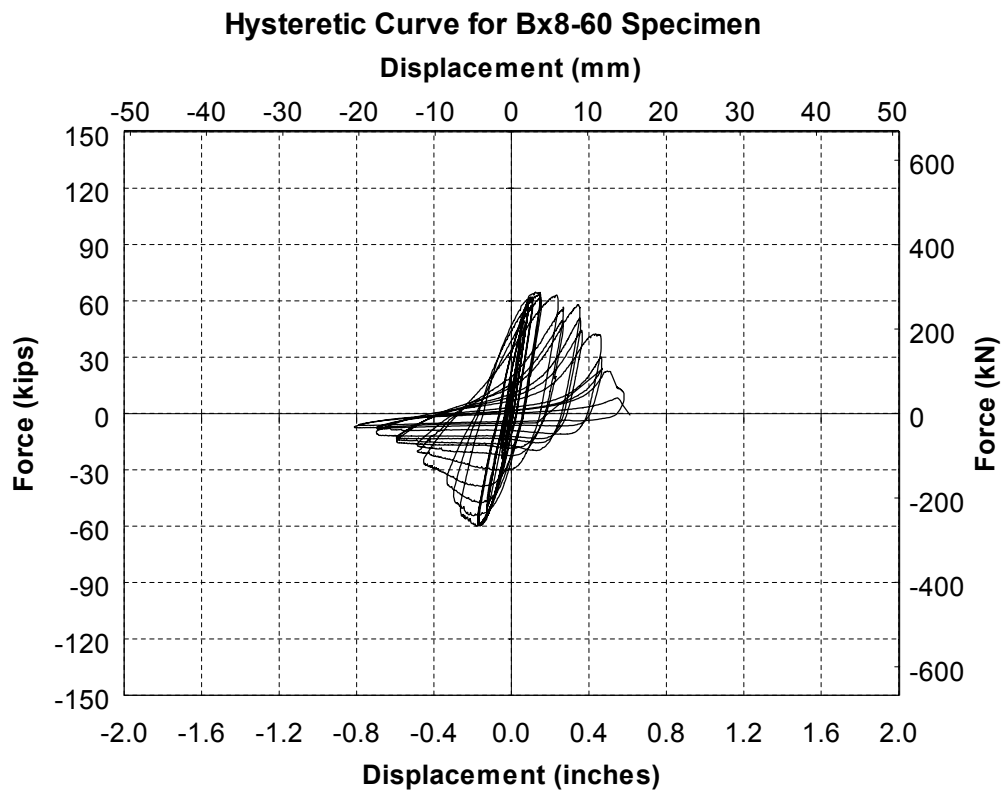
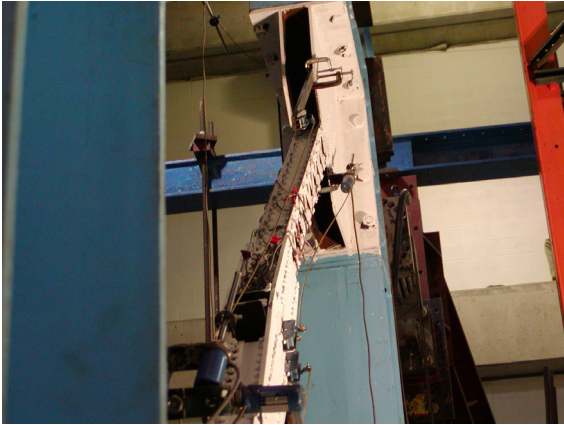


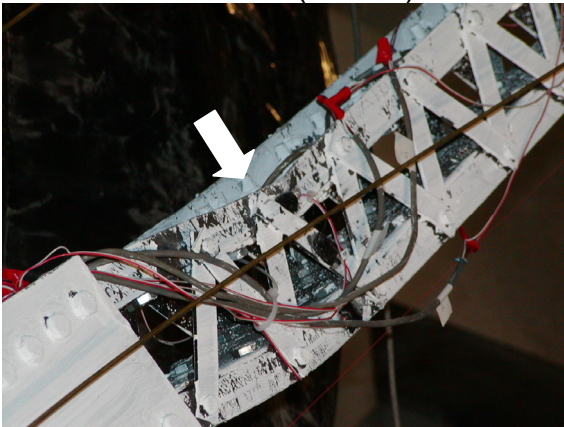
Figure 4.34 Hysteretic curve for the Bx8-60 specimen



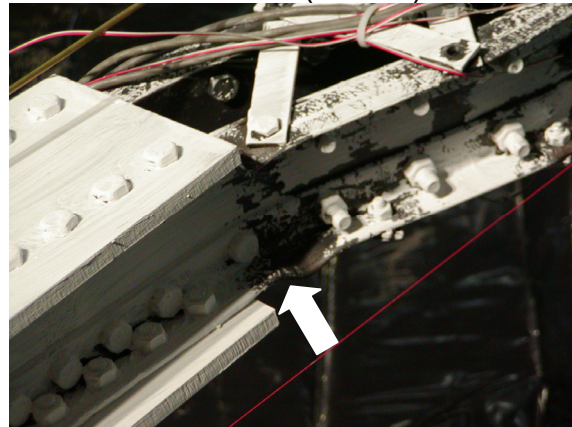
(a) Global out-of-plane buckling at  $\delta=0.27''$ (6.9mm)



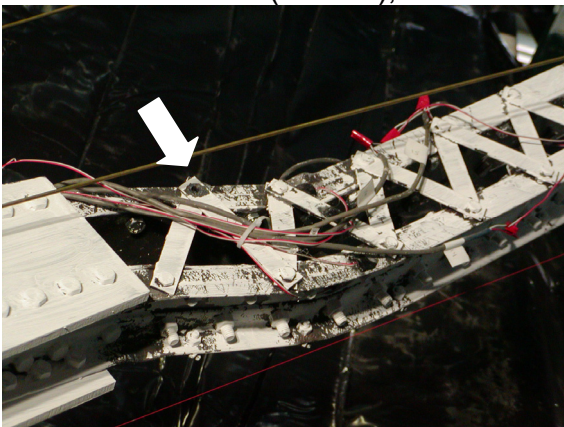
(b) Global in-plane buckling at  $\delta=0.27''$ (6.9mm)



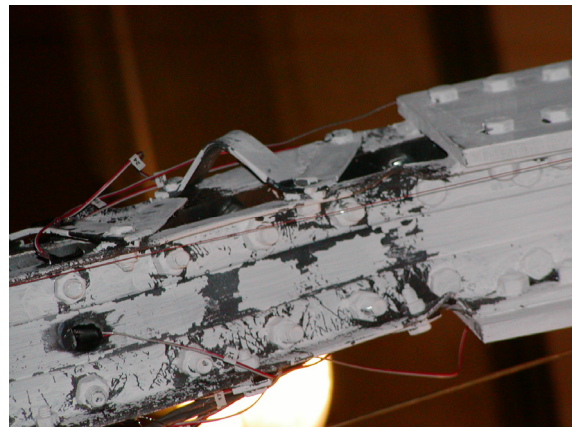
(c) Local buckling at  $\delta=0.27''$ (6.9mm), 3<sup>rd</sup>



(d) Local buckling at  $\delta=0.36''$ (9.1mm)



(e) Lacing bolt failure at  $\delta=0.36''$ (9.1mm)

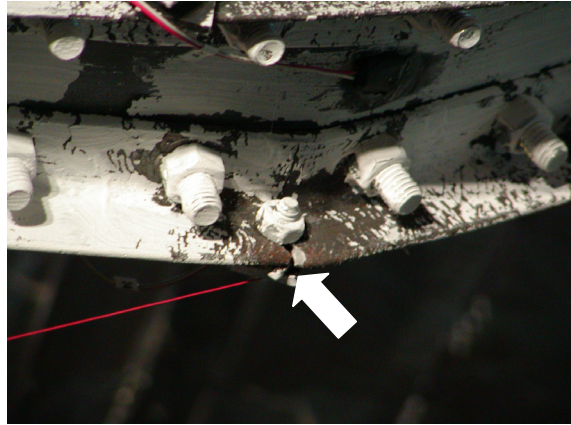


(f) Lacing buckling at  $\delta=0.36''$ (9.1mm)

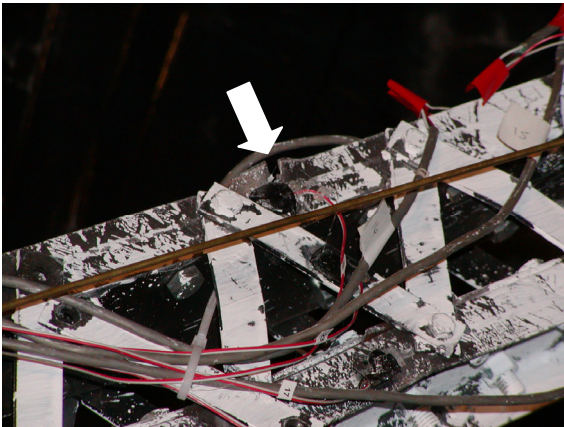
Figure 4.35 Observations made during testing of the Bx8-60 specimen



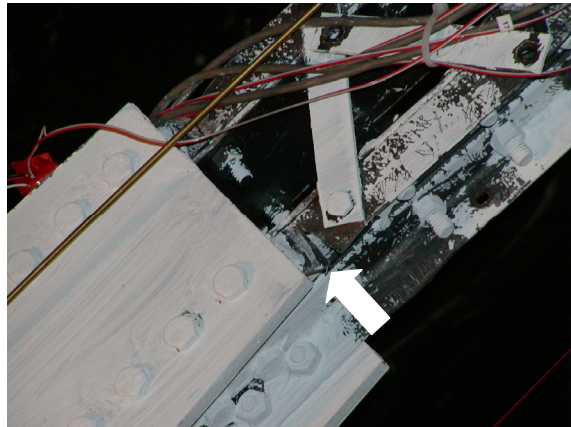
(g) Lacing buckling at  $\delta=0.45''$ (11.4mm)



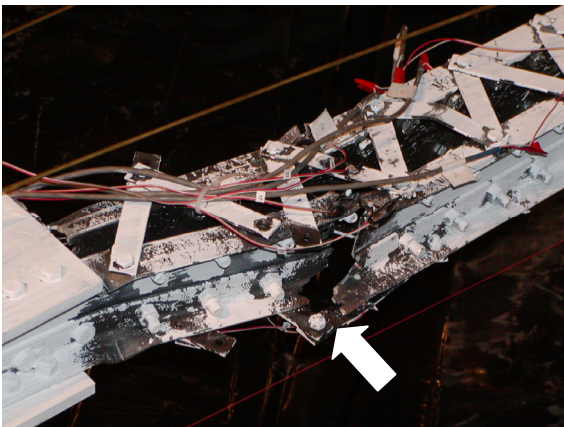
(h) Initial fracture at  $\delta=0.45''$ (11.4mm)



(i) Fracture at  $\delta=0.54''$ (13.7mm)



(j) Fracture at  $\delta=0.54''$ (13.7mm)



(k) Final fracture at  $\delta=1.63''$ (16.0mm)



(l) Global fractured shape at  $\delta=1.63''$ (16.0mm)

Figure 4.35 Observations made during testing of the Bx8-60 specimen (continued)

into an in-plane mode of buckling, as shown in Figure 4.35b. During the third compressive cycle, local buckling on the upper angles of the South segment of the specimen near the gusset-connection was also observed as shown in Figure 4.35c.

During the first compressive cycle at  $2.0 \delta_{b,exp} = 0.36''$  (9.1 mm), local buckling on the lower angles near the middle connection plate was observed as shown in Figure 4.35d. Lacing bolt failure was also observed near the gusset-connection of the South segment of the specimen as shown in Figure 4.35e. Lacing buckling was observed to start developing near the middle connection plate of the North segment in addition to the South segment of the specimen as shown in Figure 4.35f during the second compressive cycle.

During the first compressive cycle at  $2.5 \delta_{b,exp} = 0.45''$  (11.4 mm), lacing buckling was observed near the middle connection plate of the South segment as shown in Figure 4.35g. Initial fracture on the lower angle near the gusset-connection of the South segment of the specimen was observed during the first tensile cycle as shown in Figure 4.35h.

During the first tensile cycle at  $3.0 \delta_{b,exp} = 0.54''$  (13.7 mm), fractures on the both upper and lower angles near the middle connection plate of the South segment were observed as shown in Figures 4.35i and 4.35j, respectively.

During the second tensile cycle at  $3.5 \delta_{b,exp} = 0.63''$  (16.0 mm), entire fracture near the middle connection plate of the South segment of the specimen was observed as shown in Figure 4.35k. Figure 4.35l is showing global deformed shape of the specimen after fracture in tension.

#### **4.2.11 Specimen Bx8-120**

Test set-up and hysteretic curve obtained from test result for the Bx8-120 specimen are presented in Figures 4.36 and 4.37, respectively.

No evidence of buckling or yielding was observed after 9 cycles at the theoretical  $1/3 P_H$ ,  $2/3 P_H$ , and  $1.0 P_H$  (three cycles each), nor during three cycles at  $1 \frac{1}{3} P_H = 26$  kips (115.7 kN). A

decision was made to seek the experimental buckling displacement by subjecting the specimen to progressively increasing small values of the control displacement, starting from 0.12" (3.0 mm), which is corresponding to the  $1 \frac{1}{3} P_H = 26$  kips (115.7 kN). Initial global out-of-plane buckling was observed at the control displacement,  $\delta_b = 0.16$ " (4.1 mm) as shown in Figure 4.38a and the experimental buckling displacements,  $\delta_{b,exp} = 0.16$ " (4.1 mm) was identified.

Three cycles at  $1.5 \delta_{b,exp}$  instead of  $2.0 \delta_{b,exp}$  of the specimen were applied to allow better observations of buckling. During the three cycles at  $1.5 \delta_{b,exp} = 0.24$ " (6.1 mm), small frame column twisting was observed. Testing was stopped to fix the reaction frame by the addition of guidance shoes (clamped to the base foundation beam and top beam) at both ends of the specimen to prevent undesirable twisting of the reaction frame. Note that guidance shoe showed in Figure 4.38b is from the test set-up of specimen Bx16-60, but presented here for convenience. After installing guidance shoes, testing resumed and three more cycles at  $1.5 \delta_{b,exp} = 0.24$ " (6.1 mm) were applied to observe the effectiveness of these new devices on the test result. Both out-of-plane and in-plane buckling were observed during the first compressive cycle as shown in Figure 4.38c and lacing bolting failure was also observed near the North gusset-connection of the specimen as shown in Figure 4.38d. Local buckling on the lower angle near the global buckling location was observed during the third compressive cycle as shown in Figure 4.38e.

At the maximum displacements of the first compressive cycle at  $2.0 \delta_{b,exp} = 0.32$ " (8.1 mm), out-of-plane buckling behavior again permanently converted into in-plane buckling as shown in Figure 4.38f. During the first tensile cycle, a crack on the lower angle (local buckling point at  $1.5 \delta_{b,exp}$ ) was observed as shown in Figure 4.38g. During the third compressive cycle, another local buckle on the lower angles in the mid-length of the specimen was observed as shown in Figure 4.38h.

During the first compressive cycle at  $2.5 \delta_{b,exp} = 0.40$ " (10.2 mm), initial fracture on the upper angle (different from the initial crack observed during previous cycles at  $2.0 \delta_{b,exp}$ ) was observed at the mid-length of the specimen as shown in Figure 4.38i.



Figure 4.36 Test set-up for the Bx8-120 specimen

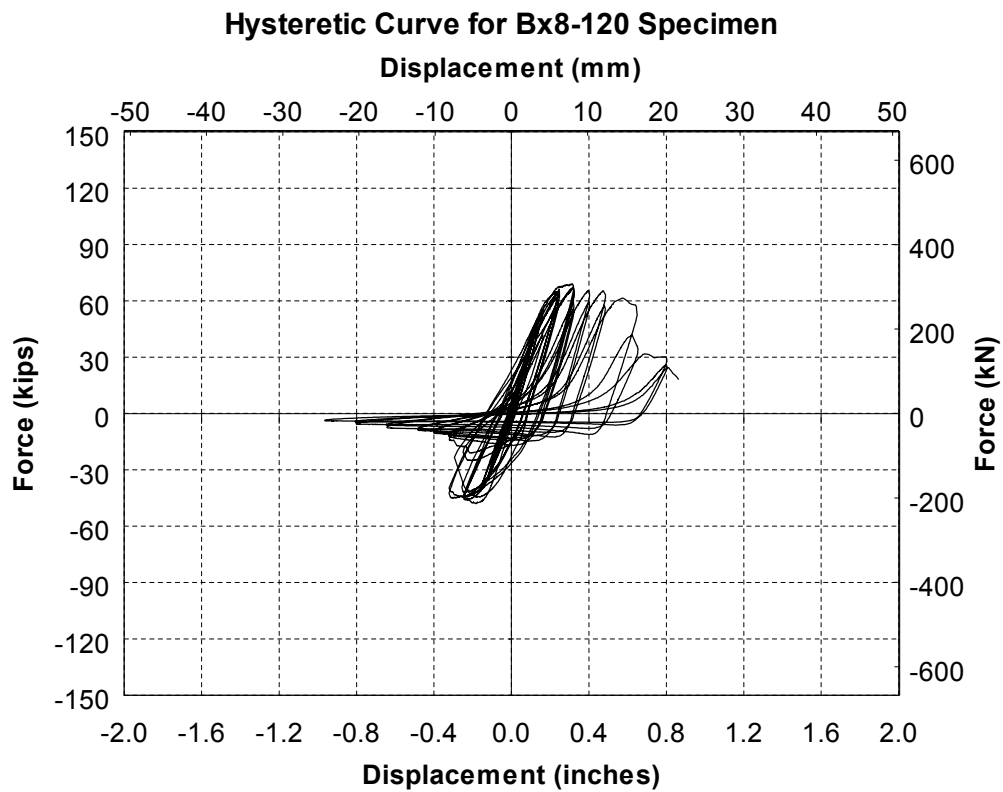
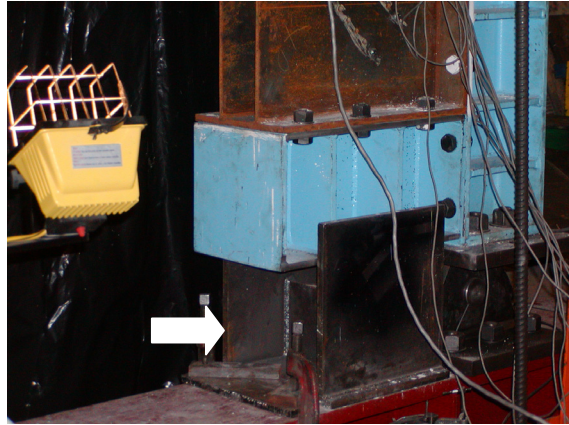


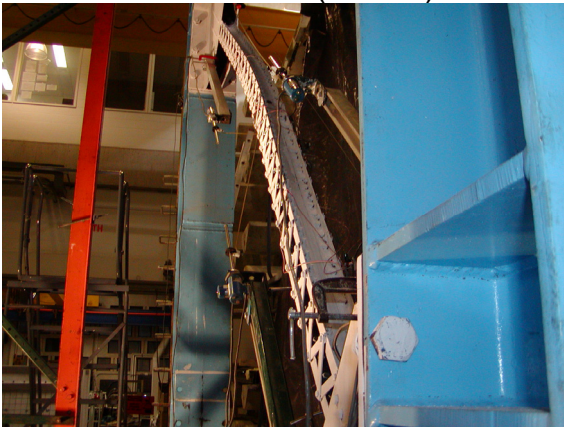
Figure 4.37 Hysteretic curve for the Bx8-120 specimen



(a) Global out-of-plane buckling at  $\delta=0.16''$  (4.1mm)



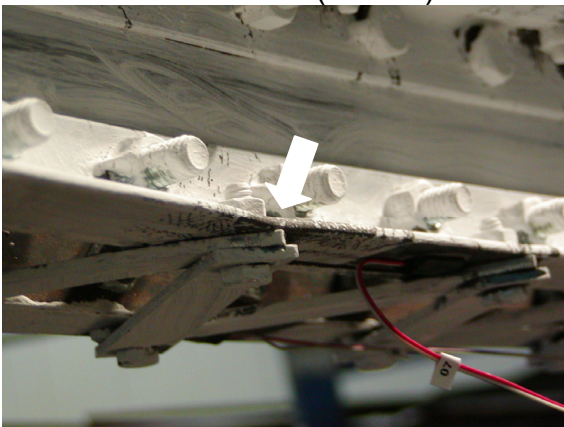
(b) Guidance shoe device



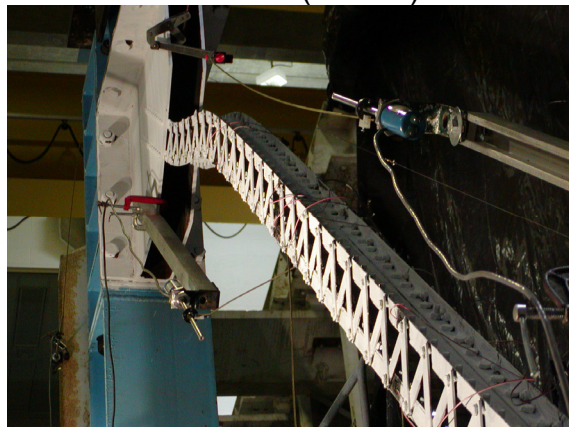
(c) Global out-of-plane buckling at  $\delta=0.24''$  (6.1mm)



(d) Lacing bolt failures at  $\delta=0.24''$  (6.1mm)

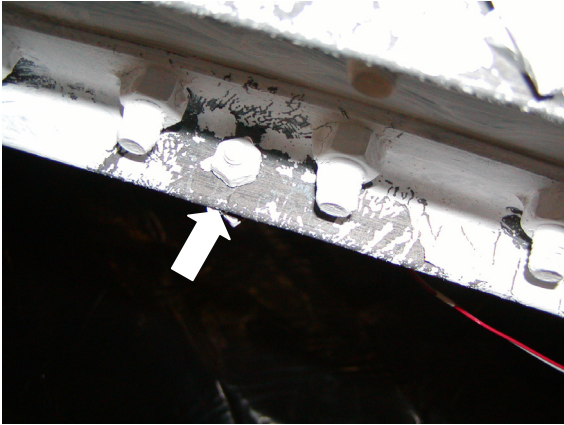


(e) Local buckling at  $\delta=0.24''$  (6.1mm)

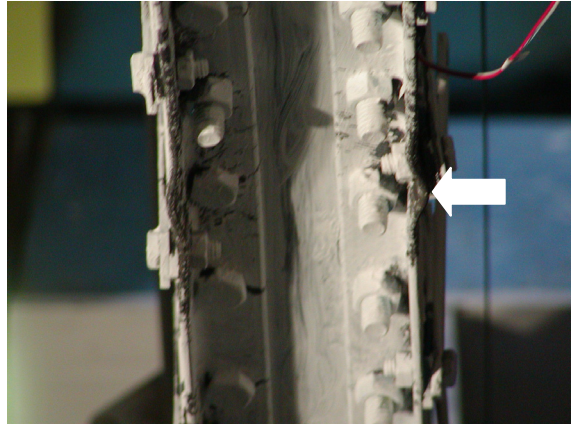


(f) Global out-of-plane buckling at  $\delta=0.32''$  (8.1mm)

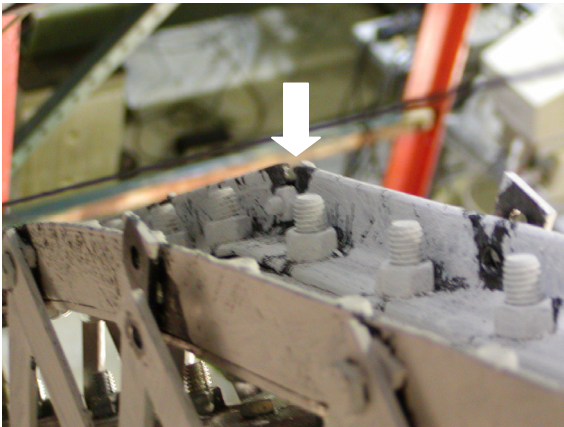
Figure 4.38 Observations made during testing of the Bx8-120 specimen



(g) Crack at  $\delta=0.32''(8.1\text{mm})$



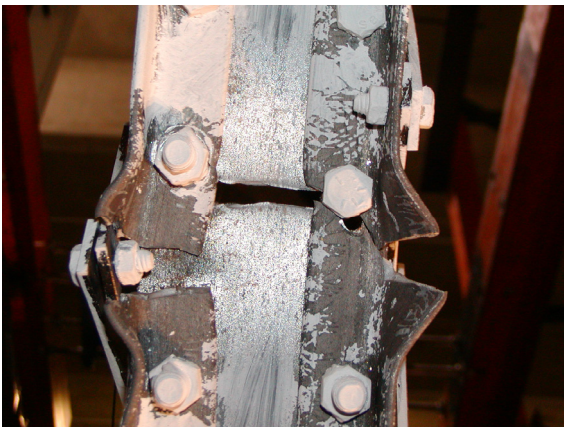
(h) Local buckling in the mid-length of the specimen at  $\delta=0.24''(6.1\text{mm})$



(i) Initial fracture at  $\delta=0.40''(10.2\text{mm})$



(j) Fracture at  $\delta=0.64''(16.3\text{mm})$



(k) Final fracture at  $\delta=0.96''(24.4\text{mm})$



(l) Global fractured shape at  $\delta=0.96''(24.4\text{mm})$

Figure 4.38 Observations made during testing of the Bx8-120 specimen (continued)

During the second tensile cycle at 4.0  $\delta_{b,exp} = 0.64''$  (16.3 mm), fracture on the upper plate at mid-length of the specimen was observed, simultaneously with a large drop in tension strength as shown in Figure 4.38j.

During the first tensile cycle at 5.0  $\delta_{b,exp} = 0.80''$  (20.3 mm), half of the gross section of the specimen fractured at the mid-length of the specimen.

During the first tensile cycle at 6.0  $\delta_{b,exp} = 0.96''$  (24.4 mm), entire fracture at mid-length of the specimen was observed as shown in Figure 4.38k. Figure 4.38l is showing global deformed shape of the specimen after fracture in tension.

#### **4.2.12 Specimen Bx16-60**

Test set-up and hysteretic curve obtained from test result for the Bx16-60 specimen are presented in Figures 4.39 and 4.40, respectively.

After the first compressive cycle at 1.0  $P_b = 66$  kips (293.7 kN), the force–displacement hysteretic curve that was monitored during the test showed some evidence of non-linear behavior. Local buckling was not clearly visible on the specimen, but subsequent test cycles indeed proved that local buckling developed at the experimental buckling displacements,  $\delta_{b,exp} = 0.20''$  (5.1 mm) corresponding to this load value.

During the first compressive cycle at 1.5  $\delta_{b,exp} = 0.30''$  (7.6 mm), visible local buckling on the lower angle of the North segment of the specimen near the gusset-connection was observed to initiate as early as displacements of 0.20'' (5.1 mm) as shown in Figure 4.41a. At the maximum displacement (0.30'' = 7.6 mm) at this compressive cycle, larger global out-of-plane buckling was observed in the South segment of the specimen as shown in Figure 4.41b. With this larger global out-of-plane buckling, several local buckling were observed: i) on the upper angles near the global buckling location (Figure 4.41b), ii) on the lower angles of the South segment near the middle connection plate (Figure 4.41c), iii) on the lower angle of the South segment near the

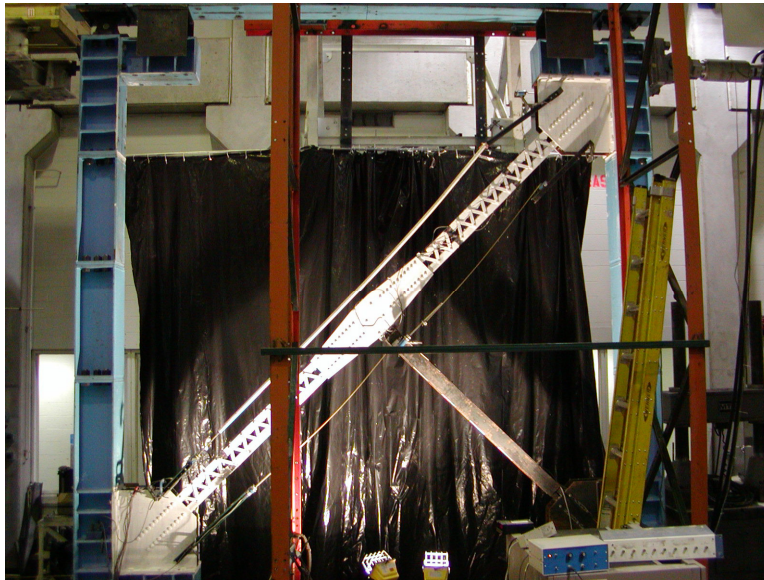


Figure 4.39 Test set-up for the Bx16-60 specimen

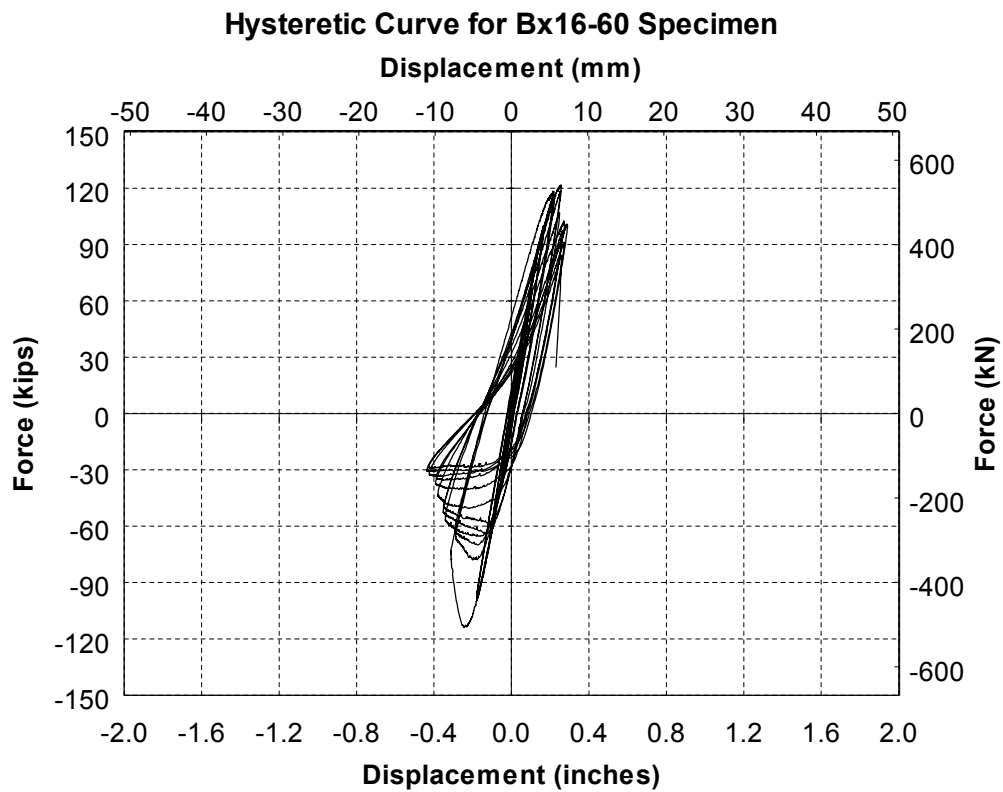
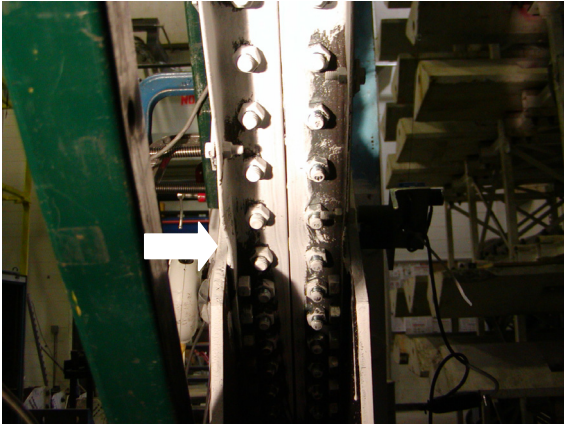
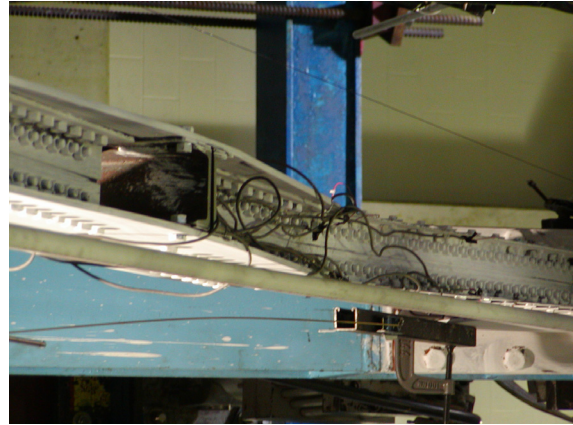


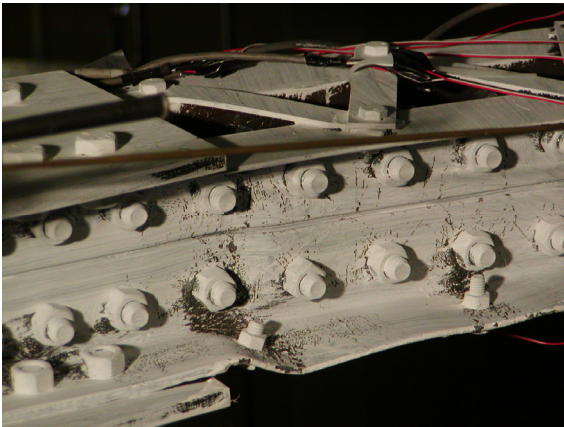
Figure 4.40 Hysteretic curve for the Bx16-60 specimen



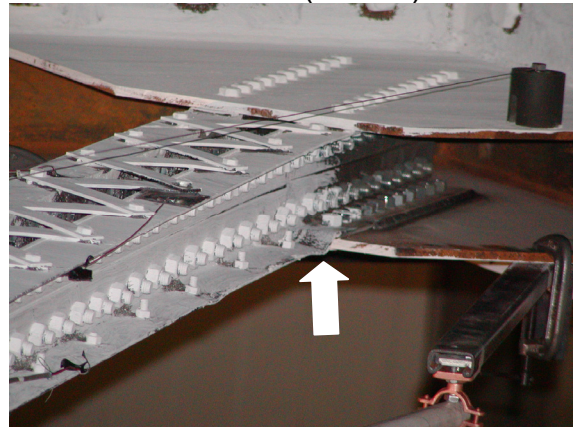
(a) Local buckling at  $\delta=0.20''$ (5.1mm)



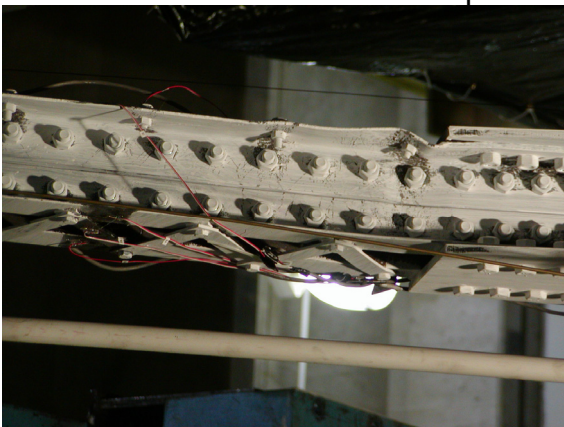
(b) Global out-of-plane and local buckling at  $\delta=0.30''$ (7.6mm)



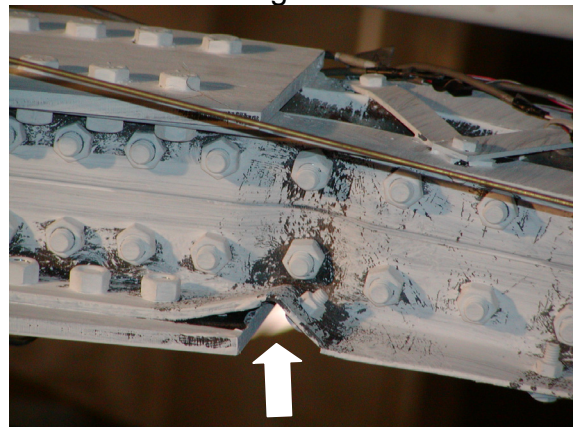
(c) Local buckling at  $\delta=0.30''$ (7.6mm) near the middle connection plate



(d) Local buckling at  $\delta=0.30''$ (7.6mm) near the South gusset-connection

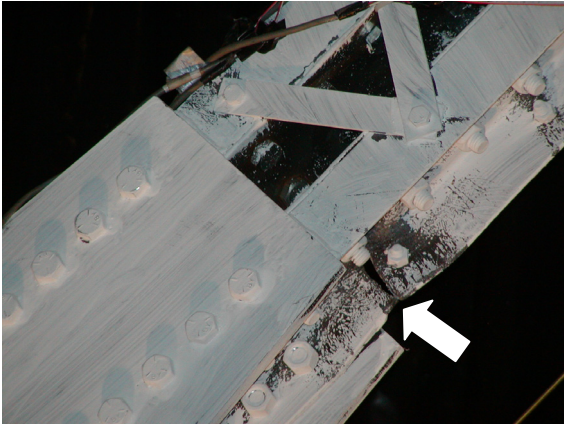


(e) Local buckling at  $\delta=0.30''$ (7.6mm) near the middle connection plate

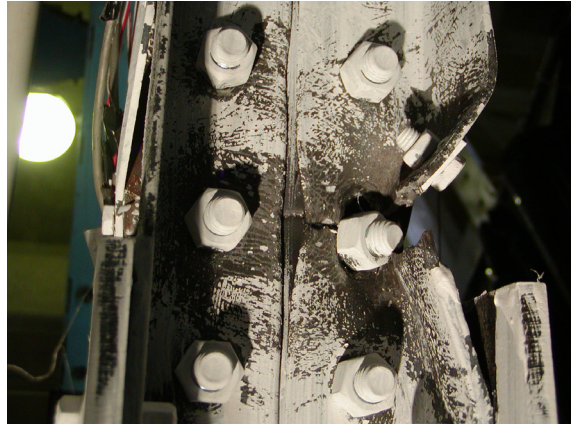


(f) Crack at  $\delta=0.40''$ (10.2mm)

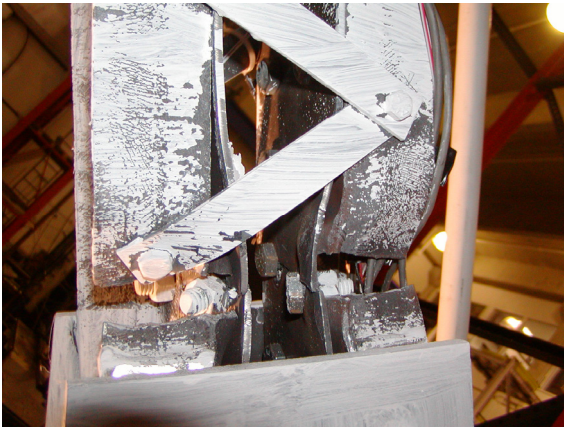
Figure 4.41 Observations made during testing of the Bx16-60 specimen



(g) Initial fracture at  $\delta=0.50''$ (12.7mm)



(h) Fracture at  $\delta=0.50''$ (12.7mm)



(i) Final fracture at  $\delta=0.60''$ (15.2mm)



(j) Global fractured shape at  $\delta=0.60''$ (15.2mm)

Figure 4.41 Observations made during testing of the Bx16-60 specimen (continued)

gusset-connection (Figure 4.41d), and iv) on the lower angles of the North segment of the specimen near the middle connection plate (Figure 4.41e).

During the first compressive cycle at  $2.0 \delta_{b,exp} = 0.40''$  (10.2 mm), a small crack on the lower angle of the South segment of the specimen near the middle connection plate was observed as shown in Figure 4.41f.

During the first tensile cycle at  $2.5 \delta_{b,exp} = 0.50''$  (12.7 mm), fracture on the lower angle of the South segment near the middle connection plate was observed as shown in Figure 4.41g and propagated significantly during the second and third tensile cycles as shown in Figure 4.41h.

During the third tensile cycle at  $3.0 \delta_{b,exp} = 0.60''$  (15.2 mm), entire fracture on the lower angle of the South segment of the specimen near the middle connection plate was observed as shown in Figure 4.41i. Figure 4.41j is showing global deformed shape of the specimen after fracture in tension.

#### **4.2.13 Specimen Bx16-120**

Test set-up and hysteretic curve obtained from test result for the Bx16-120 specimen are presented in Figures 4.42 and 4.43, respectively.

No evidence of buckling or yielding was observed after 9 cycles at the theoretical  $1/3 P_H$ ,  $2/3 P_H$ , and  $1.0 P_H = 54$  kips (240.3 kN). A decision was made to seek the experimental buckling displacement by increasing the control force, starting from  $1 \frac{1}{3} P_b = 72$  kips (320.4 kN). During the second compressive cycle at  $1 \frac{1}{3} P_b$ , local buckling on the lower angle near the South gusset-connection was observed as shown in Figure 4.44a. Again, buckling was somewhat sudden, resulting in an overshoot of the target displacement. Small but visible global out-of-plane buckling was also observed, although not shown in figure and corresponding experimental buckling displacements,  $\delta_{b,exp} = 0.28''$  (7.1 mm) was identified.

Three cycles at  $1.5 \delta_{b,exp}$  in tension and  $2.0 \delta_{b,exp}$  in compression of the specimen (i.e.,

unsymmetrical control displacements) were applied to prevent unexpected fracture during the following tensile cycle before significant buckling could be observed in compression.

During the first compressive cycle at  $2.0 \delta_{b,exp} = 0.56$  (14.2 mm), local buckling on the upper angle near the South gusset-connection was observed at  $\delta_b = 0.28''$  (7.1 mm) as shown in Figure 4.44b and larger global in-plane buckling was observed at  $\delta_b = 0.56''$  (14.2 mm) as shown in Figure 4.44c. Note that specimen buckled out-of-plane before behavior changed permanently to in-plane buckling. Local buckling on the lower angles and plate were also observed at the global buckling location during this cycle as shown in Figures 4.44d and 4.44e. During the second compressive cycle, buckling on lacings near global buckling location were observed as shown in Figure 4.44f. During the third compressive cycle, specimen strength decreased partly due to the smaller moment of inertia that developed as a consequence of lacing buckling.

During the first compressive cycle at  $3.0 \delta_{b,exp} = 0.84$  (21.3 mm), local buckling was observed on the upper angle at the 1/4 of specimen length from the North end as shown in Figure 4.44g. Due to large residual compressive deformation from the previous compressive cycle, during the first tensile cycle, local buckling was observed at the global buckling location as shown in Figure 4.44h.

During the second tensile cycle at  $4.0 \delta_{b,exp} = 1.12$  (28.4 mm), initial fracture on the lower angle at the global buckling location was observed as shown in Figure 4.44i.

During the first compressive cycle at  $5.0 \delta_{b,exp} = 1.40$  (35.6 mm), fracture on the upper angles at the global buckling point was observed as shown in Figure 4.44j. During first tensile cycle, entire fracture was observed as shown in Figure 4.44k. Figure 4.44l is showing global deformed shape of the specimen after fracture in tension.



Figure 4.42 Test set-up for the Bx16-120 specimen

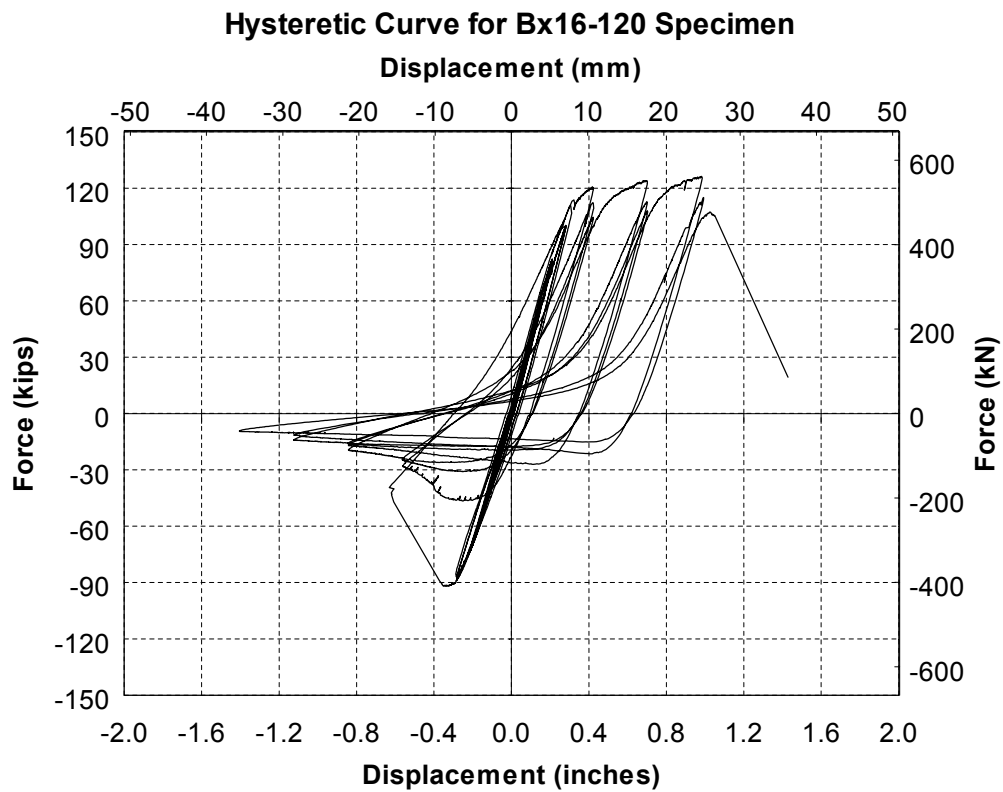
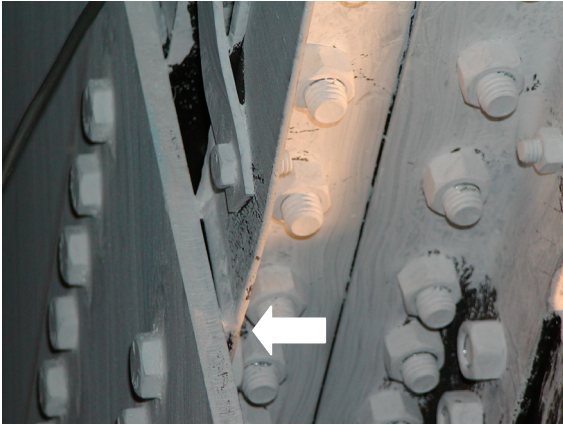
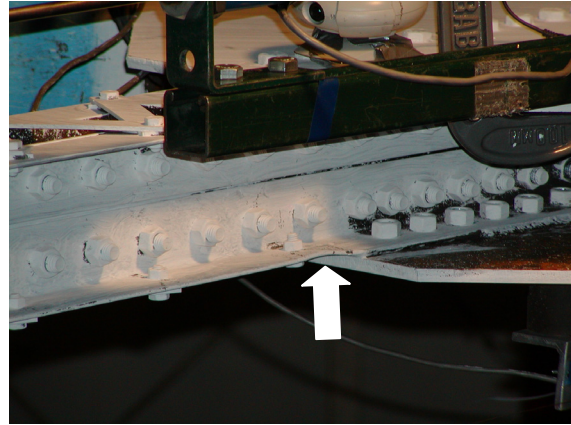


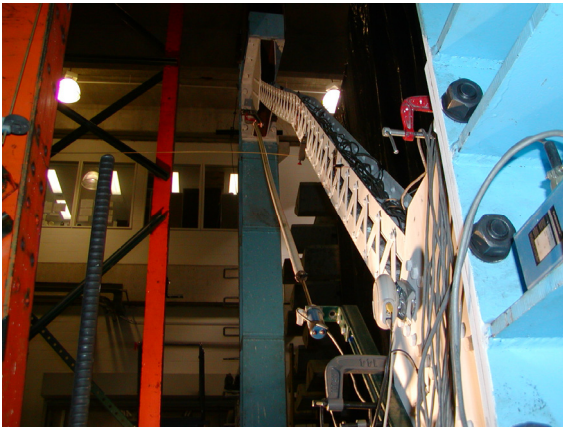
Figure 4.43 Hysteretic curve for the Bx16-120 specimen



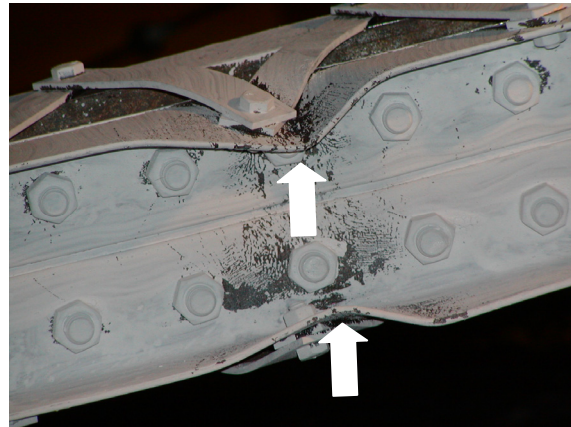
(a) Local buckling at  $\delta=0.28''$ (7.1mm)



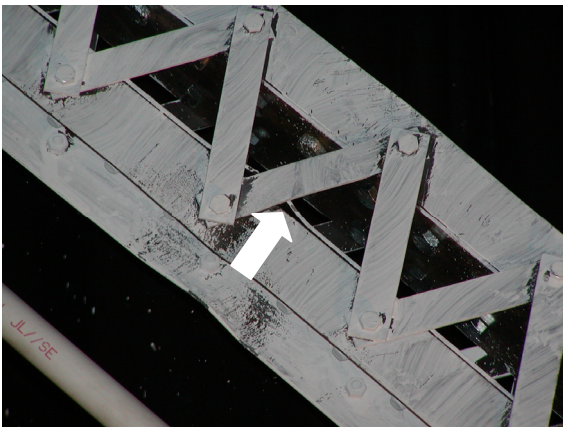
(b) Local buckling at  $\delta=0.28''$ (7.1mm)



(c) Global buckling at  $\delta=0.56''$ (14.2mm)



(d) Local buckling at  $\delta=0.56''$ (14.2mm) near the mid-length of the specimen

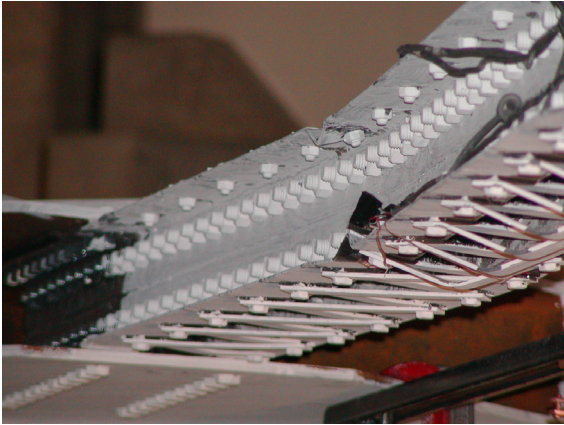


(e) Local buckling at  $\delta=0.56''$ (14.2mm) near the mid-length of the specimen



(f) Lacing buckling at  $\delta=0.56''$ (14.2mm)

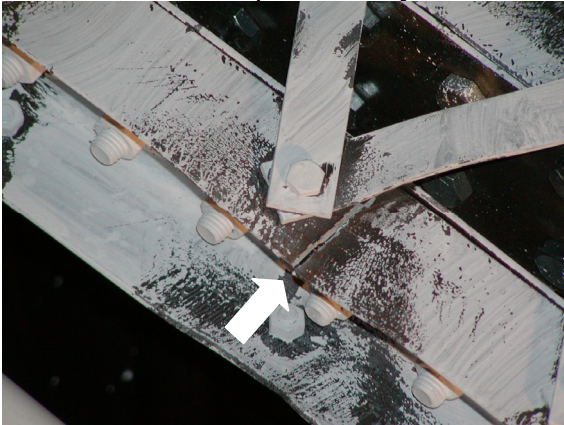
Figure 4.44 Observations made during testing of the Bx16-120 specimen



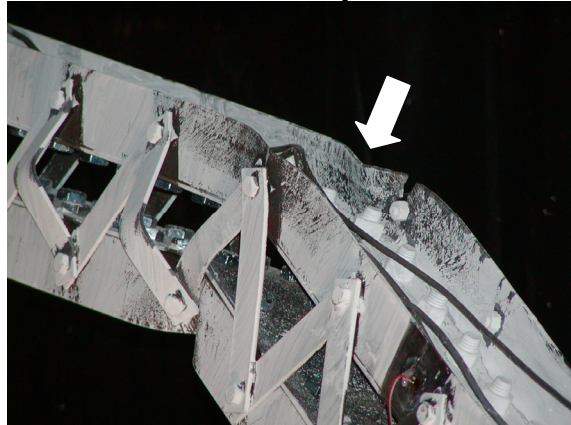
(g) Local buckling at  $\delta=0.84''$ (21.3mm)  
1<sup>st</sup> compressive cycle



(h) Local buckling at  $\delta=0.84''$ (21.3mm)  
1<sup>st</sup> tensile cycle



(i) Initial fracture at  $\delta=1.12''$ (28.4mm)  
2<sup>nd</sup> tensile cycle



(j) Fracture at  $\delta=1.40''$ (35.6mm)  
1<sup>st</sup> compressive cycle



(k) Final fracture at  $\delta=1.40''$ (35.6mm)



(l) Global fractured shape  
at  $\delta=1.40''$ (35.6mm)

Figure 4.44 Observations made during testing of the Bx16-120 specimen (continued)

## SECTION 5

### ANALYSIS OF RESULTS – HYSTERETIC BEHAVIOR

In this section, the tensile and compressive strength and hysteretic behaviors of the test results obtained from the twelve tested specimens are discussed. The tensile and compressive strengths of the specimens are compared with those predicted by the AISC LRFD Specification (AISC, 1999). Hysteretic axial force–displacement curves are reviewed in various normalized manners to observe the hysteretic behaviors of specimens obtained during the testing. Non-linear analyses are conducted and correlated with test results.

#### 5.1 Data Analyses of Test Results

##### 5.1.1 Tension Strength

Design strength of tension members is specified by the AISC LRFD Specification (AISC, 1999) as the lesser of either yielding of the gross section or fracture of the net section.

For yielding in the gross section, axial strength,  $P_n$ , is given by:

$$P_n = F_y A_g \quad (5.1 \text{ a})$$

where  $F_y$  is the specified yield stress and  $A_g$  is the gross section area.

For fracture in the net section,

$$P_n = F_u A_e \quad (5.1 \text{ b})$$

where  $F_u$  is the specified tensile strength for the type of steel used and  $A_e$  is the effective net section area specified as:

$$A_e = A_n U \quad (5.2)$$

where  $A_n$  is the net area and  $U$  is a reduction coefficient specified as:

$$U = 1 - (\bar{x}/L) \leq 0.9 \quad (5.3)$$

where  $\bar{x}$  is the connection eccentricity defined as the distance from the connection plane or face of the member to the centroid of the member section resisting the connection force, and  $L$  is the length of connection in the direction of loading. Note that in the case of staggered bolt patterns, calculation of net area,  $A_n$  is given by:

$$A_n = \sum \left[ t \left( w_n + \frac{s^2}{4g} \right) \right] \quad (5.4)$$

where  $t$  is the thickness of the each element,  $w_n$  is the effective width of the each element,  $s$  is the longitudinal center-to-center spacing (pitch) of any two consecutive holes and  $g$  is the transverse center-to-center spacing (gage) between gage lines.

Following AISC LRFD design specification per the above equations, tensile strength of each specimen was calculated. Cross sectional properties of the specimens are summarized in Table 5.1. Calculated tensile strengths using coupon yield and ultimate strengths (Table 3.4) for each specimen (instead of the specified values) are compared with results obtained from testing in Table 5.2 and graphically compared in Figure 5.1. Tensile strength of specimens with section shape “B” is limited by the net section fracture, (Eq. 5.1b), due to their relatively large number of bolt holes, while specimens with section shape “A” were able to develop gross section yielding, (Eq. 5.1a). As shown in Figure 5.1 and Table 5.2, ratios of test result to the predicted strength are 0.9 or greater, except for the Ay8-60 and Ay16-120 specimens. Note that the Ay8-60 specimen was not tested to its maximum tensile strength; recall that testing was stopped to prevent damage on the other diagonal specimen, Ay8-120, as described in SECTION 4.

Table 5.1 Cross sectional properties of the specimens

Specimen	Angles					Plates				Total			
	B In (mm)	t in (mm)	A <sub>g</sub> in <sup>2</sup> (mm <sup>2</sup> )	A <sub>n1</sub> <sup>*1</sup> in <sup>2</sup> (mm <sup>2</sup> )	A <sub>n2</sub> <sup>*1</sup> in <sup>2</sup> (mm <sup>2</sup> )	t in (mm)	D In (mm)	A <sub>g</sub> in <sup>2</sup> (mm <sup>2</sup> )	A <sub>n</sub> in <sup>2</sup> (mm <sup>2</sup> )	B In (mm)	D In (mm)	A <sub>g</sub> in <sup>2</sup> (mm <sup>2</sup> )	A <sub>n</sub> in <sup>2</sup> (mm <sup>2</sup> )
Ay8	1.5 (38.1)	0.19 (4.8)	0.53 (340.0)	0.47 (302.2)	0.47 (302.2)	0.00	0.00	0.00	0.00	3.38 (85.7)	6.50 (165.1)	2.11 (1360.0)	1.87 (1208.8)
Ay16	2.0 (50.8)	0.13 (3.2)	0.48 (312.3)	0.44 (287.1)	0.44 (287.1)	0.00	0.00	0.00	0.00	4.25 (108.0)	5.50 (139.7)	1.94 (1249.0)	1.78 (1148.2)
By8	1.0 (25.4)	0.13 (3.2)	0.23 (151.0)	0.18 (118.3)	0.20 (129.0)	0.13 (3.2)	4.75 (120.7)	0.59 (383.1)	0.50 (322.6)	4.75 (120.7)	4.75 (120.7)	2.12 (1370.0)	1.77 (1139.7)
By16	2.0 (50.8)	0.13 (3.2)	0.48 (312.3)	0.39 (253.4)	0.40 (258.1)	0.13 (3.2)	5.25 (133.4)	0.66 (423.4)	0.53 (342.7)	5.25 (133.4)	5.25 (133.4)	3.25 (2095.8)	2.65 (1708.5)
Bx8	1.0 (25.4)	0.13 (3.2)	0.23 (151.0)	0.19 (120.7)	0.19 (120.7)	0.13 (3.2)	3.00 (76.2)	0.38 (241.9)	0.28 (181.5)	4.50 (114.3)	3.00 (76.2)	1.69 (1087.7)	1.31 (845.8)
Bx16	2.0 (50.8)	0.13 (3.2)	0.48 (312.3)	0.39 (254.5)	0.43 (277.6)	0.13 (3.2)	4.13 (104.8)	0.52 (332.7)	0.39 (252.0)	6.50 (165.1)	4.13 (104.8)	2.97 (1914.4)	2.43 (1568.1)

\*1 A<sub>n</sub> was determined considering staggered hole effects, as defined in Eq. (5.4)

Table 5.1 Cross sectional properties of the specimens (continue)

Specimen	Total									
	B In (mm)	D In (mm)	A <sub>g</sub> in <sup>2</sup> (mm <sup>2</sup> )	I <sub>x</sub> in <sup>4</sup> (mm <sup>4</sup> )	I <sub>y</sub> in <sup>4</sup> (mm <sup>4</sup> )	r <sub>x</sub> in (mm)	r <sub>y</sub> in (mm)	Z <sub>x</sub> in <sup>3</sup> (mm <sup>3</sup> )	Z <sub>y</sub> in <sup>3</sup> (mm <sup>3</sup> )	
Ay8	3.375 (85.7)	6.500 (165.1)	2.108 (1360.0)	17.038 (7091594.8)	1.281 (533048.5)	2.843 (72.2)	0.779 (19.8)	5.993 (98206.7)	1.643 (26924.8)	
Ay16	4.250 (108.0)	5.500 (139.7)	1.936 (1249.0)	10.164 (4230719.6)	1.632 (679150.9)	2.291 (58.2)	0.918 (23.3)	4.436 (72693.2)	1.777 (29125.2)	
By8	4.750 (120.7)	4.750 (120.7)	2.124 (1370.0)	6.366 (2649881.2)	4.749 (1976574.0)	1.731 (44.0)	1.495 (38.0)	3.677 (60252.2)	3.176 (52037.5)	
By16	5.250 (133.4)	5.250 (133.4)	3.249 (2095.8)	12.143 (5054093.0)	3.832 (1594880.1)	1.933 (49.1)	1.086 (27.6)	6.281 (102919.3)	3.528 (57814.8)	
Bx8	4.500 (114.3)	3.000 (76.2)	1.686 (1087.7)	2.007 (835518.2)	3.384 (1408419.9)	1.091 (27.7)	1.417 (36.0)	1.840 (30146.7)	2.389 (39140.7)	
Bx16	6.500 (165.1)	4.125 (104.8)	2.967 (1914.4)	6.675 (2778194.7)	8.460 (3521467.3)	1.500 (38.1)	1.689 (42.9)	4.450 (72927.6)	5.010 (82105.6)	

Table 5.2 Tensile strength comparison

Specimen	$P_n$ , kips (kN)				Test Results
	Yield	Ratio <sup>*1</sup>	Fracture	Ratio <sup>*1</sup>	
Ay8-60 <sup>*2</sup>	107.04 (476.3)	0.77	114.67 (510.3)	0.72	82.41 (366.7)
Ay8-120	107.04 (476.3)	0.94	114.67 (510.3)	0.87	100.17 (445.7)
Ay16-60	98.81 (439.7)	0.97	103.17 (459.1)	0.93	95.83 (426.4)
Ay16-120	98.81 (439.7)	0.87	103.17 (459.1)	0.84	86.26 (383.9)
By8-60	104.67 (465.8)	0.80	92.25 (410.5)	0.91	83.85 (373.1)
By8-120	104.67 (465.8)	0.87	92.25 (410.5)	0.99	90.92 (404.6)
By16-60	160.25 (713.1)	0.81	142.22 (632.9)	0.92	130.43 (580.4)
By16-120	160.25 (713.1)	0.82	142.22 (632.9)	0.93	132.09 (587.8)
Bx8-60	84.19 (374.7)	0.77	70.47 (313.6)	0.92	64.61 (287.5)
Bx8-120	84.19 (374.7)	0.82	70.47 (313.6)	0.98	69.04 (307.2)
Bx16-60	147.09 (654.5)	0.83	132.60 (590.1)	0.92	121.57 (541.0)
Bx16-120	147.09 (654.5)	0.86	132.60 (590.1)	0.95	126.27 (561.9)

\*1 Ratio = Test result / AISC LRFD Specification.

\*2 Specimen Ay8-60 did not reach its maximum tensile strength.

### 5.1.2 Compression Strength

Buckling strengths of specimens were also calculated per the AISC LRFD Specification (AISC, 1999) considering the various limit states of global flexural buckling, local buckling, and buckling of built-up member considering shearing effect due to presence of lacings. The shearing effect of lacings proposed by Galambos (1998) was also estimated.

Two governing flexural buckling equations for compression members are specified by AISC LRFD, one for inelastic buckling and the other for elastic or Euler buckling as presented in Eq. 5.5a and 5.5b, respectively. Eq. 5.5a is an empirical relationship for the inelastic range, while Eq. 5.5b is the familiar Euler formula multiplied by 0.877. The boundary between inelastic and elastic instability is  $\lambda_c = 1.5$ .

$$\text{For } \lambda_c = \frac{KL}{r\pi} \sqrt{\frac{F_y}{E}} \leq 1.5,$$

$$P_n = A_g F_{cr} = A_g (0.658^{\lambda_c^2}) F_y \quad (5.5 \text{ a})$$

$$\text{For } \lambda_c = \frac{KL}{r\pi} \sqrt{\frac{F_y}{E}} > 1.5,$$

$$P_n = A_g F_{cr} = A_g \left[ \frac{0.877}{\lambda_c^2} \right] F_y \quad (5.5 \text{ b})$$

Axially loaded members containing elements subjected to compression having a width-thickness ratio,  $b/t$ , in excess of the AISC LRFD limitations are designed as follows:

$$\text{For } \lambda_c \sqrt{Q} \leq 1.5,$$

$$P_n = A_g F_{cr} = A_g Q (0.658^{Q\lambda_c^2}) F_y \quad (5.6 \text{ a})$$

$$\text{For } \lambda_c \sqrt{Q} > 1.5,$$

$$P_n = A_g F_{cr} = A_g \left[ \frac{0.877}{\lambda_c^2} \right] F_y \quad (5.6 \text{ b})$$

where, for unstiffened elements,  $Q = Q_s$  which is defined as follows:

For flanges, angles, and plates projection from built-up columns or other compression members:

when  $0.64/\sqrt{E/(F_y/k_c)} < b/t < 1.17/\sqrt{E/(F_y/k_c)}$ ,

$$Q_s = 1.415 - 0.65(b/t)\sqrt{(F_y/k_c)E} \quad (5.7 \text{ a})$$

when  $b/t > 1.17/\sqrt{E/(F_y/k_c)}$ ,

$$Q_s = 0.90Ek_c/[F_y(b/t)^2] \quad (5.7 \text{ b})$$

where the coefficient  $k_c$  is equal to  $4/\sqrt{h/t_w}$  for I-shaped section, and 0.763 for other sections.

For built-up compression members, the AISC LRFD Specification requires that individual components of a compression member composed of two or more shapes be connected to one another at intervals,  $a$ , such that the slenderness ratio of these individual components does not exceed three-fourths times the governing slenderness ratio of the built-up member. If the buckling mode involves relative deformations that produce shear forces in the connectors between individual shapes, the effective slenderness ratio,  $KL/r$ , is replaced by  $(KL/r)_m$  determined as follows:

For intermediate connectors that are snug-tight bolted,

$$\left(\frac{KL}{r}\right)_m = \sqrt{\left(\frac{KL}{r}\right)_0^2 + \left(\frac{a}{r_i}\right)^2} \quad (5.8 \text{ a})$$

For intermediate connectors that are welded or fully-tensioned bolted,

$$\left(\frac{KL}{r}\right)_m = \sqrt{\left(\frac{KL}{r}\right)_0^2 + 0.82 \frac{\alpha^2}{(1+\alpha^2)} \left(\frac{a}{r_{ib}}\right)^2} \quad (5.8 \text{ b})$$

Note that  $(KL/r)_m$  can be calculated either by assuming snug tight or fully-tensioned bolts. In

this study, the latter was done using the AISC LRFD Specification 3<sup>rd</sup> edition. Interestingly, section shape By specimens exhibited very little sensitivity to which method was used. For example, for the By8-60 specimen,  $(KL/r)_m$  was equal to 68.0, 66.5, and 67.7 if calculated by snug tight (1<sup>st</sup> edition to 3<sup>rd</sup> edition), fully-tensioned (1<sup>st</sup> edition), and fully-tensioned (3<sup>rd</sup> edition) of AISC LRFD Specifications, respectively. Similar variations (0.61 % larger than slenderness ratios without considering shearing effects with standard deviation of 0.80) were observed for specimens By8-120, By16-60, and By16-120 as shown in Table 5.3.

Table 5.3 Modified slenderness ratios for By specimens per different assumptions

Specimen	AISC LRFD Specifications		
	Snug tight	Fully-tensioned	
	1 <sup>st</sup> , 2 <sup>nd</sup> , 3 <sup>rd</sup> edition	1 <sup>st</sup> edition	2 <sup>nd</sup> , 3 <sup>rd</sup> edition*
	$(KL/r)_m$	$(KL/r)_m$	$(KL/r)_m$
By8-60	67.95	66.50	67.66
By16-60	71.48	71.23	71.41
By8-120	110.39	109.50	110.21
By16-120	105.14	104.97	105.09

\*  $(KL/r)_m$  values used in this study

Another approach to account for the shearing effect in a laced member consists of increasing the effective slenderness ratio as follows (Galambos, 1998):

$$\text{For } \frac{KL}{r} \geq 40, \quad K' = K \sqrt{1 + \frac{300}{(KL/r)^2}} \quad (5.9 \text{ a})$$

$$\text{For } \frac{KL}{r} < 40, \quad K' = 1.1K \quad (5.9 \text{ b})$$

In the following, results are presented first for the specimens having slenderness ratios of  $KL/r = 60$ , then for the specimens having  $KL/r = 120$ , because the way K factor is treated in these two groups of specimens is different.

The  $KL/r = 60$  specimens were originally designed assuming the theoretical slenderness ratio measured from center-line to center-line of connection gussets. Due to the actual end conditions (gusset plates and connectivity), the actual member length to use in the calculations of the accurate slenderness ratio for the specimens must be considered in the comparison between experimental results and analytical predictions. As shown in Figure 5.2, analyses using SAP 2000 show that the specimens are subjected to a bending moment diagram and are not in pure compression when the frame sways. Therefore, using the results from SAP 2000 analyses, inflection points can be determined along the braces and the distance,  $L^*$  is defined as the distance between two inflection points. The actual K factor for the specimens is therefore given by the ratio of  $L^*/L$ , where  $L$  is the distance between the first row of bolts at the face of the gusset to the same on the other gusset. Table 5.4 summarizes all of the parameters shown in Figure 5.2 for each of the specimen considered. The results in that table show that the effective length factor,  $K$  varies between 0.61 to 0.68 with an average value of 0.65.

Table 5.4 Effective length factor,  $K$  (specimens with  $KL/r = 60$ )

<b>Specimen</b>	<b><math>M1</math></b>	<b><math>M2</math></b>	<b><math>M3</math></b>	<b><math>M4</math></b>	<b><math>L</math> in (mm)</b>	<b><math>L1^*</math> in (mm)</b>	<b><math>L2^*</math> in (mm)</b>	<b><math>L^*</math> in (mm)</b>	<b><math>K</math></b>
Ay8-60	0.72	1.01	0.93	0.30	81.25 (2063.8)	23.72 (602.5)	30.72 (780.3)	54.43 (1382.5)	0.67
Ay16-60	0.82	1.17	0.80	0.25	99.75 (2533.7)	29.32 (744.7)	38.00 (965.2)	67.32 (1709.9)	0.68
By8-60	1.19	1.18	0.86	0.34	163.75 (4159.3)	40.76 (1035.3)	58.68 (1490.5)	99.44 (2525.8)	0.61
By16-60	1.22	1.52	1.18	0.38	118.00 (2997.2)	32.73 (831.3)	44.63 (1133.6)	77.36 (1964.9)	0.66
Bx8-60	1.35	1.51	1.20	0.44	114.00 (2895.6)	30.09 (764.3)	41.71 (1059.4)	71.80 (1823.7)	0.63
Bx16-60	1.72	1.78	1.32	0.49	165.00 (4191.0)	41.96 (1065.8)	60.17 (1528.3)	102.12 (2593.8)	0.62

The compression strength for the specimens named  $KL/r = 60$  calculated per the equations of AISC LRFD design specification and using the effective member length factor obtain from these SAP 2000 analyses (Table 5.4) are then compared with the test results. These results are compared in Table 5.5 and graphically presented in Figure 5.3. Note that the predicted strengths

of the specimens in Figure 5.3 were calculating using the appropriate equations corresponding to their specific buckling modes of each specimen as described in Table 5.6.

Table 5.5 Compressive strength comparison (specimens with  $KL/r = 60$ )

Specimen	$P_n$								Test
	$P_{n1}^{*1}$ Kips (kN)	Rat.	$P_{n2}^{*1}$ Kips (kN)	Rat.	$P_{n3}^{*1}$ Kips (kN)	Rat.	$P_{n4}^{*1}$ Kips (kN)	Rat.	
Ay8-60	75.31 (335.1)	1.13	75.31 (335.1)	1.13	NA	NA	NA	NA	84.79 (377.3)
Ay16-60	67.06 (298.4)	1.15	60.84 (270.8)	1.27	NA	NA	NA	NA	77.17 (343.4)
By8-60	80.98 (360.4)	0.63	80.98 (360.4)	0.63	79.56 (354.1)	0.64	79.25 (352.6)	0.64	50.80 (226.1)
By16-60	115.03 (511.9)	1.02	104.37 (464.5)	1.12	114.78 (510.8)	1.02	112.57 (500.9)	1.04	117.27 (521.8)
Bx8-60	64.71 (287.9)	0.93	64.71 (287.9)	0.93	NA	NA	NA	NA	60.06 (267.3)
Bx16-60	108.41 (482.4)	1.05	98.37 (437.7)	1.16	NA	NA	NA	NA	113.95 (507.1)

\*1  $P_{n1}$  = Eq. 5.5: LRFD global buckling

$P_{n2}$  = Eq. 5.6: LRFD global buckling

$P_{n3}$  = Eq. 5.8: LRFD global buckling + shearing effect

$P_{n4}$  = Eq. 5.9: global buckling + Galambos shearing effect

Table 5.6 Buckling mode observed at its maximum compressive forces reached  
(specimens with  $KL/r = 60$ )

Specimen	Ay8-60	Ay16-60	By8-60	By16-60	Bx8-60	Bx16-60
Buckling Mode Observed	Global Buckling	Local Buckling	Global Buckling + Shearing Effects	Local Buckling	Global Buckling	Local Buckling

As shown in Figure 5.3, the specimen strengths calculated using the AISC LRFD Specification equations match the experimentally obtained values within 20 percents except for specimen By8-60. This greater error observed for that specimen can be attributed to the fact that an initial imperfection existed at the beginning of the test of each testing. That imperfection was introduced during the testing of the specimen By8-60. Therefore, it is imperative in predicting the strength of that specimen to consider this initial imperfection greater than with otherwise has been the case if the specimen had been intact from the onset. Elastic buckling strength of compression members having initial imperfection,  $a$ , can be obtained as (Gere and Timoshenko, 1984):

$$\sigma_{\max} = \frac{P}{A_g} \left( 1 + \frac{\frac{ac}{r^2}}{1 - \frac{P}{\pi^2 EA_g} \left( \frac{L}{r} \right)^2} \right) \quad (5.10 a)$$

For the purpose of calculation, it can be rewritten as a quadratic equation with  $P/A_g$  as unknown:

$$b_1 \left( \frac{P}{A_g} \right)^2 - b_2 \left( \frac{P}{A_g} \right) + \sigma_{\max} = 0 \quad (5.10 b)$$

where,  $b_1 = \frac{1}{\pi^2 E} \left( \frac{L}{r} \right)^2$ ,  $b_2 = 1 + \frac{ac}{r^2} + \frac{\sigma_{\max}}{\pi^2 E} \left( \frac{L}{r} \right)^2$ ,  $\frac{ac}{r^2}$  is the imperfection ratio,  $a$  is the maximum initial imperfection, and  $c$  is distance from the centroidal axis to the extreme fiber on the concave side of the compressive member.

Note that the initial imperfection for specimen By8-60 was measured graphically from photographs taken of the specimen prior to testing instead of measuring it directly from the specimen in the lab. The resulting member length to initial imperfection,  $a$  is approximately 1/300. Using this information, the compressive strength of the By8-60 specimen was recalculated per Eq. 5.10b. The resulting compressive strength ratio of test result to calculated value is 0.9 as shown in Figure 5.3.

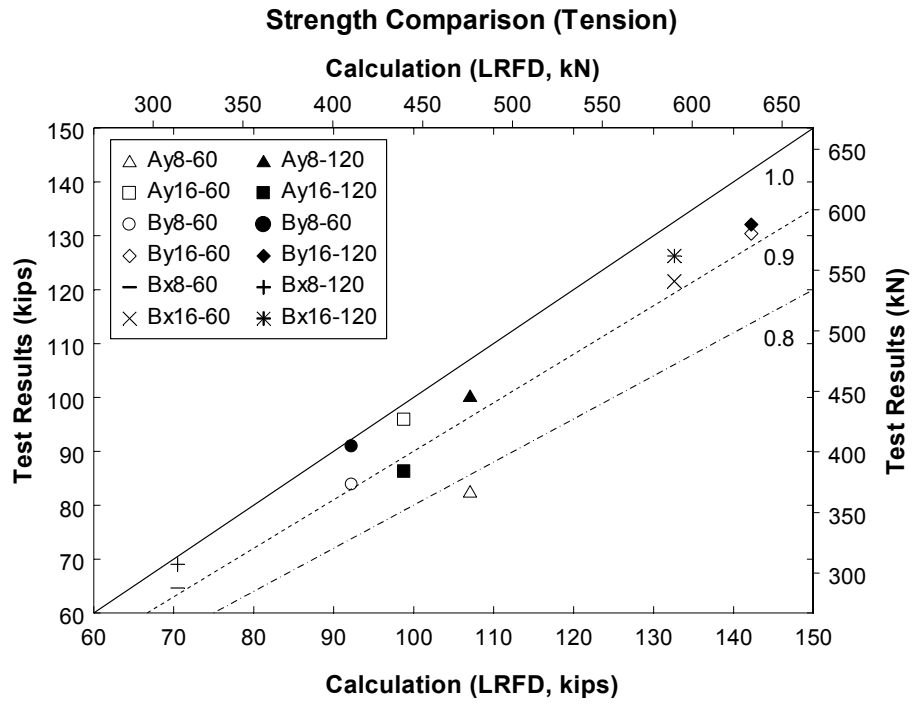


Figure 5.1 Tensile strength comparisons

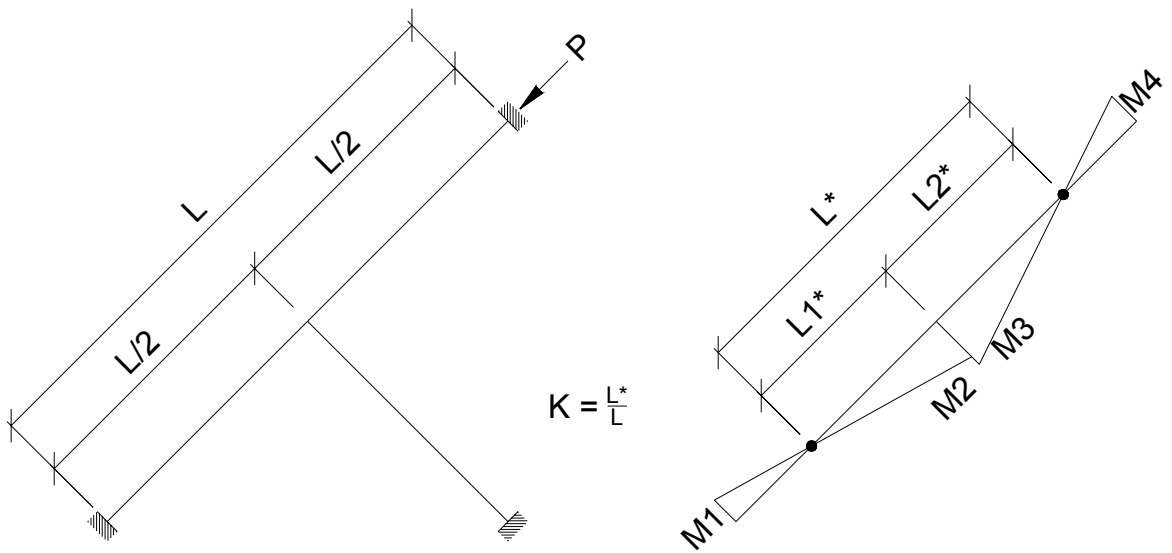


Figure 5.2 Effective length factor, K (specimens with  $KL/r = 60$ )

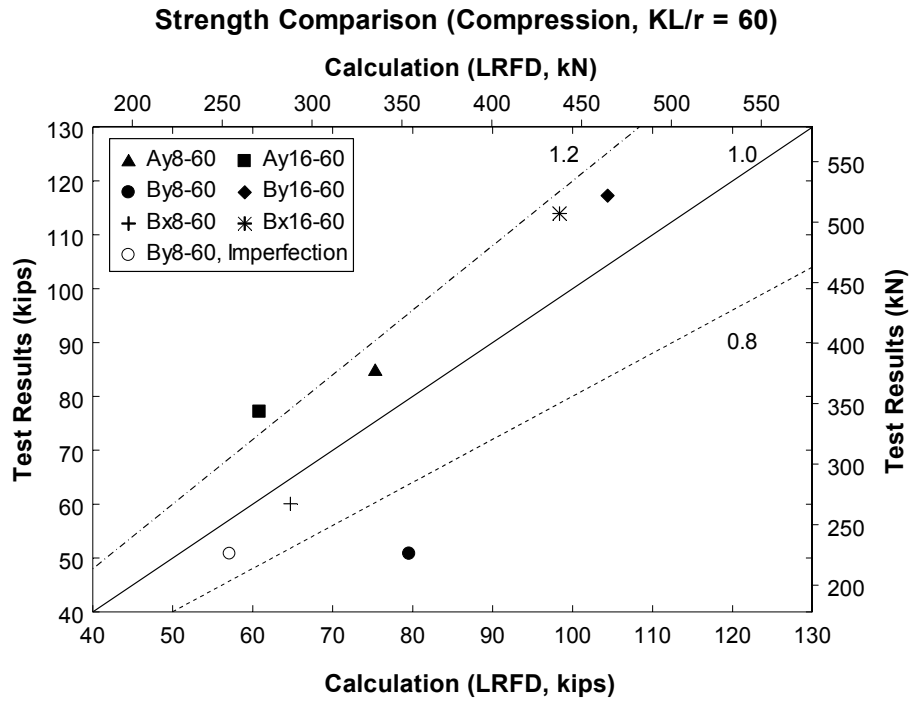


Figure 5.3 Compressive strength comparisons ( $KL/r = 60$ )

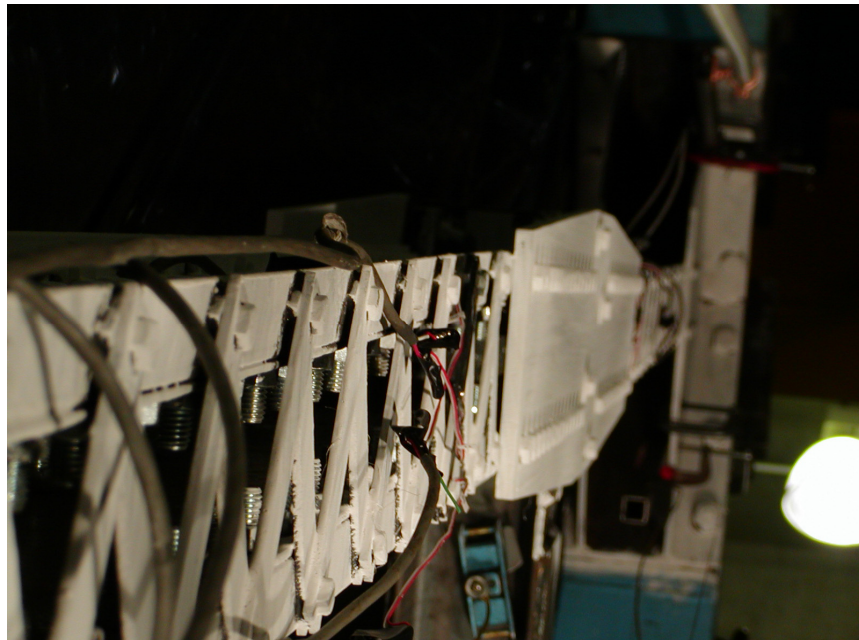


Figure 5.4 Initial imperfection of By8-60 specimen

The design compressive strengths of the specimens with  $KL/r = 120$ , predicted by the AISC LRFD Specification, were also compared with those obtained from the testing. Theoretically,  $K$  values for these specimens are 1.0 as schematically shown in Figure 5.5a. From the bending moment diagrams obtained from SAP 2000 analyses, the effective length factors,  $K$  of the specimens with  $KL/r$  of 120 were proved to be slightly larger than 1.0 (Figure 5.5b). However, in the first step the expected design compressive strength of the specimens with  $KL/r$  of 120 were calculated here with  $K$  value of 1.0. Resulting calculated values are compared with those obtained from testing in Table 5.7 and Figure 5.6. Buckling modes observed during testing for each specimen are also summarized in Table 5.8. As shown in Table 5.7 and Figure 5.6, compressive strength calculated using the AISC LRFD Specification equations underestimate the compressive strength of the test specimens having a slenderness ratio of 120 with a relatively large error (ratios vary from 1.12 to 1.45).

Table 5.7 Compressive strength comparison (specimens with  $KL/r = 120$ )

Specimen	$P_n$								Test
	$P_{n1}^{*1}$ Kips (kN)	Rat.	$P_{n2}^{*1}$ Kips (kN)	Rat.	$P_{n3}^{*1}$ Kips (kN)	Rat.	$P_{n4}^{*1}$ Kips (kN)	Rat.	
Ay8-120	48.90 (217.6)	1.14	48.90 (217.6)	1.14	NA	NA	NA	NA	55.95 (249.0)
Ay16-120	42.19 (187.7)	1.12	38.28 (170.3)	1.24	NA	NA	NA	NA	47.37 (210.8)
By8-120	46.92 (208.8)	1.42	46.92 (208.8)	1.42	46.10 (205.2)	1.44	45.92 (204.3)	1.45	66.50 (295.9)
By16-120	74.94 (333.5)	1.34	67.99 (302.6)	1.48	74.77 (332.7)	1.34	73.33 (326.3)	1.37	100.49 (447.2)
Bx8-120	38.05 (169.3)	1.26	38.05 (169.3)	1.26	NA	NA	NA	NA	48.00 (213.6)
Bx16-120	63.28 (281.6)	1.45	57.42 (255.5)	1.60	NA	NA	NA	NA	92.06 (409.7)

\*1  $P_{n1}$  = Eq. 5.5: LRFD global buckling

$P_{n2}$  = Eq. 5.6: LRFD global buckling

$P_{n3}$  = Eq. 5.8: LRFD global buckling + shearing effect

$P_{n4}$  = Eq. 5.9: global buckling + Galambos shearing effect

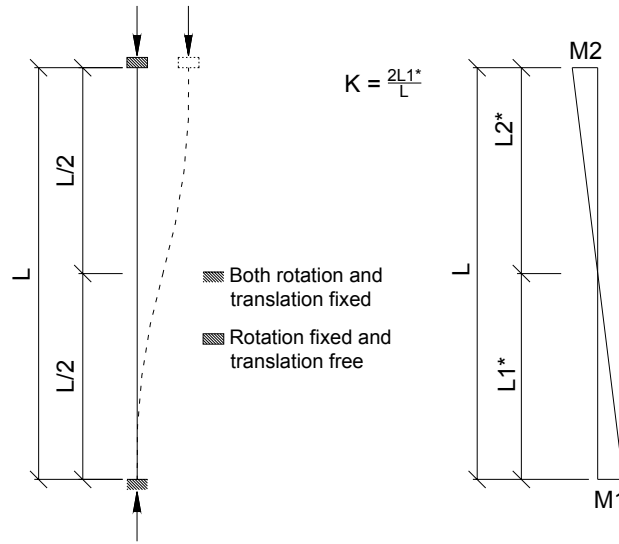
Table 5.8 Buckling mode observed at its maximum compressive forces reached  
(specimens with  $KL/r = 120$ )

Specimen	Ay8-120	Ay16-120	By8-120	By16-120	Bx8-120	Bx16-120
Buckling Mode Observed	Global Buckling	Global Buckling	Global Buckling + Shearing Effects	Global Buckling + Shearing Effects	Global Buckling	Global Buckling

Therefore, the effective length factor,  $K$  that would make the calculated strength of each specimen equal to the experimentally obtained results are calculated and presented in Table 5.9. These values of the effective length factor will be used for evaluation of low cycle fatigue fracture life of the test specimens in SECTION 6.

Table 5.9 Effective length factor,  $K$  (specimens with  $KL/r = 120$ )

Specimen	$P_n, K$								Test
	$P_{n1}$ Kips (kN)	$K_{req}$	$P_{n2}$ Kips (kN)	$K_{req}$	$P_{n3}$ Kips (kN)	$K_{req}$	$P_{n4}$ Kips (kN)	$K_{req}$	
Ay8-120	48.90 (217.6)	0.91	48.90 (217.6)	0.91	NA	NA	NA	NA	55.95 (249.0)
Ay16-120	42.19 (187.7)	0.93	38.28 (170.3)	0.87	NA	NA	NA	NA	47.37 (210.8)
By8-120	46.92 (208.8)	0.77	46.92 (208.8)	0.77	46.10 (205.2)	0.76	45.92 (204.3)	0.76	66.50 (295.9)
By16-120	74.94 (333.5)	0.79	67.99 (302.6)	0.71	74.77 (332.7)	0.79	73.33 (326.3)	0.78	100.49 (447.2)
Bx8-120	38.05 (169.3)	0.85	38.05 (169.3)	0.85	NA	NA	NA	NA	48.00 (213.6)
Bx16-120	63.28 (281.6)	0.76	57.42 (255.5)	0.68	NA	NA	NA	NA	92.06 (409.7)



(a) Theoretical  $K = 1.0$  (AISC, 1993)      (b)  $K$  from BMD (SAP 2000 Analyses)

Figure 5.5 Theoretical  $K$  value for test specimens with  $KL/r = 120$

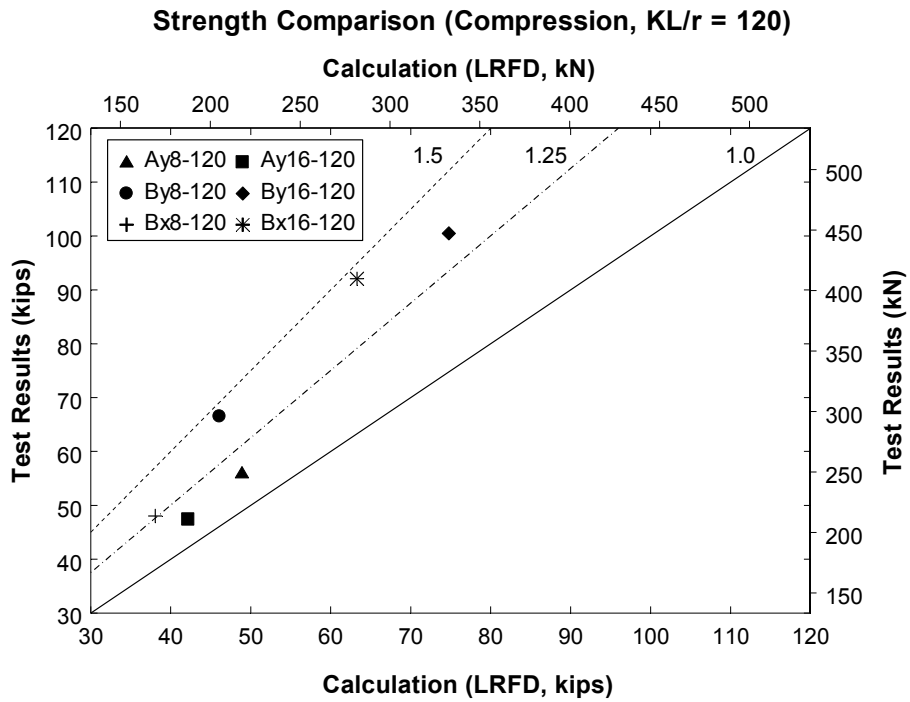


Figure 5.6 Compressive strength comparisons ( $KL/r = 120$ )

### 5.1.3 Hysteretic Curves

The deformations and corresponding forces recorded during the tests were examined to observe the hysteretic behavior of test specimens. As stated in SECTION 3, the hysteretic behavior of brace members depends on their slenderness ratios,  $KL/r$  and width-to-thickness ratios,  $b/t$ . To compare the relative hysteretic behavior of test specimens having different slenderness ratios and width-to-thickness ratios but same cross-section type (i.e. Ay, By, and Bx), four hysteretic curves are presented in each figure for a given section shape. Furthermore, to allow more general comparison of the hysteretic behavior of all the test specimens, the hysteretic curves were normalized in a few different ways.

In the following, five hysteretic curves figures are presented for each specimen section shape, presenting results in different formats, namely:

- (1) Absolute results, i.e., forces and displacements measured from the actuator and gauges during the tests, are presented. All normalized hysteretic curves are derived from these results. Forces from the test results are normalized by theoretical yield forces of test specimens calculated as  $P_y = A_g \sigma_y$ .
- (2) Displacements obtained from testing normalized by the experimentally measured buckling displacement ( $\delta_{b,exp}$ ). A secant modulus approach was used to obtain  $\delta_{b,exp}$  instead of a tangent modulus, as schematically shown in Figure 5.7. Forces from the test results are normalized by theoretical yield forces of test specimens calculated as  $P_y = A_g \sigma_y$ .
- (3) Displacements normalized by the experimental yield displacement ( $\delta_{y,exp}$ ) corresponding to the experimental buckling displacement,  $\delta_{b,exp}$ , calculated as shown in Figure 5.7. Forces from the test results are normalized by theoretical yield forces of test specimens calculated as  $P_y = A_g \sigma_y$ .
- (4) Frame drifts,  $\Delta$  (of interest in seismic design) obtained from testing. From the Transonic located at the loading point, normalized by frame height ( $H$ ) (i.e. presented as percentage of height,  $(\Delta/H) \times 100$ ). Forces from the test results are normalized by theoretical yield forces of test specimens calculated as  $P_y = A_g \sigma_y$ .

- (5) Frame drifts calculated from the diagonal displacements also presented in a normalized manner. As shown in Figure 5.8, equivalent drifts were obtained from the geometric relationships between diagonal displacements and horizontal drifts assuming rigid columns and beam on the top of the frame. Forces from the test results are normalized by theoretical yield forces of test specimens calculated as  $P_y = A_g \sigma_y$ .

Hysteretic curves normalized by experimental buckling displacements (item (2) above), are presented in Figures 5.9 to 5.14 and others are presented in Appendix C. In these figures, hysteresis of normalized diagonal displacements for specimens with  $KL/r = 60$  are presented either in terms of ‘Element’ or ‘System’ ductilities which are respectively calculated using either diagonal axial displacement of the buckled segment and the full diagonal axial displacement of both segments of the specimen (such a distinction is not necessary for the specimens with  $KL/r = 120$ ). As described in SECTION 3, specimens with  $KL/r = 60$  have essentially two identical members simultaneously tested in a frame. Displacements were measured for both the upper and lower specimens as well as for the full diagonal length. Figure 5.15 shows example hysteretic curves obtained from the testing of the By8-60 specimen. Theoretically, the summation of displacements obtained from the both upper and lower elements should be identical to the system displacements measured if gages were lined-up perfectly. Figures 5.16 and 5.17 present the theoretical relationships between elements and system displacements and ductilities for a specimen. If one of the elements remains elastic and the other one buckles in a perfectly plastic manner (Figure 5.17), the theoretical relationship between element ductility,  $\mu_{ele}$ , and system ductility,  $\mu_{sys}$ , is  $\mu_{ele} = 2\mu_{sys} - 1$ . A more complex relationship exist if strength degradation is considered. However no evidence of such a relationship was found experimentally. Instead, inelastic displacements of the system,  $\delta_{inelastic,sys}$  was often found to be close to that of element,  $\delta_{inelastic,ele}$  as shown in Figure 5.15 as an example for the By8-60 specimen. This could be partly due to the fact that during the testing, the two Temposonics installed for measuring displacements of the upper and lower specimens were not perfectly lined-up. Attempts were made to get correction factors to compensate for the geometric discordance between element and system displacements, using SAP 2000 analyses. For example, the By16-60 specimen was modeled and analyzed in the elastic range with a gauge eccentricity of  $a$  as shown in Figure

5.18. Some relationship between elements and system displacements was observed in elastic range from the analyses as shown in Figure 5.19. However, difficulties lie in finding such relationships in the inelastic range, which depends on rotations at the middle connection plate that were not measured. Even though no clear relationships could be established between elements and system displacements, the use of correction factors will not have an impact on the presentation of results in a normalized form, since the same correction factors would be applied to both non-normalized displacements  $\delta_{b,exp}$  and  $\delta$ . As indicated earlier, for the members with  $KL/r = 60$ , results are presented in two ways, i.e. either in terms of ‘Element’ or ‘System’ ductilities. In the former case, the axial deformations of the yielding half-brace are divided by the length of the half-brace. In the latter case, the axial deformations for the entire brace (including both the damaged and undamaged (or less damaged) half-braces) are divided by the full brace length. This gives somewhat different results since in all cases, damage was concentrated on only one half length (or one member), if one thinks of the  $KL/r = 60$  as two identical specimens and “series”.

To assess the adequacy of braces hysteretic behavior, capacity must be compared against demand. One way to quantify demand is in terms of displacement demands, themselves related to the design level, and the structural response modification,  $R$ , defined as the product of the ductility factor ( $R_d$ ) and the over-strength factor ( $\Omega_0$ ) of a structural system. For braced frames, the design (or evaluation) assumption also has an impact on demand. For example, with a certain ductility reduction factor,  $R_d$ , a tension-only braced frame can be designed to resist the base shear  $V$  which is obtained from dividing the forces obtained from the elastic response spectrum by  $R_d$ . Consequently, in that case, brace force is calculated dividing  $V$  by the cosine angle of the brace as shown in Figure 5.20. Alternatively, each brace force in a standard X-braced frame can be also determined by dividing  $V/2$  by the cosine angle of the brace as shown in Figure 5.21. In such a case, compression strength of the brace governs the design.

In the AISC LRFD Specification (1999), the ductility factor for braced frames is assumed to be 3. The over-strength factor specified for CBF is 2 and  $R$  factor is 6, corresponding to a ductility factor of 3. This value is shown in Figures 5.9 to 5.14 by thick vertical dotted lines which allow to assess whether the ductility capacity of specimens is sufficient to meet the specified demands.

As schematically presented in Figure 5.21, ductility capacity of the bracing members in a X-braced frame can be calculated as:

$$\mu_b = \frac{\delta_{\max}}{\delta_b} \quad (5.11 \text{ a})$$

for a compressive bracing member, and,

$$\mu_y = \frac{\delta_{\max}}{\delta_y} \quad (5.11 \text{ b})$$

for a tensile bracing member.

The relationship between compressive and tensile ductility capacities is a function of the slenderness ratio,  $KL/r$  of the bracing member. If a X-braced frame has slender bracing members, a smaller tensile ductility demand will be required compared to an X-braced frame with stockier bracing members as schematically presented in Figure 5.22. An example calculation of tensile ductility,  $\mu_y$ , corresponding to the compressive ductility,  $\mu_b$  of 3 for compressive members with slenderness ratios of 60 and 120 is schematically presented in Figure 5.23. In this figure, design stress for compression members with  $KL/r$  of 60 and 120 were taken from the AISC LRFD Specification (1999) design stress table for Gr. 50 ksi (344.5 MPa) steel. These values were divided by the design stress for a compression member with  $KL/r = 0$ , which corresponds to the tensile stress of the member, consequently these ratios can be translated into the ratio of compressive buckling displacement to tensile yield displacement ( $\delta_b / \delta_y$ ) of the bracing members. The corresponding relationships  $\delta_b = 0.77\delta_y$  and  $\delta_b = 0.35\delta_y$  are obtained for bracing members with slenderness ratios of 60 and 120, respectively, from which respective tensile ductility of 2.3 and 1.1 (corresponding to  $\delta_b$  of 3) are calculated. These values are also presented by vertical lines in the normalized hysteretic curves of Figures 5.9 to 5.14.

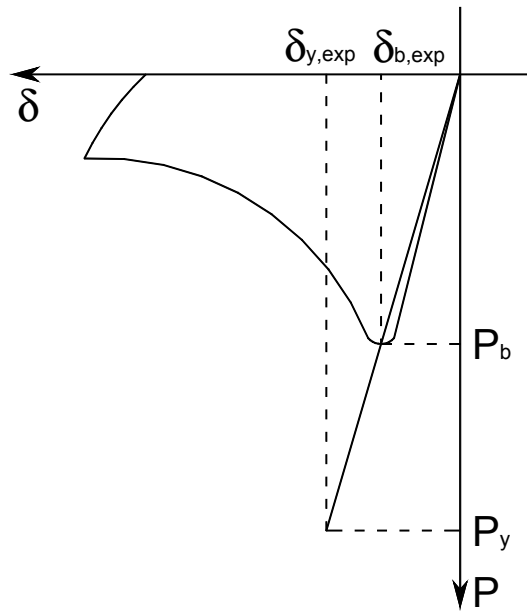
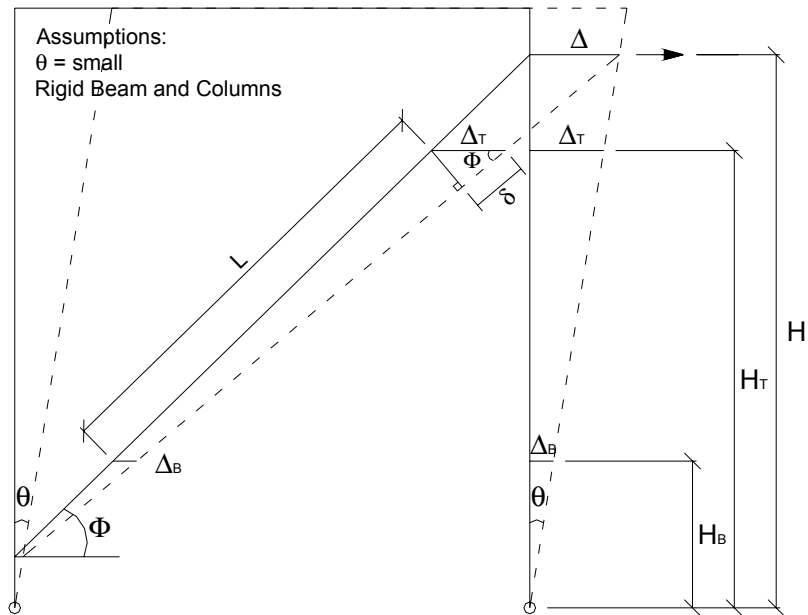


Figure 5.7 Definition of experimental buckling and yield displacement ( $\delta_{b,exp}$  and  $\delta_{y,exp}$ )



$$\begin{aligned} \delta / \cos \Phi &= \Delta_T - \Delta_B \\ \delta &= (\Delta_T - \Delta_B) \cos \Phi = (H_T \theta - H_B \theta) \\ \theta &= ((\delta / \cos \Phi) / (H_T - H_B)) \\ \therefore \Delta &= H \theta = H((\delta / \cos \Phi) / (H_T - H_B)) \end{aligned}$$

Figure 5.8 Definition of equivalent horizontal frame drift ( $\Delta$ )

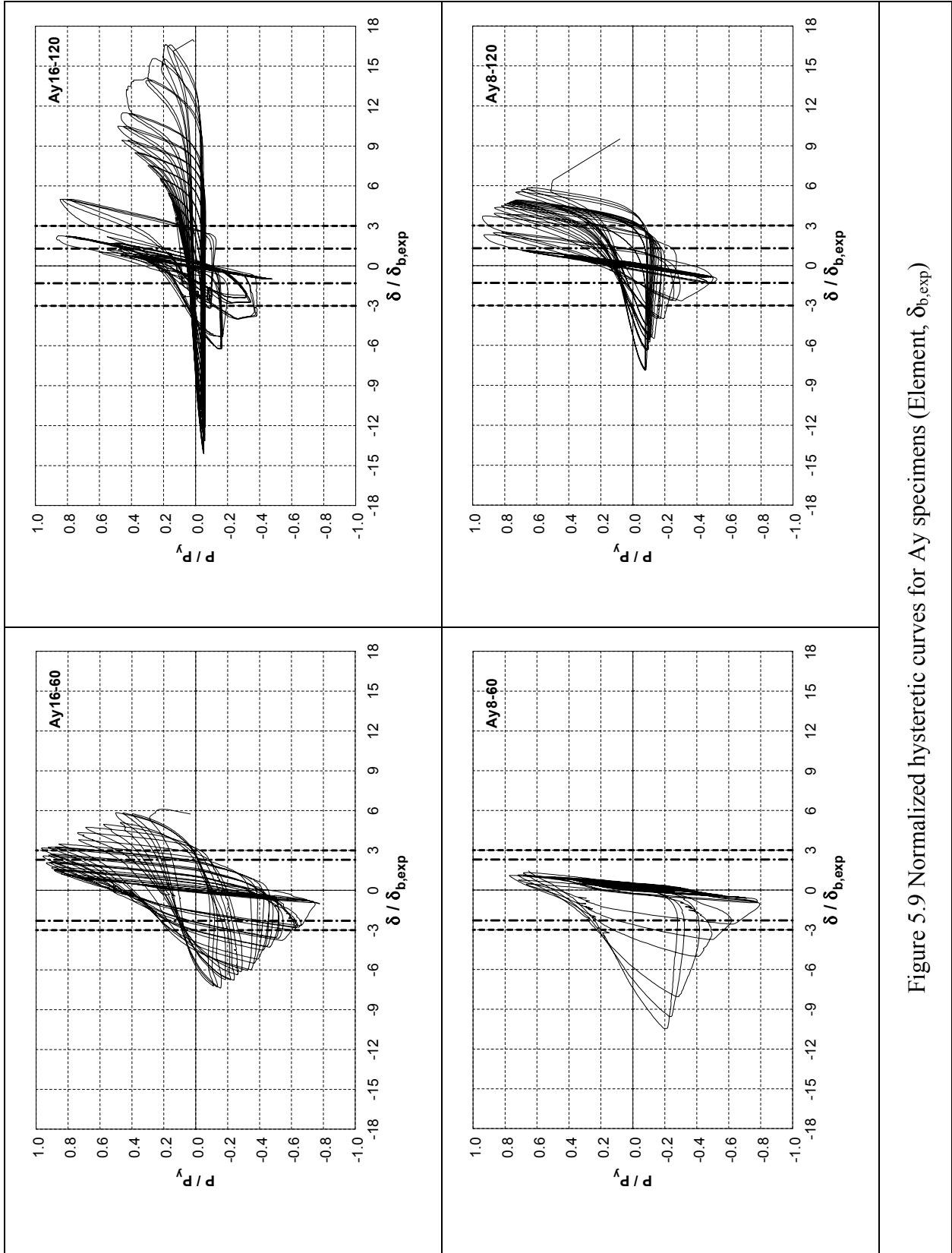


Figure 5.9 Normalized hysteretic curves for Ay specimens (Element,  $\delta_{b,exp}$ )

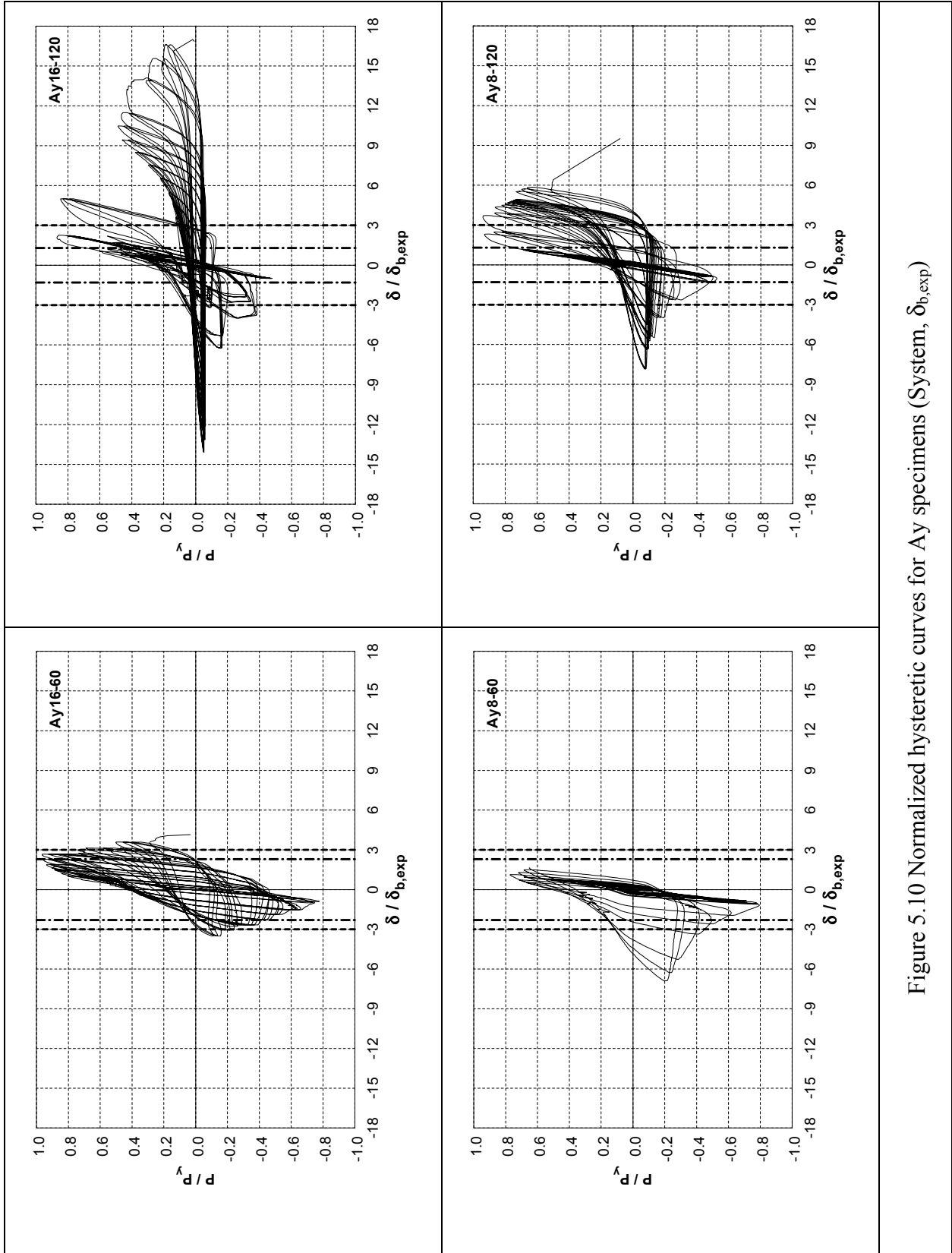


Figure 5.10 Normalized hysteretic curves for Ay specimens (System,  $\delta_{b,exp}$ )

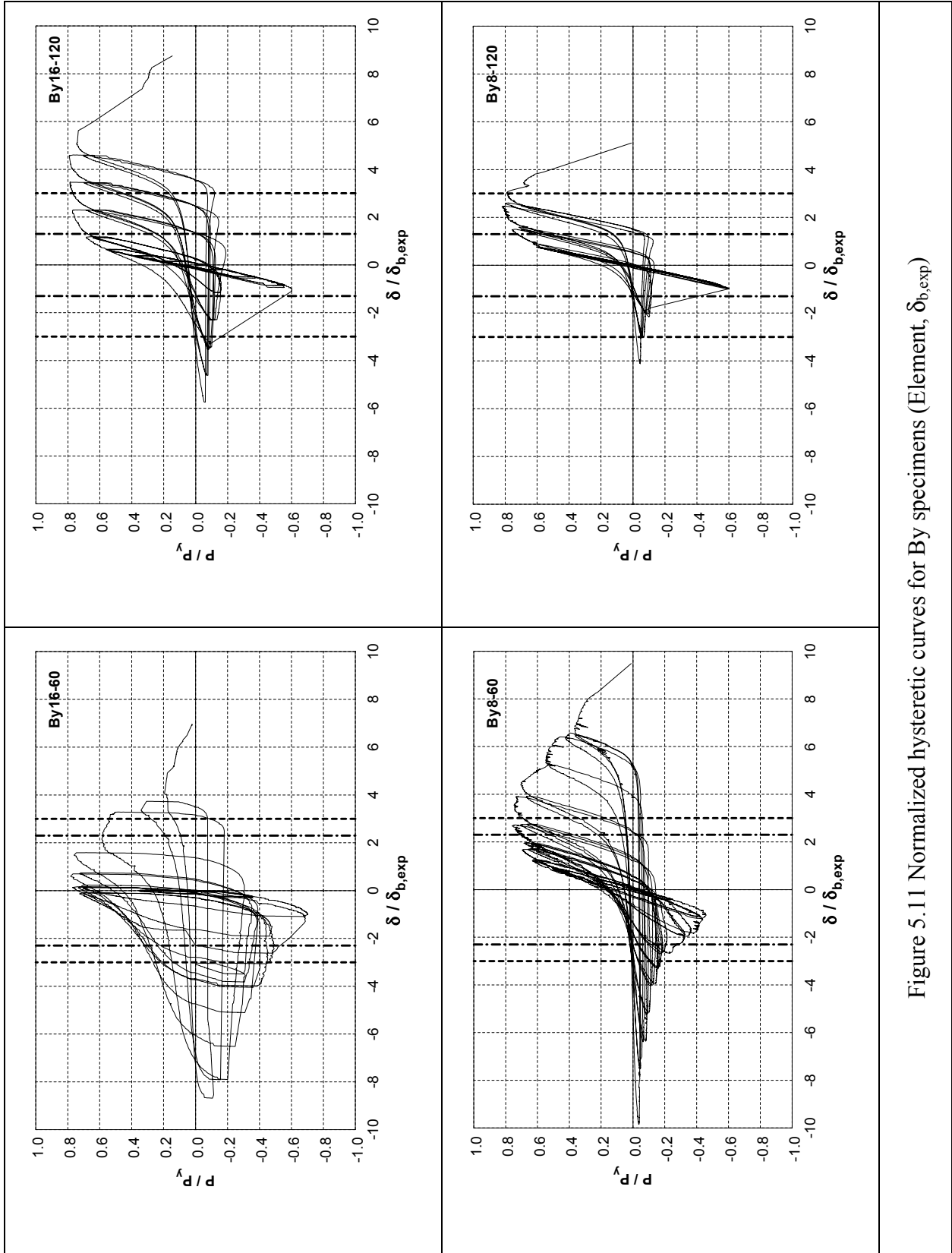


Figure 5.11 Normalized hysteretic curves for By specimens (Element,  $\delta_{b,exp}$ )

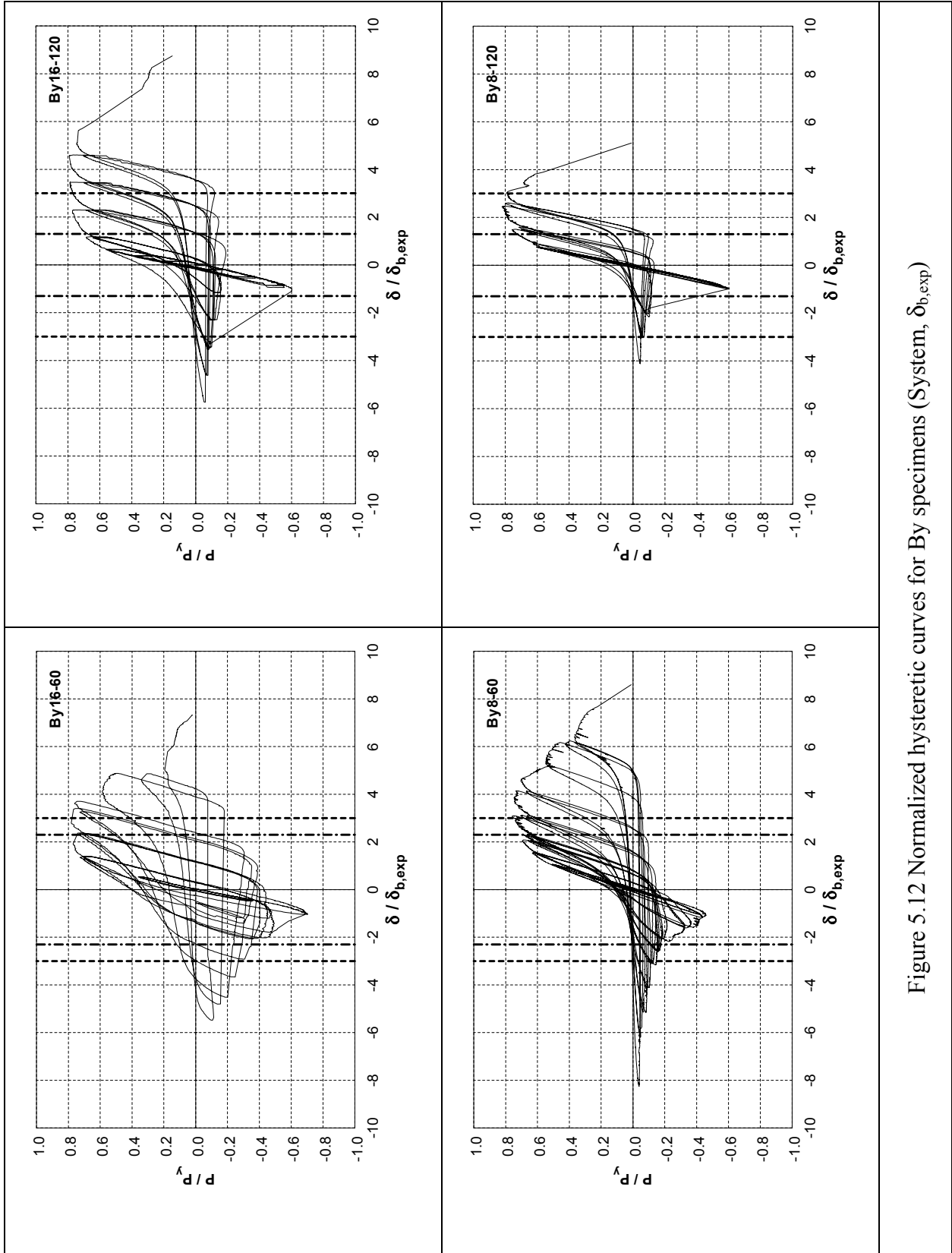


Figure 5.12 Normalized hysteretic curves for By specimens (System,  $\delta_{b,exp}$ )

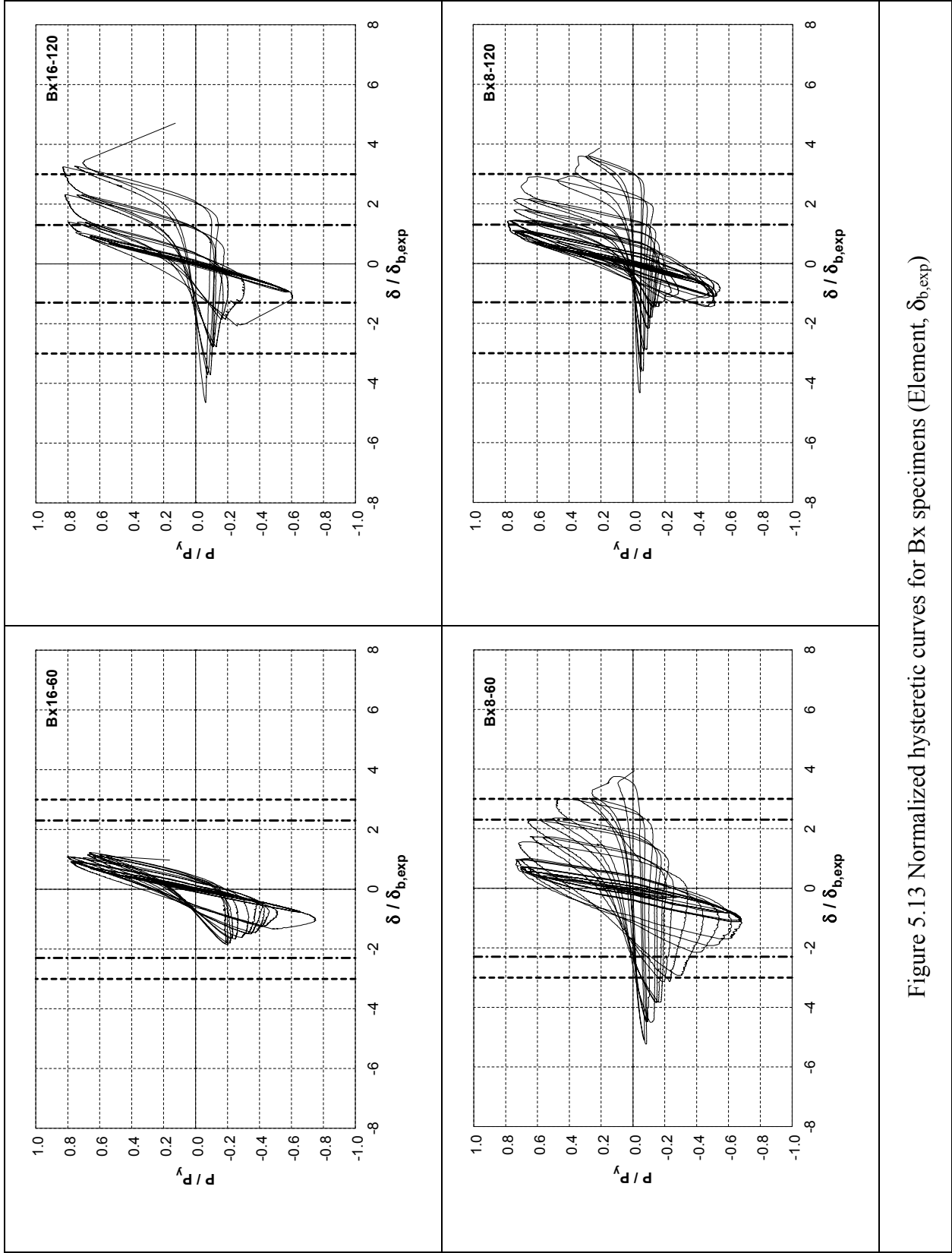


Figure 5.13 Normalized hysteretic curves for Bx specimens (Element,  $\delta_{b,exp}$ )

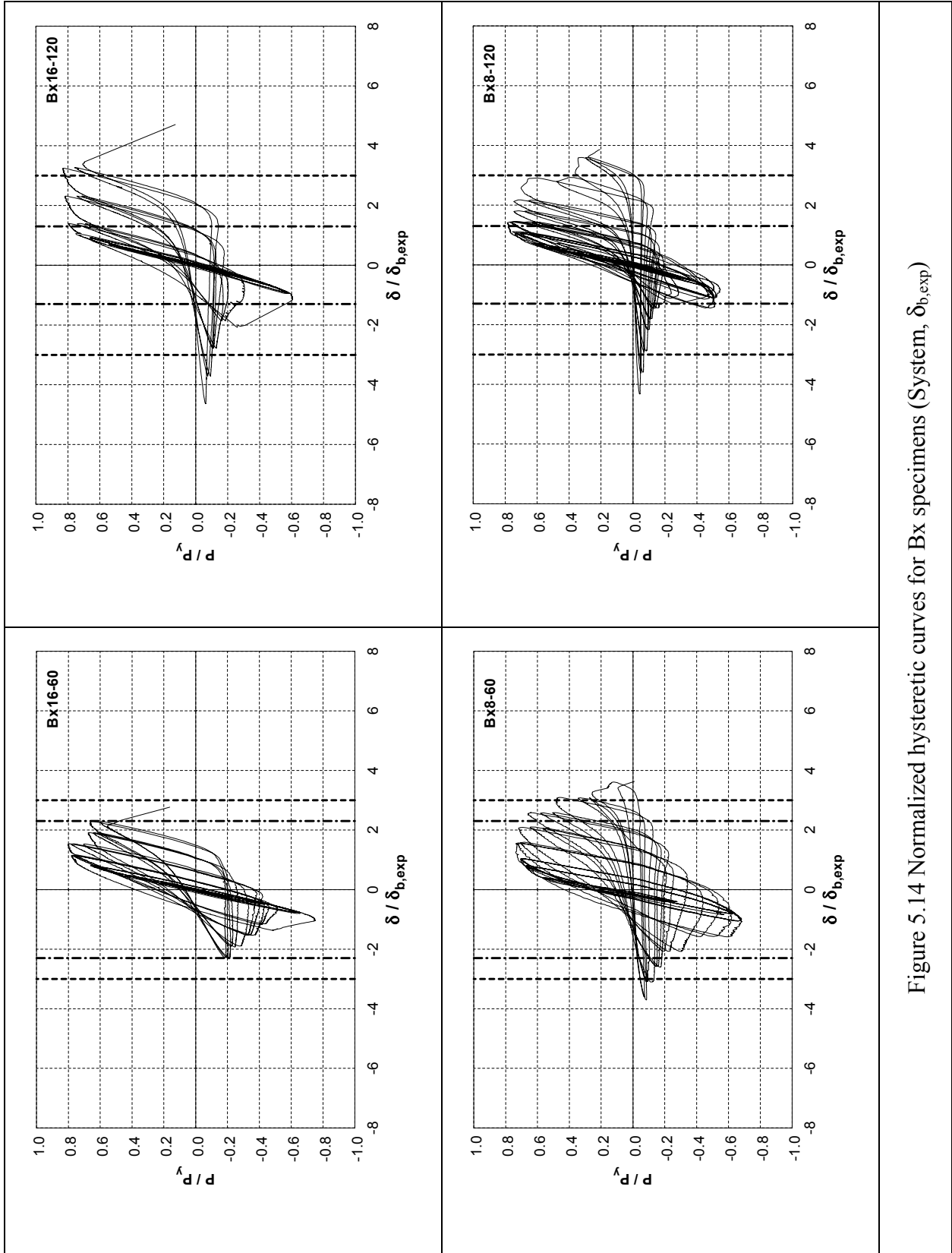
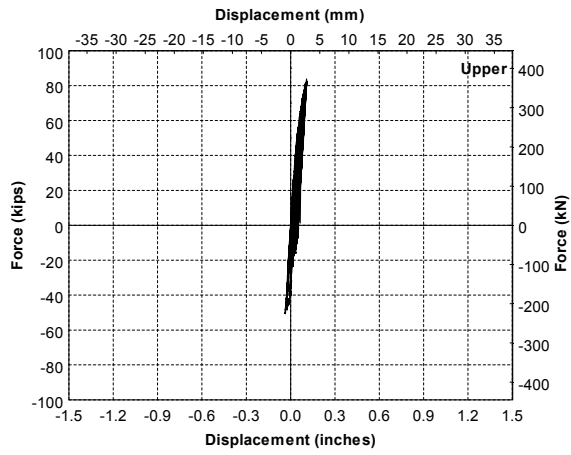
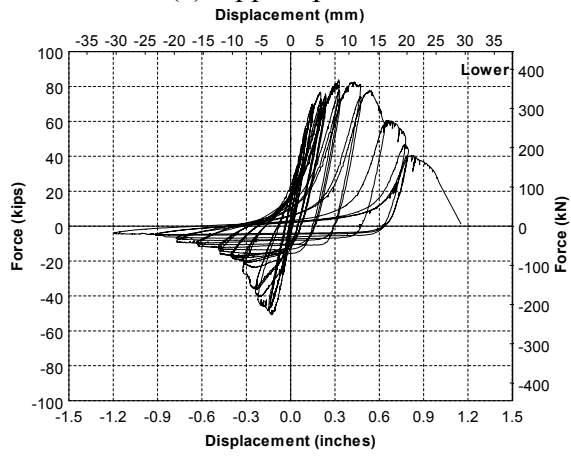


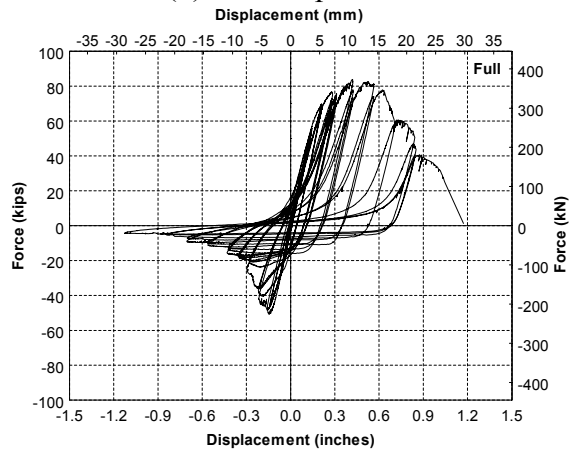
Figure 5.14 Normalized hysteretic curves for Bx specimens (System,  $\delta_{b,exp}$ )



(a) Upper specimen



(b) Lower specimen



(c) System diagonal

Figure 5.15 Hysteretic curves for By8-60 specimen

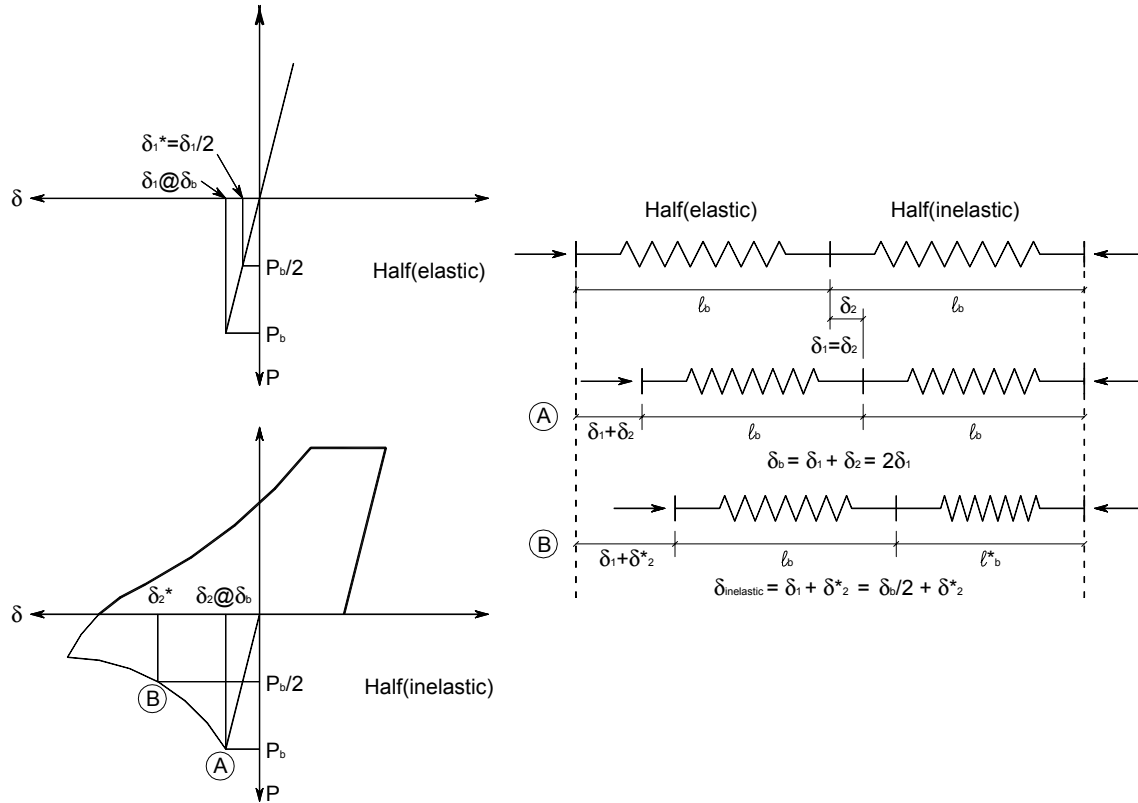
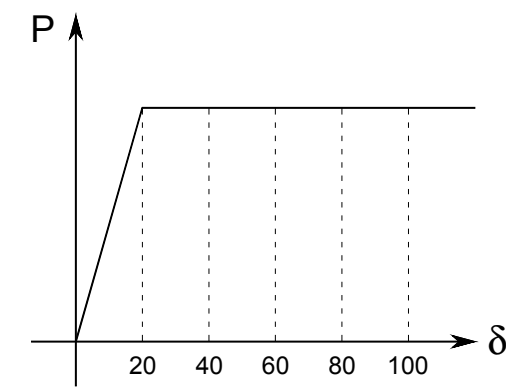


Figure 5.16 Theoretical displacements of upper and lower specimens



$\mu_{sys}$	1	2	3	4	5	...	n
$\delta_{sys}$	20	40	60	80	100	...	20n
$\delta_1$	10	10	10	10	10	...	10n
$\delta_2$	10	30	50	70	90	...	20n-1

$$\mu_{sys} = \delta_{sys} / (\delta_{1,y} + \delta_{2,y})$$

$$\mu_{ele} = \delta_2 / \delta_{2,y} = (\delta_{sys} - \delta_{y1}) / \delta_{2,y}$$

$$\mu_{sys} = n$$

$$\delta_{sys} = 20n = \delta_{1,y} + (2n - 1)\delta_{2,y}$$

$$= \delta_{1,y} + (2\mu_{sys} - 1)\delta_{2,y}$$

$$\delta_{sys} - \delta_{1,y} = (2\mu_{sys} - 1)\delta_{2,y}$$

$$\frac{\delta_{sys} - \delta_{1,y}}{\delta_{2,y}} + 1 = 2\mu_{sys}$$

$$\therefore \mu_{sys} = \frac{1}{2} \left( \frac{\delta_{sys} - \delta_1}{\delta_{2,y}} \right) + \frac{1}{2}$$

$$\mu_{sys} = \frac{1}{2} (\mu_{ele} + 1)$$

$$\mu_{ele} = 2\mu_{sys} - 1$$

Figure 5.17 Relationship between system ductility ( $\mu_{sys}$ ) and element (1 buckled brace) ductility ( $\mu_{ele}$ ) neglecting brace strength degradation

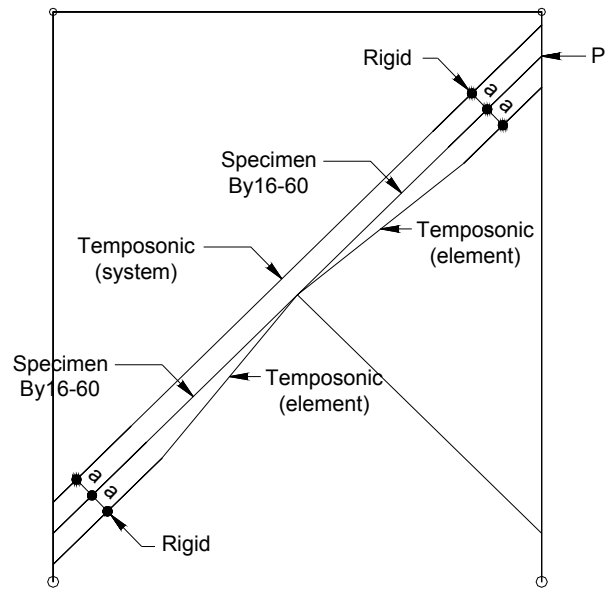


Figure 5.18 SAP 2000 model for By16-60 specimen

**Gage Eccentricity (at 0.033% frame drift)**

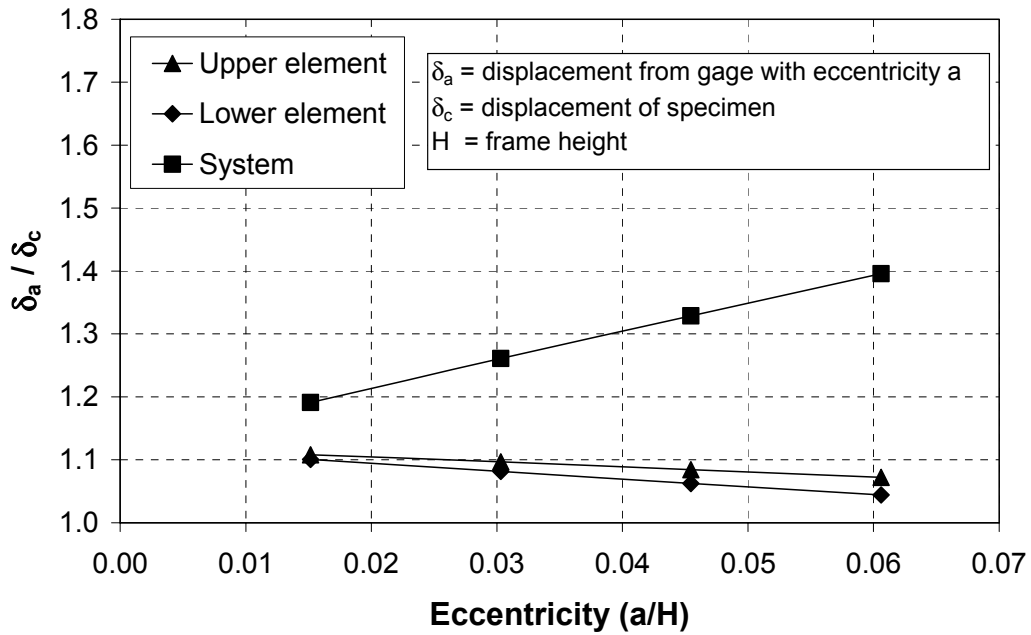


Figure 5.19 Gage correction factors from SAP 2000 analyses

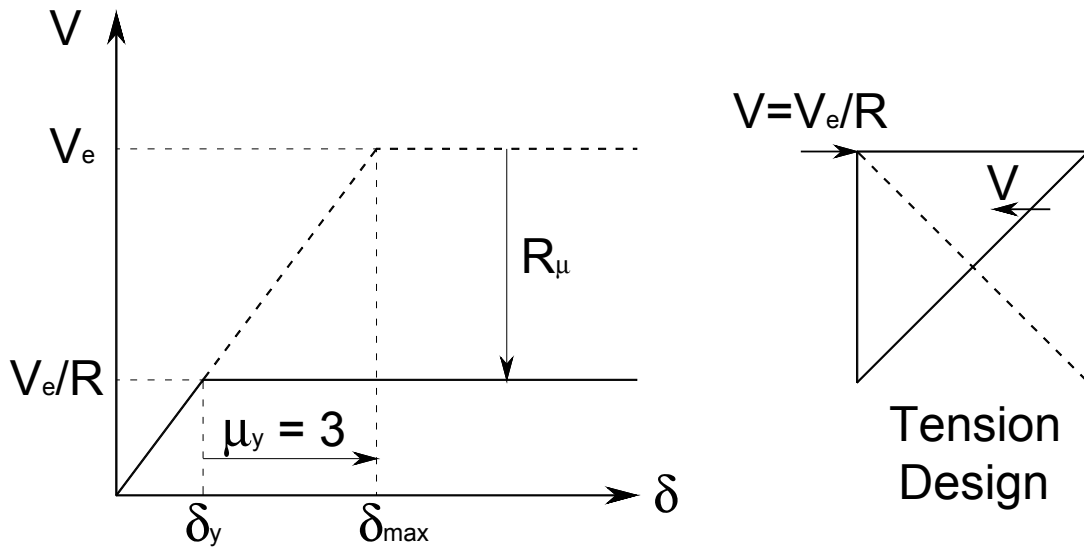


Figure 5.20 Tension only braced frame design

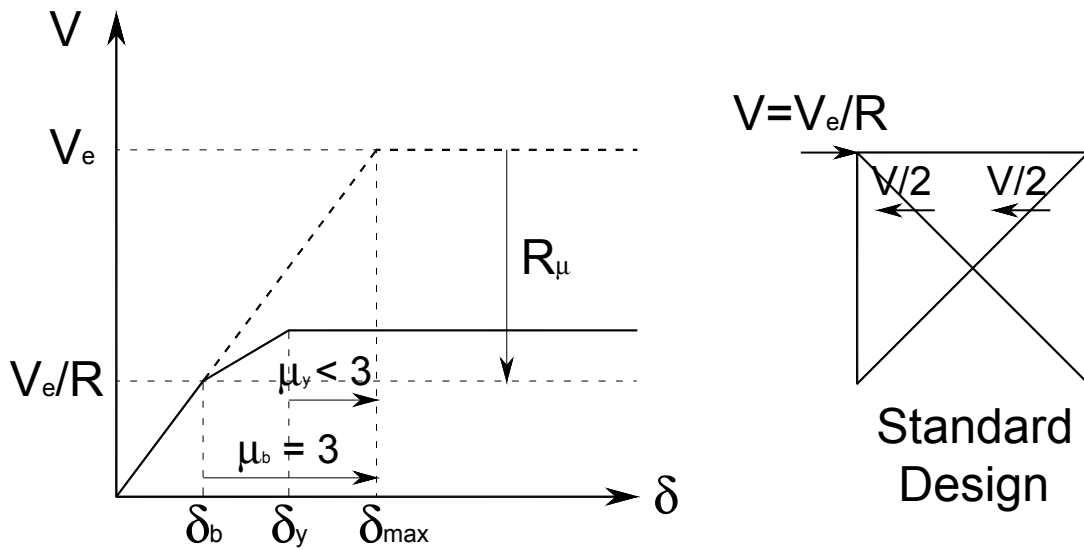


Figure 5.21 X-braced frame design

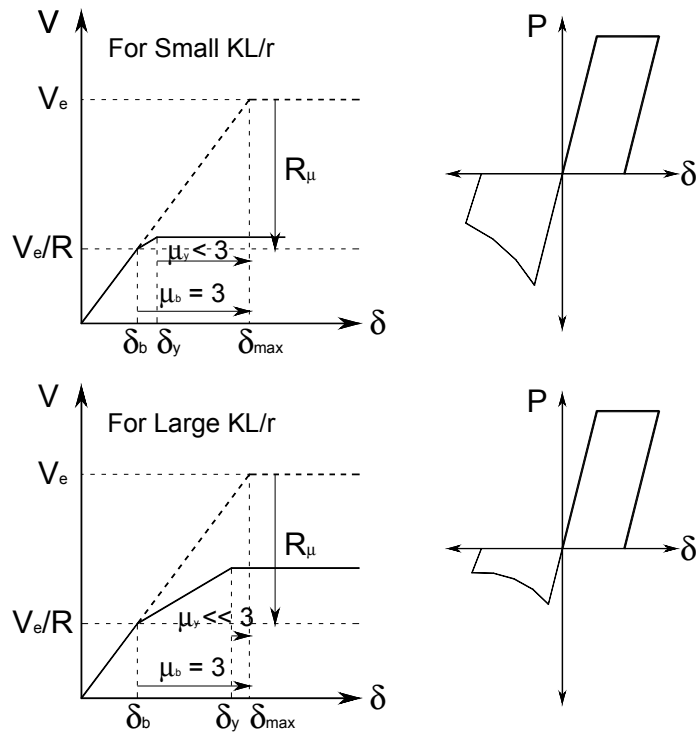


Figure 5.22 Ductility comparisons between slender and stocky braces in a X-braced frame

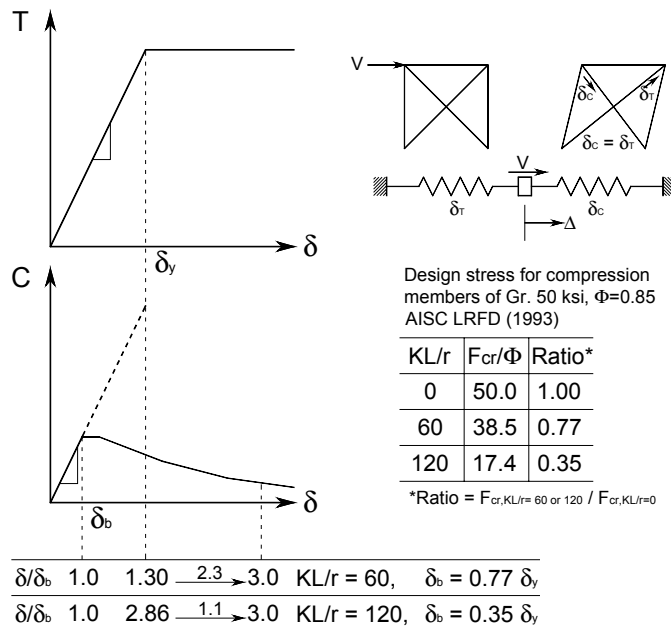


Figure 5.23 Relationship between compressive and tensile ductility

## 5.2 Non-linear Analyses

In this section, using the brace element model in DRAIN-2DX (Prakash and Powell, 1993), non-linear analyses of brace specimens are conducted. Hysteretic curves from analyses results are compared with those results obtained from testing.

### 5.2.1 Modeling

Non-linear static cyclic push-over analyses have been performed using the Ikeda and Mahin physical brace model (element No. 5), implemented in DRAIN-2DX (Prakash and Powell, 1993) by Taddei (1995). This model has been developed for solid braces of uniform cross-section (i.e. not laced members). Analyses were controlled by the axial displacements of the specimens. Note that only axial force-displacement is considered by the brace element model used (element No. 5, Taddei, 1995). As a result, compression is somewhat imperfect, since the actual test specimen was also subjected to some flexure, as indicated in the previous section. However, this effect is indirectly accounted for by doing the comparisons using the effective length factor,  $K$ , determined experimentally in calculating the displacement histories using element No. 5. Specimens having  $KL/r$  of 60 (considering the damaged half of the full brace member) were analyzed as a single member having  $K$  value of 1.0 and specimens having  $KL/r$  of 120 were analyzed with both the theoretical and the calculated (Section 5.1.2) effective length factors. As shown in Figure 5.24, specimens were modeled with both ends pinned.

### 5.2.2 Comparisons with Test Results

The hysteresis loops obtained from the analyses of all specimens using DRAIN-2DX and element No. 5 are presented in Figures 5.25 to 5.42 overlaid on top of results obtained from testing.

As described in Section 5.1.1, tensile strength of specimens with section shape “B” is limited by net section fracture while specimens with section shape “A” were able to develop gross section yielding. The brace model used for the DRAIN-2DX analyses considers only gross section

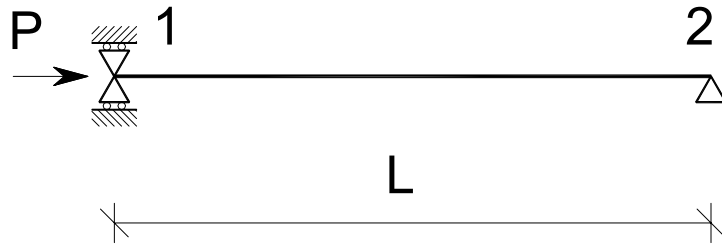


Figure 5.24 Analyses model for DRAIN-2DX

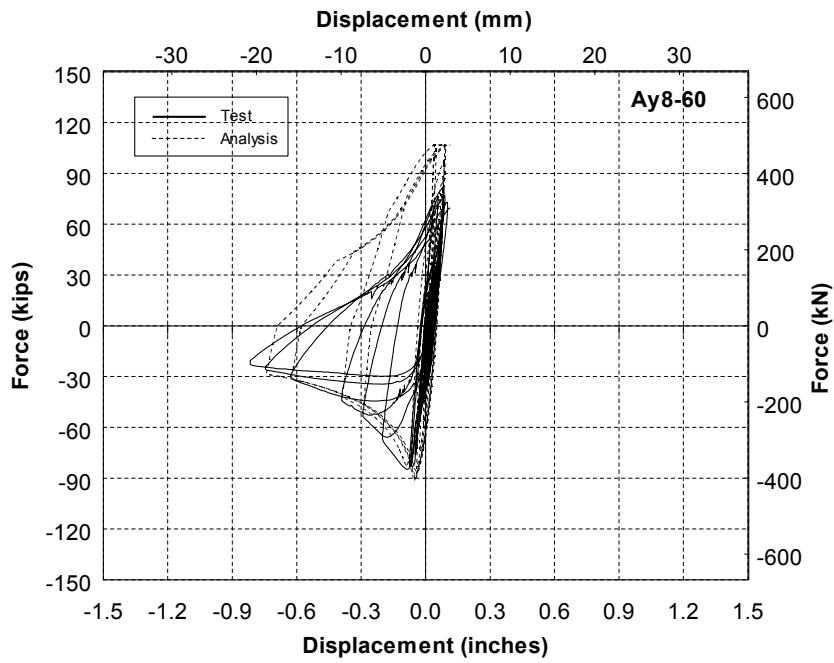


Figure 5.25 Comparison between analysis and experimental results of Ay8-60 specimen

yielding in tension. Consequently, tensile strengths of section shape “A” specimens were reasonably predicted by the DRAIN-2DX analyses, while analysis results over-estimate the tensile strengths of section shape “B” specimens. Because brace element No. 5 used for the analyses does not include a fracture criterion, strength degradation of the specimens in tension after initial fracture are not captured by the analyses, i.e., tests results show strength degradation in tension upon initial fracture, while analysis results show flat yielding plateaus when the maximum tensile strength reached.

Hysteretic behaviors in compression of section shape “A” specimens having  $KL/r$  of 60, reasonably predicted by the analyses results and compressive strengths were also reasonably predicted. Upon reloading in compression after initial buckling, the brace specimen behaved as a component with an initial deflection, and its peak buckling capacity decreased significantly in each subsequent cycle after the first buckling load, however, this behavior was not replicated by the DRAIN-2DX analysis results for the specimens having  $KL/r$  of 60 except for a few specimens for which a decrease was observed after the first buckling cycle, but for which peak buckling strength remained constant for all subsequent cycles. However, the model replicated well the compression strength degradation after the peak buckling load is reached, at increasing axial displacements.

The compressive strengths of the section shape “B” specimens having  $KL/r$  of 60 were overestimated by the analyses results with DRAIN-2DX element No. 5 which only considered Euler buckling or compression yielding as possible limit states for the first buckling strength in compression, the latter case governing in this case. Tensile strengths were also over-estimated by the DRAIN-2DX element No. 5 analyses. This is largely due to shortcoming in the modeling capabilities of element No. 5. As described earlier, the tensile strengths of section shape “B” specimens were limited by the net section fracture. For the section shape “B” specimens, net section yielding precedes gross section yielding, which itself would precede net section fracture. Although net section properties could have been input into the model instead, this could have given the wrong member axial stiffness ( $EA/L$ ). This could have been corrected by changing the modulus of elasticity accordingly, but this was not pursued since these are other significant problems anyhow with the predictions obtained with element No. 5, as described later.

Assuming that the maximum tension and compression strength of the brace calculated by element No. 5 are both limited by the tensile strength of the brace in the cases considered here, overestimation of the compressive strengths of the section shape “B” specimens having  $KL/r$  of 60 by the analyses results is therefore proportional to the ratio of net section fracture to gross section yielding in tension. Additional shortcoming in element No. 5 also exist in that the maximum strength reached in compression in successive cycles (beyond the first cycle) remains constant, contrary to experimental results which show progressive degradation. Hence, although further “tuning” of the element No. 5 input data could have been possible, it was decided not to pursue this option since it somewhat goes against the objective of using a physical brace model in the first place, and particularly because the strength degradation observed in the test specimens was substantially more severe than typically observed for monolithic braces of the type that can be modeled using element No. 5.

Compressive strengths of the section shapes “A” and “B” specimens having  $KL/r$  of 120 and overall shape of their hysteretic curves were reasonably predicted by the analyses results when the calculated effective length factors,  $K$  (Section 5.1.2) were used for the analyses. However, as described in SECTION 4, section shape “B” specimens having  $KL/r$  of 120 suffered significant compression strength degradation because buckling was accompanied by local buckling and by lacing buckling. As a result of lacing buckling, the components of the brace moved closer together, reducing the moment of inertia of the section at that location, also reducing the plastic moment at these hinges, and thus accelerating the loss in compression strength. However, this behavior was not captured by brace element No. 5 because this model does not consider local buckling and lacing buckling (i.e., this model has been developed for monolithic bracing members which do not having lacings in the member).

### **5.3 General Observations**

Twelve built-up laced bracing members having different slenderness ratios and width-to-thickness ratios were tested. Design tensile and compressive strengths of the specimens were calculated by the AISC LRFD Specification (but using actual instead of specified yield strength) and correlated with results obtained from testing. Cyclic hysteretic curves obtained from the

twelve test specimens were presented in various normalized manners. From the experimentally obtained hysteretic curves, ductility capacities of the specimens were obtained and compared with the recommended ductility demands. Hysteretic loops from the non-linear analyses were also presented and compared with those obtained from testing.

From the analysis of test results presented in this section, a number of observations can be made. First, the tensile strengths of test specimens were relatively well predicted by AISC LRFD Specification within ten percent aberration in most cases.

As generally noticed, compressive strengths of the bracing members largely depend on the effective length factor,  $K$ . From the SAP 2000 analyses of the specimens with slenderness ratio of 60, the theoretical effective length factor for these specimens was found to be, on average, 0.65. Compressive strengths of the specimens with  $KL/r = 60$  compared to within 20 percent accuracy with strengths calculated by the AISC LRFD Specification (for their appropriate buckling mode) when using this theoretical effective length. Initial imperfections had a major impact when calculating the expected compressive strength of the By8-60 specimen. The compressive strength of this specimen was approximately within 10 percent of the experimental value considering initial imperfection of the member, but only within 45 percent otherwise.

SAP 2000 analyses were also performed to establish the effective length factor,  $K$ , for specimens having a slenderness of 120. The theoretical  $K$  value of 1.0 was expected for the end conditions of these test specimens. SAP 2000 analyses showed  $K$  values slightly larger than 1.0. However, comparisons between the results obtained from testing and calculations following the AISC LRFD Specification with  $K$  value of 1.0 showed calculated values significantly underestimating (by approximately 50 percent) the compressive strength of the specimens with  $KL/r$  of 120. The reason for this discrepancy is unknown. Therefore, new effective length factors,  $K$  were calculated for which the AISC LRFD Specification would match the test results for the specimens. From these calculations, resulting effective length factor,  $K$  values for the specimens with  $KL/r$  of 120 varied from 0.76 to 0.93 (the average being 0.83). Both these calculated  $K$  values and theoretical ones ( $K = 1.0$ ) will be used for the calculations of low cycle fatigue life of the specimens in SECTION 6.

Ductility capacities obtained from the testing of specimens are presented in Table 5.10 and Figures 5.43 to 5.45. Note that the term  $\mu_y^*$  is used to quantify the tensile ductility reached before the significantly drops in tensile strength occur due to initial fracture. System capacity and demand ductilities are compared for each cross-section type.

Table 5.10 Ductility capacity comparisons

<i>Specimen</i>	$\mu_b$	$\mu_y$	$\mu_y^{*1}$	<i>Specimen</i>	$\mu_b$	$\mu_y$	$\mu_y^{*1}$
Ay16-60	4.60	4.69	2.67	Ay16-120	14.09	16.99	5.00
Ay8-60	6.89	1.65 <sup>*2</sup>	1.65 <sup>*2</sup>	Ay8-120	7.85	9.51	3.72
By16-60	5.48	7.33	3.71	By16-120	5.74	8.83	5.68
By8-60	8.26	8.60	4.67	By8-120	4.12	5.11	3.09
Bx16-60	2.29	2.77	2.29	Bx16-120	4.63	4.71	3.23
Bx8-60	3.71	3.63	2.56	Bx8-120	4.32	3.86	2.89

\*1 Ductility before relatively large strength degradation in tension after initial fracture observed.

\*2 Specimen Ay8-60 did not reach its maximum tensile strength.

For specimens having section shape “A” (Figure 5.10), specimens having KL/r of 120 had sufficient ductility to meet the ductility demand of 3.0. The specimen Ay16-60 barely met the target ductility demand of 3.0 and upon initial fracture of the specimen at experimentally obtained ductility of 2.67, tensile strength dropped rapidly. Finally, results for specimen Ay8-60 are inconclusive because that specimen was not tested in tension for reason explained earlier.

Specimens with section shape “By”, all exhibited satisfactory ductility capacity and met the target ductility demand of 3.0. Specimen By16-120 and By8-60 reached the largest ductility capacity in tension although the drop in tension strength was more sudden for the By16-120 specimen than for the By8-60 specimen. The other two specimens exhibited development and progression of fracture almost immediately after the target ductility was reached.

Specimens with section shape “Bx” exhibited the worst cyclic inelastic performance, where all specimens failed to reach the target ductility of 3.0 before starting to fracture with the exception of the Bx16-120 specimen which fractured just after reaching the target ductility of 3.0. Specimen Bx16-60 had the worst behavior of all specimens in this category as it started to develop fracture at ductility less than 2.0.

Overall, specimens with both larger slenderness and width-to-thickness ratio showed best ductility performance while the specimens with smaller slenderness and larger width-to-thickness ratio showed the worst ductility capacity. For the specimens with slenderness ratio,  $KL/r$  of 60, specimens designed with larger width-to-thickness ratios,  $b/t$ , showed lower ductility capacity than those designed with smaller  $b/t$ , because local buckling precipitated low cycle fatigue. However, comparing the ductility of the specimens with  $KL/r$  of 120, it appears that ductility capacity of the slender specimens was not much affected by the  $b/t$  ratios. Note that initial global buckling was observed during the testing of the specimens with  $KL/r$  of 120, irrespectively of their  $b/t$  ratios.

Overall, specimens with section shape “A” exhibited the most ductile behavior, and specimens with section shape “Bx” the worst.

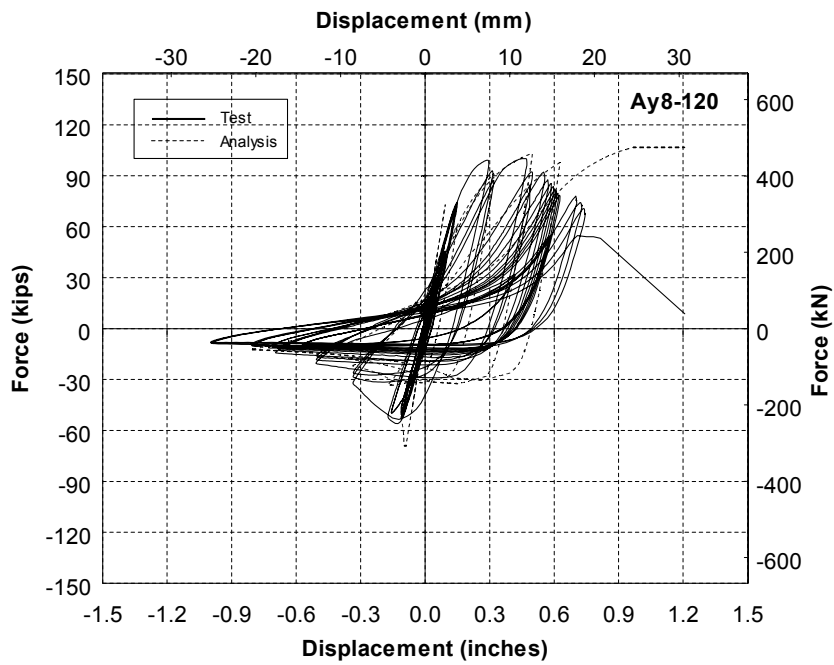


Figure 5.26 Comparison between analysis and experimental results of Ay8-120 specimen (Theoretical  $K = 1.0$ )

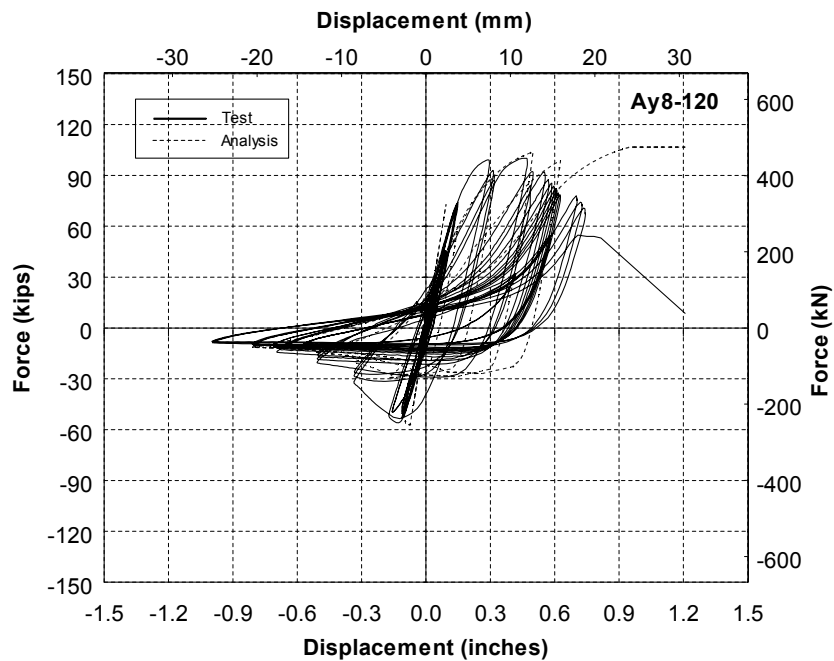


Figure 5.27 Comparison between analysis and experimental results of Ay8-120 specimen (Experimental  $K = 0.91$ )

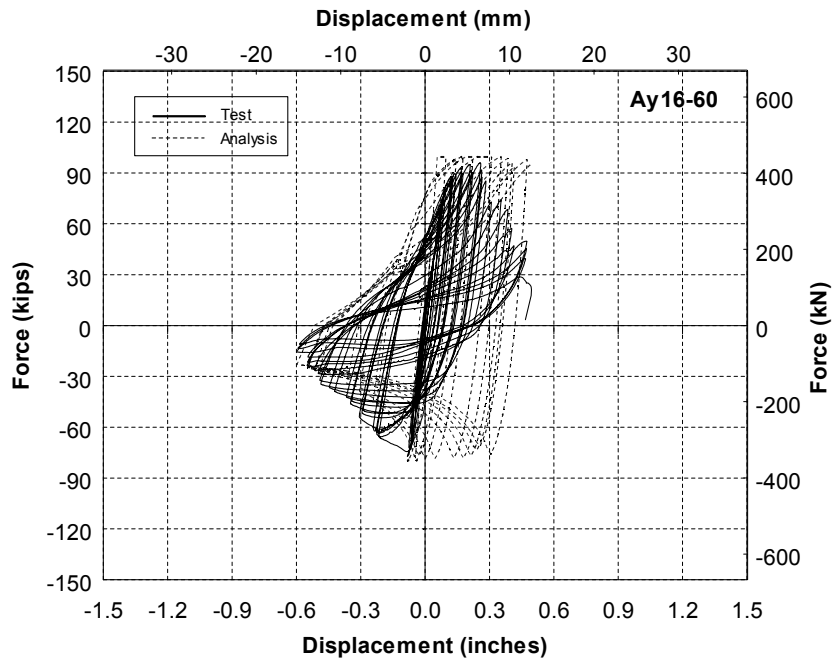


Figure 5.28 Comparison between analysis and experimental results of Ay16-60 specimen

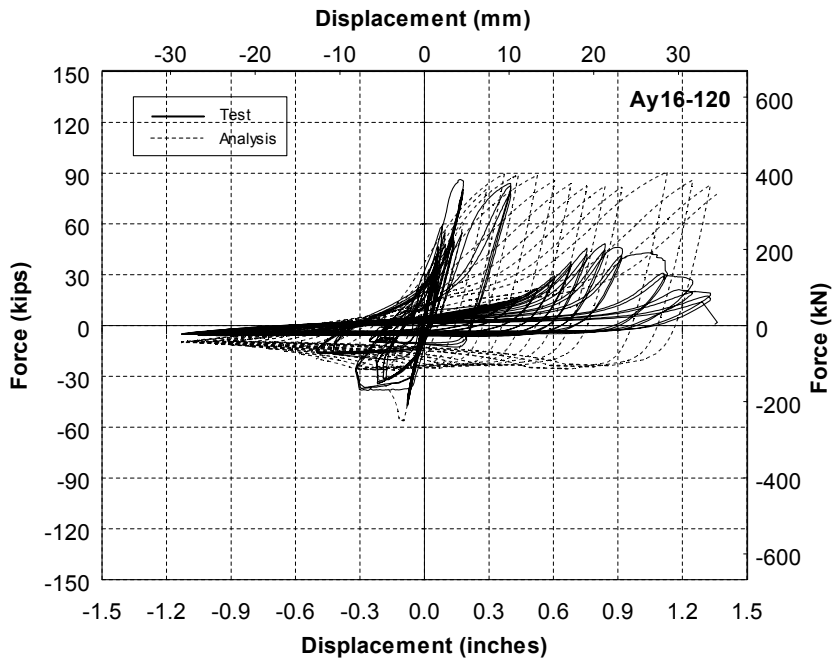


Figure 5.29 Comparison between analysis and experimental results of Ay16-120 specimen (Theoretical K = 1.0)

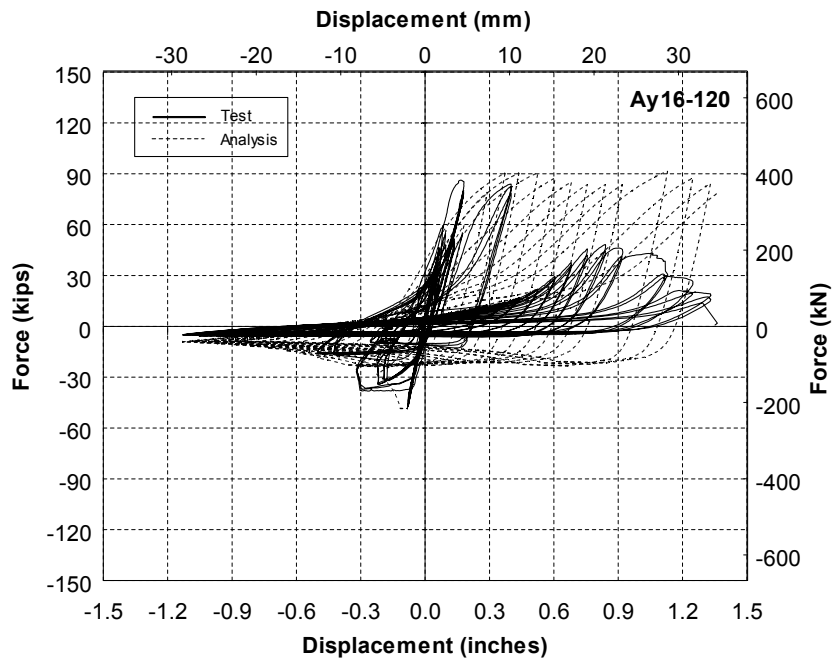


Figure 5.30 Comparison between analysis and experimental results of Ay16-120 specimen (Experimental  $K = 0.93$ )

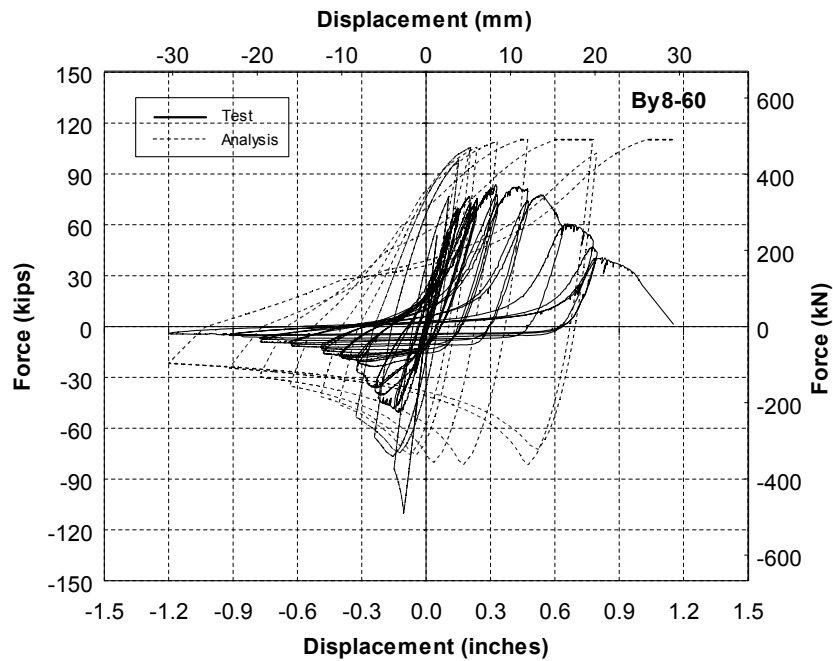


Figure 5.31 Comparison between analysis and experimental results of By8-60 specimen

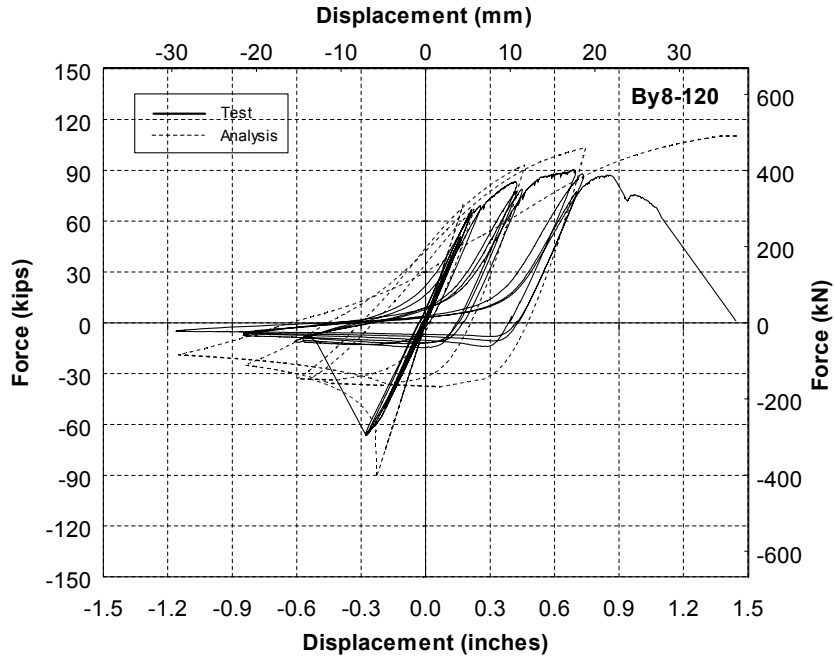


Figure 5.32 Comparison between analysis and experimental results of By8-120 specimen (Theoretical  $K = 1.0$ )

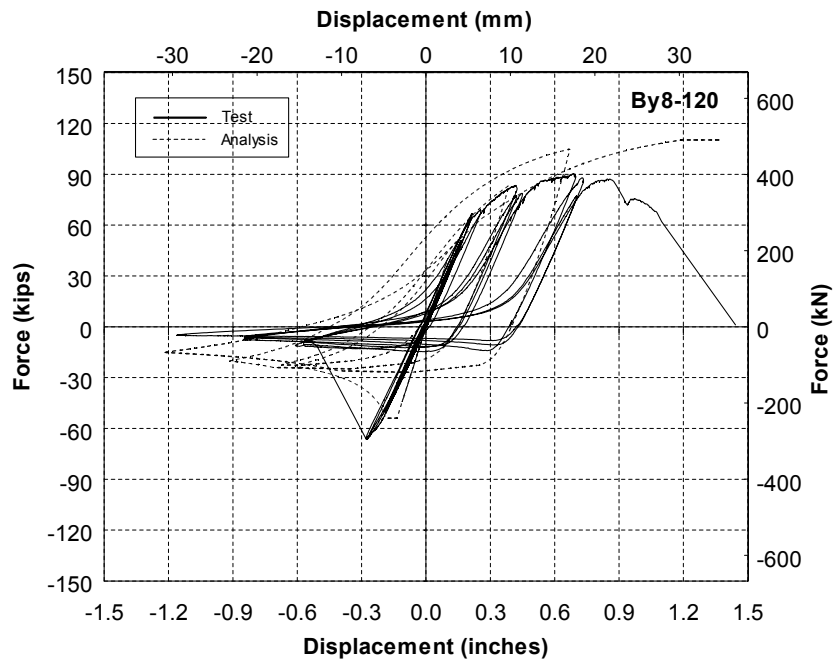


Figure 5.33 Comparison between analysis and experimental results of By8-120 specimen (Experimental  $K = 0.77$ )

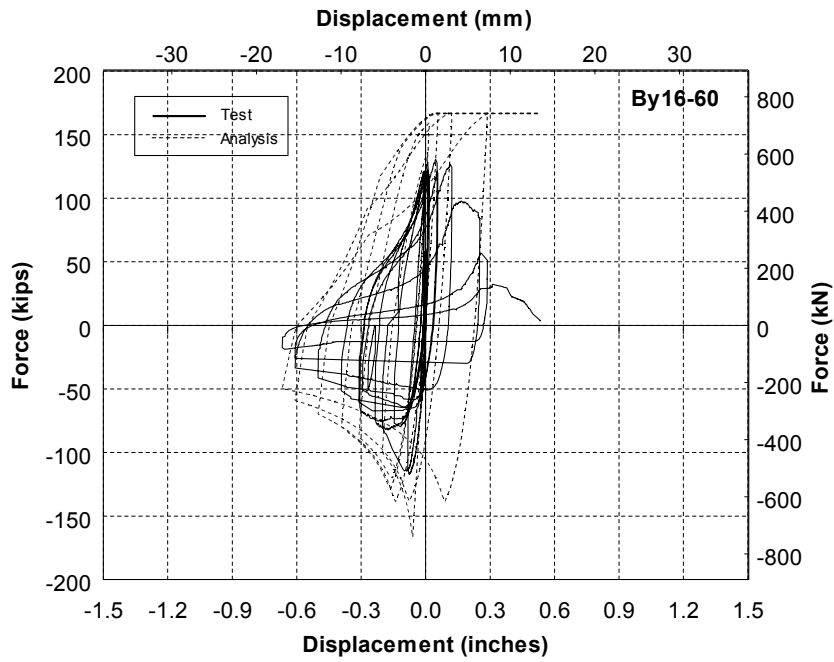


Figure 5.34 Comparison between analysis and experimental results of By16-60 specimen

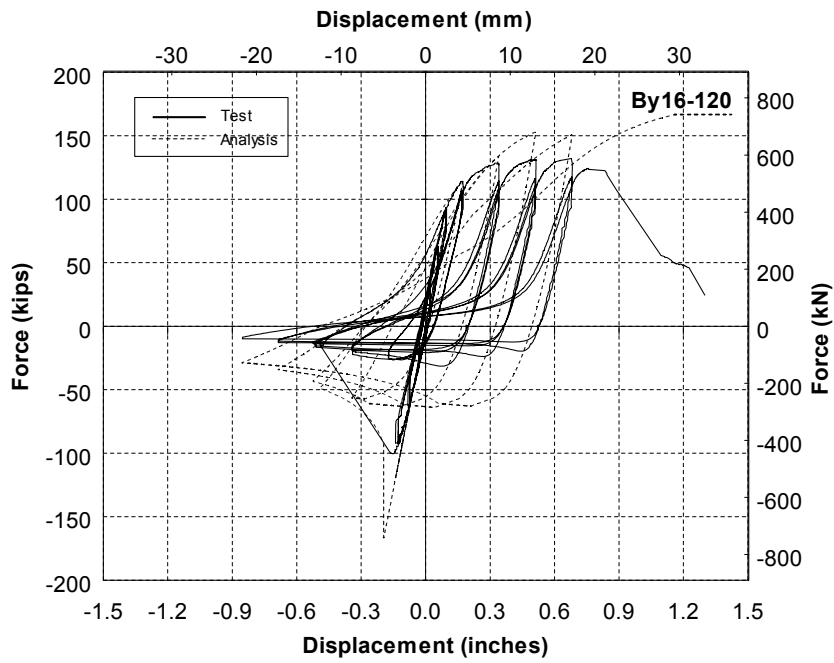


Figure 5.35 Comparison between analysis and experimental results of By16-120 specimen (Theoretical  $K = 1.0$ )

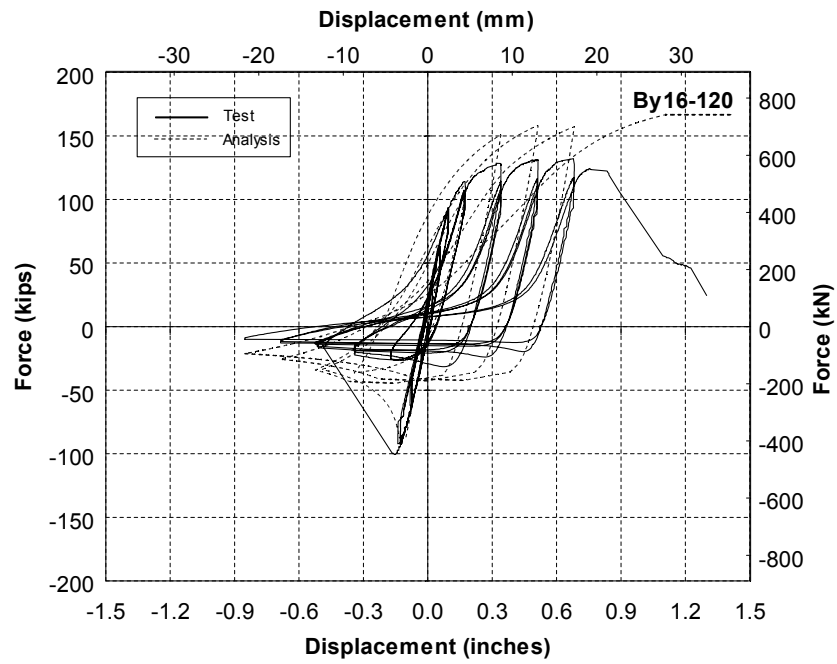


Figure 5.36 Comparison between analysis and experimental results of By16-120 specimen (Experimental  $K = 0.71$ )

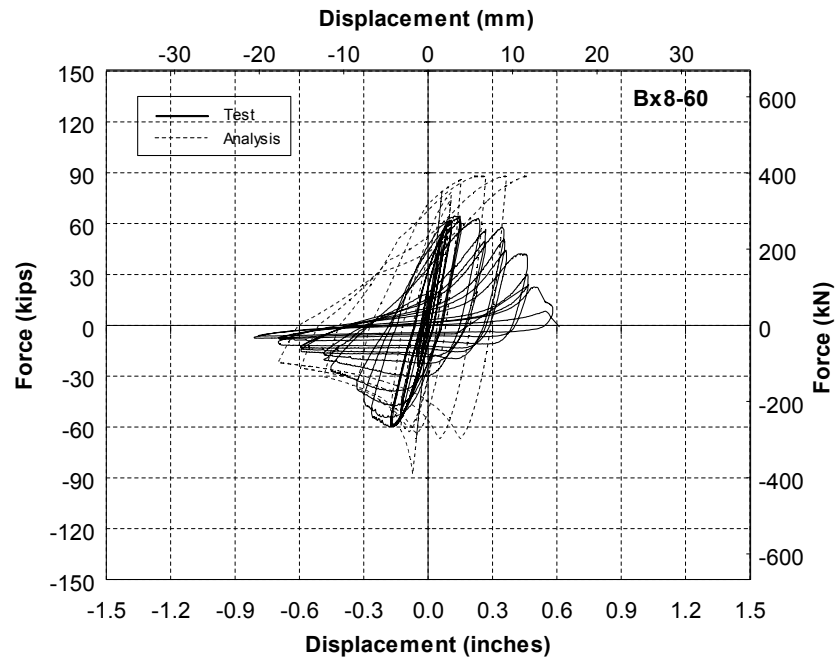


Figure 5.37 Comparison between analysis and experimental results of Bx8-60 specimen

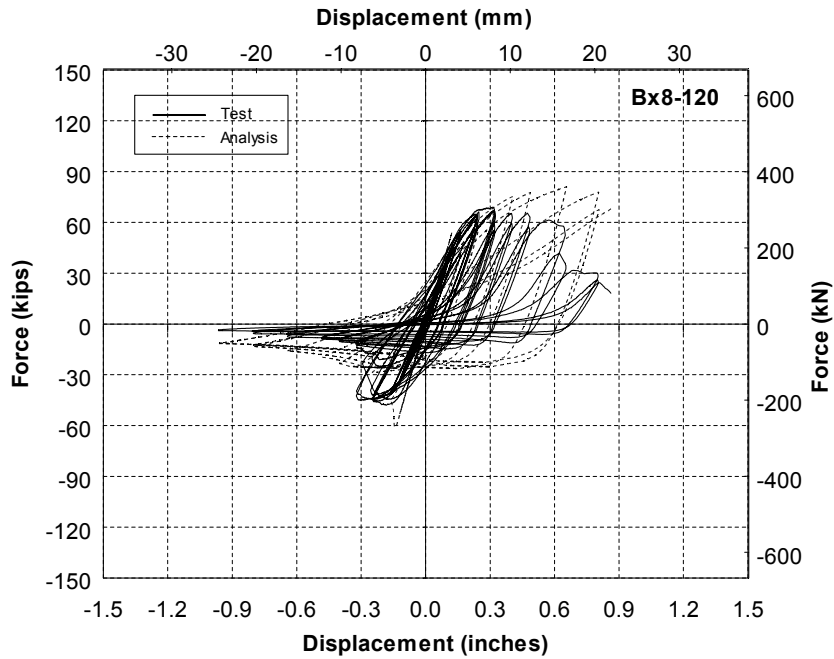


Figure 5.38 Comparison between analysis and experimental results of Bx8-120 specimen (Theoretical  $K = 1.0$ )

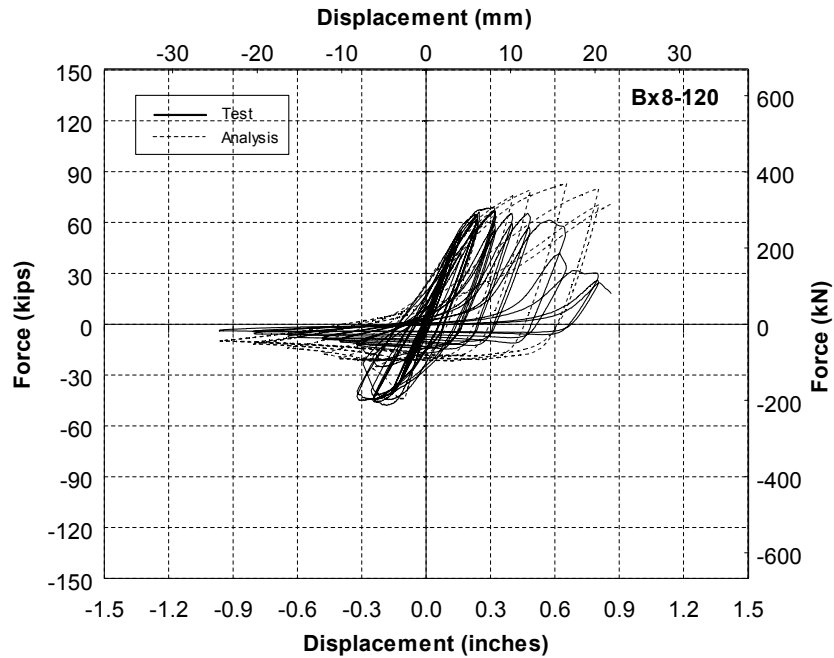


Figure 5.39 Comparison between analysis and experimental results of Bx8-120 specimen (Experimental  $K = 0.85$ )

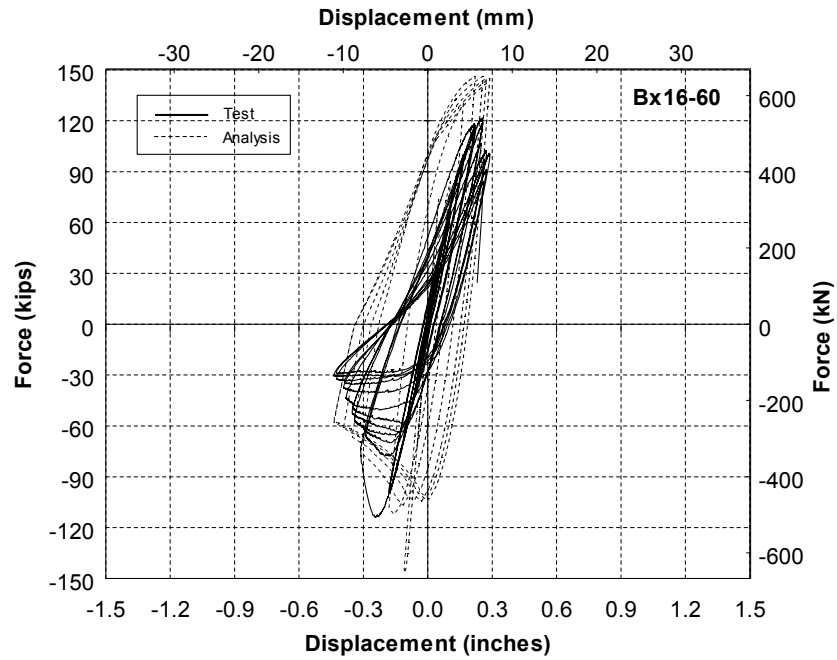


Figure 5.40 Comparison between analysis and experimental results of Bx16-60 specimen

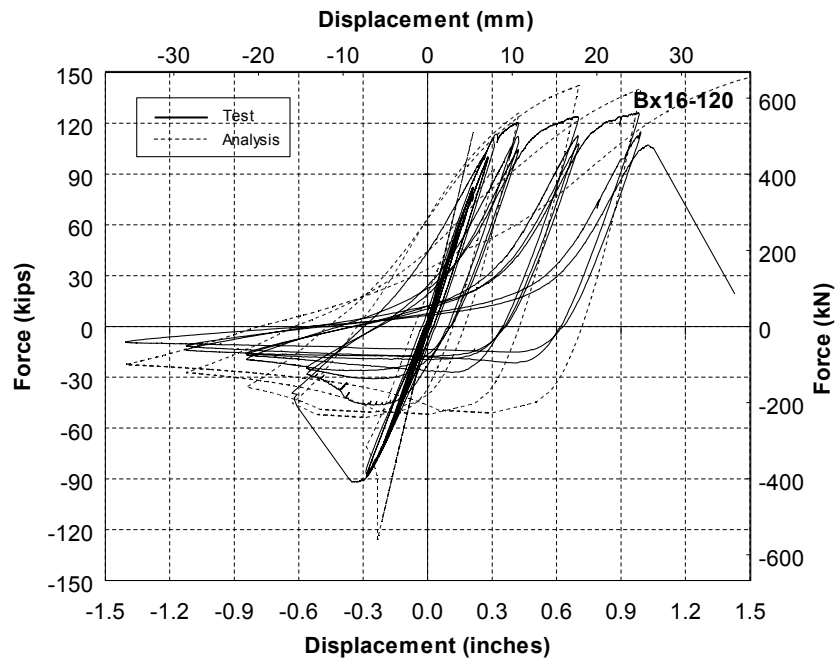


Figure 5.41 Comparison between analysis and experimental results of Bx16-120 specimen (Theoretical  $K = 1.0$ )

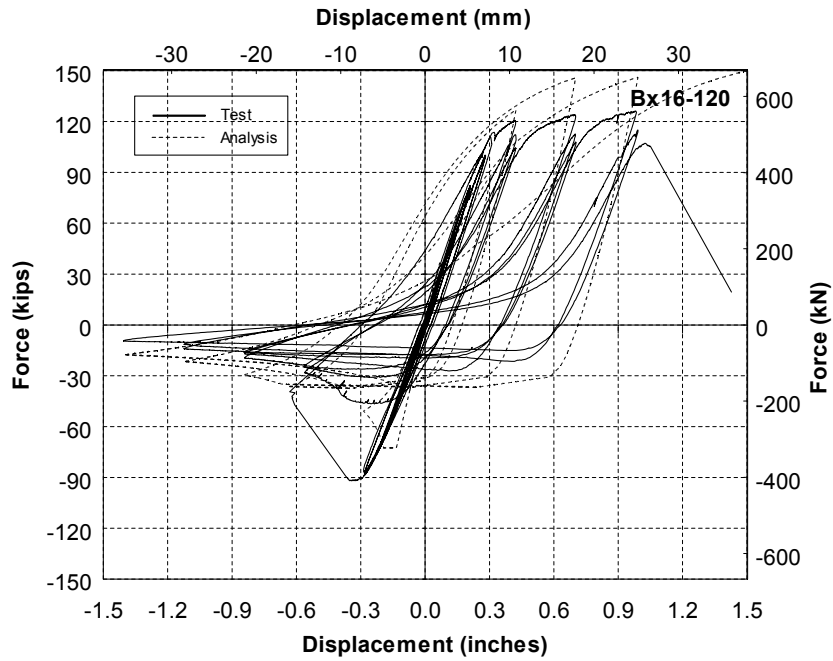


Figure 5.42 Comparison between analysis and experimental results of Bx16-120 specimen (Experimental  $K = 0.76$ )

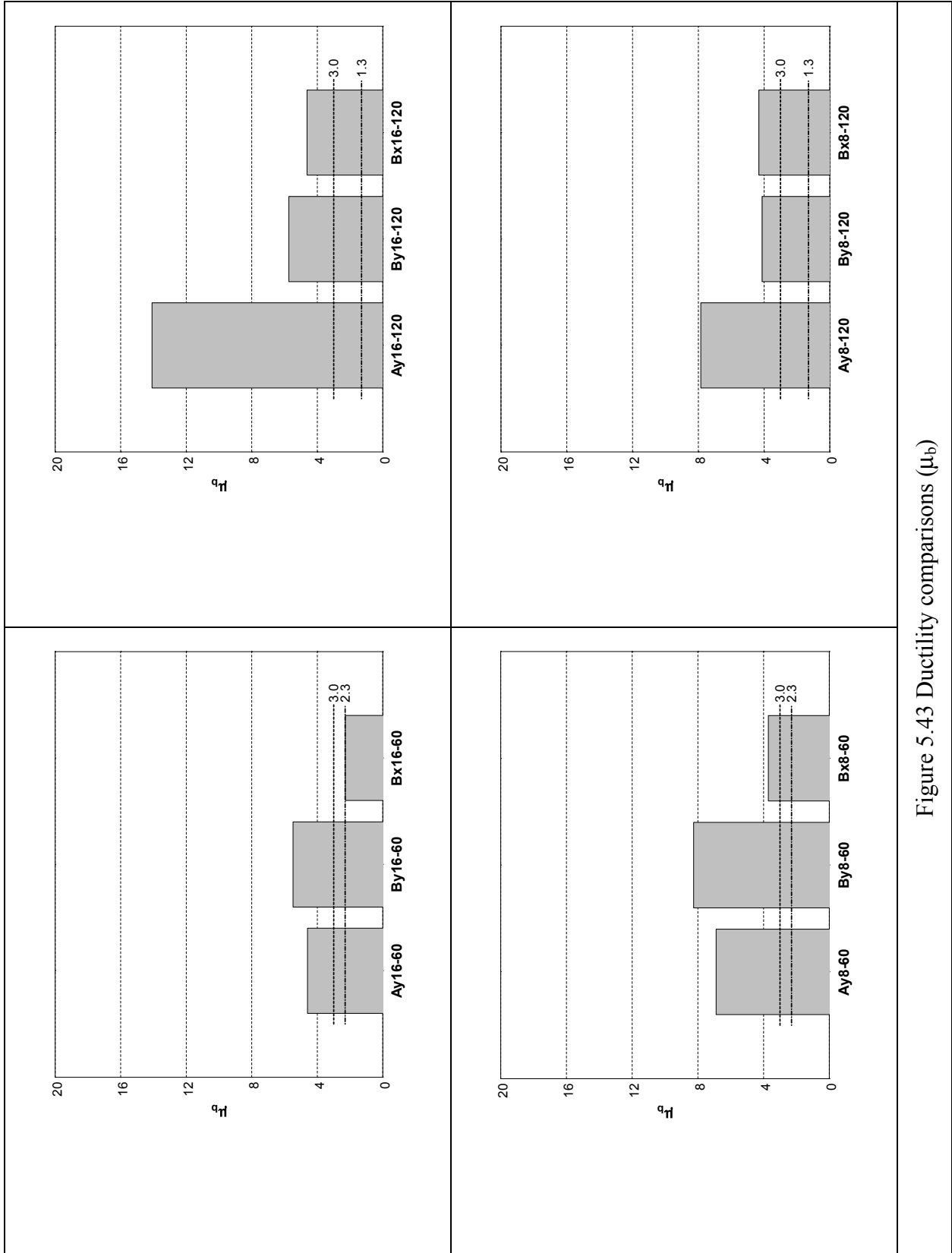


Figure 5.43 Ductility comparisons ( $\mu_b$ )

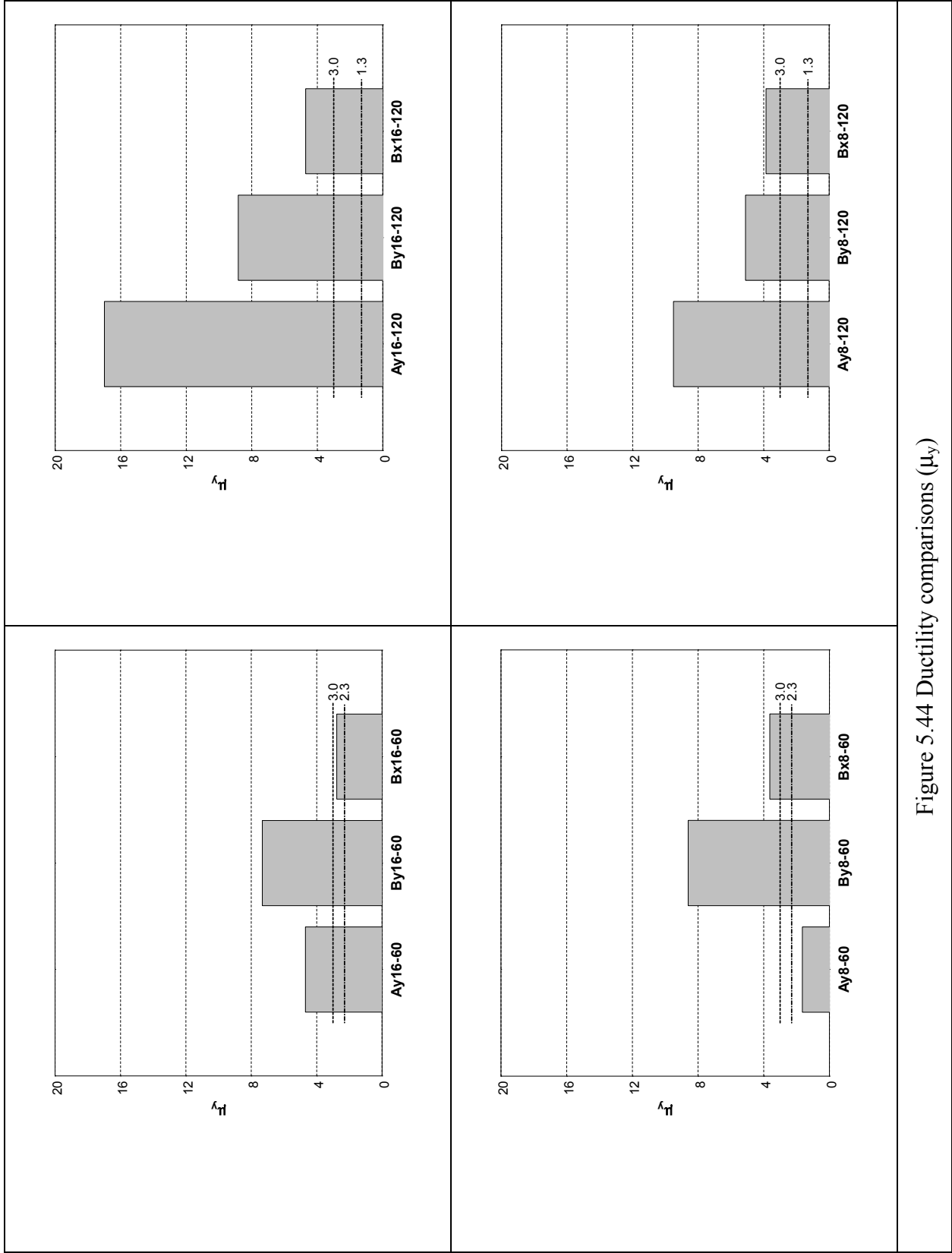


Figure 5.44 Ductility comparisons ( $\mu_y$ )

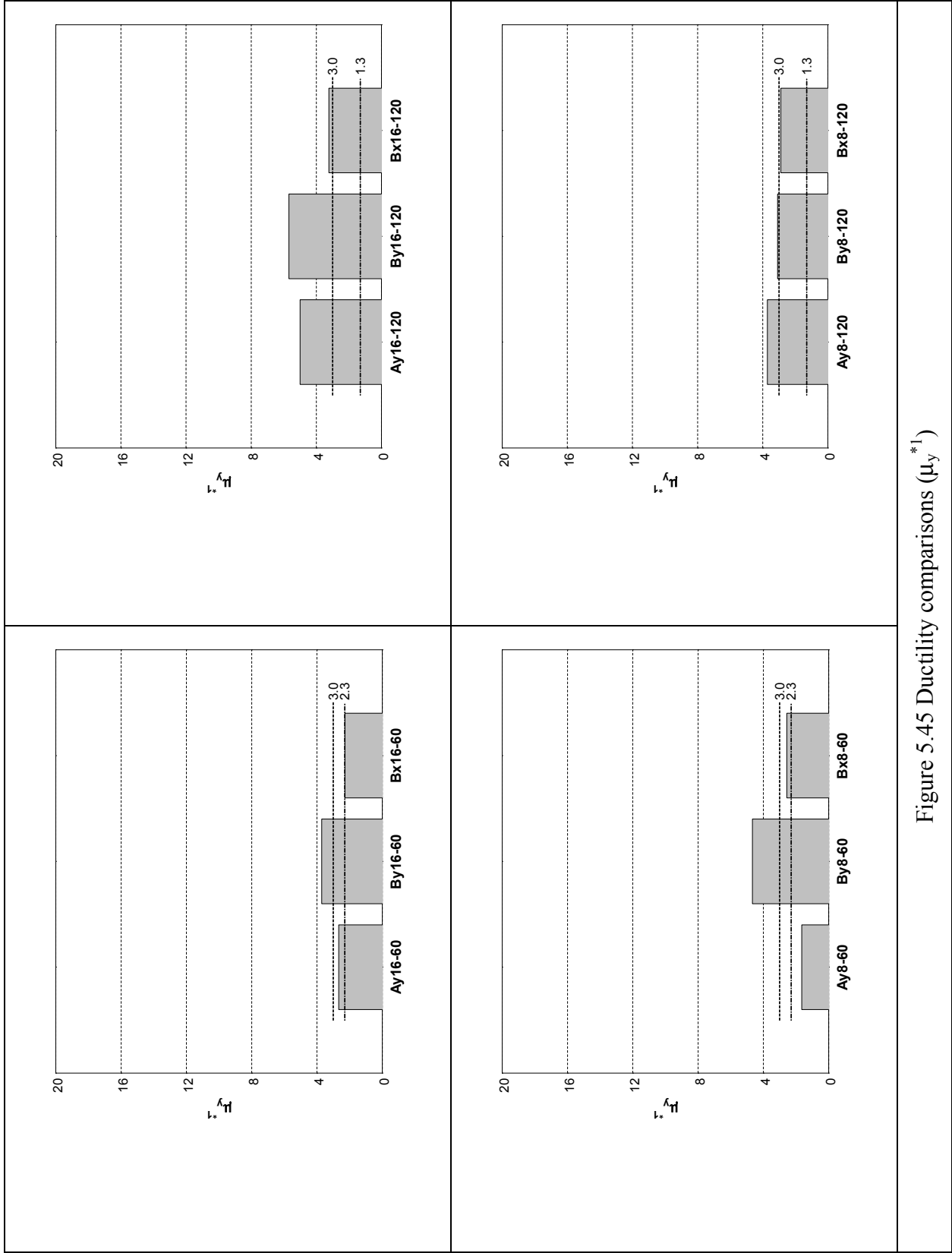


Figure 5.45 Ductility comparisons ( $\mu_y^*$ )



## SECTION 6

### ANALYSIS OF RESULTS – NORMALIZED COMPRESSION STRENGTH, NORMALIZED HYSTERETIC ENERGY, AND LOW CYCLE FATIGUE RESULTS

This section quantitatively describes the hysteretic characteristics and low cycle fatigue life of the specimens obtained from test results. Energy dissipation capacity in compression and the compressive strength degradation after buckling of the specimens are quantified and compared using the same methodology introduced in SECTION 5. Low cycle fatigue fracture life of the specimens is also quantified and compared with those predicted by the equations proposed by Tang and Goel (1987) and Archambault et al. (1995).

#### 6.1 Energy Dissipation

To assess the energy dissipation capacity of built-up laced compression members, the energy dissipated during testing by each specimen was calculated from the experimentally obtained hysteretic force-axial deformation curves of the specimens. The tension and compression energy dissipation was calculated for each cycle as a product of the compression or tension force times the axial deformation. Calculated energy dissipation was then normalized to facilitate comparison between results from the specimens. The normalized energy,  $E_C/E_{T,cal}$  or  $E_T/E_{T,cal}$  is obtained by dividing the compressive or tensile energy by the corresponding theoretical tensile energy,  $E_{T,cal}$ , defined as the energy that would have been dissipated by the member in tension if the same maximum axial displacement was reached during unloading of the member after its elongation as schematically shown in Figure 6.1 (Lee and Bruneau, 2002). Note that the term,  $E_{T,cal}$  is identical with  $E_T$  used by Lee and Bruneau (2002) and the reason for using different notation in this section is to differentiate with the calculated energy dissipation in tension obtained from testing. Here,  $E_C$  and  $E_T$  respectively represent the calculated energy dissipation in compression and tension obtained from testing. Note that the axial deformation in compression,  $\delta$ , is measured from the point of zero member force (which may not correspond to

the original zero displacement position) up to the point of maximum compressive deformation, as illustrated in Figure 6.2 (Lee and Bruneau, 2002). The resulting plots of normalized energy as a function of normalized axial deformation,  $\delta/\delta_{b,exp}$ , of the specimens are shown in Figures 6.3 to 6.8. In these figures, only normalized energy dissipation of the specimens in compression ( $E_C/E_{T,cal}$ ) is presented and others such as normalized energy dissipation in tension ( $E_T/E_{T,cal}$ ) and normalized energy dissipation of sum of tension and compression ( $(E_C+E_T)/E_{T,cal}$ ) are presented in Appendix D. Four resulting figures are presented in each figure for a given brace type, as was done for the comparisons of hysteretic curves in SECTION 5. Normalized energy ratio of each cycle of the specimens was then accumulated until the entire fracture of the specimens and results are summarized in Table 6.1 and compared in Figures 6.9 and 6.10.

Table 6.1 Cumulative energy dissipation ratios capacity of the specimens

Specimen	$\Sigma(E_C / E_{T,cal})$		$\Sigma(E_T / E_{T,cal})$		$\Sigma[(E_C+E_T) / E_{T,cal}]$	
	Element	System	Element	System	Element	System
Ay8-60* <sup>1</sup>	3.06	2.74	1.53	1.53	4.60	4.27
Ay8-120	4.02		4.78		8.79	
Ay16-60	7.61	8.43	7.53	9.46	15.14	17.89
Ay16-120	4.52		3.97		8.49	
By8-60	2.71	2.90	2.94	3.16	5.65	6.06
By8-120	1.19		1.52		2.71	
By16-60	4.78	4.80	4.39	6.34	9.17	11.22
By16-120	1.38		2.52		3.91	
Bx8-60	3.97	4.42	3.57	4.27	7.54	8.69
Bx8-120	4.31		4.78		9.09	
Bx16-60	3.47	4.30	3.05	4.43	6.51	8.72
Bx16-120	1.86		2.19		4.05	

\*1 Specimen Ay8-60 did not reach its maximum tensile strength.

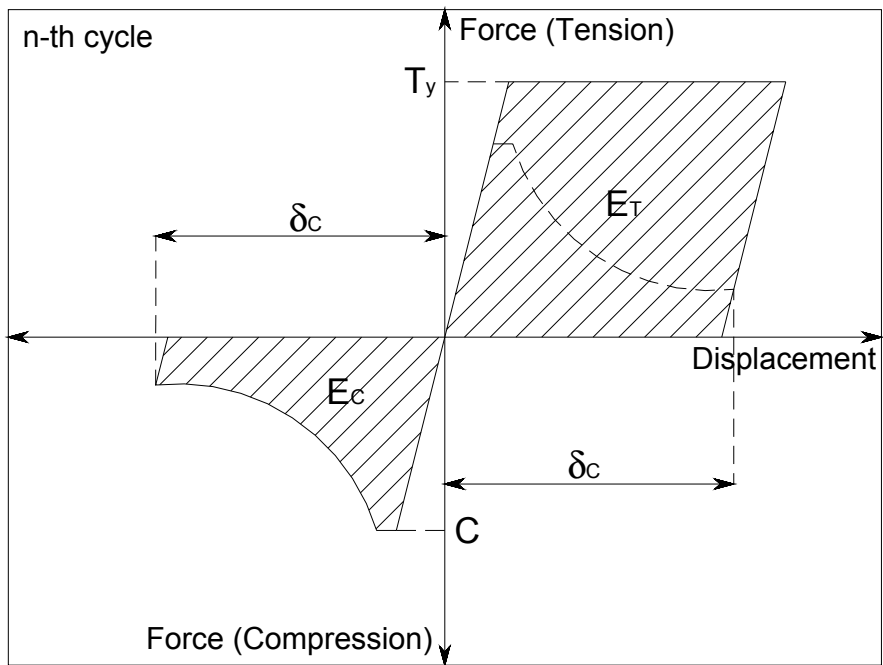


Figure 6.1 Definition of dissipated energy ratio,  $E_C / E_T$  (Lee and Bruneau, 2002)

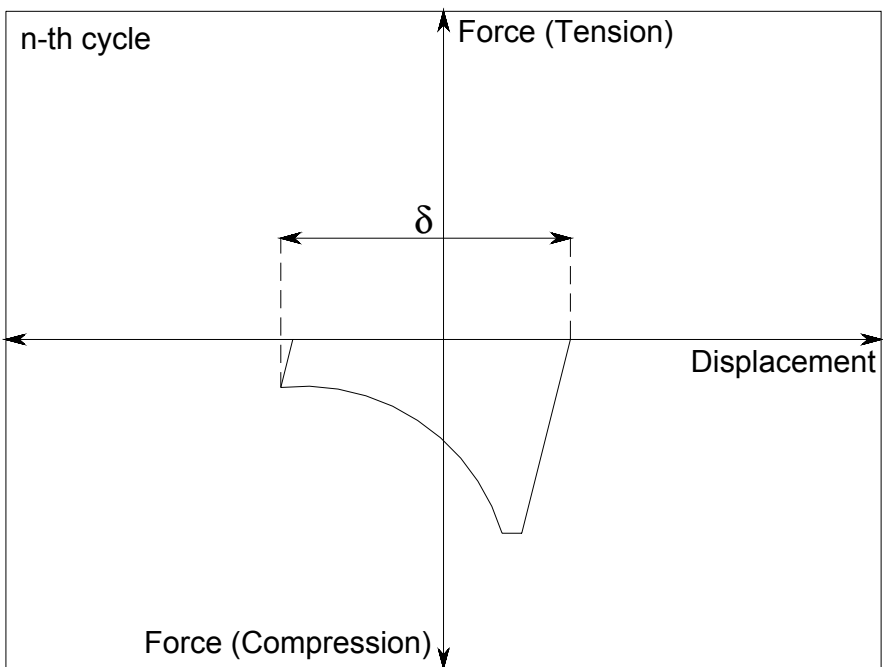


Figure 6.2 Definition of axial displacement,  $\delta$  (Lee and Bruneau, 2002)

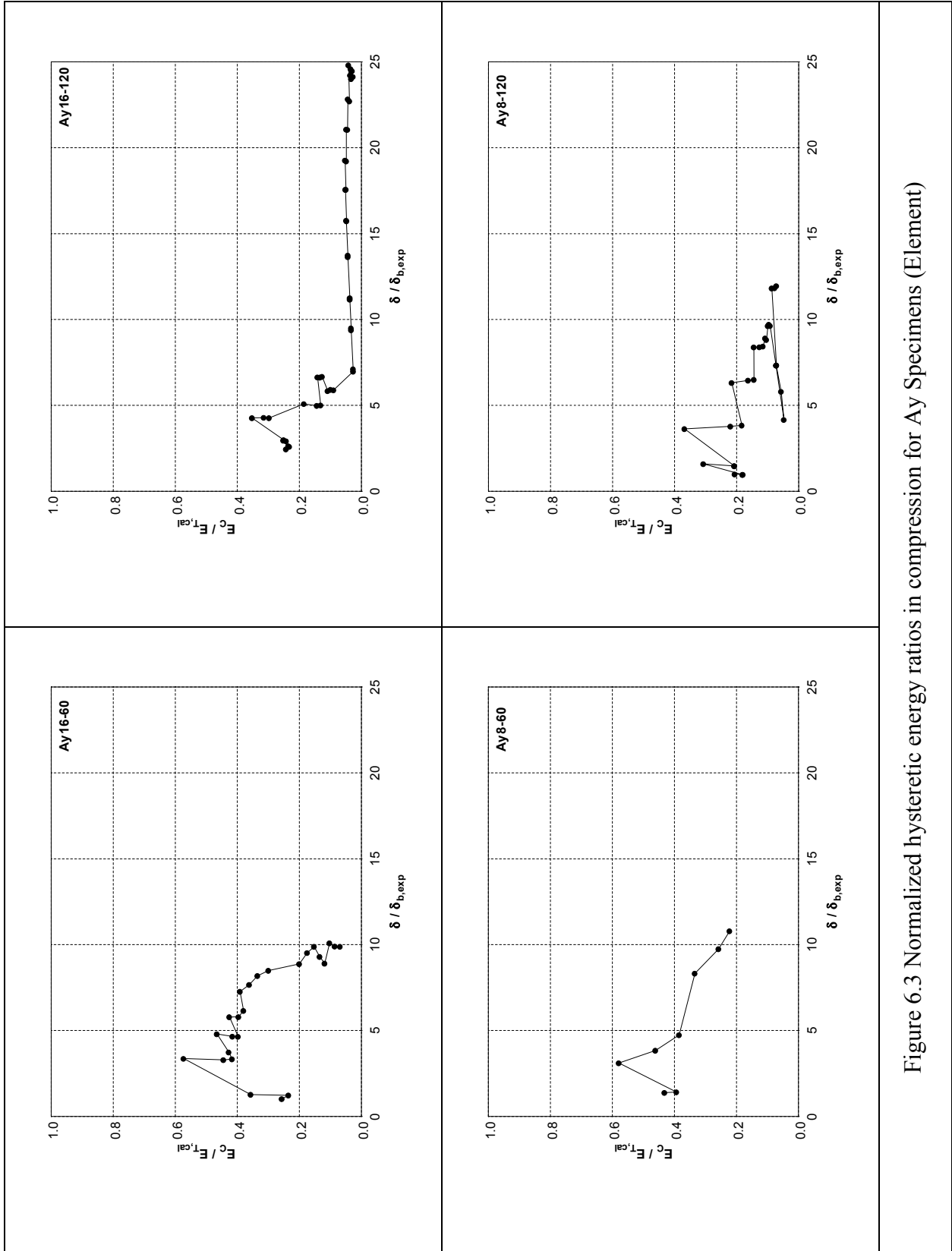


Figure 6.3 Normalized hysteretic energy ratios in compression for Ay Specimens (Element)

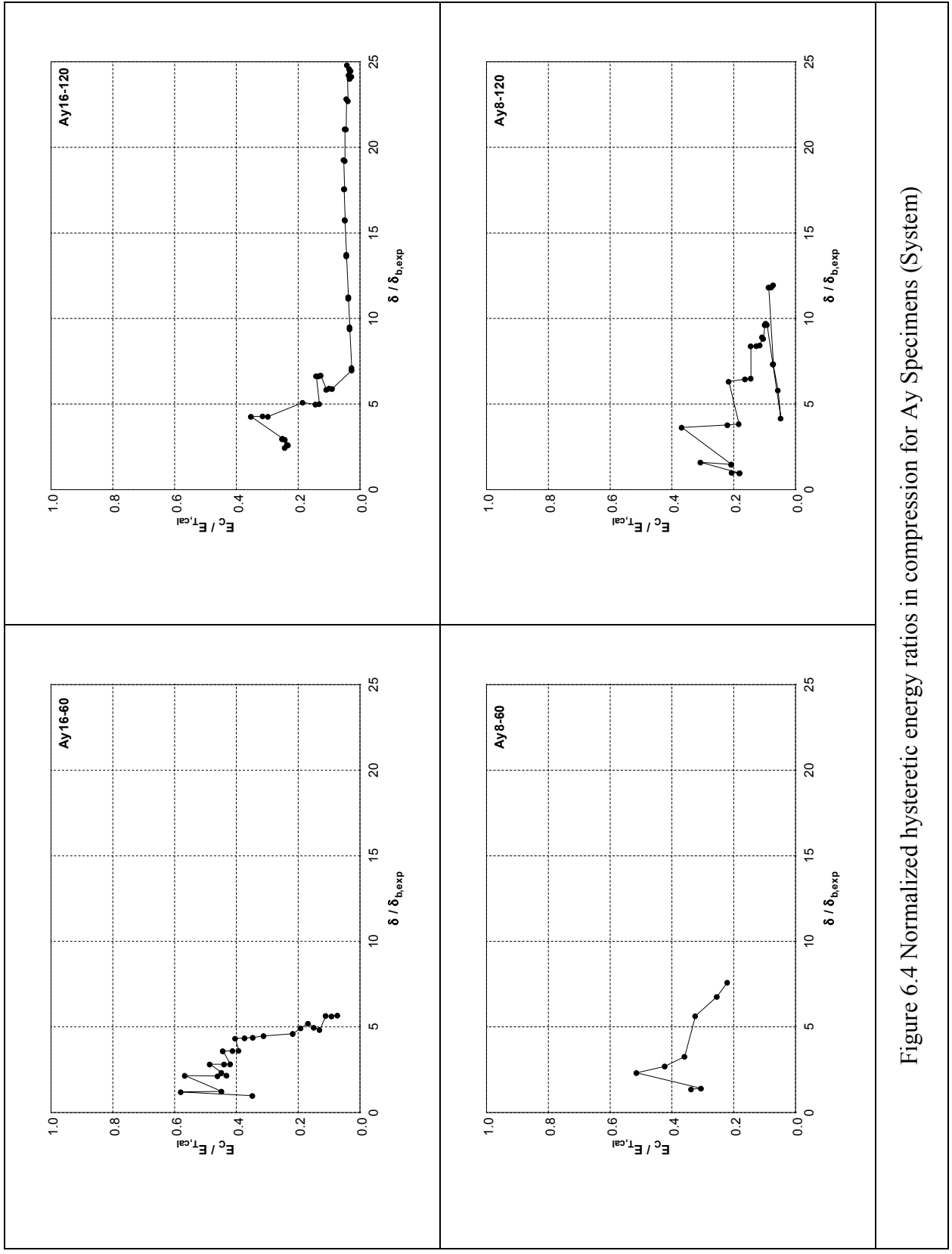


Figure 6.4 Normalized hysteretic energy ratios in compression for Ay Specimens (System)

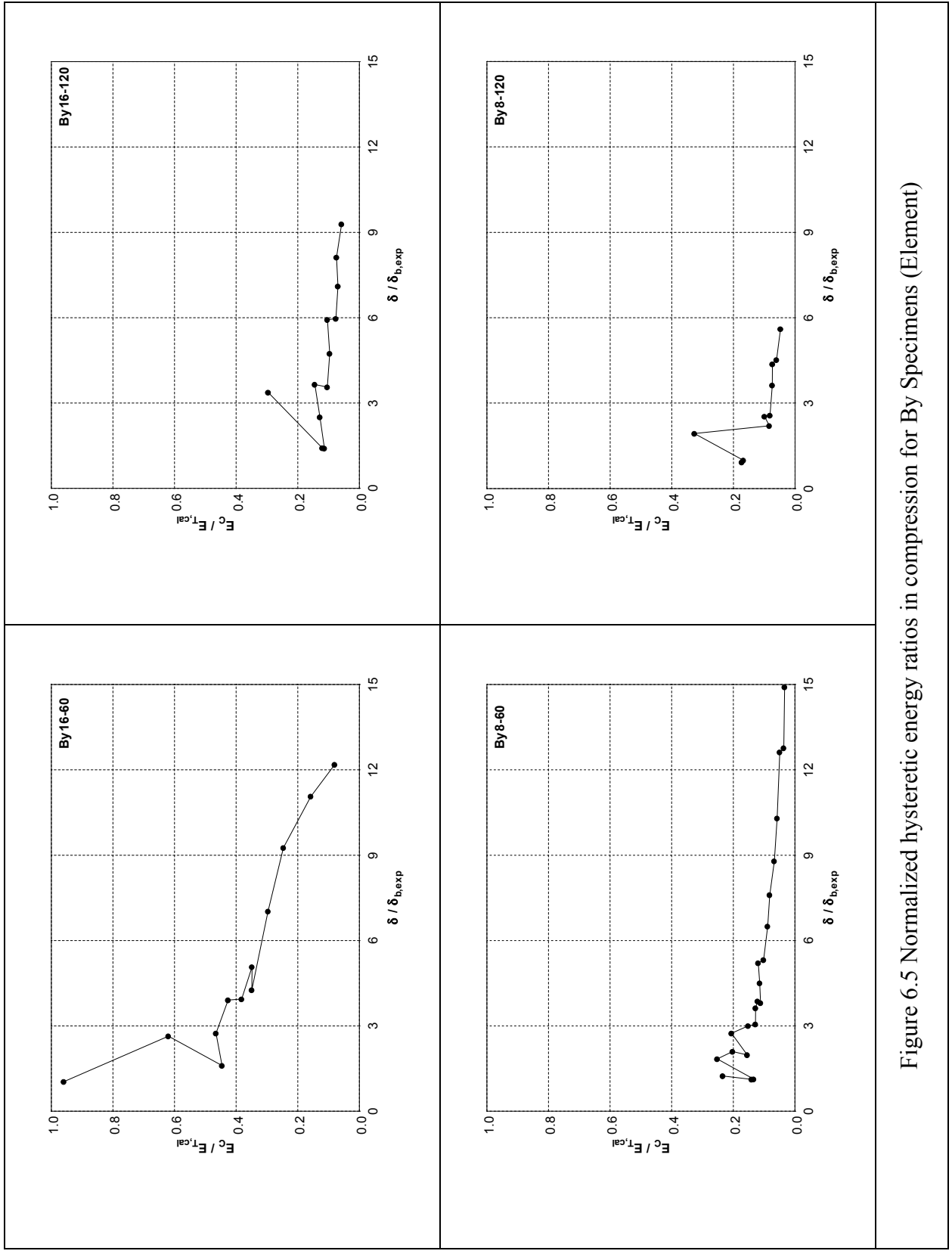


Figure 6.5 Normalized hysteretic energy ratios in compression for By Specimens (Element)

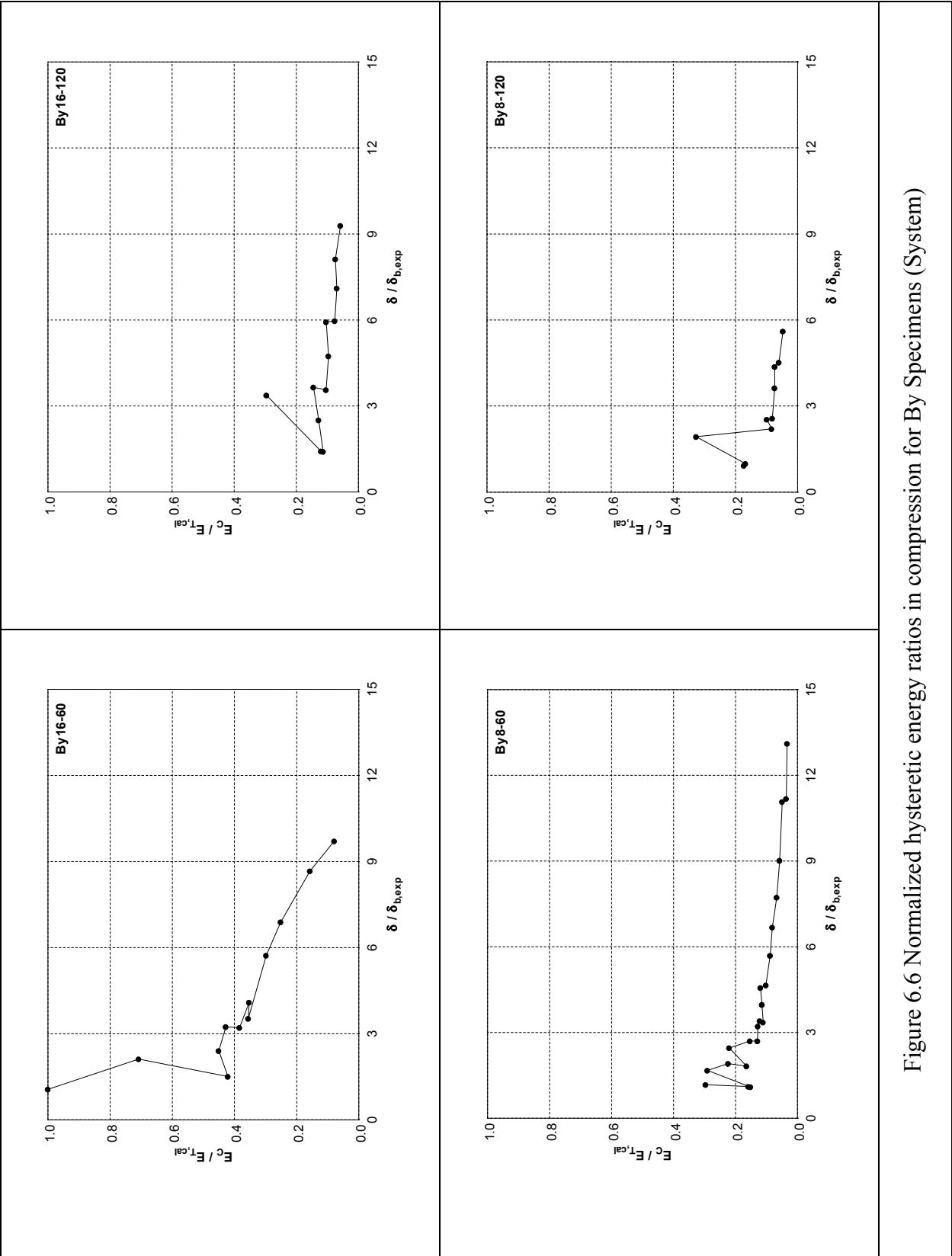


Figure 6.6 Normalized hysteretic energy ratios in compression for By Specimens (System)

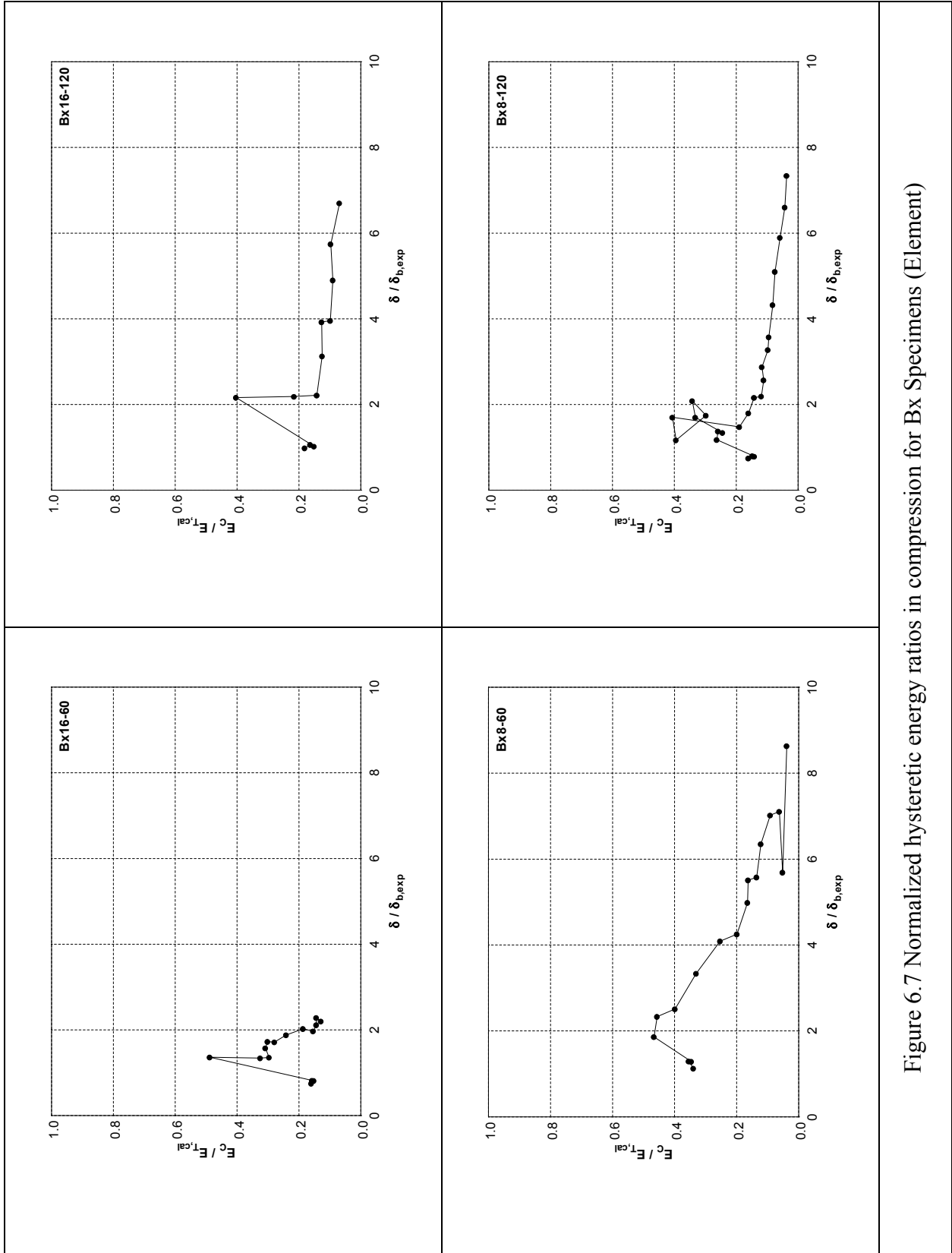


Figure 6.7 Normalized hysteretic energy ratios in compression for Bx Specimens (Element)

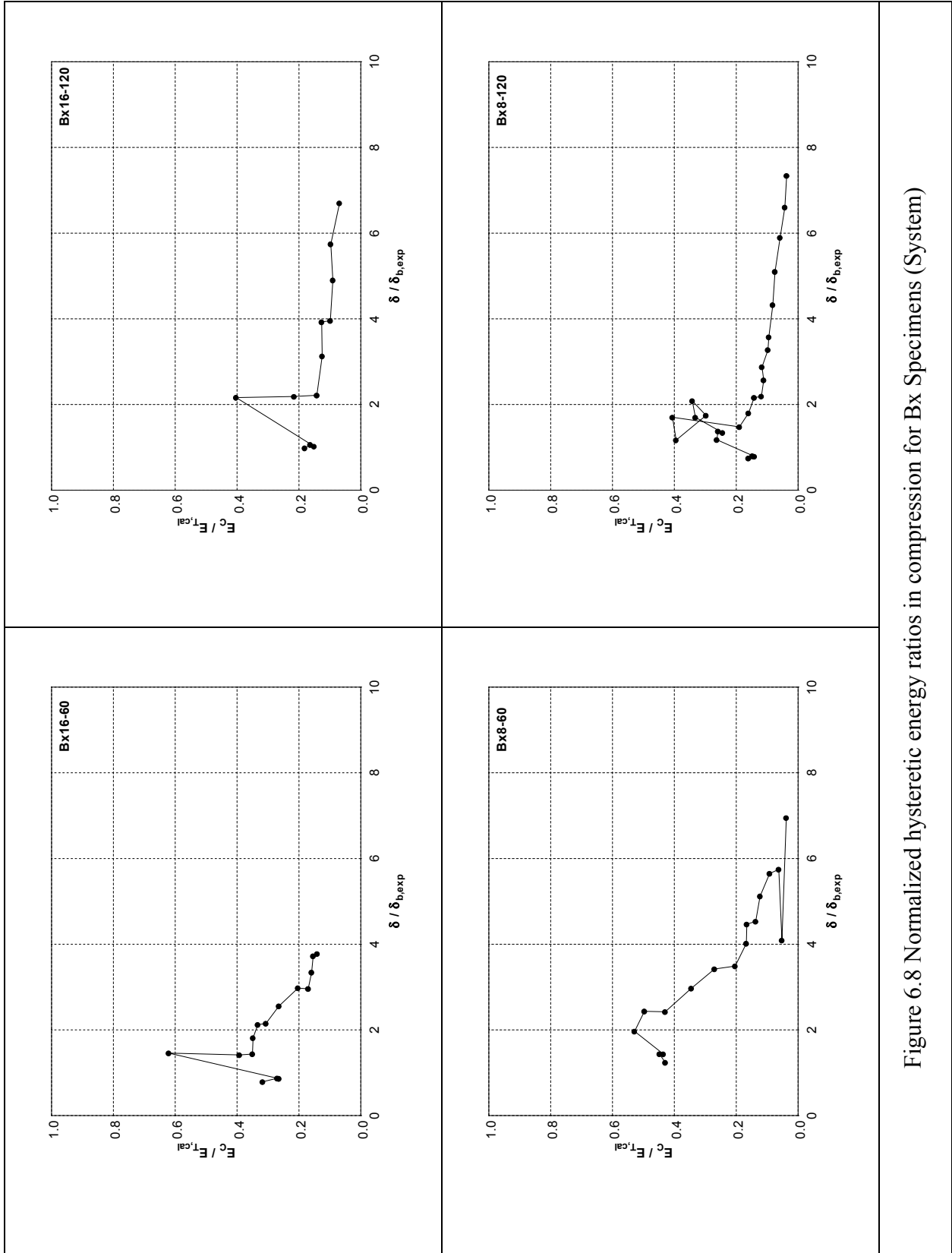


Figure 6.8 Normalized hysteretic energy ratios in compression for Bx Specimens (System)

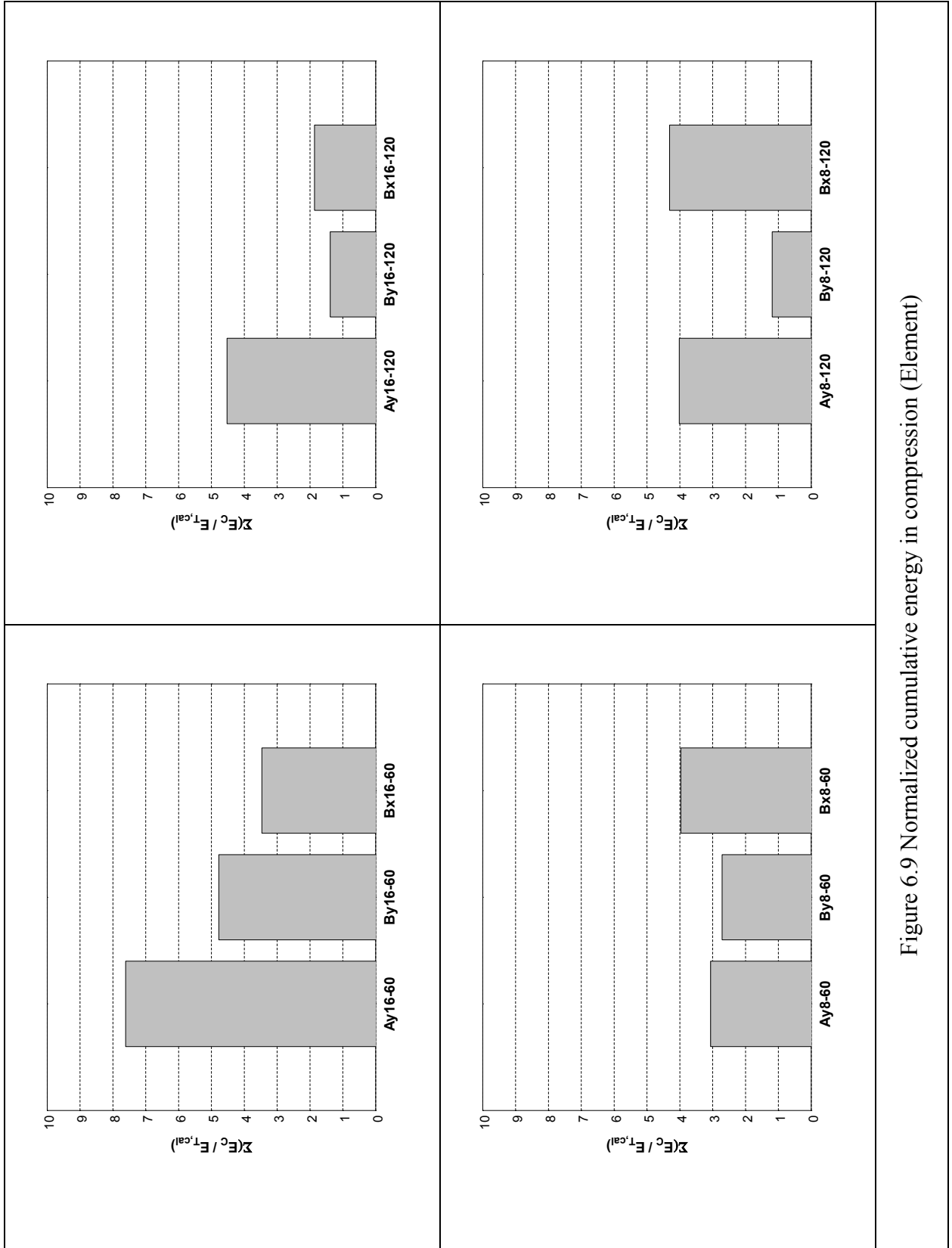


Figure 6.9 Normalized cumulative energy in compression (Element)

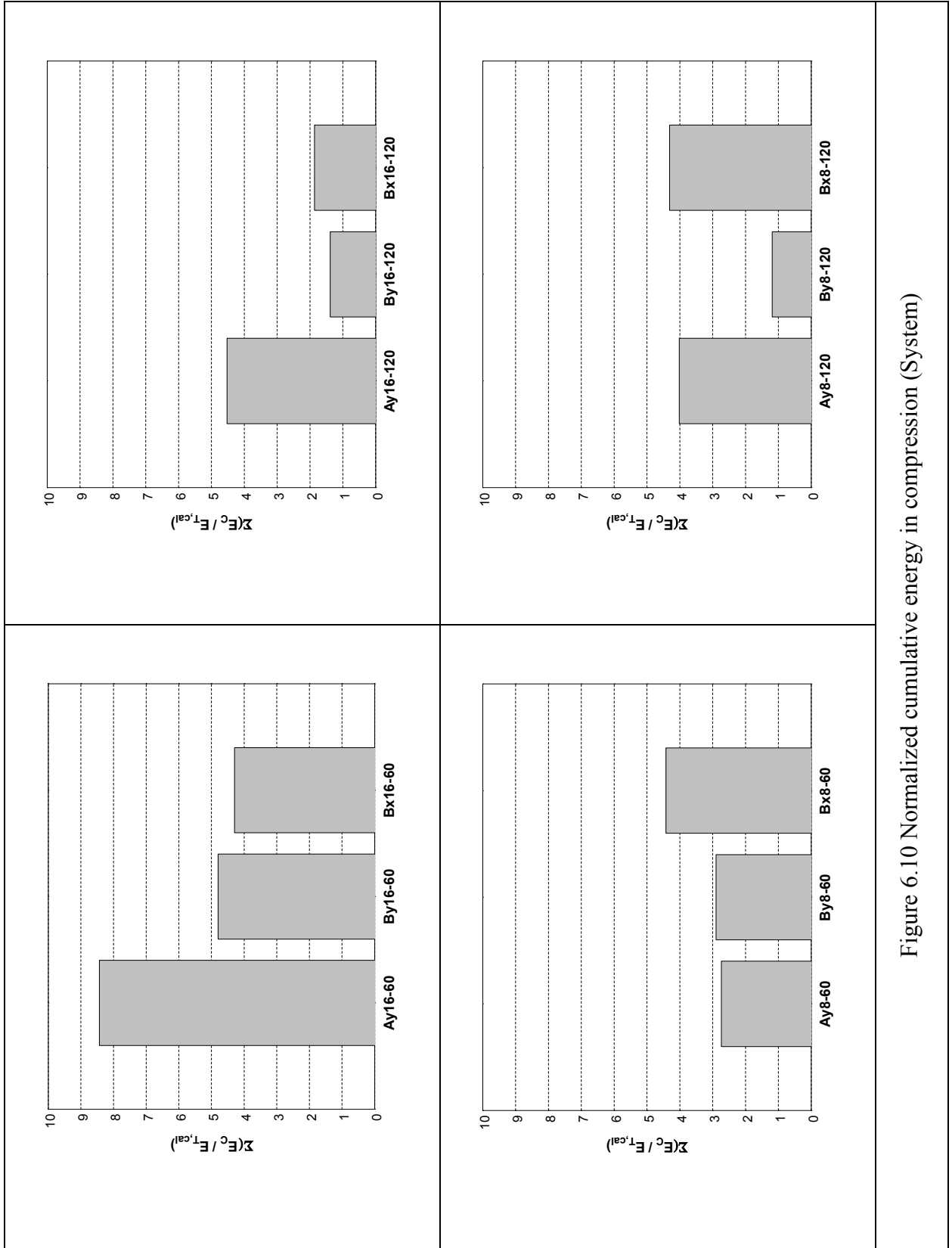


Figure 6.10 Normalized cumulative energy in compression (System)

## 6.2 Strength Degradation

Strength degradation of the compression member after buckling depends on their slenderness ratios and width-to-thickness ratios. To quantify the strength degradation of the built-up laced compression specimens upon repeated cycling loads, test results were processed following the same procedures as schematically shown in Figures 6.11 and 6.12, which were used by Lee and Bruneau (2002). The strength degradation of the specimens in compression, in terms of  $C_r''/C_r(\text{first})$ ,  $C_r''/C_r(\text{last})$ , and  $C_r''/C_r(\text{first/last})$ , were obtained at the various levels of normalized deformations (using the experimentally obtained buckling displacement,  $\delta_{b,\text{exp}}$ ) for each specimen. Resulting curves obtained from these procedures are shown in Figures 6.13 to 6.30. In these figures, strength degradation of the specimens were also compared in the same way described in the previous section.

## 6.3 Low Cycle Fatigue Fracture Life

Another factor that impacts the behavior of compression members is fracture upon low cycle fatigue under repeated cyclic loading. Upon repeated cyclic loading, the local buckling and straightening of the material at that location induce cracks that may propagate and lead to fracture. Two different fracture criteria of tubular bracing members are reviewed in this section.

### 6.3.1 *Tang and Goel Model*

Tang and Goel (1987) introduced an empirical fracture criterion for rectangular tubular bracing members. This criterion requires a special calculation of the number of cycles that contribute to fatigue life. To count these cycles, Tang and Goel established the following rules applicable to a brace axial deformation time history (referring to Figure 6.31 to help explain some of these concepts):

- (1) A full cycle is typically defined from one peak in compression to another. In-between these two compressive peaks, the brace member will typically be subjected to tension (although not always). For this discussion, displacements are taken as negative in the direction of greater

compression. For example, in Figure 6.31, full cycles are defined from point 1 to 2, 2 to 3, etc.

- (2) Only the half cycles from a compression peak to the point of maximum tension (or minimum compression) in a cycle are counted to contribute to fatigue life. In that perspective, in Figure 6.31, cycle 1-2 contributes a value of 1 to the fatigue life calculation (i.e. a displacement of  $\Delta/\Delta_y=+1$  from the point 1 at  $\Delta/\Delta_y=-1$  to the peak displacement in tension at  $\Delta/\Delta_y=0$ ).
- (3) A standard cycle is defined as the one contributing a value of 1.0 to the fatigue life calculation.
- (4) The effect of small deformations cycles (defined as deformations of less than the standard cycle, or, in other words, of less than  $\Delta_y$ ) are deemed to only have a small effect on the fatigue life of bracing members, and are ignored. For example, cycle 0-1 in Figure 6.31 would be ignored.
- (5) The amplitude of cycles proportionally contribute to fatigue life. In other words, a cycle with an amplitude of  $4\Delta_y$  is equal to 4 cycles of  $\Delta_y$ . For example, in Figure 2.32, cycle 2-3 is equivalent to two cycles 1-2.

Figure 6.32 illustrates how a complex displacement time history is decomposed in a series of standard cycles following the above rules.

Following this criterion, the following fracture life model for tubular bracing members was proposed:

$$N_f = C_s \frac{(B/D)(60)}{[(B-2t)/t]^2} \text{ for } KL/r \leq 60 \quad (6.1a)$$

$$N_f = C_s \frac{(B/D)(KL/r)}{[(B-2t)/t]^2} \text{ for } KL/r > 60 \quad (6.1b)$$

where  $N_f$  is the fracture life expressed in terms of standard cycles,  $C_s$  is a numerical coefficient obtained from the test results,  $B$  and  $D$  are respectively the gross width and depth of the section (in inches), and  $t$  is thickness of the section (in inches).

Lee and Goel (1987) reformulated this model by considering the effect of  $F_y$  and eliminating the dependency on  $KL/r$ . In this criterion,  $\Delta_f$  is used instead of  $N_f$  to quantify the fracture life of a tubular bracing member. This method proceeds per the following steps.

- (a) The hysteresis curves (P vs.  $\Delta$ ) is converted to a normalized hysteresis curves ( $P/P_y$  vs.  $\Delta/\Delta_y$ ).
- (b) The deformation amplitude (tension excursion in a cycle) is divided into two parts,  $\Delta_1$  and  $\Delta_2$ , defined at the axial load  $P_y/3$  point, as illustrated in Figure 6.33.  $\Delta_1$  is the tension deformation from the load reversal point to  $P_y/3$ , while  $\Delta_2$  is from that  $P_y/3$  point up to the unloading point.
- (c)  $\Delta_{f,exp}$  is obtained by adding 0.1 times  $\Delta_1$  to  $\Delta_2$  in each cycle and summary summing up for all cycles up to the failure (i.e., by the equation  $\Delta_f = \Sigma(0.1\Delta_1 + \Delta_2)$ ).
- (d) The theoretical fracture life,  $\Delta_f$  is expressed as follows:

$$\Delta_f = C_s \frac{(46/F_y)^{1.2}}{[(B-2t)/t]^{1.6}} \left( \frac{4B/D+1}{5} \right) \quad (6.2)$$

where  $C_s$  is an empirically obtained constant calibrated from test results, and  $F_y$  is the yield strength of the brace (ksi). The numerical constant  $C_s$ , originally given as 1335 by Lee and Goel (1987), was recalibrated using the test results of Gugerli and Goel (1982) and Lee and Goel (1987), and found to be 1560 by Hassan and Goel (1991). Fracture is assumed to occur when  $\Delta_{f,exp} = \Delta_f$ .

### 6.3.2 Archambault et al. Model

Another criterion was presented by Archambault et al. (1995). This criterion re-introduced the effect of slenderness ratio,  $KL/r$ , on the basis that, based on a review of previous test results, the Tang and Goel model was noted to underestimate the fracture life of tubular bracing members having large slenderness ratios. Two distinct trends were noted for fracture life of bracing members as a function of  $KL/r$ , depending on whether slenderness was lower or higher than 70.

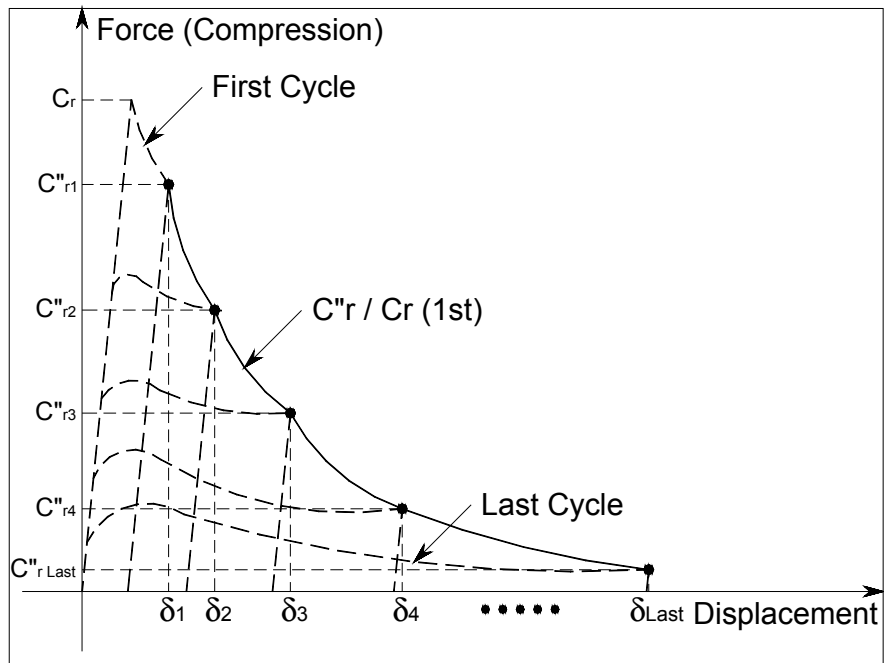


Figure 6.11 Definition of normalized buckling capacity,  $C''_r / C_r$  (1<sup>st</sup>) (Lee and Bruneau, 2002)

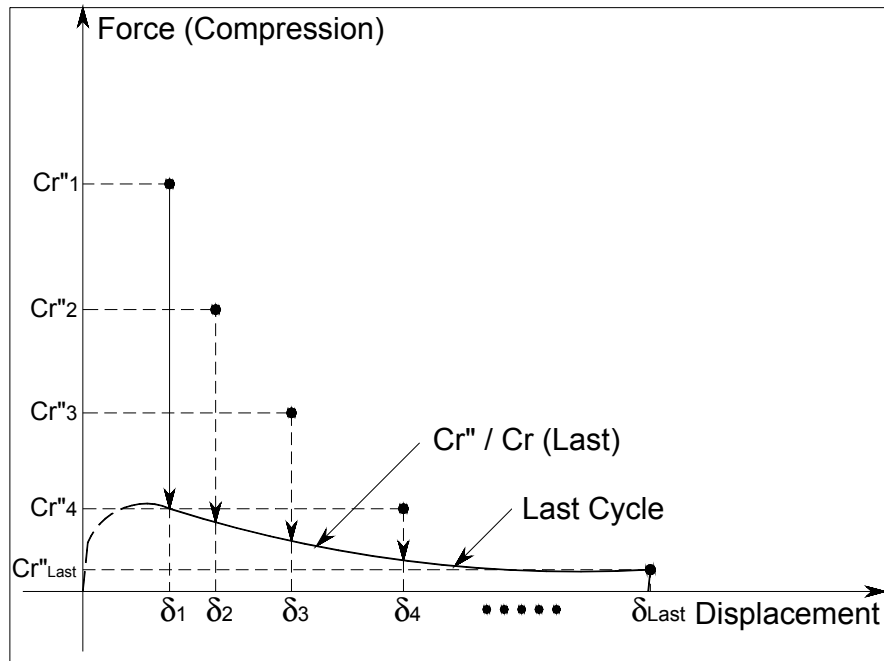


Figure 6.12 Definition of normalized buckling capacity,  $Cr'' / Cr$  (Last) (Lee and Bruneau, 2002)

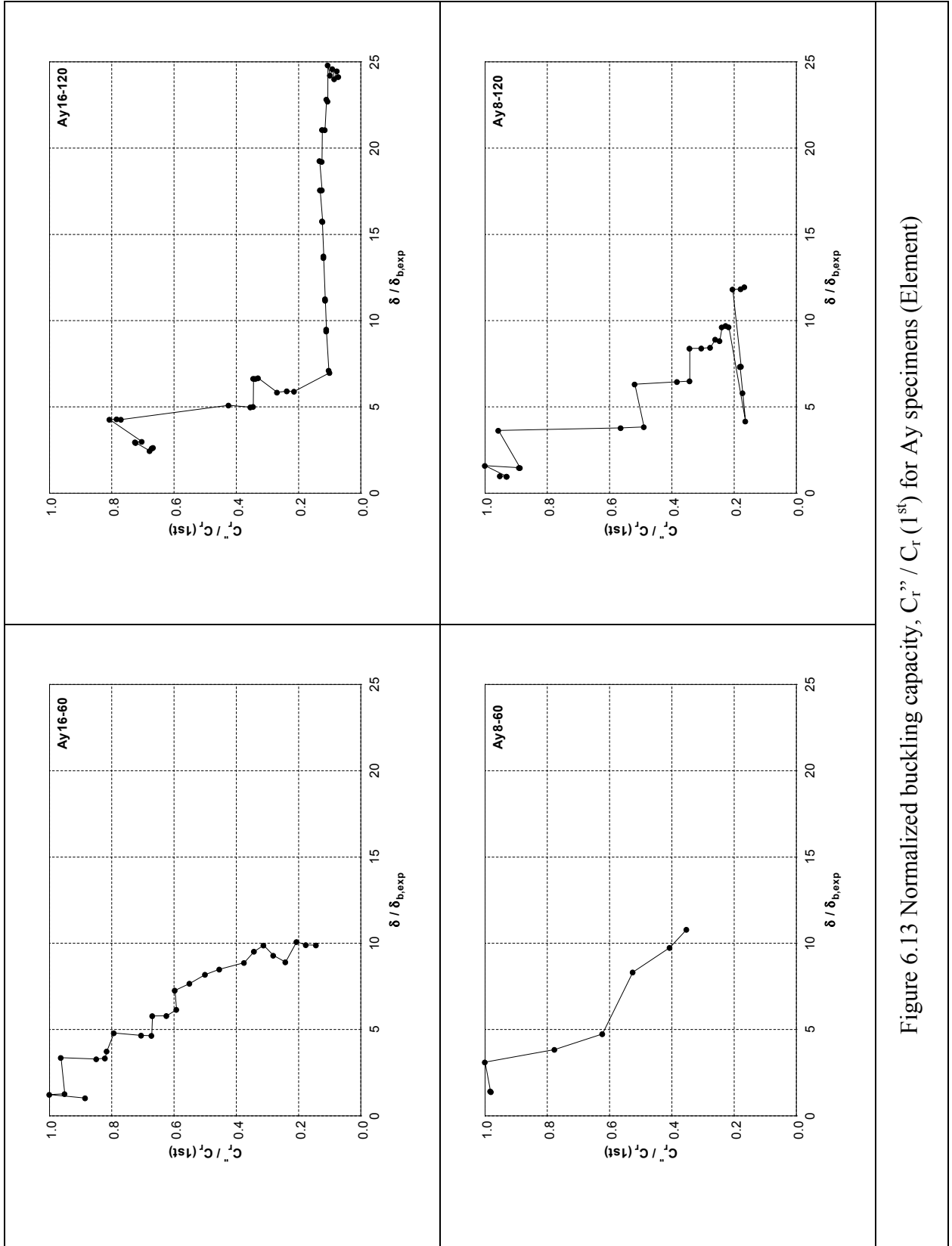


Figure 6.13 Normalized buckling capacity,  $C_r'' / C_r'(1^{st})$  for Ay specimens (Element)

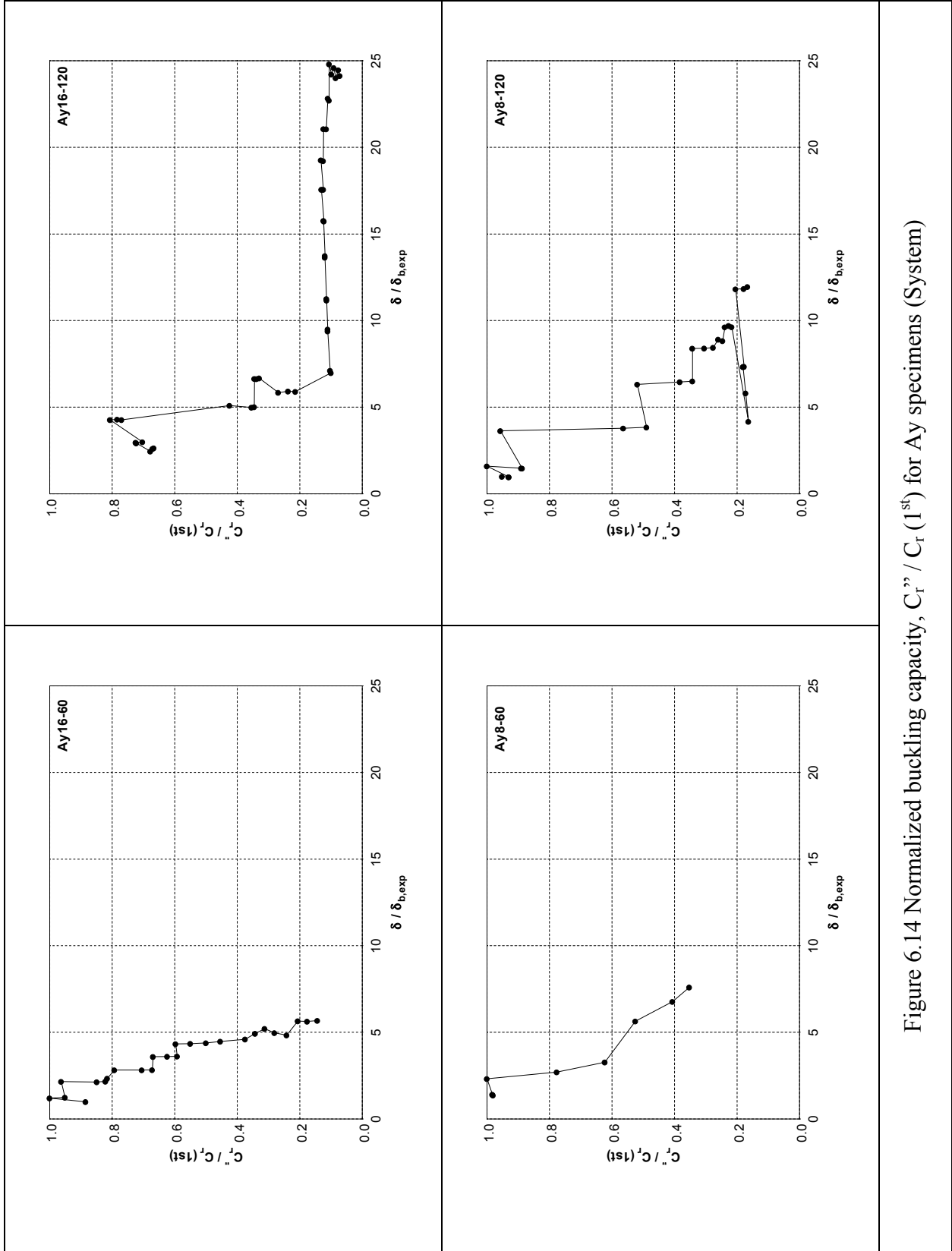


Figure 6.14 Normalized buckling capacity,  $C_r'' / C_r (1^{st})$  for Ay specimens (System)

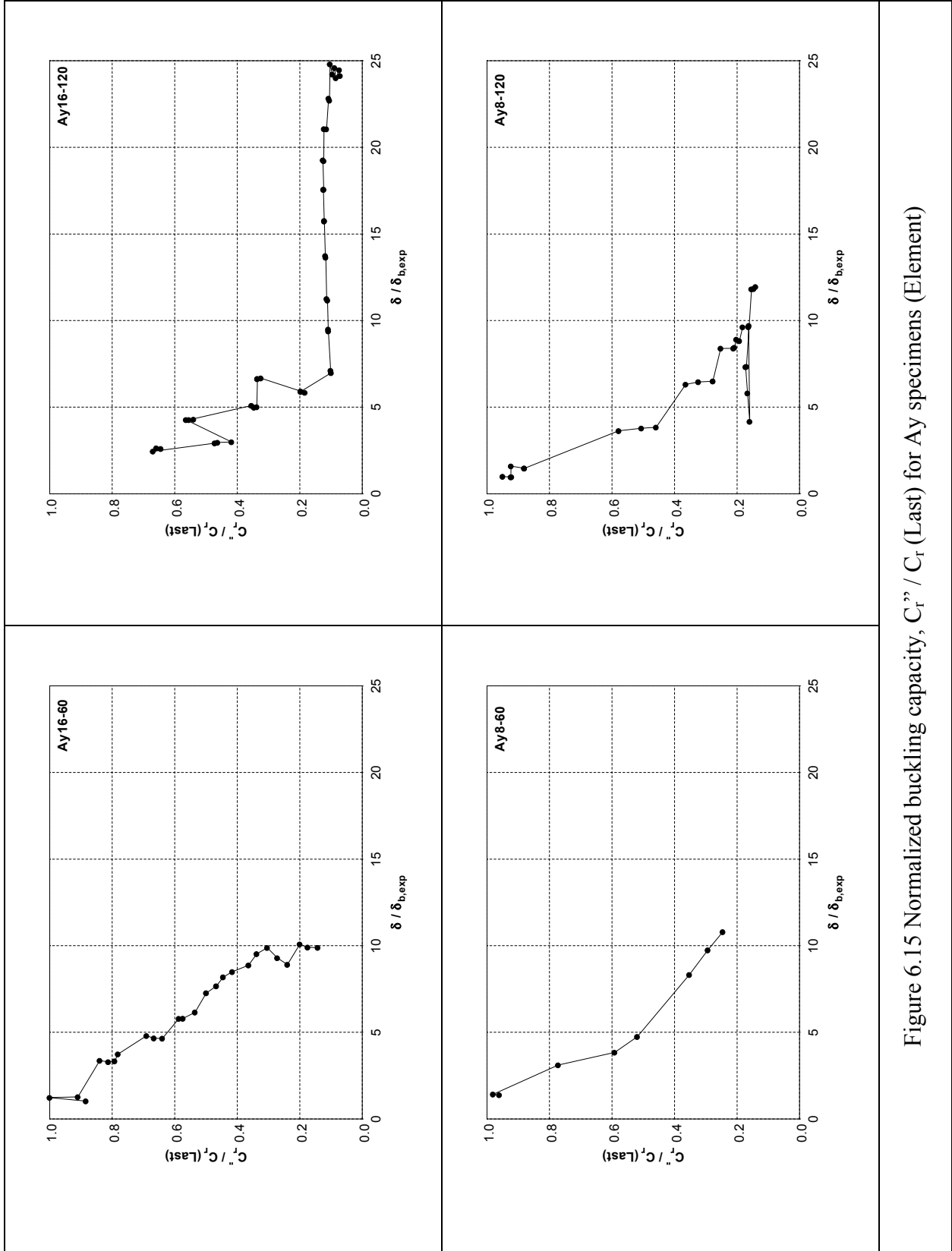


Figure 6.15 Normalized buckling capacity,  $C_r'' / C_r (\text{Last})$  for Ay specimens (Element)

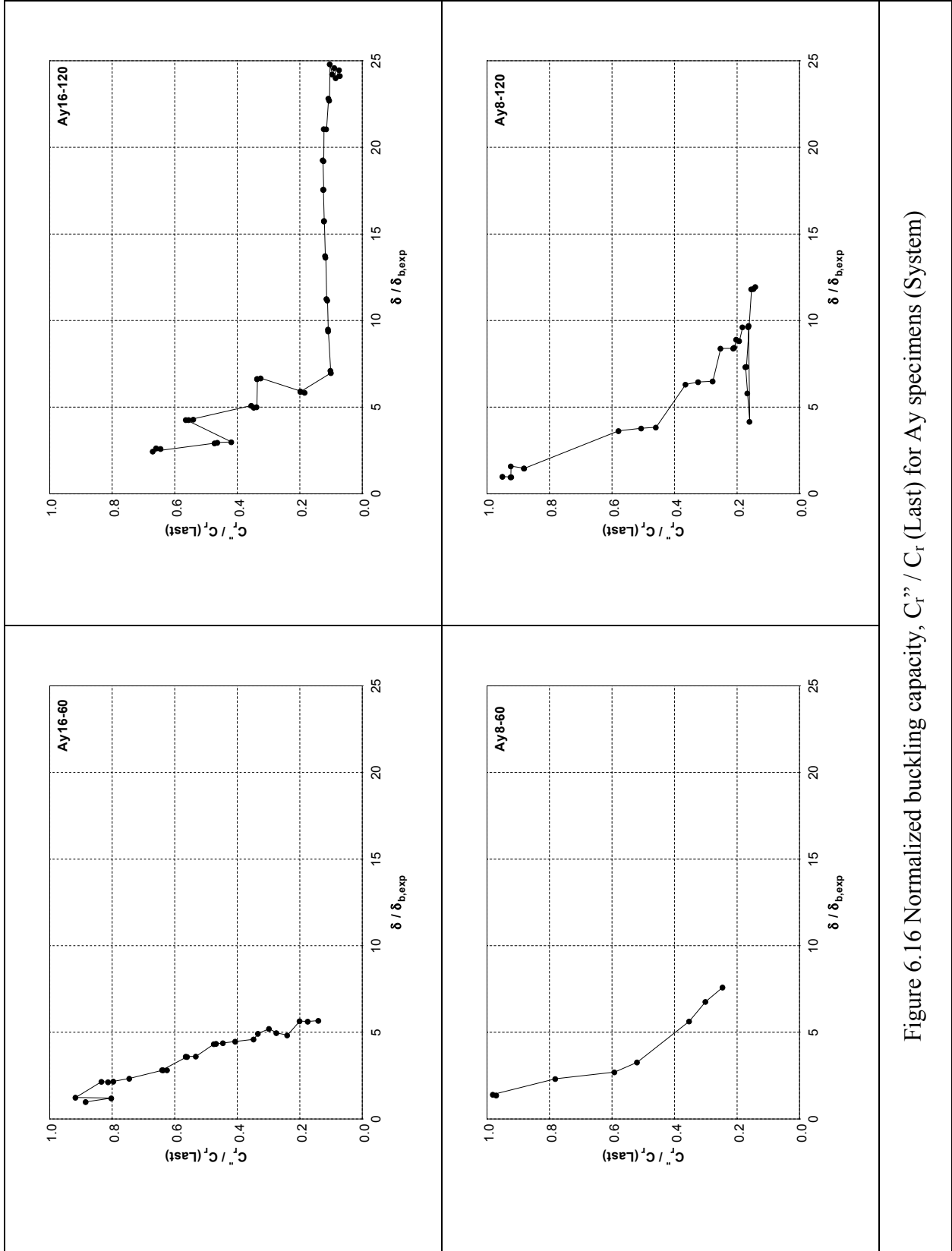


Figure 6.16 Normalized buckling capacity,  $C_r'' / C_r (\text{Last})$  for Ay specimens (System)

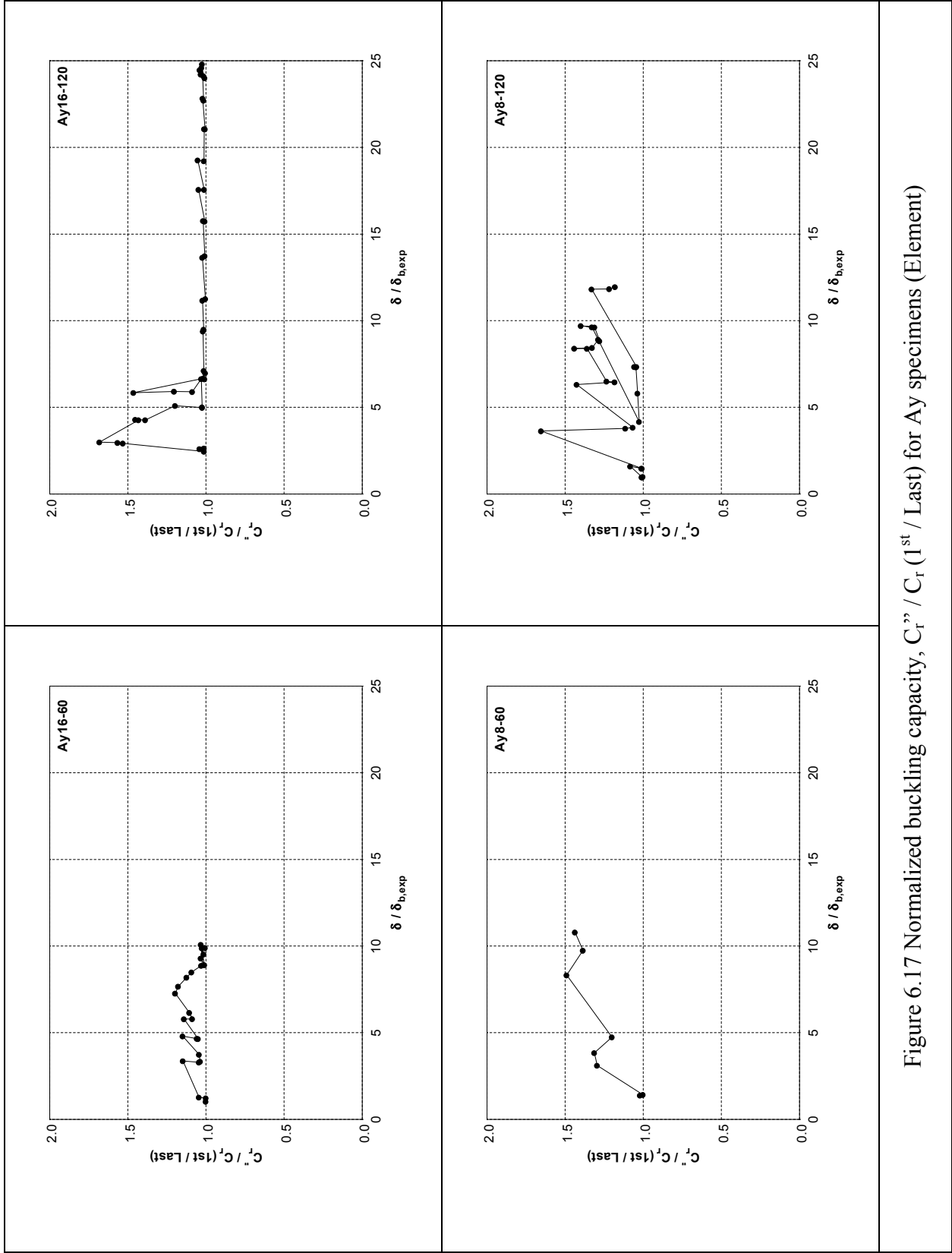


Figure 6.17 Normalized buckling capacity,  $C_r'' / C_r$  (1<sup>st</sup> / Last) for Ay specimens (Element)

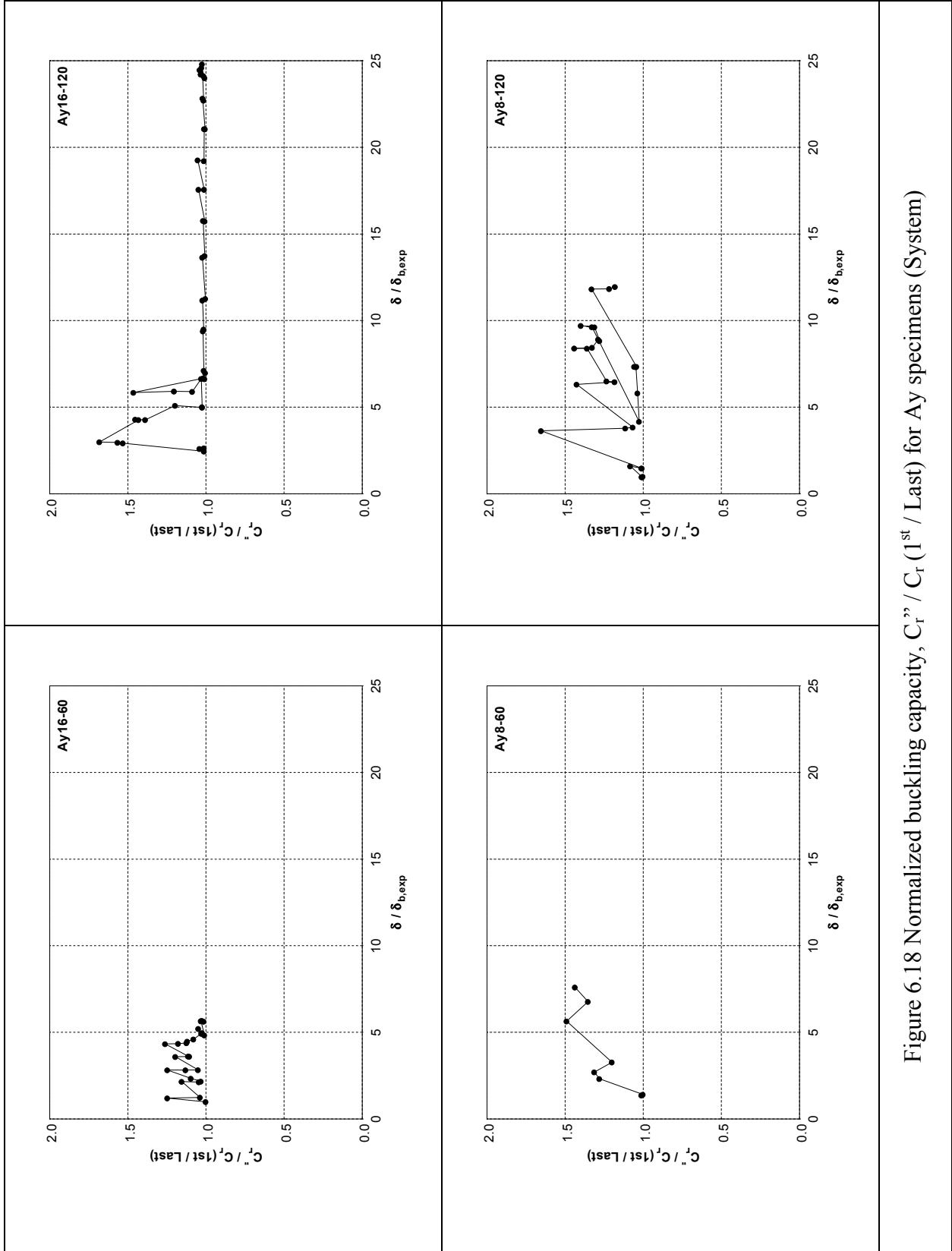


Figure 6.18 Normalized buckling capacity,  $C_r'' / C_r$  (1<sup>st</sup> / Last) for Ay specimens (System)

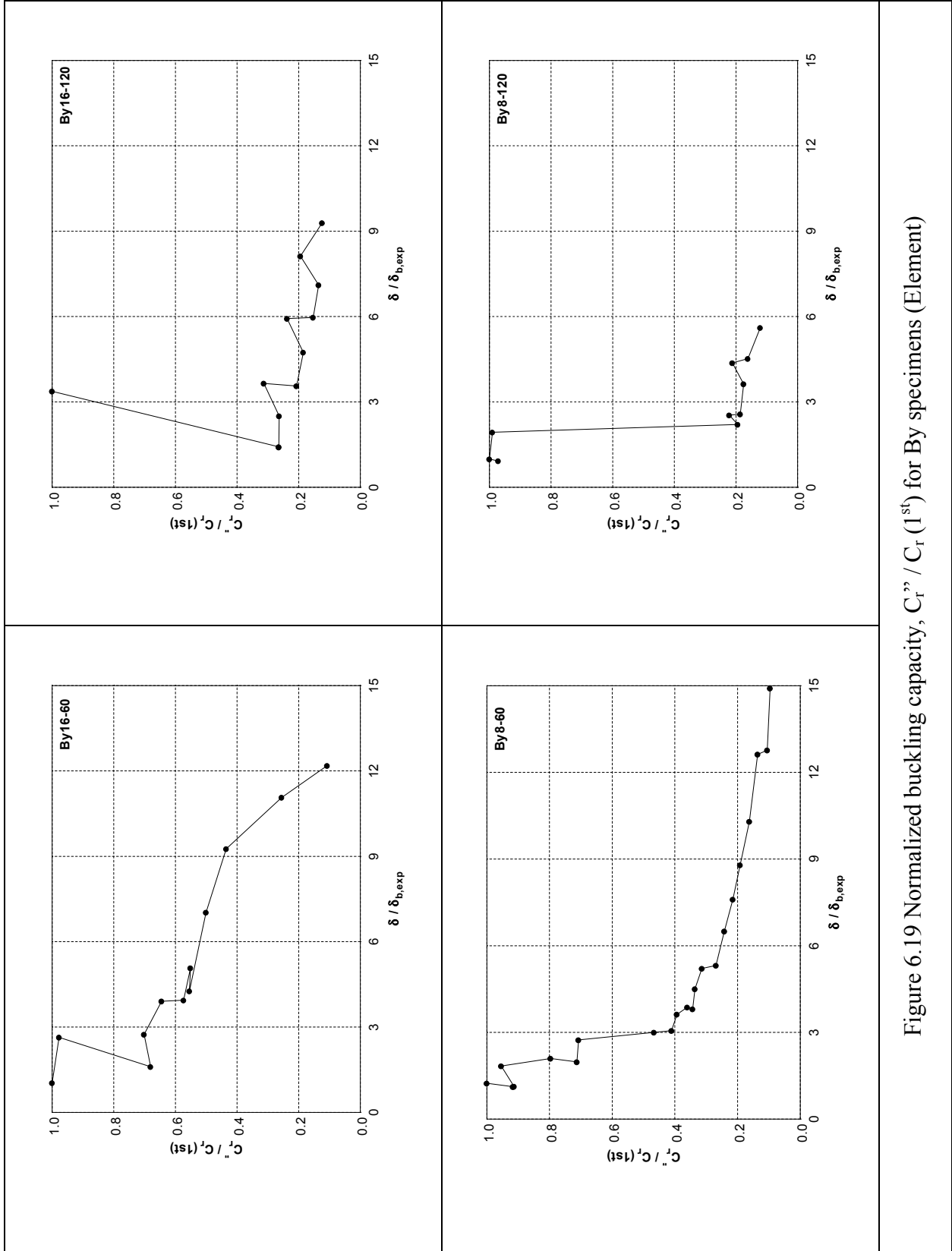


Figure 6.19 Normalized buckling capacity,  $C_r'' / C_r'(1^{st})$  for By specimens (Element)

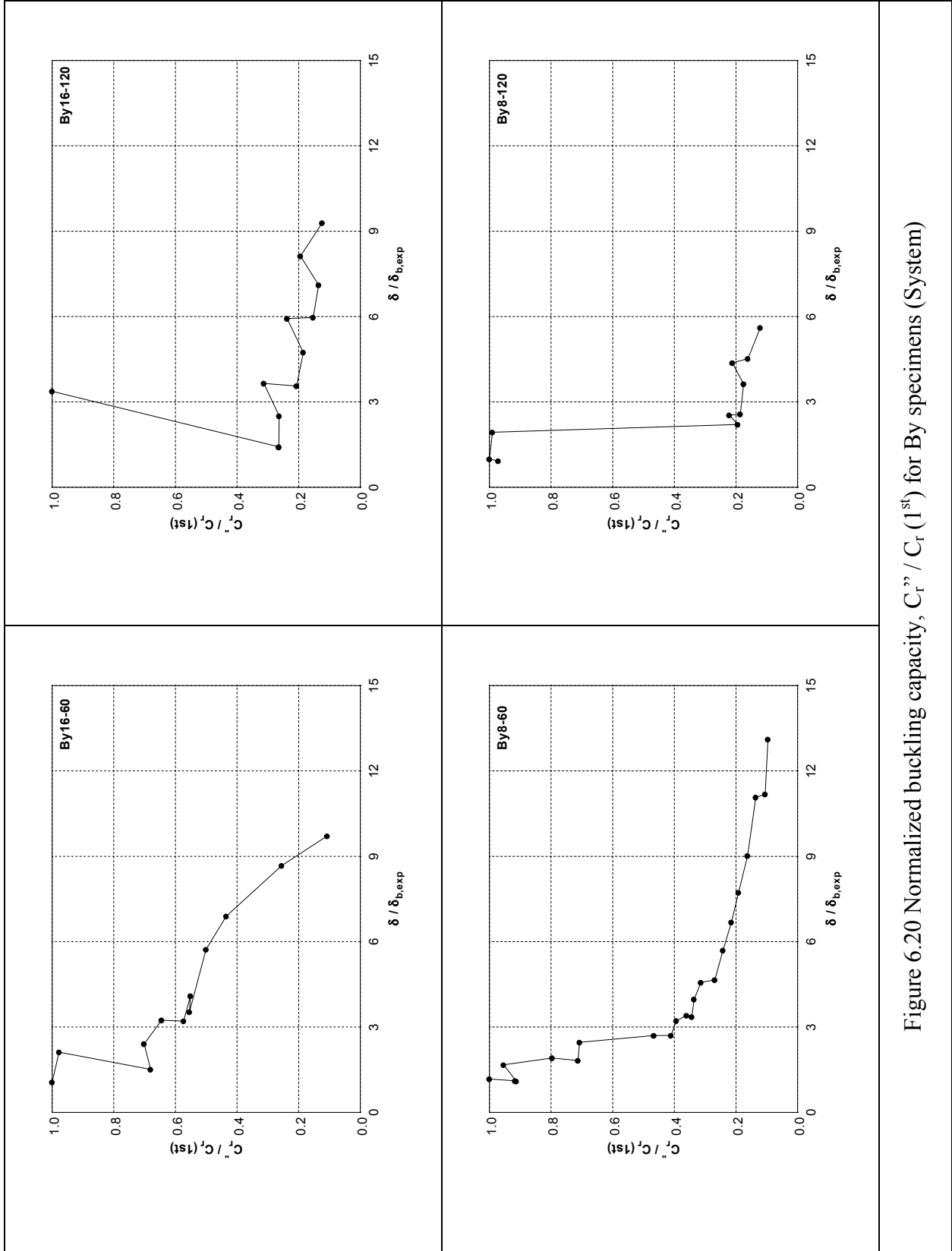


Figure 6.20 Normalized buckling capacity,  $C_r'' / C_r'(1st)$  for By specimens (System)

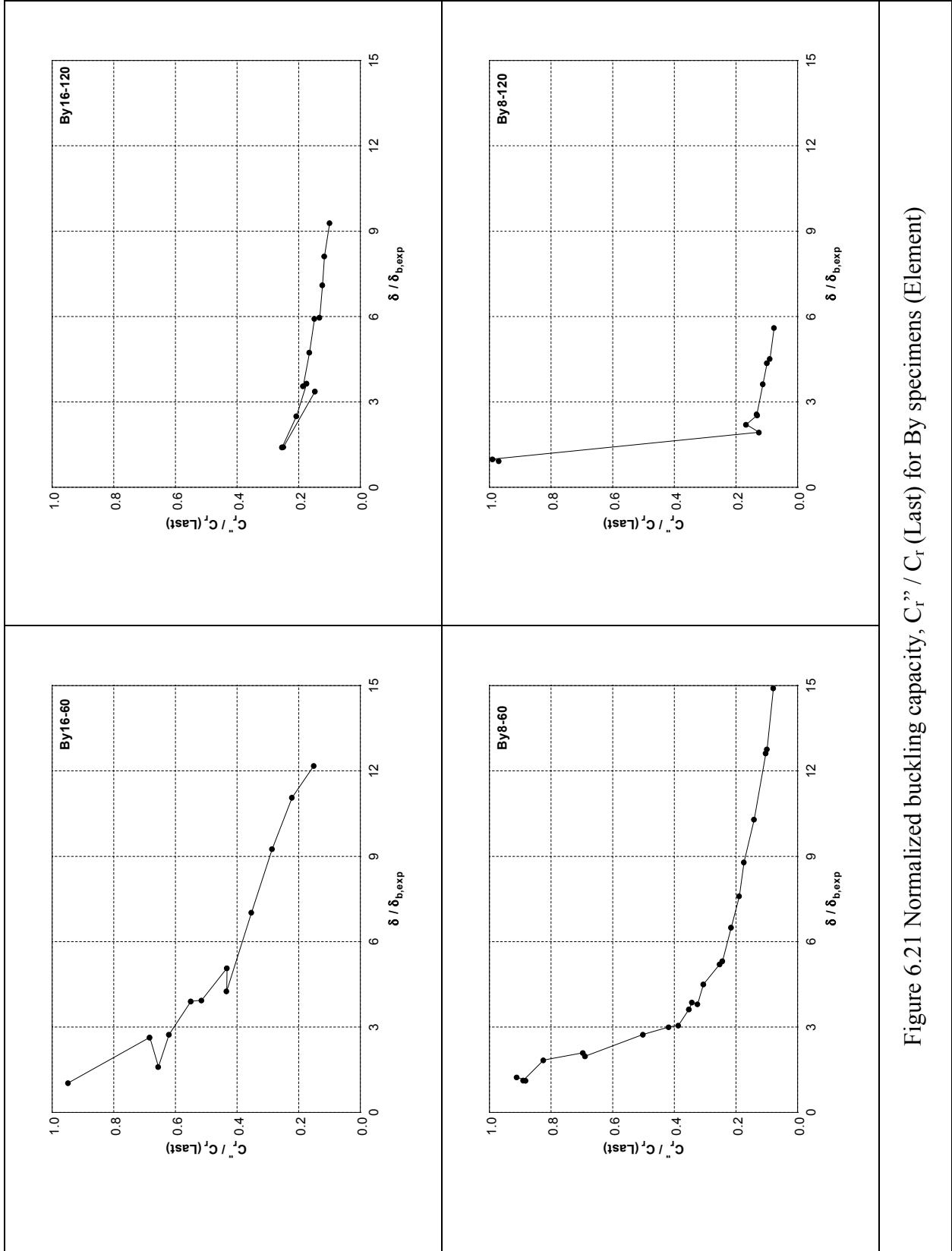


Figure 6.21 Normalized buckling capacity,  $C_r'' / C_r$  (Last) for By specimens (Element)

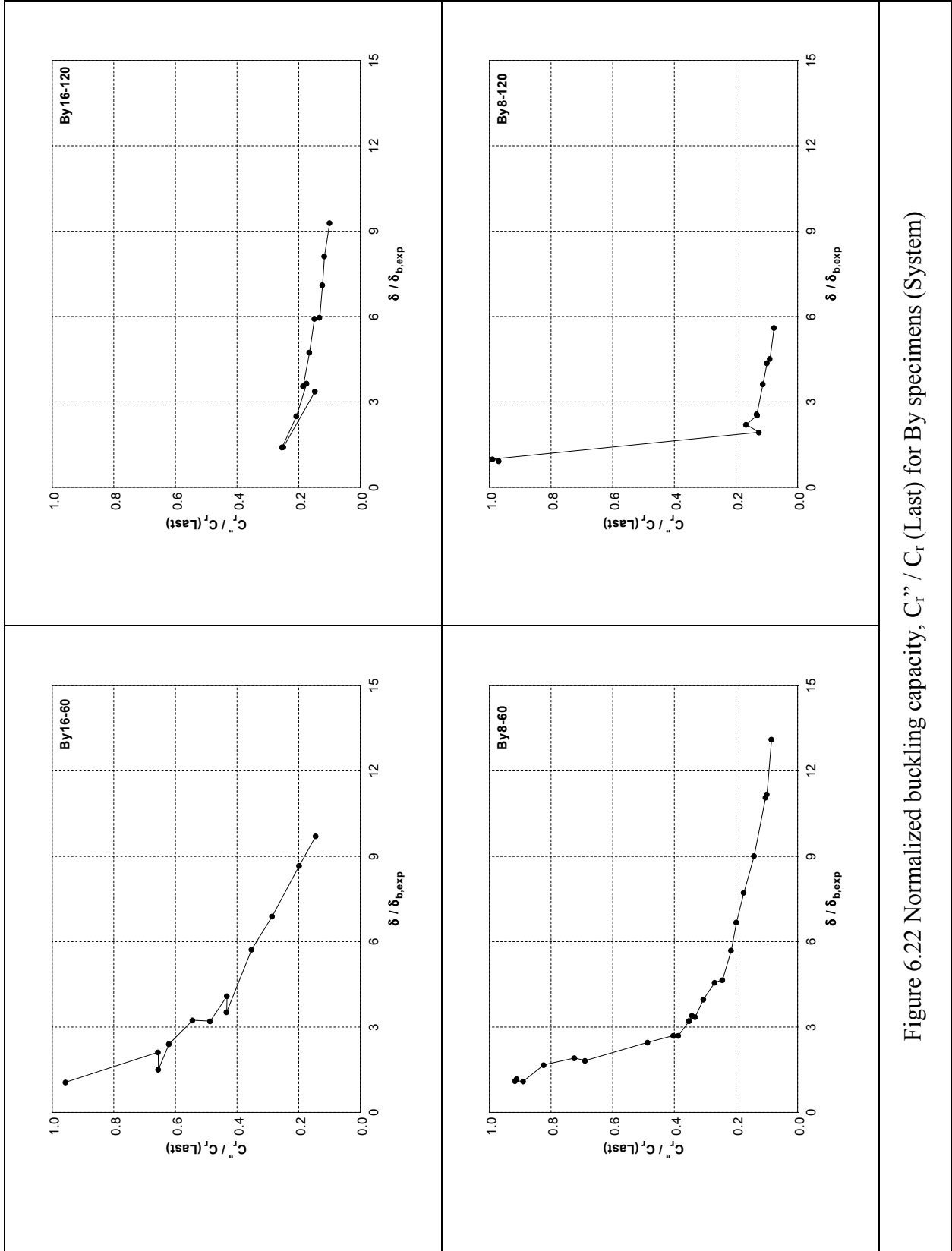


Figure 6.22 Normalized buckling capacity,  $C_r'' / C_r (\text{Last})$  for By specimens (System)

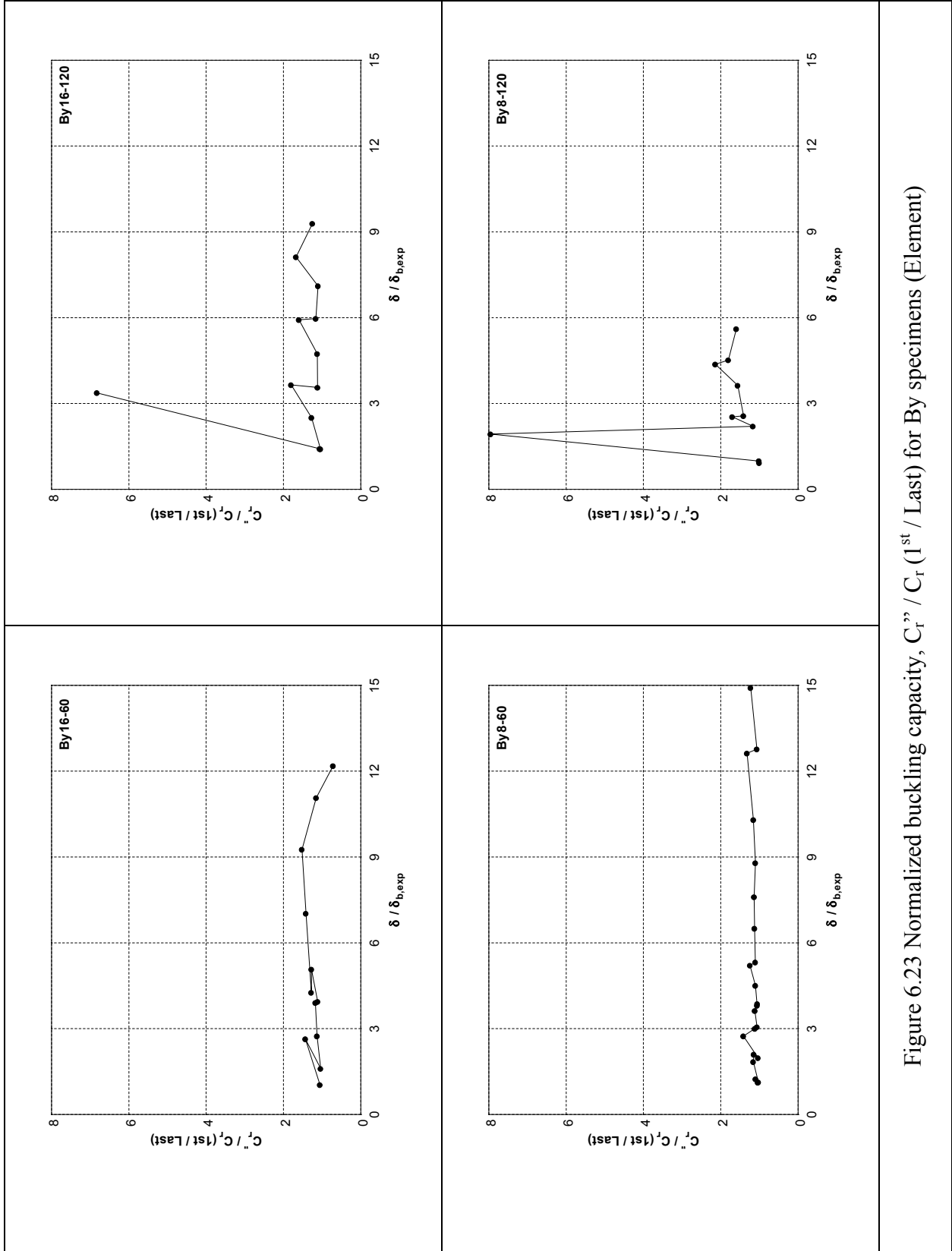


Figure 6.23 Normalized buckling capacity,  $C_r'' / C_r$  (1<sup>st</sup> / Last) for By specimens (Element)

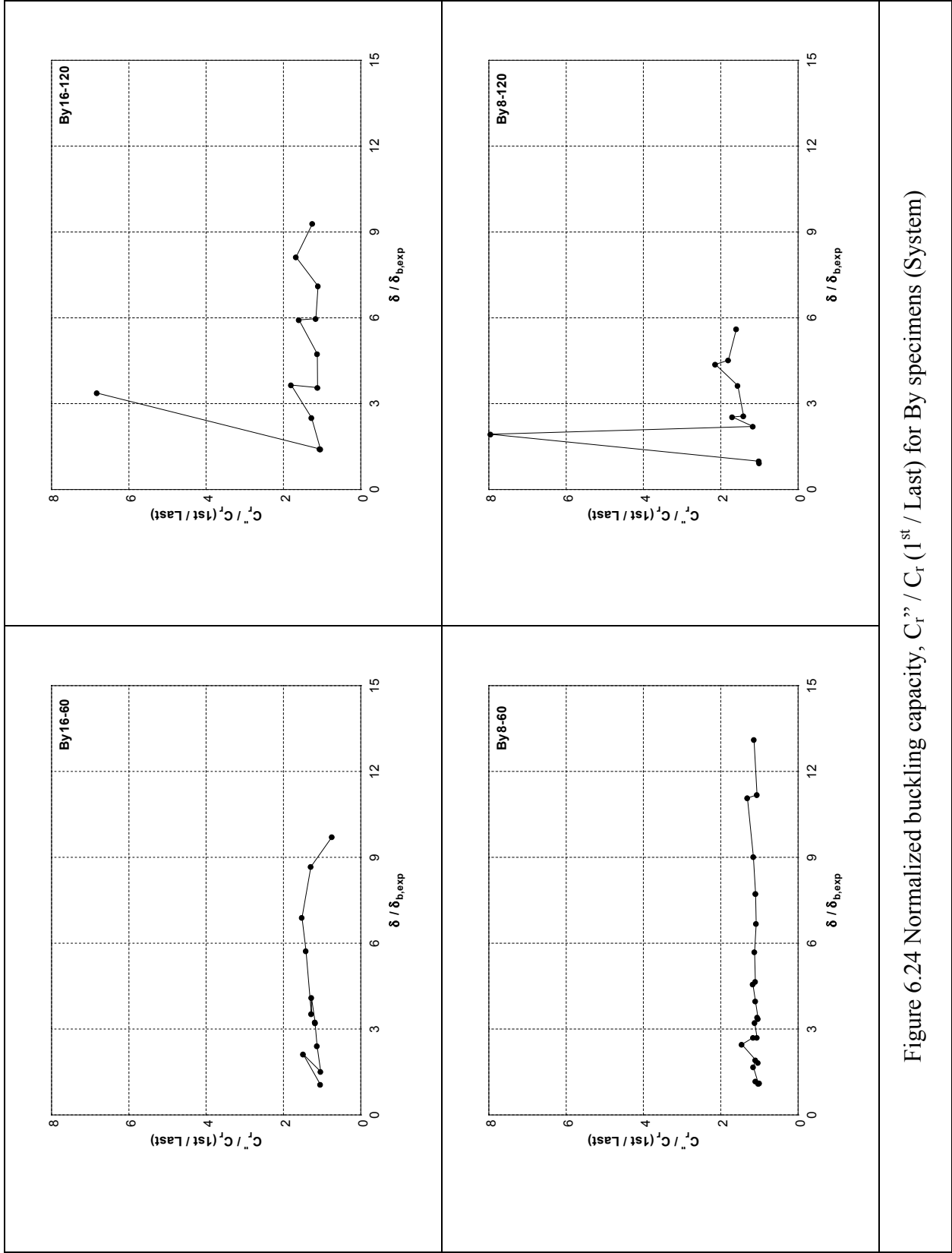


Figure 6.24 Normalized buckling capacity,  $C_r'' / C_r$  (1<sup>st</sup> / Last) for By specimens (System)

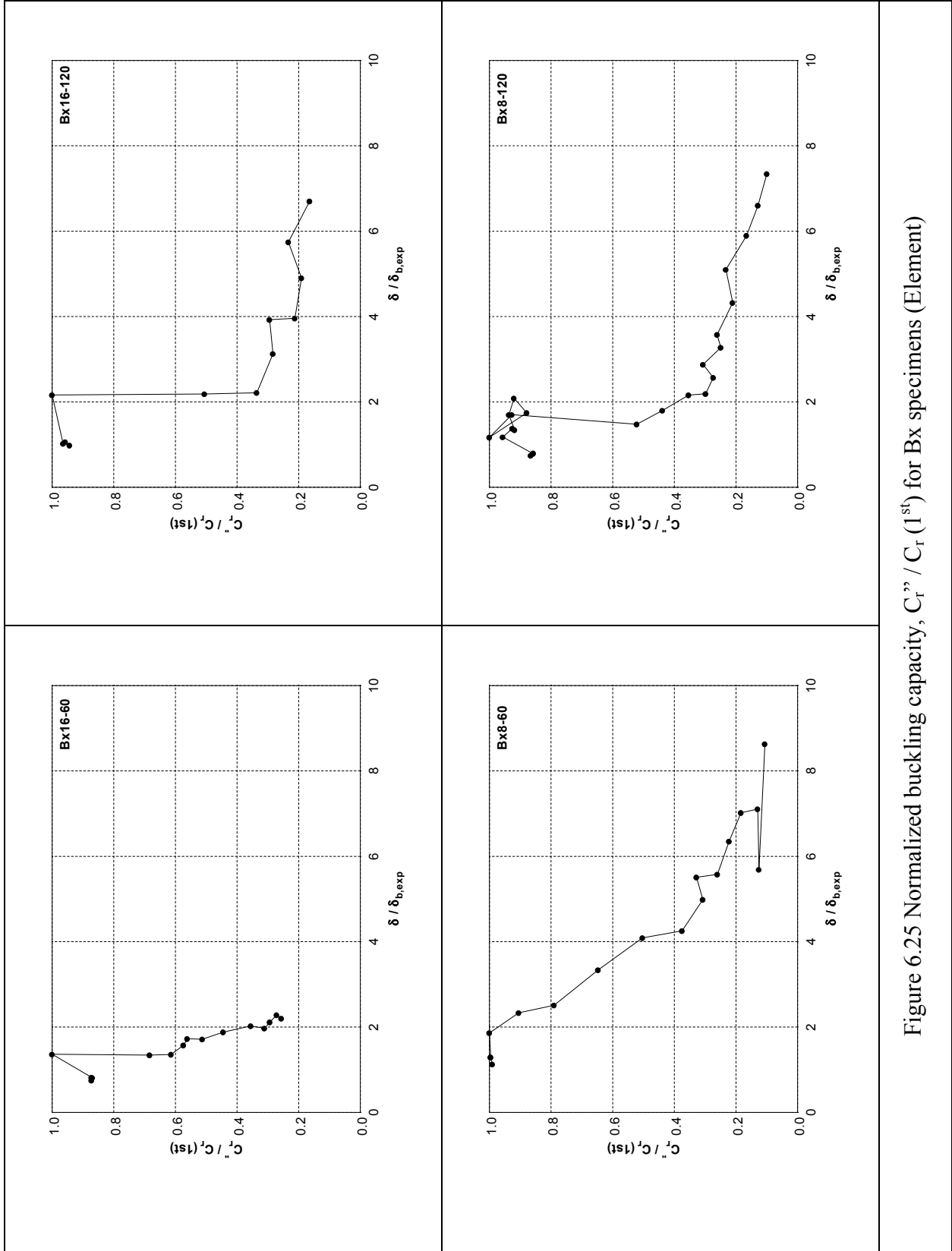


Figure 6.25 Normalized buckling capacity,  $C_r / C_r(1^{st})$  for Bx specimens (Element)

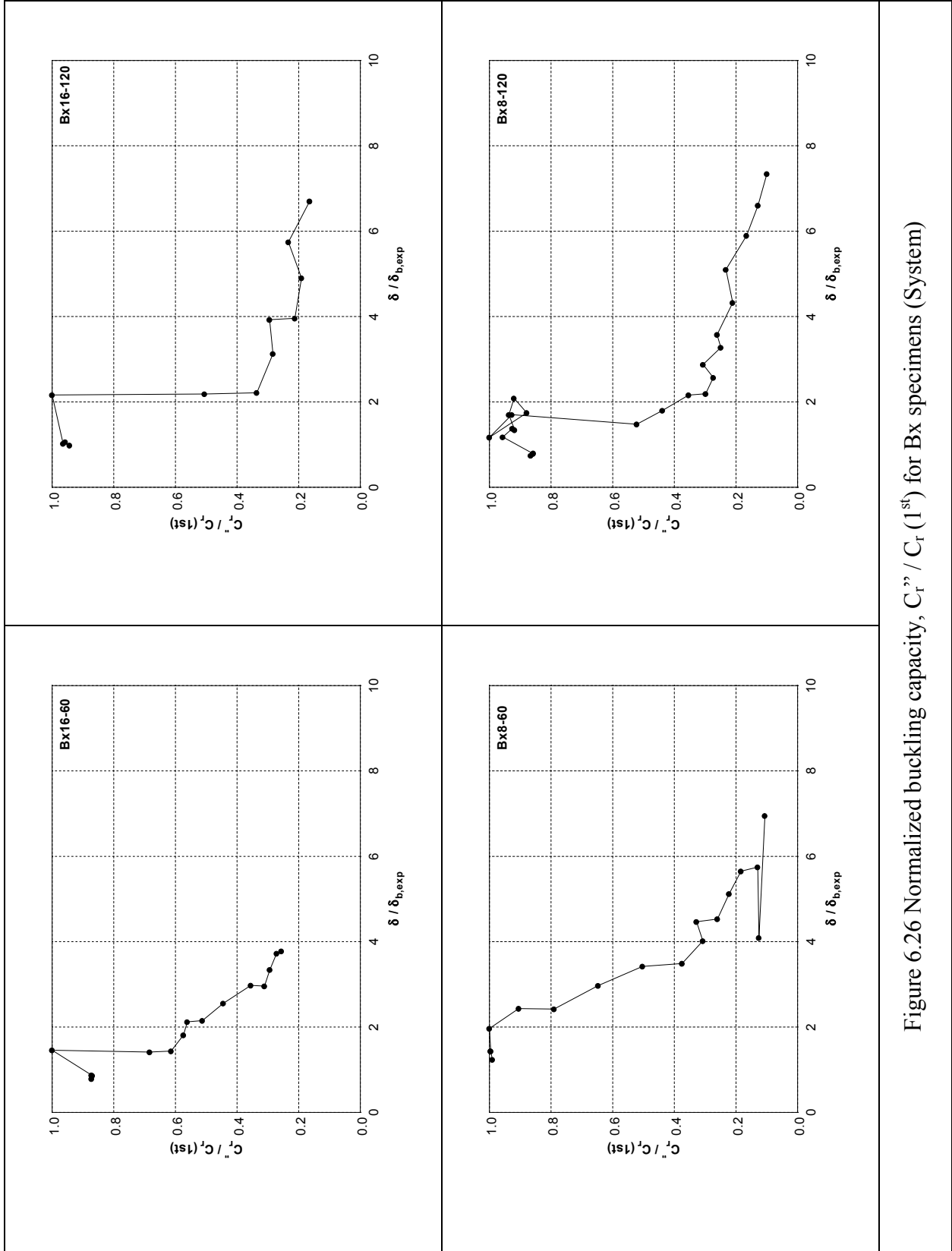


Figure 6.26 Normalized buckling capacity,  $C_r'' / C_r'(1st)$  for Bx specimens (System)

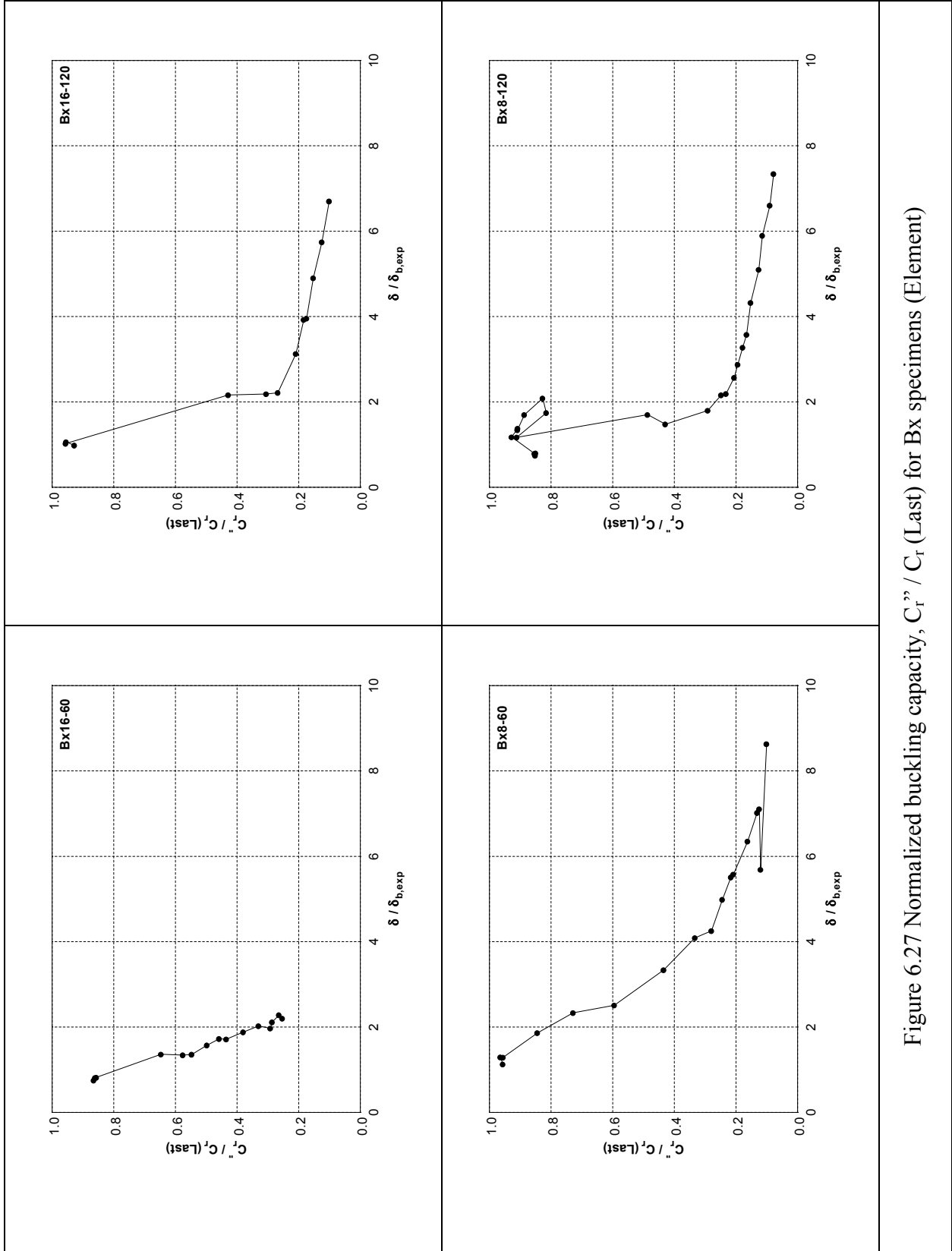


Figure 6.27 Normalized buckling capacity,  $C_r'' / C_r (\text{Last})$  for Bx specimens (Element)

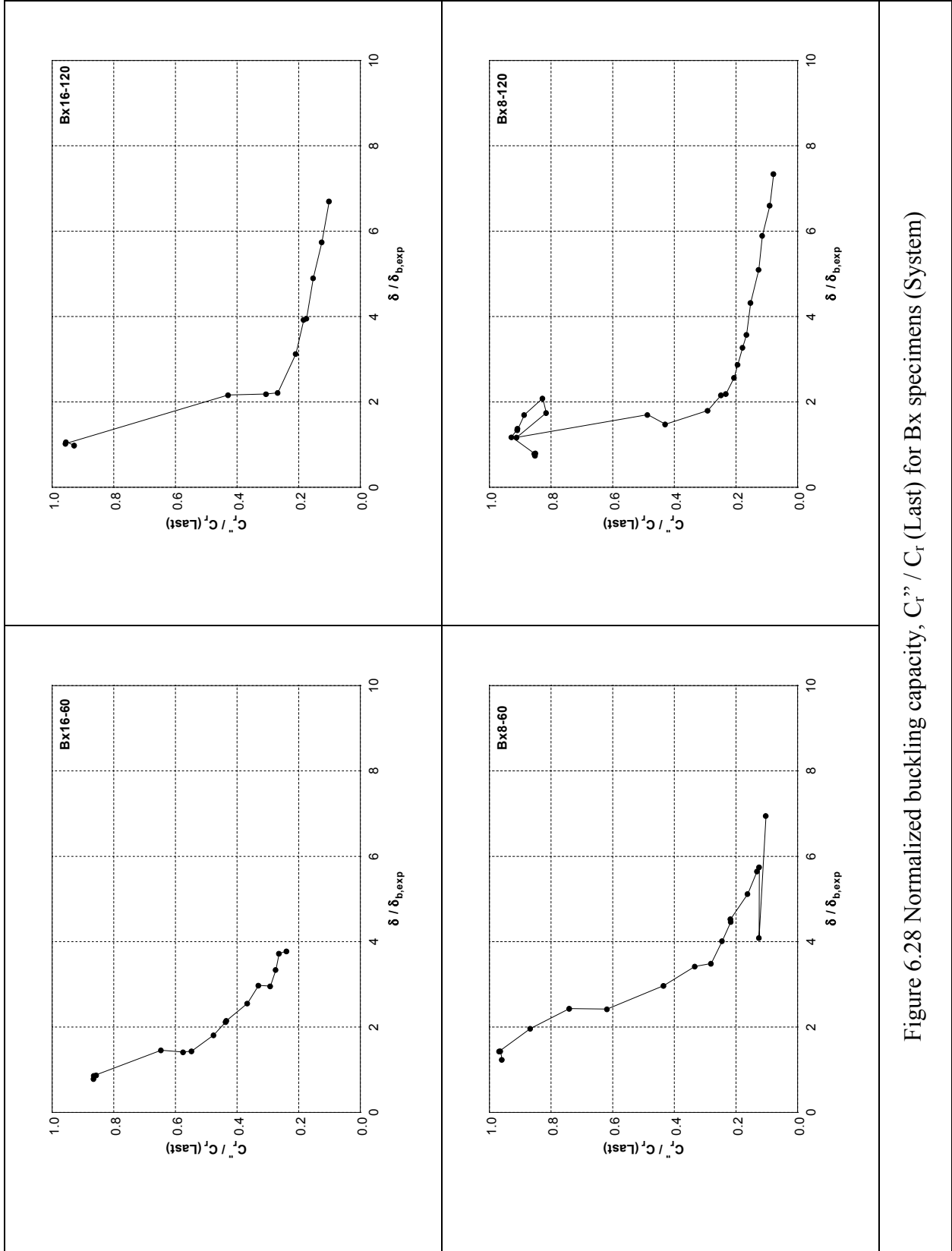


Figure 6.28 Normalized buckling capacity,  $C_r'' / C_r'(Last)$  for Bx specimens (System)

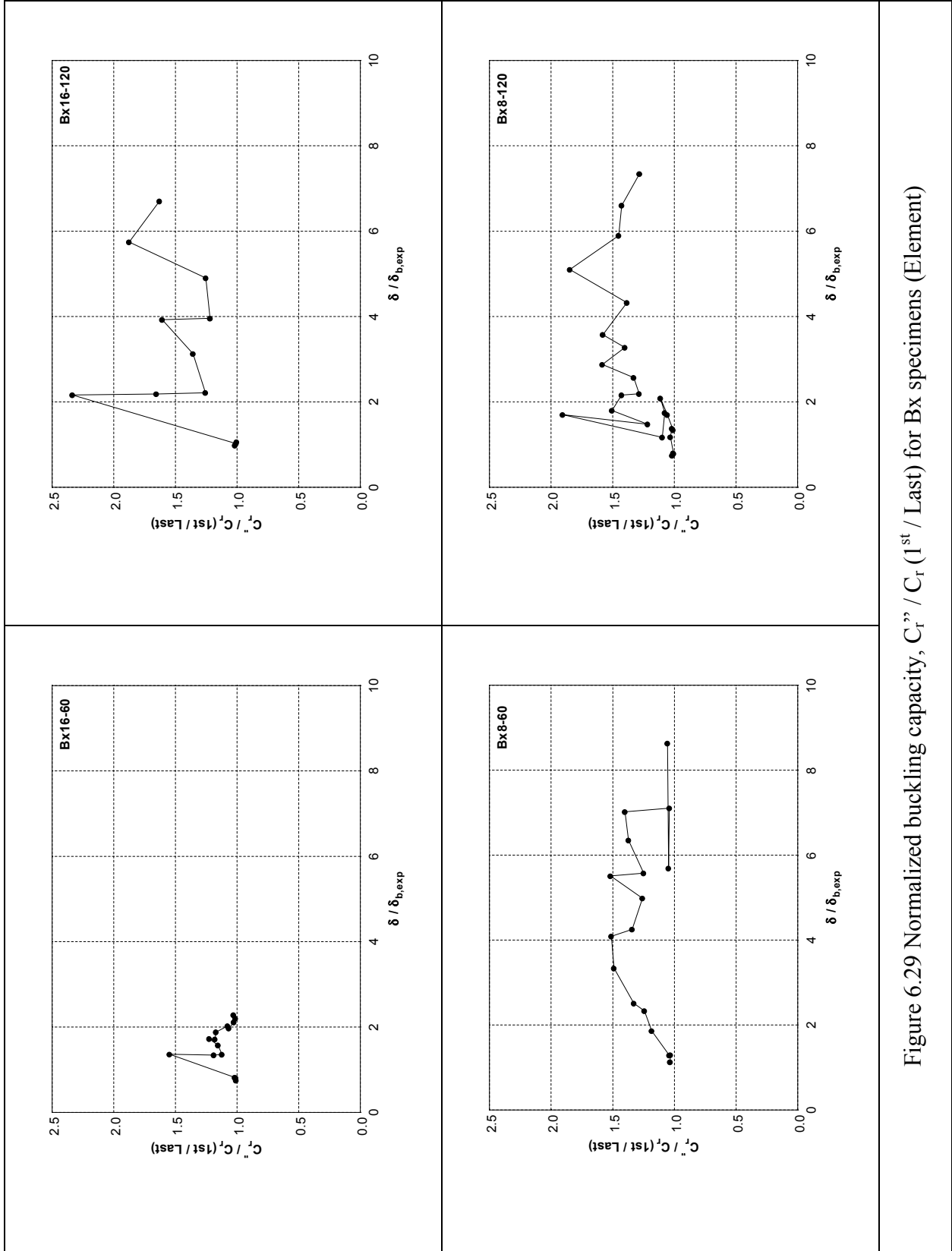


Figure 6.29 Normalized buckling capacity,  $C_r'' / C_r$  (1<sup>st</sup> / Last) for Bx specimens (Element)

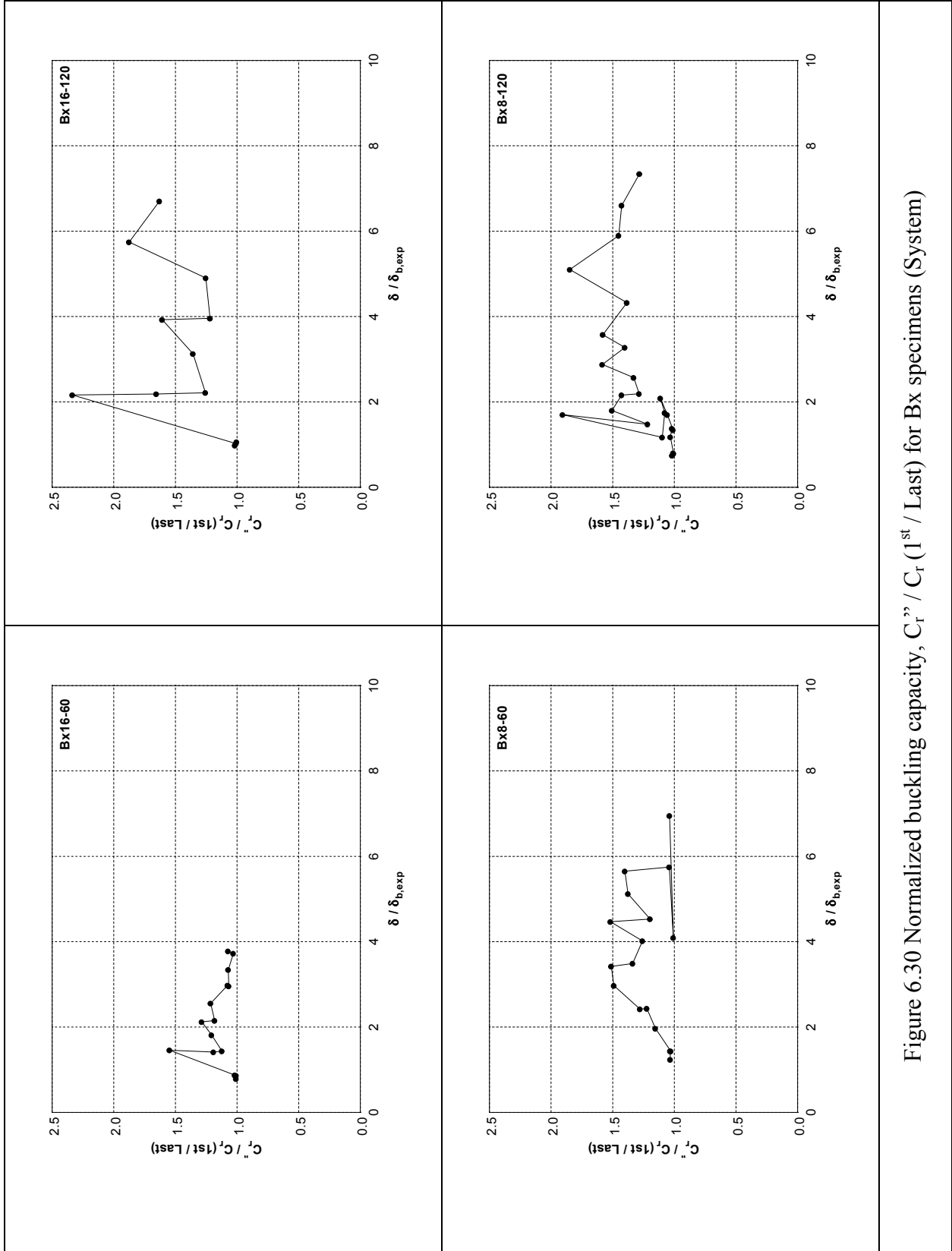


Figure 6.30 Normalized buckling capacity,  $C_r'' / C_r (1^{st} / Last)$  for Bx specimens (System)

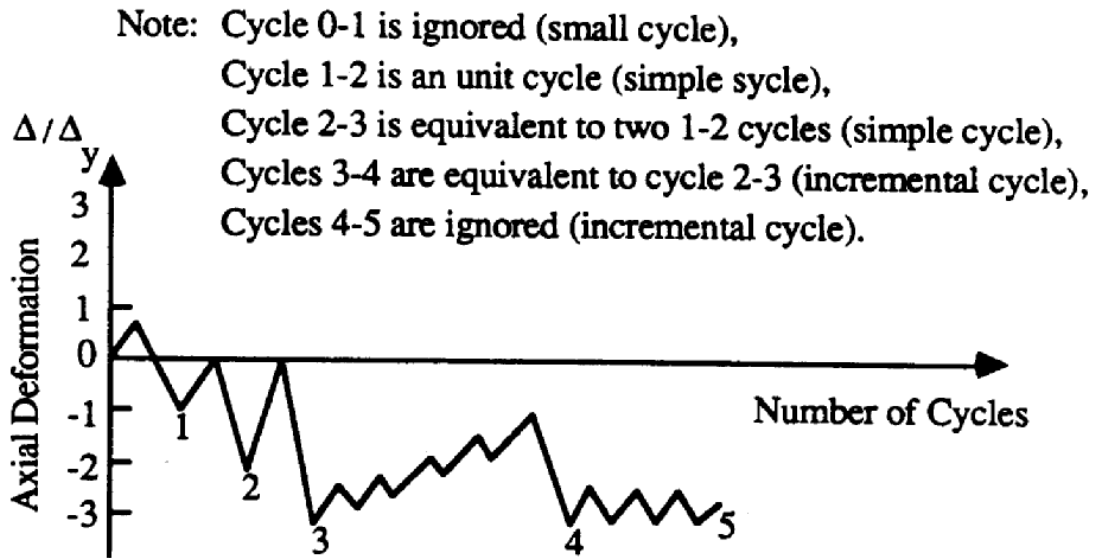


Figure 6.31 Typical cycles in a deformation history of Tang and Goel model (1987)

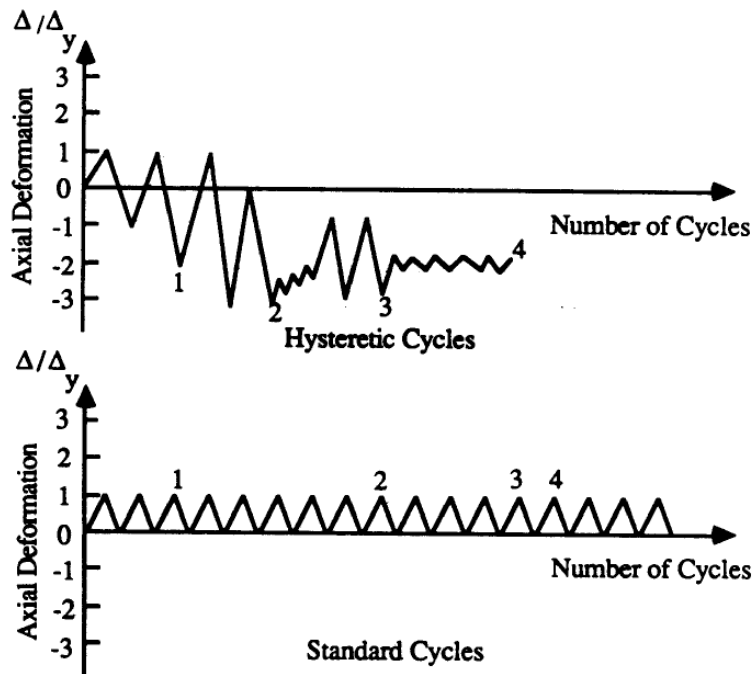


Figure 6.32 Equivalent conversion between hysteresic cycles and the standard cycles of Tang and Goel model (1987)

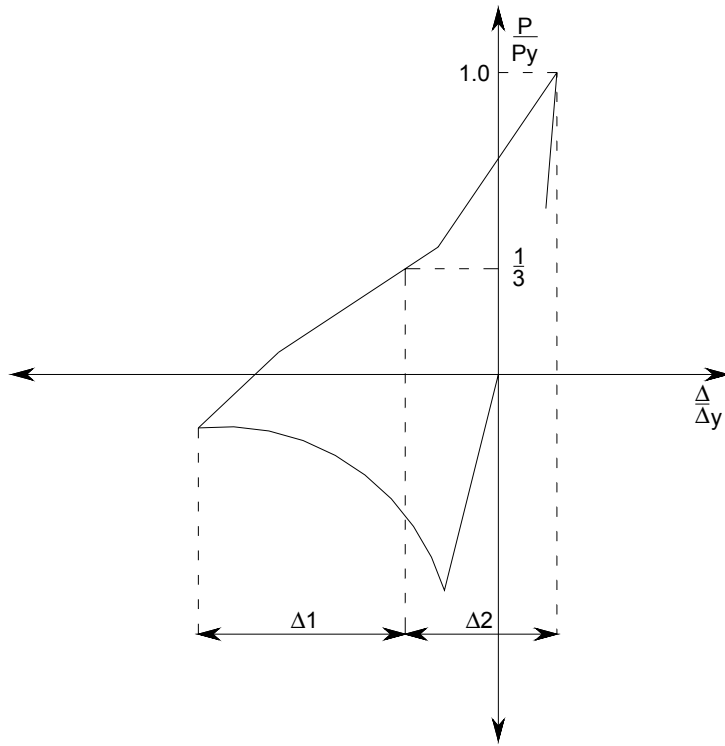


Figure 6.33 Definition of  $\Delta_1$  and  $\Delta_2$  (Lee and Goel model)

They introduced the term,  $\Delta_f^*$  (to differentiate it from  $\Delta_f$  used by Tang and Goel), and expressed fatigue life as follows:

$$\Delta_f^* = C_s \frac{(317/F_y)^{1.2}}{[(B-2t)/t]^{0.5}} \left( \frac{4B/D+1}{5} \right)^{0.8} \times (70)^2 \text{ for } KL/r < 70 \quad (6.3a)$$

$$\Delta_f^* = C_s \frac{(317/F_y)^{1.2}}{[(B-2t)/t]^{0.5}} \left( \frac{4B/D+1}{5} \right)^{0.8} \times (KL/r)^2 \text{ for } KL/r \geq 70 \quad (6.3b)$$

where the  $C_s$  value is empirically determined from the experimental results was given as 0.0257,  $F_y$  is in MPa and all dimensions are in mm units.

### 6.3.3 Fracture life of Built-up Specimens

To quantitatively access the low cycle fracture life of the built-up specimens, the experimental fracture life,  $\Delta_{f,exp}$ , of test specimens were calculated following the Tang and Goel (1987) method (also used by Archambault et al.). As described in Section 6.3.1, the experimental fracture life of bracing member was calculated from the axial force-displacement hysteretic curve normalized by tensile yield force,  $P_y$  and yield displacement,  $\delta_y$ , respectively. When calculating the experimental fracture life of the specimen, section shape “A” specimens were calculated from the hysteretic curves normalized by  $P_y$  and  $\delta_y$ , however, as described earlier, tensile strengths of the section shape “B” specimens were limited by net section fracture rather than gross section yielding. Consequently, it is more reasonable to calculate the experimental fracture life of the section shape “B” specimens from the hysteretic curves normalized by tensile force and displacement,  $P_y^*$  and  $\delta_y^*$ , corresponding to the net section criterion (Eq. 5.1b). Resulting experimental fracture life of specimens are summarized in Table 6.2 and presented in Figures 6.34.

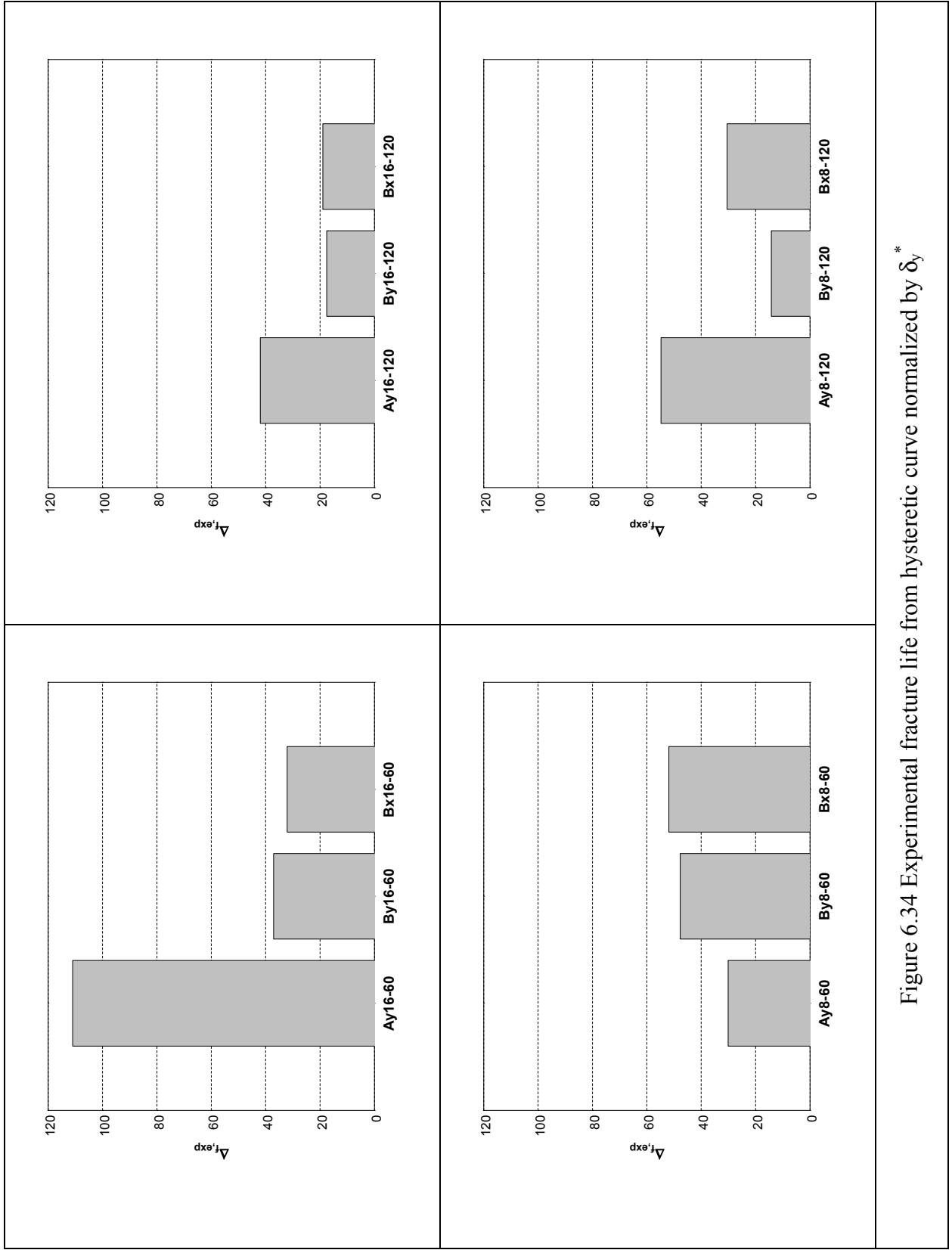


Figure 6.34 Experimental fracture life from hysteretic curve normalized by  $\delta_y^*$

Table 6.2 Experimentally obtained fracture life the specimens ( $\Delta_{f,exp}$ )

$\Delta_{f,exp}$	<b>From <math>\delta_y^*</math></b>	$\Delta_{f,exp}$	<b>From <math>\delta_y^*</math></b>
Ay16-60	111.00	Ay16-120	42.01
Ay8-60	30.12 <sup>*1</sup>	Ay8-120	54.80
$\Delta_{f,exp}$	<b>From <math>\delta_y^*</math></b>	$\Delta_{f,exp}$	<b>From <math>\delta_y^*</math></b>
By16-60	37.13	By16-120	17.54
By8-60	47.74	By8-120	14.25
$\Delta_{f,exp}$	<b>From <math>\delta_y^*</math></b>	$\Delta_{f,exp}$	<b>From <math>\delta_y^*</math></b>
Bx16-60	32.09	Bx16-120	18.99
Bx8-60	51.93	Bx8-120	30.51

\*1 Specimen Ay8-60 did not reach its maximum tensile strength.

Using proposed equations of the fracture life of bracing members by Tang and Goel (1987, Eq. 6.2) and Archambault et al. (1995, Eq. 6.3), fracture life of test specimens were calculated and resulting values are summarized in Table 6.3, then compared with those obtained from experimental results in Figure 6.35. For application of these equations to the built-up brace specimens, the brace shape factor term,  $[(4B/D+1)/5]$ , was ignored; while it was noted to have an impact on the fracture life of monolithic tubular bracing members, it is not applicable for built-up bracing members made of angles, plates, and lacings. When calculating the width-to-thickness ratio term in these equations, b/t ratios of angles of the specimens (i.e., 8 and 16) were used instead of using the term,  $[(B-2t)/t]$ .

Table 6.3 Predicted fracture life the specimens ( $\Delta_f$  and  $\Delta_f^*$ )

	$\Delta_f$	$\Delta_f^*$		$\Delta_f$	$\Delta_f^*$
Ay16-60	14.8	24.4	Ay16-120	14.8	51.0
Ay8-60	37.9	28.7	Ay8-120	37.9	52.7
	$\Delta_f$	$\Delta_f^*$		$\Delta_f$	$\Delta_f^*$
By16-60	18.1	28.7	By16-120	18.1	32.5
By8-60	59.3	40.7	By8-120	59.3	59.0
	$\Delta_f$	$\Delta_f^*$		$\Delta_f$	$\Delta_f^*$
Bx16-60	12.8	21.8	Bx16-120	12.8	31.1
Bx8-60	43.5	31.7	Bx8-120	43.5	54.7

$\Delta_f$ : Tang and Goel (1987)

$\Delta_f^*$ : Archambault et al. (1995)

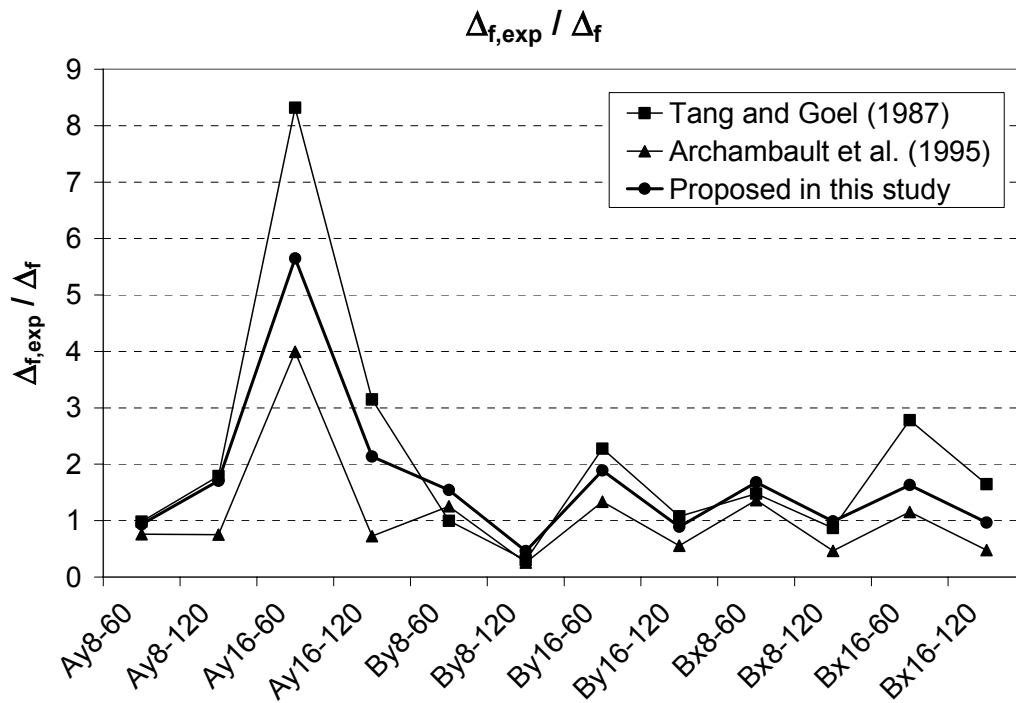


Figure 6.35 Comparisons of fracture life of the specimens

As shown in Figure 6.35, Tang and Goel model underestimated the fracture life of the test specimens while Archambault et al. model overestimated. As described earlier, these fracture criteria were developed to predict the fracture life of tubular bracing members, and it is therefore not surprising that they do not provide accurate estimates of the fracture life of built-up brace specimens. To improve predictions of the fracture life of built-up brace member, it is possible to develop a new model applicable for the built-up bracing members, and calibrated using the experimental data obtained in this study.

As shown in Figure 6.35, the Archambault et al. model under-estimated the experimental fracture life of the built-up specimens for 8 out of 11 specimens (recall that the twelfth specimen is Ay8-60 for which testing was stopped before fracture), with an average experimental to predicted fracture life ratio of 1.12 and a standard deviation of 1.03. Conservatively, the Tang and Goel model over-estimated the experimentally obtained fracture life for 7 out of 11 specimens, with an average ratio of 2.24 and a standard deviation of 2.19. The new model proposed for the built-up bracing members needed to be calibrated to be between these two models, i.e., safer than the

Archambault model and less conservative than the Tang and Goel mode. As described above, the Archambault model more closely predicted the fracture life of the specimens than the Tang and Goel model, and development of the new model was therefore based on the Archambault et al. model (Eq. 6.3). As described earlier, the Archambault et al. model mainly differ with the Tang and Goel model in that it considers the impact of slenderness ratio of the bracing member on fracture life. However, for the built-up brace specimens in this study, slenderness ratio was not found to have an impact on fracture life, as shown in Table 6.3, and effect of slenderness ratio was therefore ignored in the new model. Additionally the shape factor term,  $[(4B/D+1)/5]$ , was removed as done before for consistency because this term considers the width-to-depth ratio of tubular bracing member on the fracture life, which is not applicable for built-up braces. As a result, Eq. 6.3 was simplified to:

$$\Delta_f^{**} = C_s \frac{(46/F_y)^{1.2}}{(b/t)^{0.5}} \quad (6.4)$$

where, yield stress,  $F_y$  in ksi and the width-to-thickness term,  $[(B-2t)/t]$ , in Eq. 6.3 was simplified as  $(b/t)$ .

The effect of yield stress (i.e., the term  $(46/F_y)^{1.2}$  in Eq. 6.4) was not changed for lack of better data. Then, best values for the numerical coefficient term,  $C_s$ , and exponent to the width-to-thickness term,  $(b/t)^{0.5}$ , were sought to find the equation that best predicted the fracture life of built-up brace members. The resulting equation was found to be:

$$\Delta_f^{**} = C_s \frac{(46/F_y)^{1.2}}{[b/t]^{0.7}} \quad (6.5)$$

where the numerical coefficient  $C_s$  is 155.

Using Eq. 6.5, fracture life was calculated for the test specimens and results are also presented in Figure 6.35 (thicker line). The fracture life of the built-up bracing member thus obtained are

safer than predicted by the Archambault et al. model and less conservative than by the Tang and Goel model, with an average ratio of experimental to predicted fracture life of 1.78 and a standard deviation of 1.38.

#### **6.4 General Observations**

In this section, hysteretic characteristics such as energy dissipation, strength degradation, and low cycle fatigue life of the specimens obtained from test results of the specimens were quantitatively obtained. Energy dissipation capacity and strength degradation after buckling of the specimens in compression were quantified. Low cycle fatigue fracture life of the specimens was also calculated. From the analysis of test results presented in this section, a number of observations can be made.

First, it was established that the normalized energy dissipation,  $E_C/E_T$ , of built-up brace specimens typically decreases with increasing normalized displacements,  $\delta/\delta_{b,exp}$ , and dropped more rapidly for specimens having larger slenderness ratio. This is a similar trend to what was observed for monolithic braces by Lee and Bruneau (2002).

In addition, experimental results here show that when a bracing member is designed with a smaller width-to-thickness ratio,  $b/t$ , the normalized cumulative energy ratio decreases more significantly (a generally observed trend with the exception of specimens Bx for  $KL/r$  of 120 only). For the specimens having  $KL/r$  of 120, as shown in Figures 6.2 to 6.7, this trend was consistent regardless of the section shapes. The “Ay” and “By” specimens having  $b/t$  ratio of 16 experienced more inelastic cycles and deformation, consequently dissipated more cumulative compressive energy than the specimens having  $b/t$  ratio of 8. For the “Ay” and “By” specimens having  $KL/r$  of 60, comparisons of the cumulative energy ratios between specimens having  $b/t$  ratios of 8 and 16 is not possible, because testing of the Ay8-60 specimens stopped before the fracture of the specimen, and the By8-60 specimen would have been able to dissipate more normalized energy ratio during its first few cycles after buckling if not for its initial imperfection. Additionally, for the “Bx” specimens having  $KL/r$  of 60, the difference of the cumulative energy ratios between Bx8-60 ( $b/t$  ratio of 8) and Bx16-60 ( $b/t$  ratio of 16) was relatively small,

approximately within 10 percent, and consequently no general trend is observed in their cumulative energy ratios.

Second, the normalized compressive strength degradation,  $C_r''/C_r(\text{first})$  and  $C_r''/C_r(\text{last})$ , of the specimens having  $KL/r$  of 120 was more severe than that of specimens having  $KL/r$  of 60, as shown in Figures 6.13 to 6.30. At the normalized displacement,  $\delta/\delta_{b,\text{exp}}$ , of 5, the normalized compressive strength of specimens having  $KL/r$  of 120 drops 50 to 60 percent of the maximum value for the section shape “A” specimens and 70 to 80 percent for the section shape “B” specimens. For the section shape “A” and “B” specimens having slenderness ratio of 60, the corresponding reductions are 30 to 40 percent, and 50 to 70 percent in most cases. Additionally, slopes of the degradation, from the initial buckling to the normalized displacement,  $\delta/\delta_{b,\text{exp}}$ , of 5, were steeper for the specimens having  $KL/r$  of 120. This is a similar trend to what was observed for monolithic braces by Lee and Bruneau (2002).

Third, it was found that specimens having smaller  $KL/r$  of 60 and  $b/t$  ratio of 8 experienced more inelastic cycles until the entire fracture of the specimens. Section shape “B” specimens also showed similar trends with Ay specimens, except for the case of specimens By8-120 ( $KL/r = 120$ ,  $b/t = 8$ ) and By16-120 ( $KL/r = 120$ ,  $b/t = 16$ ). In this case, the specimen having larger  $b/t$  ratio (By16-120) showed approximately 19 percent larger low cycle fatigue fracture capacity than that having smaller  $b/t$  ratio (By8-60).

## CHAPTER 7

### SUMMARY AND CONCLUSIONS

#### 7.1 Summary

The objective of the research project reported here is to provide better knowledge on the seismic behavior of built-up laced members, supported by experimental results, and that can be broadly applicable to many structures that share similar structural characteristics and details.

Commonly encountered built-up brace details and configurations have been collected from actual bridges having laced members. Using this information, a limited experimental program was designed and conducted to investigate the hysteretic behavior of typical built-up compression members. Strength capacity of the specimens obtained from the testing was correlated with the predicted strength with AISC LRFD Specification (1999). Assessments of hysteretic properties such as ductility capacity, energy dissipation capacity, and strength degradation after buckling of the specimen were performed. Non-linear pushover analyses were also conducted and correlated with test results. The low cycle fatigue life of the specimens was quantified and compared with that predicted from models by other researchers.

#### 7.2 Conclusions

From the experimental data obtained from the testing of twelve laced built-up bracing members, and analyses of these results, the following conclusions can be made.

- (a) The experimentally obtained tensile strengths of the built-up bracing members matched relatively well those predicted using equations from the AISC LRFD Specification. When calculating the compressive strength of the built-up bracing members using the AISC LRFD Specification, the theoretical effective length factor,  $K$ , of 0.65 was found to more accurately match the experimental results for X-braced configuration. In single brace configuration, although the calculated effective length factors varied from 0.76 to 0.93, the theoretical

length factor,  $K$ , of 1.0 resulted in slightly under-estimating the compressive strength for the members in single braced configuration. Note that the full clear diagonal length should be used for the member length when calculating the compressive strength with above theoretical length factors.

- (b) Built-up bracing members having both larger slenderness and width-to-thickness ratio showed best ductility performance, while the bracing members having smaller slenderness and larger width-to-thickness ratio showed the worst ductility capacity. In built-up bracing members having smaller slenderness ratio and large width-to-thickness ratios, lower ductility capacity arises because local buckling precipitates low cycle fatigue. However, note that for the built-up bracing members having larger slenderness ratio, ductility capacity was not much affected by the  $b/t$  ratios.
- (c) Built-up bracing members with section shape “A” (forming I shapes) exhibited more ductile behavior than those with section shape “B” (forming box shapes). This is because buckling of the lacing that occurred in plastic hinge locations after buckling of the brace in section shape “B” built-up bracing members worsened the strength degradation in compression, while built-up bracing member with section shape “A” without lacing buckling behaved more closely to the monolithic bracing members.
- (d) The normalized energy dissipation ratio,  $E_C/E_T$  and the normalized compressive strength degradation,  $C_r''/C_r(\text{first})$  and  $C_r''/C_r(\text{last})$  of built-up brace members typically decrease with increasing normalized displacements  $\delta/\delta_{b,exp}$ , and the ratios for specimens having larger slenderness ratio dropped more rapidly than those for specimens having smaller slenderness ratio. Lacing buckling in built-up bracing members greatly affect strength degradation because as a result of lacing buckling, the components of the brace moved closer together, reducing the moment of inertia of the section at that location, also reducing the plastic moment at these hinges, and thus accelerating according by the loss in compression strength.

- (e) When a built-up bracing member is designed with smaller width-to-thickness ratio,  $b/t$ , and larger slenderness ratio,  $KL/r$ , then the normalized cumulative energy ratio decreases; this is a similar trend to what was observed for monolithic braces by Lee and Bruneau (2002).
- (f) Tensile and compressive strengths of section shape “A” built-up bracing members having small slenderness ratio were reasonably predicted by the analyses using DRAIN-2DX brace element No. 5, while analysis results over-estimated both tensile and compressive strengths of section shape “B” built-up bracing member having small slenderness ratio. This is because DRAIN-2DX element No. 5 only considers Euler buckling or compression yielding as possible limit states for the first buckling strength in compression, the latter case governing in this study for section shape “B”. Hysteretic behaviors in compression of built-up bracing members having  $KL/r$  of 60, were reasonably predicted by the analysis results, however, peak buckling capacity decrease after first buckling load was not replicated by the DRAIN-2DX analyses. Compressive strengths of built-up bracing members having large slenderness ratio, and overall shape of their hysteretic curves, were reasonably predicted by the analyses results when the calculated effective length factors,  $K$ , were used for the analyses. However, section shape “B” built-up bracing members having  $KL/r$  of 120 suffered significant compression strength degradation as described in (d) above. Again, this behavior was not captured by brace element No. 5 because this model does not consider local buckling and lacing buckling (nor does it include a fracture criterion).
- (g) Built-up bracing members having smaller slenderness ratio,  $KL/r$ , and width-to-thickness ratio,  $b/t$ , experienced larger number of inelastic cycles than those having larger slenderness ratio and width-to-thickness ratio. Proposed low cycle fracture life criteria by other researchers, Tang and Goel (1987) and Archambault et al. (1995), respectively over- and under-estimated the fracture life of built-up bracing members. A new criterion was proposed in this study applicable for estimating the low cycle fracture life of the built-up bracing members, which is safer than the Archambault et al. model and less conservative than the Tang and Goel model.

- (h) Although the laced built-up bracing members having smaller slenderness ratio dissipated substantial energy dissipation and experienced lots of inelastic cycles, these members failed to reach the target ductility of 3.0 before starting to fracture, while built-up bracing members having larger slenderness ratio had sufficient ductility to meet the ductility demand of 3.0 in most cases, although their normalized cumulative energy dissipation and fracture life capacities were much less than those having smaller slenderness ratio.
- (i) Built-up laced bracing members having larger slenderness ratio were shown to have less ductility capacity than monolithic bracing members (Lee and Bruneau, 2002), while those having smaller slenderness ratio showed ductility capacity comparable to monolithic bracing members. On average, the tested built-up bracing members with section shape “B” dissipated less normalized cumulative energy than monolithic bracing members, however those with section shape “A” dissipated slightly more normalized cumulative energy.

### **7.3 Recommendations for Future Research**

The results obtained from this study are valid within the context for which the tests were conducted. While useful results are obtained, there remains a significant need for future research. More specifically, the results show that improvements are needed in the DRAIN-2DX analysis model to enhance prediction of the hysteretic behavior of built-up bracing members. Likewise, more analytical and experimental study on the behavior of built-up bracing members is desirable, in particular to account for effects of random cyclic loading, boundary conditions effects, and damage accumulation. More specifically:

- (a) The brace element model (element No. 5) in DRAIN-2DX can be improved to better predict the tensile and compressive strengths of compressive members, particularly for bolted members for which net section behavior can be significant. The hysteretic behavior of built-up bracing members could be better modeled by introducing specific failure modes for net-section fracture of the member, and simple models for the progressive strength degradation in compression. Furthermore, since local buckling effect and fracture life have a dominant

impact on the hysteretic behavior of bracing members, some methods to model these behaviors into the physical brace elements should be implemented in brace element No.5.

- (b) Although loading protocol used in this study followed the procedure prescribed by the ATC 24 loading protocol, and is valid, the hysteretic behavior of built-up bracing members would likely be different if subjected to random cyclic loading. The effect of random cycle loading should therefore be studied, although this would be the case in a general sense, not just in the perspective of the cyclic hysteretic behavior of built-up compression members.
- (c) The effect of different boundary conditions should be investigated. It might even be partly accountable for the fact that the buckling axis changed direction during the testing of section shape Bx specimens, an observed behavior which was unsolved in this study, and that was also observed from the other similar research.
- (d) In this study, two different section shapes of built-up laced bracing members were selected and tested. These were selected further to a review of existing truss bridges having built-up bracing members in their sub-structures. From the limited comparisons of hysteretic behavior between these two section shapes, it was found that the configuration of a built-up bracing member may also have an effect on hysteretic behavior. Therefore, it would be worthwhile to investigate the hysteretic behaviors of built-up compressive members having other section configurations. Additionally, the behavior of X-braced frames having built-up bracing members, rather than the study of the built-up bracing members themselves, might also be of interest for engineers involved in the seismic retrofit of steel truss bridges.
- (e) For the seismic retrofit of steel built-up bracing members, designers sometimes consider the rigidity of gusset connections, which introduce flexure at the end of the members, and treat the laced built-up members as beam-columns. Although this effect was indirectly accounted for by doing the comparisons using the effective length factor,  $K$ , development or modification of the axial force-moment interaction relationship applicable for the built-up compression members should be investigated, using previous test results and results of this study (see Uang and Kleiser, 1997, for some work on this topic).

- (f) Damage accumulation process is an important issue in low cycle fracture life of the steel built-up members. As observed in this study, qualitative change of buckling mode (from out-of-plane to in-plane) can happen during the inelastic loading process. This area should be further investigated.
  
- (g) Further research in general on the seismic behavior of concentrically braced frame is sorely needed, as revealed by the literature review and finding of this study. Important topics include the need to reassess the relevance of  $KL/r$  as a design criterion to ensure satisfactory seismic response, and the development of better models to predict fracture life and other key limit states for braces.

## CHAPTER 8

### REFERENCES

American Institute of Steel Constructions, Inc. (1999), “Load and Resistance Factor Design Specification for Structural Steel Buildings”, AISC, Chicago, Illinois.

Applied Technology Council (1992), “Guidelines for Cyclic Seismic Testing of Components of Steel Structures”, *Report No. ATC-24*, ATC, Redwood City, California.

Archambault, Marie-Hélène, Tremblay, Robert and Filiatrault, André (1995), Étude du Comportement Séismique des Contreventements Ductiles en X Avec Profilés Tubulaires en Acier”, *Rapport No. EPM/GCS-1995-09*, Département de Génie Civil Section Structures, École Polytechnique, Montréal, Quebec, Canada.

ASTM (1997), “Standard Specification for Commercial Steel Sheet, Carbon, Cold-Rolled”, A 366/A 336M-97, American Society for Testing and Materials, Philadelphia, Pennsylvania.

Caltrans, (1995), “A Guideline for Seismic Retrofit Evaluation and Design of Latticed Members and Their Connections on San Francisco – Oakland Bay Bridge”, *Caltrans Report*, Division of Structure, California Department of Transportation, Sacramento, California.

Dameron, R. A., Maxwell, J. S. and Dunham, R. S. (1997), “Pre-Test Analysis of Three UCSD Laced Member Tests and Laced Member Modeling Recommendations, *Report to Caltrans Laced Member Research Project Team*, September, ANATECH, San Diego, California.

Dietrich, Adrienne M. and Itani, Ahmad M., “Cyclic Behavior of Built-up and Perforated Steel Members on the San Francisco–Oakland Bay Bridge”, *Report No. CCEER 99-9*, June, Center for Civil Engineering Earthquake Research, University of Nevada, Reno, Nevada.

Galambos, Theodore V. (1998), “Guide to Stability Design Criteria for Metal Structures, 5<sup>th</sup> edition”, John Willey & Sons, New York, New York.

Gere, James M. and Timoshenko, Stephen P. (1984), “Mechanics of Material second edition”, Brooks/Cole Engineering Division, Wadsworth, Inc., Belmont, California.

Gugerli, H. and Goel, S. C. (1982), “Inelastic Cyclic Behavior of Steel Bracing Members”, *Report No. UMEE 82R1*, January, Department of Civil Engineering, The University of Michigan, Ann Arbor, Michigan.

Hassan, O. F. and Goel, S. C. (1991), “Modeling of Bracing Members and Seismic Behavior of Concentrically Braced Steel Structures”, *Report No. UMCE 91-1*, January, Department of Civil Engineering, The University of Michigan, Ann Arbor, Michigan.

Itani, Ahmad M., Vesco, Timothy D., and Dietrich, Adrienne M. and, “Cyclic Behavior of As-Built Laced Members with End Gusset Plates on the San Francisco–Oakland Bay Bridge”, *Report No. CCEER 98-01*, March, Center for Civil Engineering Earthquake Research, University of Nevada, Reno, Nevada.

Ketchum, Milo Smith (1920), “The Design of Highway Bridges of Steel, Timber and Concrete,” McGraw-Hill Co., New York, New York.

Kunz, F. C. (1915), “Design of Steel Bridges; Theory and Practice for use of Civil Engineers and Students,” McGraw-Hill Co., New York, New York.

Lee, Kangmin. and Bruneau, Michel (2002), “Review of Energy Dissipation of Compression Members in Concentrically Braced Frames”, *Report No. MCEER-02-0005*, October, Multidisciplinary Center for Earthquake Engineering Research, State University of New York, Buffalo, New York.

Lee, S. and Goel, S. C. (1987), “Seismic Behavior of Hollow and Concrete-Filled Square Tubular Bracing Members”, *Report No. UMEE 87-11*, December, Department of Civil Engineering, The University of Michigan, Ann Arbor, Michigan.

Prakash, V. and Powell, G. H. (1993), “DRAIN-2DX, DRAIN-3DX and DRAIN-BUILDING, Base Program Design Documentation”, *Report No. UCB/SEMM-93/16*, December, Structural Engineering Mechanics and Materials, University of California, Berkeley, California.

Roeder, Charles W., Leon, Roberto T., and Preece, F. Robert, (1994), “Strength, Stiffness and Ductility of Older Steel Structures under Seismic Loading”, *Report No. SGEM 94-4*, December, Department of Civil Engineering, University of Washington, Seattle, Washington.

Taddei, Pascal (1995), “Implementation of the Refined Physical Theory Model of Braced Steel Frames in NONSPEC and DRAIN-2DX”, August, Department of Civil Engineering, The University of Ottawa, Ottawa, Ontario, Canada.

Tang, Xiaodong and Goel, Subhash C. (1987), “Seismic Analysis and Design Considerations of Braced Steel Structures”, *Report No. UMCE 87-4*, April, Department of Civil Engineering, The University of Michigan, Ann Arbor, Michigan.

Uang, Chia-Ming and Kleiser, Michael (1997), “Cyclic Performance of As-Built Latticed Members for the San Francisco-Oakland Bay Bridge,” *Report No. SSRP-97/01*, June, Division of Structural Engineering, University of California, San Diego, La Jolla, California.



# **APPENDIX A**

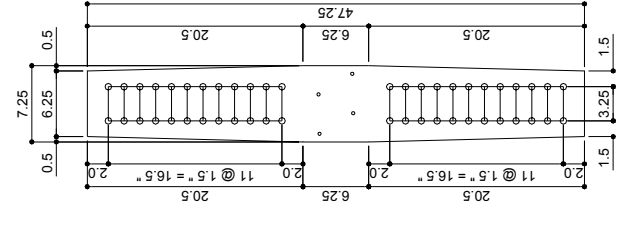
## **Drawings for Specimens and Boundary Frames**



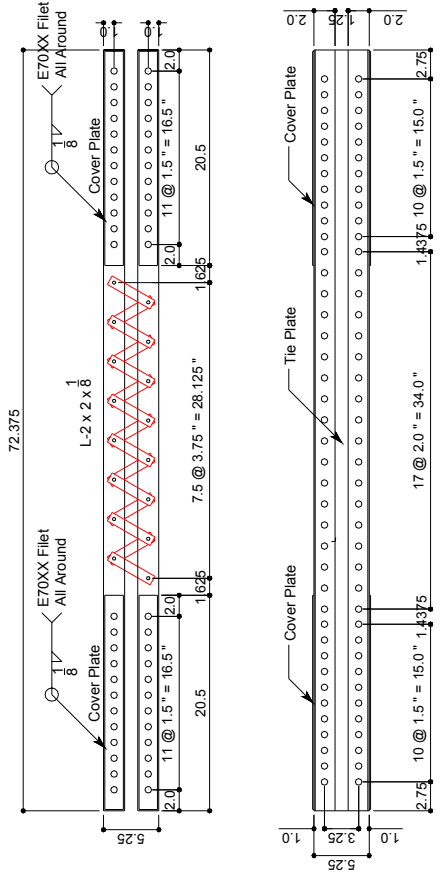
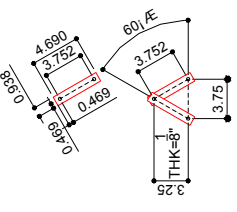




Middle Connection Plate:  $\frac{3}{8}$ " Thk.  
 $\phi 2$ " A307 Bolts with  $\phi 2$ " Holes



Lacings Plates:  $\frac{1}{8}$ " x  $16$ "  
 $\phi 16$ " dia. A307 Bolts with  $\phi 16$ " Holes



Cover Plates:  $\frac{1}{8}$ " x  $14$ " x  $20\frac{3}{8}$ "  
 $\phi 2$ " dia. A307 Bolts with  $\phi 2$ " Holes  
 Tie Plates(short):  $\frac{1}{8}$ " x  $5\frac{1}{4}$ " x  $72\frac{3}{8}$ "  
 $\phi 2$ " dia. A307 Bolts with  $\phi 2$ " Holes

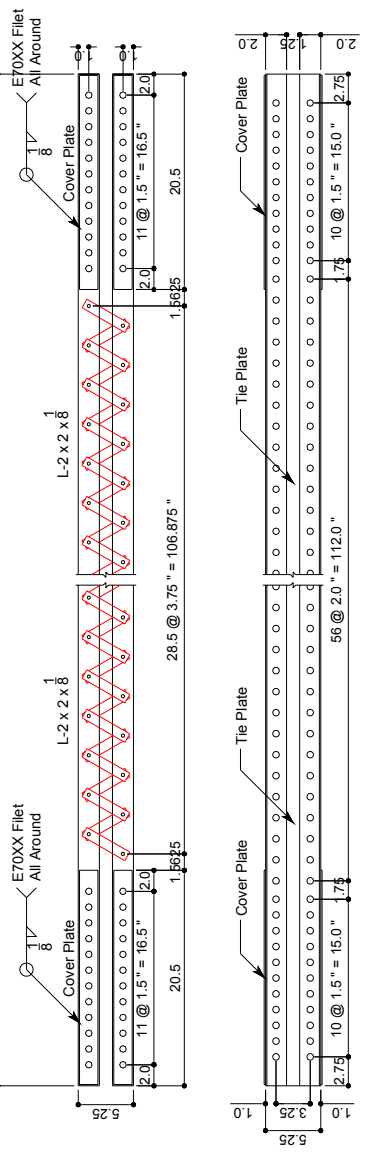


Figure A.4 Drawings for the specimen By16





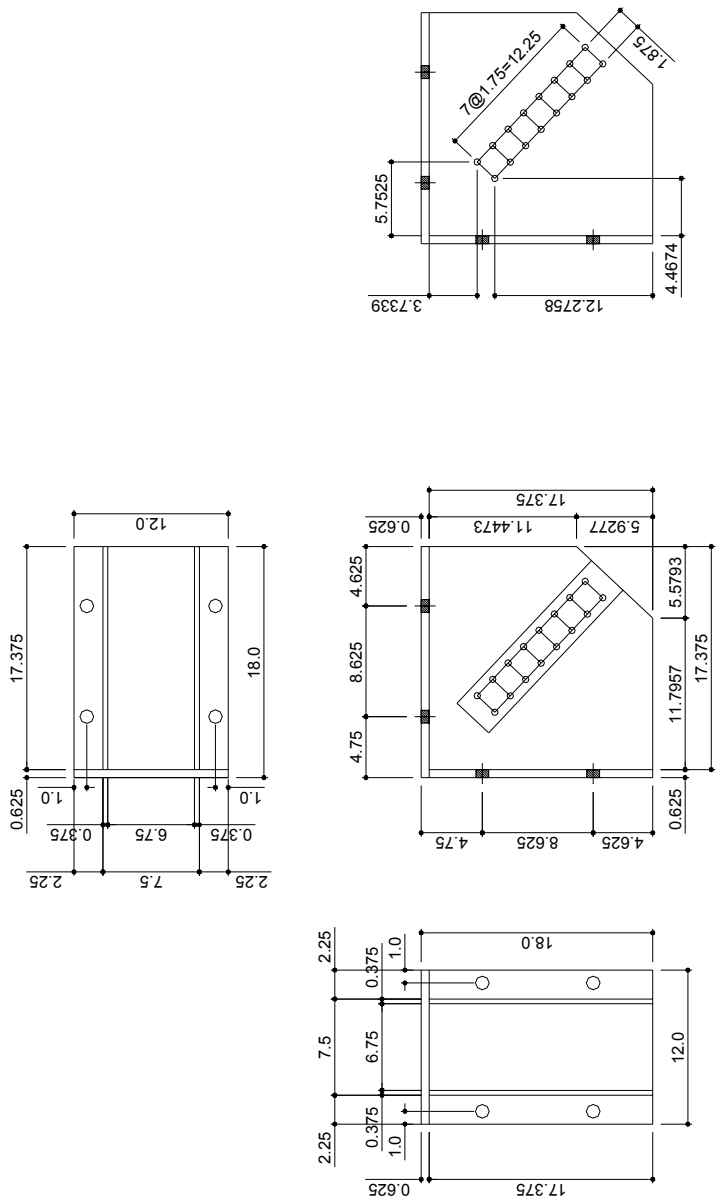


Figure A.7 Drawings for the gusset of the specimen Ay8

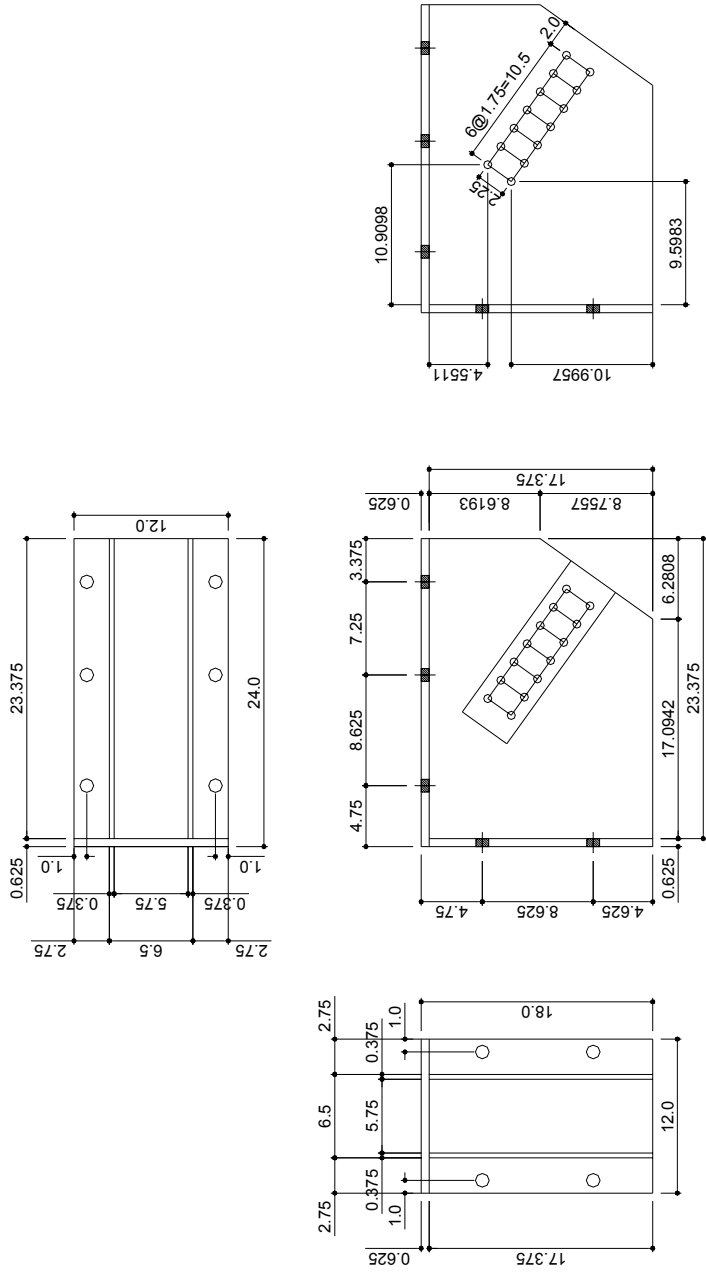


Figure A.8 Drawings for the gusset of the specimen Ay16

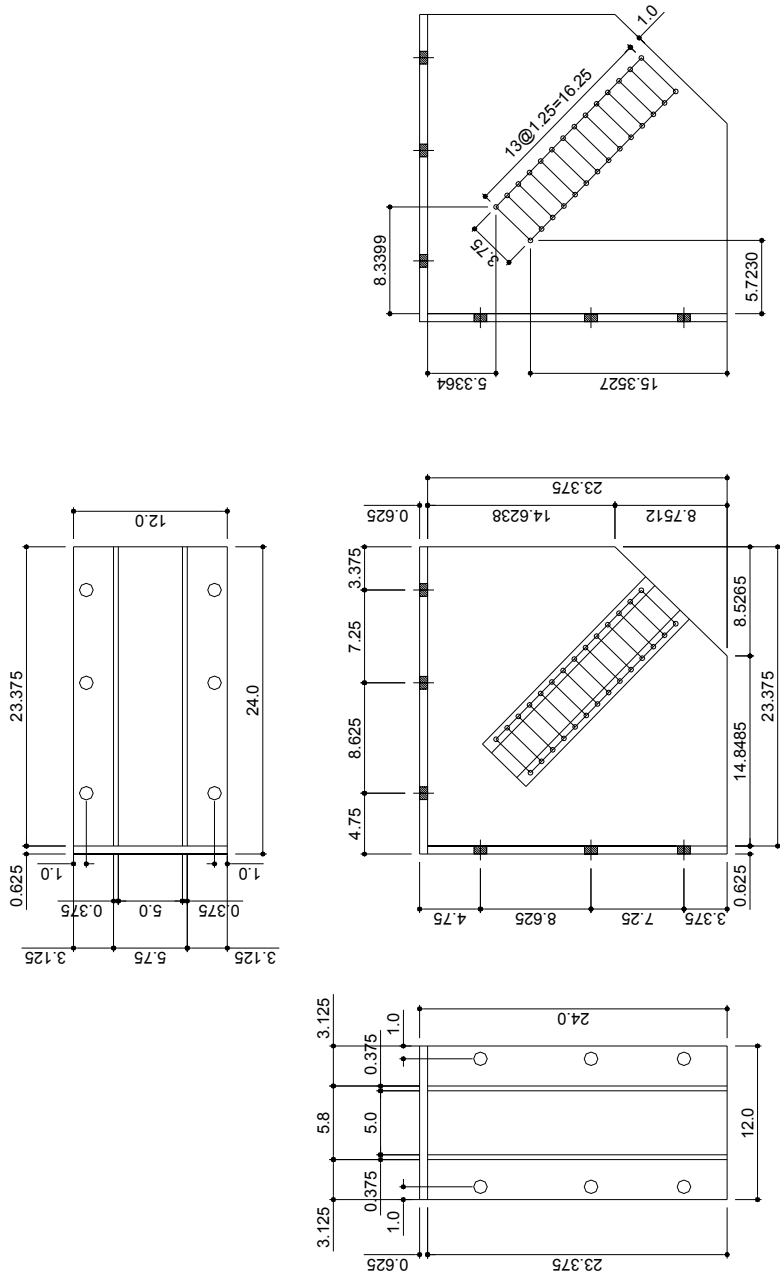


Figure A.9 Drawings for the gusset of the specimen By8

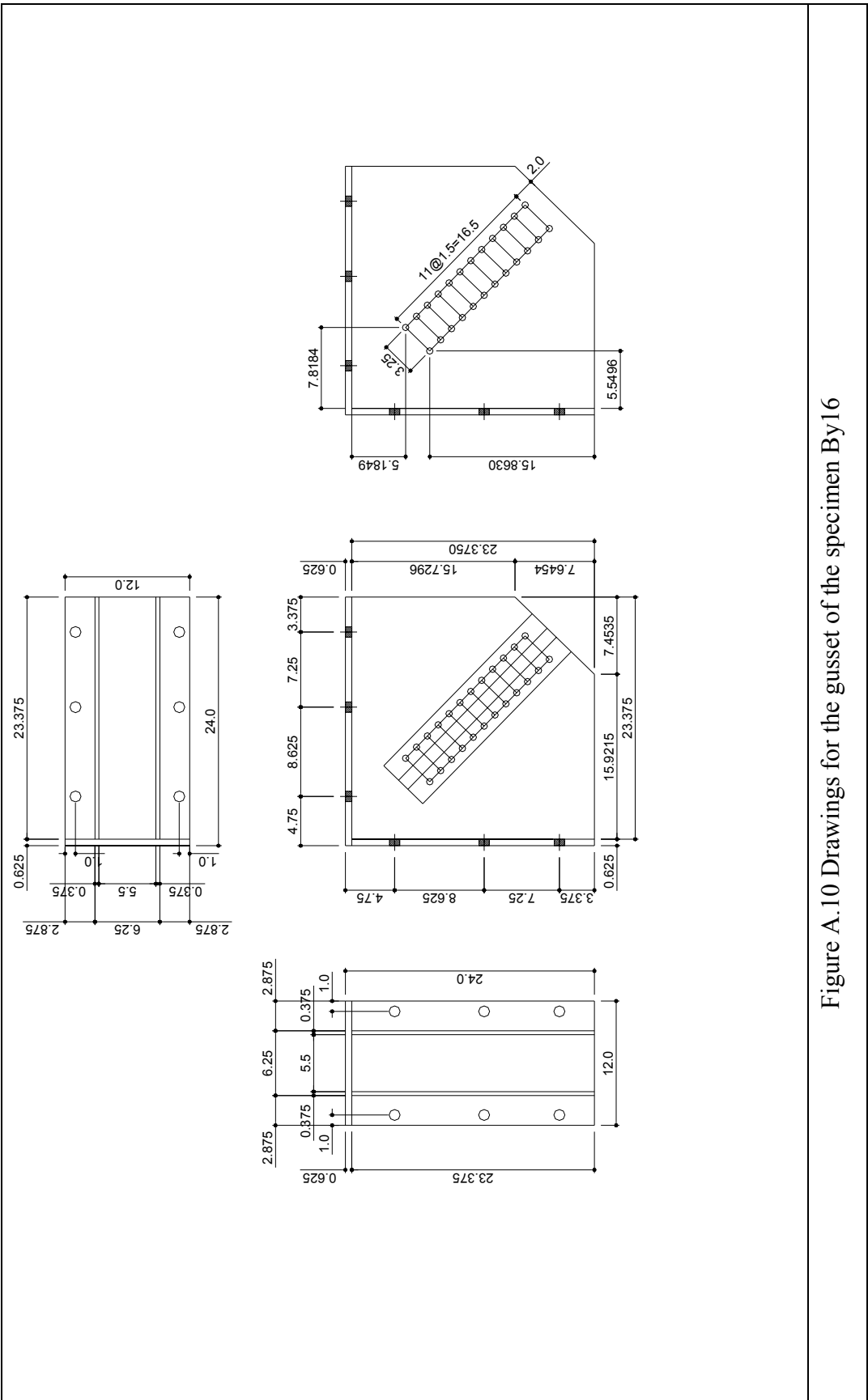


Figure A.10 Drawings for the gusset of the specimen By16

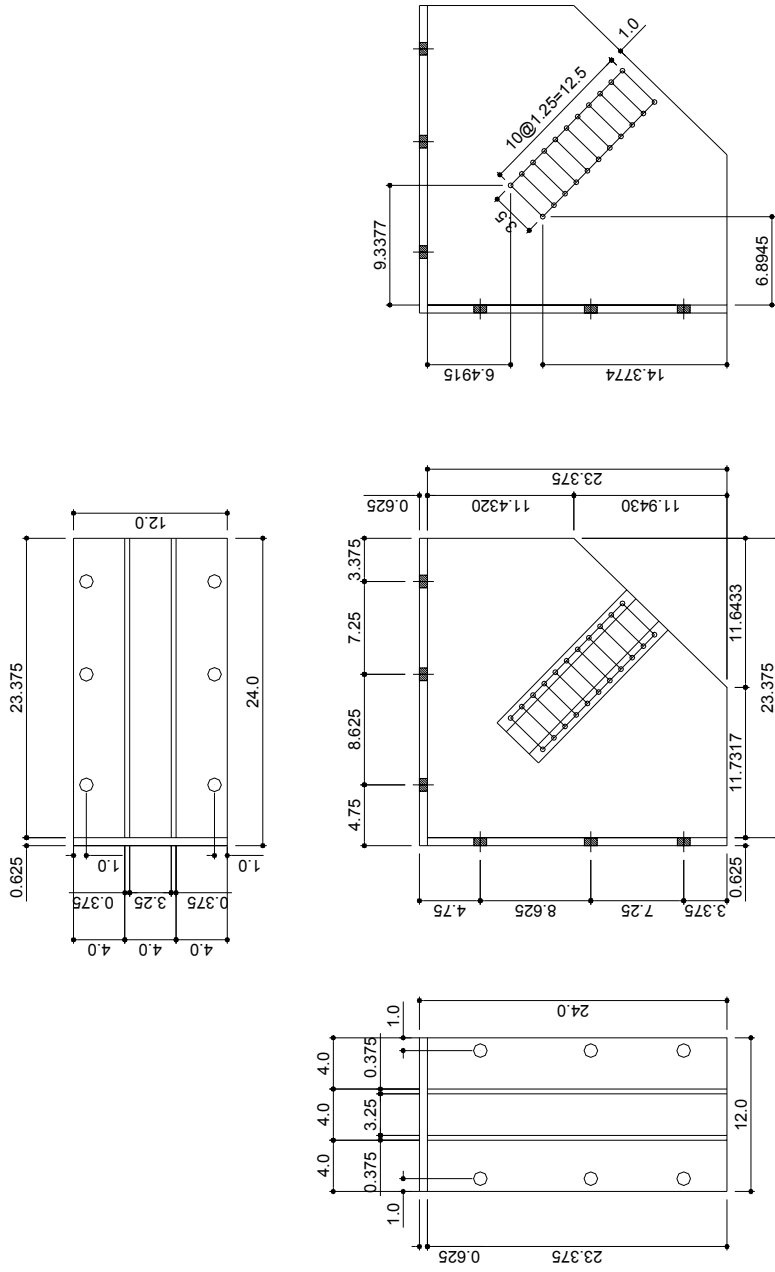


Figure A.11 Drawings for the gusset of the specimen Bx8



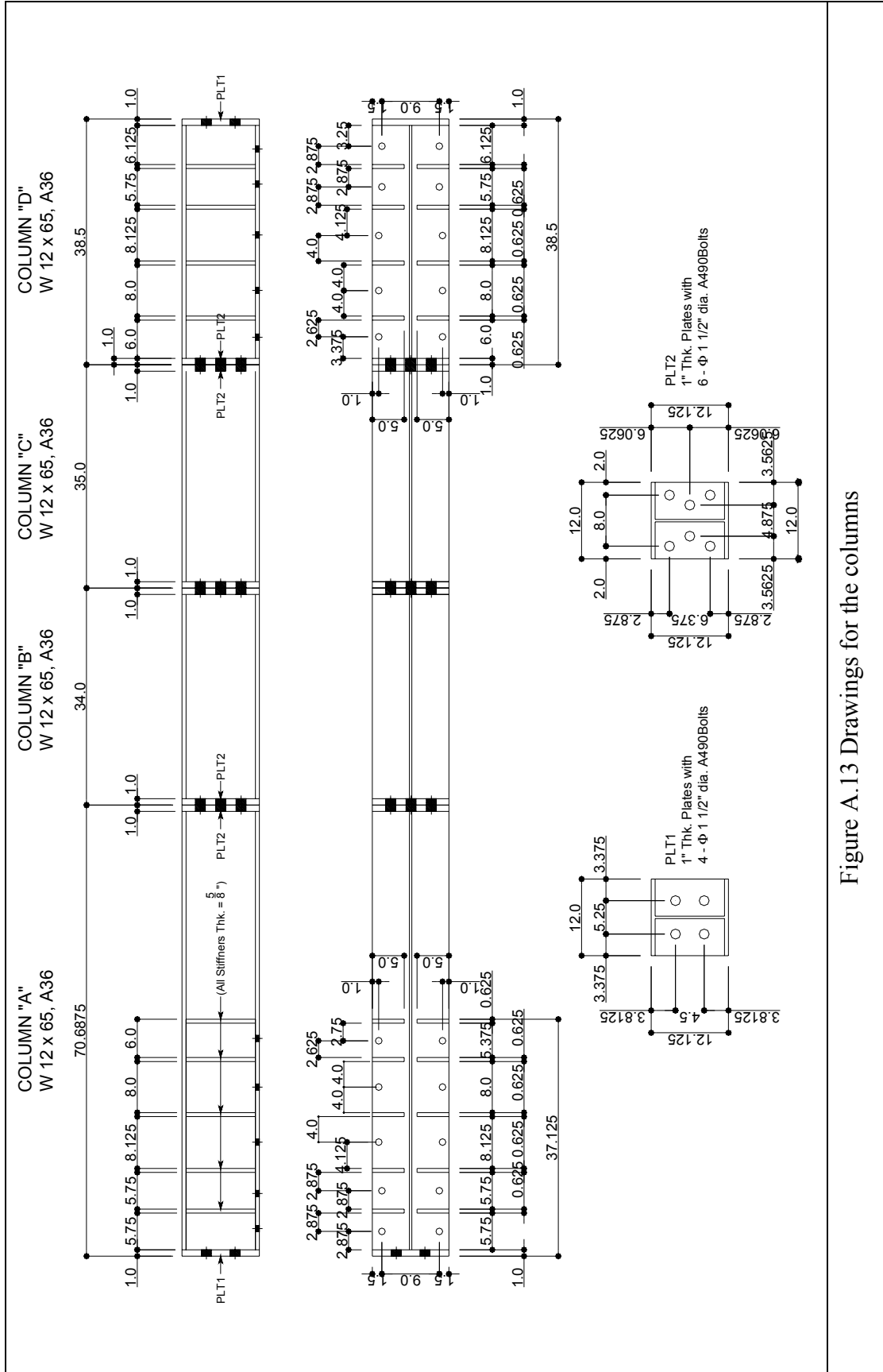


Figure A.13 Drawings for the columns

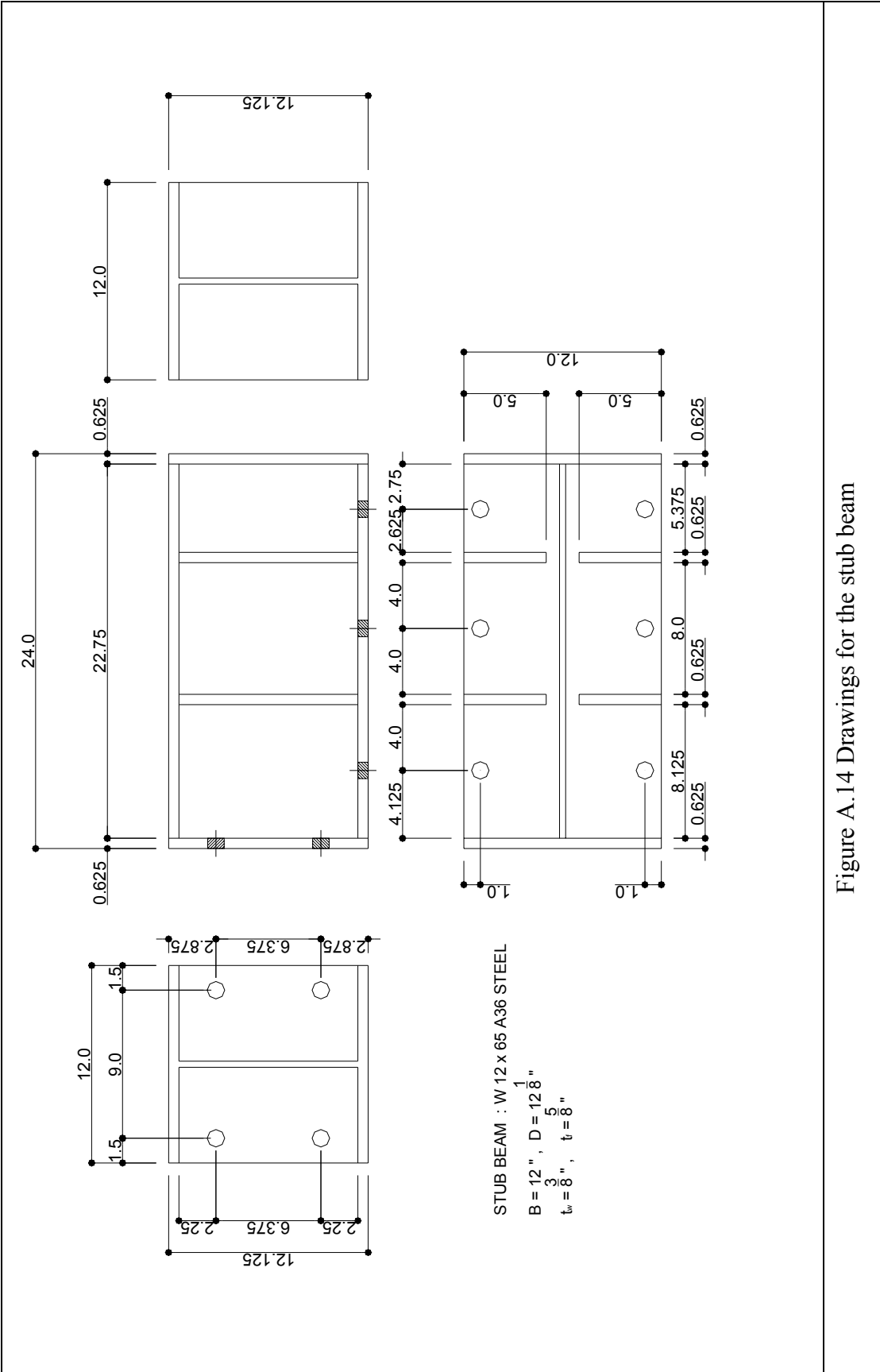


Figure A.14 Drawings for the stub beam

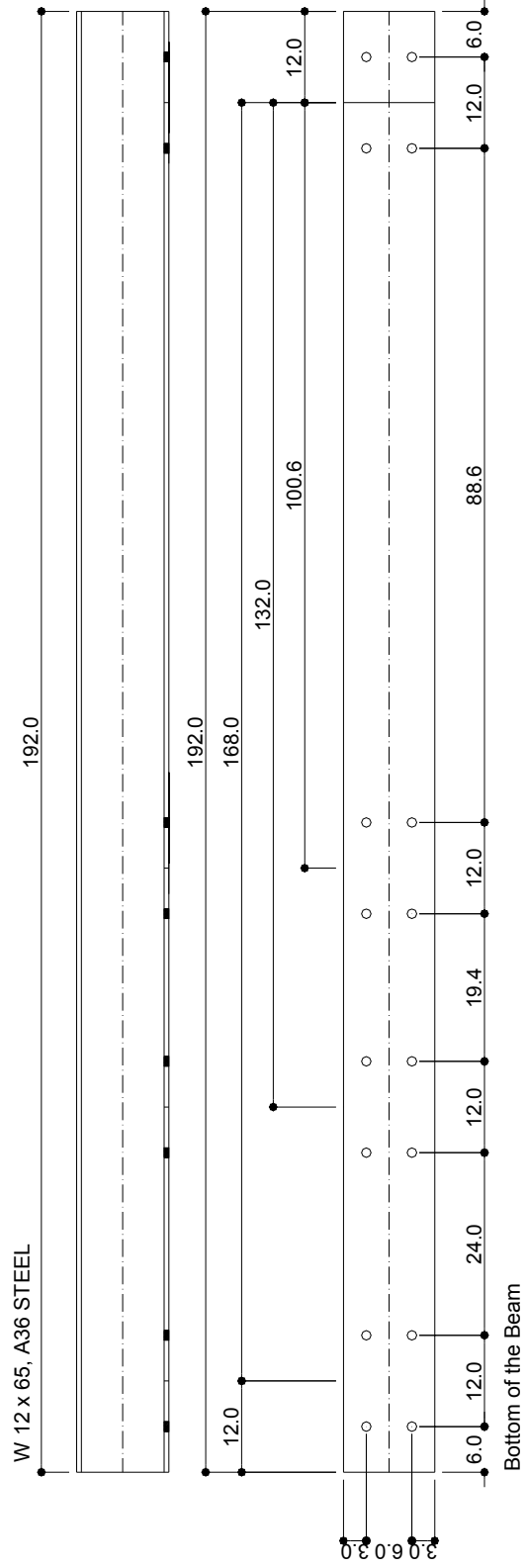


Figure A.15 Drawings for the top beam

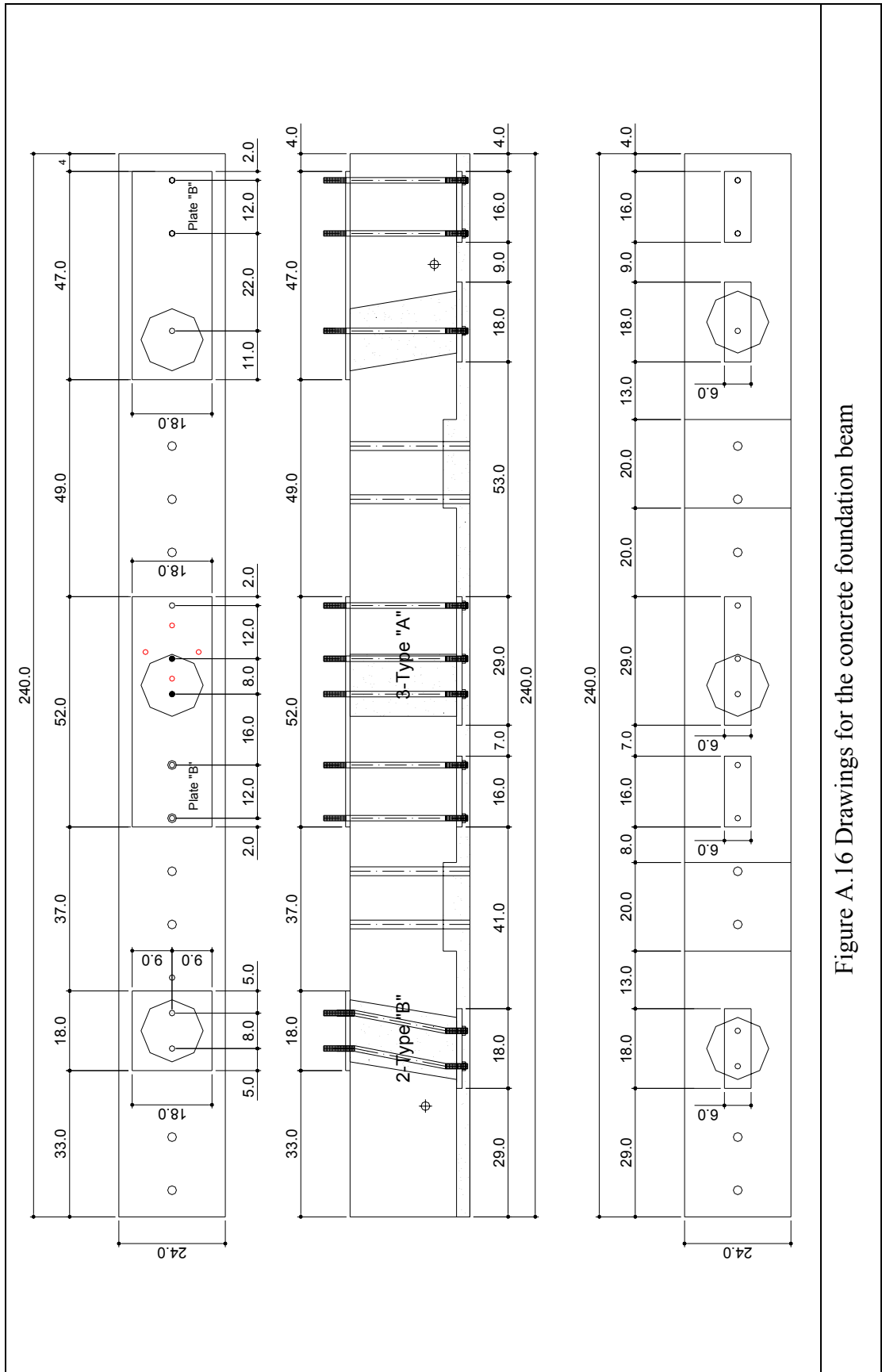


Figure A.16 Drawings for the concrete foundation beam

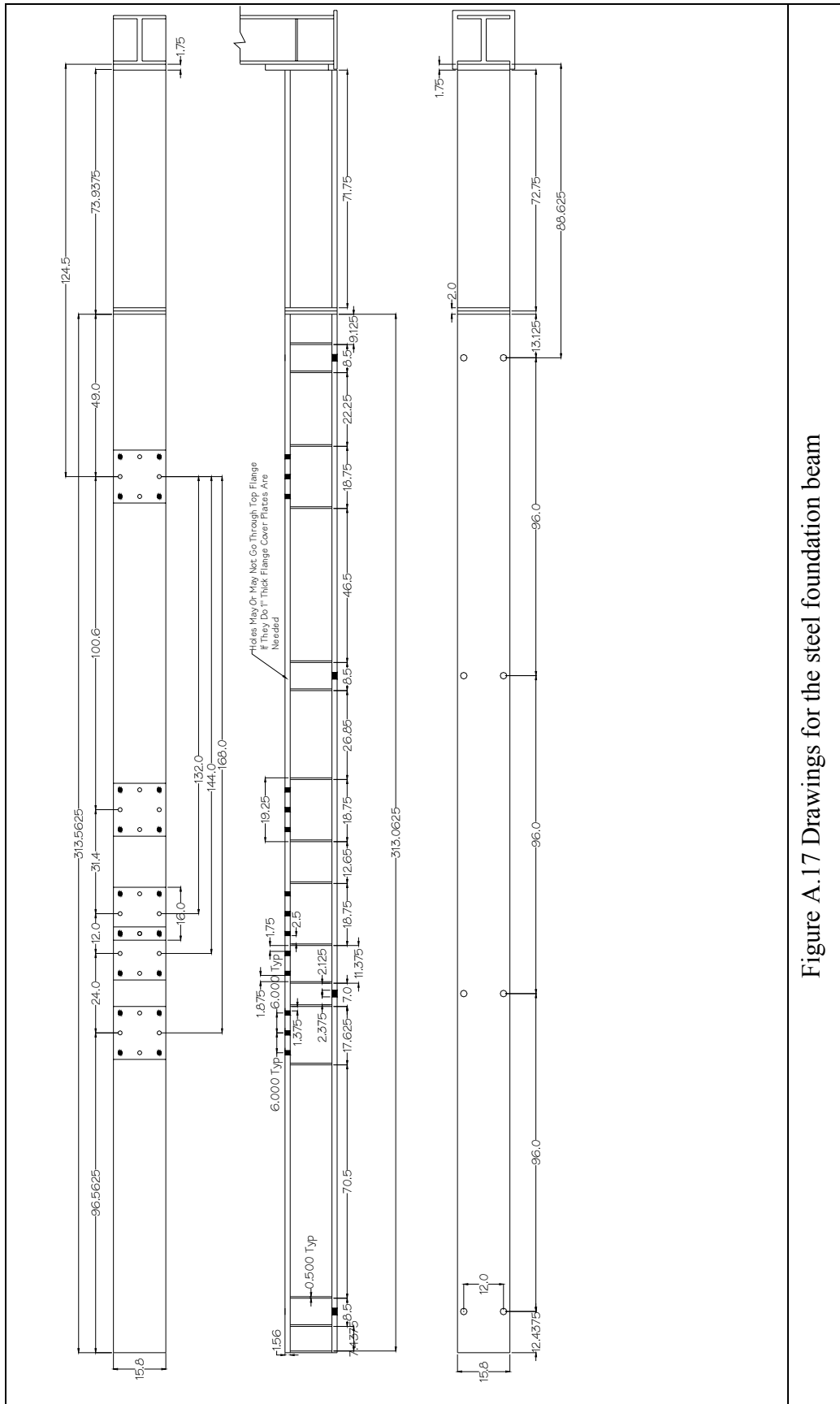


Figure A.17 Drawings for the steel foundation beam





## **APPENDIX B**

### **Experimental Observations Made During Testing**

Table B.1 Observations made during testing of the Ay8-60 specimen

CYCLE NO.	CONTROL DATA	$\Delta/\Delta_{b,exp}$	OBSERVATIONS
1 – 2	$\Delta = 0.2"$ (5.08 mm)	0.2	Control data, $\Delta$ = Equivalent horizontal buckling frame drift Elastic Cycles
3 – 4	$\Delta = 0.3"$ (7.62 mm)	0.3	Elastic Cycles
5 – 6	$\Delta = 0.4"$ (10.16 mm)	0.4	Elastic Cycles
7 – 8	$\Delta = 0.5"$ (12.70 mm)	0.5	Elastic Cycles
9 – 10	$\Delta = 0.65"$ (16.51 mm)	0.65	Elastic Cycles
11 – 12	$\Delta = 0.8"$ (20.32 mm)	0.8	Elastic Cycles
13 – 15	$\Delta = 1.0"$ (25.40 mm)	1.0	@-13: Global buckling
16 – 18	$\Delta = 1.2"$ (30.48 mm)	1.2	@-16: Local buckling Testing was stopped without fracture to prevent severe damage on the other diagonal specimen (Ay8-120)

Table B.2 Observations made during testing of the Ay8-120 specimen

CYCLE NO.	CONTROL DATA	$\delta/\delta_{b,exp}$	OBSERVATIONS
1 – 2	$\delta = 0.015''$ (0.38 mm)	0.1	Control data, $\delta$ = Diagonal axial displacement Elastic cycles
3 – 5	$\delta = 0.037''$ (0.94 mm)	0.23	Elastic cycles
6 – 8	$\delta = 0.064''$ (1.63 mm)	0.4	Elastic cycles
9 – 11	$\delta = 0.121''$ (3.07 mm)	0.75	Elastic cycles
12 – 14	$\delta = 0.16''$ (4.06 mm)	1.0	@-12: Global buckling at the mid-length of the specimen
15 – 17	$\delta = 0.32''$ (8.13 mm)	2.0	@-15: Larger buckling at the mid-length of the specimen with local buckling
18 – 20	$\delta = 0.48''$ (12.19 mm)	3.0	Buckling matured
21 – 22	$\delta = 0.64''$ (16.26 mm)	4.0	@+21: Initial fracture on the angle
23 – 27	$\delta = 0.72''$ (18.29 mm)	4.5	Fracture getting worse
28 – 30	$\delta = 0.80''$ (20.32 mm)	5.0	Fracture getting worse
31 – 34	$\delta = 0.96''$ (24.38 mm)	6.0	@+38: Entire fracture

Table B.3 Observations made during testing of the Ay16-60 specimen

CYCLE NO.	CONTROL DATA	$\delta/\delta_{b,exp}$	OBSERVATIONS
1 – 3	$\delta = 0.074''$ (1.87 mm)	1/3	Control data, $\delta =$ Diagonal displacement Elastic cycles
4 – 6	$\delta = 0.147''$ (3.73 mm)	2/3	@-4: Local buckling on the angle near the gusset-connection of the North segment of the specimen (West – lower)
7 – 10	$\delta = 0.22''$ (5.61 mm)	1.0	@-7: Local buckling on the angle near the middle connection plate of the North segment of the specimen (West – upper)
11 – 13	$\delta = 0.275''$ (7.00 mm)	1.25	1.5 $\delta_{b,exp}$ N + 1.0 $\delta_{b,exp}$ S @-11: Local buckling on the angle near the gusset-connection of the North segment of the specimen (East – lower) @-11: Local buckling on the angle near the middle connection plate of the North segment of the specimen (West – lower)
14 – 16	$\delta = 0.330''$ (8.38 mm)	1.5	2.0 $\delta_{b,exp}$ N + 1.0 $\delta_{b,exp}$ S Local buckling was getting worse
17 – 20	$\delta = 0.385''$ (9.78 mm)	1.75	2.5 $\delta_{b,exp}$ N + 1.0 $\delta_{b,exp}$ S @+20: Fracture on the angle near the middle connection plate of the North segment of the specimen (West – lower)
21 – 23	$\delta = 0.440''$ (11.18 mm)	2.0	3.0 $\delta_{b,exp}$ N + 1.0 $\delta_{b,exp}$ S @+20: Fracture was getting worse @+22: Fracture on the angle near the middle connection plate of the North segment of the specimen (East – upper)
24	$\delta = 0.495''$ (12.57 mm)	2.0	3.5 $\delta_{b,exp}$ N + 1.0 $\delta_{b,exp}$ S
25 – 26	$\delta = 0.550''$ (13.97 mm)	2.5	4.0 $\delta_{b,exp}$ N + 1.0 $\delta_{b,exp}$ S Fractures were getting worse
27	$\delta = 0.660''$ (16.76 mm)	3.0	5.0 $\delta_{b,exp}$ N + 1.0 $\delta_{b,exp}$ S @+27: Entire Fracture on the lower angle near the middle connection plate of the North segment of the specimen

Table B.4 Observations made during testing of the Ay16-120 specimen

CYCLE NO.	CONTROL DATA	$\delta/\delta_{b,exp}$	OBSERVATIONS
1 – 6	1/3 $\delta_b$ 2/3 $\delta_b$	1/3 2/3	Control data, $\delta$ = Entire diagonal displacement Elastic cycles 1/3 $\delta_b$ = 0.029" (= 0.74mm), 2/3 $\delta_b$ = 0.058" (= 1.47mm)
7 – 9	1.0 $\delta_b$	1.0	@-7: Global buckling was observed and $\delta_{b,exp}$ = 0.088" (2.24 mm) was identified
10 - 12	$\delta$ = 0.131" (3.33 mm)	1.5	@-10: Local buckling on angle near the South gusset-connection @-10: Global and Local buckling near the mid-length of the specimen
13 - 15	$\delta$ = 0.175" (4.45 mm)	2.0	
16 - 18	$\delta$ = 0.263" (6.68 mm)	3.0	@-16: Local buckling on the lower angle at the 1/3 member length from South end of the specimen
19 - 21	$\delta$ = 0.263" (6.68 mm)	3.0	During controller set-up, unexpected force was applied in compression with larger buckling without data acquisition @-19: Local buckling near the mid-length of the specimen
22 - 24	$\delta$ = 0.350" (8.89 mm)	4.0	
25 - 27	$\delta$ = 0.350" (8.89 mm)	4.0	Three comparison cycles without axial load
28 - 30	$\delta$ = 0.438" (11.05 mm)	5.0	@+28: Initial fracture near the mid-length of the specimen (West – lower)
31 – 40	$\delta$	6.0 to 10.0	Fractures were getting worse
41 – 42	$\delta$ = 0.963" (24.46 mm)	11.0	@+41: Fracture on the upper angles near the South gusset-connection
43 – 44	$\delta$ = 1.050" (26.67 mm)	12.0	@+43: Fracture on lower angle at the 1/3 of the member length from the South end of the specimen
45 – 46	$\delta$ = 1.138" (28.91 mm)	13.0	
47 – 48	$\delta$ = 1.226" (31.14 mm)	14.0	14.0 $\delta_{b,exp}$ in tension and 13.0 $\delta_{b,exp}$ in compression (actuator stroke problem)
49 – 50	$\delta$ = 1.313" (33.35 mm)	15.0	15.0 $\delta_{b,exp}$ in tension and 13.0 $\delta_{b,exp}$ in compression
51 – 52	$\delta$ = 1.401" (35.59 mm)	16.0	16.0 $\delta_{b,exp}$ in tension and 13.0 $\delta_{b,exp}$ in compression @+51: Failure in a bolt near the initial fracture location
53	$\delta$ = 1.488" (37.80 mm)	17.0	17.0 $\delta_{b,exp}$ in tension and 13.0 $\delta_{b,exp}$ in compression @+53: Entire fracture

Table B.5 Observations made during testing of the By8-60 specimen

CYCLE NO.	CONTROL DATA	$\delta/\delta_{b,exp}$	OBSERVATIONS
1 - 3	$P_H = 18$ kips (80.1 kN)	0.5	Control data : Horizontal Force Elastic cycles $P_H @ 1/3 \delta_b = 18$ kips (80.1 kN),
4 - 6	$\delta = 0.14''$ (3.56 mm)	1.0	@-4: Global buckling
7 - 9	$\delta = 0.21''$ (5.33 mm)	1.5	@-7: Larger global buckling in the North segment of the Specimen @+7: Yielding cracks in the North segment of the Specimen
10 - 12	$\delta = 0.28''$ (7.11 mm)	2.0	@-10: Lacing buckling -North specimen: West 6 <sup>th</sup> lacing from top (@0.21"=5.33mm) 2 <sup>nd</sup> 4 <sup>th</sup> 6 <sup>th</sup> 8 <sup>th</sup> (@0.28"=7.11mm) -North specimen: East 2 <sup>nd</sup> lacing from top (@0.21"=5.33mm) 3 <sup>rd</sup> 5 <sup>th</sup> 7 <sup>th</sup> (@0.28"=7.11mm) @-11: Force drop due to lacing buckling @-12: Local buckling on upper angle in the North segment of the Specimen
13 - 15	$\delta = 0.35''$ (8.89 mm)	2.5	@-14: Lacing bolting failure on the East 2 <sup>nd</sup> lacing
16 - 18	$\delta = 0.42''$ (10.67 mm)	3.0	@-17: Lacing buckling East 3 <sup>rd</sup> lacing (North segment) @-17: Local buckling on the angle near 5 <sup>th</sup> lacing bolt location @-18: Fracture on the lower angle near 5 <sup>th</sup> lacing @+18: Lacing bolt failure East 3 <sup>rd</sup> lacing (North segment) West 5 <sup>th</sup> lacing (North segment)
19 - 20	$\delta = 0.56''$ (14.22 mm)	4.0	
21 - 22	$\delta = 0.70''$ (17.78 mm)	5.0	@+21: 2 angles completely fractured near the 4 <sup>th</sup> and 5 <sup>th</sup> lacing
23 - 24	$\delta = 0.84''$ (21.34 mm)	6.0	@+23: 4 angles completely fractured near the 4 <sup>th</sup> and 5 <sup>th</sup> lacing
25	$\delta = 1.12''$ (28.45 mm)	8.0	@+25: Entire fracture

Table B.6 Observations made during testing of the By8-120 specimen

CYCLE NO.	CONTROL DATA	$\delta/\delta_{b,exp}$	OBSERVATIONS
1 – 9	Horizontal $P_H$	0.18 0.36 0.61	Control data : Horizontal Force Elastic cycles $P_H$ @1/3 $\delta_b$ =10 kips (44.5kN), $P_H$ @2/3 $\delta_b$ =20 kips (89.0kN) $P_H$ @1.0 $\delta_b$ =33 kips (146.85kN)
10 – 12	$\delta = 0.28''$ (7.11 mm)	1.0	@10: $P_H = 42.0$ kips (186.90 kN) @11: $P_H = 43.5$ kips (193.58 kN) @12: $P_H = 45.0$ kips (200.25 kN) @-12: Large buckling @-12: Lacing bolt failures West: 4 <sup>th</sup> and 5 <sup>th</sup> from the South East: 3 <sup>rd</sup> , 5 <sup>th</sup> , and 6 <sup>th</sup> from the South @-12: Lacing buckling West 2 <sup>nd</sup> and 12 <sup>th</sup> from the South East 5 <sup>th</sup> and 9 <sup>th</sup> from the South @-12: Local buckling on the lower angles near the global buckling location
13 - 15	$\delta = 0.56''$ (14.22 mm)	2.0	2.0 $\delta_{b,exp}$ in compression, 1.5 $\delta_{b,exp}$ in tension
16 - 18	$\delta = 0.84''$ (21.34 mm)	3.0	3.0 $\delta_{b,exp}$ in compression, 2.5 $\delta_{b,exp}$ in tension @+16: Fracture on the lower angle near the 7 <sup>th</sup> lacing from the South of the specimen @-17: Fracture on the angle near the global buckling location
19	$\delta = 1.12''$ (28.45 mm)	4.0	4.0 $\delta_{b,exp}$ both tension and compression @-19: Fracture on the lower angles near the gusset-connection @+19: Entire fracture near the global buckling location

Table B.7 Observations made during testing of the By16-60 specimen

CYCLE NO.	CONTROL DATA	$\delta/\delta_{b,exp}$	OBSERVATIONS
1 – 3	$P_H = 39$ kips (173.55kN)	0.44	Control data : Horizontal Force $P_H @ 1/3 \delta_b = 39$ kips (173.55kN) Elastic cycles
4 – 6	$\delta = 0.16''$ (4.06 mm)	1.0	Control data : Horizontal Force $P_H @ 2/3 \delta_b = 77$ kips (342.65kN) @-4: Local buckling on the upper angle near the middle connection plate @-4: Local buckling on the lower angles near the gusset-connection @+4: Strength degradation
7 – 9	$\delta = 0.24''$ (6.10 mm)	1.5	@-7: Local buckling on the plate near the gusset-connection @-9: Local buckling on the upper angle near the gusset-connection
10 – 12	$\delta = 0.32''$ (8.13 mm)	2.0	
13 – 14	$\delta = 0.40''$ (10.20 mm)	2.5	@-13: Lacing bolt failure West: 1 <sup>st</sup> from the North @+13: Initial fracture on the lower angle near the gusset-connection
15	$\delta = 0.48''$ (10.67 mm)	3.0	@+13: Entire fracture @ 0.6" (15.2 mm)

Table B.8 Observations made during testing of the By16-120 specimen

CYCLE NO.	CONTROL DATA	$\delta/\delta_{b,exp}$	OBSERVATIONS
1 – 9	Horizontal $P_H$	0.21 0.42 0.82	Control data : Horizontal Force Elastic cycles $P_H$ @ 1/3 $\delta_b=20$ kips (89.0kN), $P_H$ @ 2/3 $\delta_b=40$ kips (178.0kN) $P_H$ @ 1.0 $\delta_b=60$ kips (267.0kN)
10 – 12	0.17" (4.32 mm)	1.0	@-10: Large global buckling near the mid-length of the specimen at 70 kips (311.5 kN) @-10: Local buckling on upper angles near the global buckling @-10: Local buckling on lower angles near both the South and North gusset-connections @+10: Yielding cracks
13 – 15	0.34" (8.64 mm)	2.0	@-13: Local buckling was getting more severe @-14: Local buckling on the upper angles near the North gusset-connection
16 – 18	0.51" (12.95 mm)	3.0	
19 – 20	0.68" (17.27 mm)	4.0	@-19: Fracture on the lower angle near the global buckling @-20: Lacing buckling 1 <sup>st</sup> lacing from the top 24 <sup>th</sup> lacing from the top @+20: Fracture on the upper angle near the global buckling
21	0.85" (21.59 mm)	5.0	@+21: Entire fracture near the global buckling

Table B.9 Observations made during testing of the Bx8-60 specimen

CYCLE NO.	CONTROL DATA	$\delta/\delta_{b,exp}$	OBSERVATIONS
1 – 6	Horizontal $P_H$	0.39 0.78	Control data : Horizontal Force Elastic cycles $P_H @ 1/3 \delta_b = 29$ kips (129.1kN), $P_H @ 2/3 \delta_b = 58$ kips (258.1kN)
7 – 9	0.18" (4.57 mm)	1.0	@-7: Global out-of-plane buckling
10 – 12	0.27 (6.86 mm)	1.5	@-10: Out-of-plane buckling in the South segment @-11: In-plane buckling in the South segment @-12: Local buckling on the upper angles near the South gusset-connection
13 – 15	0.36" (9.14 mm)	2.0	@-13: Local buckling on lower angle near the middle connection plate in the South segment @-13: Lacing buckling the middle connection plate in the North segment @-13: Lacing bolt failure near the South gusset-connection
16 – 18	0.45" (11.43 mm)	2.5	@-16: Lacing buckling near the middle connection plate in the South segment @+16: Fracture on the lower angle near the South gusset-connection
19 – 21	0.54" (13.72 mm)	3.0	@+19: Fracture on both lower and upper angles near the middle connection plate in the South segment
22 – 23	0.63" (16.00 mm)	3.5	@+22: Fracture on entire three angles near the middle connection plate in the South segment @+23: Entire fracture

Table B.10 Observations made during testing of the Bx8-120 specimen

CYCLE NO.	CONTROL DATA	$\delta/\delta_{b,exp}$	OBSERVATIONS
1 – 12	Horizontal $P_H$	0.188 0.375 0.563 0.75	Control data : Horizontal Force Elastic cycles $P_H @ 1/3 \delta_b = 6.5 \text{kips (28.9kN)}$ , $P_H @ 2/3 \delta_b = 13.0 \text{kips (57.9kN)}$ $P_H @ 1.0 \delta_b = 19.5 \text{kips (86.8kN)}$ , $P_H @ 1 \frac{1}{3} \delta_b = 26 \text{kips (115.7kN)}$
13 – 15	0.16" (4.06 mm)	1.0	@-13: Global out-of-plane buckling
16 – 18	0.24" (6.10 mm)	1.5	Frame column twisting
19 – 21	0.24" (6.10 mm)	1.5	@-19: Both out-of-plane and in-plane buckling @-19: Lacing bolt failure near the North gusset-connection @-21: Local buckling on the lower angle near the global buckling location
22 – 24	0.32" (8.13 mm)	2.0	@+22: Crack observed near the local global buckling location @-24: Local buckling on the upper angle near the global buckling location
25 – 26	0.40" (10.16 mm)	2.5	@-25: Initial fracture on the upper angle near the global buckling location
27 – 28	0.48" (12.19 mm)	3.0	
29 – 30	0.64" (16.26 mm)	4.0	@-29: Fracture on the upper plate near the global buckling location
31 – 32	0.80" (20.32 mm)	5.0	@-31: Half section fracture near the global buckling location
33	0.96" (24.38 mm)	6.0	@-33: Entire fracture

Table B.11 Observations made during testing of the Bx16-60 specimen

CYCLE NO.	CONTROL DATA	$\delta/\delta_{b,exp}$	OBSERVATIONS
1 – 6	Horizontal $P_H$	0.335 0.665	Control data : Horizontal Force Elastic cycles $P_H @ 1/3 \delta_b = 22$ kips (97.9kN) $P_H @ 2/3 \delta_b = 44.0$ kips (195.8kN)
7 – 9	0.2" (5.08 mm)	1.0	@-7: Local buckling was observed at $P @ 1.0 \delta_b = 66.0$ kips (293.7kN)
10 – 12	0.3" (7.62 mm)	1.5	@-10: Local buckling on the lower angle near the North gusset-connection at $\delta = 0.20$ " (5.08 mm) @-10: Global out-of-plane buckling near the middle connection of the North segment of the specimen at $\delta = 0.30$ " (7.62 mm) @-10: Local buckling on the upper angle near the global buckling location @-10: Local buckling on the lower angles near the middle connection of the South segment of the specimen @-10: Local buckling on the lower angles near the South gusset-connection
13 – 15	0.4" (10.16 mm)	2.0	@-13: Crack on the lower angle near the middle connection of the South segment of the specimen
16 – 18	0.5" (12.70 mm)	2.5	@+16: Initial fracture on the lower angle near the middle connection of the South segment of the specimen
19 – 21	0.6" (15.24 mm)	3.0	@+21: Entire fracture

Table B.12 Observations made during testing of the Bx16-120 specimen

CYCLE NO.	CONTROL DATA	$\delta/\delta_{b,exp}$	OBSERVATIONS
1 – 9	Horizontal $P_H$	0.25 0.50 0.75	Control data : Horizontal Force Elastic cycles $P_H @ 1/3 \delta_b = 18.0$ kips (80.1kN) $P_H @ 2/3 \delta_b = 36.0$ kips (160.2kN) $P_H @ 1.0 \delta_b = 54.0$ kips (240.3kN)
10 – 12	0.28" (7.11 mm)	1.0	@-11: Global out-of-plane buckling @-11: Local buckling on the lower angle near the South gusset-connection
13 – 15	0.56" (14.22 mm)	2.0	@-13: Local buckling on both lower and upper angles near the South gusset-connection at $\delta=0.28"$ (7.11mm) @-13: Larger global buckling at $\delta=0.56"$ (7.11mm), starting out-of-plane buckling and changed into in-plane buckling @-13: Local buckling on the angle and plate near the global buckling location @-14: Lacing buckling
16 – 18	0.84" (21.34 mm)	3.0	@-16: Local buckling on the upper angle near the 1/4 of the specimen length from the North @-16: Local buckling on the upper angle near the global buckling location @-18: Local buckling on the lower angle near the 1/4 of the specimen length from the North
19 – 20	1.12" (28.15 mm)	4.0	@+20: Initial fracture on the lower angle near the global buckling location
21	1.4" (35.56 mm)	5.0	@+21: Entire fracture near global buckling



## **APPENDIX C**

### **Hysteretic Curves from Test Results**

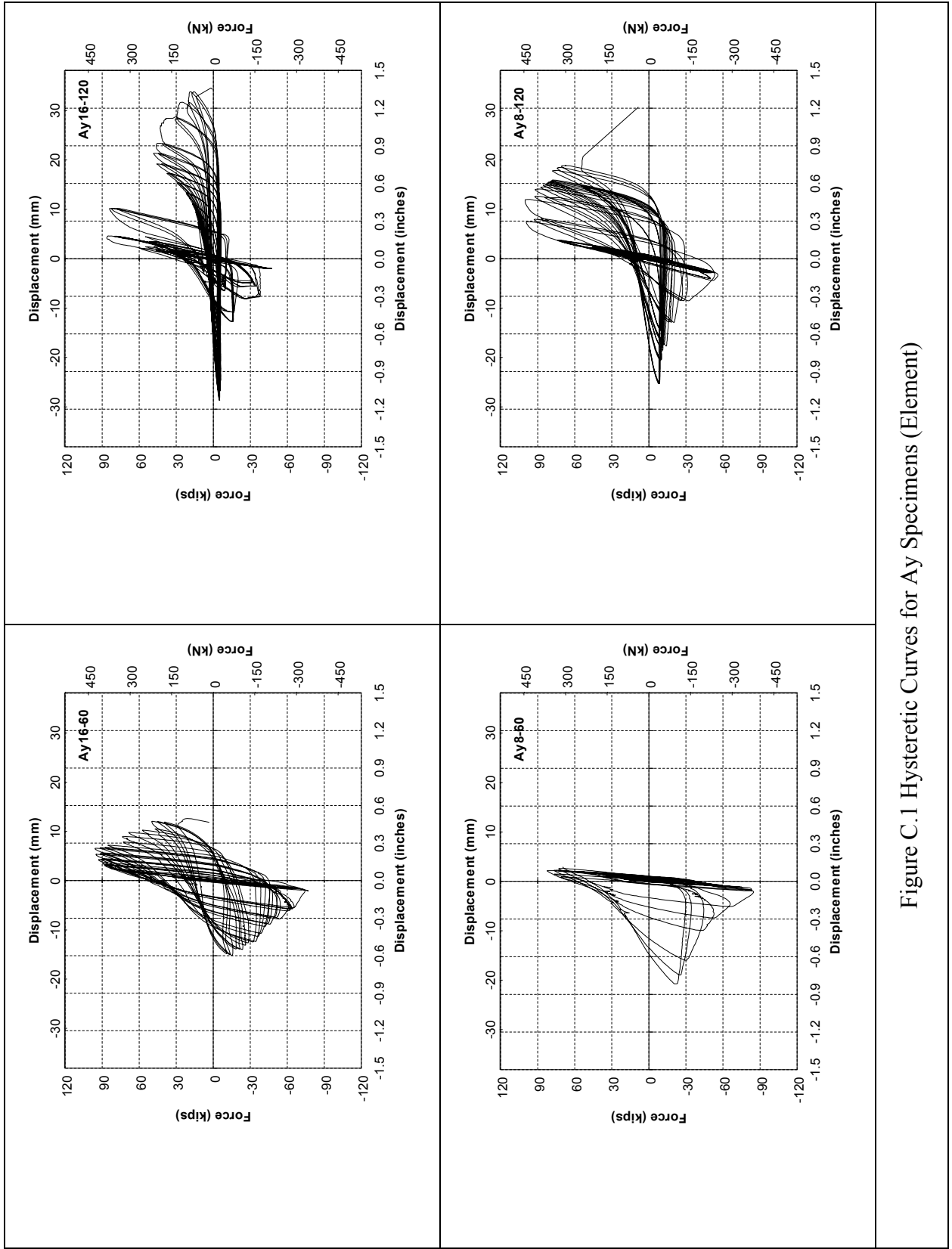


Figure C.1 Hysteretic Curves for Ay Specimens (Element)

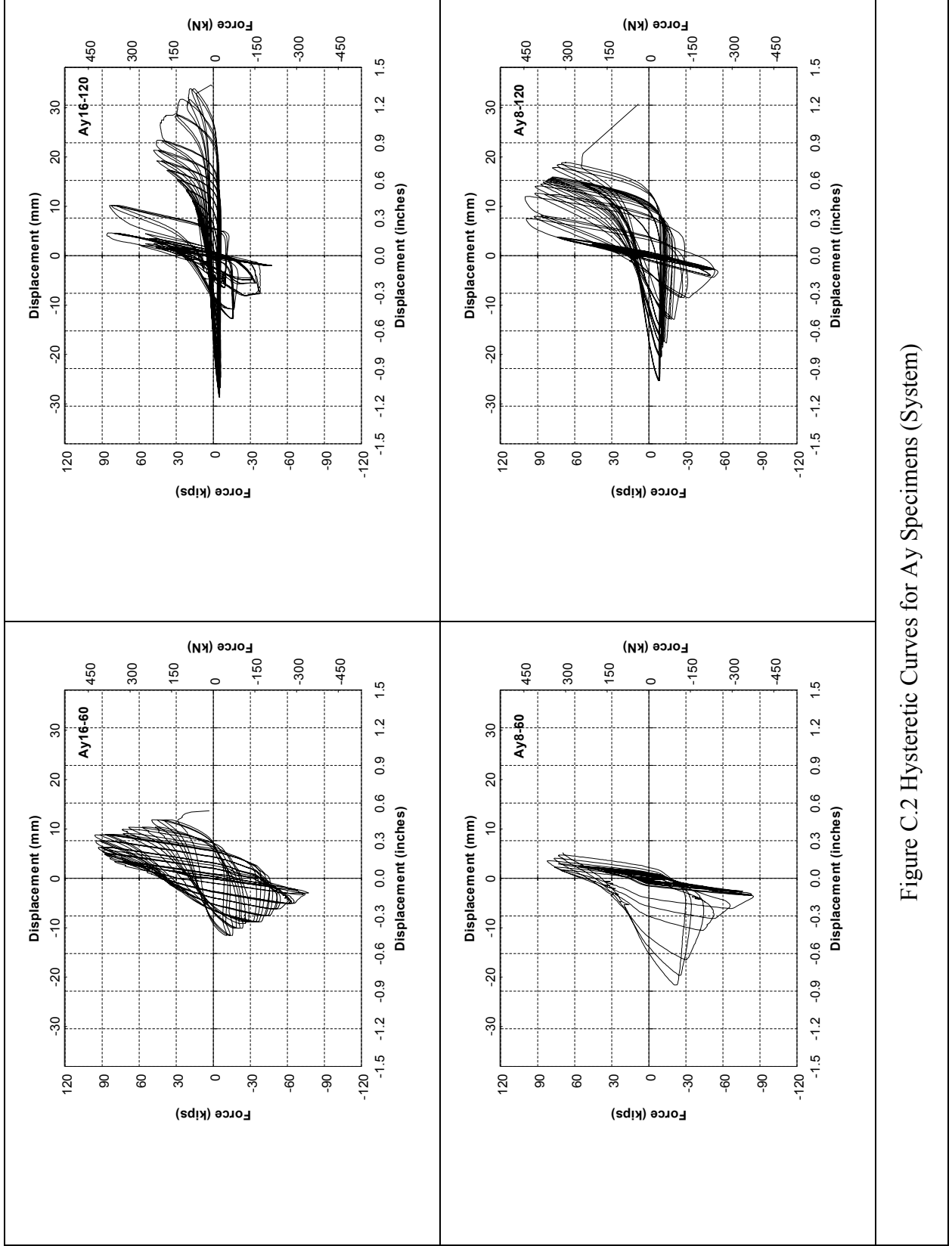


Figure C.2 Hysteretic Curves for Ay Specimens (System)

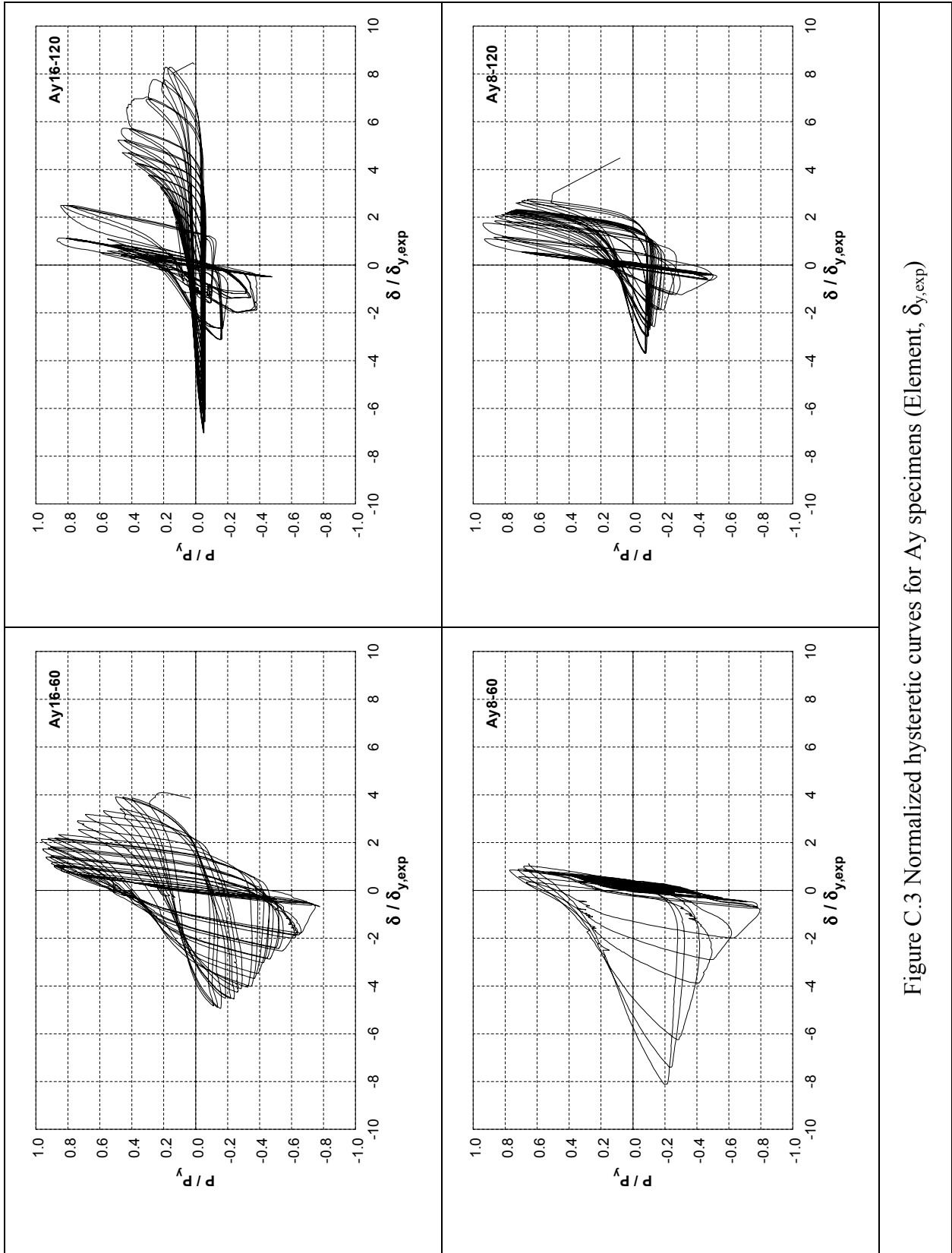


Figure C.3 Normalized hysteretic curves for Ay specimens (Element,  $\delta_{y,exp}$ )

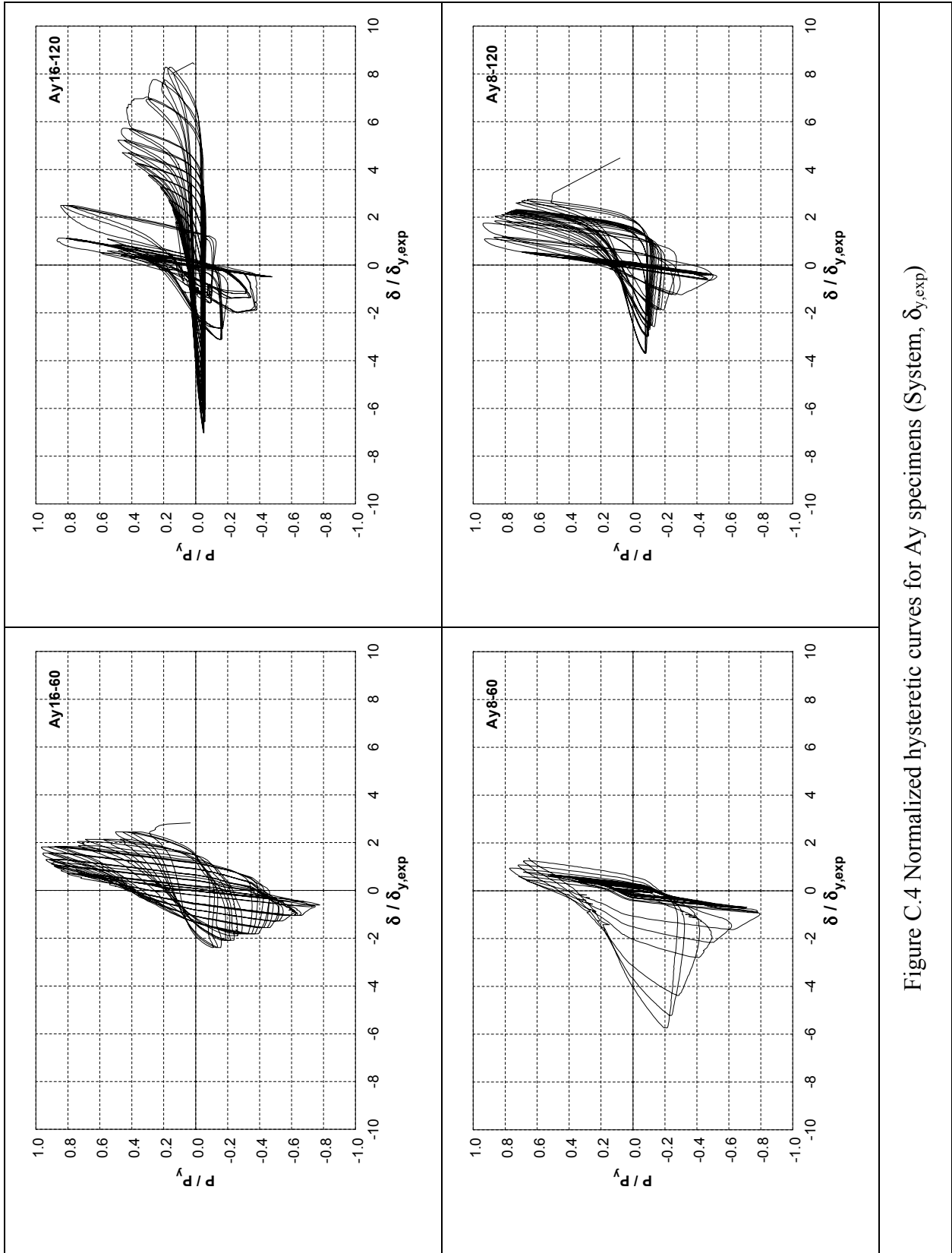


Figure C.4 Normalized hysteretic curves for Ay specimens (System,  $\delta_{y,exp}$ )

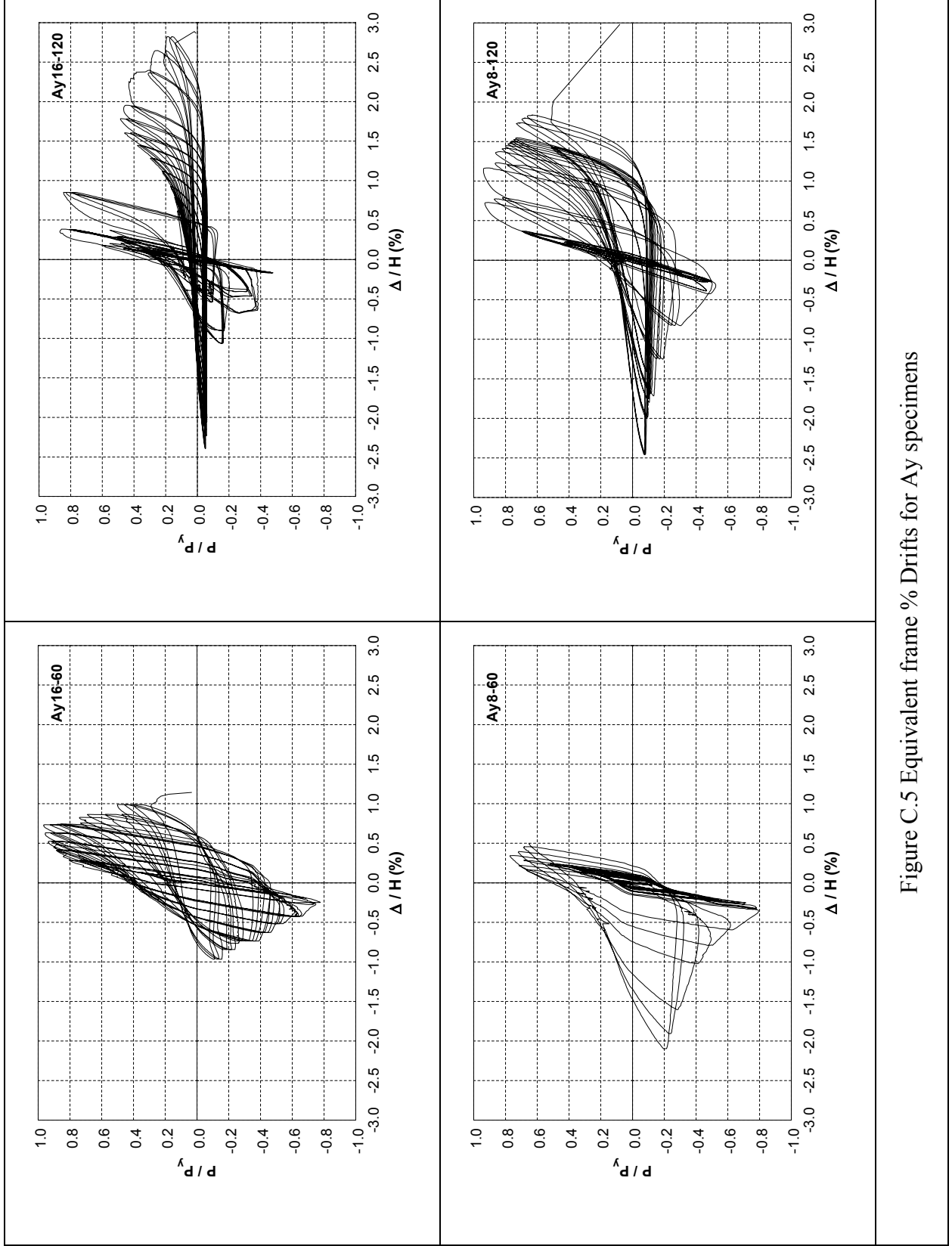


Figure C.5 Equivalent frame % Drifts for Ay specimens

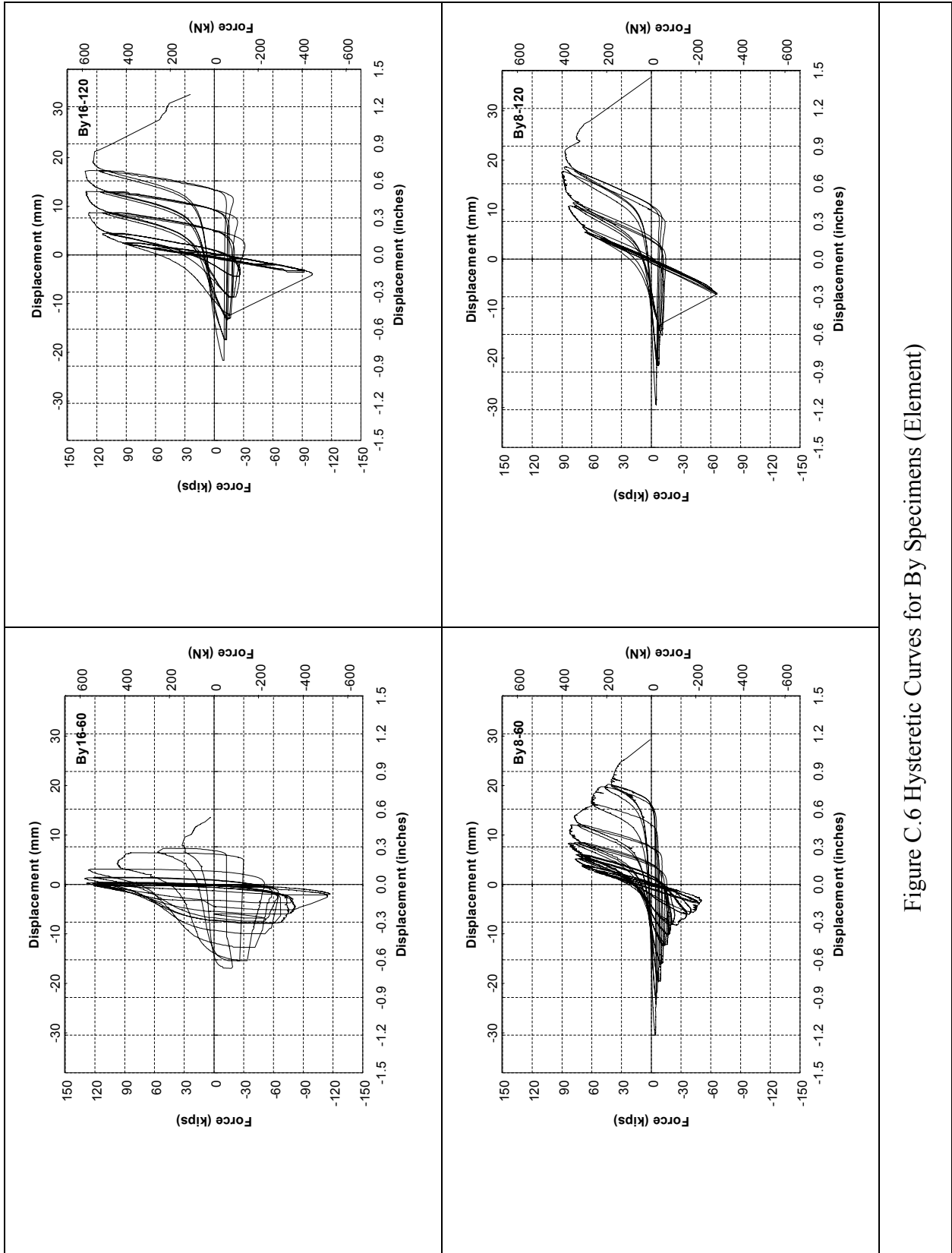


Figure C.6 Hysteretic Curves for By Specimens (Element)

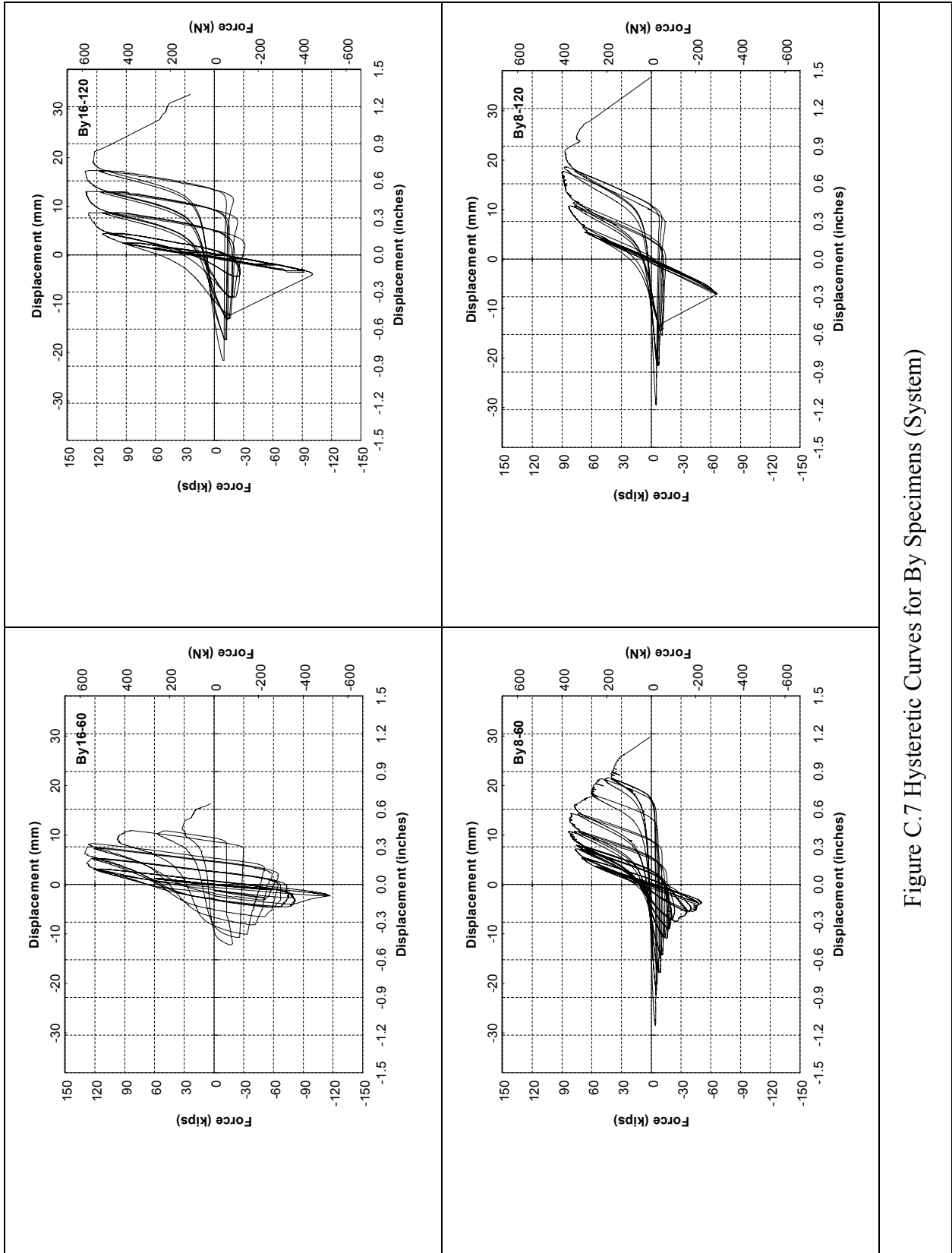


Figure C.7 Hysteretic Curves for By Specimens (System)

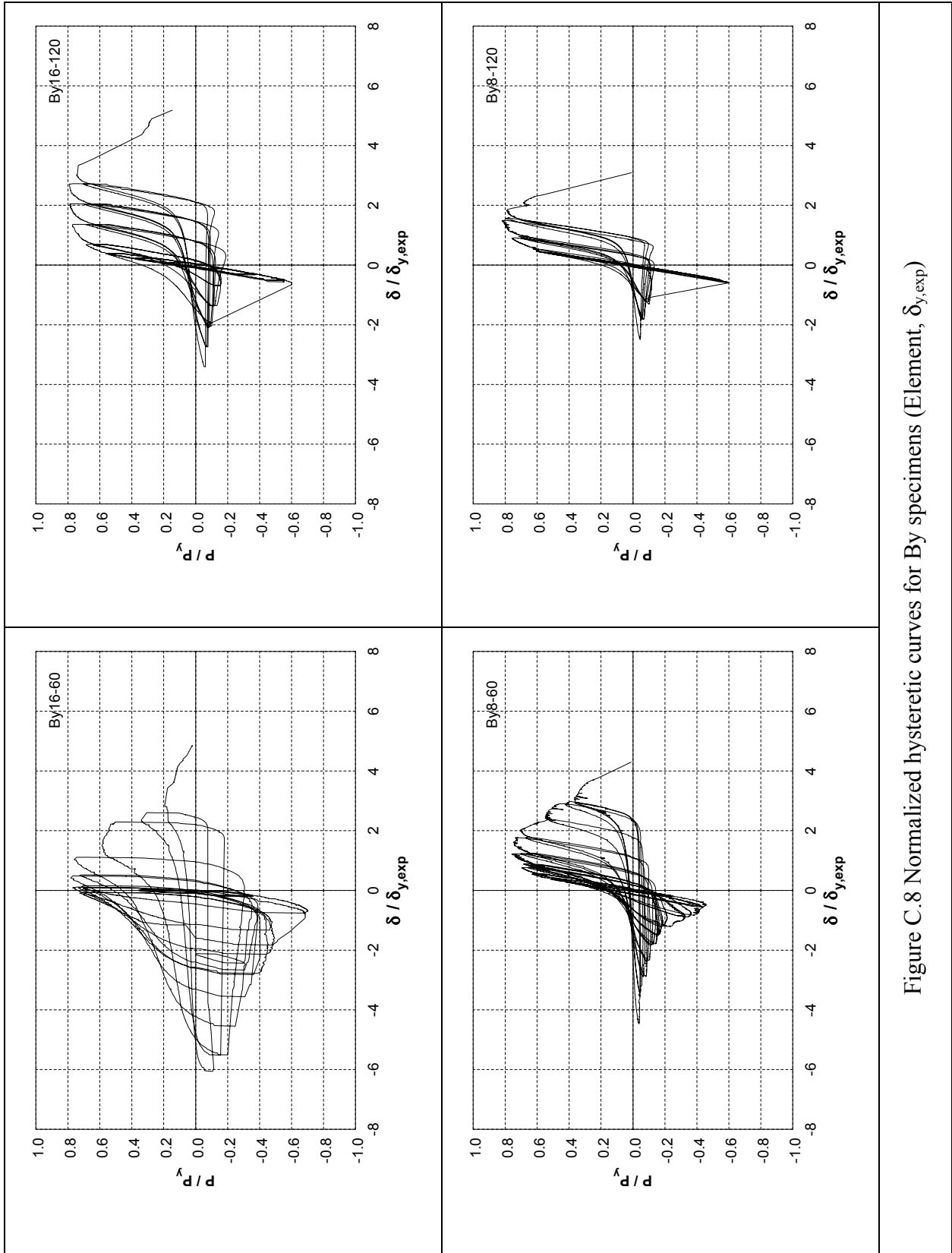


Figure C.8 Normalized hysteretic curves for By specimens (Element,  $\delta_{y,exp}$ )

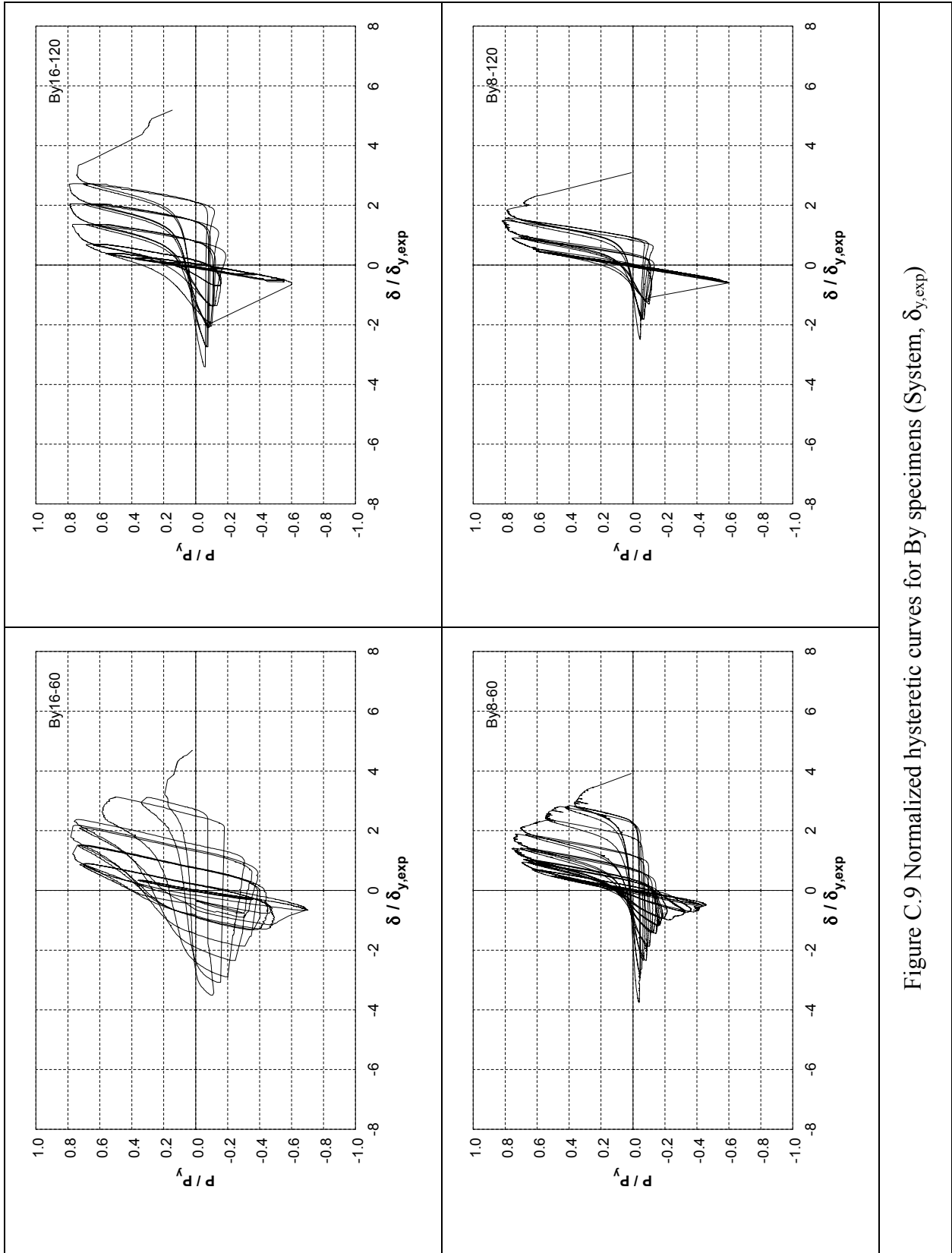


Figure C.9 Normalized hysteretic curves for By specimens (System,  $\delta_{y,exp}$ )

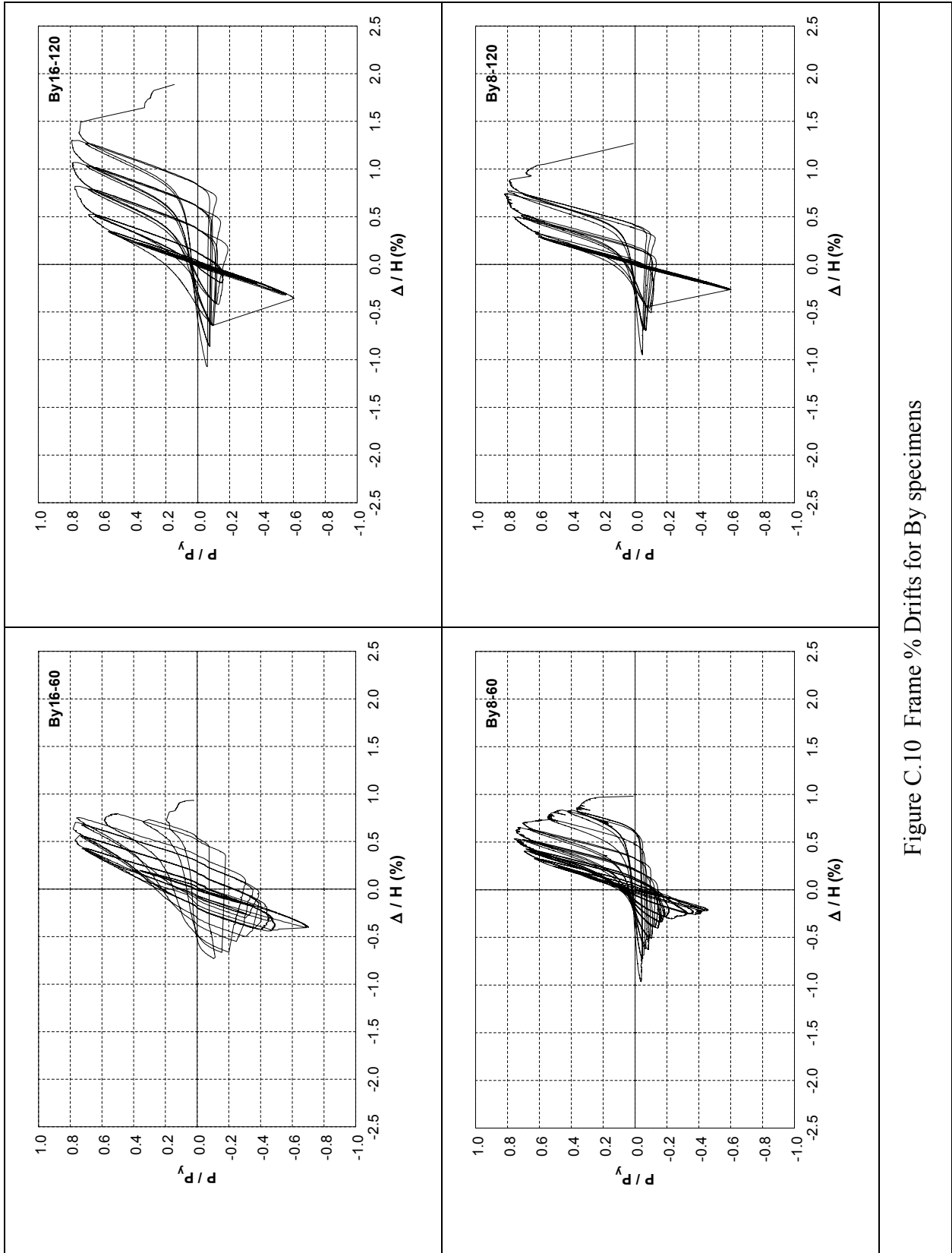


Figure C.10 Frame % Drifts for By specimens

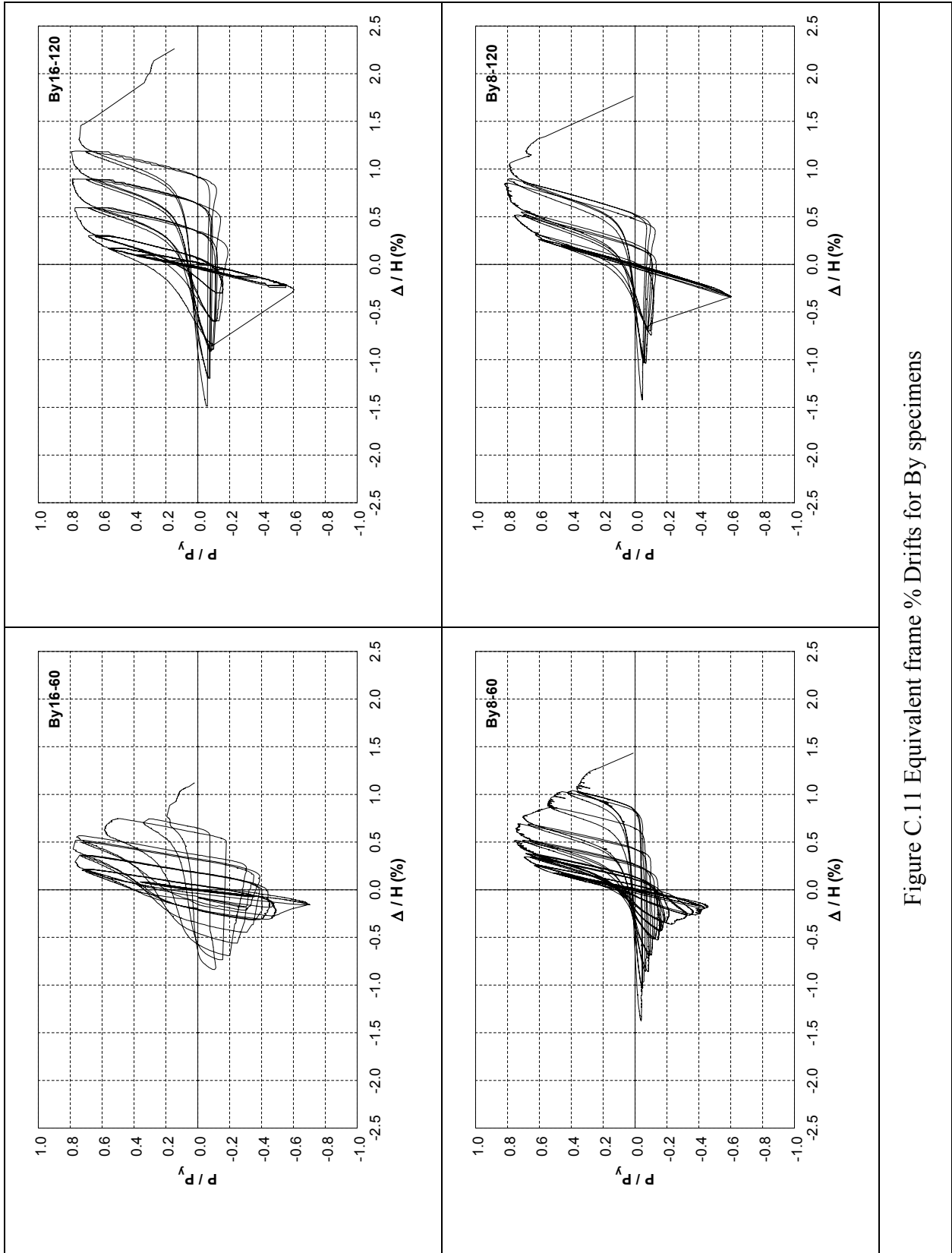


Figure C.11 Equivalent frame % Drifts for By specimens

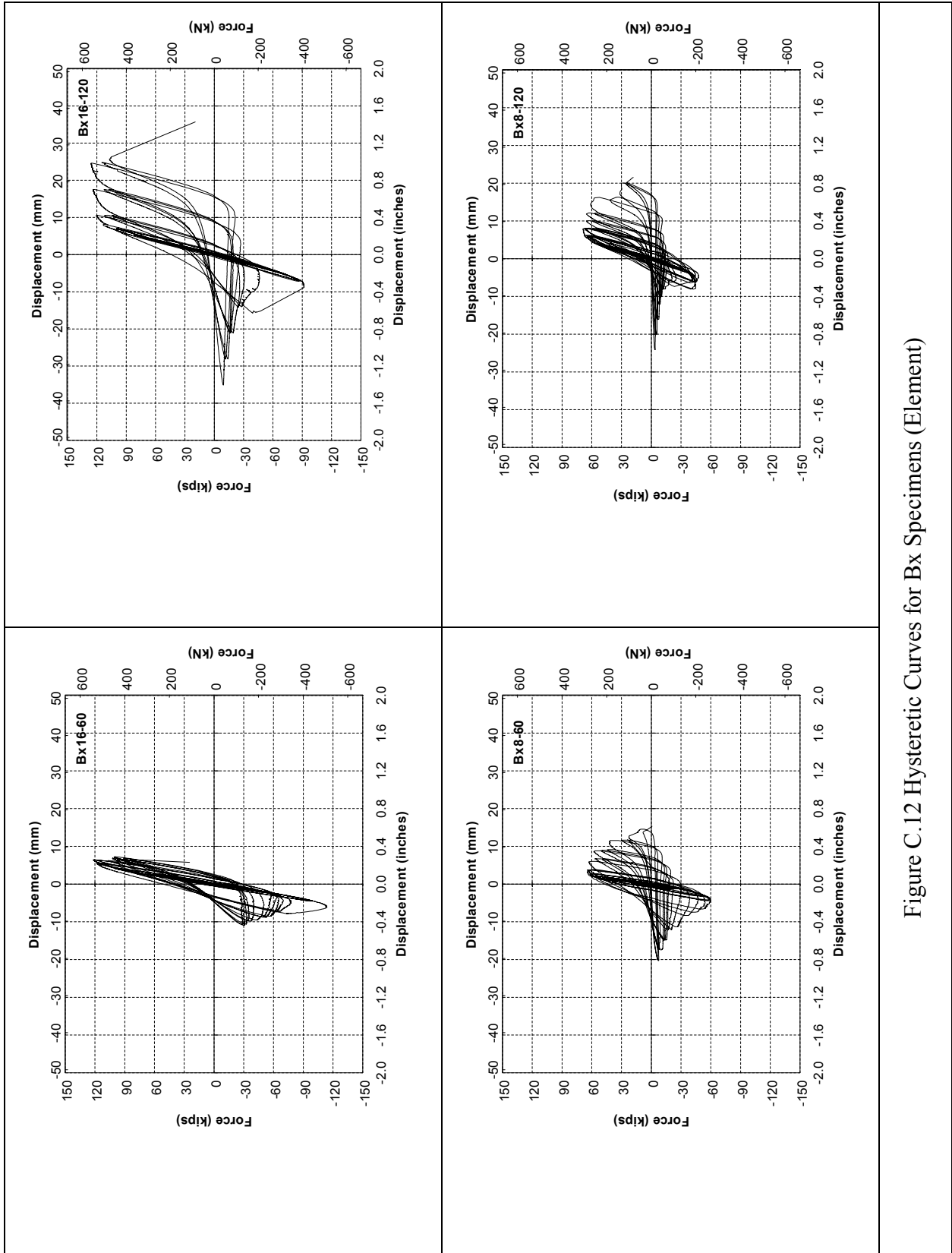


Figure C.12 Hysteretic Curves for Bx Specimens (Element)

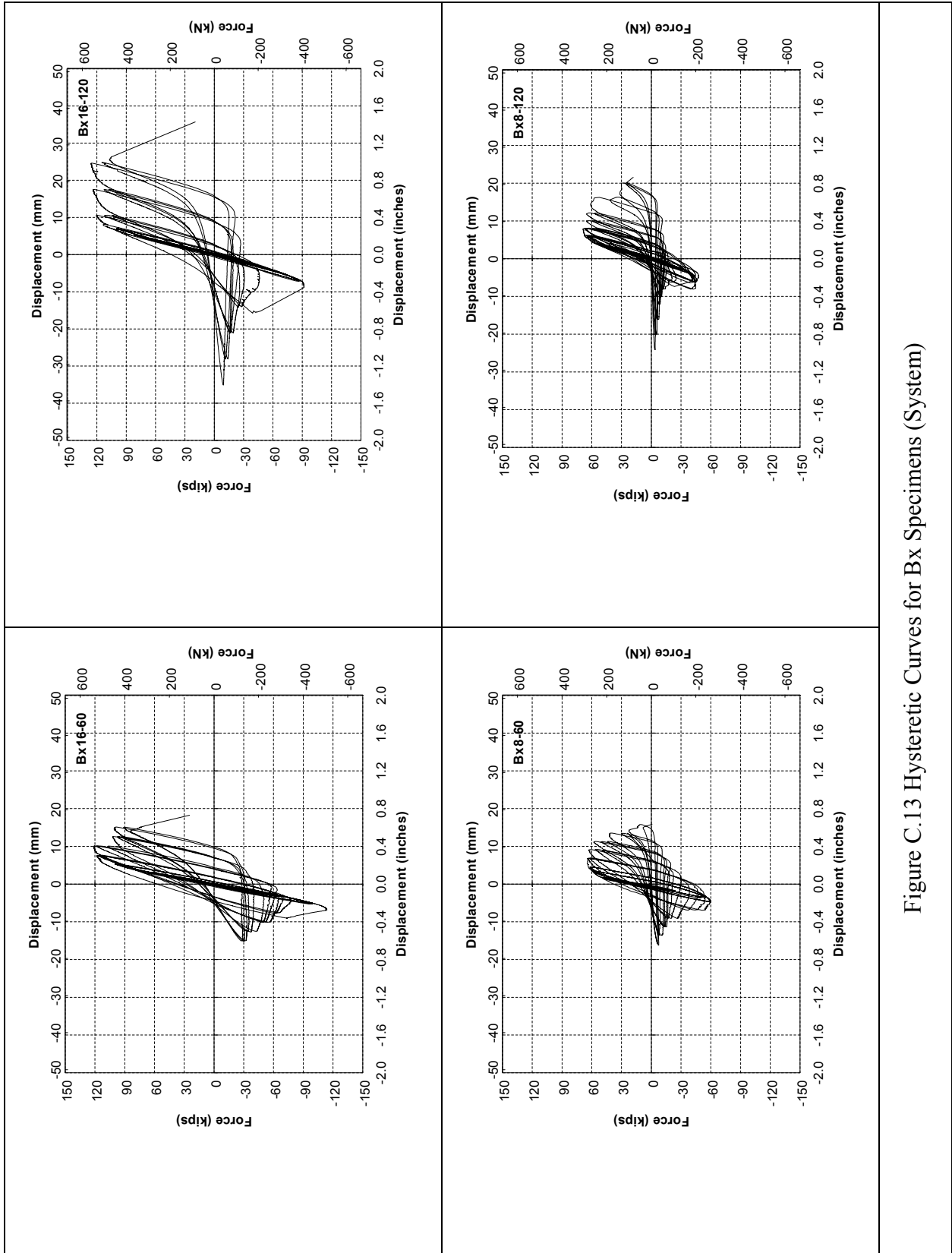


Figure C.13 Hysteretic Curves for Bx Specimens (System)

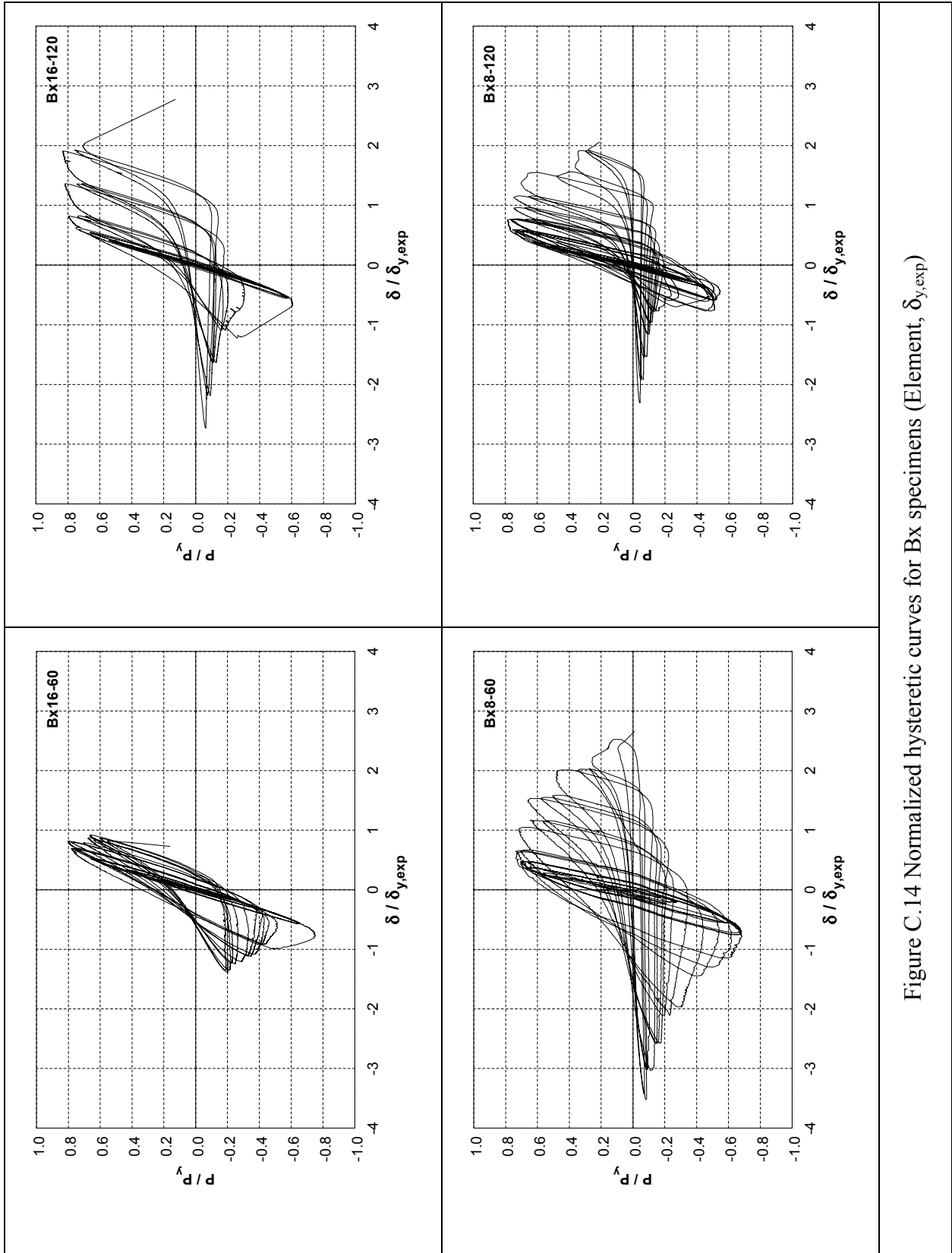


Figure C.14 Normalized hysteretic curves for Bx specimens (Element,  $\delta_{y,exp}$ )

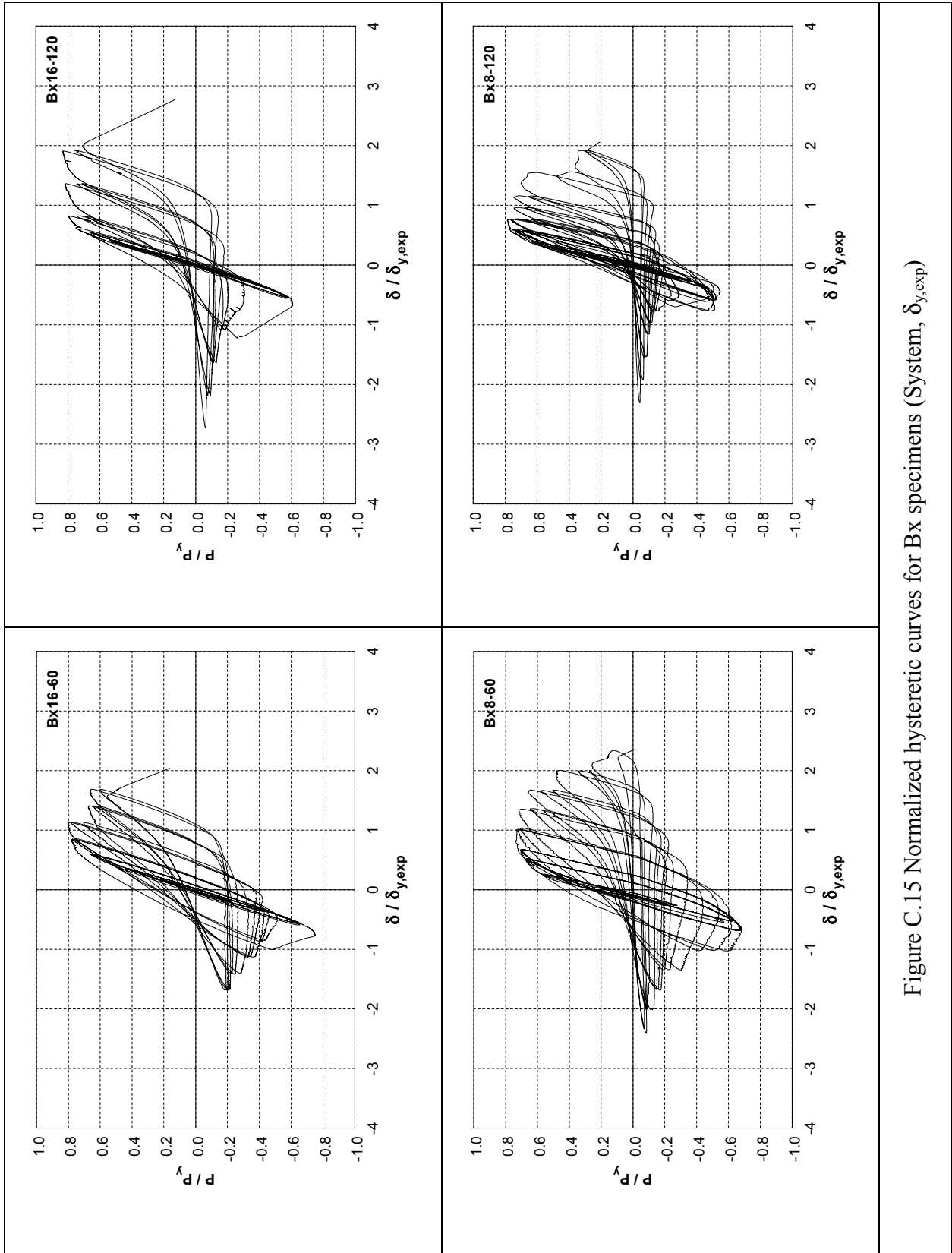


Figure C.15 Normalized hysteretic curves for Bx specimens (System,  $\delta_{y,exp}$ )

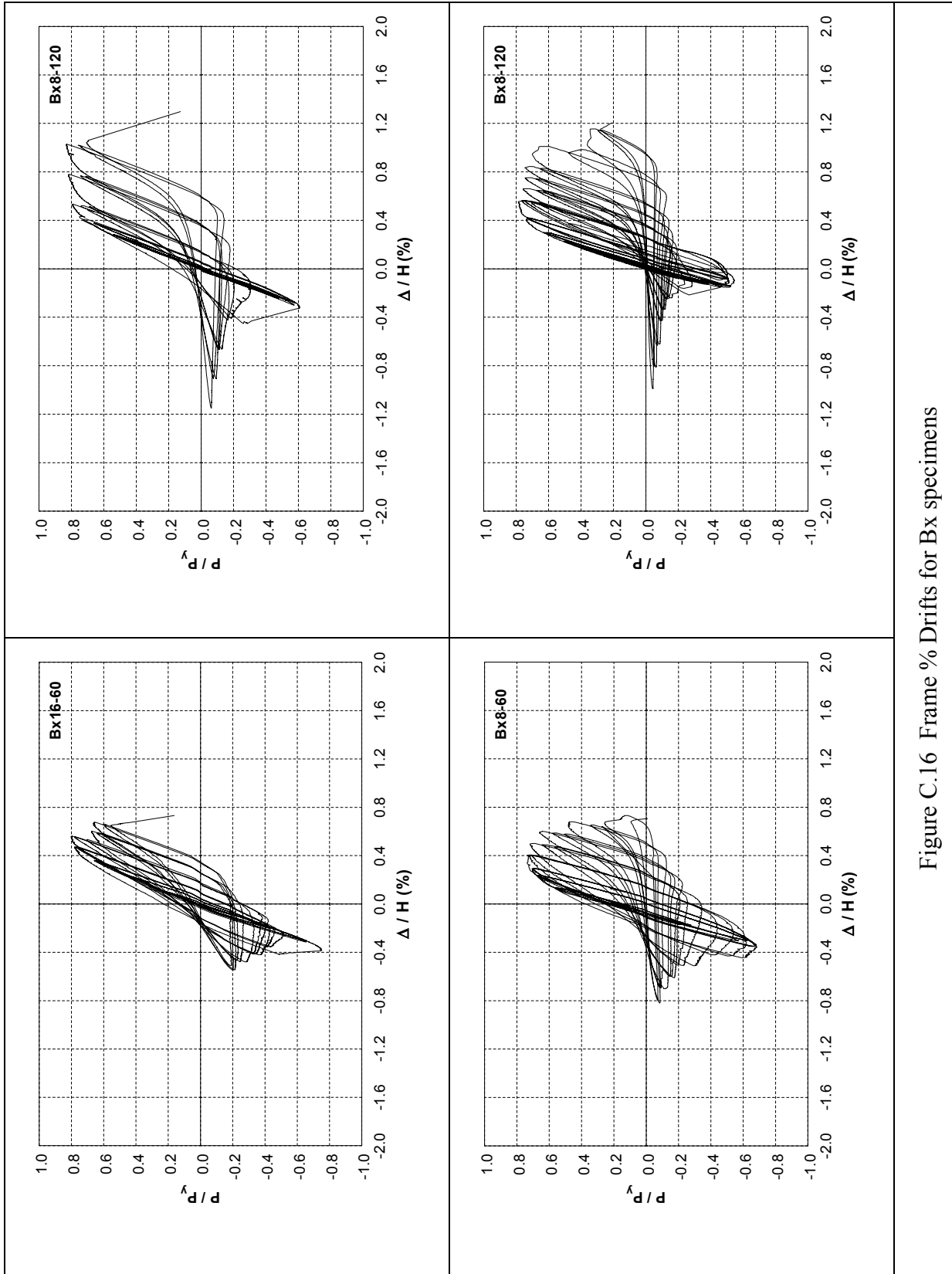


Figure C.16 Frame % Drifts for Bx specimens

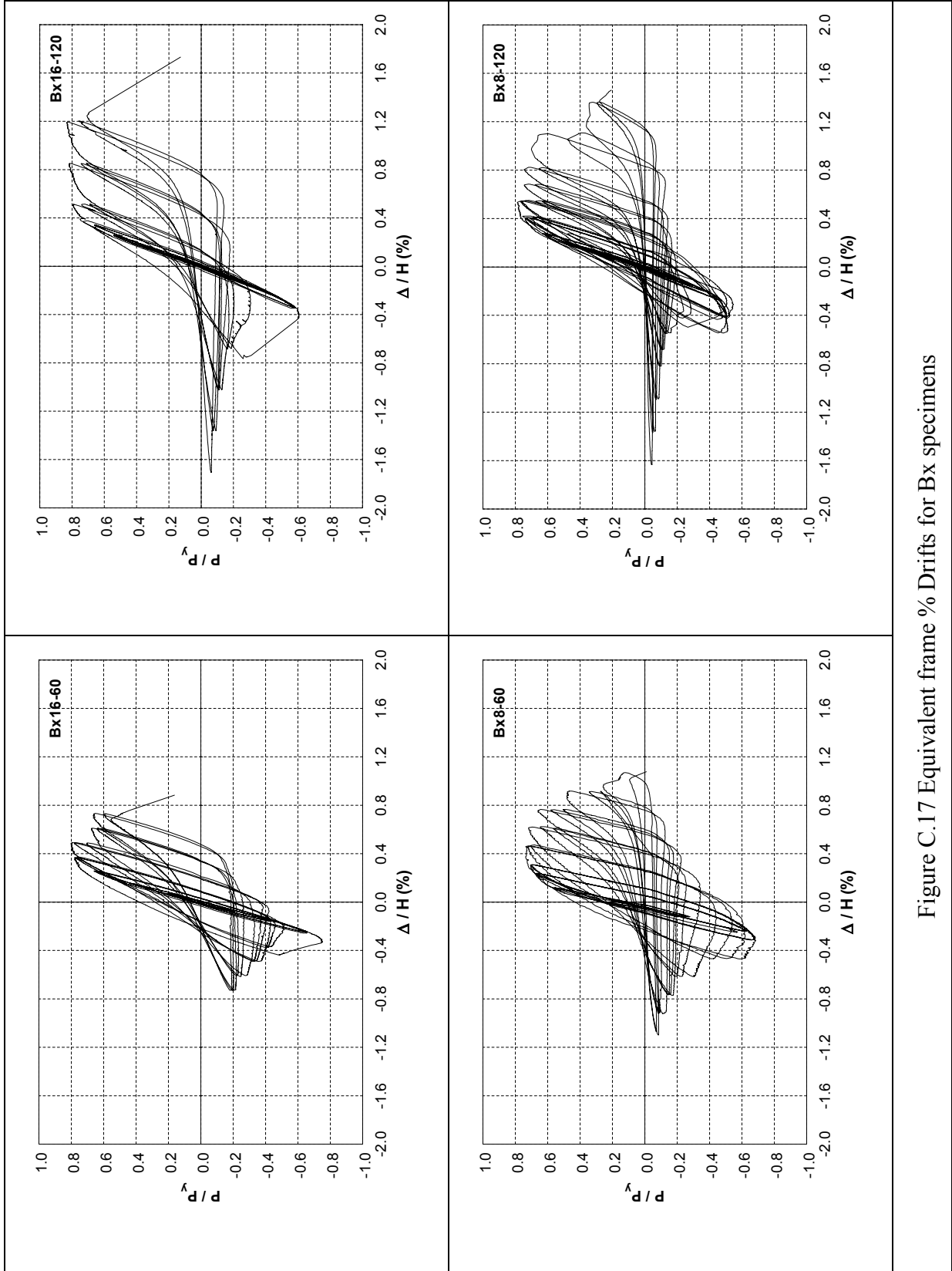


Figure C.17 Equivalent frame % Drifts for Bx specimens

## **APPENDIX D**

### **Normalized Energy Dissipation of Specimens**

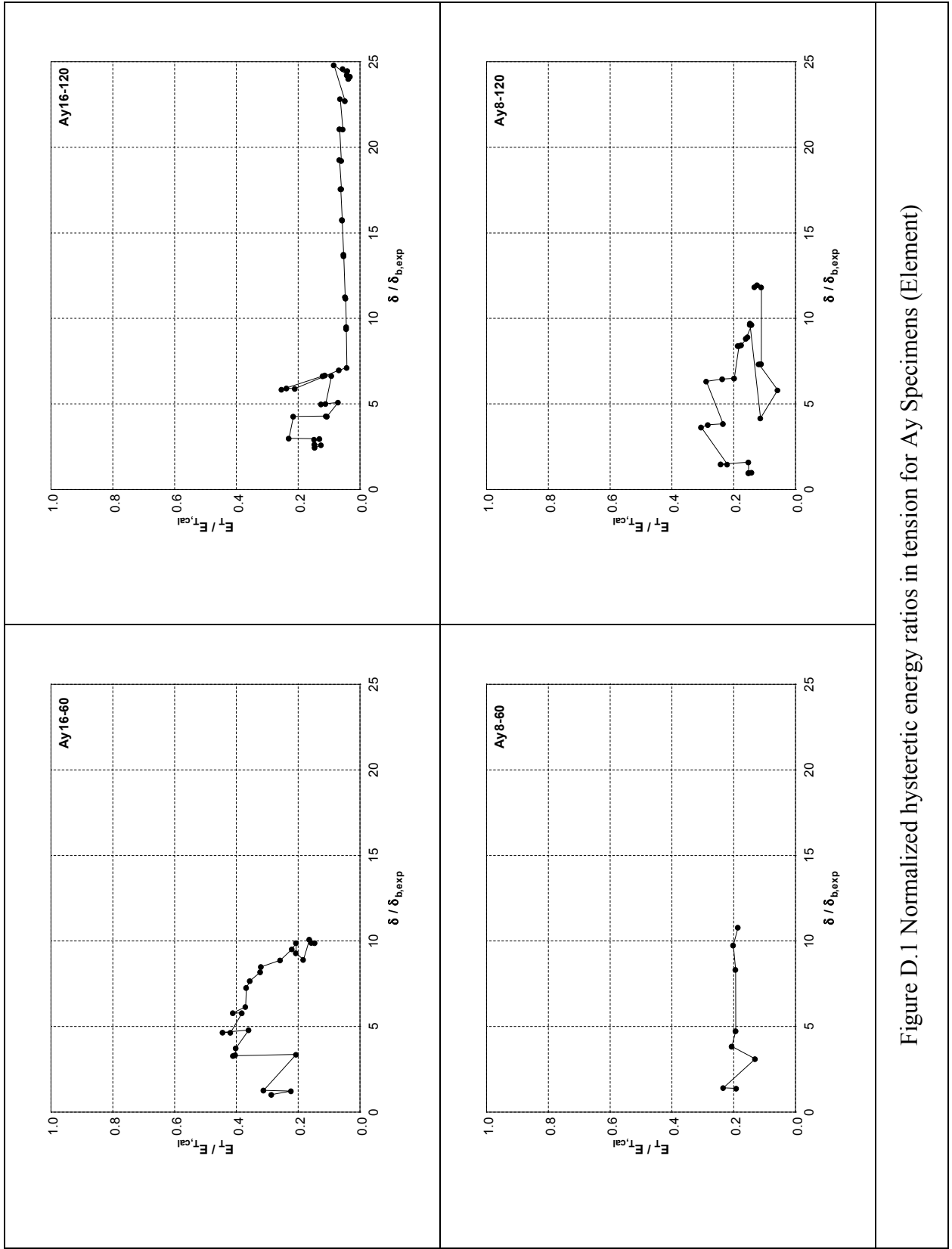


Figure D.1 Normalized hysteretic energy ratios in tension for Ay Specimens (Element)

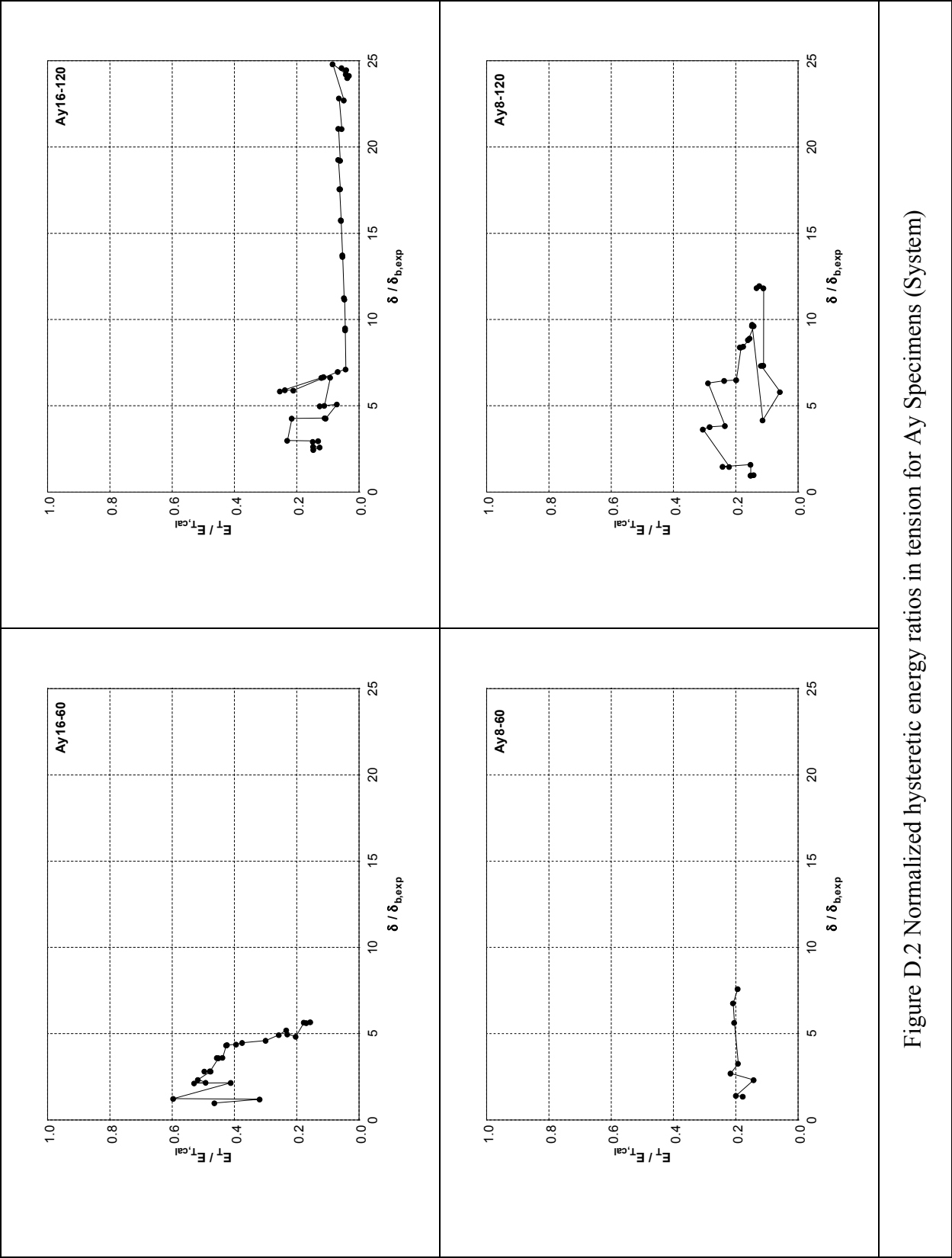


Figure D.2 Normalized hysteretic energy ratios in tension for Ay Specimens (System)

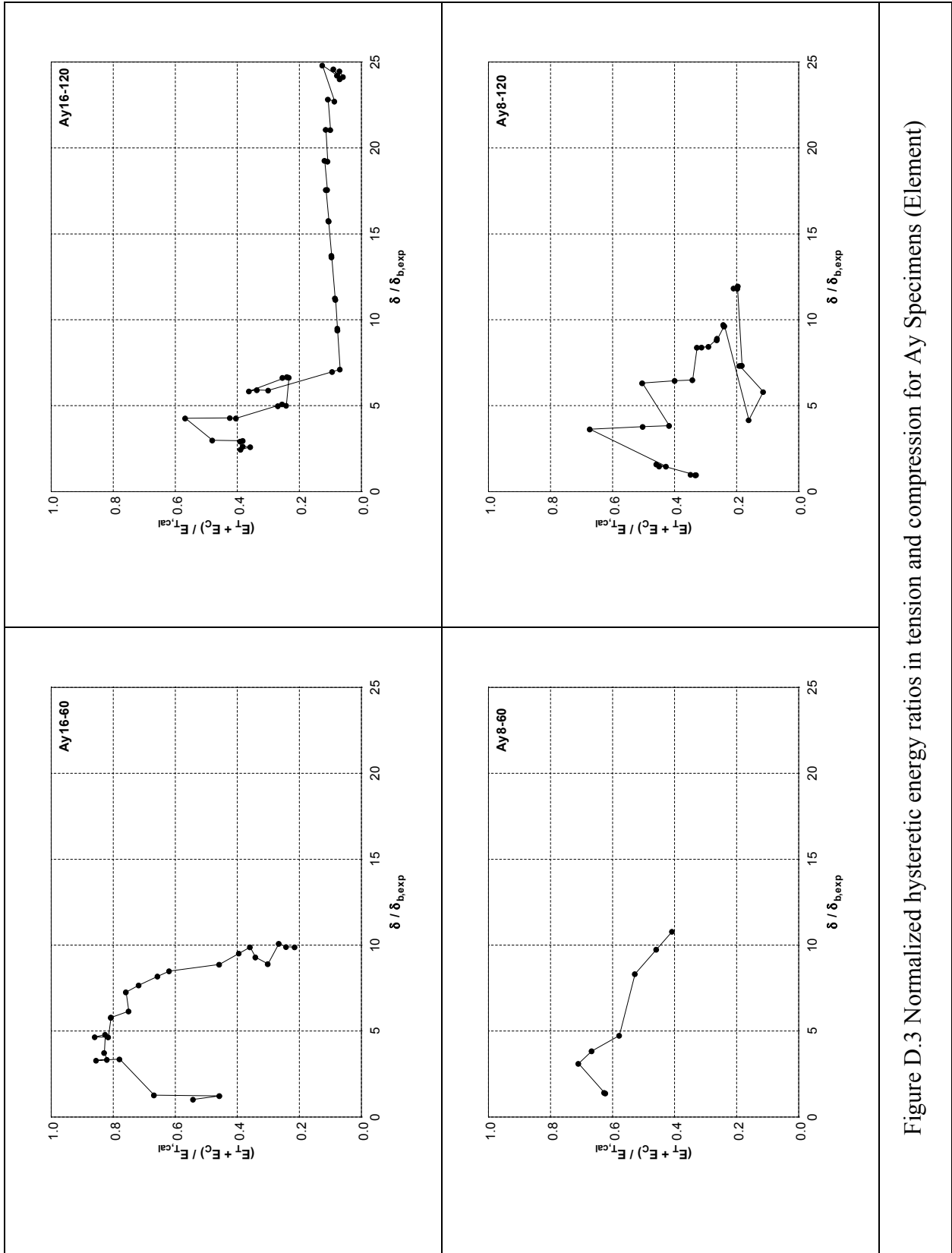


Figure D.3 Normalized hysteretic energy ratios in tension and compression for Ay Specimens (Element)

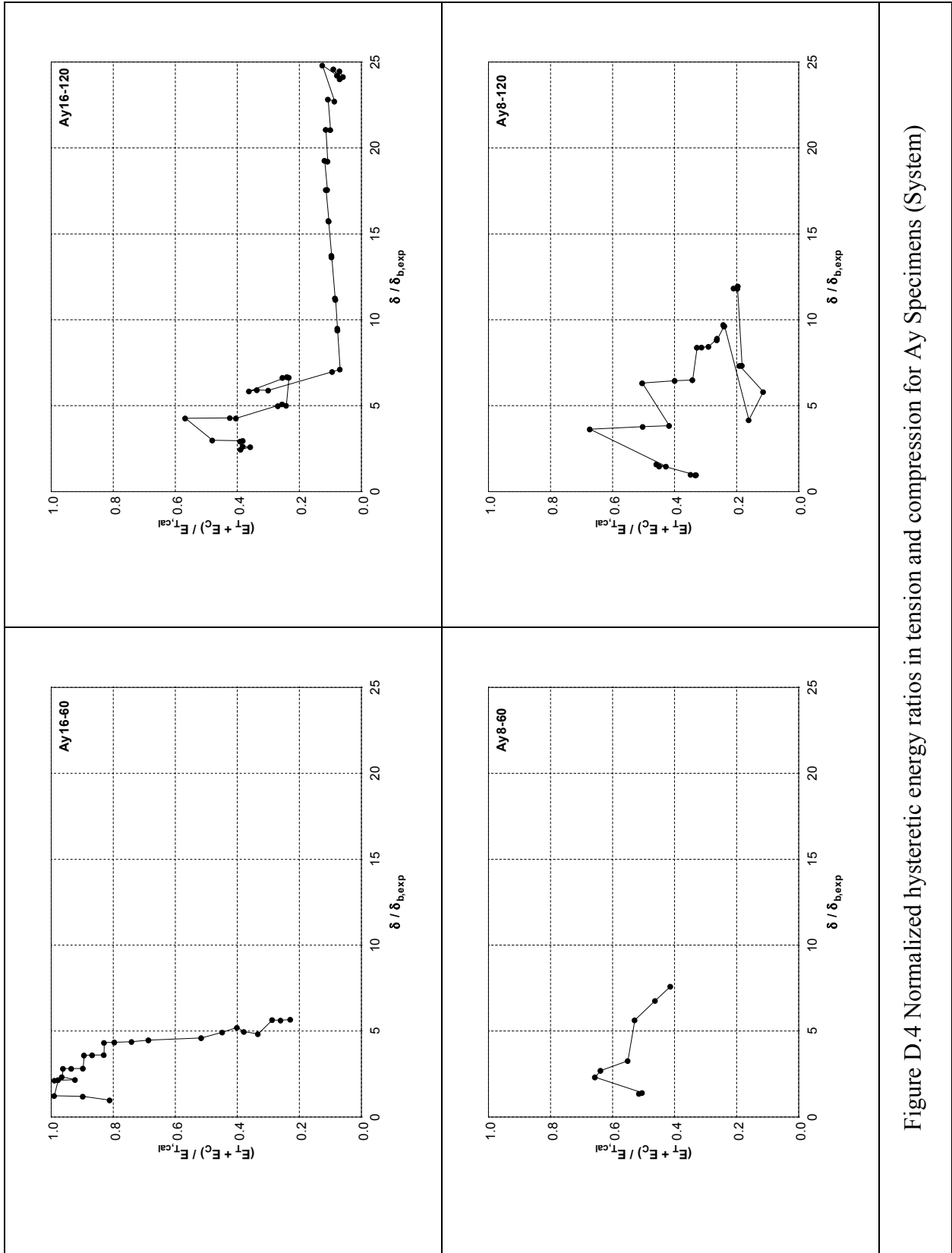


Figure D.4 Normalized hysteretic energy ratios in tension and compression for Ay Specimens (System)

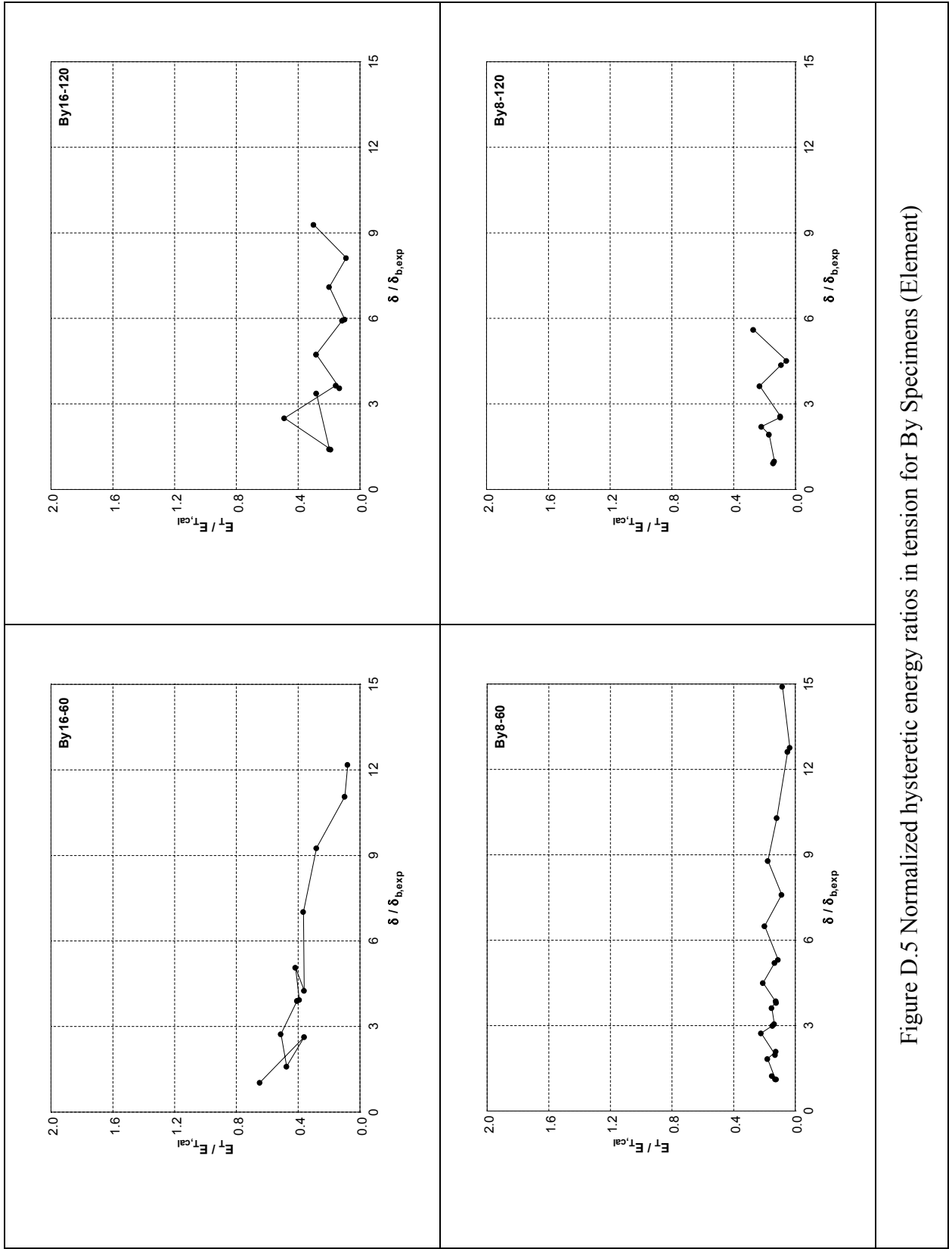


Figure D.5 Normalized hysteretic energy ratios in tension for By Specimens (Element)

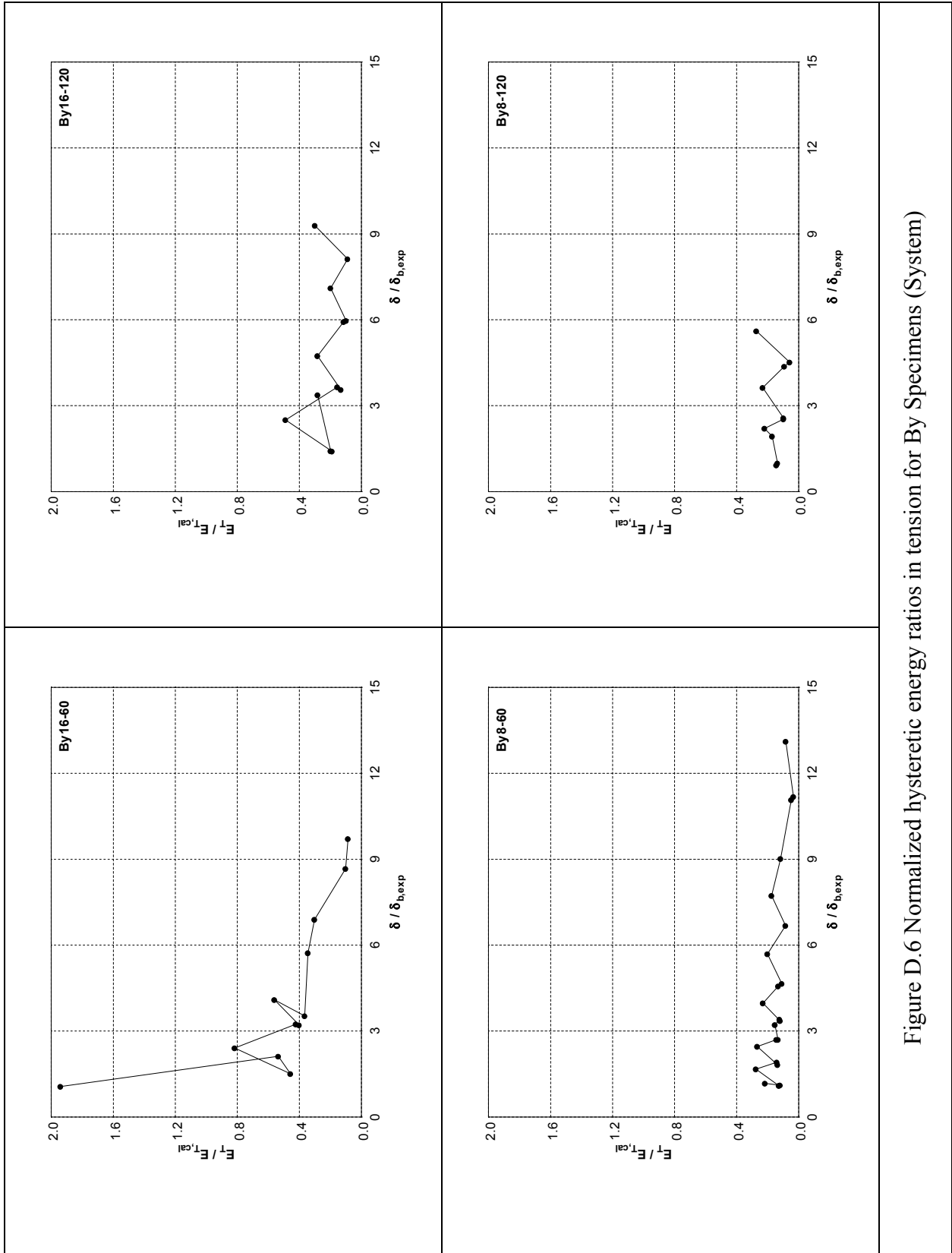


Figure D.6 Normalized hysteretic energy ratios in tension for By Specimens (System)

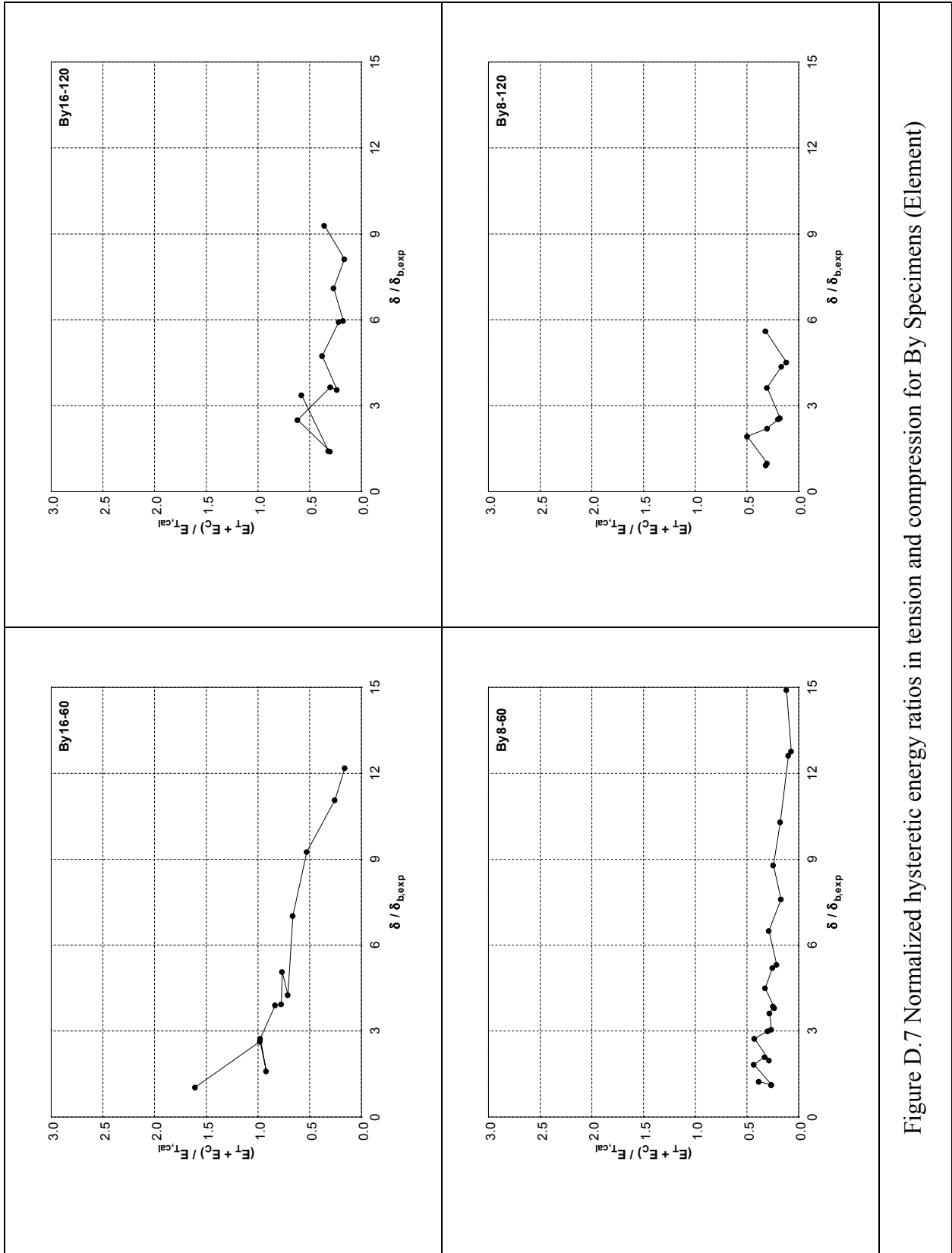


Figure D.7 Normalized hysteretic energy ratios in tension and compression for By Specimens (Element)

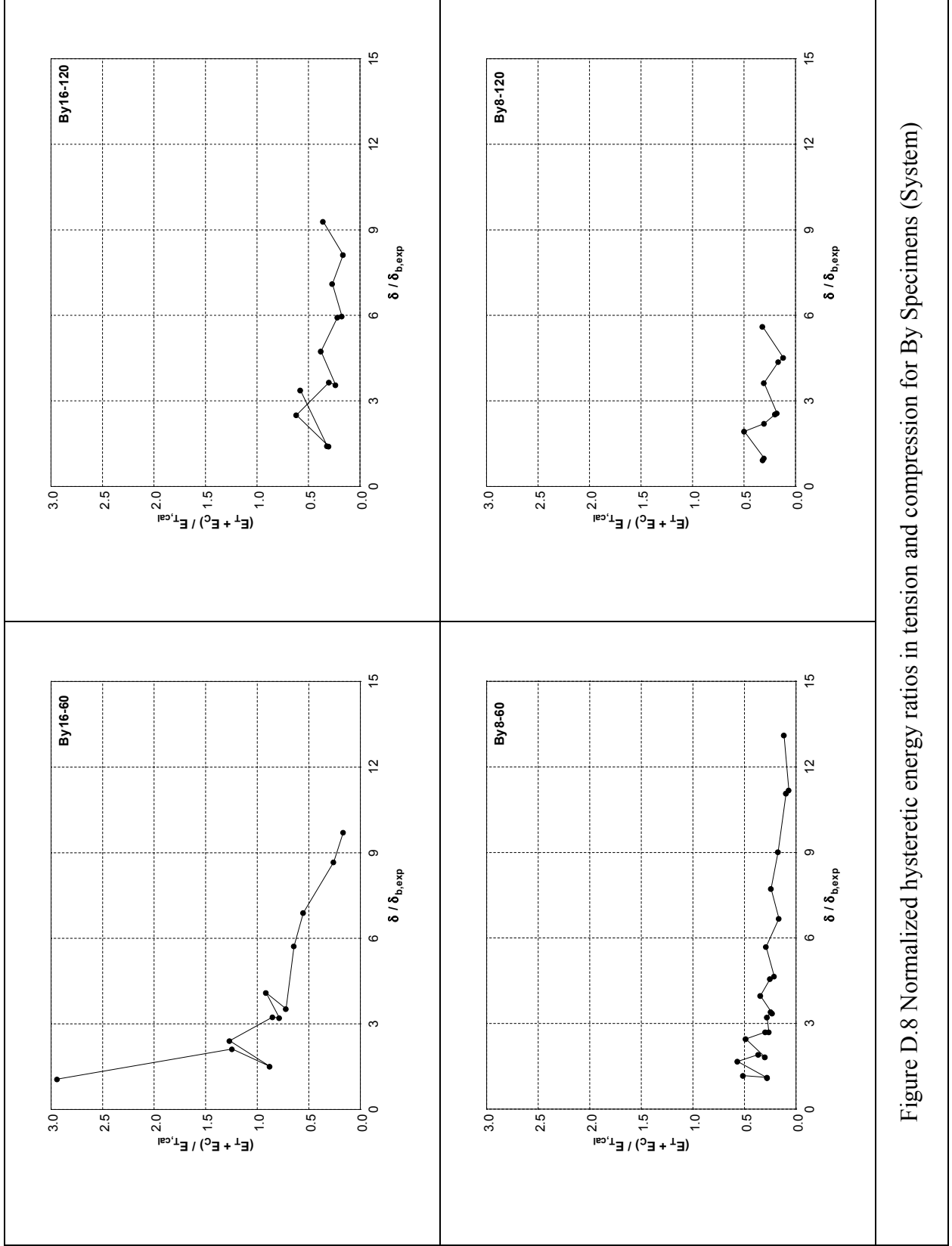


Figure D.8 Normalized hysteretic energy ratios in tension and compression for By Specimens (System)

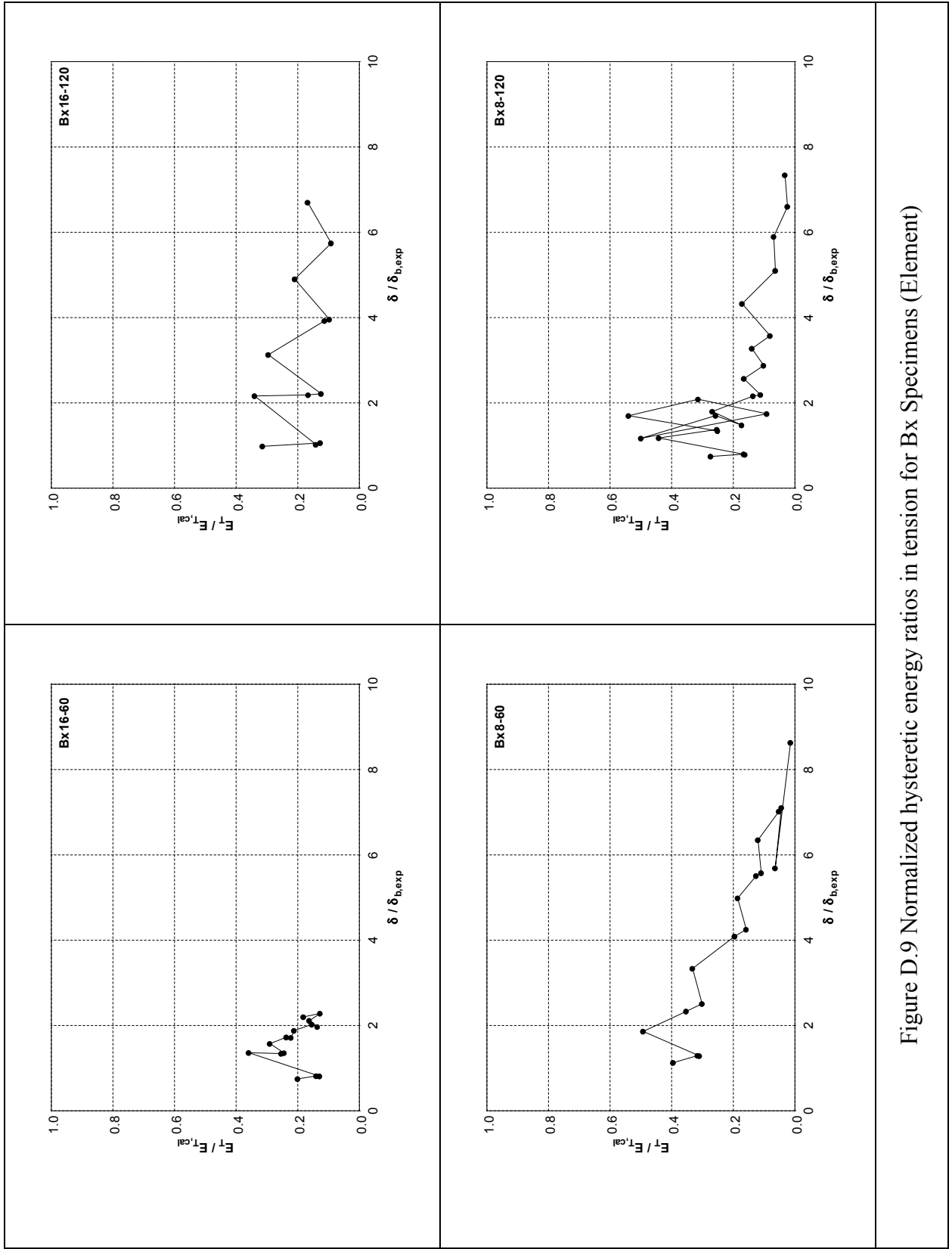


Figure D.9 Normalized hysteretic energy ratios in tension for Bx Specimens (Element)

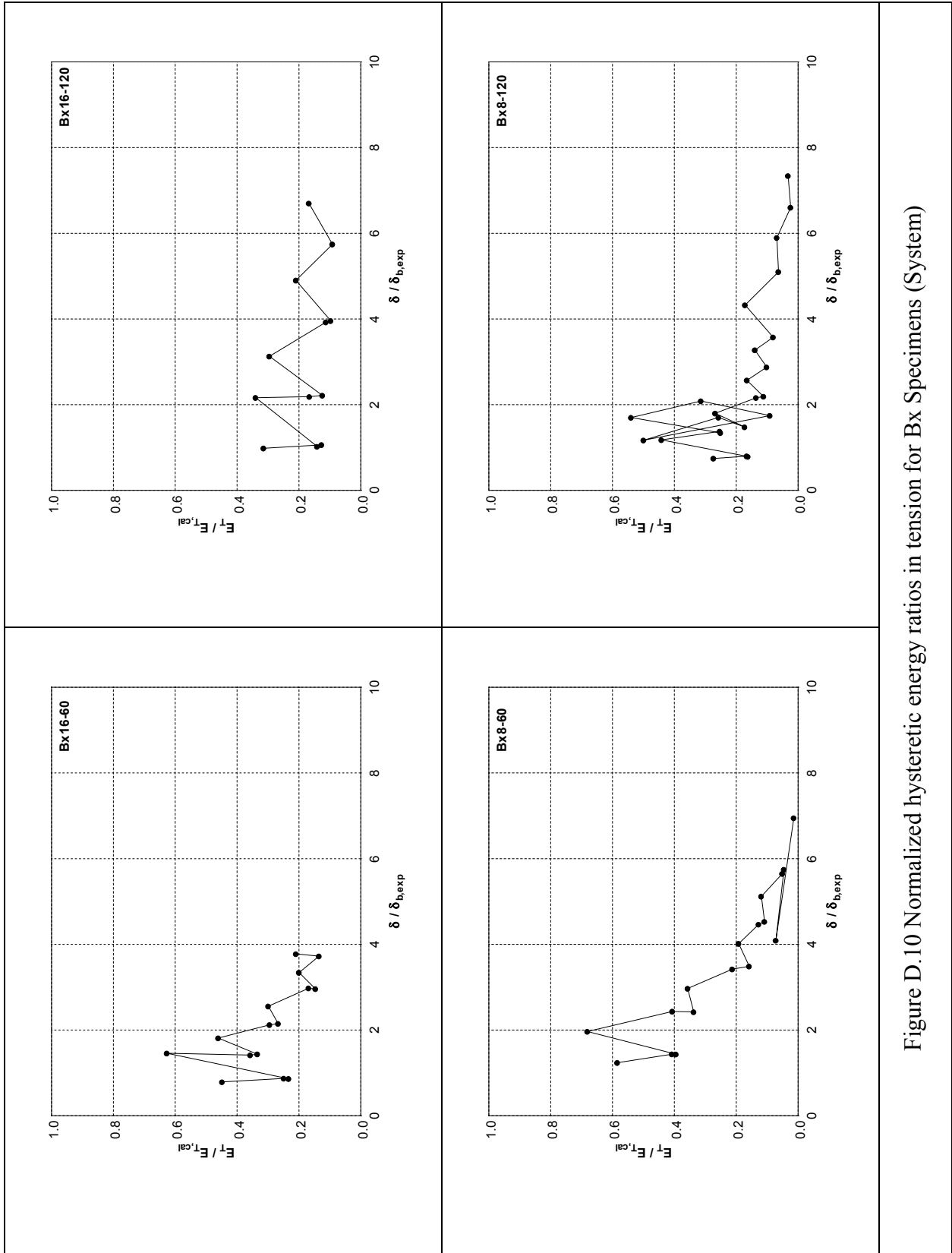


Figure D.10 Normalized hysteretic energy ratios in tension for Bx Specimens (System)

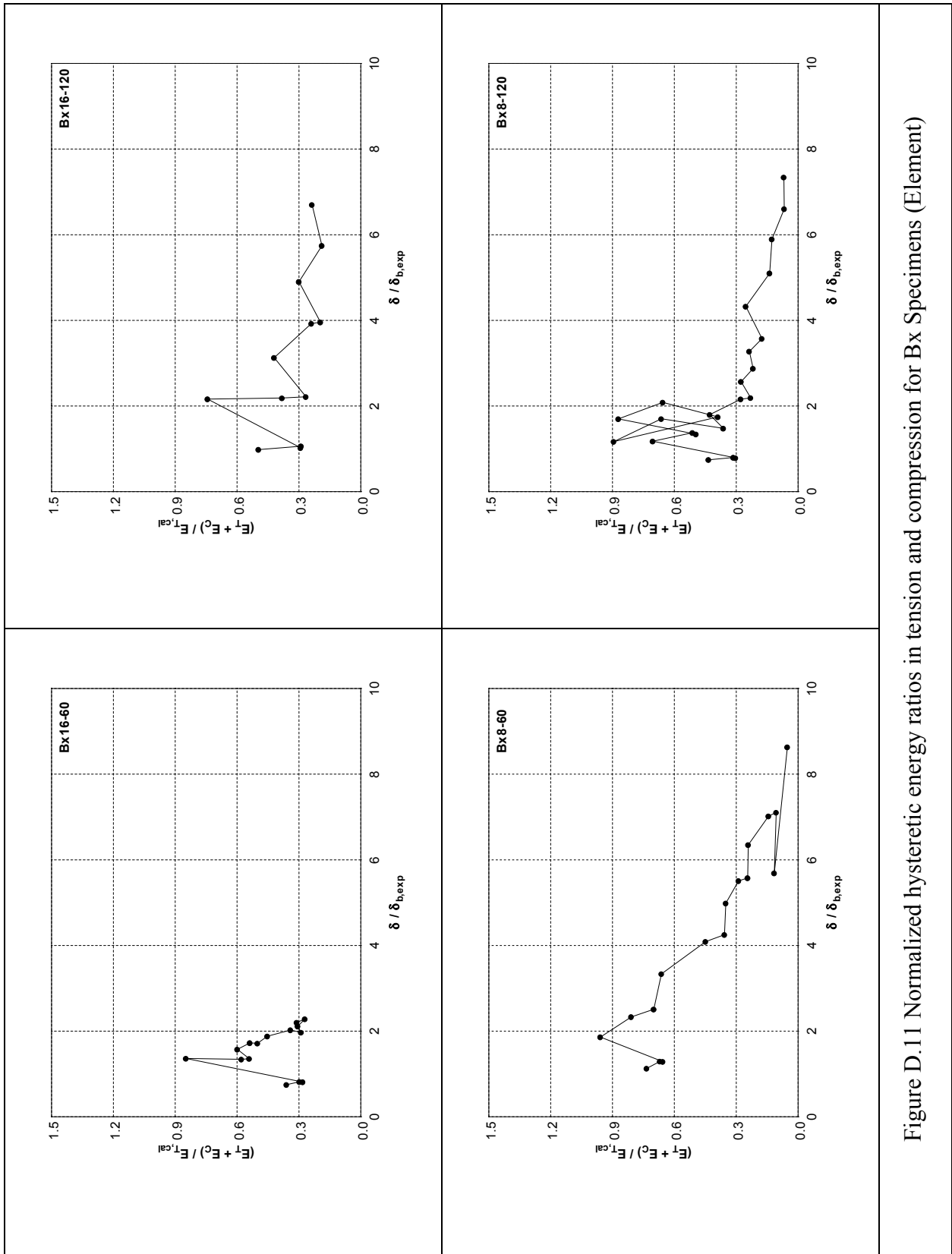


Figure D.11 Normalized hysteretic energy ratios in tension and compression for Bx Specimens (Element)

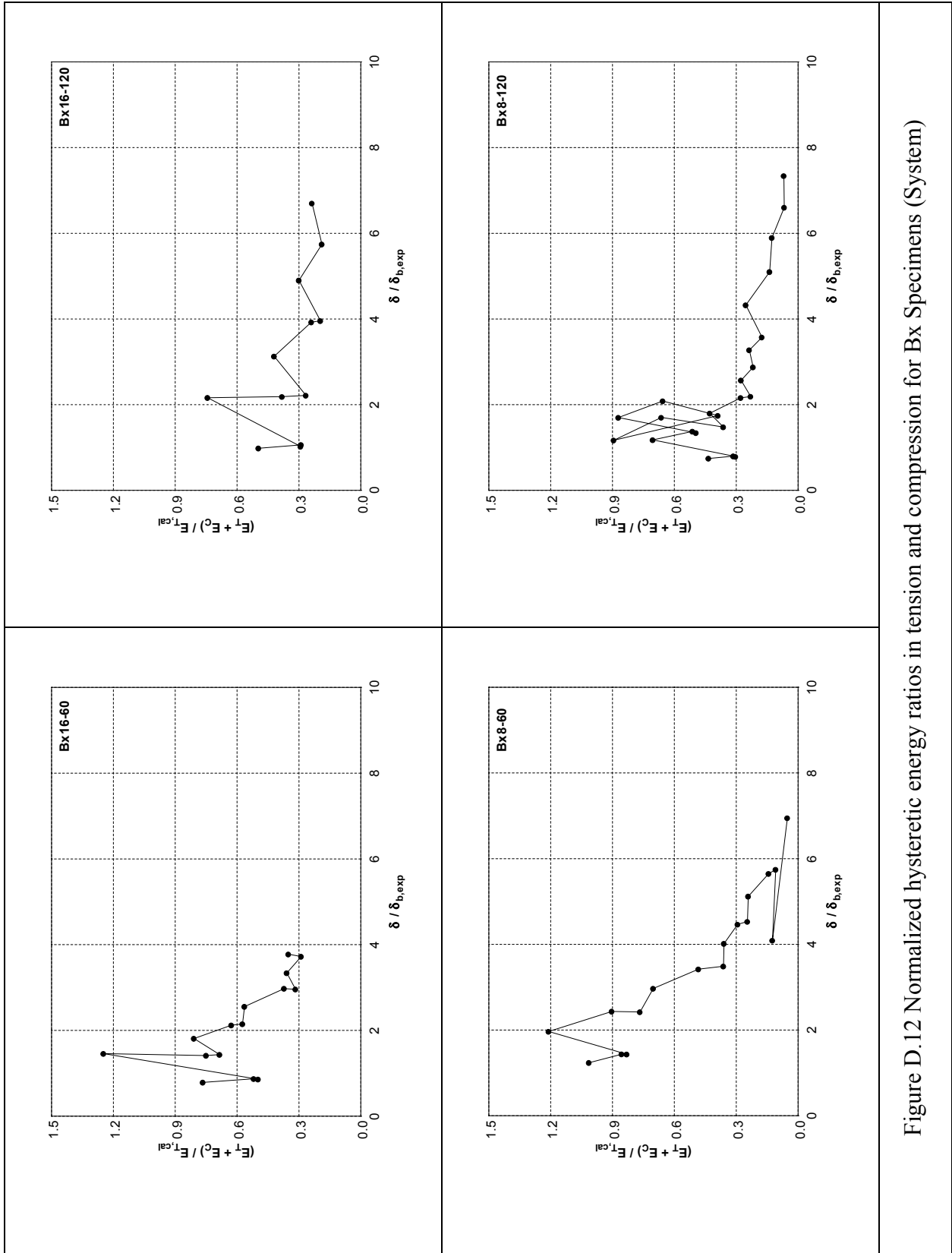


Figure D.12 Normalized hysteretic energy ratios in tension and compression for Bx Specimens (System)

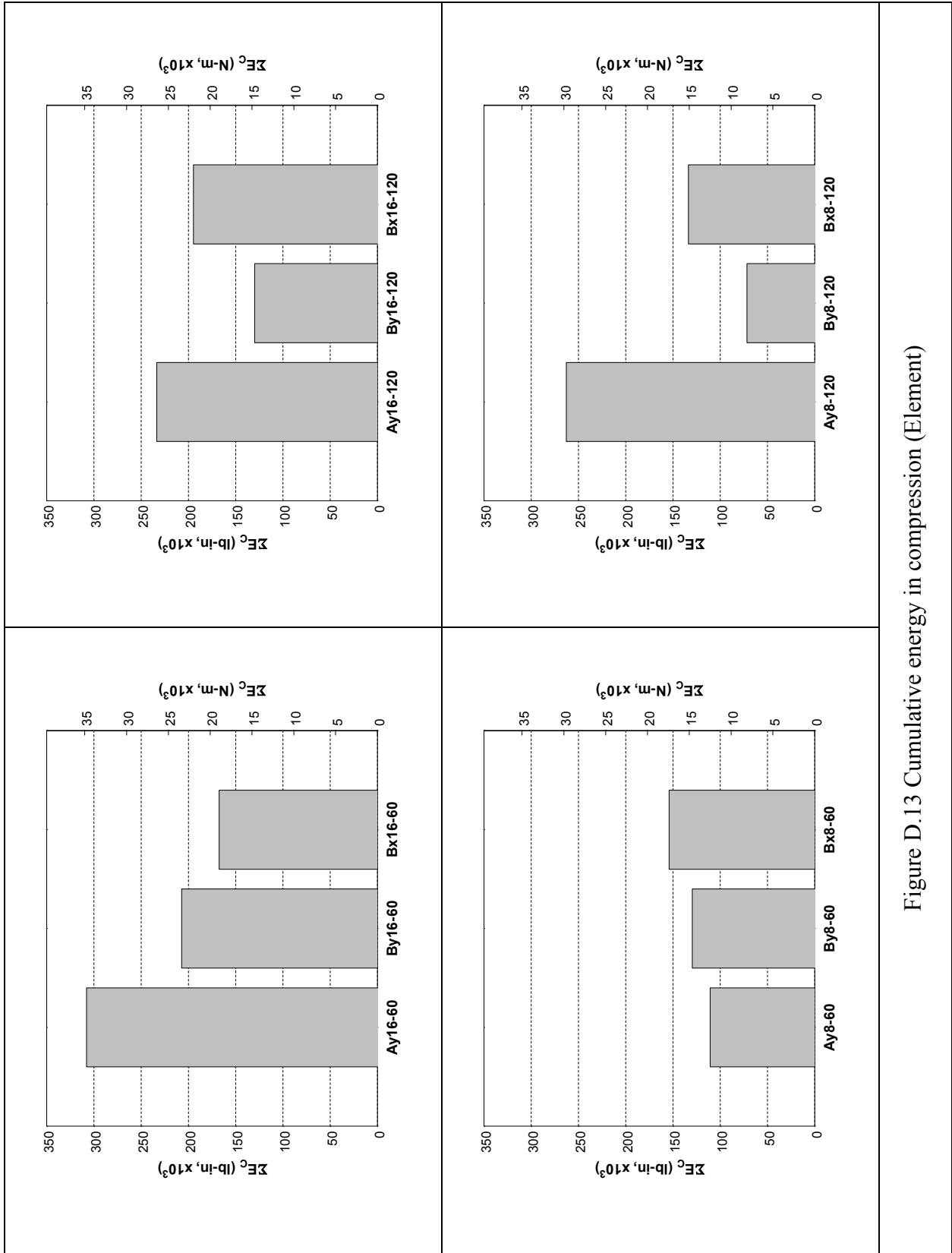


Figure D.13 Cumulative energy in compression (Element)

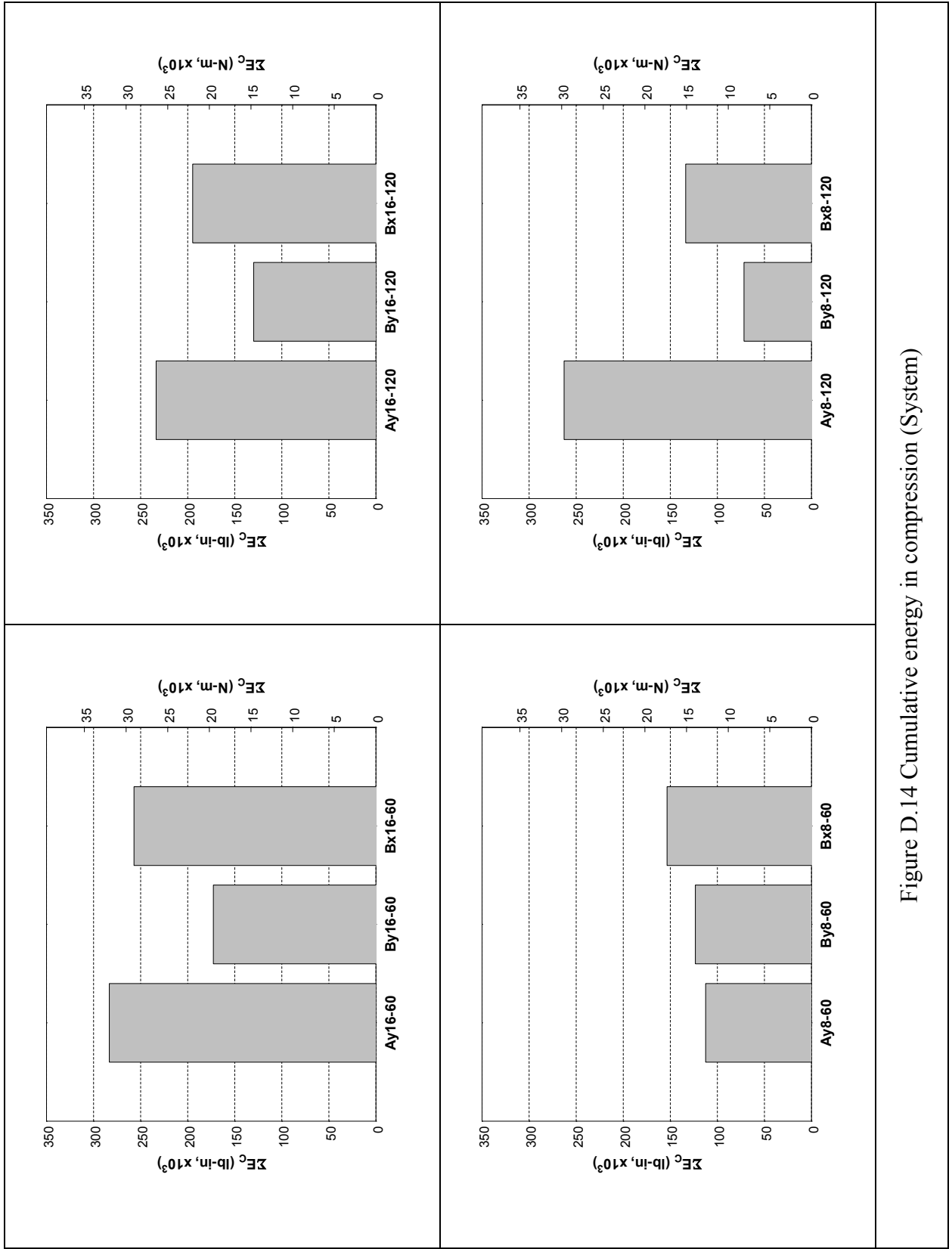


Figure D.14 Cumulative energy in compression (System)

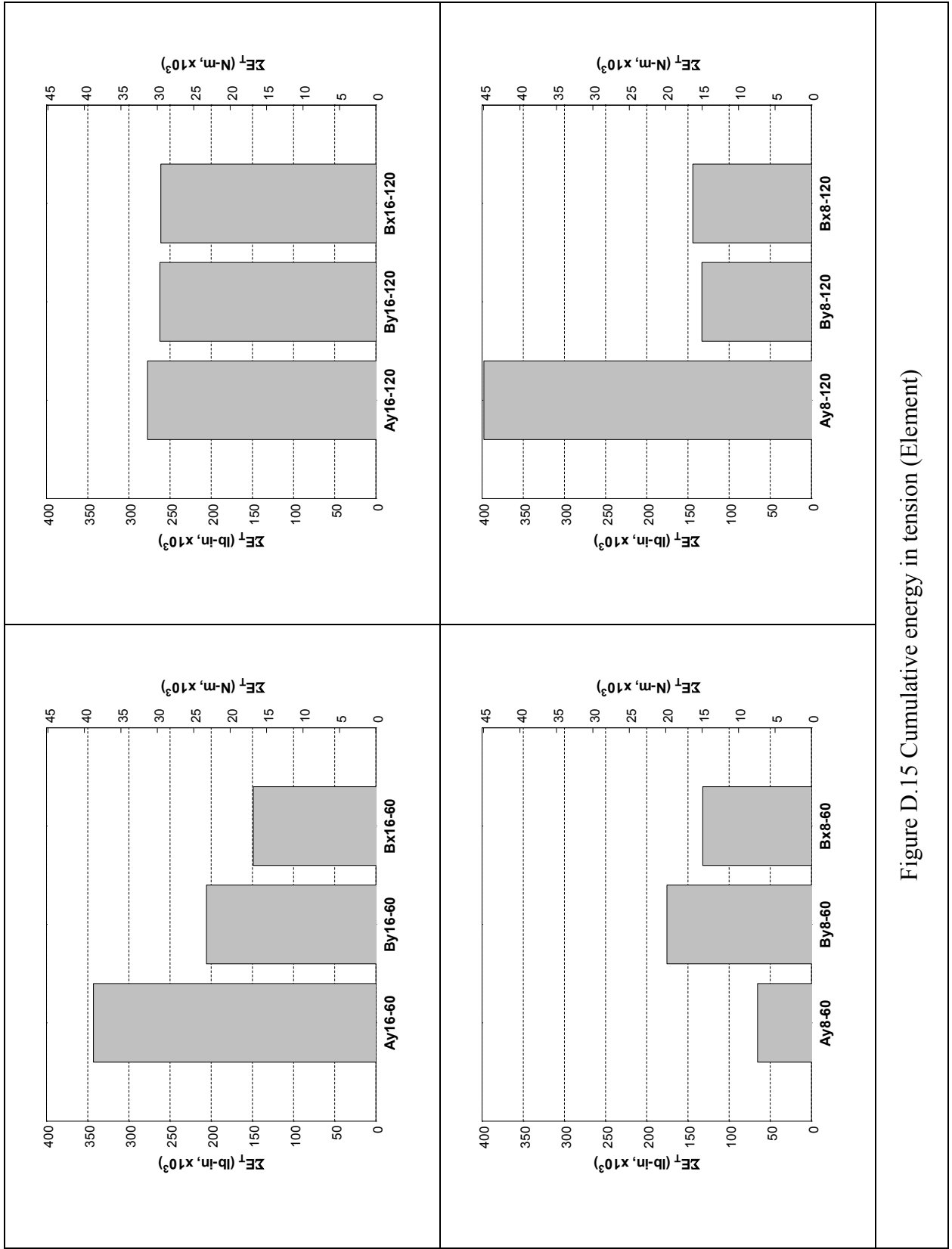


Figure D.15 Cumulative energy in tension (Element)

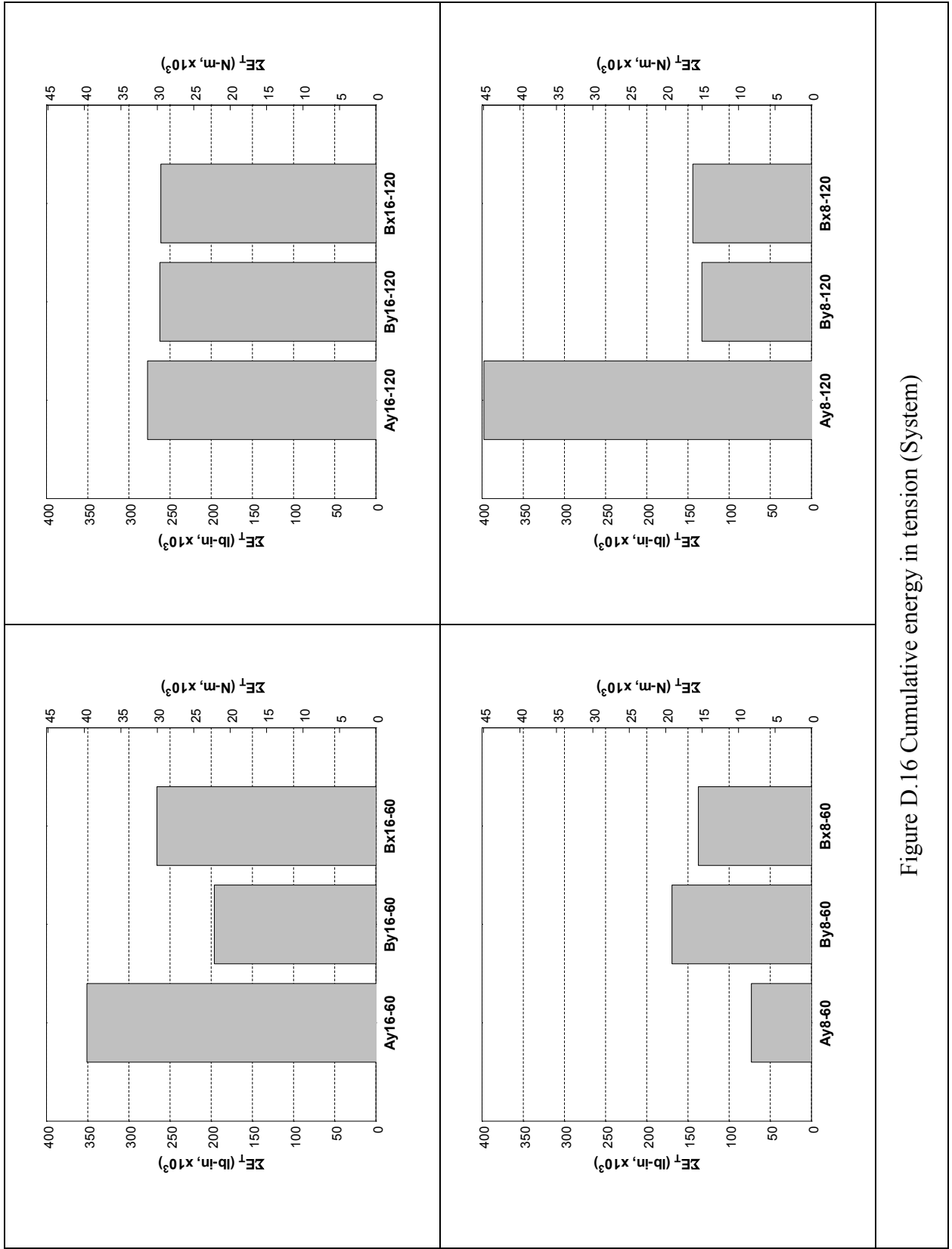


Figure D.16 Cumulative energy in tension (System)

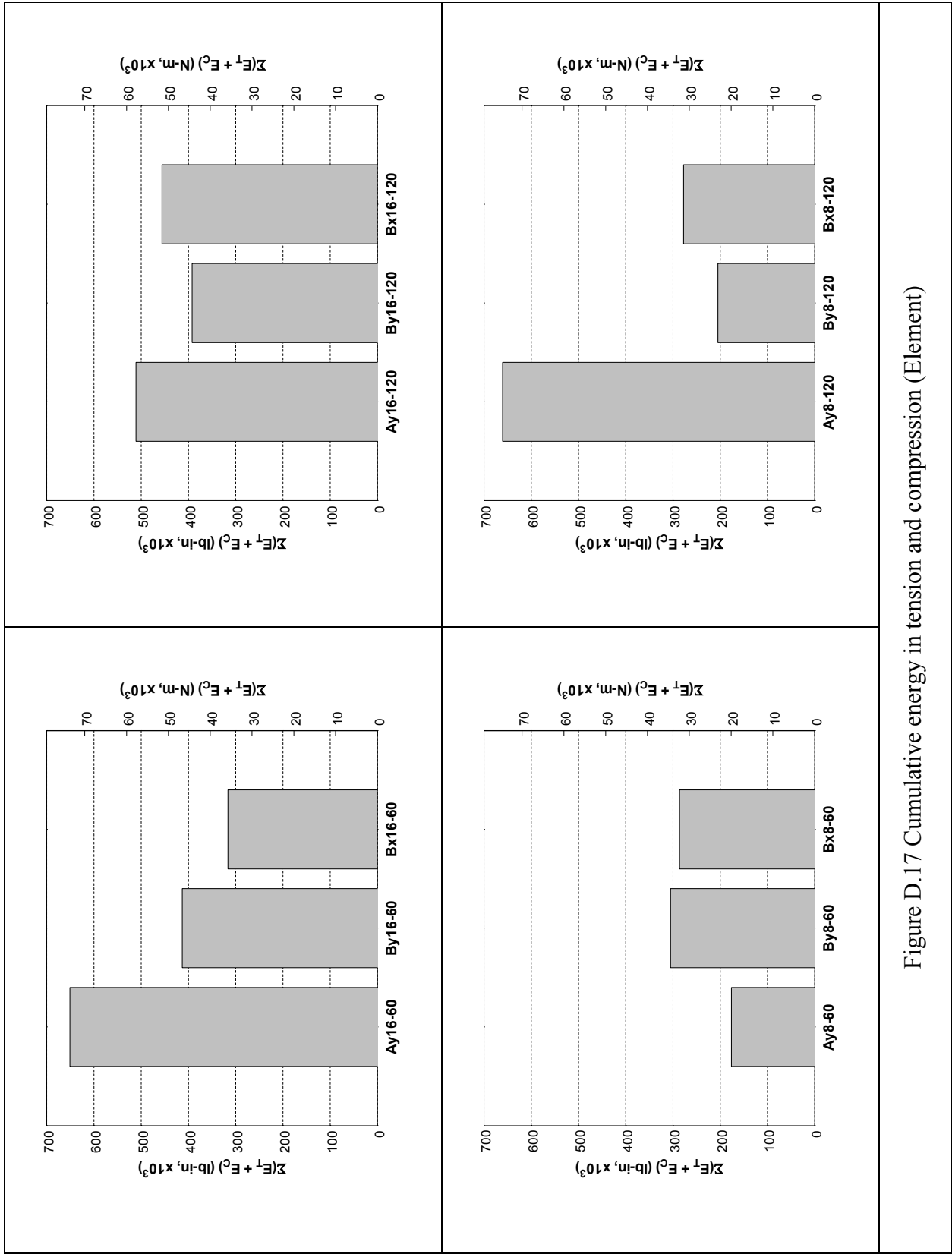


Figure D.17 Cumulative energy in tension and compression (Element)

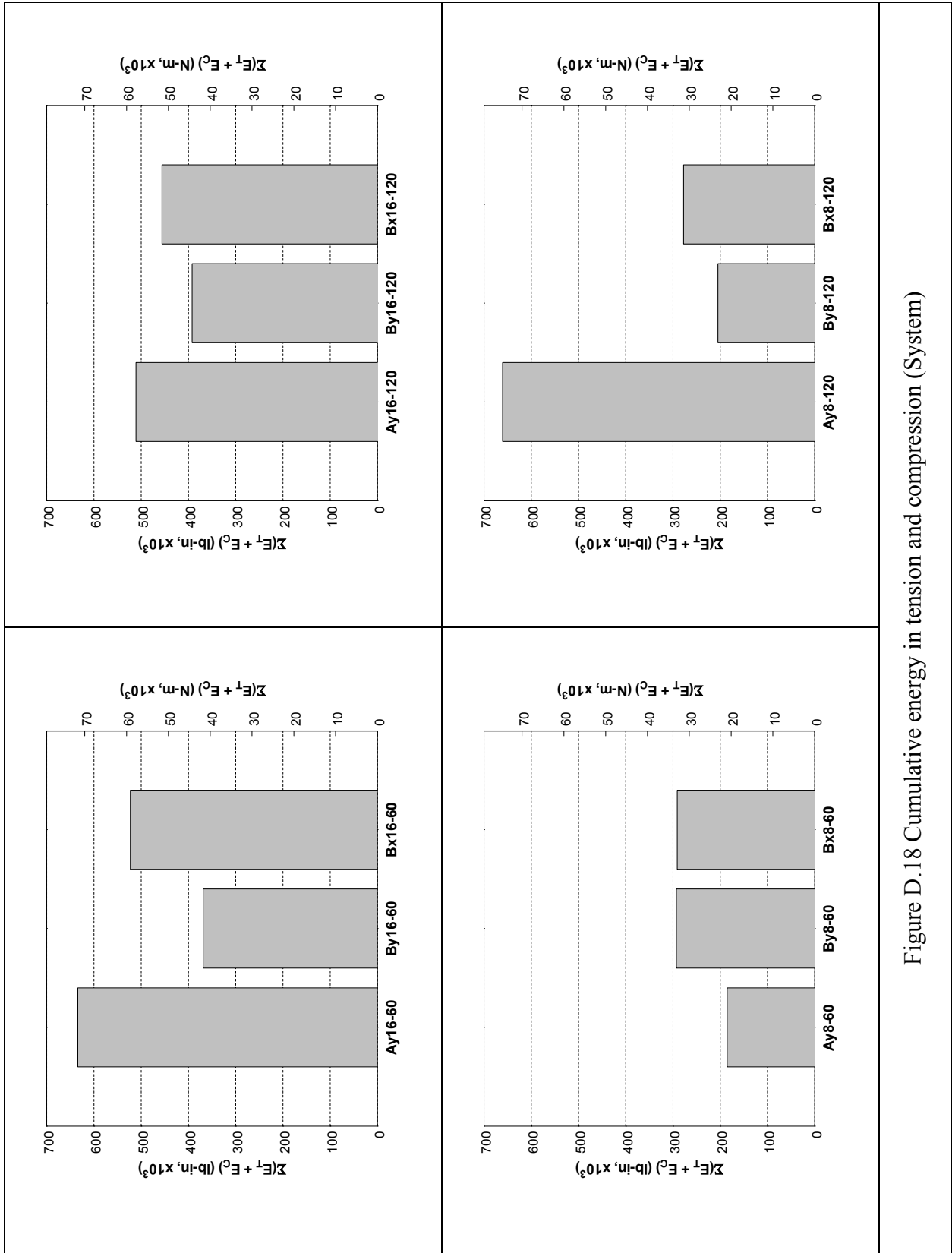


Figure D.18 Cumulative energy in tension and compression (System)

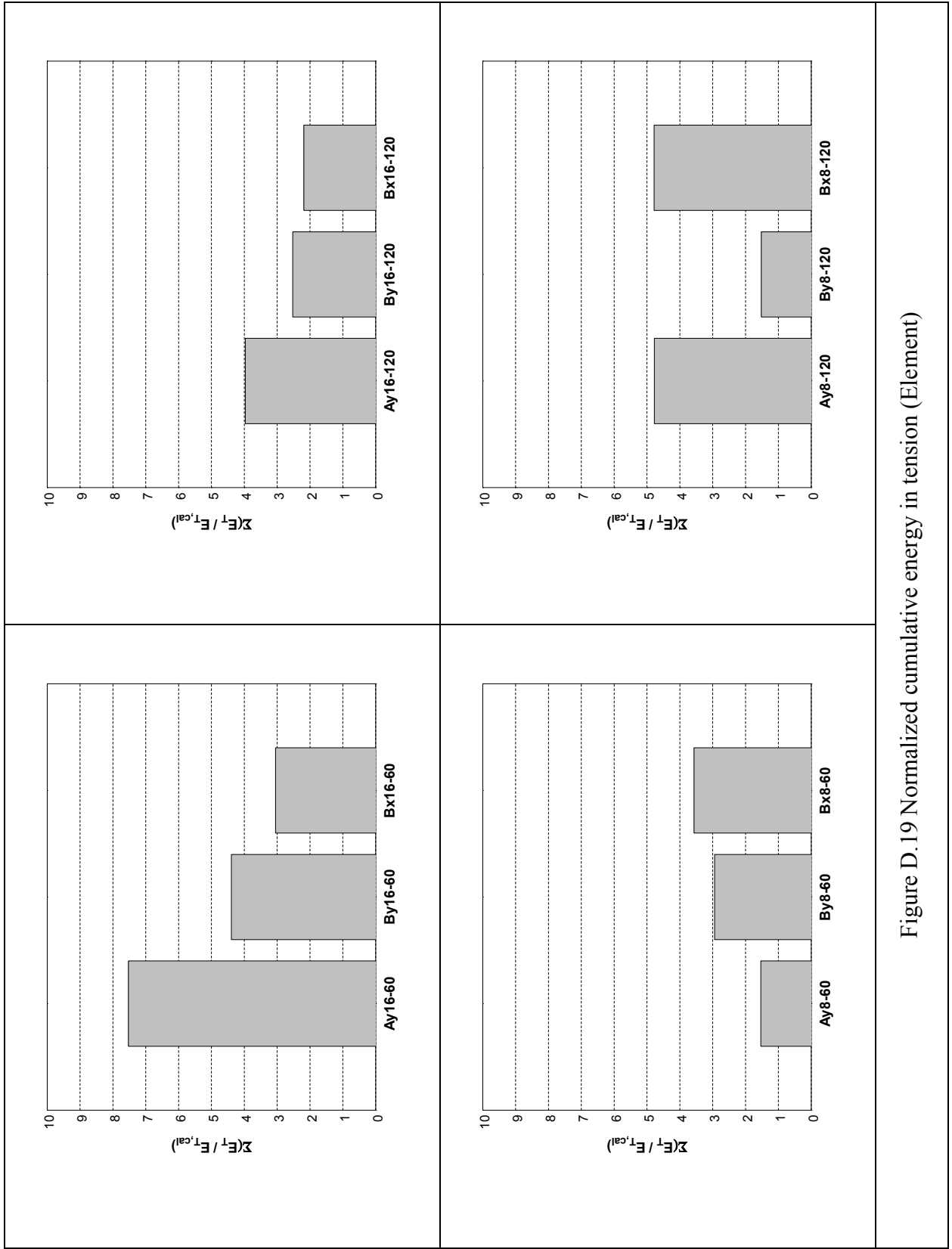


Figure D.19 Normalized cumulative energy in tension (Element)

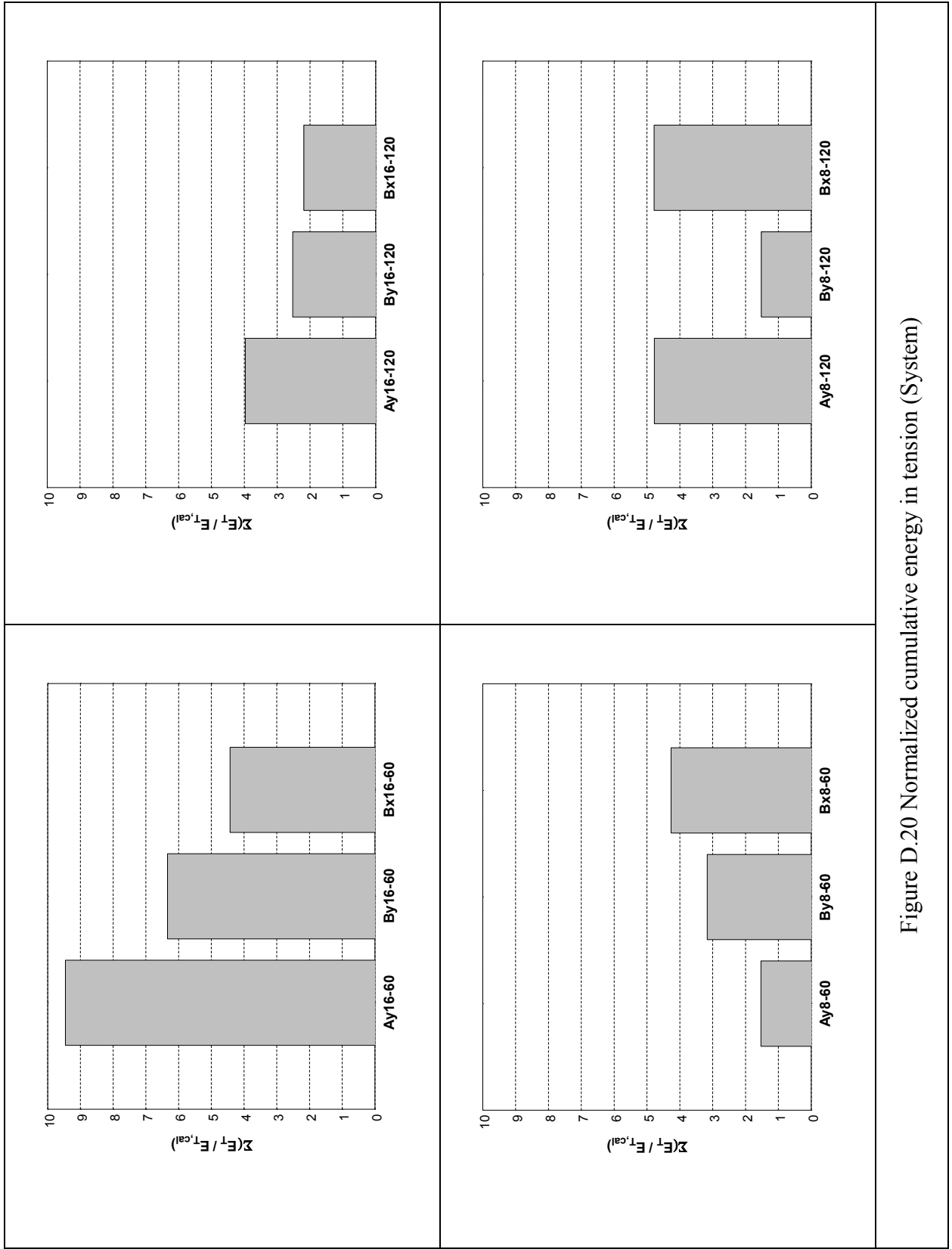


Figure D.20 Normalized cumulative energy in tension (System)

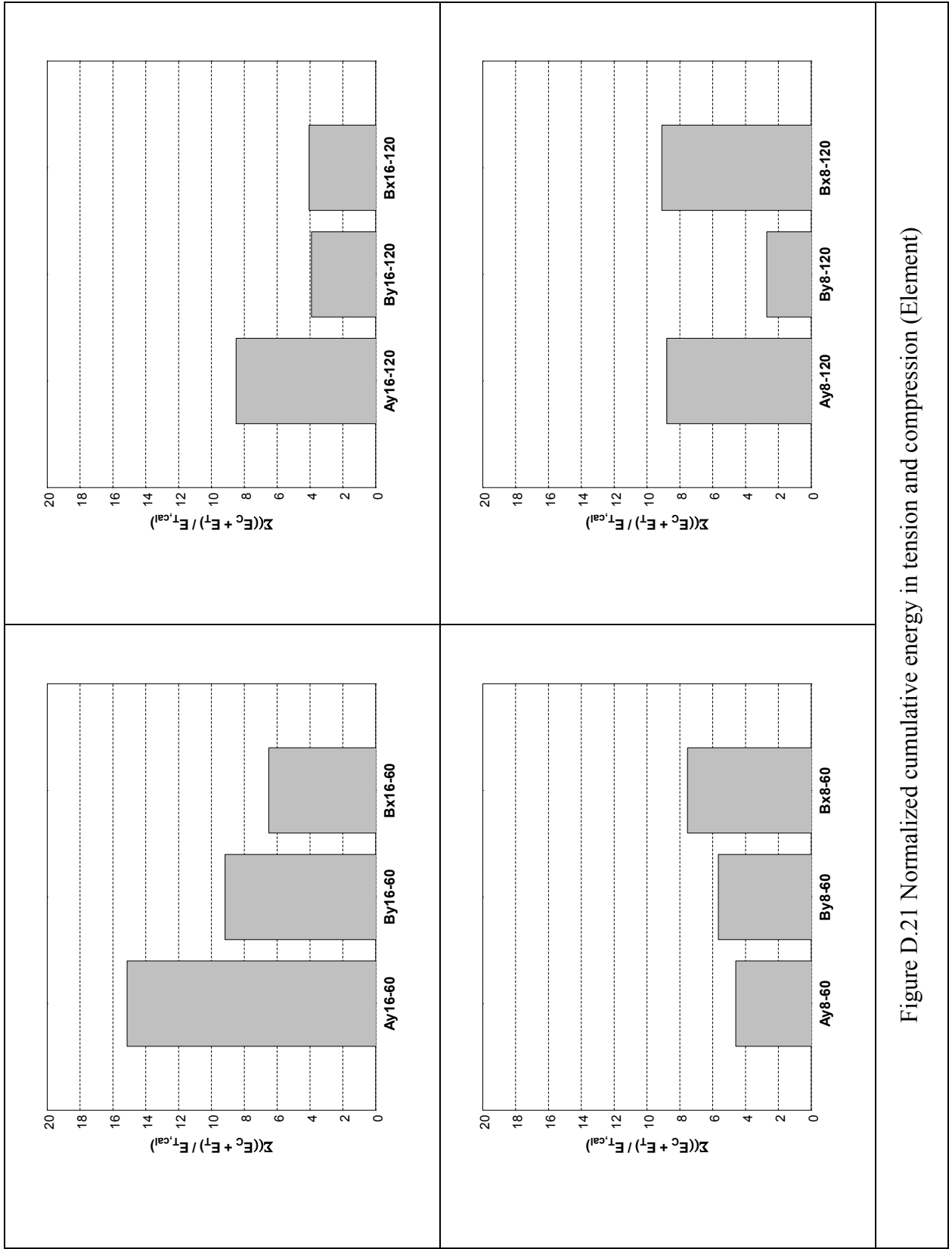


Figure D.21 Normalized cumulative energy in tension and compression (Element)

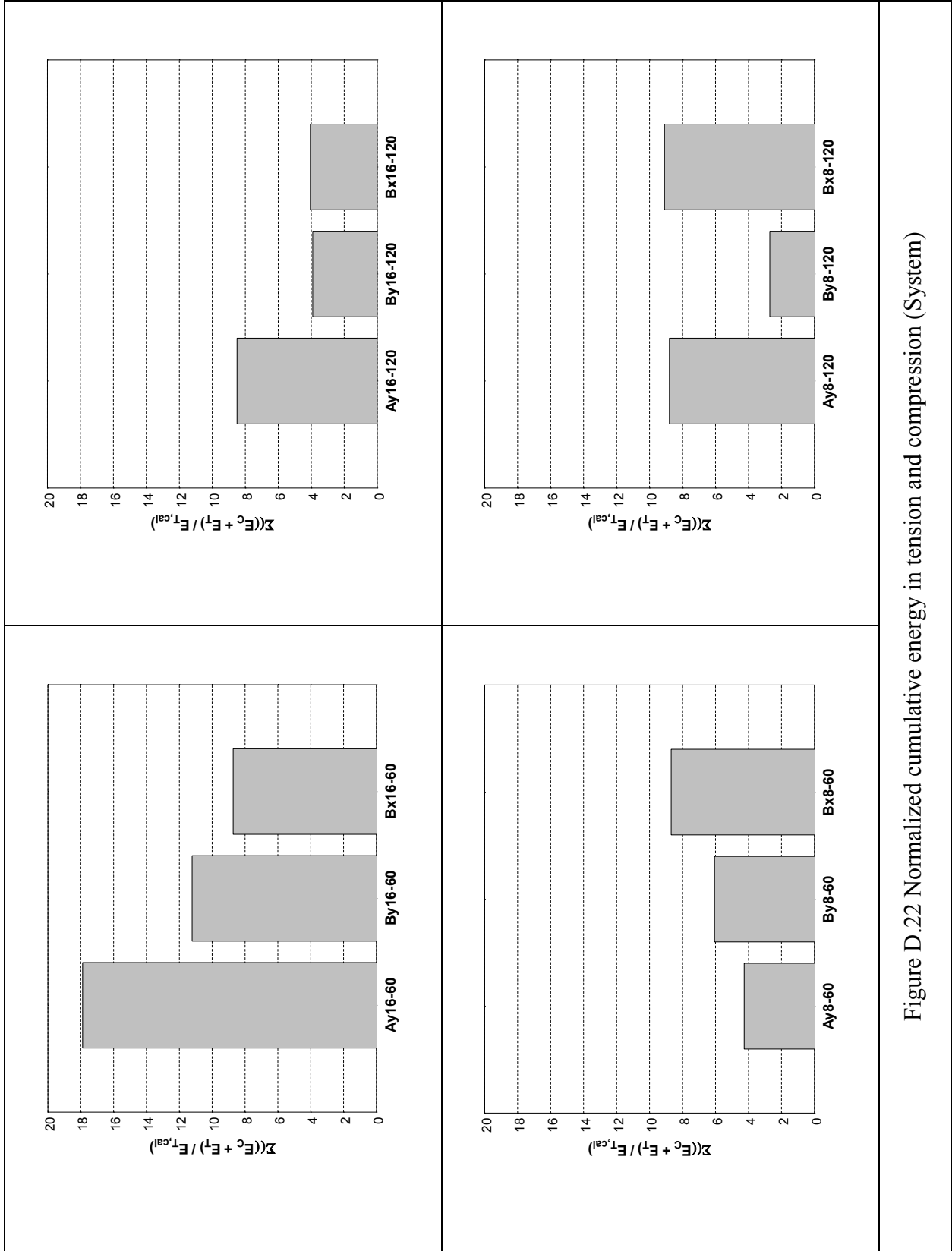


Figure D.22 Normalized cumulative energy in tension and compression (System)



## **Multidisciplinary Center for Earthquake Engineering Research List of Technical Reports**

The Multidisciplinary Center for Earthquake Engineering Research (MCEER) publishes technical reports on a variety of subjects related to earthquake engineering written by authors funded through MCEER. These reports are available from both MCEER Publications and the National Technical Information Service (NTIS). Requests for reports should be directed to MCEER Publications, Multidisciplinary Center for Earthquake Engineering Research, State University of New York at Buffalo, Red Jacket Quadrangle, Buffalo, New York 14261. Reports can also be requested through NTIS, 5285 Port Royal Road, Springfield, Virginia 22161. NTIS accession numbers are shown in parenthesis, if available.

- NCEER-87-0001 "First-Year Program in Research, Education and Technology Transfer," 3/5/87, (PB88-134275, A04, MF-A01).
- NCEER-87-0002 "Experimental Evaluation of Instantaneous Optimal Algorithms for Structural Control," by R.C. Lin, T.T. Soong and A.M. Reinhorn, 4/20/87, (PB88-134341, A04, MF-A01).
- NCEER-87-0003 "Experimentation Using the Earthquake Simulation Facilities at University at Buffalo," by A.M. Reinhorn and R.L. Ketter, to be published.
- NCEER-87-0004 "The System Characteristics and Performance of a Shaking Table," by J.S. Hwang, K.C. Chang and G.C. Lee, 6/1/87, (PB88-134259, A03, MF-A01). This report is available only through NTIS (see address given above).
- NCEER-87-0005 "A Finite Element Formulation for Nonlinear Viscoplastic Material Using a Q Model," by O. Gyebi and G. Dasgupta, 11/2/87, (PB88-213764, A08, MF-A01).
- NCEER-87-0006 "Symbolic Manipulation Program (SMP) - Algebraic Codes for Two and Three Dimensional Finite Element Formulations," by X. Lee and G. Dasgupta, 11/9/87, (PB88-218522, A05, MF-A01).
- NCEER-87-0007 "Instantaneous Optimal Control Laws for Tall Buildings Under Seismic Excitations," by J.N. Yang, A. Akbarpour and P. Ghaemmaghami, 6/10/87, (PB88-134333, A06, MF-A01). This report is only available through NTIS (see address given above).
- NCEER-87-0008 "IDARC: Inelastic Damage Analysis of Reinforced Concrete Frame - Shear-Wall Structures," by Y.J. Park, A.M. Reinhorn and S.K. Kunnath, 7/20/87, (PB88-134325, A09, MF-A01). This report is only available through NTIS (see address given above).
- NCEER-87-0009 "Liquefaction Potential for New York State: A Preliminary Report on Sites in Manhattan and Buffalo," by M. Budhu, V. Vijayakumar, R.F. Giese and L. Baumgras, 8/31/87, (PB88-163704, A03, MF-A01). This report is available only through NTIS (see address given above).
- NCEER-87-0010 "Vertical and Torsional Vibration of Foundations in Inhomogeneous Media," by A.S. Veletsos and K.W. Dotson, 6/1/87, (PB88-134291, A03, MF-A01). This report is only available through NTIS (see address given above).
- NCEER-87-0011 "Seismic Probabilistic Risk Assessment and Seismic Margins Studies for Nuclear Power Plants," by Howard H.M. Hwang, 6/15/87, (PB88-134267, A03, MF-A01). This report is only available through NTIS (see address given above).
- NCEER-87-0012 "Parametric Studies of Frequency Response of Secondary Systems Under Ground-Acceleration Excitations," by Y. Yong and Y.K. Lin, 6/10/87, (PB88-134309, A03, MF-A01). This report is only available through NTIS (see address given above).
- NCEER-87-0013 "Frequency Response of Secondary Systems Under Seismic Excitation," by J.A. HoLung, J. Cai and Y.K. Lin, 7/31/87, (PB88-134317, A05, MF-A01). This report is only available through NTIS (see address given above).
- NCEER-87-0014 "Modelling Earthquake Ground Motions in Seismically Active Regions Using Parametric Time Series Methods," by G.W. Ellis and A.S. Cakmak, 8/25/87, (PB88-134283, A08, MF-A01). This report is only available through NTIS (see address given above).

- NCEER-87-0015 "Detection and Assessment of Seismic Structural Damage," by E. DiPasquale and A.S. Cakmak, 8/25/87, (PB88-163712, A05, MF-A01). This report is only available through NTIS (see address given above).
- NCEER-87-0016 "Pipeline Experiment at Parkfield, California," by J. Isenberg and E. Richardson, 9/15/87, (PB88-163720, A03, MF-A01). This report is available only through NTIS (see address given above).
- NCEER-87-0017 "Digital Simulation of Seismic Ground Motion," by M. Shinozuka, G. Deodatis and T. Harada, 8/31/87, (PB88-155197, A04, MF-A01). This report is available only through NTIS (see address given above).
- NCEER-87-0018 "Practical Considerations for Structural Control: System Uncertainty, System Time Delay and Truncation of Small Control Forces," J.N. Yang and A. Akbarpour, 8/10/87, (PB88-163738, A08, MF-A01). This report is only available through NTIS (see address given above).
- NCEER-87-0019 "Modal Analysis of Nonclassically Damped Structural Systems Using Canonical Transformation," by J.N. Yang, S. Sarkani and F.X. Long, 9/27/87, (PB88-187851, A04, MF-A01).
- NCEER-87-0020 "A Nonstationary Solution in Random Vibration Theory," by J.R. Red-Horse and P.D. Spanos, 11/3/87, (PB88-163746, A03, MF-A01).
- NCEER-87-0021 "Horizontal Impedances for Radially Inhomogeneous Viscoelastic Soil Layers," by A.S. Veletsos and K.W. Dotson, 10/15/87, (PB88-150859, A04, MF-A01).
- NCEER-87-0022 "Seismic Damage Assessment of Reinforced Concrete Members," by Y.S. Chung, C. Meyer and M. Shinozuka, 10/9/87, (PB88-150867, A05, MF-A01). This report is available only through NTIS (see address given above).
- NCEER-87-0023 "Active Structural Control in Civil Engineering," by T.T. Soong, 11/11/87, (PB88-187778, A03, MF-A01).
- NCEER-87-0024 "Vertical and Torsional Impedances for Radially Inhomogeneous Viscoelastic Soil Layers," by K.W. Dotson and A.S. Veletsos, 12/87, (PB88-187786, A03, MF-A01).
- NCEER-87-0025 "Proceedings from the Symposium on Seismic Hazards, Ground Motions, Soil-Liquefaction and Engineering Practice in Eastern North America," October 20-22, 1987, edited by K.H. Jacob, 12/87, (PB88-188115, A23, MF-A01). This report is available only through NTIS (see address given above).
- NCEER-87-0026 "Report on the Whittier-Narrows, California, Earthquake of October 1, 1987," by J. Pantelic and A. Reinhorn, 11/87, (PB88-187752, A03, MF-A01). This report is available only through NTIS (see address given above).
- NCEER-87-0027 "Design of a Modular Program for Transient Nonlinear Analysis of Large 3-D Building Structures," by S. Srivastav and J.F. Abel, 12/30/87, (PB88-187950, A05, MF-A01). This report is only available through NTIS (see address given above).
- NCEER-87-0028 "Second-Year Program in Research, Education and Technology Transfer," 3/8/88, (PB88-219480, A04, MF-A01).
- NCEER-88-0001 "Workshop on Seismic Computer Analysis and Design of Buildings With Interactive Graphics," by W. McGuire, J.F. Abel and C.H. Conley, 1/18/88, (PB88-187760, A03, MF-A01). This report is only available through NTIS (see address given above).
- NCEER-88-0002 "Optimal Control of Nonlinear Flexible Structures," by J.N. Yang, F.X. Long and D. Wong, 1/22/88, (PB88-213772, A06, MF-A01).
- NCEER-88-0003 "Substructuring Techniques in the Time Domain for Primary-Secondary Structural Systems," by G.D. Manolis and G. Juhn, 2/10/88, (PB88-213780, A04, MF-A01).
- NCEER-88-0004 "Iterative Seismic Analysis of Primary-Secondary Systems," by A. Singhal, L.D. Lutes and P.D. Spanos, 2/23/88, (PB88-213798, A04, MF-A01).

- NCEER-88-0005 "Stochastic Finite Element Expansion for Random Media," by P.D. Spanos and R. Ghanem, 3/14/88, (PB88-213806, A03, MF-A01).
- NCEER-88-0006 "Combining Structural Optimization and Structural Control," by F.Y. Cheng and C.P. Pantelides, 1/10/88, (PB88-213814, A05, MF-A01).
- NCEER-88-0007 "Seismic Performance Assessment of Code-Designed Structures," by H.H-M. Hwang, J-W. Jaw and H-J. Shau, 3/20/88, (PB88-219423, A04, MF-A01). This report is only available through NTIS (see address given above).
- NCEER-88-0008 "Reliability Analysis of Code-Designed Structures Under Natural Hazards," by H.H-M. Hwang, H. Ushiba and M. Shinozuka, 2/29/88, (PB88-229471, A07, MF-A01). This report is only available through NTIS (see address given above).
- NCEER-88-0009 "Seismic Fragility Analysis of Shear Wall Structures," by J-W Jaw and H.H-M. Hwang, 4/30/88, (PB89-102867, A04, MF-A01).
- NCEER-88-0010 "Base Isolation of a Multi-Story Building Under a Harmonic Ground Motion - A Comparison of Performances of Various Systems," by F-G Fan, G. Ahmadi and I.G. Tadjbakhsh, 5/18/88, (PB89-122238, A06, MF-A01). This report is only available through NTIS (see address given above).
- NCEER-88-0011 "Seismic Floor Response Spectra for a Combined System by Green's Functions," by F.M. Lavelle, L.A. Bergman and P.D. Spanos, 5/1/88, (PB89-102875, A03, MF-A01).
- NCEER-88-0012 "A New Solution Technique for Randomly Excited Hysteretic Structures," by G.Q. Cai and Y.K. Lin, 5/16/88, (PB89-102883, A03, MF-A01).
- NCEER-88-0013 "A Study of Radiation Damping and Soil-Structure Interaction Effects in the Centrifuge," by K. Weissman, supervised by J.H. Prevost, 5/24/88, (PB89-144703, A06, MF-A01).
- NCEER-88-0014 "Parameter Identification and Implementation of a Kinematic Plasticity Model for Frictional Soils," by J.H. Prevost and D.V. Griffiths, to be published.
- NCEER-88-0015 "Two- and Three- Dimensional Dynamic Finite Element Analyses of the Long Valley Dam," by D.V. Griffiths and J.H. Prevost, 6/17/88, (PB89-144711, A04, MF-A01).
- NCEER-88-0016 "Damage Assessment of Reinforced Concrete Structures in Eastern United States," by A.M. Reinhorn, M.J. Seidel, S.K. Kunnath and Y.J. Park, 6/15/88, (PB89-122220, A04, MF-A01). This report is only available through NTIS (see address given above).
- NCEER-88-0017 "Dynamic Compliance of Vertically Loaded Strip Foundations in Multilayered Viscoelastic Soils," by S. Ahmad and A.S.M. Israil, 6/17/88, (PB89-102891, A04, MF-A01).
- NCEER-88-0018 "An Experimental Study of Seismic Structural Response With Added Viscoelastic Dampers," by R.C. Lin, Z. Liang, T.T. Soong and R.H. Zhang, 6/30/88, (PB89-122212, A05, MF-A01). This report is available only through NTIS (see address given above).
- NCEER-88-0019 "Experimental Investigation of Primary - Secondary System Interaction," by G.D. Manolis, G. Juhn and A.M. Reinhorn, 5/27/88, (PB89-122204, A04, MF-A01).
- NCEER-88-0020 "A Response Spectrum Approach For Analysis of Nonclassically Damped Structures," by J.N. Yang, S. Sarkani and F.X. Long, 4/22/88, (PB89-102909, A04, MF-A01).
- NCEER-88-0021 "Seismic Interaction of Structures and Soils: Stochastic Approach," by A.S. Veletsos and A.M. Prasad, 7/21/88, (PB89-122196, A04, MF-A01). This report is only available through NTIS (see address given above).
- NCEER-88-0022 "Identification of the Serviceability Limit State and Detection of Seismic Structural Damage," by E. DiPasquale and A.S. Cakmak, 6/15/88, (PB89-122188, A05, MF-A01). This report is available only through NTIS (see address given above).

- NCEER-88-0023 "Multi-Hazard Risk Analysis: Case of a Simple Offshore Structure," by B.K. Bhartia and E.H. Vanmarcke, 7/21/88, (PB89-145213, A05, MF-A01).
- NCEER-88-0024 "Automated Seismic Design of Reinforced Concrete Buildings," by Y.S. Chung, C. Meyer and M. Shinozuka, 7/5/88, (PB89-122170, A06, MF-A01). This report is available only through NTIS (see address given above).
- NCEER-88-0025 "Experimental Study of Active Control of MDOF Structures Under Seismic Excitations," by L.L. Chung, R.C. Lin, T.T. Soong and A.M. Reinhorn, 7/10/88, (PB89-122600, A04, MF-A01).
- NCEER-88-0026 "Earthquake Simulation Tests of a Low-Rise Metal Structure," by J.S. Hwang, K.C. Chang, G.C. Lee and R.L. Ketter, 8/1/88, (PB89-102917, A04, MF-A01).
- NCEER-88-0027 "Systems Study of Urban Response and Reconstruction Due to Catastrophic Earthquakes," by F. Kozin and H.K. Zhou, 9/22/88, (PB90-162348, A04, MF-A01).
- NCEER-88-0028 "Seismic Fragility Analysis of Plane Frame Structures," by H.H-M. Hwang and Y.K. Low, 7/31/88, (PB89-131445, A06, MF-A01).
- NCEER-88-0029 "Response Analysis of Stochastic Structures," by A. Kardara, C. Bucher and M. Shinozuka, 9/22/88, (PB89-174429, A04, MF-A01).
- NCEER-88-0030 "Nonnormal Accelerations Due to Yielding in a Primary Structure," by D.C.K. Chen and L.D. Lutes, 9/19/88, (PB89-131437, A04, MF-A01).
- NCEER-88-0031 "Design Approaches for Soil-Structure Interaction," by A.S. Veletsos, A.M. Prasad and Y. Tang, 12/30/88, (PB89-174437, A03, MF-A01). This report is available only through NTIS (see address given above).
- NCEER-88-0032 "A Re-evaluation of Design Spectra for Seismic Damage Control," by C.J. Turkstra and A.G. Tallin, 11/7/88, (PB89-145221, A05, MF-A01).
- NCEER-88-0033 "The Behavior and Design of Noncontact Lap Splices Subjected to Repeated Inelastic Tensile Loading," by V.E. Sagan, P. Gergely and R.N. White, 12/8/88, (PB89-163737, A08, MF-A01).
- NCEER-88-0034 "Seismic Response of Pile Foundations," by S.M. Mamoon, P.K. Banerjee and S. Ahmad, 11/1/88, (PB89-145239, A04, MF-A01).
- NCEER-88-0035 "Modeling of R/C Building Structures With Flexible Floor Diaphragms (IDARC2)," by A.M. Reinhorn, S.K. Kunnath and N. Panahshahi, 9/7/88, (PB89-207153, A07, MF-A01).
- NCEER-88-0036 "Solution of the Dam-Reservoir Interaction Problem Using a Combination of FEM, BEM with Particular Integrals, Modal Analysis, and Substructuring," by C-S. Tsai, G.C. Lee and R.L. Ketter, 12/31/88, (PB89-207146, A04, MF-A01).
- NCEER-88-0037 "Optimal Placement of Actuators for Structural Control," by F.Y. Cheng and C.P. Pantelides, 8/15/88, (PB89-162846, A05, MF-A01).
- NCEER-88-0038 "Teflon Bearings in Aseismic Base Isolation: Experimental Studies and Mathematical Modeling," by A. Mokha, M.C. Constantinou and A.M. Reinhorn, 12/5/88, (PB89-218457, A10, MF-A01). This report is available only through NTIS (see address given above).
- NCEER-88-0039 "Seismic Behavior of Flat Slab High-Rise Buildings in the New York City Area," by P. Weidlinger and M. Ettouney, 10/15/88, (PB90-145681, A04, MF-A01).
- NCEER-88-0040 "Evaluation of the Earthquake Resistance of Existing Buildings in New York City," by P. Weidlinger and M. Ettouney, 10/15/88, to be published.
- NCEER-88-0041 "Small-Scale Modeling Techniques for Reinforced Concrete Structures Subjected to Seismic Loads," by W. Kim, A. El-Attar and R.N. White, 11/22/88, (PB89-189625, A05, MF-A01).

- NCEER-88-0042 "Modeling Strong Ground Motion from Multiple Event Earthquakes," by G.W. Ellis and A.S. Cakmak, 10/15/88, (PB89-174445, A03, MF-A01).
- NCEER-88-0043 "Nonstationary Models of Seismic Ground Acceleration," by M. Grigoriu, S.E. Ruiz and E. Rosenblueth, 7/15/88, (PB89-189617, A04, MF-A01).
- NCEER-88-0044 "SARCF User's Guide: Seismic Analysis of Reinforced Concrete Frames," by Y.S. Chung, C. Meyer and M. Shinozuka, 11/9/88, (PB89-174452, A08, MF-A01).
- NCEER-88-0045 "First Expert Panel Meeting on Disaster Research and Planning," edited by J. Pantelic and J. Stoyke, 9/15/88, (PB89-174460, A05, MF-A01).
- NCEER-88-0046 "Preliminary Studies of the Effect of Degrading Infill Walls on the Nonlinear Seismic Response of Steel Frames," by C.Z. Chrysostomou, P. Gergely and J.F. Abel, 12/19/88, (PB89-208383, A05, MF-A01).
- NCEER-88-0047 "Reinforced Concrete Frame Component Testing Facility - Design, Construction, Instrumentation and Operation," by S.P. Pessiki, C. Conley, T. Bond, P. Gergely and R.N. White, 12/16/88, (PB89-174478, A04, MF-A01).
- NCEER-89-0001 "Effects of Protective Cushion and Soil Compliancy on the Response of Equipment Within a Seismically Excited Building," by J.A. HoLung, 2/16/89, (PB89-207179, A04, MF-A01).
- NCEER-89-0002 "Statistical Evaluation of Response Modification Factors for Reinforced Concrete Structures," by H.H-M. Hwang and J-W. Jaw, 2/17/89, (PB89-207187, A05, MF-A01).
- NCEER-89-0003 "Hysteretic Columns Under Random Excitation," by G-Q. Cai and Y.K. Lin, 1/9/89, (PB89-196513, A03, MF-A01).
- NCEER-89-0004 "Experimental Study of 'Elephant Foot Bulge' Instability of Thin-Walled Metal Tanks," by Z-H. Jia and R.L. Ketter, 2/22/89, (PB89-207195, A03, MF-A01).
- NCEER-89-0005 "Experiment on Performance of Buried Pipelines Across San Andreas Fault," by J. Isenberg, E. Richardson and T.D. O'Rourke, 3/10/89, (PB89-218440, A04, MF-A01). This report is available only through NTIS (see address given above).
- NCEER-89-0006 "A Knowledge-Based Approach to Structural Design of Earthquake-Resistant Buildings," by M. Subramani, P. Gergely, C.H. Conley, J.F. Abel and A.H. Zaghaw, 1/15/89, (PB89-218465, A06, MF-A01).
- NCEER-89-0007 "Liquefaction Hazards and Their Effects on Buried Pipelines," by T.D. O'Rourke and P.A. Lane, 2/1/89, (PB89-218481, A09, MF-A01).
- NCEER-89-0008 "Fundamentals of System Identification in Structural Dynamics," by H. Imai, C-B. Yun, O. Maruyama and M. Shinozuka, 1/26/89, (PB89-207211, A04, MF-A01).
- NCEER-89-0009 "Effects of the 1985 Michoacan Earthquake on Water Systems and Other Buried Lifelines in Mexico," by A.G. Ayala and M.J. O'Rourke, 3/8/89, (PB89-207229, A06, MF-A01).
- NCEER-89-R010 "NCEER Bibliography of Earthquake Education Materials," by K.E.K. Ross, Second Revision, 9/1/89, (PB90-125352, A05, MF-A01). This report is replaced by NCEER-92-0018.
- NCEER-89-0011 "Inelastic Three-Dimensional Response Analysis of Reinforced Concrete Building Structures (IDARC-3D), Part I - Modeling," by S.K. Kunnath and A.M. Reinhorn, 4/17/89, (PB90-114612, A07, MF-A01). This report is available only through NTIS (see address given above).
- NCEER-89-0012 "Recommended Modifications to ATC-14," by C.D. Poland and J.O. Malley, 4/12/89, (PB90-108648, A15, MF-A01).
- NCEER-89-0013 "Repair and Strengthening of Beam-to-Column Connections Subjected to Earthquake Loading," by M. Corazao and A.J. Durrani, 2/28/89, (PB90-109885, A06, MF-A01).

- NCEER-89-0014 "Program EXKAL2 for Identification of Structural Dynamic Systems," by O. Maruyama, C-B. Yun, M. Hoshiya and M. Shinozuka, 5/19/89, (PB90-109877, A09, MF-A01).
- NCEER-89-0015 "Response of Frames With Bolted Semi-Rigid Connections, Part I - Experimental Study and Analytical Predictions," by P.J. DiCorso, A.M. Reinhorn, J.R. Dickerson, J.B. Radzinski and W.L. Harper, 6/1/89, to be published.
- NCEER-89-0016 "ARMA Monte Carlo Simulation in Probabilistic Structural Analysis," by P.D. Spanos and M.P. Mignolet, 7/10/89, (PB90-109893, A03, MF-A01).
- NCEER-89-P017 "Preliminary Proceedings from the Conference on Disaster Preparedness - The Place of Earthquake Education in Our Schools," Edited by K.E.K. Ross, 6/23/89, (PB90-108606, A03, MF-A01).
- NCEER-89-0017 "Proceedings from the Conference on Disaster Preparedness - The Place of Earthquake Education in Our Schools," Edited by K.E.K. Ross, 12/31/89, (PB90-207895, A012, MF-A02). This report is available only through NTIS (see address given above).
- NCEER-89-0018 "Multidimensional Models of Hysteretic Material Behavior for Vibration Analysis of Shape Memory Energy Absorbing Devices, by E.J. Graesser and F.A. Cozzarelli, 6/7/89, (PB90-164146, A04, MF-A01).
- NCEER-89-0019 "Nonlinear Dynamic Analysis of Three-Dimensional Base Isolated Structures (3D-BASIS)," by S. Nagarajaiah, A.M. Reinhorn and M.C. Constantinou, 8/3/89, (PB90-161936, A06, MF-A01). This report has been replaced by NCEER-93-0011.
- NCEER-89-0020 "Structural Control Considering Time-Rate of Control Forces and Control Rate Constraints," by F.Y. Cheng and C.P. Pantelides, 8/3/89, (PB90-120445, A04, MF-A01).
- NCEER-89-0021 "Subsurface Conditions of Memphis and Shelby County," by K.W. Ng, T-S. Chang and H-H.M. Hwang, 7/26/89, (PB90-120437, A03, MF-A01).
- NCEER-89-0022 "Seismic Wave Propagation Effects on Straight Jointed Buried Pipelines," by K. Elhadi and M.J. O'Rourke, 8/24/89, (PB90-162322, A10, MF-A02).
- NCEER-89-0023 "Workshop on Serviceability Analysis of Water Delivery Systems," edited by M. Grigoriu, 3/6/89, (PB90-127424, A03, MF-A01).
- NCEER-89-0024 "Shaking Table Study of a 1/5 Scale Steel Frame Composed of Tapered Members," by K.C. Chang, J.S. Hwang and G.C. Lee, 9/18/89, (PB90-160169, A04, MF-A01).
- NCEER-89-0025 "DYNA1D: A Computer Program for Nonlinear Seismic Site Response Analysis - Technical Documentation," by Jean H. Prevost, 9/14/89, (PB90-161944, A07, MF-A01). This report is available only through NTIS (see address given above).
- NCEER-89-0026 "1:4 Scale Model Studies of Active Tendon Systems and Active Mass Dampers for Aseismic Protection," by A.M. Reinhorn, T.T. Soong, R.C. Lin, Y.P. Yang, Y. Fukao, H. Abe and M. Nakai, 9/15/89, (PB90-173246, A10, MF-A02). This report is available only through NTIS (see address given above).
- NCEER-89-0027 "Scattering of Waves by Inclusions in a Nonhomogeneous Elastic Half Space Solved by Boundary Element Methods," by P.K. Hadley, A. Askar and A.S. Cakmak, 6/15/89, (PB90-145699, A07, MF-A01).
- NCEER-89-0028 "Statistical Evaluation of Deflection Amplification Factors for Reinforced Concrete Structures," by H.H.M. Hwang, J-W. Jaw and A.L. Ch'ng, 8/31/89, (PB90-164633, A05, MF-A01).
- NCEER-89-0029 "Bedrock Accelerations in Memphis Area Due to Large New Madrid Earthquakes," by H.H.M. Hwang, C.H.S. Chen and G. Yu, 11/7/89, (PB90-162330, A04, MF-A01).
- NCEER-89-0030 "Seismic Behavior and Response Sensitivity of Secondary Structural Systems," by Y.Q. Chen and T.T. Soong, 10/23/89, (PB90-164658, A08, MF-A01).
- NCEER-89-0031 "Random Vibration and Reliability Analysis of Primary-Secondary Structural Systems," by Y. Ibrahim, M. Grigoriu and T.T. Soong, 11/10/89, (PB90-161951, A04, MF-A01).

- NCEER-89-0032 "Proceedings from the Second U.S. - Japan Workshop on Liquefaction, Large Ground Deformation and Their Effects on Lifelines, September 26-29, 1989," Edited by T.D. O'Rourke and M. Hamada, 12/1/89, (PB90-209388, A22, MF-A03).
- NCEER-89-0033 "Deterministic Model for Seismic Damage Evaluation of Reinforced Concrete Structures," by J.M. Bracci, A.M. Reinhorn, J.B. Mander and S.K. Kunnath, 9/27/89, (PB91-108803, A06, MF-A01).
- NCEER-89-0034 "On the Relation Between Local and Global Damage Indices," by E. DiPasquale and A.S. Cakmak, 8/15/89, (PB90-173865, A05, MF-A01).
- NCEER-89-0035 "Cyclic Undrained Behavior of Nonplastic and Low Plasticity Silts," by A.J. Walker and H.E. Stewart, 7/26/89, (PB90-183518, A10, MF-A01).
- NCEER-89-0036 "Liquefaction Potential of Surficial Deposits in the City of Buffalo, New York," by M. Budhu, R. Giese and L. Baumgrass, 1/17/89, (PB90-208455, A04, MF-A01).
- NCEER-89-0037 "A Deterministic Assessment of Effects of Ground Motion Incoherence," by A.S. Veletsos and Y. Tang, 7/15/89, (PB90-164294, A03, MF-A01).
- NCEER-89-0038 "Workshop on Ground Motion Parameters for Seismic Hazard Mapping," July 17-18, 1989, edited by R.V. Whitman, 12/1/89, (PB90-173923, A04, MF-A01).
- NCEER-89-0039 "Seismic Effects on Elevated Transit Lines of the New York City Transit Authority," by C.J. Costantino, C.A. Miller and E. Heymsfield, 12/26/89, (PB90-207887, A06, MF-A01).
- NCEER-89-0040 "Centrifugal Modeling of Dynamic Soil-Structure Interaction," by K. Weissman, Supervised by J.H. Prevost, 5/10/89, (PB90-207879, A07, MF-A01).
- NCEER-89-0041 "Linearized Identification of Buildings With Cores for Seismic Vulnerability Assessment," by I-K. Ho and A.E. Aktan, 11/1/89, (PB90-251943, A07, MF-A01).
- NCEER-90-0001 "Geotechnical and Lifeline Aspects of the October 17, 1989 Loma Prieta Earthquake in San Francisco," by T.D. O'Rourke, H.E. Stewart, F.T. Blackburn and T.S. Dickerman, 1/90, (PB90-208596, A05, MF-A01).
- NCEER-90-0002 "Nonnormal Secondary Response Due to Yielding in a Primary Structure," by D.C.K. Chen and L.D. Lutes, 2/28/90, (PB90-251976, A07, MF-A01).
- NCEER-90-0003 "Earthquake Education Materials for Grades K-12," by K.E.K. Ross, 4/16/90, (PB91-251984, A05, MF-A05). This report has been replaced by NCEER-92-0018.
- NCEER-90-0004 "Catalog of Strong Motion Stations in Eastern North America," by R.W. Busby, 4/3/90, (PB90-251984, A05, MF-A01).
- NCEER-90-0005 "NCEER Strong-Motion Data Base: A User Manual for the GeoBase Release (Version 1.0 for the Sun3)," by P. Friberg and K. Jacob, 3/31/90 (PB90-258062, A04, MF-A01).
- NCEER-90-0006 "Seismic Hazard Along a Crude Oil Pipeline in the Event of an 1811-1812 Type New Madrid Earthquake," by H.H.M. Hwang and C-H.S. Chen, 4/16/90, (PB90-258054, A04, MF-A01).
- NCEER-90-0007 "Site-Specific Response Spectra for Memphis Sheahan Pumping Station," by H.H.M. Hwang and C.S. Lee, 5/15/90, (PB91-108811, A05, MF-A01).
- NCEER-90-0008 "Pilot Study on Seismic Vulnerability of Crude Oil Transmission Systems," by T. Ariman, R. Dobry, M. Grigoriu, F. Kozin, M. O'Rourke, T. O'Rourke and M. Shinozuka, 5/25/90, (PB91-108837, A06, MF-A01).
- NCEER-90-0009 "A Program to Generate Site Dependent Time Histories: EQGEN," by G.W. Ellis, M. Srinivasan and A.S. Cakmak, 1/30/90, (PB91-108829, A04, MF-A01).
- NCEER-90-0010 "Active Isolation for Seismic Protection of Operating Rooms," by M.E. Talbott, Supervised by M. Shinozuka, 6/8/9, (PB91-110205, A05, MF-A01).

- NCEER-90-0011 "Program LINEARID for Identification of Linear Structural Dynamic Systems," by C-B. Yun and M. Shinozuka, 6/25/90, (PB91-110312, A08, MF-A01).
- NCEER-90-0012 "Two-Dimensional Two-Phase Elasto-Plastic Seismic Response of Earth Dams," by A.N. Yiagos, Supervised by J.H. Prevost, 6/20/90, (PB91-110197, A13, MF-A02).
- NCEER-90-0013 "Secondary Systems in Base-Isolated Structures: Experimental Investigation, Stochastic Response and Stochastic Sensitivity," by G.D. Manolis, G. Juhn, M.C. Constantinou and A.M. Reinhorn, 7/1/90, (PB91-110320, A08, MF-A01).
- NCEER-90-0014 "Seismic Behavior of Lightly-Reinforced Concrete Column and Beam-Column Joint Details," by S.P. Pessiki, C.H. Conley, P. Gergely and R.N. White, 8/22/90, (PB91-108795, A11, MF-A02).
- NCEER-90-0015 "Two Hybrid Control Systems for Building Structures Under Strong Earthquakes," by J.N. Yang and A. Danielians, 6/29/90, (PB91-125393, A04, MF-A01).
- NCEER-90-0016 "Instantaneous Optimal Control with Acceleration and Velocity Feedback," by J.N. Yang and Z. Li, 6/29/90, (PB91-125401, A03, MF-A01).
- NCEER-90-0017 "Reconnaissance Report on the Northern Iran Earthquake of June 21, 1990," by M. Mehrain, 10/4/90, (PB91-125377, A03, MF-A01).
- NCEER-90-0018 "Evaluation of Liquefaction Potential in Memphis and Shelby County," by T.S. Chang, P.S. Tang, C.S. Lee and H. Hwang, 8/10/90, (PB91-125427, A09, MF-A01).
- NCEER-90-0019 "Experimental and Analytical Study of a Combined Sliding Disc Bearing and Helical Steel Spring Isolation System," by M.C. Constantinou, A.S. Mokha and A.M. Reinhorn, 10/4/90, (PB91-125385, A06, MF-A01). This report is available only through NTIS (see address given above).
- NCEER-90-0020 "Experimental Study and Analytical Prediction of Earthquake Response of a Sliding Isolation System with a Spherical Surface," by A.S. Mokha, M.C. Constantinou and A.M. Reinhorn, 10/11/90, (PB91-125419, A05, MF-A01).
- NCEER-90-0021 "Dynamic Interaction Factors for Floating Pile Groups," by G. Gazetas, K. Fan, A. Kaynia and E. Kausel, 9/10/90, (PB91-170381, A05, MF-A01).
- NCEER-90-0022 "Evaluation of Seismic Damage Indices for Reinforced Concrete Structures," by S. Rodriguez-Gomez and A.S. Cakmak, 9/30/90, PB91-171322, A06, MF-A01).
- NCEER-90-0023 "Study of Site Response at a Selected Memphis Site," by H. Desai, S. Ahmad, E.S. Gazetas and M.R. Oh, 10/11/90, (PB91-196857, A03, MF-A01).
- NCEER-90-0024 "A User's Guide to Strongmo: Version 1.0 of NCEER's Strong-Motion Data Access Tool for PCs and Terminals," by P.A. Friberg and C.A.T. Susch, 11/15/90, (PB91-171272, A03, MF-A01).
- NCEER-90-0025 "A Three-Dimensional Analytical Study of Spatial Variability of Seismic Ground Motions," by L-L. Hong and A.H.-S. Ang, 10/30/90, (PB91-170399, A09, MF-A01).
- NCEER-90-0026 "MUMOID User's Guide - A Program for the Identification of Modal Parameters," by S. Rodriguez-Gomez and E. DiPasquale, 9/30/90, (PB91-171298, A04, MF-A01).
- NCEER-90-0027 "SARCF-II User's Guide - Seismic Analysis of Reinforced Concrete Frames," by S. Rodriguez-Gomez, Y.S. Chung and C. Meyer, 9/30/90, (PB91-171280, A05, MF-A01).
- NCEER-90-0028 "Viscous Dampers: Testing, Modeling and Application in Vibration and Seismic Isolation," by N. Makris and M.C. Constantinou, 12/20/90 (PB91-190561, A06, MF-A01).
- NCEER-90-0029 "Soil Effects on Earthquake Ground Motions in the Memphis Area," by H. Hwang, C.S. Lee, K.W. Ng and T.S. Chang, 8/2/90, (PB91-190751, A05, MF-A01).

- NCEER-91-0001 "Proceedings from the Third Japan-U.S. Workshop on Earthquake Resistant Design of Lifeline Facilities and Countermeasures for Soil Liquefaction, December 17-19, 1990," edited by T.D. O'Rourke and M. Hamada, 2/1/91, (PB91-179259, A99, MF-A04).
- NCEER-91-0002 "Physical Space Solutions of Non-Proportionally Damped Systems," by M. Tong, Z. Liang and G.C. Lee, 1/15/91, (PB91-179242, A04, MF-A01).
- NCEER-91-0003 "Seismic Response of Single Piles and Pile Groups," by K. Fan and G. Gazetas, 1/10/91, (PB92-174994, A04, MF-A01).
- NCEER-91-0004 "Damping of Structures: Part 1 - Theory of Complex Damping," by Z. Liang and G. Lee, 10/10/91, (PB92-197235, A12, MF-A03).
- NCEER-91-0005 "3D-BASIS - Nonlinear Dynamic Analysis of Three Dimensional Base Isolated Structures: Part II," by S. Nagarajaiah, A.M. Reinhorn and M.C. Constantinou, 2/28/91, (PB91-190553, A07, MF-A01). This report has been replaced by NCEER-93-0011.
- NCEER-91-0006 "A Multidimensional Hysteretic Model for Plasticity Deforming Metals in Energy Absorbing Devices," by E.J. Graesser and F.A. Cozzarelli, 4/9/91, (PB92-108364, A04, MF-A01).
- NCEER-91-0007 "A Framework for Customizable Knowledge-Based Expert Systems with an Application to a KBES for Evaluating the Seismic Resistance of Existing Buildings," by E.G. Ibarra-Anaya and S.J. Fenves, 4/9/91, (PB91-210930, A08, MF-A01).
- NCEER-91-0008 "Nonlinear Analysis of Steel Frames with Semi-Rigid Connections Using the Capacity Spectrum Method," by G.G. Deierlein, S-H. Hsieh, Y-J. Shen and J.F. Abel, 7/2/91, (PB92-113828, A05, MF-A01).
- NCEER-91-0009 "Earthquake Education Materials for Grades K-12," by K.E.K. Ross, 4/30/91, (PB91-212142, A06, MF-A01). This report has been replaced by NCEER-92-0018.
- NCEER-91-0010 "Phase Wave Velocities and Displacement Phase Differences in a Harmonically Oscillating Pile," by N. Makris and G. Gazetas, 7/8/91, (PB92-108356, A04, MF-A01).
- NCEER-91-0011 "Dynamic Characteristics of a Full-Size Five-Story Steel Structure and a 2/5 Scale Model," by K.C. Chang, G.C. Yao, G.C. Lee, D.S. Hao and Y.C. Yeh," 7/2/91, (PB93-116648, A06, MF-A02).
- NCEER-91-0012 "Seismic Response of a 2/5 Scale Steel Structure with Added Viscoelastic Dampers," by K.C. Chang, T.T. Soong, S-T. Oh and M.L. Lai, 5/17/91, (PB92-110816, A05, MF-A01).
- NCEER-91-0013 "Earthquake Response of Retaining Walls; Full-Scale Testing and Computational Modeling," by S. Alampalli and A-W.M. Elgamal, 6/20/91, to be published.
- NCEER-91-0014 "3D-BASIS-M: Nonlinear Dynamic Analysis of Multiple Building Base Isolated Structures," by P.C. Tsopelas, S. Nagarajaiah, M.C. Constantinou and A.M. Reinhorn, 5/28/91, (PB92-113885, A09, MF-A02).
- NCEER-91-0015 "Evaluation of SEAOC Design Requirements for Sliding Isolated Structures," by D. Theodossiou and M.C. Constantinou, 6/10/91, (PB92-114602, A11, MF-A03).
- NCEER-91-0016 "Closed-Loop Modal Testing of a 27-Story Reinforced Concrete Flat Plate-Core Building," by H.R. Somaprasad, T. Toksoy, H. Yoshiyuki and A.E. Aktan, 7/15/91, (PB92-129980, A07, MF-A02).
- NCEER-91-0017 "Shake Table Test of a 1/6 Scale Two-Story Lightly Reinforced Concrete Building," by A.G. El-Attar, R.N. White and P. Gergely, 2/28/91, (PB92-222447, A06, MF-A02).
- NCEER-91-0018 "Shake Table Test of a 1/8 Scale Three-Story Lightly Reinforced Concrete Building," by A.G. El-Attar, R.N. White and P. Gergely, 2/28/91, (PB93-116630, A08, MF-A02).
- NCEER-91-0019 "Transfer Functions for Rigid Rectangular Foundations," by A.S. Veletsos, A.M. Prasad and W.H. Wu, 7/31/91, to be published.

- NCEER-91-0020 "Hybrid Control of Seismic-Excited Nonlinear and Inelastic Structural Systems," by J.N. Yang, Z. Li and A. Daniellians, 8/1/91, (PB92-143171, A06, MF-A02).
- NCEER-91-0021 "The NCEER-91 Earthquake Catalog: Improved Intensity-Based Magnitudes and Recurrence Relations for U.S. Earthquakes East of New Madrid," by L. Seeber and J.G. Armbruster, 8/28/91, (PB92-176742, A06, MF-A02).
- NCEER-91-0022 "Proceedings from the Implementation of Earthquake Planning and Education in Schools: The Need for Change - The Roles of the Changemakers," by K.E.K. Ross and F. Winslow, 7/23/91, (PB92-129998, A12, MF-A03).
- NCEER-91-0023 "A Study of Reliability-Based Criteria for Seismic Design of Reinforced Concrete Frame Buildings," by H.H.M. Hwang and H-M. Hsu, 8/10/91, (PB92-140235, A09, MF-A02).
- NCEER-91-0024 "Experimental Verification of a Number of Structural System Identification Algorithms," by R.G. Ghanem, H. Gavin and M. Shinozuka, 9/18/91, (PB92-176577, A18, MF-A04).
- NCEER-91-0025 "Probabilistic Evaluation of Liquefaction Potential," by H.H.M. Hwang and C.S. Lee," 11/25/91, (PB92-143429, A05, MF-A01).
- NCEER-91-0026 "Instantaneous Optimal Control for Linear, Nonlinear and Hysteretic Structures - Stable Controllers," by J.N. Yang and Z. Li, 11/15/91, (PB92-163807, A04, MF-A01).
- NCEER-91-0027 "Experimental and Theoretical Study of a Sliding Isolation System for Bridges," by M.C. Constantinou, A. Kartoum, A.M. Reinhorn and P. Bradford, 11/15/91, (PB92-176973, A10, MF-A03).
- NCEER-92-0001 "Case Studies of Liquefaction and Lifeline Performance During Past Earthquakes, Volume 1: Japanese Case Studies," Edited by M. Hamada and T. O'Rourke, 2/17/92, (PB92-197243, A18, MF-A04).
- NCEER-92-0002 "Case Studies of Liquefaction and Lifeline Performance During Past Earthquakes, Volume 2: United States Case Studies," Edited by T. O'Rourke and M. Hamada, 2/17/92, (PB92-197250, A20, MF-A04).
- NCEER-92-0003 "Issues in Earthquake Education," Edited by K. Ross, 2/3/92, (PB92-222389, A07, MF-A02).
- NCEER-92-0004 "Proceedings from the First U.S. - Japan Workshop on Earthquake Protective Systems for Bridges," Edited by I.G. Buckle, 2/4/92, (PB94-142239, A99, MF-A06).
- NCEER-92-0005 "Seismic Ground Motion from a Haskell-Type Source in a Multiple-Layered Half-Space," A.P. Theoharis, G. Deodatis and M. Shinozuka, 1/2/92, to be published.
- NCEER-92-0006 "Proceedings from the Site Effects Workshop," Edited by R. Whitman, 2/29/92, (PB92-197201, A04, MF-A01).
- NCEER-92-0007 "Engineering Evaluation of Permanent Ground Deformations Due to Seismically-Induced Liquefaction," by M.H. Baziar, R. Dobry and A-W.M. Elgamel, 3/24/92, (PB92-222421, A13, MF-A03).
- NCEER-92-0008 "A Procedure for the Seismic Evaluation of Buildings in the Central and Eastern United States," by C.D. Poland and J.O. Malley, 4/2/92, (PB92-222439, A20, MF-A04).
- NCEER-92-0009 "Experimental and Analytical Study of a Hybrid Isolation System Using Friction Controllable Sliding Bearings," by M.Q. Feng, S. Fujii and M. Shinozuka, 5/15/92, (PB93-150282, A06, MF-A02).
- NCEER-92-0010 "Seismic Resistance of Slab-Column Connections in Existing Non-Ductile Flat-Plate Buildings," by A.J. Durrani and Y. Du, 5/18/92, (PB93-116812, A06, MF-A02).
- NCEER-92-0011 "The Hysteretic and Dynamic Behavior of Brick Masonry Walls Upgraded by Ferrocement Coatings Under Cyclic Loading and Strong Simulated Ground Motion," by H. Lee and S.P. Prawel, 5/11/92, to be published.
- NCEER-92-0012 "Study of Wire Rope Systems for Seismic Protection of Equipment in Buildings," by G.F. Demetriades, M.C. Constantinou and A.M. Reinhorn, 5/20/92, (PB93-116655, A08, MF-A02).

- NCEER-92-0013 "Shape Memory Structural Dampers: Material Properties, Design and Seismic Testing," by P.R. Witting and F.A. Cozzarelli, 5/26/92, (PB93-116663, A05, MF-A01).
- NCEER-92-0014 "Longitudinal Permanent Ground Deformation Effects on Buried Continuous Pipelines," by M.J. O'Rourke, and C. Nordberg, 6/15/92, (PB93-116671, A08, MF-A02).
- NCEER-92-0015 "A Simulation Method for Stationary Gaussian Random Functions Based on the Sampling Theorem," by M. Grigoriu and S. Balopoulou, 6/11/92, (PB93-127496, A05, MF-A01).
- NCEER-92-0016 "Gravity-Load-Designed Reinforced Concrete Buildings: Seismic Evaluation of Existing Construction and Detailing Strategies for Improved Seismic Resistance," by G.W. Hoffmann, S.K. Kunnath, A.M. Reinhorn and J.B. Mander, 7/15/92, (PB94-142007, A08, MF-A02).
- NCEER-92-0017 "Observations on Water System and Pipeline Performance in the Limón Area of Costa Rica Due to the April 22, 1991 Earthquake," by M. O'Rourke and D. Ballantyne, 6/30/92, (PB93-126811, A06, MF-A02).
- NCEER-92-0018 "Fourth Edition of Earthquake Education Materials for Grades K-12," Edited by K.E.K. Ross, 8/10/92, (PB93-114023, A07, MF-A02).
- NCEER-92-0019 "Proceedings from the Fourth Japan-U.S. Workshop on Earthquake Resistant Design of Lifeline Facilities and Countermeasures for Soil Liquefaction," Edited by M. Hamada and T.D. O'Rourke, 8/12/92, (PB93-163939, A99, MF-E11).
- NCEER-92-0020 "Active Bracing System: A Full Scale Implementation of Active Control," by A.M. Reinhorn, T.T. Soong, R.C. Lin, M.A. Riley, Y.P. Wang, S. Aizawa and M. Higashino, 8/14/92, (PB93-127512, A06, MF-A02).
- NCEER-92-0021 "Empirical Analysis of Horizontal Ground Displacement Generated by Liquefaction-Induced Lateral Spreads," by S.F. Bartlett and T.L. Youd, 8/17/92, (PB93-188241, A06, MF-A02).
- NCEER-92-0022 "IDARC Version 3.0: Inelastic Damage Analysis of Reinforced Concrete Structures," by S.K. Kunnath, A.M. Reinhorn and R.F. Lobo, 8/31/92, (PB93-227502, A07, MF-A02).
- NCEER-92-0023 "A Semi-Empirical Analysis of Strong-Motion Peaks in Terms of Seismic Source, Propagation Path and Local Site Conditions, by M. Kamiyama, M.J. O'Rourke and R. Flores-Berrones, 9/9/92, (PB93-150266, A08, MF-A02).
- NCEER-92-0024 "Seismic Behavior of Reinforced Concrete Frame Structures with Nonductile Details, Part I: Summary of Experimental Findings of Full Scale Beam-Column Joint Tests," by A. Beres, R.N. White and P. Gergely, 9/30/92, (PB93-227783, A05, MF-A01).
- NCEER-92-0025 "Experimental Results of Repaired and Retrofitted Beam-Column Joint Tests in Lightly Reinforced Concrete Frame Buildings," by A. Beres, S. El-Borgi, R.N. White and P. Gergely, 10/29/92, (PB93-227791, A05, MF-A01).
- NCEER-92-0026 "A Generalization of Optimal Control Theory: Linear and Nonlinear Structures," by J.N. Yang, Z. Li and S. Vongchavalitkul, 11/2/92, (PB93-188621, A05, MF-A01).
- NCEER-92-0027 "Seismic Resistance of Reinforced Concrete Frame Structures Designed Only for Gravity Loads: Part I - Design and Properties of a One-Third Scale Model Structure," by J.M. Bracci, A.M. Reinhorn and J.B. Mander, 12/1/92, (PB94-104502, A08, MF-A02).
- NCEER-92-0028 "Seismic Resistance of Reinforced Concrete Frame Structures Designed Only for Gravity Loads: Part II - Experimental Performance of Subassemblages," by L.E. Aycaardi, J.B. Mander and A.M. Reinhorn, 12/1/92, (PB94-104510, A08, MF-A02).
- NCEER-92-0029 "Seismic Resistance of Reinforced Concrete Frame Structures Designed Only for Gravity Loads: Part III - Experimental Performance and Analytical Study of a Structural Model," by J.M. Bracci, A.M. Reinhorn and J.B. Mander, 12/1/92, (PB93-227528, A09, MF-A01).

- NCEER-92-0030 "Evaluation of Seismic Retrofit of Reinforced Concrete Frame Structures: Part I - Experimental Performance of Retrofitted Subassemblages," by D. Choudhuri, J.B. Mander and A.M. Reinhorn, 12/8/92, (PB93-198307, A07, MF-A02).
- NCEER-92-0031 "Evaluation of Seismic Retrofit of Reinforced Concrete Frame Structures: Part II - Experimental Performance and Analytical Study of a Retrofitted Structural Model," by J.M. Bracci, A.M. Reinhorn and J.B. Mander, 12/8/92, (PB93-198315, A09, MF-A03).
- NCEER-92-0032 "Experimental and Analytical Investigation of Seismic Response of Structures with Supplemental Fluid Viscous Dampers," by M.C. Constantinou and M.D. Symans, 12/21/92, (PB93-191435, A10, MF-A03). This report is available only through NTIS (see address given above).
- NCEER-92-0033 "Reconnaissance Report on the Cairo, Egypt Earthquake of October 12, 1992," by M. Khater, 12/23/92, (PB93-188621, A03, MF-A01).
- NCEER-92-0034 "Low-Level Dynamic Characteristics of Four Tall Flat-Plate Buildings in New York City," by H. Gavin, S. Yuan, J. Grossman, E. Pekelis and K. Jacob, 12/28/92, (PB93-188217, A07, MF-A02).
- NCEER-93-0001 "An Experimental Study on the Seismic Performance of Brick-Infilled Steel Frames With and Without Retrofit," by J.B. Mander, B. Nair, K. Wojtkowski and J. Ma, 1/29/93, (PB93-227510, A07, MF-A02).
- NCEER-93-0002 "Social Accounting for Disaster Preparedness and Recovery Planning," by S. Cole, E. Pantoja and V. Razak, 2/22/93, (PB94-142114, A12, MF-A03).
- NCEER-93-0003 "Assessment of 1991 NEHRP Provisions for Nonstructural Components and Recommended Revisions," by T.T. Soong, G. Chen, Z. Wu, R-H. Zhang and M. Grigoriu, 3/1/93, (PB93-188639, A06, MF-A02).
- NCEER-93-0004 "Evaluation of Static and Response Spectrum Analysis Procedures of SEAOC/UBC for Seismic Isolated Structures," by C.W. Winters and M.C. Constantinou, 3/23/93, (PB93-198299, A10, MF-A03).
- NCEER-93-0005 "Earthquakes in the Northeast - Are We Ignoring the Hazard? A Workshop on Earthquake Science and Safety for Educators," edited by K.E.K. Ross, 4/2/93, (PB94-103066, A09, MF-A02).
- NCEER-93-0006 "Inelastic Response of Reinforced Concrete Structures with Viscoelastic Braces," by R.F. Lobo, J.M. Bracci, K.L. Shen, A.M. Reinhorn and T.T. Soong, 4/5/93, (PB93-227486, A05, MF-A02).
- NCEER-93-0007 "Seismic Testing of Installation Methods for Computers and Data Processing Equipment," by K. Kosar, T.T. Soong, K.L. Shen, J.A. HoLung and Y.K. Lin, 4/12/93, (PB93-198299, A07, MF-A02).
- NCEER-93-0008 "Retrofit of Reinforced Concrete Frames Using Added Dampers," by A. Reinhorn, M. Constantinou and C. Li, to be published.
- NCEER-93-0009 "Seismic Behavior and Design Guidelines for Steel Frame Structures with Added Viscoelastic Dampers," by K.C. Chang, M.L. Lai, T.T. Soong, D.S. Hao and Y.C. Yeh, 5/1/93, (PB94-141959, A07, MF-A02).
- NCEER-93-0010 "Seismic Performance of Shear-Critical Reinforced Concrete Bridge Piers," by J.B. Mander, S.M. Waheed, M.T.A. Chaudhary and S.S. Chen, 5/12/93, (PB93-227494, A08, MF-A02).
- NCEER-93-0011 "3D-BASIS-TABS: Computer Program for Nonlinear Dynamic Analysis of Three Dimensional Base Isolated Structures," by S. Nagarajaiah, C. Li, A.M. Reinhorn and M.C. Constantinou, 8/2/93, (PB94-141819, A09, MF-A02).
- NCEER-93-0012 "Effects of Hydrocarbon Spills from an Oil Pipeline Break on Ground Water," by O.J. Helweg and H.H.M. Hwang, 8/3/93, (PB94-141942, A06, MF-A02).
- NCEER-93-0013 "Simplified Procedures for Seismic Design of Nonstructural Components and Assessment of Current Code Provisions," by M.P. Singh, L.E. Suarez, E.E. Matheu and G.O. Maldonado, 8/4/93, (PB94-141827, A09, MF-A02).
- NCEER-93-0014 "An Energy Approach to Seismic Analysis and Design of Secondary Systems," by G. Chen and T.T. Soong, 8/6/93, (PB94-142767, A11, MF-A03).

- NCEER-93-0015 "Proceedings from School Sites: Becoming Prepared for Earthquakes - Commemorating the Third Anniversary of the Loma Prieta Earthquake," Edited by F.E. Winslow and K.E.K. Ross, 8/16/93, (PB94-154275, A16, MF-A02).
- NCEER-93-0016 "Reconnaissance Report of Damage to Historic Monuments in Cairo, Egypt Following the October 12, 1992 Dahshur Earthquake," by D. Sykora, D. Look, G. Croci, E. Karaesmen and E. Karaesmen, 8/19/93, (PB94-142221, A08, MF-A02).
- NCEER-93-0017 "The Island of Guam Earthquake of August 8, 1993," by S.W. Swan and S.K. Harris, 9/30/93, (PB94-141843, A04, MF-A01).
- NCEER-93-0018 "Engineering Aspects of the October 12, 1992 Egyptian Earthquake," by A.W. Elgamal, M. Amer, K. Adalier and A. Abul-Fadl, 10/7/93, (PB94-141983, A05, MF-A01).
- NCEER-93-0019 "Development of an Earthquake Motion Simulator and its Application in Dynamic Centrifuge Testing," by I. Krstelj, Supervised by J.H. Prevost, 10/23/93, (PB94-181773, A-10, MF-A03).
- NCEER-93-0020 "NCEER-Taisei Corporation Research Program on Sliding Seismic Isolation Systems for Bridges: Experimental and Analytical Study of a Friction Pendulum System (FPS)," by M.C. Constantinou, P. Tsopelas, Y-S. Kim and S. Okamoto, 11/1/93, (PB94-142775, A08, MF-A02).
- NCEER-93-0021 "Finite Element Modeling of Elastomeric Seismic Isolation Bearings," by L.J. Billings, Supervised by R. Shepherd, 11/8/93, to be published.
- NCEER-93-0022 "Seismic Vulnerability of Equipment in Critical Facilities: Life-Safety and Operational Consequences," by K. Porter, G.S. Johnson, M.M. Zadeh, C. Scawthorn and S. Eder, 11/24/93, (PB94-181765, A16, MF-A03).
- NCEER-93-0023 "Hokkaido Nansei-oki, Japan Earthquake of July 12, 1993, by P.I. Yanev and C.R. Scawthorn, 12/23/93, (PB94-181500, A07, MF-A01).
- NCEER-94-0001 "An Evaluation of Seismic Serviceability of Water Supply Networks with Application to the San Francisco Auxiliary Water Supply System," by I. Markov, Supervised by M. Grigoriu and T. O'Rourke, 1/21/94, (PB94-204013, A07, MF-A02).
- NCEER-94-0002 "NCEER-Taisei Corporation Research Program on Sliding Seismic Isolation Systems for Bridges: Experimental and Analytical Study of Systems Consisting of Sliding Bearings, Rubber Restoring Force Devices and Fluid Dampers," Volumes I and II, by P. Tsopelas, S. Okamoto, M.C. Constantinou, D. Ozaki and S. Fujii, 2/4/94, (PB94-181740, A09, MF-A02 and PB94-181757, A12, MF-A03).
- NCEER-94-0003 "A Markov Model for Local and Global Damage Indices in Seismic Analysis," by S. Rahman and M. Grigoriu, 2/18/94, (PB94-206000, A12, MF-A03).
- NCEER-94-0004 "Proceedings from the NCEER Workshop on Seismic Response of Masonry Infills," edited by D.P. Abrams, 3/1/94, (PB94-180783, A07, MF-A02).
- NCEER-94-0005 "The Northridge, California Earthquake of January 17, 1994: General Reconnaissance Report," edited by J.D. Goltz, 3/11/94, (PB94-193943, A10, MF-A03).
- NCEER-94-0006 "Seismic Energy Based Fatigue Damage Analysis of Bridge Columns: Part I - Evaluation of Seismic Capacity," by G.A. Chang and J.B. Mander, 3/14/94, (PB94-219185, A11, MF-A03).
- NCEER-94-0007 "Seismic Isolation of Multi-Story Frame Structures Using Spherical Sliding Isolation Systems," by T.M. Al-Hussaini, V.A. Zayas and M.C. Constantinou, 3/17/94, (PB94-193745, A09, MF-A02).
- NCEER-94-0008 "The Northridge, California Earthquake of January 17, 1994: Performance of Highway Bridges," edited by I.G. Buckle, 3/24/94, (PB94-193851, A06, MF-A02).
- NCEER-94-0009 "Proceedings of the Third U.S.-Japan Workshop on Earthquake Protective Systems for Bridges," edited by I.G. Buckle and I. Friedland, 3/31/94, (PB94-195815, A99, MF-A06).

- NCEER-94-0010 "3D-BASIS-ME: Computer Program for Nonlinear Dynamic Analysis of Seismically Isolated Single and Multiple Structures and Liquid Storage Tanks," by P.C. Tsopelas, M.C. Constantinou and A.M. Reinhorn, 4/12/94, (PB94-204922, A09, MF-A02).
- NCEER-94-0011 "The Northridge, California Earthquake of January 17, 1994: Performance of Gas Transmission Pipelines," by T.D. O'Rourke and M.C. Palmer, 5/16/94, (PB94-204989, A05, MF-A01).
- NCEER-94-0012 "Feasibility Study of Replacement Procedures and Earthquake Performance Related to Gas Transmission Pipelines," by T.D. O'Rourke and M.C. Palmer, 5/25/94, (PB94-206638, A09, MF-A02).
- NCEER-94-0013 "Seismic Energy Based Fatigue Damage Analysis of Bridge Columns: Part II - Evaluation of Seismic Demand," by G.A. Chang and J.B. Mander, 6/1/94, (PB95-18106, A08, MF-A02).
- NCEER-94-0014 "NCEER-Taisei Corporation Research Program on Sliding Seismic Isolation Systems for Bridges: Experimental and Analytical Study of a System Consisting of Sliding Bearings and Fluid Restoring Force/Damping Devices," by P. Tsopelas and M.C. Constantinou, 6/13/94, (PB94-219144, A10, MF-A03).
- NCEER-94-0015 "Generation of Hazard-Consistent Fragility Curves for Seismic Loss Estimation Studies," by H. Hwang and J-R. Huo, 6/14/94, (PB95-181996, A09, MF-A02).
- NCEER-94-0016 "Seismic Study of Building Frames with Added Energy-Absorbing Devices," by W.S. Pong, C.S. Tsai and G.C. Lee, 6/20/94, (PB94-219136, A10, A03).
- NCEER-94-0017 "Sliding Mode Control for Seismic-Excited Linear and Nonlinear Civil Engineering Structures," by J. Yang, J. Wu, A. Agrawal and Z. Li, 6/21/94, (PB95-138483, A06, MF-A02).
- NCEER-94-0018 "3D-BASIS-TABS Version 2.0: Computer Program for Nonlinear Dynamic Analysis of Three Dimensional Base Isolated Structures," by A.M. Reinhorn, S. Nagarajaiah, M.C. Constantinou, P. Tsopelas and R. Li, 6/22/94, (PB95-182176, A08, MF-A02).
- NCEER-94-0019 "Proceedings of the International Workshop on Civil Infrastructure Systems: Application of Intelligent Systems and Advanced Materials on Bridge Systems," Edited by G.C. Lee and K.C. Chang, 7/18/94, (PB95-252474, A20, MF-A04).
- NCEER-94-0020 "Study of Seismic Isolation Systems for Computer Floors," by V. Lambrou and M.C. Constantinou, 7/19/94, (PB95-138533, A10, MF-A03).
- NCEER-94-0021 "Proceedings of the U.S.-Italian Workshop on Guidelines for Seismic Evaluation and Rehabilitation of Unreinforced Masonry Buildings," Edited by D.P. Abrams and G.M. Calvi, 7/20/94, (PB95-138749, A13, MF-A03).
- NCEER-94-0022 "NCEER-Taisei Corporation Research Program on Sliding Seismic Isolation Systems for Bridges: Experimental and Analytical Study of a System Consisting of Lubricated PTFE Sliding Bearings and Mild Steel Dampers," by P. Tsopelas and M.C. Constantinou, 7/22/94, (PB95-182184, A08, MF-A02).
- NCEER-94-0023 "Development of Reliability-Based Design Criteria for Buildings Under Seismic Load," by Y.K. Wen, H. Hwang and M. Shinozuka, 8/1/94, (PB95-211934, A08, MF-A02).
- NCEER-94-0024 "Experimental Verification of Acceleration Feedback Control Strategies for an Active Tendon System," by S.J. Dyke, B.F. Spencer, Jr., P. Quast, M.K. Sain, D.C. Kaspari, Jr. and T.T. Soong, 8/29/94, (PB95-212320, A05, MF-A01).
- NCEER-94-0025 "Seismic Retrofitting Manual for Highway Bridges," Edited by I.G. Buckle and I.F. Friedland, published by the Federal Highway Administration (PB95-212676, A15, MF-A03).
- NCEER-94-0026 "Proceedings from the Fifth U.S.-Japan Workshop on Earthquake Resistant Design of Lifeline Facilities and Countermeasures Against Soil Liquefaction," Edited by T.D. O'Rourke and M. Hamada, 11/7/94, (PB95-220802, A99, MF-E08).

- NCEER-95-0001 “Experimental and Analytical Investigation of Seismic Retrofit of Structures with Supplemental Damping: Part I - Fluid Viscous Damping Devices,” by A.M. Reinhorn, C. Li and M.C. Constantinou, 1/3/95, (PB95-266599, A09, MF-A02).
- NCEER-95-0002 “Experimental and Analytical Study of Low-Cycle Fatigue Behavior of Semi-Rigid Top-And-Seat Angle Connections,” by G. Pekcan, J.B. Mander and S.S. Chen, 1/5/95, (PB95-220042, A07, MF-A02).
- NCEER-95-0003 “NCEER-ATC Joint Study on Fragility of Buildings,” by T. Anagnos, C. Rojahn and A.S. Kiremidjian, 1/20/95, (PB95-220026, A06, MF-A02).
- NCEER-95-0004 “Nonlinear Control Algorithms for Peak Response Reduction,” by Z. Wu, T.T. Soong, V. Gattulli and R.C. Lin, 2/16/95, (PB95-220349, A05, MF-A01).
- NCEER-95-0005 “Pipeline Replacement Feasibility Study: A Methodology for Minimizing Seismic and Corrosion Risks to Underground Natural Gas Pipelines,” by R.T. Eguchi, H.A. Seligson and D.G. Honegger, 3/2/95, (PB95-252326, A06, MF-A02).
- NCEER-95-0006 “Evaluation of Seismic Performance of an 11-Story Frame Building During the 1994 Northridge Earthquake,” by F. Naeim, R. DiSulio, K. Benuska, A. Reinhorn and C. Li, to be published.
- NCEER-95-0007 “Prioritization of Bridges for Seismic Retrofitting,” by N. Basöz and A.S. Kiremidjian, 4/24/95, (PB95-252300, A08, MF-A02).
- NCEER-95-0008 “Method for Developing Motion Damage Relationships for Reinforced Concrete Frames,” by A. Singhal and A.S. Kiremidjian, 5/11/95, (PB95-266607, A06, MF-A02).
- NCEER-95-0009 “Experimental and Analytical Investigation of Seismic Retrofit of Structures with Supplemental Damping: Part II - Friction Devices,” by C. Li and A.M. Reinhorn, 7/6/95, (PB96-128087, A11, MF-A03).
- NCEER-95-0010 “Experimental Performance and Analytical Study of a Non-Ductile Reinforced Concrete Frame Structure Retrofitted with Elastomeric Spring Dampers,” by G. Pekcan, J.B. Mander and S.S. Chen, 7/14/95, (PB96-137161, A08, MF-A02).
- NCEER-95-0011 “Development and Experimental Study of Semi-Active Fluid Damping Devices for Seismic Protection of Structures,” by M.D. Symans and M.C. Constantinou, 8/3/95, (PB96-136940, A23, MF-A04).
- NCEER-95-0012 “Real-Time Structural Parameter Modification (RSPM): Development of Innervated Structures,” by Z. Liang, M. Tong and G.C. Lee, 4/11/95, (PB96-137153, A06, MF-A01).
- NCEER-95-0013 “Experimental and Analytical Investigation of Seismic Retrofit of Structures with Supplemental Damping: Part III - Viscous Damping Walls,” by A.M. Reinhorn and C. Li, 10/1/95, (PB96-176409, A11, MF-A03).
- NCEER-95-0014 “Seismic Fragility Analysis of Equipment and Structures in a Memphis Electric Substation,” by J-R. Huo and H.H.M. Hwang, 8/10/95, (PB96-128087, A09, MF-A02).
- NCEER-95-0015 “The Hanshin-Awaji Earthquake of January 17, 1995: Performance of Lifelines,” Edited by M. Shinozuka, 11/3/95, (PB96-176383, A15, MF-A03).
- NCEER-95-0016 “Highway Culvert Performance During Earthquakes,” by T.L. Youd and C.J. Beckman, available as NCEER-96-0015.
- NCEER-95-0017 “The Hanshin-Awaji Earthquake of January 17, 1995: Performance of Highway Bridges,” Edited by I.G. Buckle, 12/1/95, to be published.
- NCEER-95-0018 “Modeling of Masonry Infill Panels for Structural Analysis,” by A.M. Reinhorn, A. Madan, R.E. Valles, Y. Reichmann and J.B. Mander, 12/8/95, (PB97-110886, MF-A01, A06).
- NCEER-95-0019 “Optimal Polynomial Control for Linear and Nonlinear Structures,” by A.K. Agrawal and J.N. Yang, 12/11/95, (PB96-168737, A07, MF-A02).

- NCEER-95-0020 “Retrofit of Non-Ductile Reinforced Concrete Frames Using Friction Dampers,” by R.S. Rao, P. Gergely and R.N. White, 12/22/95, (PB97-133508, A10, MF-A02).
- NCEER-95-0021 “Parametric Results for Seismic Response of Pile-Supported Bridge Bents,” by G. Mylonakis, A. Nikolaou and G. Gazetas, 12/22/95, (PB97-100242, A12, MF-A03).
- NCEER-95-0022 “Kinematic Bending Moments in Seismically Stressed Piles,” by A. Nikolaou, G. Mylonakis and G. Gazetas, 12/23/95, (PB97-113914, MF-A03, A13).
- NCEER-96-0001 “Dynamic Response of Unreinforced Masonry Buildings with Flexible Diaphragms,” by A.C. Costley and D.P. Abrams, 10/10/96, (PB97-133573, MF-A03, A15).
- NCEER-96-0002 “State of the Art Review: Foundations and Retaining Structures,” by I. Po Lam, to be published.
- NCEER-96-0003 “Ductility of Rectangular Reinforced Concrete Bridge Columns with Moderate Confinement,” by N. Wehbe, M. Saiidi, D. Sanders and B. Douglas, 11/7/96, (PB97-133557, A06, MF-A02).
- NCEER-96-0004 “Proceedings of the Long-Span Bridge Seismic Research Workshop,” edited by I.G. Buckle and I.M. Friedland, to be published.
- NCEER-96-0005 “Establish Representative Pier Types for Comprehensive Study: Eastern United States,” by J. Kulicki and Z. Prucz, 5/28/96, (PB98-119217, A07, MF-A02).
- NCEER-96-0006 “Establish Representative Pier Types for Comprehensive Study: Western United States,” by R. Imbsen, R.A. Schamber and T.A. Osterkamp, 5/28/96, (PB98-118607, A07, MF-A02).
- NCEER-96-0007 “Nonlinear Control Techniques for Dynamical Systems with Uncertain Parameters,” by R.G. Ghanem and M.I. Bujakov, 5/27/96, (PB97-100259, A17, MF-A03).
- NCEER-96-0008 “Seismic Evaluation of a 30-Year Old Non-Ductile Highway Bridge Pier and Its Retrofit,” by J.B. Mander, B. Mahmoodzadegan, S. Bhadra and S.S. Chen, 5/31/96, (PB97-110902, MF-A03, A10).
- NCEER-96-0009 “Seismic Performance of a Model Reinforced Concrete Bridge Pier Before and After Retrofit,” by J.B. Mander, J.H. Kim and C.A. Ligozio, 5/31/96, (PB97-110910, MF-A02, A10).
- NCEER-96-0010 “IDARC2D Version 4.0: A Computer Program for the Inelastic Damage Analysis of Buildings,” by R.E. Valles, A.M. Reinhorn, S.K. Kunnath, C. Li and A. Madan, 6/3/96, (PB97-100234, A17, MF-A03).
- NCEER-96-0011 “Estimation of the Economic Impact of Multiple Lifeline Disruption: Memphis Light, Gas and Water Division Case Study,” by S.E. Chang, H.A. Seligson and R.T. Eguchi, 8/16/96, (PB97-133490, A11, MF-A03).
- NCEER-96-0012 “Proceedings from the Sixth Japan-U.S. Workshop on Earthquake Resistant Design of Lifeline Facilities and Countermeasures Against Soil Liquefaction, Edited by M. Hamada and T. O’Rourke, 9/11/96, (PB97-133581, A99, MF-A06).
- NCEER-96-0013 “Chemical Hazards, Mitigation and Preparedness in Areas of High Seismic Risk: A Methodology for Estimating the Risk of Post-Earthquake Hazardous Materials Release,” by H.A. Seligson, R.T. Eguchi, K.J. Tierney and K. Richmond, 11/7/96, (PB97-133565, MF-A02, A08).
- NCEER-96-0014 “Response of Steel Bridge Bearings to Reversed Cyclic Loading,” by J.B. Mander, D-K. Kim, S.S. Chen and G.J. Premus, 11/13/96, (PB97-140735, A12, MF-A03).
- NCEER-96-0015 “Highway Culvert Performance During Past Earthquakes,” by T.L. Youd and C.J. Beckman, 11/25/96, (PB97-133532, A06, MF-A01).
- NCEER-97-0001 “Evaluation, Prevention and Mitigation of Pounding Effects in Building Structures,” by R.E. Valles and A.M. Reinhorn, 2/20/97, (PB97-159552, A14, MF-A03).
- NCEER-97-0002 “Seismic Design Criteria for Bridges and Other Highway Structures,” by C. Rojahn, R. Mayes, D.G. Anderson, J. Clark, J.H. Hom, R.V. Nutt and M.J. O’Rourke, 4/30/97, (PB97-194658, A06, MF-A03).

- NCEER-97-0003 "Proceedings of the U.S.-Italian Workshop on Seismic Evaluation and Retrofit," Edited by D.P. Abrams and G.M. Calvi, 3/19/97, (PB97-194666, A13, MF-A03).
- NCEER-97-0004 "Investigation of Seismic Response of Buildings with Linear and Nonlinear Fluid Viscous Dampers," by A.A. Seleemah and M.C. Constantinou, 5/21/97, (PB98-109002, A15, MF-A03).
- NCEER-97-0005 "Proceedings of the Workshop on Earthquake Engineering Frontiers in Transportation Facilities," edited by G.C. Lee and I.M. Friedland, 8/29/97, (PB98-128911, A25, MR-A04).
- NCEER-97-0006 "Cumulative Seismic Damage of Reinforced Concrete Bridge Piers," by S.K. Kunnath, A. El-Bahy, A. Taylor and W. Stone, 9/2/97, (PB98-108814, A11, MF-A03).
- NCEER-97-0007 "Structural Details to Accommodate Seismic Movements of Highway Bridges and Retaining Walls," by R.A. Imbsen, R.A. Schamber, E. Thorkildsen, A. Kartoum, B.T. Martin, T.N. Rosser and J.M. Kulicki, 9/3/97, (PB98-108996, A09, MF-A02).
- NCEER-97-0008 "A Method for Earthquake Motion-Damage Relationships with Application to Reinforced Concrete Frames," by A. Singhal and A.S. Kiremidjian, 9/10/97, (PB98-108988, A13, MF-A03).
- NCEER-97-0009 "Seismic Analysis and Design of Bridge Abutments Considering Sliding and Rotation," by K. Fishman and R. Richards, Jr., 9/15/97, (PB98-108897, A06, MF-A02).
- NCEER-97-0010 "Proceedings of the FHWA/NCEER Workshop on the National Representation of Seismic Ground Motion for New and Existing Highway Facilities," edited by I.M. Friedland, M.S. Power and R.L. Mayes, 9/22/97, (PB98-128903, A21, MF-A04).
- NCEER-97-0011 "Seismic Analysis for Design or Retrofit of Gravity Bridge Abutments," by K.L. Fishman, R. Richards, Jr. and R.C. Divito, 10/2/97, (PB98-128937, A08, MF-A02).
- NCEER-97-0012 "Evaluation of Simplified Methods of Analysis for Yielding Structures," by P. Tsopelas, M.C. Constantinou, C.A. Kircher and A.S. Whittaker, 10/31/97, (PB98-128929, A10, MF-A03).
- NCEER-97-0013 "Seismic Design of Bridge Columns Based on Control and Repairability of Damage," by C-T. Cheng and J.B. Mander, 12/8/97, (PB98-144249, A11, MF-A03).
- NCEER-97-0014 "Seismic Resistance of Bridge Piers Based on Damage Avoidance Design," by J.B. Mander and C-T. Cheng, 12/10/97, (PB98-144223, A09, MF-A02).
- NCEER-97-0015 "Seismic Response of Nominally Symmetric Systems with Strength Uncertainty," by S. Balopoulou and M. Grigoriu, 12/23/97, (PB98-153422, A11, MF-A03).
- NCEER-97-0016 "Evaluation of Seismic Retrofit Methods for Reinforced Concrete Bridge Columns," by T.J. Wipf, F.W. Klaiber and F.M. Russo, 12/28/97, (PB98-144215, A12, MF-A03).
- NCEER-97-0017 "Seismic Fragility of Existing Conventional Reinforced Concrete Highway Bridges," by C.L. Mullen and A.S. Cakmak, 12/30/97, (PB98-153406, A08, MF-A02).
- NCEER-97-0018 "Loss Assessment of Memphis Buildings," edited by D.P. Abrams and M. Shinozuka, 12/31/97, (PB98-144231, A13, MF-A03).
- NCEER-97-0019 "Seismic Evaluation of Frames with Infill Walls Using Quasi-static Experiments," by K.M. Mosalam, R.N. White and P. Gergely, 12/31/97, (PB98-153455, A07, MF-A02).
- NCEER-97-0020 "Seismic Evaluation of Frames with Infill Walls Using Pseudo-dynamic Experiments," by K.M. Mosalam, R.N. White and P. Gergely, 12/31/97, (PB98-153430, A07, MF-A02).
- NCEER-97-0021 "Computational Strategies for Frames with Infill Walls: Discrete and Smeared Crack Analyses and Seismic Fragility," by K.M. Mosalam, R.N. White and P. Gergely, 12/31/97, (PB98-153414, A10, MF-A02).

- NCEER-97-0022 "Proceedings of the NCEER Workshop on Evaluation of Liquefaction Resistance of Soils," edited by T.L. Youd and I.M. Idriss, 12/31/97, (PB98-155617, A15, MF-A03).
- MCEER-98-0001 "Extraction of Nonlinear Hysteretic Properties of Seismically Isolated Bridges from Quick-Release Field Tests," by Q. Chen, B.M. Douglas, E.M. Maragakis and I.G. Buckle, 5/26/98, (PB99-118838, A06, MF-A01).
- MCEER-98-0002 "Methodologies for Evaluating the Importance of Highway Bridges," by A. Thomas, S. Eshenaur and J. Kulicki, 5/29/98, (PB99-118846, A10, MF-A02).
- MCEER-98-0003 "Capacity Design of Bridge Piers and the Analysis of Overstrength," by J.B. Mander, A. Dutta and P. Goel, 6/1/98, (PB99-118853, A09, MF-A02).
- MCEER-98-0004 "Evaluation of Bridge Damage Data from the Loma Prieta and Northridge, California Earthquakes," by N. Basoz and A. Kiremidjian, 6/2/98, (PB99-118861, A15, MF-A03).
- MCEER-98-0005 "Screening Guide for Rapid Assessment of Liquefaction Hazard at Highway Bridge Sites," by T. L. Youd, 6/16/98, (PB99-118879, A06, not available on microfiche).
- MCEER-98-0006 "Structural Steel and Steel/Concrete Interface Details for Bridges," by P. Ritchie, N. Kaulh and J. Kulicki, 7/13/98, (PB99-118945, A06, MF-A01).
- MCEER-98-0007 "Capacity Design and Fatigue Analysis of Confined Concrete Columns," by A. Dutta and J.B. Mander, 7/14/98, (PB99-118960, A14, MF-A03).
- MCEER-98-0008 "Proceedings of the Workshop on Performance Criteria for Telecommunication Services Under Earthquake Conditions," edited by A.J. Schiff, 7/15/98, (PB99-118952, A08, MF-A02).
- MCEER-98-0009 "Fatigue Analysis of Unconfined Concrete Columns," by J.B. Mander, A. Dutta and J.H. Kim, 9/12/98, (PB99-123655, A10, MF-A02).
- MCEER-98-0010 "Centrifuge Modeling of Cyclic Lateral Response of Pile-Cap Systems and Seat-Type Abutments in Dry Sands," by A.D. Gadre and R. Dobry, 10/2/98, (PB99-123606, A13, MF-A03).
- MCEER-98-0011 "IDARC-BRIDGE: A Computational Platform for Seismic Damage Assessment of Bridge Structures," by A.M. Reinhorn, V. Simeonov, G. Mylonakis and Y. Reichman, 10/2/98, (PB99-162919, A15, MF-A03).
- MCEER-98-0012 "Experimental Investigation of the Dynamic Response of Two Bridges Before and After Retrofitting with Elastomeric Bearings," by D.A. Wendichansky, S.S. Chen and J.B. Mander, 10/2/98, (PB99-162927, A15, MF-A03).
- MCEER-98-0013 "Design Procedures for Hinge Restrainers and Hinge Sear Width for Multiple-Frame Bridges," by R. Des Roches and G.L. Fenves, 11/3/98, (PB99-140477, A13, MF-A03).
- MCEER-98-0014 "Response Modification Factors for Seismically Isolated Bridges," by M.C. Constantinou and J.K. Quarshie, 11/3/98, (PB99-140485, A14, MF-A03).
- MCEER-98-0015 "Proceedings of the U.S.-Italy Workshop on Seismic Protective Systems for Bridges," edited by I.M. Friedland and M.C. Constantinou, 11/3/98, (PB2000-101711, A22, MF-A04).
- MCEER-98-0016 "Appropriate Seismic Reliability for Critical Equipment Systems: Recommendations Based on Regional Analysis of Financial and Life Loss," by K. Porter, C. Scawthorn, C. Taylor and N. Blais, 11/10/98, (PB99-157265, A08, MF-A02).
- MCEER-98-0017 "Proceedings of the U.S. Japan Joint Seminar on Civil Infrastructure Systems Research," edited by M. Shinozuka and A. Rose, 11/12/98, (PB99-156713, A16, MF-A03).
- MCEER-98-0018 "Modeling of Pile Footings and Drilled Shafts for Seismic Design," by I. PoLam, M. Kapuskar and D. Chaudhuri, 12/21/98, (PB99-157257, A09, MF-A02).

- MCEER-99-0001 "Seismic Evaluation of a Masonry Infilled Reinforced Concrete Frame by Pseudodynamic Testing," by S.G. Buonopane and R.N. White, 2/16/99, (PB99-162851, A09, MF-A02).
- MCEER-99-0002 "Response History Analysis of Structures with Seismic Isolation and Energy Dissipation Systems: Verification Examples for Program SAP2000," by J. Scheller and M.C. Constantinou, 2/22/99, (PB99-162869, A08, MF-A02).
- MCEER-99-0003 "Experimental Study on the Seismic Design and Retrofit of Bridge Columns Including Axial Load Effects," by A. Dutta, T. Kokorina and J.B. Mander, 2/22/99, (PB99-162877, A09, MF-A02).
- MCEER-99-0004 "Experimental Study of Bridge Elastomeric and Other Isolation and Energy Dissipation Systems with Emphasis on Uplift Prevention and High Velocity Near-source Seismic Excitation," by A. Kasalanati and M. C. Constantinou, 2/26/99, (PB99-162885, A12, MF-A03).
- MCEER-99-0005 "Truss Modeling of Reinforced Concrete Shear-flexure Behavior," by J.H. Kim and J.B. Mander, 3/8/99, (PB99-163693, A12, MF-A03).
- MCEER-99-0006 "Experimental Investigation and Computational Modeling of Seismic Response of a 1:4 Scale Model Steel Structure with a Load Balancing Supplemental Damping System," by G. Pekcan, J.B. Mander and S.S. Chen, 4/2/99, (PB99-162893, A11, MF-A03).
- MCEER-99-0007 "Effect of Vertical Ground Motions on the Structural Response of Highway Bridges," by M.R. Button, C.J. Cronin and R.L. Mayes, 4/10/99, (PB2000-101411, A10, MF-A03).
- MCEER-99-0008 "Seismic Reliability Assessment of Critical Facilities: A Handbook, Supporting Documentation, and Model Code Provisions," by G.S. Johnson, R.E. Sheppard, M.D. Quilici, S.J. Eder and C.R. Scawthorn, 4/12/99, (PB2000-101701, A18, MF-A04).
- MCEER-99-0009 "Impact Assessment of Selected MCEER Highway Project Research on the Seismic Design of Highway Structures," by C. Rojahn, R. Mayes, D.G. Anderson, J.H. Clark, D'Appolonia Engineering, S. Gloyd and R.V. Nutt, 4/14/99, (PB99-162901, A10, MF-A02).
- MCEER-99-0010 "Site Factors and Site Categories in Seismic Codes," by R. Dobry, R. Ramos and M.S. Power, 7/19/99, (PB2000-101705, A08, MF-A02).
- MCEER-99-0011 "Restrainer Design Procedures for Multi-Span Simply-Supported Bridges," by M.J. Randall, M. Saiidi, E. Maragakis and T. Isakovic, 7/20/99, (PB2000-101702, A10, MF-A02).
- MCEER-99-0012 "Property Modification Factors for Seismic Isolation Bearings," by M.C. Constantinou, P. Tsopelas, A. Kasalanati and E. Wolff, 7/20/99, (PB2000-103387, A11, MF-A03).
- MCEER-99-0013 "Critical Seismic Issues for Existing Steel Bridges," by P. Ritchie, N. Kauh and J. Kulicki, 7/20/99, (PB2000-101697, A09, MF-A02).
- MCEER-99-0014 "Nonstructural Damage Database," by A. Kao, T.T. Soong and A. Vender, 7/24/99, (PB2000-101407, A06, MF-A01).
- MCEER-99-0015 "Guide to Remedial Measures for Liquefaction Mitigation at Existing Highway Bridge Sites," by H.G. Cooke and J. K. Mitchell, 7/26/99, (PB2000-101703, A11, MF-A03).
- MCEER-99-0016 "Proceedings of the MCEER Workshop on Ground Motion Methodologies for the Eastern United States," edited by N. Abrahamson and A. Becker, 8/11/99, (PB2000-103385, A07, MF-A02).
- MCEER-99-0017 "Quindío, Colombia Earthquake of January 25, 1999: Reconnaissance Report," by A.P. Asfura and P.J. Flores, 10/4/99, (PB2000-106893, A06, MF-A01).
- MCEER-99-0018 "Hysteretic Models for Cyclic Behavior of Deteriorating Inelastic Structures," by M.V. Sivaselvan and A.M. Reinhorn, 11/5/99, (PB2000-103386, A08, MF-A02).

- MCEER-99-0019 "Proceedings of the 7<sup>th</sup> U.S.- Japan Workshop on Earthquake Resistant Design of Lifeline Facilities and Countermeasures Against Soil Liquefaction," edited by T.D. O'Rourke, J.P. Bardet and M. Hamada, 11/19/99, (PB2000-103354, A99, MF-A06).
- MCEER-99-0020 "Development of Measurement Capability for Micro-Vibration Evaluations with Application to Chip Fabrication Facilities," by G.C. Lee, Z. Liang, J.W. Song, J.D. Shen and W.C. Liu, 12/1/99, (PB2000-105993, A08, MF-A02).
- MCEER-99-0021 "Design and Retrofit Methodology for Building Structures with Supplemental Energy Dissipating Systems," by G. Pekcan, J.B. Mander and S.S. Chen, 12/31/99, (PB2000-105994, A11, MF-A03).
- MCEER-00-0001 "The Marmara, Turkey Earthquake of August 17, 1999: Reconnaissance Report," edited by C. Scawthorn; with major contributions by M. Bruneau, R. Eguchi, T. Holzer, G. Johnson, J. Mander, J. Mitchell, W. Mitchell, A. Papageorgiou, C. Scaethorn, and G. Webb, 3/23/00, (PB2000-106200, A11, MF-A03).
- MCEER-00-0002 "Proceedings of the MCEER Workshop for Seismic Hazard Mitigation of Health Care Facilities," edited by G.C. Lee, M. Ettouney, M. Grigoriu, J. Hauer and J. Nigg, 3/29/00, (PB2000-106892, A08, MF-A02).
- MCEER-00-0003 "The Chi-Chi, Taiwan Earthquake of September 21, 1999: Reconnaissance Report," edited by G.C. Lee and C.H. Loh, with major contributions by G.C. Lee, M. Bruneau, I.G. Buckle, S.E. Chang, P.J. Flores, T.D. O'Rourke, M. Shinozuka, T.T. Soong, C-H. Loh, K-C. Chang, Z-J. Chen, J-S. Hwang, M-L. Lin, G-Y. Liu, K-C. Tsai, G.C. Yao and C-L. Yen, 4/30/00, (PB2001-100980, A10, MF-A02).
- MCEER-00-0004 "Seismic Retrofit of End-Sway Frames of Steel Deck-Truss Bridges with a Supplemental Tendon System: Experimental and Analytical Investigation," by G. Pekcan, J.B. Mander and S.S. Chen, 7/1/00, (PB2001-100982, A10, MF-A02).
- MCEER-00-0005 "Sliding Fragility of Unrestrained Equipment in Critical Facilities," by W.H. Chong and T.T. Soong, 7/5/00, (PB2001-100983, A08, MF-A02).
- MCEER-00-0006 "Seismic Response of Reinforced Concrete Bridge Pier Walls in the Weak Direction," by N. Abo-Shadi, M. Saiidi and D. Sanders, 7/17/00, (PB2001-100981, A17, MF-A03).
- MCEER-00-0007 "Low-Cycle Fatigue Behavior of Longitudinal Reinforcement in Reinforced Concrete Bridge Columns," by J. Brown and S.K. Kunnath, 7/23/00, (PB2001-104392, A08, MF-A02).
- MCEER-00-0008 "Soil Structure Interaction of Bridges for Seismic Analysis," I. PoLam and H. Law, 9/25/00, (PB2001-105397, A08, MF-A02).
- MCEER-00-0009 "Proceedings of the First MCEER Workshop on Mitigation of Earthquake Disaster by Advanced Technologies (MEDAT-1), edited by M. Shinozuka, D.J. Inman and T.D. O'Rourke, 11/10/00, (PB2001-105399, A14, MF-A03).
- MCEER-00-0010 "Development and Evaluation of Simplified Procedures for Analysis and Design of Buildings with Passive Energy Dissipation Systems," by O.M. Ramirez, M.C. Constantinou, C.A. Kircher, A.S. Whittaker, M.W. Johnson, J.D. Gomez and C. Chrysostomou, 11/16/01, (PB2001-105523, A23, MF-A04).
- MCEER-00-0011 "Dynamic Soil-Foundation-Structure Interaction Analyses of Large Caissons," by C-Y. Chang, C-M. Mok, Z-L. Wang, R. Settgast, F. Waggoner, M.A. Ketchum, H.M. Gonnermann and C-C. Chin, 12/30/00, (PB2001-104373, A07, MF-A02).
- MCEER-00-0012 "Experimental Evaluation of Seismic Performance of Bridge Restrainers," by A.G. Vlassis, E.M. Maragakis and M. Saiid Saiidi, 12/30/00, (PB2001-104354, A09, MF-A02).
- MCEER-00-0013 "Effect of Spatial Variation of Ground Motion on Highway Structures," by M. Shinozuka, V. Saxena and G. Deodatis, 12/31/00, (PB2001-108755, A13, MF-A03).
- MCEER-00-0014 "A Risk-Based Methodology for Assessing the Seismic Performance of Highway Systems," by S.D. Werner, C.E. Taylor, J.E. Moore, II, J.S. Walton and S. Cho, 12/31/00, (PB2001-108756, A14, MF-A03).

- MCEER-01-0001 "Experimental Investigation of P-Delta Effects to Collapse During Earthquakes," by D. Vian and M. Bruneau, 6/25/01, (PB2002-100534, A17, MF-A03).
- MCEER-01-0002 "Proceedings of the Second MCEER Workshop on Mitigation of Earthquake Disaster by Advanced Technologies (MEDAT-2)," edited by M. Bruneau and D.J. Inman, 7/23/01, (PB2002-100434, A16, MF-A03).
- MCEER-01-0003 "Sensitivity Analysis of Dynamic Systems Subjected to Seismic Loads," by C. Roth and M. Grigoriu, 9/18/01, (PB2003-100884, A12, MF-A03).
- MCEER-01-0004 "Overcoming Obstacles to Implementing Earthquake Hazard Mitigation Policies: Stage 1 Report," by D.J. Alesch and W.J. Petak, 12/17/01, (PB2002-107949, A07, MF-A02).
- MCEER-01-0005 "Updating Real-Time Earthquake Loss Estimates: Methods, Problems and Insights," by C.E. Taylor, S.E. Chang and R.T. Eguchi, 12/17/01, (PB2002-107948, A05, MF-A01).
- MCEER-01-0006 "Experimental Investigation and Retrofit of Steel Pile Foundations and Pile Bents Under Cyclic Lateral Loadings," by A. Shama, J. Mander, B. Blabac and S. Chen, 12/31/01, (PB2002-107950, A13, MF-A03).
- MCEER-02-0001 "Assessment of Performance of Bolu Viaduct in the 1999 Duzce Earthquake in Turkey" by P.C. Roussis, M.C. Constantinou, M. Erdik, E. Durukal and M. Dicleli, 5/8/02, (PB2003-100883, A08, MF-A02).
- MCEER-02-0002 "Seismic Behavior of Rail Counterweight Systems of Elevators in Buildings," by M.P. Singh, Rildova and L.E. Suarez, 5/27/02. (PB2003-100882, A11, MF-A03).
- MCEER-02-0003 "Development of Analysis and Design Procedures for Spread Footings," by G. Mylonakis, G. Gazetas, S. Nikolaou and A. Chauncey, 10/02/02, (PB2004-101636, A13, MF-A03, CD-A13).
- MCEER-02-0004 "Bare-Earth Algorithms for Use with SAR and LIDAR Digital Elevation Models," by C.K. Huyck, R.T. Eguchi and B. Houshmand, 10/16/02, (PB2004-101637, A07, CD-A07).
- MCEER-02-0005 "Review of Energy Dissipation of Compression Members in Concentrically Braced Frames," by K.Lee and M. Bruneau, 10/18/02, (PB2004-101638, A10, CD-A10).
- MCEER-03-0001 "Experimental Investigation of Light-Gauge Steel Plate Shear Walls for the Seismic Retrofit of Buildings" by J. Berman and M. Bruneau, 5/2/03, (PB2004-101622, A10, MF-A03, CD-A10).
- MCEER-03-0002 "Statistical Analysis of Fragility Curves," by M. Shinozuka, M.Q. Feng, H. Kim, T. Uzawa and T. Ueda, 6/16/03, (PB2004-101849, A09, CD-A09).
- MCEER-03-0003 "Proceedings of the Eighth U.S.-Japan Workshop on Earthquake Resistant Design of Lifeline Facilities and Countermeasures Against Liquefaction," edited by M. Hamada, J.P. Bardet and T.D. O'Rourke, 6/30/03, (PB2004-104386, A99, CD-A99).
- MCEER-03-0004 "Proceedings of the PRC-US Workshop on Seismic Analysis and Design of Special Bridges," edited by L.C. Fan and G.C. Lee, 7/15/03, (PB2004-104387, A14, CD-A14).
- MCEER-03-0005 "Urban Disaster Recovery: A Framework and Simulation Model," by S.B. Miles and S.E. Chang, 7/25/03, (PB2004-104388, A07, CD-A07).
- MCEER-03-0006 "Behavior of Underground Piping Joints Due to Static and Dynamic Loading," by R.D. Meis, M. Maragakis and R. Siddharthan, 11/17/03.
- MCEER-03-0007 "Seismic Vulnerability of Timber Bridges and Timber Substructures," by A.A. Shama, J.B. Mander, I.M. Friedland and D.R. Allicock, 12/15/03.
- MCEER-04-0001 "Experimental Study of Seismic Isolation Systems with Emphasis on Secondary System Response and Verification of Accuracy of Dynamic Response History Analysis Methods," by E. Wolff and M. Constantinou, 1/16/04.

- MCEER-04-0002 “Tension, Compression and Cyclic Testing of Engineered Cementitious Composite Materials,” by K. Kesner and S.L. Billington, 3/1/04.
- MCEER-04-0003 “Cyclic Testing of Braces Laterally Restrained by Steel Studs to Enhance Performance During Earthquakes,” by O.C. Celik, J.W. Berman and M. Bruneau, 3/16/04.
- MCEER-04-0004 “Methodologies for Post Earthquake Building Damage Detection Using SAR and Optical Remote Sensing: Application to the August 17, 1999 Marmara, Turkey Earthquake,” by C.K. Huyck, B.J. Adams, S. Cho, R.T. Eguchi, B. Mansouri and B. Houshmand, 6/15/04.
- MCEER-04-0005 “Nonlinear Structural Analysis Towards Collapse Simulation: A Dynamical Systems Approach,” by M.V. Sivaselvan and A.M. Reinhorn, 6/16/04.
- MCEER-04-0006 “Proceedings of the Second PRC-US Workshop on Seismic Analysis and Design of Special Bridges,” edited by G.C. Lee and L.C. Fan, 6/25/04.
- MCEER-04-0007 “Seismic Vulnerability Evaluation of Axially Loaded Steel Built-up Laced Members,” by K. Lee and M. Bruneau, 6/30/04.



MULTIDISCIPLINARY CENTER FOR EARTHQUAKE ENGINEERING RESEARCH

*A National Center of Excellence in Advanced Technology Applications*

University at Buffalo, State University of New York

Red Jacket Quadrangle • Buffalo, New York 14261

Phone: (716) 645-3391 • Fax: (716) 645-3399

E-mail: [mceer@mceermail.buffalo.edu](mailto:mceer@mceermail.buffalo.edu) • WWW Site <http://mceer.buffalo.edu>



University at Buffalo *The State University of New York*

ISSN 1520-295X